UNIVERSITÀ DEGLI STUDI DI TRIESTE
e
UNIVERSITÀ CA' FOSCARI DI VENEZIA

XXXII CICLO DEL DOTTORATO DI RICERCA IN

CHIMICA

SYNTHESIS OF TRIPHENYLENES FOR SUPRAMOLECULAR APPLICATIONS

Settore scientifico-disciplinare: **Chim/06**

PhD CANDIDATE
GIACOMO BERTON

COORDINATOR
PROF. BARBARA MILANI

SUPERVISOR
PROF. ALESSANDRO SCARSO

CO-SUPERVISOR
PROF. FABRIZIO FABRIS

ACADEMIC YEAR 2018/2019

General Index

Introduction

I.1 Supramolecular Capsules and Cages

At the beginning of modern chemistry, the focus of the research has been the intimate understanding of the chemical reactivity, firstly looking at new ways to describe chemical connectivity, then optimizing the creation and cleavage of different covalent bonds, moving over time to intrinsically less reactive molecules in order to obtain new chemical species, like drugs, and new materials, like polymers, that revolutionized the human society.

More or less one hundred years later, by observing the biological systems, chemists realized that the molecules of life were dispatching many of their functions by simply interacting with the target site through weak interactions, without having their chemical connectivity modified, playing a role as entire species thanks to specific functional groups. With this lesson coming from Nature, the scientific community learned to pay particular attention not only to the covalent modifications of molecules in order to explore the connectivity of molecules, but also to the different interactions occurring between molecules *via* non-covalent weak bindings.

To study these interactions and exploit this knowledge to develop new systems that could mimic typical features of biological systems present in Nature and, possibly, use them to our advantage, a new branch of chemistry came forth: Supramolecular Chemistry.

Within this newly born science, which is now a grown-up adult in its forties, it is now possible to browse through memories album of supramolecular recognition where three major periods of evolution can be recognized.[1]

The first period characterized the 80s and consisted into in depth studies of synthetic receptors, aimed at understanding the thermodynamic properties of binding, mostly involving bimolecular systems. Trimolecular systems at that time were less studied, apart examples related to the investigation of the allosteric effect,[2] and partially cooperativity effect.[3,4]

In the 90s, a higher level of complexity in host-guest systems was achieved with studies like template effects on bimolecular[5] and trimolecular[6,7,8] systems. The receptors started to become larger and more complex, displaying concave structures like clefts,[9] armatures,[10] tweezers,[11,12] bowls[13] and others,[14] with the general thought that a receptor could be created to surround the target molecule and recognizing it through weak intermolecular forces. The strategy of using self-complementary compounds to create host systems instead of a large covalent host molecule started to be considered in the late 90s, obtaining the first examples of “encapsulation complexes”.[1]

On the other side, several large host systems based on covalent structures like carcerands[15] and cryptophanes[16] appeared on the stage, showing the first examples of molecular cages. Later, the discovery and application of the dynamic covalent chemistry allowed the formation at the equilibrium of covalent bonds,[17,18] making easier the preparation of closed host systems forming stable cages.[19,20]

From that moment, the third period begun with a proliferation of supramolecular receptors, mainly composed by two or more concave hemispheres, held together by weak interactions

to form capsules, or by covalent bonds to form cages. At the same time, the knowledge gathered in this field helped to put the basis for molecular machines (Figure 1).[21]

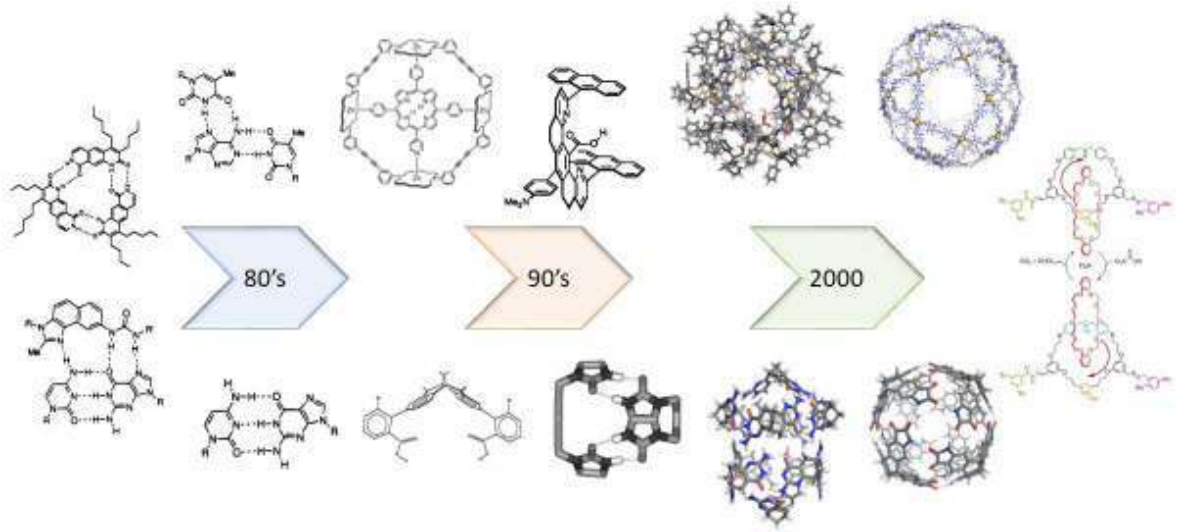

Figure 1: Schematic representation of the three different time-stages of supramolecular chemistry and recognition.

Very recently, the implementation of specific molecular structures like photochromic units[22] and catalytic units, spurred the development of supramolecular systems characterized by reversible properties like modulation of shape, size and position by external stimuli as well as the advent of supramolecular catalysis.[23,24] The latter is still a fast-growing part of supramolecular chemistry, where the recognition of reaction intermediates, or ideally transition states, by host systems enable strong acceleration of organic transformations, clearly resembling what occurring in enzymes.

In particular for supramolecular catalysis, the development of closed host systems is peculiar to allow a full solvation of the substrate, which is a fundamental pre-requisite for its recognition (substrate selectivity), activation and pre-orientation, stabilization of intermediates (often charged species), product selective formation and possible release of the product and uptake of a new molecule of substrate to obtain turnover properties.

All the work done in this field so far would have been impossible without the discovery and exploitation of weak interactions, such as hydrogen bonds, ionic interactions, metal-ligand coordination, ion-π and π-π interactions, hydrophobic effect and, more recently, halogen bonds. All these intermolecular forces, observed also in all biological processes taking places in Nature, are fundamental tools for the development of self-assembling systems from simple entities to form capsules with different sizes and shapes. Nowadays, chemists mastering weak intermolecular interactions are just limited by their imagination when seeking for new recognition systems.

I.1.1 Hydrogen Bonded Capsules

When talking about capsules held together by hydrogen bonds,[25] the most iconic examples are those developed by Rebek, in particular the so-called "tennis ball" and "soft ball" in virtue of their shape resembling specific sports balls, characterized by the use of glycoluril moieties[26] to create supramolecular structures. The very first H-bonded supramolecular

capsule was obtained conjugating two glycoluril units on a central aromatic core giving rise to the tennis ball (Scheme 1).[27]

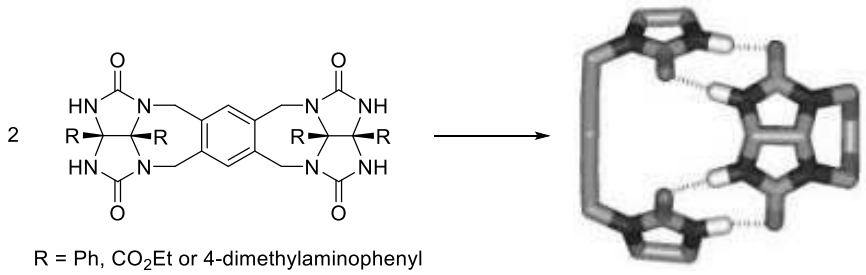

Scheme 1: Self-assembly in solution of Rebek's "tennis ball" capsule. Adapted from [1].

The glycoluril substituents granted curvature to the monomer and the possibility to establish eight hydrogen bonds between two identical molecules. The result is a small ball-shaped capsule (thus the nickname), with a 50 Å^3 cavity capable of hosting guests like methane, ethane, ethylene, and noble gases. Larger guests such as propane, allene, and isobutylene were excluded from the cavity being too large to fit the cavity.[28]

By expanding the aromatic skeleton, larger capsules known as "softballs" were obtained (Scheme 2).[29,30]

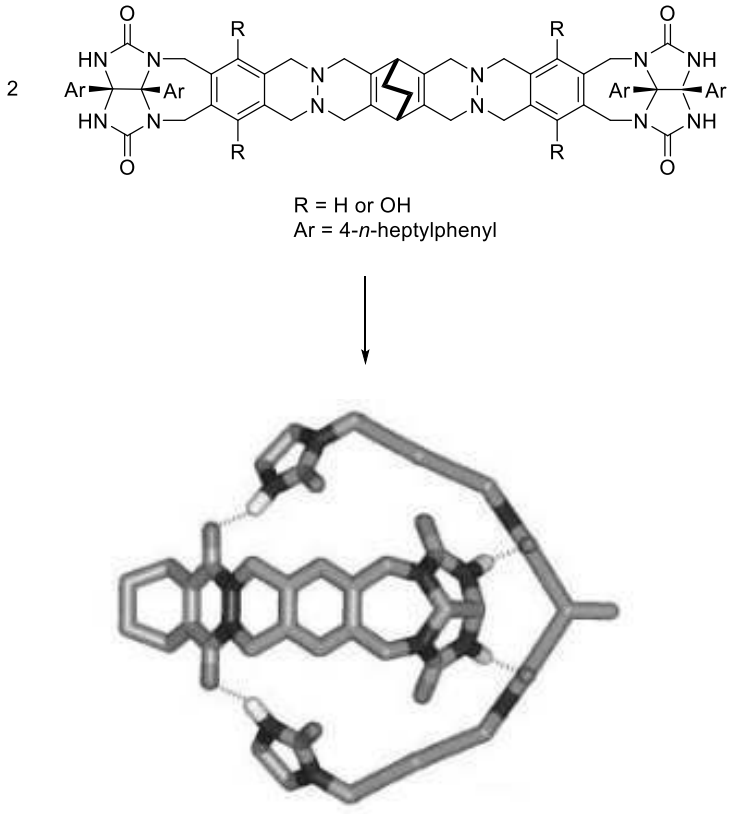

Scheme 2: Self-assembly in solution of Rebek's "softball" capsule. Adapted from [1].

The general idea is similar to the "tennis ball", but this time the cavity is larger (in the range 240-320 Å^3), as function of the spacer units between the glycoluril moieties, enabeling to accommodate even two copies of guests as large as benzene at the same time.[31]

Over the years, in the literature appeared several interesting examples of dimeric capsules, like calix[4]arene provided with four ureas moieties on the upper rim, able to aggregate in the presence of a guest,[32] or an imide-substituted resorcin[4]arene cavitand,[33] that in the presence of suitable guests dimerize into a cylindrical capsule capable of binding elongated guests.

Self-assembling through H-bond is not limited to dimeric systems, and concomitantly capsules composed by more than two monomers came to stage. One fundamental example reported by Atwood was the resorcin[4]arene, able to form hexameric structures in the solid state as well as in solution held by 60 hydrogen bonds, comprising also the participation of eight water molecules.[34] Recent examples of beautiful H-bonded capsules, in particular characterized by the use of enantiopure building blocks, have appeared in the literature. One elegant example was reported by Wärnmark and Orentas, where the combination of double and triple hydrogen bonds between isocytosine units, embedded in an enantiomerically pure bicyclic framework, enabled the formation of a chiral decameric capsule in carbon disulphide (Scheme 3).[35]

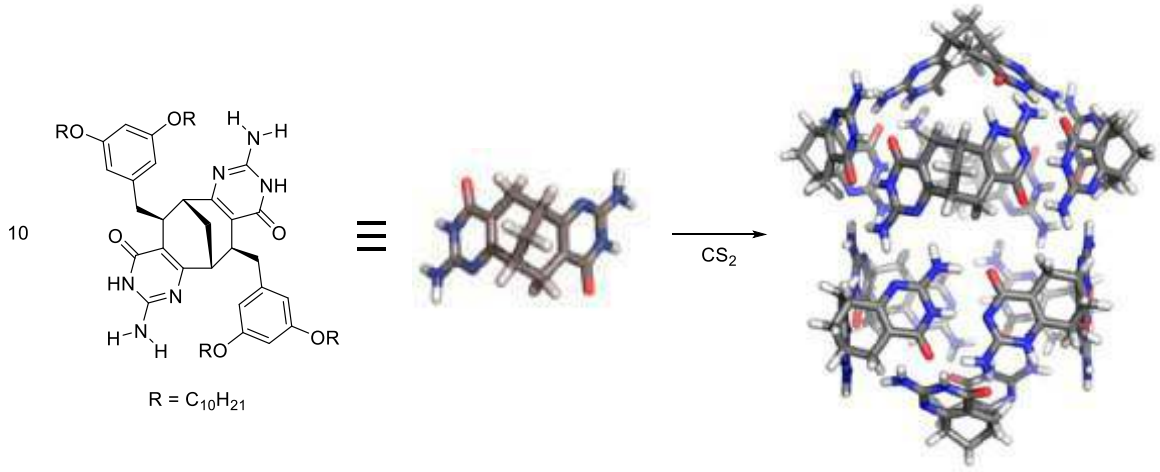

Scheme 3: Scheme of Orentas's monomer and self-assembly into a decameric H-bonded chiral enantiopure capsule in carbon disulphide. Adapted from [35].

In solution, the C_2 enantiopure monomer tautomerizes into three different forms with different hydrogen bonding donor-acceptor patterns, thus breaking its intrinsic symmetry. The formed chiral decameric aggregate resembles a tube, capped by two C_2-symmetric monomers, and demonstrated to host one partially solvated C_{60} molecule. Since the tautomerization of the monomer depends on the solvent, the aggregation is highly solvent dependent.

Another example of chiral capsule from chiral H-bonding building blocks was reported in 2016 by Mastalerz and co-workers. The combination of four enantiomerically pure C_3-symmetric building blocks designed to associate into a single geometric orientation provided a chiral cube-shaped capsule in apolar solvents (Scheme 4).[36]

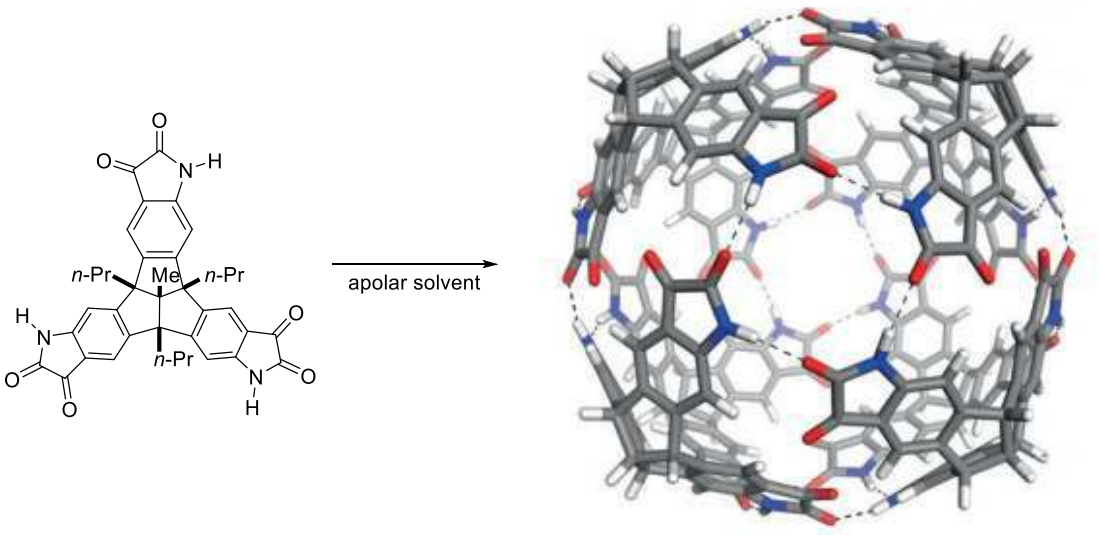

Scheme 4: Mastalerz chiral monomer and self-assembling into a tetrameric enantiopure cubic capsule. Adapted from [36].

The use of an enantiopure monomer was vital for the formation of the capsule. Indeed, when the racemate monomer was used under identical experimental conditions, only a large amount of ill-defined aggregates was observed. The large cavity of 2300 $Å^3$ allowed to bind cationic species, like the very large tetrahexadecylammonium cation.

One last example, brought by Markiewicz and Jenczak, consisted in the use of derivatives of the trimesic acid bearing three amino acids connected through amide bonds. The C_3-symmetric enantiopure monomers aggregated in nonpolar solvents into an octameric enantiopure capsule held together by the formation of 48 hydrogen bonds (Scheme 5).[37]

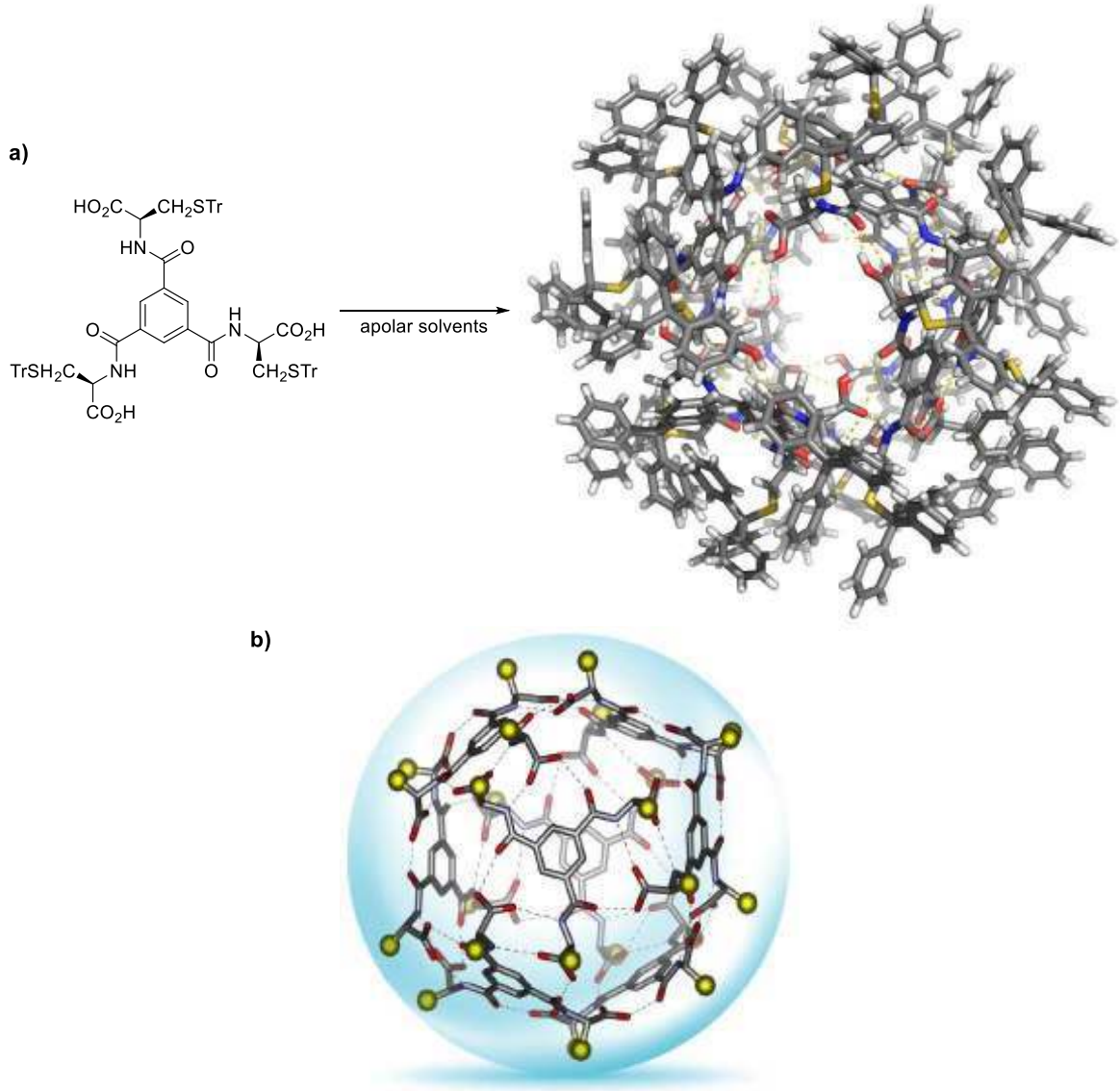

Scheme 5: a) *tris*-amino acid functionalized monomer forming a octameric capsule and b) simplified structure of the octamer. Adapted from [37].

The obtained amino acids-based nano-capsules resulted to be stable at high and low temperatures and in the presence of a base, probably thanks to the large hydrogen bonding network. With a cavity volume of 1.719 Å^3, the octamer enabled to host both C_{60} and C_{70}, with a preferential and selective binding toward the latter when in the presence of a mixture of the two guests due to structural complementarity.

It is important to note that almost all the known H-bonded supramolecular capsules are stable in apolar solvents and typical solvents for their investigation, specifically by NMR spectroscopy, are chlorinated solvents.

I.1.2 Metal-Ligand-Based Supramolecular Capsules

Hydrogen bonds are an effective way to create capsules in solution, and together with metal-ligand coordination they represent the most common methods for the preparation of self-assembling supramolecular capsules in solution. While in the case of hydrogen bonds

there is the need of curved molecules to create the final closed structure, when using a metal-ligand interaction the curvature can be created by metal centres with different coordination geometries, while flat ligand molecules can act as panels or edges for the capsule.

One of the most iconic examples of metal-ligand capsules was reported by the group of Fujita, which proposed the preparation of water-soluble coordination cages combining a triangular *p*-substituted *tris*-pyridine ligand with a triazine core and different *cis*-protected square-planar palladium or platinum complexes (Scheme 6).[38]

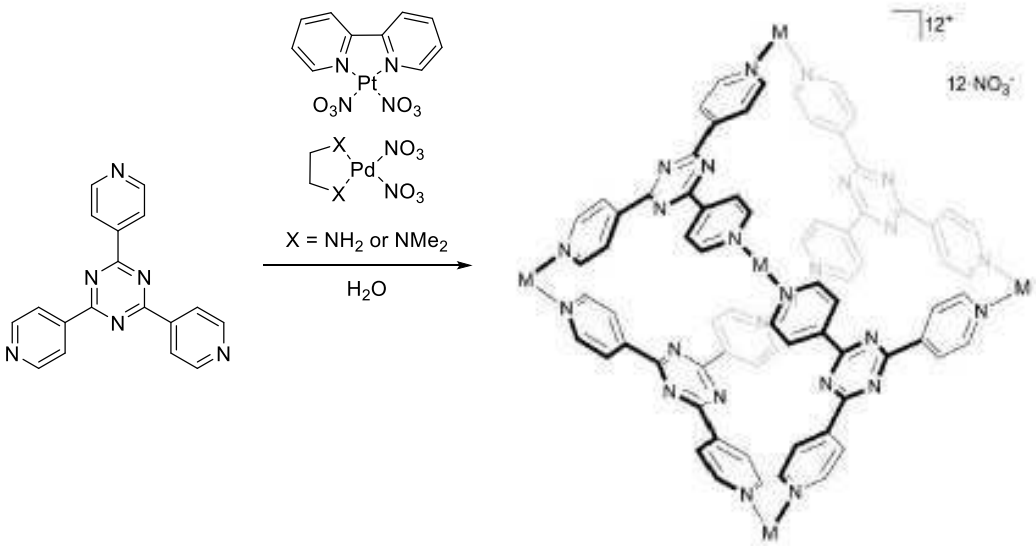

Scheme 6: Formation of Fujita's octahedral capsule in water through the coordination between a *tris*-pyridine ligand and Pt or Pd complexes as metal corners.

This capsule showed landmark host-guest properties, being able to host up to three molecules of guests, showing the first examples of supramolecular catalysis with impressive product selectivity properties for a very wide range of chemical reactions.[39]

During the years, Fujita developed many metal-ligand capsules, trying to make them very large and roomy by carefully choosing the geometry of the ligands and the coordinating metals. A record was reached with the creation of a $M_{30}L_{60}$ icosidodecahedron assembly starting from a pyridine substituted thiophene and a palladium salt in DMF (Scheme 7).[40]

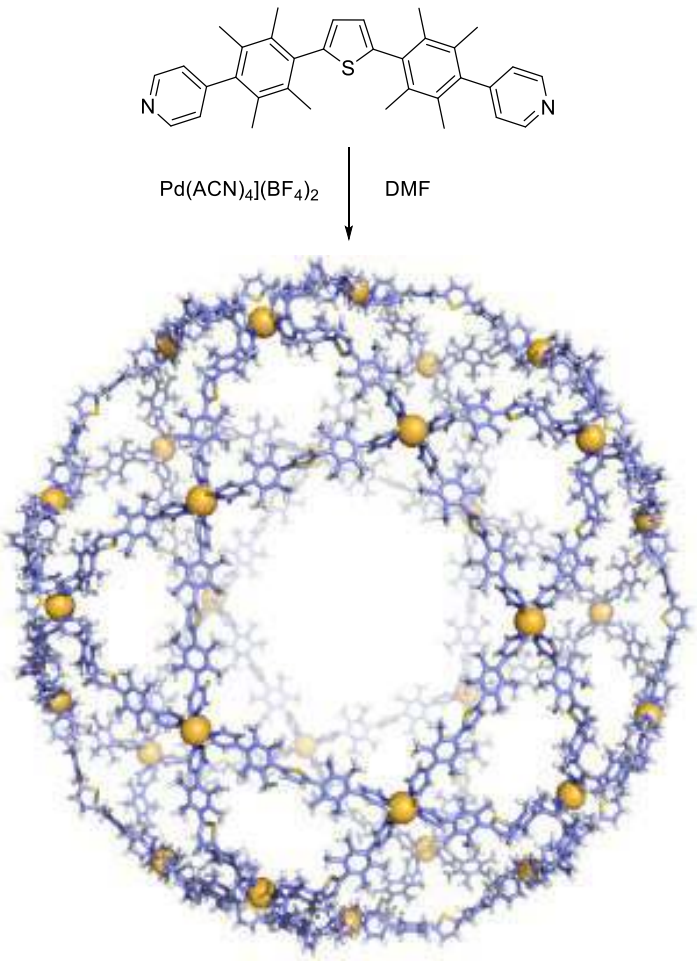

Scheme 7: Formation of Fujita's icosidodecahedral capsules in DMF through coordination between a bis-pyridine ligand and Pd corners. Adapted from [40].

The structure was confirmed by X-rays diffraction, which was possible only after months of slow vapor diffusion of AcO*i*Pr in a DMSO solution of the capsules, affording a single crystal suitable for analysis. With a diameter of 8.2 nm and an amazing volume of 157000 $Å^3$, this capsule is a very promising host for large objects, like proteins or nanoparticles.

Another seminal example in this field is the tetrahedral capsule developed by Raymond by connecting four bis-catecholamide ligands and four metal centres of gallium(III), that is soluble in water thanks to the presence of several negative charges (Scheme 8).[41,42]

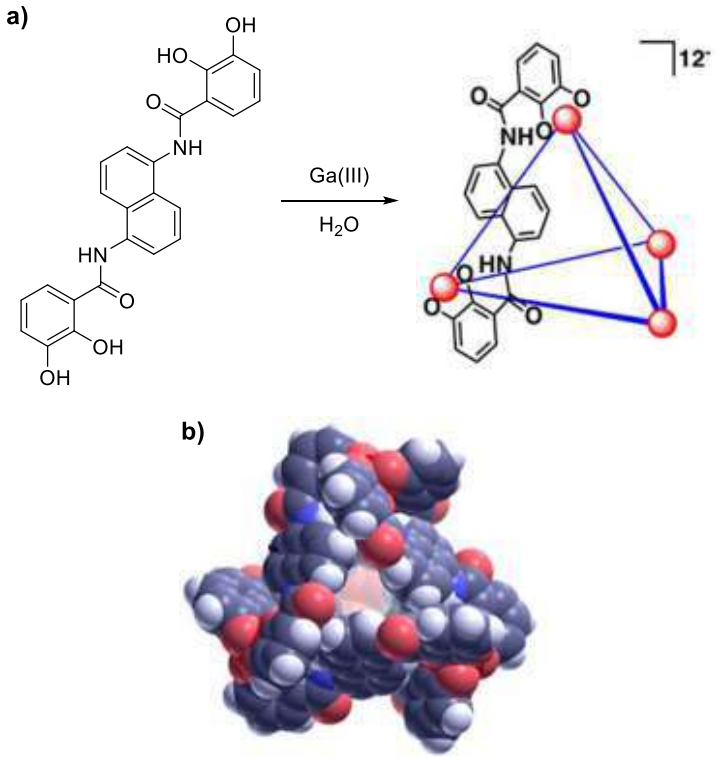

Scheme 8: a) Self-assembling of the Raymond's capsule in water forming a tetrahedral capsule and b) molecular model of the capsule. Adapted from [42].

The nano-capsule is chiral due to the asymmetry arising by the coordination of three catechol units on octahedral Ga(III) corners, and exists as racemate mixture of ΔΔΔΔ or ΛΛΛΛ, depending on the orientation of the octahedral propeller-like complexes at the vertices of the capsule. Due to the anionic nature of Raymond's capsule, encapsulation of cationic guests like tetraethylammonium was achieved easily, spurring the stabilization of cationic intermediate species for a wide range of chemical transformations. In fact, this aggregate is mostly famous for its astonishing catalytic activities. For instance, the capsule promoted electro-cyclizations and sigmatropic rearrangements, like the aza-Cope, *via* molecular confinement and constriction within the cavity with rate accelerations up to 850-fold (Scheme 9).[43] This reactivity was also observed in a stereoselective fashion, with enantiomeric excesses up to 78% when using the enantiopure ΔΔΔΔ capsule.[44]

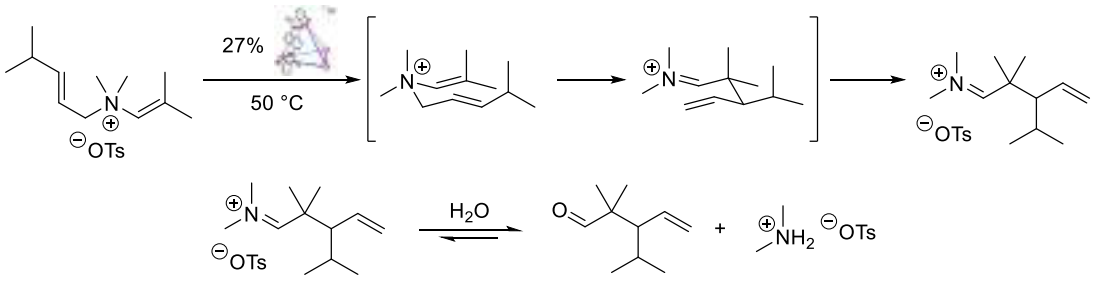

Scheme 9: Aza-Cope rearrangement promoted by Raymond's capsule.

To prove the role of the electrostatic charge of the capsule and its implication in the catalysis, an isostructural capsule bearing eight negative charges instead of twelve was obtained by replacing Ga(III) with Si(IV) cations.[45] The capsules where tested in the aza-Cope rearrangement of allyl-vinyl-ammonium cations and in the Nazarov cyclization. While

they showed identical rete acceleration in performing the aza-Cope rearrangement reaction, driven by simple constrictive binding, the results were largely different for the Nazarov cyclization, where the generation and stabilization of a carbocation as intermediate species within the capsule is crucial (Scheme 10).

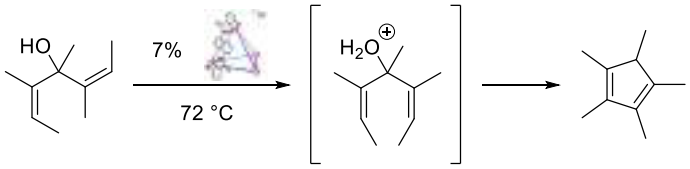

Scheme 10: Example of Nazarov cyclization promoted by Raymond's Ga(III) and Si(IV) capsules.

Indeed, the Ga(III) capsule, bearing twelve negative charges, demonstrated to accelerate the reaction rate of about 2000000-fold,[46] 680-fold higher than the Si(IV) capsule, thus demonstrating the crucial role of the anionic charge of the host in the stabilization of cation intermediates.

I.1.3 Hydrophobic Driven Capsule Formation

Water is the most abundant solvent on earth, and the medium in which all the biochemical reactions take place and where several different kinds of organisms live. During the years, some research groups decided to exploit the hydrophobic effect for the preparation of self-assembling capsules and molecular containers to use them as nanocarriers or nanoreactors.[47]

Taking inspiration by previous works,[48,49] Gibb and co-workers managed to obtain, through a six synthetic steps procedure, gram quantities of a water-soluble deep-cavity cavitand based on the functionalization of a shallow bowl-shaped resorcin[4]arene unit, adorned with aromatic walls and overall eight carboxylic acid moieties (Scheme 11).[50]

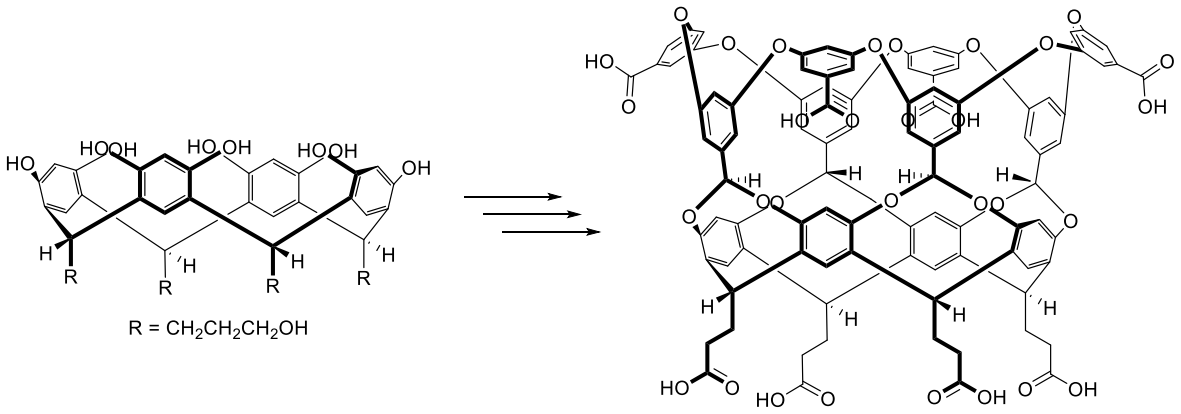

Scheme 11: Staring resorcin[4]arene substrate and final Gibb's octa-acid deep-cavity cavitand that provide capsules in water in the presence of suitable hydrophobic guests.

This molecule and its derivatives, soluble at concentrations greater than one hundred millimolar at pH 9, is able to bind apolar guests in the cavity and to self-assemble into well-defined supramolecular entities via the hydrophobic effect, taking advantage of its hydrophilic outer surface and hydrophobic inner cavity. In the presence of linear alkanes the cavitand can form different aggregates in water solution, with stoichiometries that

depend on the guest's length: 1:1 with methane, ethane, *n*-heptane and *n*-octane, a mixture of 1:1 and 2:2 complexes with propane, *n*-butane, and *n*-hexane, and a dimeric capsular assembly for *n*-pentane (2:2) as well as for longer chain alkanes C9 to C14 (2:1) (Scheme 12).[51,52]

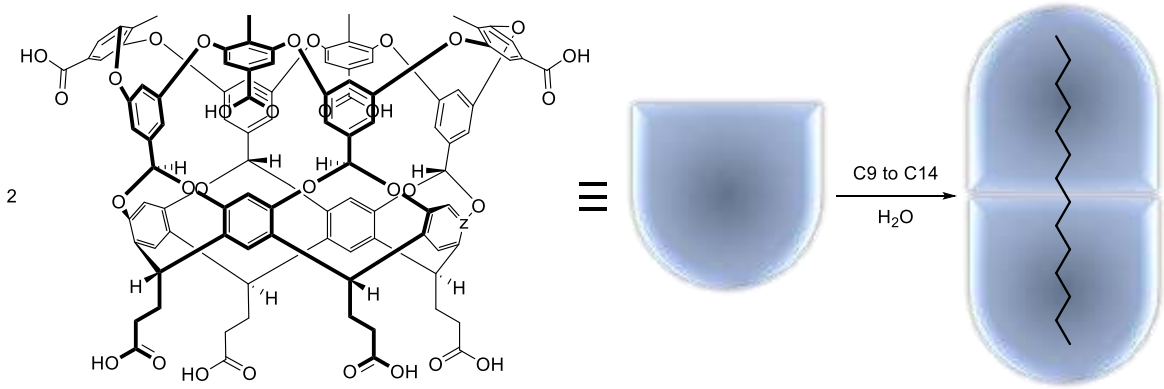

Scheme 12: Self-assemble of TEMOA into a 2:1 dimeric capsular aggregate in water in the presence of long- alkanes.

I.1.4 Ion-Pairing Capsules

Coulombic interactions (charge-charge) are intrinsically strong intermolecular interactions that are very sensitive to the polarity of the medium and to the presence of other ionic species in solution (ionic strength of the solution). Because of its higher complexity and, differently from the H-bond, lack of directionality, the electrostatic interaction has been much less exploited compared to other interactions for the development of self-assembling capsular systems. To date, in the literature there are no more than three classes of this kind of aggregate, witnessing the difficulty to obtain such supramolecular nano-systems.

One of the first examples of ion-pairing capsules was reported by Reinhoudt and Timmerman, who reported the obtainment of a hemi-spherical assembly based on tetra-pyridinium porphyrin capped with a tetra-sulfonate decorated calix[4]arene (Scheme 13).[53]

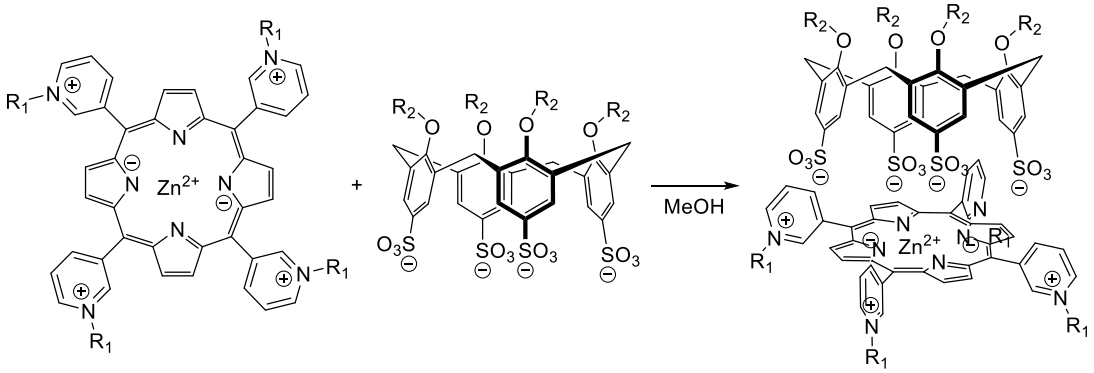

Scheme 13: Tetra-pyridinium porphyrin and tetra-sulfonate calix[4]arene self-assemble in methanol.

This interaction took place in a polar solvent, such as methanol or methanol and water (up to 45% molar fraction). The aggregation process was analysed, and it was confirmed to be entropy driven, with a 1:1 stoichiometry, displaying in methanol a very large K_a around 10^7 M^{-1}. Addition of salts like tetrabutylammonium perchlorate in concentration 4500 times

higher than the capsule produced a decrease of the binding constant of only 10 times, giving a great idea on the possible strength of this kind of aggregates.

I.1.5 Halogen Bonded Capsules

Halogen bond is a recently disclosed weak intermolecular interaction, similar to a Lewis acid-base interaction, given by the interaction of a σ-donor (*i.e.* amines, pyridines) with a halogen atom bearing a so-called σ-hole, a positively charged anisotropy in the electronic cloud caused by a strong electron-withdrawing group bonded to the halogen, typically a fluorine-substituted aromatic ring. A few years ago, Diederich and collaborators decided to use this interaction to create a series of supramolecular capsules, which were studied in the solid phase as well as in solution and in the gas phase (Figure 2).[54]

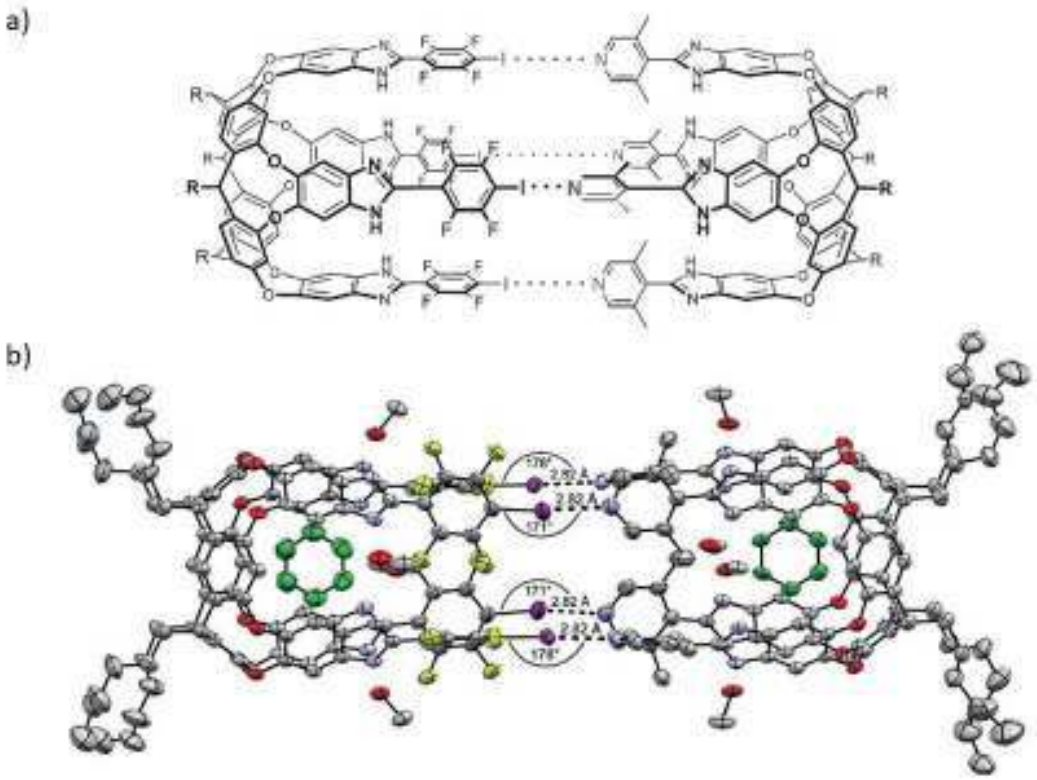

Figure 2: One of the halogen bonded capsules developed by Diederich's group. a) Line-drawing structure of halogen bonded capsule (R = C_6H_{13}); b) ORTEP single-crystal X-ray structure of the same capsule. Halogen bonds are highlighted with dashed lines. Adapted from [54].

The capsules, composed by two complementary resorcin[4]arene derivatives with remarkable K_a up to $2.11 \cdot 10^5$ M^{-1} in apolar solvent, showed to bind suitable guests like *N*-methylpyridinium tosilate, while an elongated version of the capsule was able to host up to three molecules of 1,4-dithiane.

I.1.6 Covalent Cages

As previously discussed, the first examples of covalent molecular containers were reported in the early 90s, by connecting two resorcin[4]arene cavitands with covalent linkers. The resulting structures displayed spherical cavities suitable for hosting of small guest.[55]

Examples of such molecules were called carcerands by their creator, Cram, to put emphasis on the high kinetic stability of the host-guest complexes obtained by heating together hosts and guests or by covalently assembling the host around the guest, exploiting the template effect in a shell-closing reaction (Figure 3).[56]

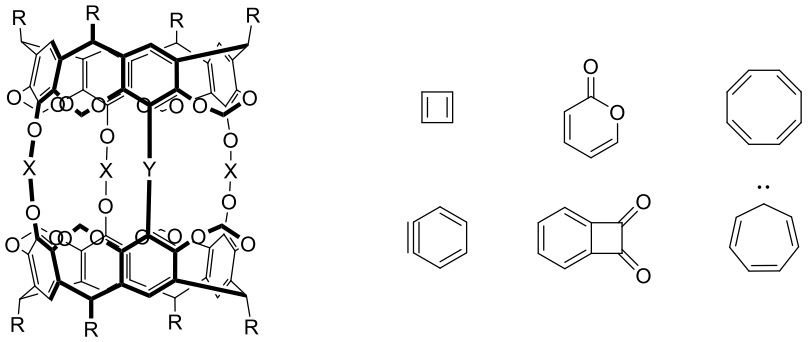

R = CH_2CH_2Ph, X = CH_2, Y = 2H
or
R = CH_2CH_2Ph, X = $(CH_2)_4$, Y = $-O(CH_2)_4O-$
or
R = $(CH_2)_4CH_3$, X = $(CH_2)_4$, Y = $-O(CH_2)_4O-$

Figure 3: Examples of Cram's carcerands and reactive molecules stabilized as guests.

The properties of the trapped guest were different from those in bulk solution, so different that Cram started to talk about a new phase of matter.[57] Carcerands were able to stabilize reactive molecules upon encapsulation, like cyclobutadiene,[58] whose existence was proved before only in an argon matrix at 8 K.[59]

Later on, an example of covalent cage came from the group of Kobayashi, which reported a new structure based on two resorcin[4]arene units connected using dynamic boronic ester bonds between boronic acid modified resorcin[4]arenes and bis-catechol containing bridging units (Figure 4).[60]

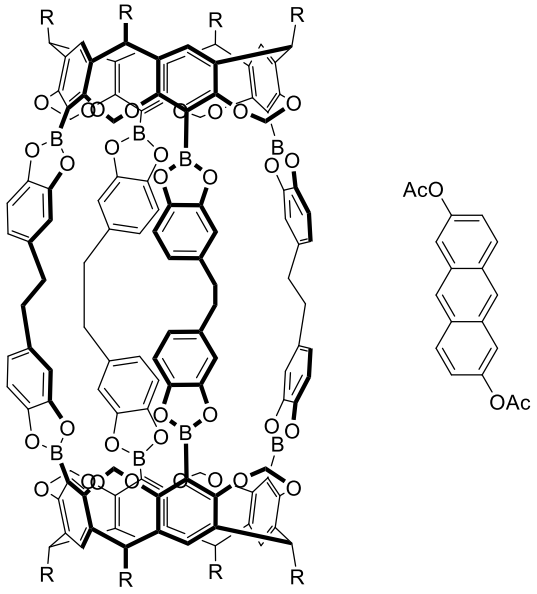

R = $(CH_2)_6CH_3$

Figure 4: Kobayashi's covalent cage and the proper guest, 2,6-diacetoxyanthracene.

The covalent cage was able to reversibly bind 2,6-diacetoxyanthracene, that, when encapsulated, upon irradiation did not undergo photodimerization or photooxygenation. The photodimerization did not take place due to the impossibility for the capsule to host more than one molecule of guest at a time, while the authors explained the absence of photooxygenation due to a high energy transition state within the capsule, which, with its bent structure within the constricted space of the cavity, would be too energetically high.

I.2 Triphenylenes

Triphenylene is a symmetric and planar polycyclic aromatic hydrocarbon consisting in four fused benzene rings, which is commonly substituted in the highlighted positions 2, 3, 6, 7, 10 and 11 (Figure 5).

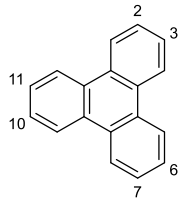

Figure 5: Structure of triphenylene. The most substituted positions of triphenylene are highlighted.

The discovery of triphenylene is dated back in 1880, when it was isolated by Schultz from the pyrolysis product of benzene,[61] which was synthesized by Berthelot thirteen years before.[62] However, the first real synthesis of triphenylene was reported in 1907 when Mannich obtained this polycyclic aromatic compound in two steps: condensation of cyclohexanone with sulphuric acid in methanol to achieve 1,2,3,4,5,6,7,8,9,10,11,12-dodecahydrotriphenylene with 8% yield, followed by dehydrogenation catalyzed by copper or zinc powder (Scheme 14).[63]

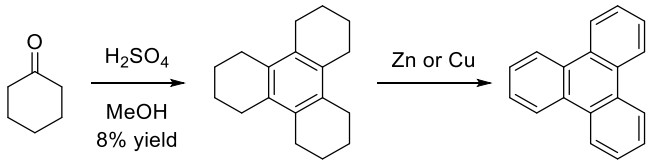

Scheme 14: Mannich synthesis of triphenylene.

The first studies on triphenylene were aimed more to unveiling its physical properties rather than its reactivity, since it showed fluorescence and strong absorbance in the UV region. The peculiar electronic distribution of triphenylene makes it the most similar molecule to benzene among all the polycyclic aromatic hydrocarbons.[64]

Nowadays, there are many strategies for the synthesis of triphenylene derivatives, symmetrical and unsymmetrical ones, that can be divided into six categories. In Scheme 15, the six strategies are reported using solid lines to show the isolated intermediates, while dashed bonds highlight the molecular portions that are added in the last step of the syntheses.[65]

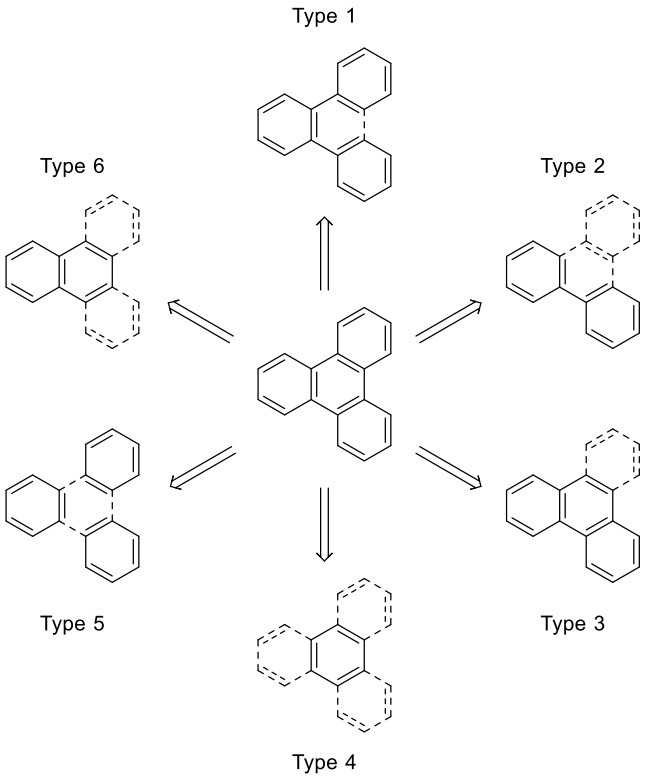

Scheme 15: The six methods for triphenylene synthesis. Dashed bonds highlight the molecular fragments that are added in the last step of the synthesis. Adapted from [65].

Type 1 strategy consists in the cyclization of a terphenyl involving oxidative methods or photocyclization. An example can be the synthesis of 2,3,6,7-tetrakis(hexyloxy)triphenylene obtained after a Suzuki coupling followed by oxidation or treatment with light (Scheme 16).[66]

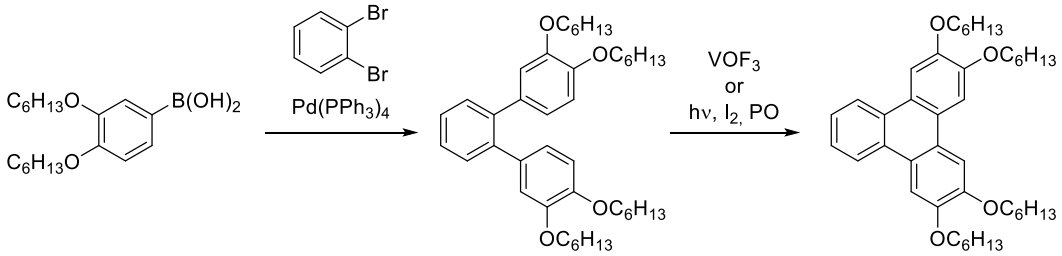

Scheme 16: Example of Type 1 strategy, the synthesis of 2,3,6,7-tetrakis(hexyloxy)triphenylene.

It is interesting to notice that propylene oxide (PO) can be used as acid scavenger to improve the triphenylene yield when a combination of iodine and light is used to perform the cyclization.[67]

Type 2 strategy relies on a precursor containing two of the final aromatic rings, connected through a biaryl bond. Usually, the reactions involved in a type 2 synthesis are palladium catalyzed cross-coupling,[68] Diels-Alder cycloaddition,[69] and oxidative cyclization (Scheme 17).[70]

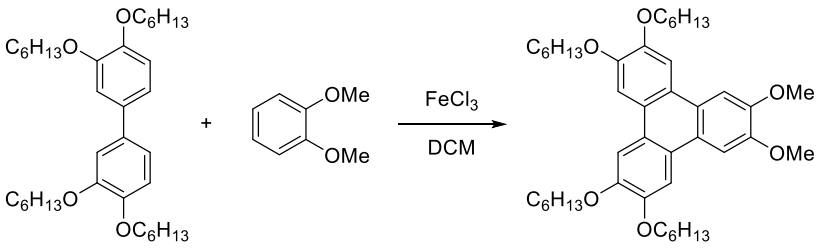

Scheme 17: Example of Type 2 strategy involving an oxidative cyclization.

Type 1 and 2 strategies share the same type of reactions, and in both cases the cyclization is characterized by moderate yields due to the formation of possible isomers.

Starting form a naphthalene core, the Type 3 strategy is based on the addition of the other two peripheric rings mainly through a Diels-Alder reaction, with general moderate yields (Scheme 18).[71]

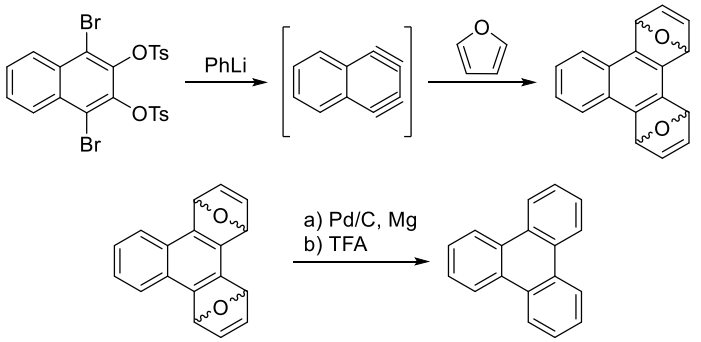

Scheme 18: Example of synthesis of triphenylene through Diels-Alder reaction using a Type 3 strategy.

Classical Friedel-Craft reactions from functionalized naphthalene can also be involved for Type 3 strategy, but yields are always from moderate to low.[72]

Type 4 strategy considers a phenanthrene derivative as a key intermediate which is converted to a triphenylene through the insertion of the fourth ring. Diels-Alder reactions[73] and photocyclization[74] are usually involved when considering this strategy, but also Friedel-Craft reactions proved useful (Scheme 19).[75]

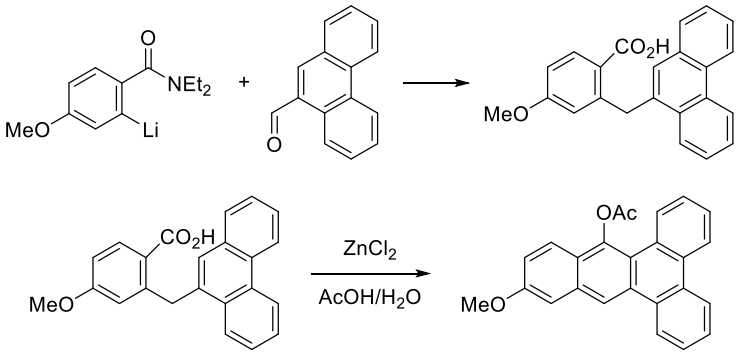

Scheme 19: Example of a Type 4 synthesis of triphenylene through a Friedel-Craft reaction.

In the last synthetic step of the reaction in Scheme 19, a ketone intermediate is formed before enolization and acetylation. Other methods, like condensations[76] and Wittig reactions,[77] proved to be viable to achieve a triphenylene from a phenanthrene.

Since the Mannich synthesis of triphenylene, the trimerization reactions are the oldest method for the preparation of triphenylenes and are the subjects of Type 5 strategy. Among this strategy, oxidative trimerizations of catechol derivatives are the most exploited, involving iron(III) chloride,[78] molybdenum(V) chloride[79] or vanadium(V) oxychloride as oxidising agents.[80] Moreover, Grignard reagents[81] or transition metals catalysts proved to be efficient in the trimerization of aryl derivatives as well (Scheme 20).[82]

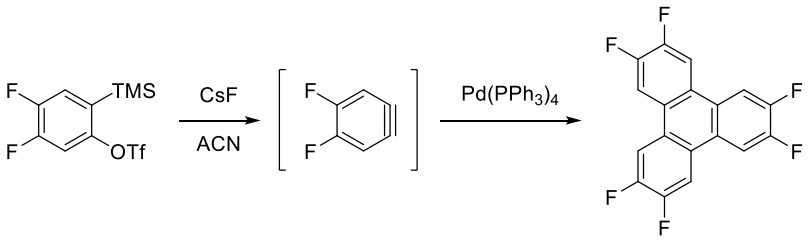

Scheme 20: Palladium catalyzed trimerization of aryl derivative as example of Type 5 strategies.

The last synthetic approach, Type 6, consists in the formation of all the peripheral rings in just one synthetic step. These reactions are challenging, nevertheless in the literature are reported examples involving catalyzed cyclizations,[83] Diels-Alder reactions[84] or photochemical cyclizations (Scheme 21).[85]

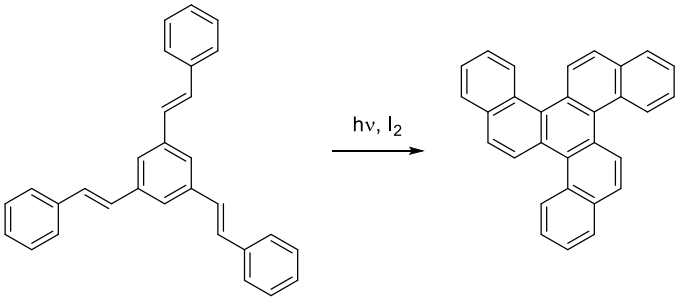

Scheme 21: Example of photochemical cyclization to triphenylene in one step, belonging to the Type 6 strategies.

During the years, triphenylene analogous have been created to expand the properties of such molecule. Among them, worth to notice are aza-triphenylenes, benzotrithiophenes, benzotrifuranes and truxenes.

Aza-triphenylenes are usually prepared through condensation of hexaaminobenzene with 1,2-dicarbonyl derivatives,[86] or condensation of hexaketocyclohexane with 1,2-diaminoethylene derivatives (Scheme 22).[87]

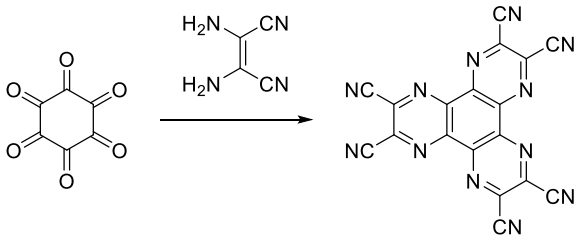

Scheme 22: Synthesis of aza-triphenylenes *via* ketone-amine condensation.

Aza-triphenylene derivatives are among the smallest two-dimensional *N*-containing polyheterocyclic aromatic systems and are used for the synthesis of larger polyheterocyclic systems, as well as materials for the creation of optical devices.[88]

Benzotrithiophenes are obtained with a Type 1 strategy, simply using a thiophene analogue of terphenyl (Scheme 23).[89]

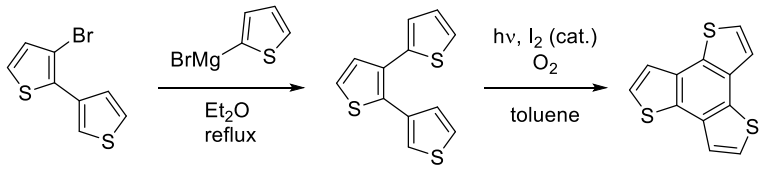

Scheme 23: Synthesis of benzotrithiophenes.

For what regards benzotrifuranes, a Type 6 strategy is involved in the synthesis (Scheme 24).[90]

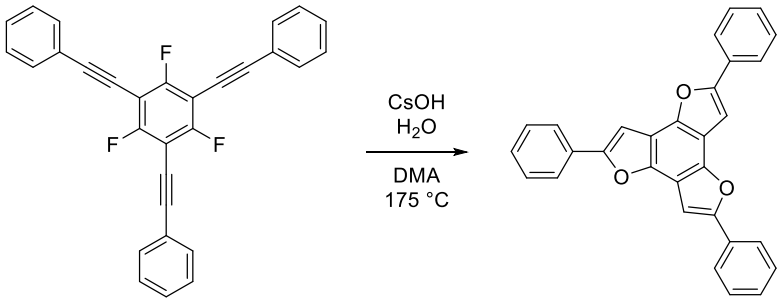

Scheme 24: Aryl-benzotrifurane synthesis.

Benzotrithiophenes and benzotrifuranes are characterized by a C_3-symmetry and are exploited as building blocks for π-conjugated materials due their shape and delocalized π-surface, that confers optical and self-assembling properties.[91]

Truxene and derivatives are usually obtained with a Type 5 strategy from the condensation of 1-indanone, 1,3-dioxoindan[92] or indole (Scheme 25).[93]

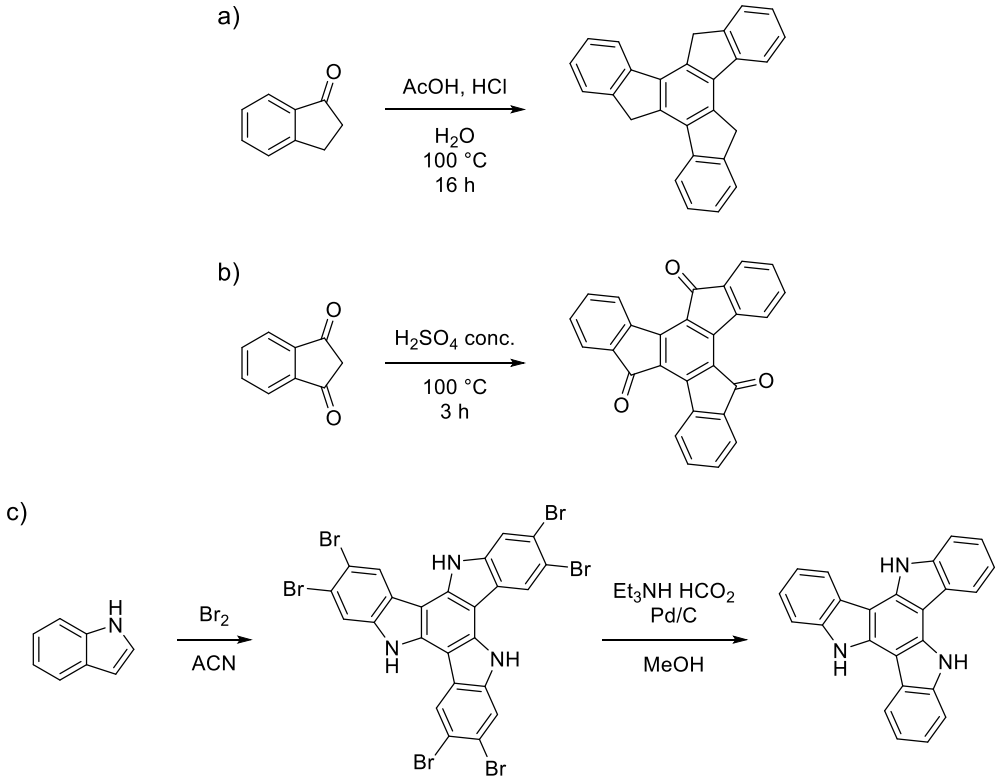

Scheme 25: a) synthesis of truxene, b) truxenone and c) triazatruxene.

The reported uses of truxene and derivatives are numerous, at least a dozen, many similar to the uses of triphenylene: non-linear opticals (NLO), two photon absorption (TPA), transistors, organic photovoltaics (OPVs), organic light-emitting diodes (OLEDs), molecular resists, lasers, organo-gels, fluorescent probes, self-assembling systems, molecular wires, liquid crystals and dynamic nuclear polarisation.[94]

I.2.1 Triphenylenes for Liquid Crystals Applications

Discotic liquid crystals (DLCs) are peculiar examples of state of the matter characterized by the self-organization of disk-like molecules through π-π interactions. In the majority of the cases, DLCs form a columnar mesophase where the molecules stack one on the top of the other forming columns, which self-organize into different two-dimensional lattice, in an ordered or disordered (aperiodical) fashion (Figure 6).[95]

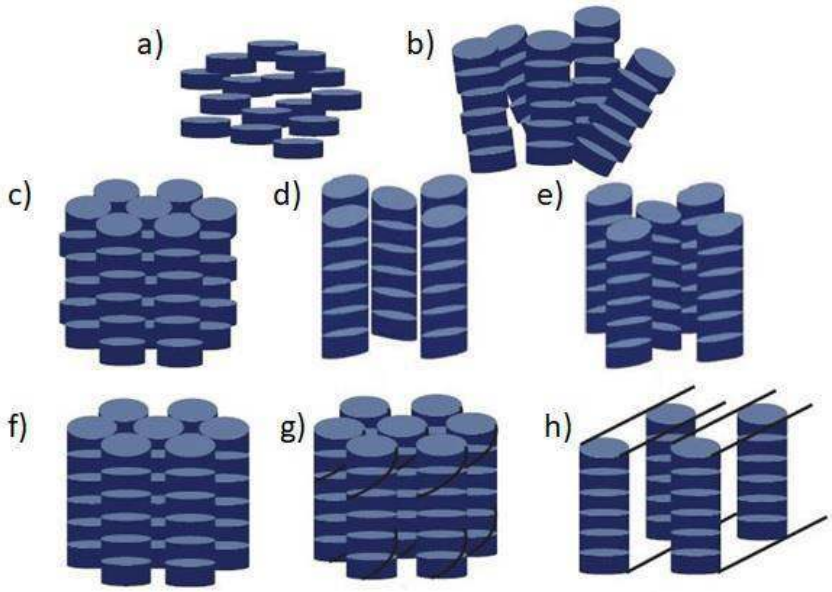

Figure 6: Different mesophases formed by disc-like molecules. a) discotic nematic; b) columnar nematic; c) hexagonal columnar; d) rectangular columnar; e) columnar oblique; f) columnar plastic; g) columnar helical; h) columnar lamellar phase. Adapted from [95].

For their self-aggregation ability, discotic molecules can be exploited for device applications like photovoltaic,[96] light-emitting diodes,[97] memory elements and sensors.[98]

The columns formed by discotic molecules display charge transfer properties through the pillar core, formed by the staked π systems, which is sensitive to structural defect. This property comes from the core-core separation in the columnar mesophase, usually around 3.5 Å, that allows a good overlapping of the π orbitals. The flexible aliphatic chains surrounding the core act as insulation, thus interactions between neighbouring columns are limited and the charge migration in these materials is almost mono-dimensional (Figure 7).[95]

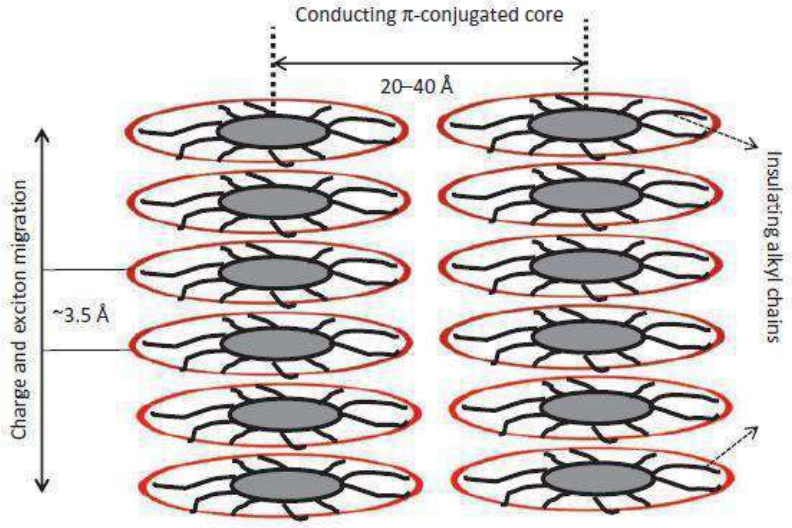

Figure 7: Representation of charge transfer in columnar discotic systems. Adapted from [95].

Due to this wide π orbital overlapping, the band width reaches values close to 1.1 eV, similar to graphite.[99] Suitable molecules for the creation of DLCs are those provided by rigid

aromatic cores, based on benzene, triphenylene, pyrene, perylene, porphyrin, phthalocyanine or hexabenzocoronene. Among them, triphenylene has been recognized as a potential starting material for DLCs since 1978,[100] and since then, hundreds of triphenylenes based DLCs have been prepared.

The properties of such derivatives proved to be significantly influenced by the nature of the substituents surrounding the triphenylenic core. Indeed, varying only one of the attached chains often resulted in dramatic changes of phase behaviour and physical properties.[101,102]

Substituted triphenylenes for DLCs can be divided into three main classes: symmetrical triphenylene hexaethers, symmetrical triphenylene hexaesters, and unsymmetrical hexasubstituted triphenylene derivatives, which are usually synthetized through Type 5 strategy. In addition to these classes, symmetrical and unsymmetrical triphenylene-based dimers, trimers, oligomers and polymers can be found as well.

Regarding the first two classes of triphenylenes, symmetrical hexaethers and hexaesters, these are obtained from a common hexahydroxytriphenylene unit, **HHTP**, which can be easily transformed into the desired products by nucleophilic substitution reactions on the phenolic units in good to high yields (Scheme 26).[95]

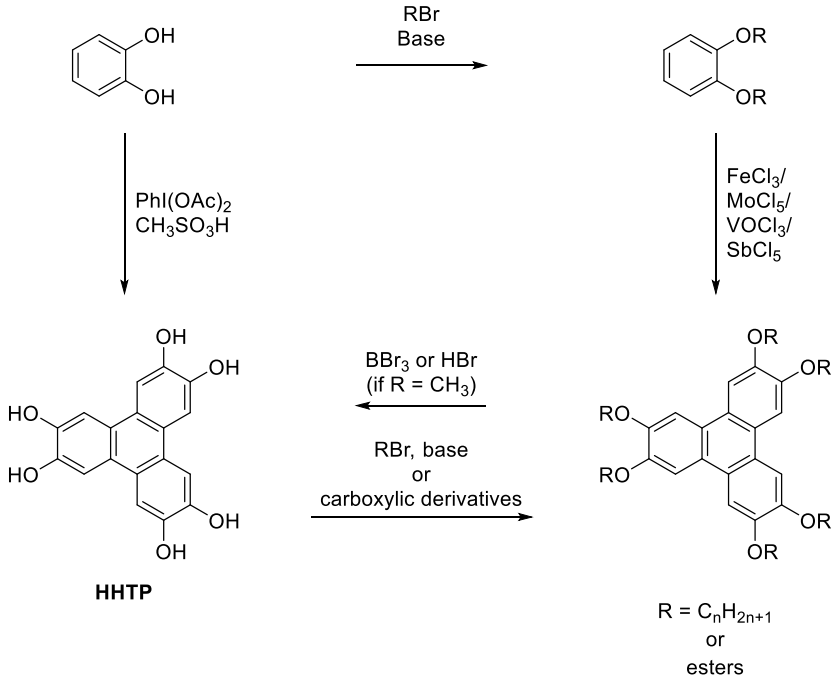

Scheme 26: Classic synthesis of **HHTP** and symmetric hexasubstituted triphenylenes.

The synthetic challenge increases when considering unsymmetrical hexasubstituted triphenylene derivatives. Indeed, by relying on statistical methods or multi-step reactions for the control of the product distribution, the yields decrease inevitably (Scheme 27).[95]

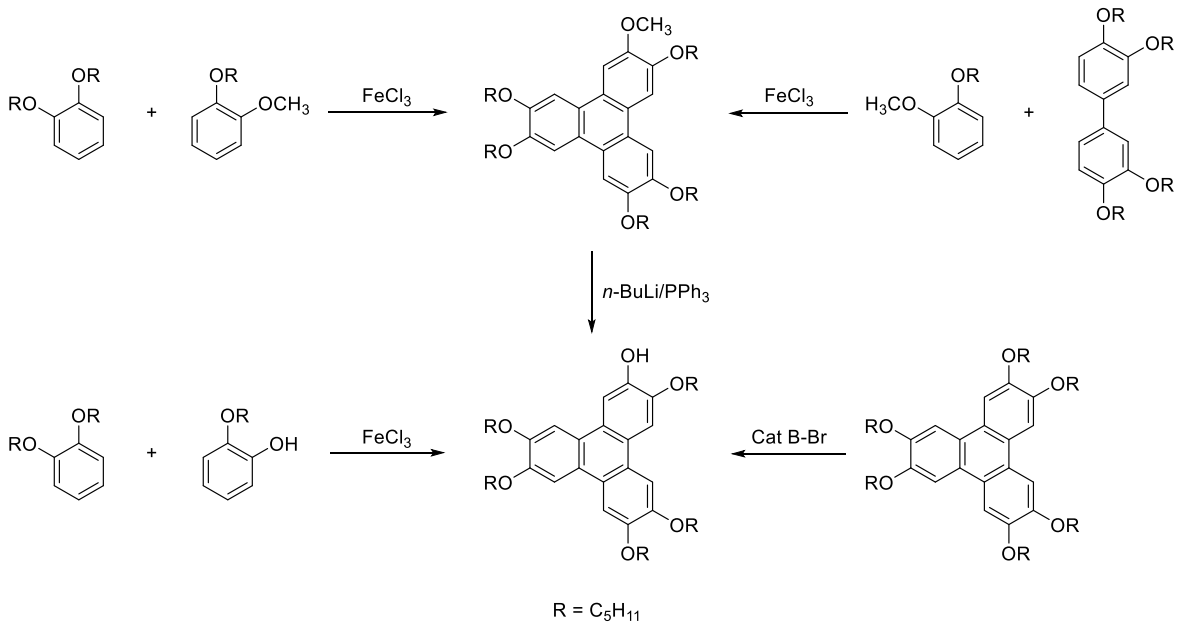

Scheme 27: Different synthetic pathways for the synthesis of asymmetric substituted 2-hydroxy-3,6,7,8,9-pentaalkoxytriphenylenes.

The R groups in Scheme 27 can vary to afford different products, but the strategy remains the same.

Very interesting, and very challenging, is the synthesis of symmetric and unsymmetrical triphenylenes bearing two different substituents, respectively C_3 and C_S symmetric derivatives, that can be achieved with two different strategies: oxidation of guaiacol derivatives,[103] or dealkylation of hexaethers with bromo containing boranes (Scheme 28).[104,105]

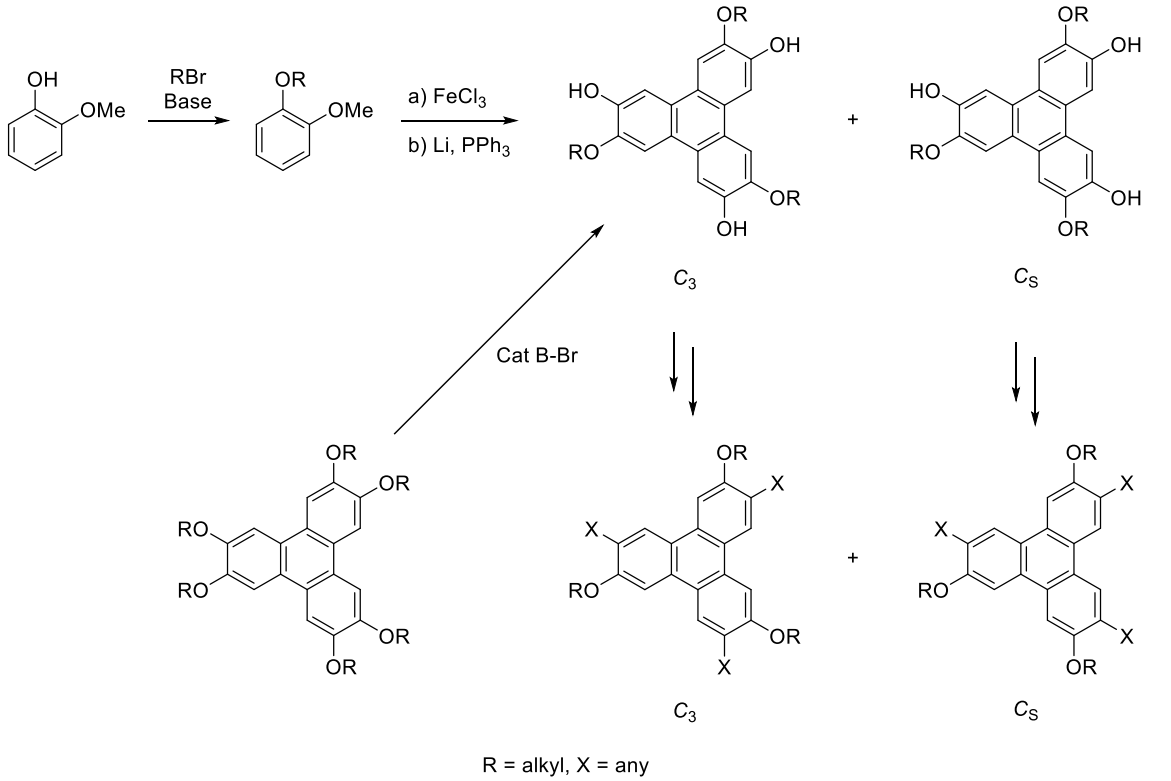

Scheme 28: Synthesis of symmetrical (C_3) and unsymmetrical (C_S) mixed tail triphenylenes.

Among the two possible stereoisomers, the C_3 product provides the most useful structure, with alternating substituents on the phenolic O atoms of the triphenylenes. Unfortunately, yields decrease dramatically using the oxidation pathway, since only 25% of the product consists in the C_3 isomer. On the other side, the use of bromo-borane derivatives, which affords only the C_3 isomer, has been limited due to their toxicity.

I.2.2 Triphenylenes in Supramolecular Chemistry

Although the main applications for triphenylene are the development of liquid crystals, in the recent years many scientists started to look at triphenylene as a useful scaffold in supramolecular chemistry. This is challenging, because with respect to more common intrinsically concave macrocycles (cyclophanes, calixarenes, resorcinarenes, pillararenes, tweezers) and containers (cryptophanes, metallocages), triphenylene units are flat and, due to this, less prone to host other molecules. However, by attaching the right substituent to the central aromatic unit, hosts based on triphenylene core can be obtained and can beneficiate by the presence of a flat electron-rich surface and up to six peripheral interacting substituents. Moreover, the UV-Visible and fluorescence emission properties of triphenylenes can provide a host that could monitor the binding of the guest.[106]

The first examples in the literature of host-guest applications of triphenylenes took inspiration from the use of triphenylenes in liquid crystals, with the self-assembly of columns through the formation of donor-acceptor π-complexes, using triphenylene as host and donor in combination with planar electron-poor molecules as acceptors. Such systems exploited triphenylene hexaethers as π-donors and 2,4,7-trinitrofluorenone,[107] *hexa*-azatriphenylenes,[108] or hexa-azatriphenylene triimides as π-acceptors (Figure 8).[109]

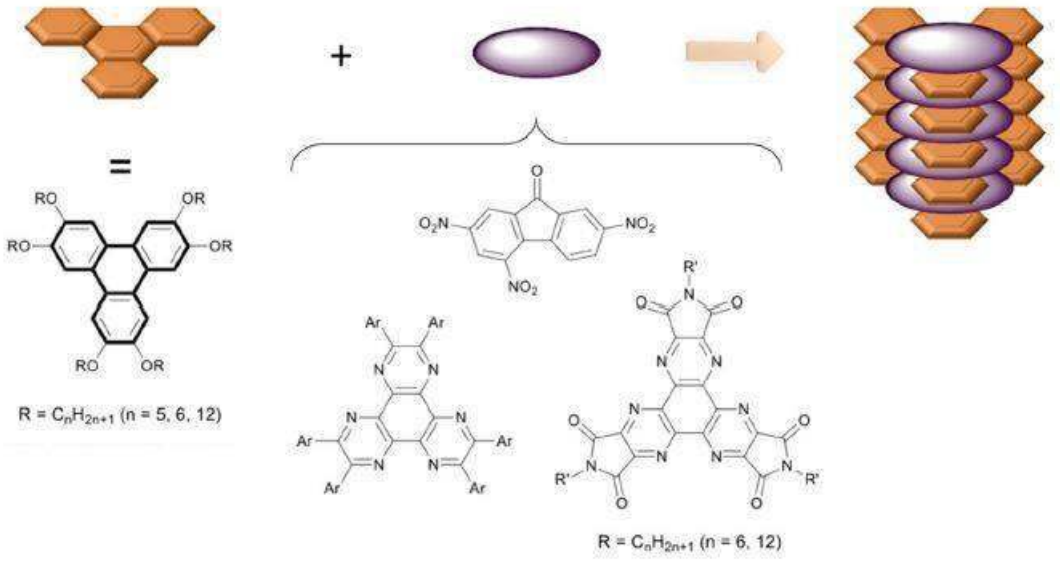

Figure 8: First examples of host-guest application of triphenylene derivates for the creation of donor-acceptor π-complexes. Adapted from [106].

In the last twenty years, a variety of triphenylene based receptors has been synthesized mainly for the recognition of flat molecules. Two categories can be detected among these

receptors: triphenylenes cavitands bearing three all-*syn* substituents and triphenylenes bearing six substituents.

The first concave triphenylenic receptor as cavitand was obtained by Waldvogel and Rebek Jr. through the connection of three catechol ketals through a Type 5 strategy (Scheme 29).[110]

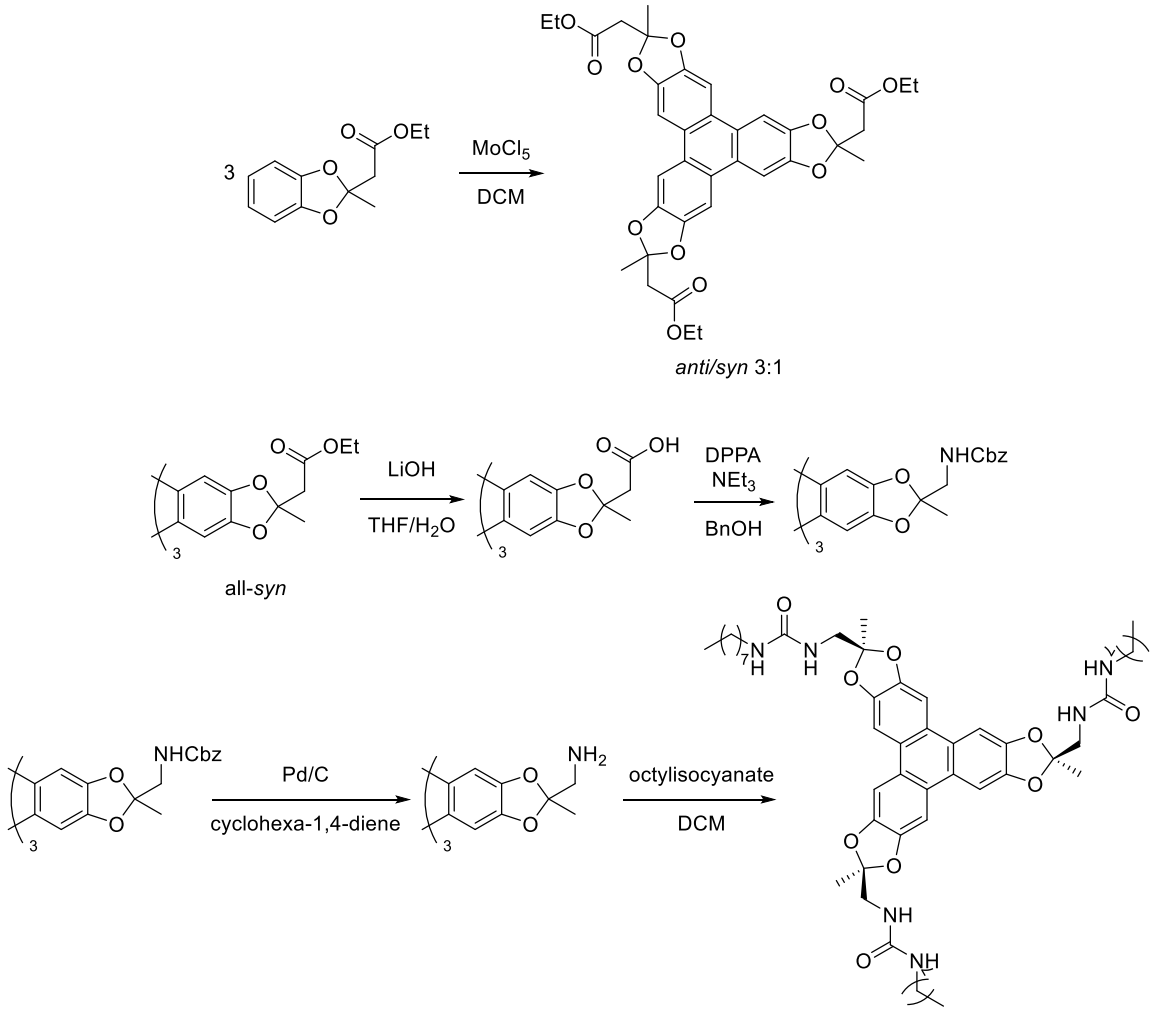

Scheme 29: Synthesis of the first *all*-syn triphenylenic receptor.

The *tris*-substituted all-*syn* triphenylene, isolated and separated from the statistically more abundant *anti, anti, syn* isomer, was characterized by the presence of three substituents around the flat cavity, separated 11 Å each other. Some years later, another similar all-*syn* substituted triphenylene endowed with rigid *tris*-urea units proved to bind selectively alkylated oxopurines in CD_2Cl_2, like caffeine ($K_a = 3.6 \cdot 10^4$ M^{-1}) or 8-methoxycaffeine ($K_a = 9.2 \cdot 10^3$ M^{-1}) with good selectivity and affinity (Figure 9).[111,112]

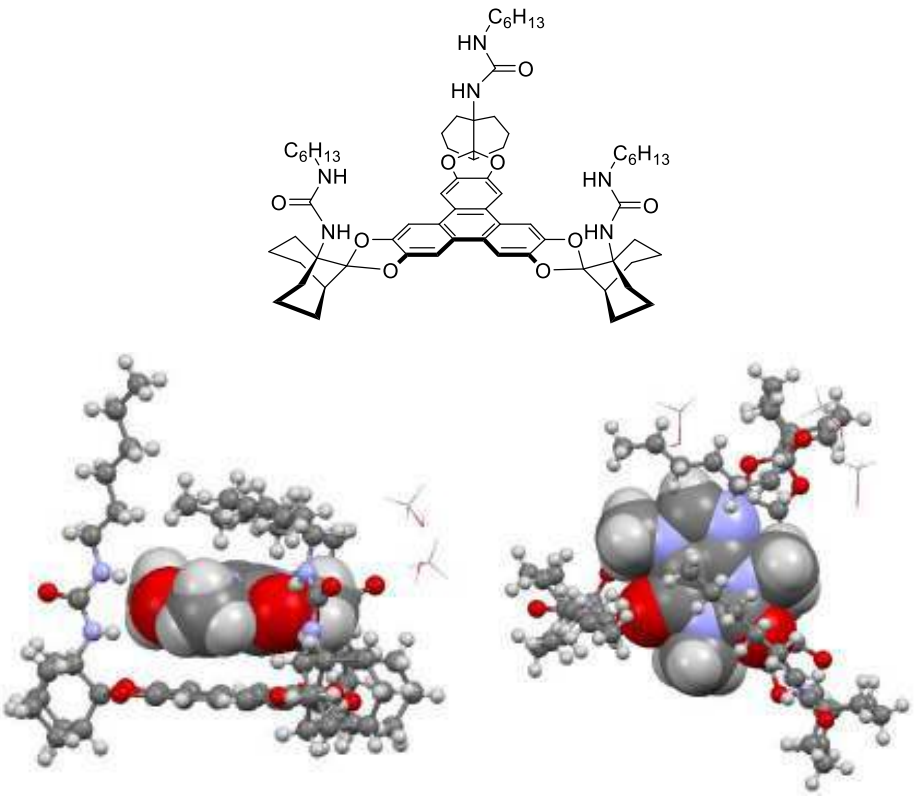

Figure 9: Structure of the triphenylenic receptor with rigid *tris*-urea units (top) and X-ray structure (side and top view) of the host with bound caffeine (bottom).

X-ray diffraction confirmed the interaction between the triphenylene host and caffeine also in the solid state, with the guest bound to the urea moieties through multiple hydrogen bonds. Moreover, caffeine lies at 3.4 Å from the triphenylenic core, at optimal distance for π-π interactions.

By attaching chiral substituents to the urea, the resulting receptors showed reversible enantiofacial differentiation of caffeine.[113,114] Similar tris-ketal-urea derivatives were also employed in the liquid-liquid extraction of radio-labelled xanthine,[115] or for the detection of trinitrotoluene (TNT).[116]

Another cavitand receptor for electron poor nitro-compounds was reported by Anzenbacher Jr. and Král, which proposed an all-*syn* C_3-symmetric triphenylene endowed with three Tröger's bases that was prepared using a Type 5 strategy, very similar to the original Mannich synthesis of triphenylene (Scheme 30).[117]

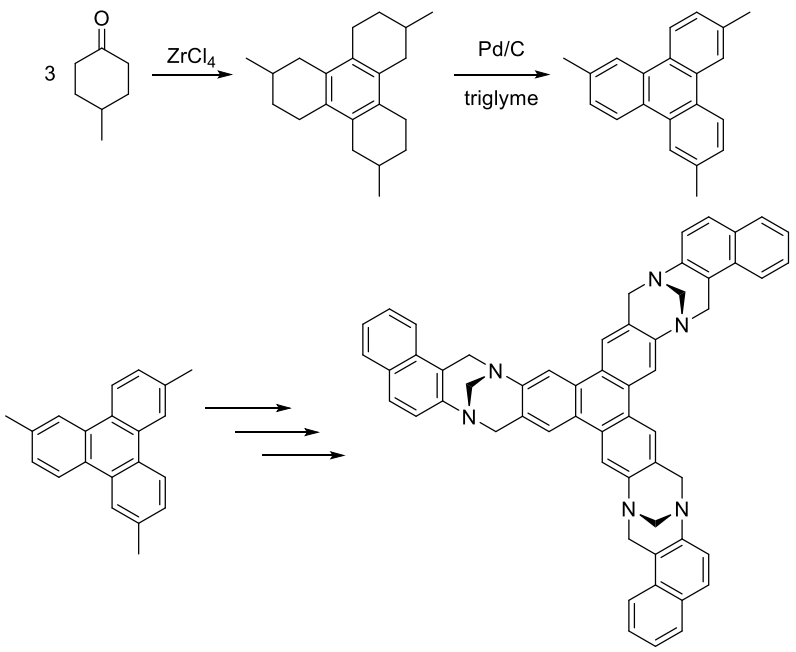

Scheme 30: Synthesis of the precursor and structure of all-*syn* C_3-symmetric triphenylene endowed with three Tröger's bases.

This receptor, with a cavity of about 700 Å^3, turned out to easily host two molecules of nitrobenzene in the solid state. This result was possible not only in virtue of the large cavity, but also because of the strong edge-to-face π-π contacts between electron-poor guests with the triphenylene and the naphthalene moieties of the host. As a consequence of the binding of the guest, the fluorescence emission of the triphenylene decreased, thus allowing the detection of such molecules in solution. In DCM the binding showed a different stoichiometry, with a 1:1 ratio for the selective recognition of trinitrotoluene (TNT, K_a = 2.03 M^{-1}) and a similar affinity for 2,4-dinitrotoluene and 2,6-dinitrotoluene, with K_a = 1.46 and 2.13 M^{-1}, respectively. Similar results were obtained using ethanol as solvent.

Hexasubstituted triphenylene receptors, also known as multivalent receptors due to the ability to offer up to six binding sites for the guests, are usually easier to make generally in less than three synthetic steps.[106]

In the first example from Bibal, **HHTP** was endowed with six phosphoryl moieties to promote the interaction with the guests through hydrogen bonds (Scheme 31).[118]

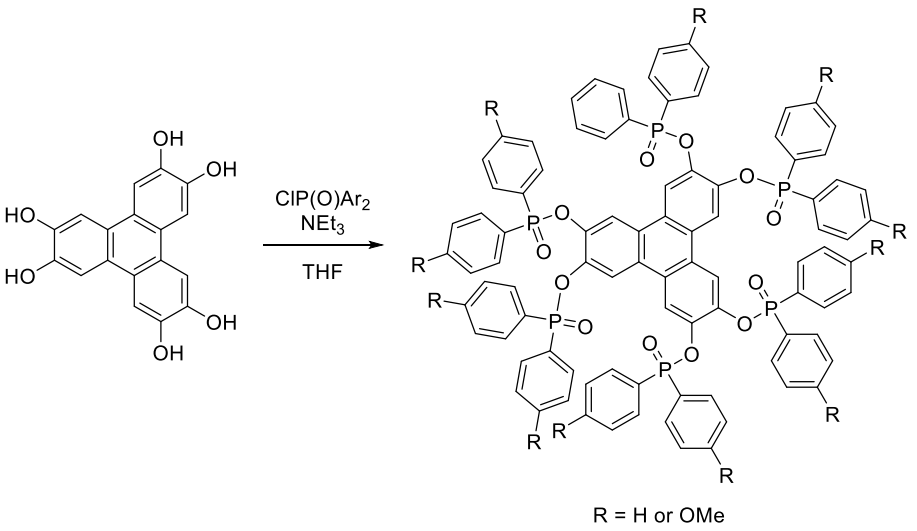

Scheme 31: Synthesis of the hexa-phosphoryl triphenylene.

The combined action of hydrogen bonds and π-π interactions allowed this receptor to interact with catechol and similar derivatives in $CDCl_3$ with a 1:2 stoichiometry, while phenol and related compounds were not recognized, being only monodentate H-bonding species. Molecular calculations showed that the first guest is able to interact with both hydrogen bond and π-π interactions with the triphenylenic ring positioning on the top of the core, while the second guest molecule is able to establish just hydrogen bonds with the host, laying in the peripheric portion of the receptor. These calculations can explain the great experimental difference between first and second association constants, that can be as high as two orders of magnitude depending on the guest.

A multivalent receptor was prepared by Bhalla and Kumar consisting in a hexacarbazole triphenylene obtained using Suzuki-Miyaura couplings over hexabromotriphenylene (Scheme 32).[119]

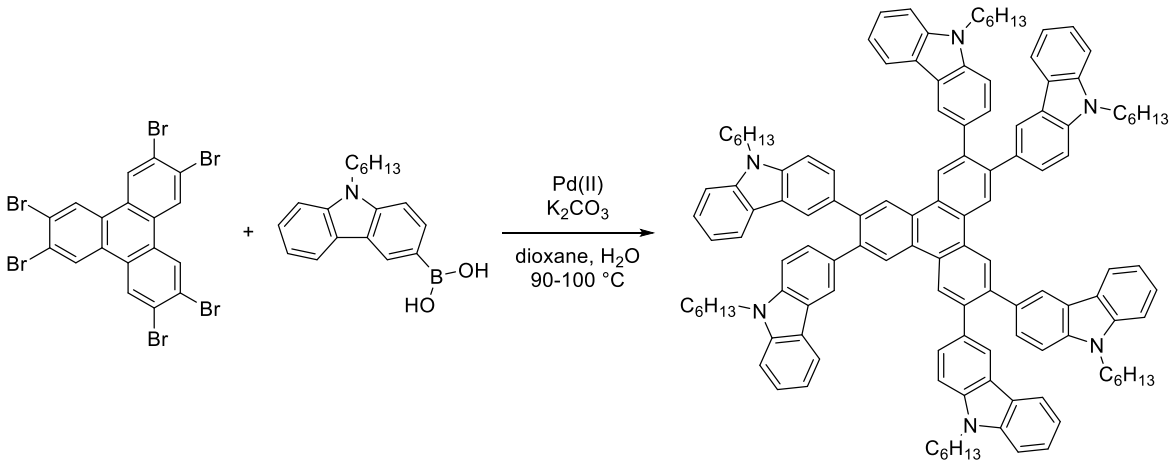

Scheme 32: Synthesis of the hexacarbazole triphenylene receptor using Suzuki-Miyaura coupling.

In polar solvent, this electron-rich receptor does not aggregate, enabling a strong fluorescence emission. Therefore, in a THF/water solution (95:5), nitroaromatic guests like TNT and picric acid can interact with the receptor and quench its fluorescence. This fluorescence quenching was strong enough to detect picric acid at 400 nM concentration,

and by coating a TLC plate with this receptor, the naked-eye detection of picric acid was possible with a lower limit of 14 pg·cm^{-2}.

Bhalla and Kumar reported also another HHTP derivative suitable as receptor, obtained by reaction with propargyl bromide and a thermal azide-alkyne cycloaddition (TAAC, "click" reaction) with hexyl azide (Scheme 33).[120]

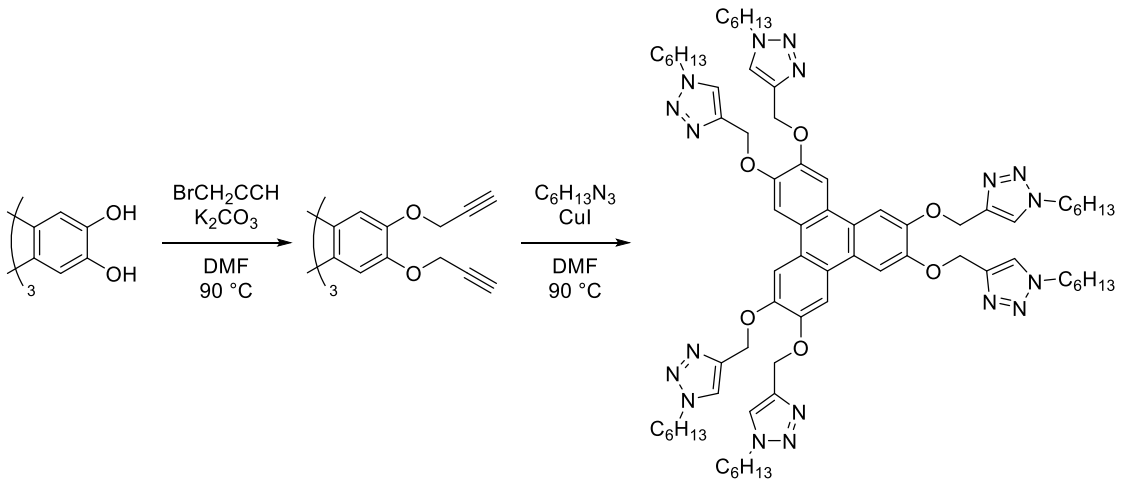

Scheme 33: Synthesis of another receptor for nitro-aromatic compounds through addition of propargyl bromide and TAAC reaction.

This triphenylene demonstrated to behave as a liquid crystal (forming hexagonal columnar phases) providing an organogel when in cyclohexane thanks to dipole-dipole and π-π interactions between the 1,2,3-triazoles units. Moreover, its fluorescence was quenched upon addition of different nitro-aromatic compounds, such as dinitrotoluene, dinitrobenzene, nitrotoluene, and benzoquinone, making it feasible as receptor for such electron poor molecules.

The detection with triphenylenic receptors is not limited only in organic solvents, but with the right substituents such molecules can become water-soluble and start working as receptor in aqueous media. By connecting six carboxylate moieties to the HHTP, Bibal and co-workers obtained a water-soluble triphenylene able to host biological ammonium targets (Scheme 34).[121]

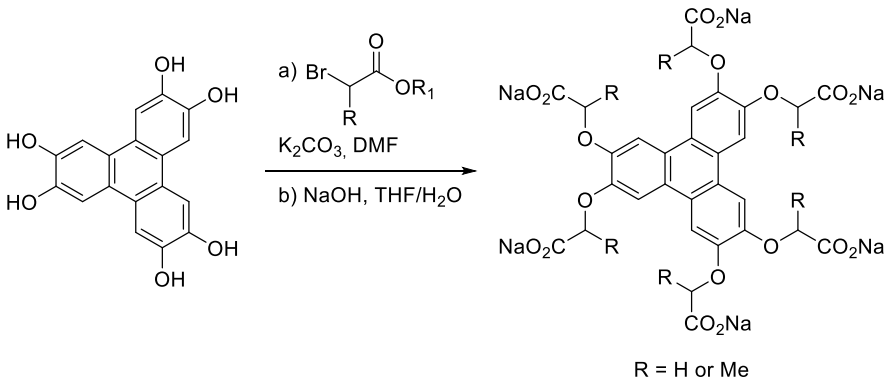

Scheme 34: Synthesis of Bibal's water-soluble triphenylenic receptor for biological ammonium targets.

In buffered medium, this receptor demonstrated to recognize protonated *D*-glucosamine and acetylcholine with moderate binding constant (respectively, K_a = 87 and 94 M^{-1}), having

as only interaction the electrostatic interaction between ammonium and carboxylate. However, when catecholamines like dopamine, *L*-noradrenaline and *L*-adrenaline and serotonin bearing aromatic groups were considered, the interaction was one order of magnitude higher (K_a = ~ 200 M^{-1}). Molecular calculations demonstrated that biological ammonium species provided with aromatic rings could establish π-π interactions over the ionic interactions, strengthening the host-guest interaction (Figure 10).[122]

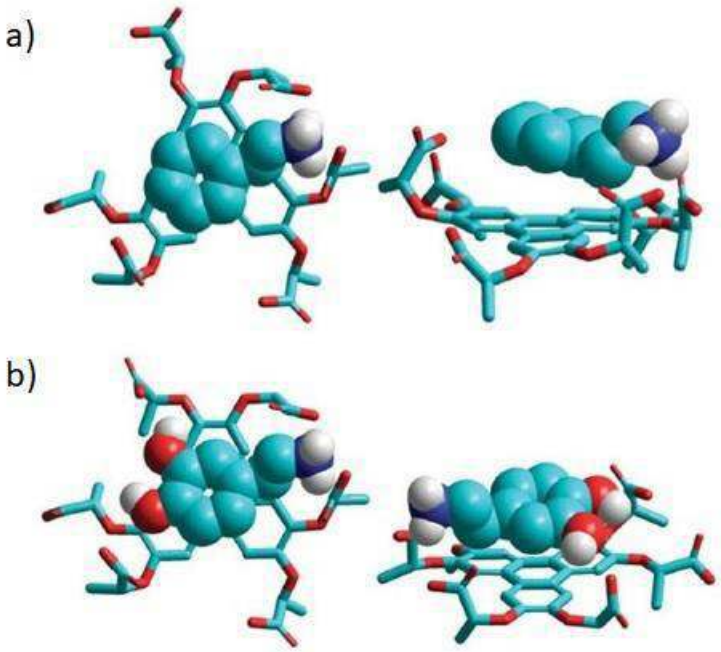

Figure 10: Energy-minimized structure of the water soluble triphenylene receptor with a) phenethylamonium and b) dopamine. Adapted from [122].

It is worth noting that the receptor showed interesting binding selectivity. In fact, similar guests like choline, *D*-glucose and *L*-dopa, did not show binding due to enhanced hydrophilicity, lack of ammonium and presence of repulsive carboxylate group, respectively.

Triphenylene based molecules have been used also for the coordination of metals ions in solution, even if in this case the triphenylenic core had the main role to hold together the metal coordinating moieties, without partaken actively to the interaction with the metals. In the first example, a triphenylene endowed with six iminoquinoline groups was created to bind zinc(II) ions in THF/H_2O (95:5) (Figure 11).[123]

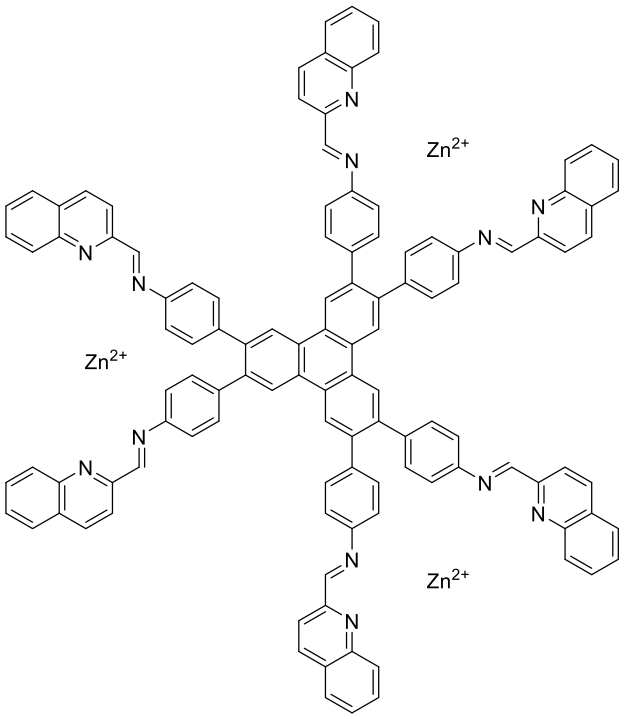

Figure 11: Structure of triphenylene, provided of six iminoquinoline groups, to bind zinc(II).

Due to an effect called intramolecular photo-induced electron transfer (PET), this molecule does not show fluorescence, but in the presence of zinc(II) ions, the formation of a 1:3 complex quenches the PET and triggers the fluorescence, creating a selective fluorescence sensor for Zn^{2+} with a detection limit of 1 µM.

Another example comes from the previously described hexatriazole triphenylene that proved to bind copper(II) ions in DMSO (Figure 12).[124]

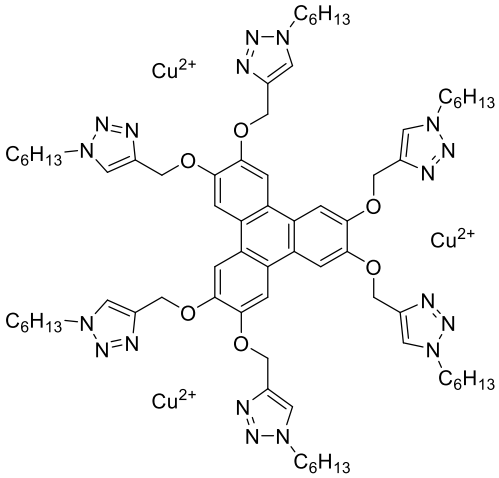

Figure 12: Structure of triphenylene comprising six triazole groups for copper(II) binding.

The action of this sensor is opposite to what previously seen for the zinc(II) sensor, with the fluorescence being quenched by the presence of copper(II) ions. Interestingly, the complex itself can act as a sensor for cyanide, since demetallation induced by CN^- form the latter causes the triphenylene fluorescence to increase. Cyanide ions were detected in tap water and human blood serum by using a TLC coated with the sensor, with a 5 µM detection limit.

In just one example in the literature, triphenylene was used as structural unit to build a dimeric hydrogen bonded capsule. This capsule, created by Rebek Jr. and nicknamed ‘‘jelly doughnut”, consisted in a triphenylene unit bearing three self-complementary *all-syn tris*-glycoluril moieties. In solution, two triphenylenic monomers can interact with each other establishing up to twelve hydrogen bonds between each other forming a flat capsule (Scheme 35).[125]

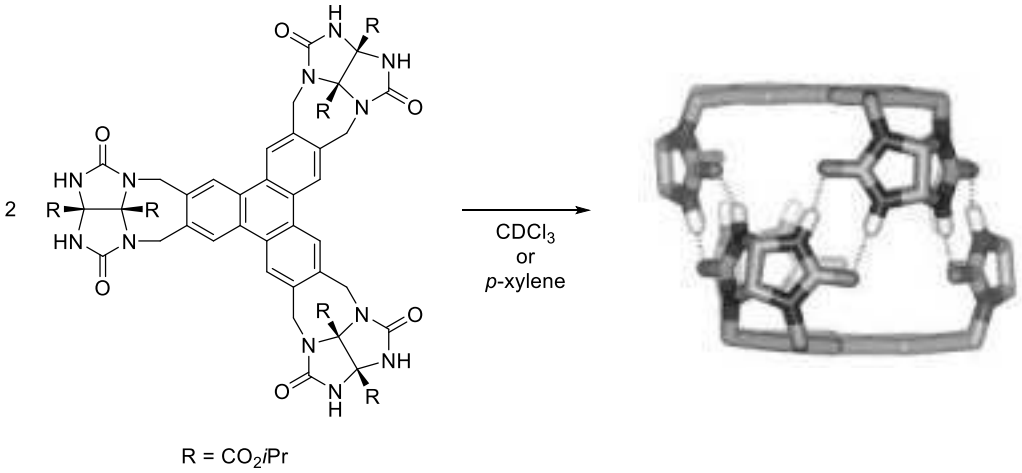

Scheme 35: Triphenylenic monomer with glycoluril units and the dimeric “Jelly doughnut” self-assembled capsule. Adapted from [1].

With a volume of c.a. 240 Å^3, this flattened nano-container can host benzene in $CDCl_3$ or cyclohexane in *p*-xylene. In particular, cyclohexane, with a volume of 239 Å^3, fits perfectly the cavity and promotes van der Waals interactions with the walls of the host, contributing to the enthalpy-driven encapsulation. In addition, the exchange process of cyclohexane in and out from the cavity is slow, with a half-time of 2.5 hours due to the necessity to break several H-bonds to open up the capsule.

I.3 Our Contribution

Although the reported examples testify the possibility of using triphenylene-based molecules for supramolecular applications, with the only exceptions of Rebek Jr. “jelly doughnut”, at the best of our knowledge nobody ever used triphenylene for the creation of supramolecular capsules or cages. Conversely, so far, the use of triphenylenes in supramolecular chemistry has been largely limited for the obtainment of single molecular receptors, probably due to the “flatness” of the molecule.

To overcome this problematic and develop supramolecular spherical objects having this molecule as precursor, C_3-symmetric triphenylenes with alternate substituents could be the answer, since these groups can be oriented to one side or the other of the aromatic panel, giving three-dimensionality to an object that otherwise would be rather flat.

The availability of a C_3-symmetric triphenylenes with readily interchangeable substituents could be of great interest for the creation of capsules or cages. Indeed, by choosing each time the right side-chain with the desired functionalization, triphenylene molecules could start interacting with each other and form aggregates using the desired interaction. With

this method, many supramolecular products could be obtained, all starting from the same, simple, precursor.

For this reason, this Doctoral Thesis starts with the development of a novel synthesis of a C_3-symmetric triphenylenes, 3,7,11-tris(benzyloxy)triphenylene-2,6,10-triol, a versatile compound able to sustain a large number of modifications thanks to the free phenolic units and the easily cleavable benzyl moieties (Figure 13).

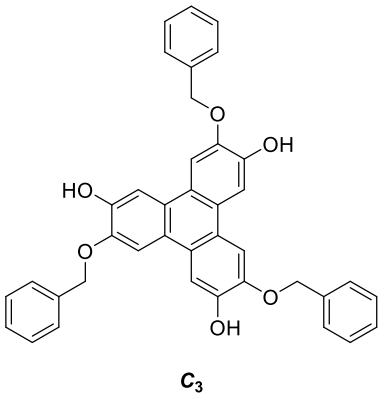

Figure 13: Structure of 3,7,11-tris(benzyloxy)triphenylene-2,6,10-triol, core of this thesis.

By endowing this molecule with different substituents and performing the right modifications, a number of molecules were created to form covalent and coordination cages, self-assembled capsules and micelles through weak intermolecular forces for many possible applications, obtaining the required sphericity through the involvement of several triphenylene molecules together.

More specifically, the introduction of alkyl thiol chains allowed the formation of sulphide and disulphide covalent cages (Chapter 4), while by insertion of pyridine moieties through Mannich reaction it was possible to obtain transition metal coordination cages upon addition of metal corners (Chapter 5). The creation of a *tris*-acid from the original scaffold allowed the investigation of self-aggregation capsules through hydrogen bonds between carboxylic acids (Chapter 6), and the functionalization with charged polytails attached to the central triphenylenic core, alternated with apolar substituents, allowed solubilization in water with the formation of very small micelles (Chapter 7). Moreover, the interaction between positively charged and negatively charged triphenylenes permitted the creation of peculiar ionic hetero-dimeric capsules (Chapter 8). Figure 14 resumes the work reported in this work.

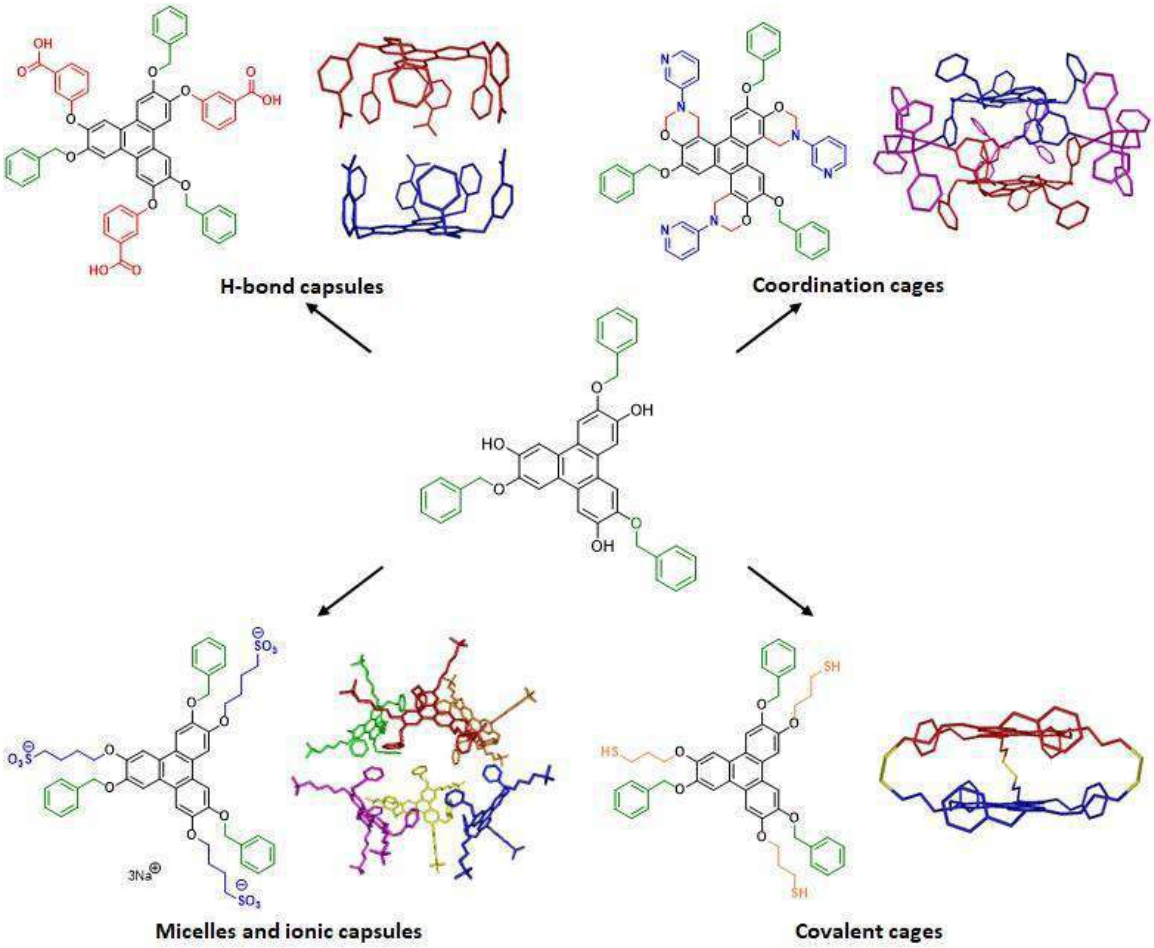

Figure 14: Various applications of C_3-symmetric triphenylenes in supramolecular chemistry and recognition reported in this Doctoral Thesis.

I.4 Bibliography

1 F. Hof, S. L. Craig, C. Nuckolls, J. Rebek, Jr., *Angew. Chem. Int. Ed.*, **2002**, *41*, 1488-1508.

2 J. Rebek, Jr., *Acc. Chem. Res.*, **1984**, *17*, 258-264.

3 S. C. Zimmerman, B. F. Duerr, *J. Org. Chem.*, **1992**, *57*, 2215-2217.

4 S. C. Zimmerman, P. Schmitt, *J. Am. Chem. Soc.*, **1995**, *117*, 10769-10770.

5 T. R. Kelly, C. Zhao, G. J. Bridger, *J. Am. Chem. Soc.*, **1989**, *111*, 3744-3745.

6 S. Anderson, H. L. Anderson, J. K. M. Sanders, *Acc. Chem. Res.*, **1993**, *26*, 469-475.

7 R. Hoss, F. Vögtle, *Angew. Chem. Int.*, **1994**, *33*, 375-384.

8 F. Diederich, P. J. Stang in *Templated Organic Synthesi*s, Wiley-VCH, Weinheim, **1999**.

9 J. Rebek, Jr., *Science*, **1987**, *235*, 1478-1484.

10 J. C. Adrian, Jr., C. S. Wilcox, *J. Am. Chem. Soc.*, **1989**, *111*, 8055-8057.

11 S. Zimmerman, W. Wu, *J. Am. Chem. Soc.*, **1989**, *111*, 8054-8055.

12 S. P. Brown, T. Schaller, U. P. Seelbach, F. Koziol, C. Ochsenfeld, F.- G. Klärner, H. W. Spiess, *Angew. Chem. Int. Ed.*, **2001**, *40*, 717-720.

13 P. G. E. Sanderson, J. D. Kilburn, W. C. Still, *J. Am. Chem. Soc.*, **1989**, *111*, 8314-8315.

14 R. P. Dixon, S. J. Gelb, A. D. Hamilton, *J. Am. Chem. Soc.*, **1992**, *114*, 365-366.

15 D. J. Cram, H.-J. Choi, J. A. Bryant, C. B. Knobler, *J. Am. Chem. Soc.*, **1992**, *114*, 7748-7765.

16 J. Canceill, L. Lacombe, A. Collet, *J. Am. Chem. Soc.*, **1986**, *108*, 4230-4232.

17 S. J. Rowan, S. J. Cantrill, G. R. L. Cousins, J. K. M. Sanders, J. F. Stoddart, *Angew. Chem. Int. Ed.*, **2002**, *41*, 898-952.

18 Y. Jin, C. Yu, R. J. Denman, W. Zhang, *Chem. Soc. Rev.,* 2013, **42**, 6634-6654.

19 M. Mastalerz, *Acc. Chem. Res.*, **2018**, *51*, 2411-2422.

20 T. Hasell, A. I. Cooper, *Nat. Rev. Mater.*, **2016**, *1*, 16053.

21 S. Erbas-Cakmak, D. A. Leigh, C. T. McTernan, A. L. Nussbaumer, *Chem. Rev.*, **2015**, *115*, 10081-10206.

22 Ling Wang, Quan Li, *Chem. Soc. Rev.*, **2018**, *47*, 1044-1097.

23 M. Raynal, P. Ballester, A. Vidal-Ferran, P. W. N. M. van Leeuwen, *Chem. Soc. Rev.,* **2014**, *43*, 1660-1733; M. Raynal, P. Ballester, A. Vidal-Ferran, P. W. N. M. van Leeuwen, *Chem. Soc. Rev.,* **2014**, *43*, 1734-1787.

24 A. Scarso, G. Borsato, J. Rebek, Jr "Capsule and Cavitands: Synthetic Catalysts of Nanometric Dimension" in *Selective Nanocatalysts and Nanoscience: Concepts for Heterogeneous and Homogeneous Catalysis* Wiley-VCH, **2011**, pp. 105-168

25 A. Scarso, G. Borsato "Self-Assembly of Organic Supramolecular Capsules" in "*Supramolecular Chemistry: from Molecules to Nanomaterials"*, J.W. Steed and P.A.

Gale (eds). John Wiley & Sons Ltd, Chichester, UK, ISBN 9780470746400, **2012**, pp. 2085-2114

26 A. E. Rowan, J. A. A. W. Elemans, R. J. M. Nolte, *Acc. Chem. Res.*, **1999**, *32*, 995-1006.

27 R. Wyler, J. de Mendoza, J. Rebek, Jr., *Angew. Chem. Int. Ed.*, **1993**, *32*, 1699-1701.

28 N. Branda, R. Wyler, J. Rebek, Jr., *Science*, **1994**, *263*, 1267-1268.

29 R. S. Meissner, J. Rebek, Jr., J. de Mendoza, *Science*, **1995**, *270*, 1485-1488.

30 M. Rivera, T. Martin, J. Rebek, Jr., *J. Am. Chem. Soc.*, **1998**, *120*, 819-820.

31 J. Kang, J. Rebek, Jr., *Nature*, **1996**, *382*, 239-241.

32 K. D. Shimizu, J. Rebek, Jr., *Proc. Natl. Acad. Sci. USA*, **1995**, *92*, 12403-12407.

33 T. Heinz, D. M. Rudkevich, J. Rebek, Jr., *Nature*, **1998**, *394*, 764-766.

34 L. R. MacGillivray, J. L. Atwood, *Nature*, **1997**, *389*, 469-472.

35 D. Račkauskaite,˙K.-E. Bergquist, Q. Shi, A. Sundin, E. Butkus, K. Wärnmark, E. Orentas, *J. Am. Chem. Soc.*, **2015**, *137*, 10536-10546.

36 D. Beaudoin, F. Rominger, M. Mastalerz, *Angew. Chem. Int. Ed.*, **2016**, *55*, 15599-15603.

37 G. Markiewicz, A. Jenczak, M. Kołodziejski, J. J. Holstein, J. K.M. Sanders, A. R. Stefankiewicz, *Nat. Commun.*, **2017**, *8*, 15109.

38 M. Fujita, K. Umemoto, M. Yoshizawa, N. Fujita, T. Kusukawa, K. Biradha, *Chem. Commun.*, **2001**, 509-518.

39 M. Yoshizawa, J. K. Klosterman, M. Fujita, *Angew. Chem. Int. Ed.*, **2009**, *48*, 3418-3438.

40 D. Fujita, Y. Ueda, S. Sato, H. Yokoyama, N. Mizuno, T. Kumasaka, M. Fujita, *Chem.*, **2016**, *1*, 91-101.

41 D. L. Caulder, R. E. Powers, T. N. Parac, K. N. Raymond, *Angew. Chem. Int. Ed.*, **1998**, *37*, 1840-1843.

42 C. M. Hong, R. G. Bergman, K. N. Raymond, F. D. Toste, *Acc. Chem. Res.*, **2018**, *51*, 2447-2455.

43 D. Fiedler, R. G. Bergman, K. N. Raymond, *Angew. Chem. Int. Ed.*, **2004**, *116*, 6916-6919.

44 C. J. Brown, R. G. Bergman, K. N. Raymond, *J. Am. Chem. Soc.*, **2009**, *131*, 17530-17531.

45 C. M. Hong, M. Morimoto, E. A. Kapustin, N. Alzakhem, R. G. Bergman, K. N. Raymond, F. D. Toste, *J. Am. Chem. Soc.*, **2018**, *140*, 6591-6595.

46 C. Hastings, M. D. Pluth, R. G. Bergman, K. N. Raymond, *J. Am. Chem. Soc.*, **2010**, *132*, 6938-6940.

47 J. H. Jordan, B. C. Gibb, *Chem. Soc. Rev.,* **2015**, *44*, 547-585.

48 H. Xi, C. L. D. Gibb, E. D. Stevens, B. C. Gibb, *Chem. Commun.*, **1998**, 1743-1744.

49 J. O. Green, J. H. Baird, B. C. Gibb, *Org. Lett.*, **2000**, *2*, 3845-3848.

50 S. Liu, S. E. Whisenhunt-Ioup, C. L. D. Gibb, B. C. Gibb, *Supramol. Chem.*, **2011**, *23*, 480-485.

51 C. L. D. Gibb, B. C. Gibb, *Chem. Commun.*, **2007**, 1635-1637.

52 H. Gan, C. J. Benjamin, B. C. Gibb, *J. Am. Chem. Soc.*, **2011**, *133*, 4770-4773.

53 R. Fiammengo, P. Timmerman, J. Huskens, K. Versluis, A. J. R. Heck, D. N. Reinhoudt, *Tetrahedron*, **2002**, *58*, 757-764.

54 O. Dumele, B. Schreib, U. Warzok, N. Trapp, C. A. Schalley, F. Diederich, *Angew. Chem. Int. Ed.*, **2017**, *56*, 1152-1157.

55 D. J. Cram, S. Karbach, Y. H. Kim, L. Baczynskyj, G. W. Kalleymeyn, *J. Am. Chem. Soc.*, **1985**, *107*, 2575-2576.

56 M. L. C. Quan, D. J. Cram, *J. Am. Chem. Soc.*, **1991**, *113*, 2754-2755.

57 J. C. Sherman, D. J. Cram, *J. Am. Chem. Soc.*, **1989**, *111*, 4527-4528.

58 D. J. Cram, M. E. Tanner, R. Thomas, *Angew. Chem. Int. Ed.*, **1991**, *30*, 1024-1027.

59 O. L. Chapman, C. L. Mcintosh, J. Pacansky, *J. Am. Chem. Soc.*, **1973**, *95*, 614-617.

60 N. Nishimura, K. Kobayashi, *J. Org. Chem.*, **2010**, *75*, 6079-6085.

61 H. Schmidt, G. Schultz, *Ann.*, **1880**, *203*, 118.

62 M. Berthelot, *Ann.*, **1867**, *142*, 257.

63 C. Mannich, *Ber.*, **1907**, *40*, 153; **1907**, *40*, 159.

64 C. M. Buess, D. D. Lawson, *Chem. Rev.*, **1960**, 313-327.

65 D. Perez, E. Guitian, *Chem. Soc. Rev.*, **2004**, *33*, 274-283.

66 H. Meier, B. Rose, *J. Prakt. Chem.*, **1998**, *340*, 536-543.

67 R. Freudenmann, B. Behnisch, M. Hanack, *J. Mater. Chem.*, **2001**, *11*, 1618-1624.

68 J. W. Goodby, M. Hird, K. J. Toyne, T. Watson, *J. Chem. Soc., Chem. Commun.*, **1994**, 1701-1702.

69 H. Hart, C. Y. Lai, G. C. Nwokogu, S. Shamoulian, *Tetrahedron*, **1987**, *43*, 5203-5224

70 N. Boden, R. J. Bushby, A. N. Cammidge, *J. Chem. Soc., Chem. Commun.*, **1994**, 465-466.

71 G. W. Gribble, R. B. Perni, K. D. Onan, *J. Org. Chem.*, **1985**, *50*, 2934-2939.

72 A. U. Rahman, O. L. Tombesi, *Chem. Ber.*, **1966**, *99*, 1805-1809.

73 J. Moursounidis, D. Wege, *Aust. J. Chem.*, **1988**, *41*, 235-249.

74 W. H. Laarhoven, J. A. M. Van Broekhoven, *Tetrahedron Lett.*, **1970**, *11*, 73-76.

75 R. G. Harvey, E. Aboshkara, J. Pataki, *Tetrahedron*, **1997**, *53*, 15947-15956.

76 K. B. Sukumaran, R. G. Harvey, *J. Org. Chem.*, **1981**, *46*, 2740-2745.

77 C. Yang, D. Yang, R. G. Harvey, *Synlett*, **1992**, 799-800.

78 M. Piattelli, E. Fattorusso, R. A. Nicolaus, S. Magno, *Tetrahedron*, **1965**, *21*, 3229-3236.

79 S. Kumar, M. Manickam, *Chem. Commun.*, **1997**, 1615-1666

80 S. Kumar, S. K. Varshney, *Synthesis*, **2001**, 305-311.

81 H. Heaney, P. Lees, *Tetrahedron Lett.*, **1964**, *5*, 3049-3052.

82 D. Peña, S. Escudero, D. Pérez, E. Guitián, L. Castedo, *Angew. Chem. Int. Ed.*, **1998**, *37*, 2659-2661.

83 P. Canonne and A. Regnault, *Tetrahedron Lett.*, **1969**, *4*, 243-246.

84 W. E. Billups, D. J. McCord and B. R. Maughon, *J. Am. Chem. Soc.*, **1994**, *116*, 8831-8832.

85 G. W. Winter, U. Langjahr, H. Meier, J. Merkuschev and J. Juriew, *Chem. Ber.*, **1984**, *117*, 2452-2463.

86 D. Z. Rogers, *J. Org. Chem.*, **1986**, *51*, 3904-3905.

87 J. T. Rademacher, K. Kanakarajan and A. W. Czarnik, *Synthesis*, **1994**, 378-380.

88 J. L. Segura, R. Juárez, M. Ramos, C. Seoane, *Chem. Soc. Rev.*, **2015**, *44*, 6850-6885.

89 Y. Nicolas, P. Blanchard, E. Levillain, M. Allain, N. Mercier, J. Roncali, *Org. Lett.*, **2004**, *6*, 273‑276.

90 R. B. Ferreira, J. M. Figueroa, D. E. Fagnani, K. A. Abboud, R. K. Castellano, *Chem. Commun.,* **2017**, *53*, 9590-9593.

91 A. L. Kanibolotsky, I. F. Perepichka, P. J. Skabara, *Chem. Soc. Rev.*, **2010**, *39*, 2695‑2728.

92 E. V. Dehmlow, T. Kelle, *Synth. Commun.*, **1997**, *27*, 2021-2031.

93 N. Robertson, S. Parsons, E.J. MacLean, R.A. Coxall, A.R. Mount, *J. Mater. Chem*., **2000**, *10*, 2043-2047.

94 F. Goubard, F. Dumur, *RSC Adv.*, **2015**, *5*, 3521-3551.

95 S. Kumar Pal, S. Setia, B.S. Avinash, S. Kumar, *Liquid Crystals*, **2013**, *40*, 1769–1816.

96 L. Schmidt-Mende, A. Fechtenkotter, K. Mullen, E. Moons, R. H. Friend, J. D. MacKenzie, *Science*, **2001**, *293*, 1119-1122.

97 T. Hassheider, S. A. Benning, H. S. Kitzerow, M. F. Achard, H. Bock, *Angew. Chem., Int. Ed.*, **2001**, *40*, 2060-2063.

98 S. Kumar, *Chem. Soc. Rev.*, **2006**, *35*, 83-109.

99 X. Crispin, J. Cornil, R. Friedlein, K. K. Okudaira, V. Lemaur, A. Crispin, G. Kestemont, M. Lehmann, M. Fahlman, R. Lazzaroni, Y. Geerts, G. Wendin, N. Ueno, J.-L. Brédas, W. R. Salaneck, *J. Am. Chem. Soc.*, **2004**, *126*, 11889-11899.

100 J. Billard, J. C. Dubois, N. H. Tinh, A. Zann, *Nouv. J. Chimie*, **1978**, *2*, 535‑540.

101 J. A. Rego, S. Kumar, H. Ringsdorf, *Chem. Mater.*, **1996**, *8*, 1402‑1409.

102 A. Kettner, J. H. Wendorff, *Liq. Cryst.*, **1999**, *26*, 483‑487.

103 K.-Q. Zhao, Y. Gao, W.-H. Yu, P. Hu, B.-Q. Wang, B. Heinrich, B. Donnio, *Eur. J. Org. Chem*., **2016**, *16*, 2802-2814.

104 P. T. Wright, I. Gillies, J. D. Kilburn, *Synthesis*, **1997**, *9*, 1007-1009.

105 S. Kumar, M. Manickam, *Synthesis*, **1998**, *8*, 1119-1122.

106 D. Sonet, B. Bibal, *Tetrahedron Lett.*, **2019**, *60*, 872-884.

107 W. Kranig, C. Boeffel, H.W. Spiess, O. Karthaus, H. Ringsdorf, R. Wüstefeld, *Liq. Cryst.*, **1990**, *8*, 375-388

108 E.O. Arikainen, N. Boden, R.J. Bushby, O.R. Lozman, J.G. Vinter, A. Wood, *Angew. Chem. Int. Ed.*, **2000**, *39*, 2333-2336.

109 L.M. Klivansky, D. Hanifi, G. Koshkakaryan, D.R. Holycross, E.K. Gorski, Q. Wu, M. Chai, Y. Liu, *Chem. Sci.*, **2012**, *3*, 2009-2014.

110 S. R. Waldvogel, A. R. Wartini, P. H. Rasmussen, J. Rebek Jr., *Tetrahedron Lett.*, **1999**, *40*, 3515-3518.

111 S. R. Waldvogel, R. Fröhlich, C. A. Schalley, *Angew. Chem. Int. Ed.*, **2000**, *39*, 2472-2475.

112 C. Siering, H. Kerschbaumer, M. Nieger, S. R. Waldvogel, *Org. Lett.*, **2006**, *8*, 1471-1474.

113 M. C. Schopohl, C. Siering, O. Kataeva, S. R. Waldvogel, *Angew. Chem. Int. Ed.*, **2003**, *42*, 2620-2623.

114 C. Siering, S. Grimme, S. R. Waldvogel, *Chem. Eur. J.*, **2005**, *11*, 1877-1888.

115 M. Bomkamp, C. Siering, K. Landrock, H. Stephan, R. Fröhlich, S. R. Waldvogel, *Chem. Eur. J.*, **2007**, *13*, 3724-3732.

116 R. Orghici, U. Willer, M. Gierszewska, S. R. Waldvogel, W. Schade, *Appl. Phys. B*, **2008**, *90*, 355-360.

117 L. Mosca, J. Cejka, B. Dolensky, M. Havlik, M. Jakubek, R. Kaplanek, V. Kral, P. Anzenbacher Jr., *Chem. Commun.*, **2016**, *52*, 10664-10667.

118 C.Givelet, B. Tinant, L. Van Meervelt, T. Buffeteau, N. Marchand-Geneste, B. Bibal, *J. Org. Chem.*, **2009**, *74*, 652-659.

119 V. Bhalla, H. Arora, H. Singh, M. Kumar, *Dalton. Trans.*, **2013**, *42*, 969-974.

120 V. Bhalla, H. Singh, M. Kumar, S.K. Prasad, *Langmuir*, **2011**, *27*, 15275-15281.

121 C. Givelet, T. Buffeteau, F. Arnaud-Neu, V. Huscher-Bruder, B. Bibal, *J. Org. Chem.*, **2009**, *74*, 5059-5062.

122 C. Givelet, B. Bibal, *Org. Biomol. Chem.*, **2011**, *9*, 7457-7460.

123 V. Bhalla, H. Arora, A. Dhir, M. Kumar, *Chem. Commun.*, **2012**, *48*, 4722-4724.

124 V. Bhalla, H. Singh, M. Kumar, *Dalton. Trans.*, **2012**, *41*, 11413-11418.

125 R. M. Grotzfeld, N. Branda, J. Rebek Jr., *Science*, **1996**, *271*, 487-489.

1 Development of a New Synthetic Routes to C_3-triphenylenes

As reported in the Introduction, in the last decade scientists interested in triphenylene functionalization put a lot of effort in the obtainment of alternated and hemi-*O*-alkylated hexahydroxy triphenylenes for various applications. Different synthetic approaches were investigated, mainly involving palladium-catalyzed reactions such as annulation of *o*-iodobiphenyls with arynes,[1,2] [2+2+2] cycloadditions of arynes,[3] and Suzuki cross-couplings with 2-bromophenylboronic esters.[4] For all those methods, yields were very variable depending on the substitutions on the aromatic rings.

In 1997, the first example of hemi-*O*-alkylated hexahydroxytriphenylenes from fully *O*-alkylated derivatives of the **HHTP** was reported by Kilburn and co-workers, that selectively debenzylated 2,3,6,7,10,11-hexakis(benzyloxy)triphenylene using 9-bromo-9-borabicyclo[3.3.1]nonane (9-Br-BBN), achieving the corresponding C_3-trisubstituted triphenylene with a 29% yield starting from veratrole (Scheme 1).[5]

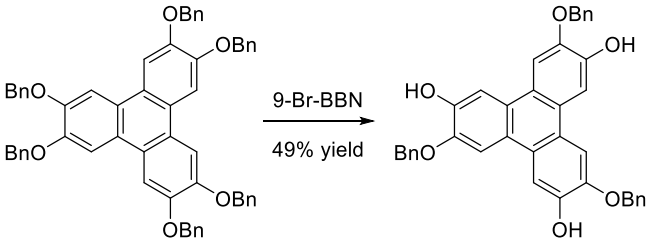

Scheme 1: Kilburn's hemi-*O*-alkylated hexahydroxytriphenylene synthesis forming predominantly the C_3 isomer.

In a similar methodology, hexa-*n*-pentyl substituted triphenylene was partially de-alkylated using B-bromocatecholborane with good selectivity towards the C_3 product, which was obtained in 60% yield.[6] The crucial step of the whole route was the regioselective formation of the *vic*-hydroxy-alkoxy moiety in the hemi-*O*-alkylated hexahydroxytriphenylene. Indeed, trials of stoichiometric controlled alkylation of the hexahydroxytriphenylene afforded only complex mixtures of randomly substituted products. However, both the above reported methodologies were characterized by the use of toxic and expensive reagents like B-bromocatecholborane and 9-Br-BBN, with rather limited availability on the market, thus making these methods largely impractical.

In 2016, Donnio and co-workers reported the synthesis of 2,6,10-triaryltriphenylenes, using a hemi-*O*-alkylated hexahydroxytriphenylenes as intermediate, obtained through a more traditional oxidation reaction from a guaiacol derivative bearing an alkyl substituent (Scheme 2).[7]

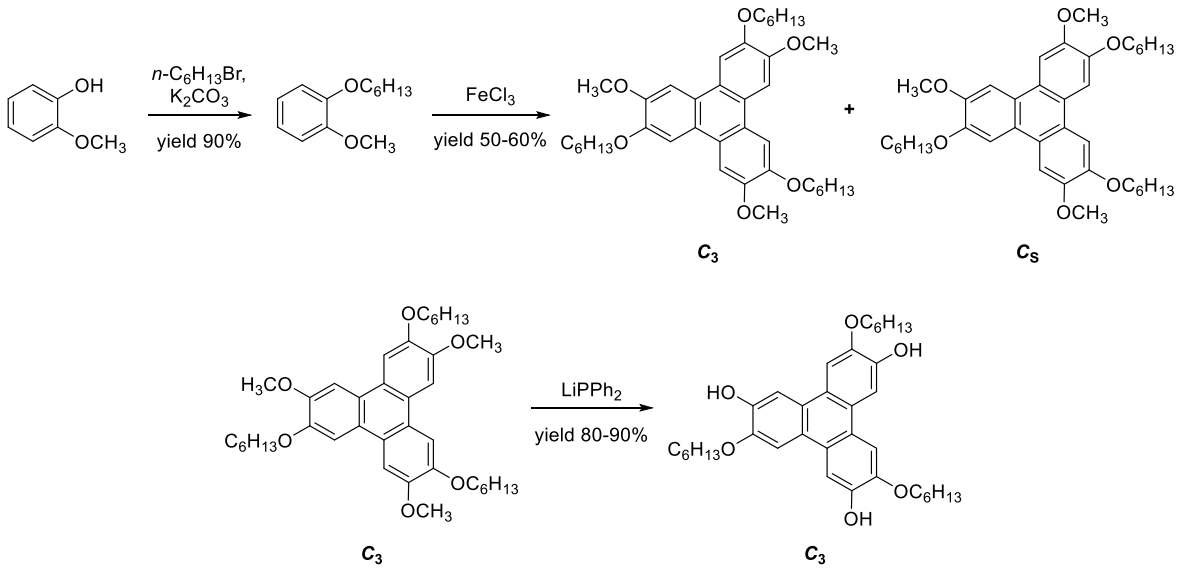

Scheme 2: Donnio's hemi-*O*-alkylated hexahydroxytriphenylene synthesis.

The problem with this methodology lies in the oxidation step, which gave both C_3 and C_S isomers with a 1:3 statistical distribution, dramatically lowering the total yield to 10% starting from guaiacol.

According to the general interest in the preparation of C_3-symmetric hexa-substituted triphenylenes and looking for a much simpler and convenient method based on safer, available and economical reagents, we started working on alternative reaction pathways.

1.1 Protected *O*-Alkyl Catechols as Triphenylenes Precursors

Since the simplest alkyloxy substituted triphenylene, hexamethoxytriphenylene, can be obtained by oxidation of veratrole in high yields,[8] the first considered idea was to synthesize a protected guaiacol with an *O*-alkyl group on the hydroxyl position, followed by oxidation to the corresponding triphenylene and subsequent deprotection to obtain the hemi-*O*-alkylated hexahydroxytriphenylene. The choice of ethers as protective group was due to the required presence of electron donating group in the aromatic ring to favour the oxidation reaction (Scheme 3).

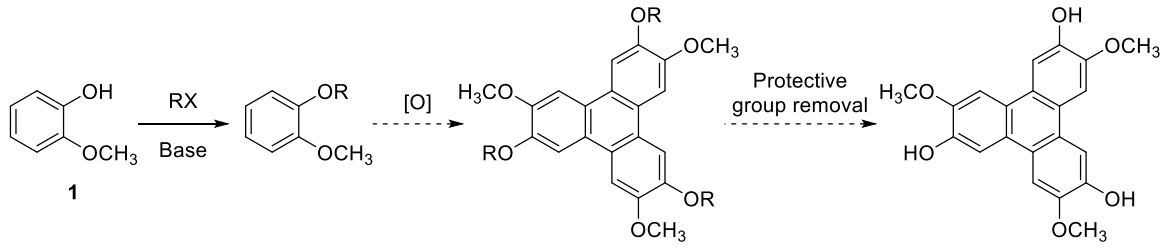

Scheme 3: Hemi-*O*-alkylated hexahydroxytriphenylenes through oxidation of veratrole and subsequent removal of protective groups.

This methodology is very similar to the one reported by Donnio *et al.*, but we wanted to modify the procedure introducing a protective group removable under much milder conditions to make the reaction easier, avoiding the use of lithium diphenylphosphide, an air sensitive reagent that needs to be freshly prepared right before use.

The first protective group added to the guaiacol was the benzyl, due to its easy cleavage under reductive conditions. 1-(Benzyloxy)-2-methoxybenzene, **3**, was obtained reacting guaiacol with 1.5 equivalents of benzyl bromide in the presence of K_2CO_3, in refluxing acetone, under inert atmosphere overnight (Scheme 4).[9]

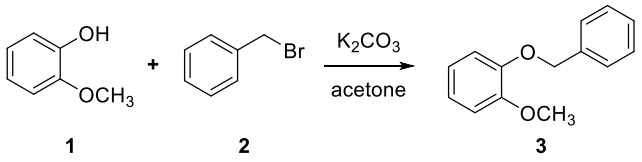

1 **2** **3**

Scheme 4: Synthesis of 1-(benzyloxy)-2-methoxybenzene, **3.**

The product was isolated in quantitative yield after filtration and concentration in *vacuum* of the resulting solution, requiring no further purification for the following steps.

The previously obtained substrate **3** was treated with anhydrous iron(III) chloride and concentrated sulphuric acid in DCM, under inert atmosphere, at room temperature (Scheme 5).[8] After 3 hours, TLC analysis displayed the absence of starting material in the mixture.

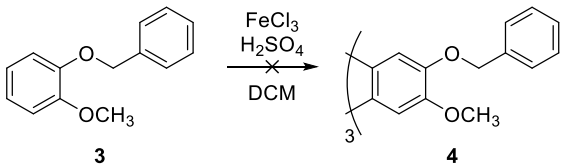

3 **4**

Scheme 5: Reaction on substrate **3** with iron (III) chloride to form **4**.

^{1}H NMR and ^{13}C NMR analysis after flash-chromatography of the crude reaction mixture revealed only the presence of monomer and/or dimeric units bearing an oxidized benzyl function. Indeed, the benzyl group could not resist such harsh oxidative conditions, leading to the corresponding benzoic ester, thus deactivating the aromatic ring and hampering the oxidation reaction.

The second protective group that we decided to test was the methoxymethyl (MOM), which is easily removable under mild acidic conditions. 1-Methoxy-2-(methoxymethoxy)benzene, **6**, was obtained by reaction between guaiacol and 1.5 equivalents of chloromethyl methyl ether (MOMCl), in DCM in the presence of *N,N*-diisopropylethylamine, under inert atmosphere (Scheme 6).[10]

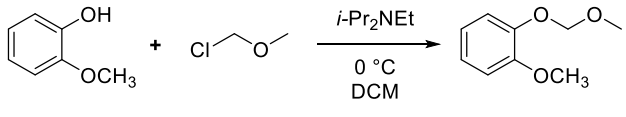

1 **5** **6**

Scheme 6: Synthesis of 1-methoxy-2-(methoxymethoxy)benzene, **6**.

The reaction was carried out at 0 °C for 1 h, eventually warmed to room temperature overnight, affording the desired product **6** in 92% yield.

Since the iron(III) chloride oxidation step involves harsh acidic conditions that are not compatible with the delicate MOM protecting group,[8] milder experimental conditions were chosen for the cyclization of **6**. The latter was treated with molybdenum(V) chloride in DCM at 0 °C under inert atmosphere (Scheme 7).[11] TLC analysis of the crude evidenced complete

consumption of the substrate after 30 minutes, with concomitant formation of more retained derivatives.

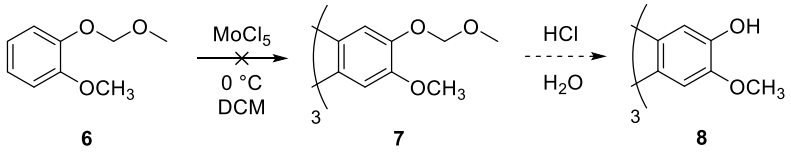

Scheme 7: Reaction between substrate **6** and molybdenum(V) chloride.

Treatment with aqueous 1 M HCl, followed by extractive work-up and flash chromatography of the crude product led to the isolation of significant amounts of an aromatic derivative, whose ^{1}H NMR and 2D NMR spectra were not in agreement with the expected triphenylene structure, rather with the structure **9** reported in Scheme 8, together with some other minor isomers not shown in the scheme. The aromatic compound **9** is presumably formed after cleavage of the acetal moiety of **6**, with consequent release of formaldehyde, responsible for the aromatic substitution on the more activated positions of the two aromatic rings, in *meta* position with respect to the methyl moiety.

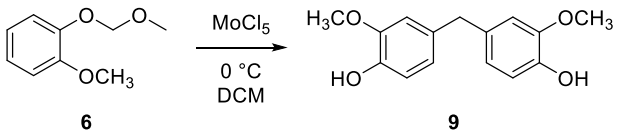

Scheme 8: Side reaction between substrate **6** and molybdenum(V) chloride.

Molecule **9** is an interesting intermediate for the preparation of anti-inflammatory quebecol and its derivatives.[12] Anyway, this synthetic pathway is far from being convenient for our purposes and no further investigations were undertaken.

The last suitable protective group for the oxidative cyclization reaction for the formation of the triphenylene unit was the *tert*-butoxy moiety, which is considered more resistant to oxidative environments. Two different strategies to convert guaiacol into 1-(*tert*-butoxy)-2-methoxybenzene were considered and tested: a Suzuki cross-coupling reaction and the reaction of guaiacol with *tert*-butyl chloride in the presence of elemental Zn.

1-Bromo-2-methoxyphenol and sodium *tert*-butoxide were allowed to react in the presence of palladium(II) acetate and tri-*tert*-butyl phosphonium tetrafluoroborate, HP(^{t}Bu)$_3$BF$_4$, in *p*-xylene at 120 °C, under inert atmosphere (Scheme 9).[13]

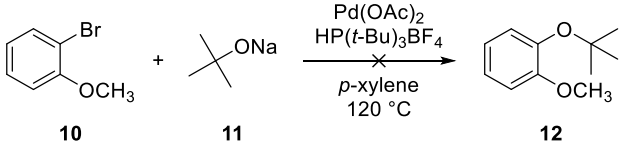

Scheme 9: Synthesis of 1-(*tert*-butoxy)-2-methoxybenzene, **12**, *via* Buchwald-Hartwig Coupling.

The reaction was monitored by TLC and NMR analysis for 2 days, without evidences of the formation of the desired product.

After the failure of the first approach, the reaction with *tert*-butyl chloride was considered. In order to synthesize 1-(*tert*-butoxy)-2-methoxybenzene, **12**, guaiacol was dissolved in *tert*-

butyl chloride and zinc powder was added to the solution, under inert atmosphere at room temperature (Scheme 10).[14]

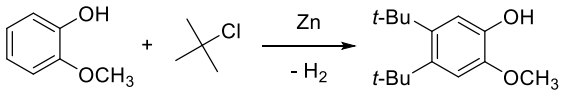

1 13 14

Scheme 10: *tert*-butylation of guaiacol with tert-butyl chloride and zinc.

TLC analysis of the crude revealed complete conversion of the starting guaiacol after 2 hours, nevertheless, despite our expectations, after purification of the crude product by flash chromatography, the main product resulted 4,5-di-*tert*-butyl-2-methoxyphenol (19% yield) with no traces of the desired product. The formation of this compound can be imputed to the initial formation of the desired product, which generates zinc(II) chloride as co-product. This salt acts as a Lewis acid, promoting the formation of *tert*-butyl carbocations, that can be more conveniently captured by the nucleophilic aromatic ring.

Although in the literature are reported several other methods for phenols *tert*-butylation, those options were not further investigated because the evidences experienced revealed the *tert*-butyl to be too reactive in the perspective of the use of oxidants able to impart acidic character to the reaction media.

The strategy to obtain a hemi-*O*-alkylated hexahydroxytriphenylene by simple removal of one protective group from a bis-*O*-alkylated trimethoxytriphenylene turned out to be not a suitable approach, mainly due to the liability of the protecting group considered during the cyclization reaction, or the lack of protected precursors. More stable protective groups were therefore required, and because of this we abandoned this synthetic pathway, opting for the use of ketals as alternative protecting groups.

1.2 Catechol Ketals as Triphenylenes precursors

Careful analysis of the literature reported by Waldvogel and co-workers[11] revealed that ketals of catechol can trimerize under chemical and electrochemical oxidation conditions. Furthermore, ketals can be reductively opened[15,16,17] thus enabling the formation of alternated triphenylenes. According to these assumptions, the ketal moieties of hexahydroxytriphenylene may act as precursors for hemi-*O*-alkylated hexahydroxytriphenylene (Scheme 11).

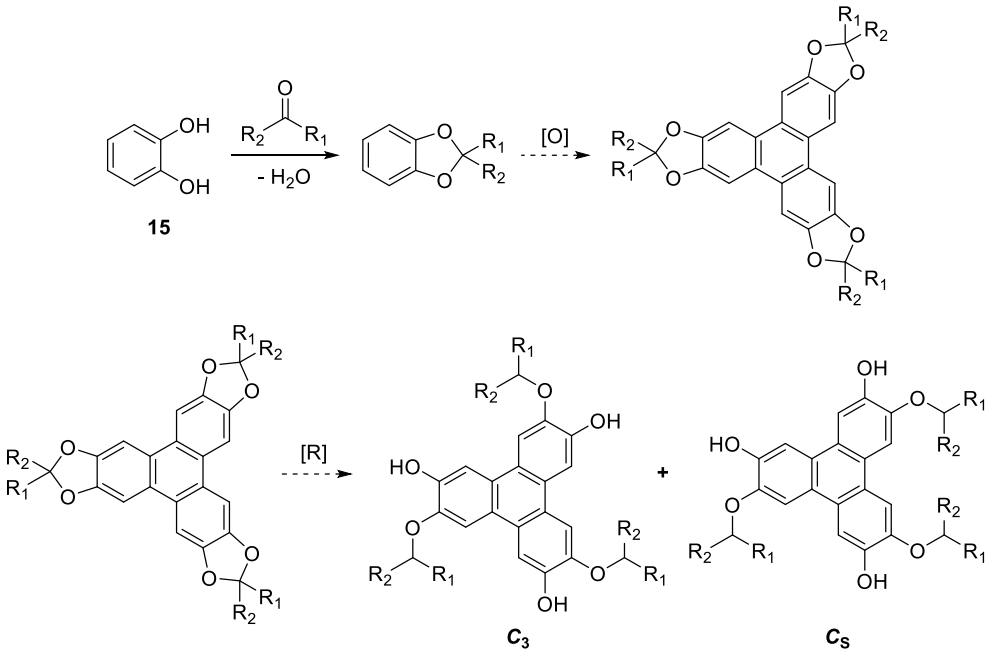

Scheme 11: Hemi-*O*-alkylated hexahydroxytriphenylenes via ketals opening.

The atom economy of this method is also higher than the previous ones, since there is no loss of protecting group and the opened ketal remains part of the final molecule. For this purpose, the acetal of catechol with benzaldehyde was prepared, and lately oxidized with several methods. It is worth to notice that, on the basis of statistical considerations, if the three acetal ring-opening reactions are independent one to the other, the C_3 product will be always disfavoured for the C_S with an expected ratio of 1:3 between the two.

2-Phenylbenzo[*d*][1,3]dioxole, **17**, was synthesized by condensation reaction between catechol and 1.0 equivalent of benzaldehyde in toluene, with *p*-toluensulphonic acid as acidic catalyst, under azeotropic removal of water for 48 hours (Scheme 12).[18]

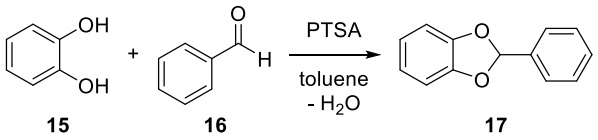

Scheme 12: Synthesis of 2-phenylbenzo[*d*][1,3]dioxole, **17**.

Reduced pressure distillation of the crude reaction mixture to remove the excess of benzaldehyde gave the product in 20% yield. The low yield of the reaction could be imputable to the small scale of the reaction itself and the side oxidation of benzaldehyde to benzoic acid.

The availability of acetal **17** allowed to test both chemical and electrochemical oxidative trimerization to obtain the corresponding hexahydroxytriphenylene benzylidene.

Chemical oxidative trimerizations of **17** were attempted using the two possible oxidants reported in the literature: iron(III) chloride[8] and molybdenum(V) chloride.[11]

At first, substrate **17** was subjected to oxidation using anhydrous iron(III) chloride in DCM, in the presence of concentrated sulphuric acid under inert atmosphere at room temperature (Scheme 13).[19]

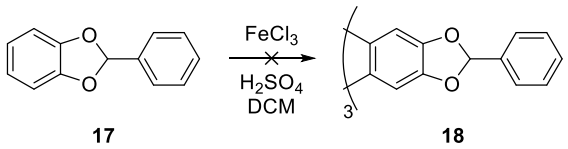

Scheme 13: Chemical oxidation of molecule **17** with iron(III) chloride.

Disappointingly, no triphenylene products were observed by ^{1}H NMR analysis after 4 hours. Furthermore, catechol resonances were not present in the NMR spectra and the typical singlet resonance of benzaldehyde was still present in large amount, together with some benzoic acid. This suggested that iron(III) chloride and the catalytic amount of sulfuric acid were able to cleave the acetal moiety due to the adventious presence of moisture, with subsequent catechol and benzaldehyde oxidation to quinone and benzoic acid. The intense colour of the solution also supported this hypothesis.

A further attempt to trimerize **17** was performed with anhydrous molybdenum(V) chloride in DCM, under inert atmosphere at 0 °C (Scheme 14).[11]

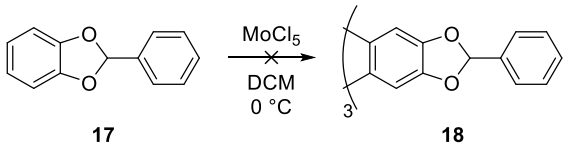

Scheme 14: Chemical oxidation of molecule **17** with molybdenum (V) chloride**.**

TLC analysis of the crude displayed complete consumption of the reagent after 30 minutes. However, after work-up of the reaction mixture the ^{1}H NMR analysis revealed a complex mixture in which trimer and benzaldehyde acetal resonances were not present. Once again, the highly coloured solution suggested the presence of quinones indicating that the acetal was completely hydrolysed, and the resulting benzaldehyde and catechol were oxidized.

Since the chemical oxidations did not work on **17** due to the acidic nature of the reagents and promoters, an alternative electrochemical oxidative trimerization was considered. Using platinum electrodes, a solution of **17** in anhydrous ACN, in the presence of tetrabutylammonium tetrafluoroborate as electrolyte, under inert atmosphere at 0 °C was subjected to a current of 0.016 A/cm^{2} (Scheme 15).[20,21]

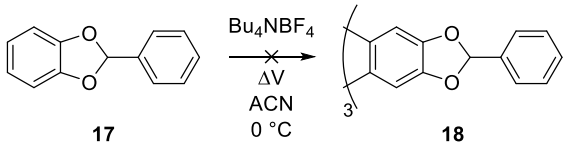

Scheme 15: Electrochemical oxidation of molecule **17**.

The reaction was monitored by TLC analysis, which revealed the presence of substrate **17** after 4 hours of experiment, although ^{1}H and ^{13}C NMR suggested that the acetal was partially opened, according to the observation of signals attributed to the benzyl moiety. Signals diagnostic of the formation of triphenylene were not detected. In any case, the reaction was further continued for 3.5 hours, observing the formation of large amounts of

a brown precipitate, that was isolated, washed and analysed. The ^{1}H NMR spectrum revealed the polymeric nature of the precipitate, whose structure was tentatively assessed as **19**, which is presumably formed by the polymerization of the reductively opened acetal (Scheme 16).

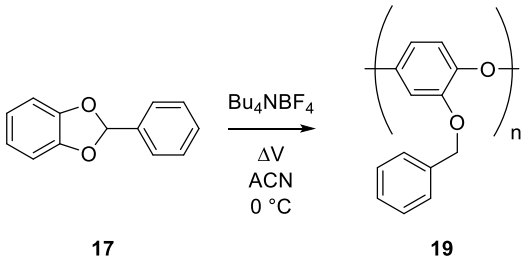

17 **19**

Scheme 16: Electrochemical polymerization of **17**.

Even if the expected triphenylene was not obtained with this method, the reaction will be subjected to further investigations, since there is reason to believe that it could afford cyclic oligomeric aromatic poly-ethers with n = 5, 6, or 7, potentially useful for supramolecular applications.

1.3 Synthesis of Ketals from Hexahydroxytriphenylene

Due to the difficulties found in the trimerization of catechol ketals (especially for acetal **17**), we decided to reverse the steps synthesizing at first the triphenylene core with known methods and introducing later on the ketal moieties.

Veratrole was oxidized with anhydrous iron(III) chloride in the presence of concentrated sulphuric acid under inert atmosphere, at room temperature (Figure 17).[1,8]

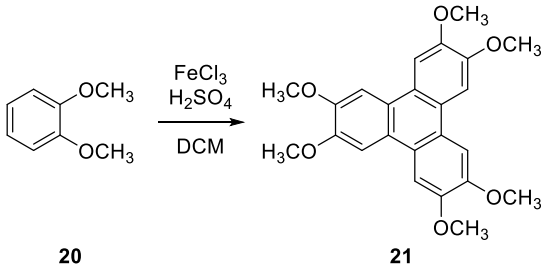

20 **21**

Figure 17: Synthesis of 2,3,6,7,10,11-hexamethoxytriphenylene, **21**.

After 3 hours, the product **21** was precipitated with methanol from the reaction mixture as a white powder, pure enough for the following derivatizations (80% yield). This reaction was further easily scaled-up to 10 grams of starting material, with no loss on the yield demonstrating the robustness of the method.

For the removal of the methyl ether moieties to obtain the hexahydroxytriphenylene (**HHTP**) for further functionalization, a suspension of **21** in a 1:1 v/v mixture of 48% aqueous hydrobromic acid and acetic acid was purged, maintained under inert atmosphere and refluxed overnight (Figure 18).[1,8]

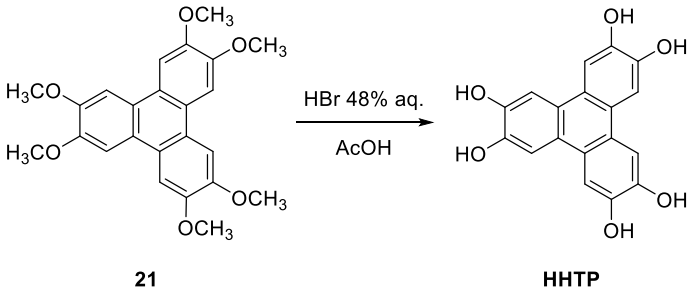

Figure 18: Synthesis of 2,3,6,7,10,11-hexahydroxytriphenylene, **HHTP**.

The tan solid that separated spontaneously from the reaction mixture was filtered off and recrystallized from aqueous acetic acid, treated with activated charcoal to afford colourless crystals of **HHTP** with a 60% yield. Without the treatment with activated charcoal, the yield can rise up to 95%, obtaining the product with a suitable NMR purity.

In order to synthesize tri-*O,O*-benzylidene-2,3,6,7,10,11-hexahydroxytriphenylene, **18**, three different approaches were undertaken. At first, the formation of **18** was attempted refluxing **HHTP** with 1.3 equivalents of benzaldehyde in the presence of scandium(III) triflate as Lewis acid catalyst, under inert atmosphere, with azeotropic removal of water in the presence of 3 Å molecular sieves (Scheme 19).[22]

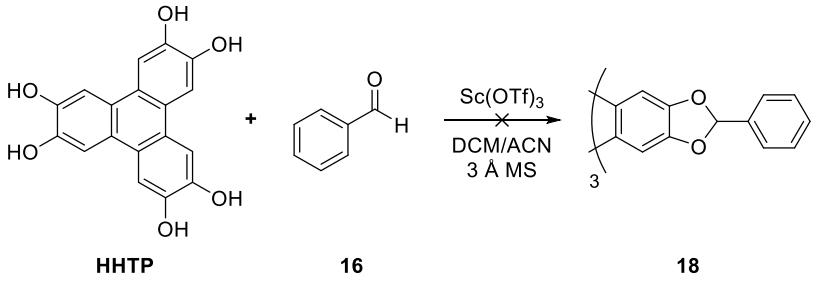

Scheme 19: First attempt of synthesis of molecule **18** with $Sc(OTf)_3$ as Lewis acid.

Even after prolonged reflux, ^{1}H NMR analysis showed negligible amounts of product **18**, whose isolation was not attempted. The second approach involved a transacetalization between **HHTP** and benzaldehyde dimethoxy acetal, used as solvent, employing *p*-toluensulphonic acid as acidic catalyst under inert atmosphere at 100 °C (Scheme 20).

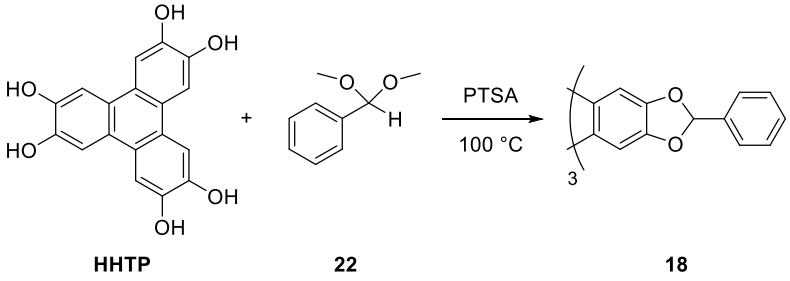

Scheme 20: Synthesis of **18** with benzaldehyde dimethoxy acetal and PTSA.

After 4 days under reflux, the reaction mixture was cooled, neutralized and extracted to afford a crude containing large amounts of benzaldehyde dimethoxy acetal, which was removed under reduced pressure. Finally, the residue was purified by flash chromatography, affording product **18** in only 8% yield.

The last methodology tested involved removal of water with 3 Å molecular sieves from the condensed azeotropic vapours of a refluxing solution of toluene containing **HHTP**, a large excess of benzaldehyde (48 equivalents) and a catalytic amount of *p*-toluensulphonic acid (PTSA) (Scheme 21).[18]

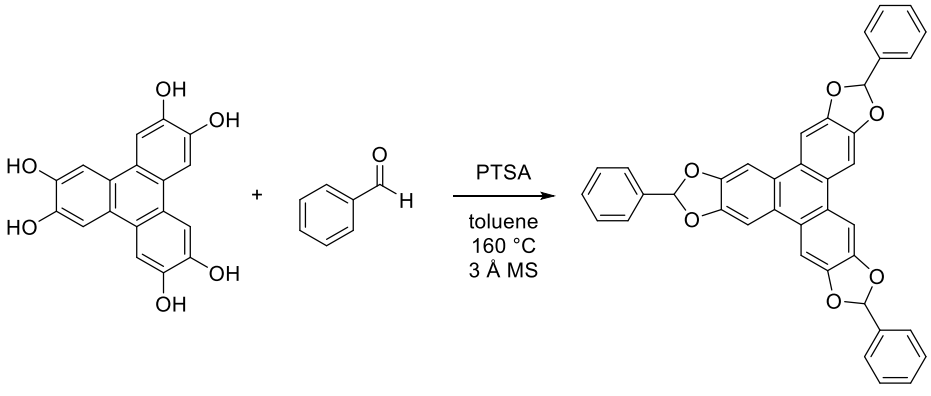

HHTP **16** **18**

Scheme 21: Synthesis of tri-*O,O*-benzylidene-2,3,6,7,10,11-hexahydroxytriphenylene, **18**, with benzaldehyde and PTSA.

The reaction was run under reflux for 96 hours, then the mixture was neutralized, dried and concentrated. Precipitation with Et_2O allowed the recovery of a first amount of product form the benzaldehyde solution. *Vacuum* distillation of the excess of benzaldehyde and a further precipitation with Et_2O afforded a second amount of product, as well as the recovery of most of the aldehyde used in the reaction. The final overall yield was 80%.

1.3.1 Investigation on the Stereochemistry of the Acetalization Reaction

HHTP is a perfectly planar molecule, as well as its alkylated derivatives. On the contrary, when acetal moieties are introduced, as for molecule **18**, the three phenyl rings are protruding from the plane of the triphenylene moiety in two possible relative dispositions: one with all the substituents on the same side of the plane (*syn* isomer), and the other with two substituents on the same side and one on the opposite side of the plane (*anti* isomer) (Scheme 22).

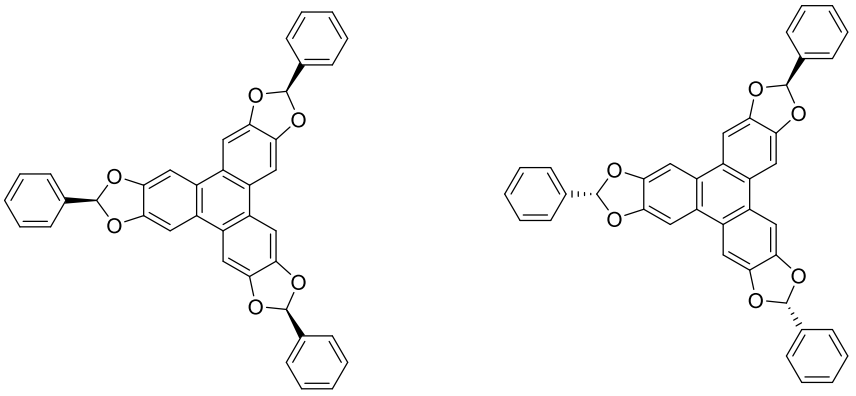

Syn ***Anti***

Scheme 22: *Syn* and *anti* isomers of molecule **18**.

Statistically, their ratio should be 3:1 in favour of the *anti* isomer, because once the first acetal is formed, the second has a 50% chance to lay on the same side of the plane and the third another 50% chance, thus reducing the possibility to obtain the *syn* product to 25% (50% of the 50%). This, of course, if the formation of an acetal does not influence the formation of the following ones. Unfortunately, for the molecule **18**, the *syn* and *anti* isomers are characterized by both ^{1}H NMR and ^{13}C NMR spectra that are perfectly isochronous. Moreover, despite several attempts, the separation of the two isomers by flash chromatography turned out not to be feasible. To better understand the stereochemistry of the reaction, trying to figure out if the three acetalization steps were independent one to the other, we decided to introduce a fluorine atom on the *para* position of the benzylidene, believing that this could be sufficient to spectroscopically differentiate by ^{19}F NMR the two isomers.

Since the first attempt of synthesis of the *p*-fluorinated derivative of **18**, **23**, following the same methodology using *p*-fluorobenzaldehyde in place of benzaldehyde did not work, we decided to prepare 1-(dibromomethyl)-4-fluorobenzene as a more electrophilic analogue of the *p*-fluoro-benzaldehyde to be reacted with **HHTP** under basic conditions.

The synthesis of 1-(dibromomethyl)-4-fluorobenzene, **25**, was achieved by reacting *p*-fluorobenzaldehyde with bromotriphenylphosphonium bromide in anhydrous ACN at 60 °C for 3.5 hours (Scheme 23).[23]

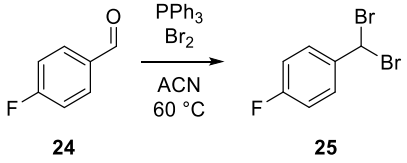

Scheme 23: Synthesis of 1-(dibromomethyl)-4-fluorobenzene, **25**.

After the work-up, the product was obtained as a pale-yellow oil in 71% yield, pure enough for the following steps.

Once product **25** was obtained, it was reacted with **HHTP** in DMF in the presence of K_2CO_3 at 60° C for 48 hours (Scheme 24).

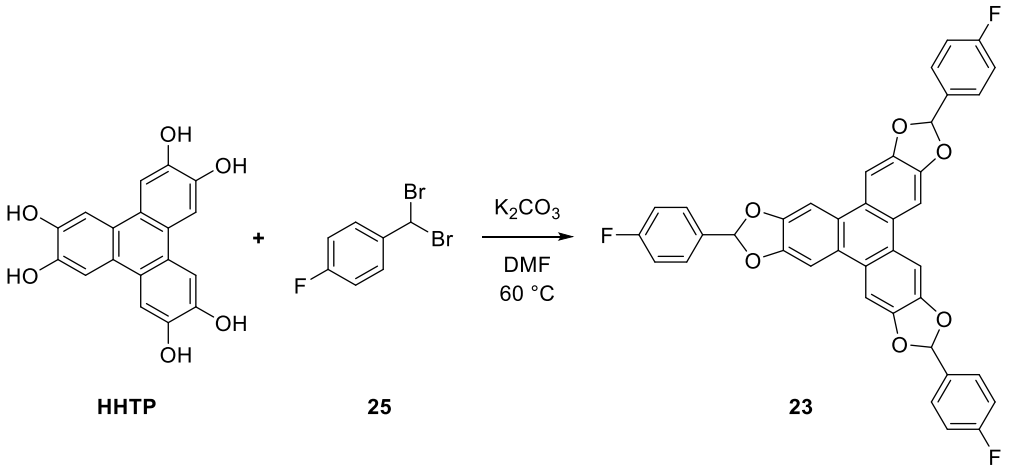

Scheme 24: Reaction between **HHTP** and **25** to achieve the product **23**.

After work-up and flash chromatography of the crude, product **23** was isolated in 7% total yield. With this synthetic method the yield results very low probably due to stability problems of **HHTP** in basic environments. Indeed, **HHTP** in the presence of adventious oxygen in the system can quickly oxidize to quinonic forms.

Even though the ^{1}H NMR ^{13}C NMR did not result useful for the differentiation and quantification of the two isomers due to isochronism of the signals of the *syn* and *anti* stereoisomers, $^{19}F\{^{1}H\}$ NMR of the product revealed the presence of three resonances in the range -110.17 - -110.22 ppm, one for the *syn* and two for the *anti* isomer (Figure 1).

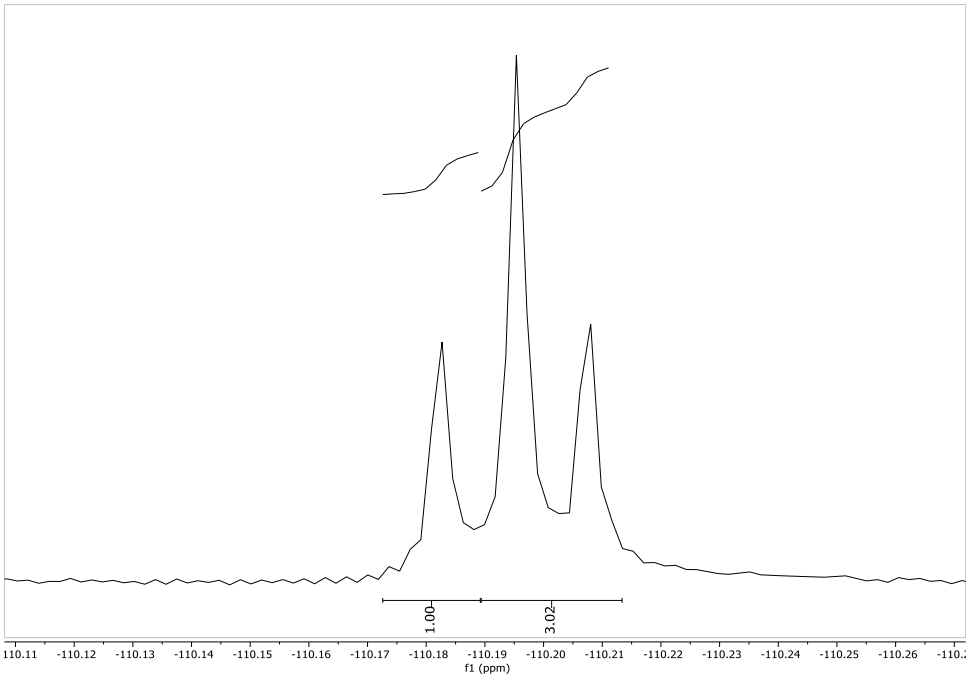

Figure 1: $^{19}F\{^{1}H\}$ NMR of the reaction crude of molecule **23**. Detail of the signals at -110.2 ppm.

Although column chromatography could not provide a full separation of the isomers, two enriched fractions in the two isomers enabled the peaks assignment (Figure 2).

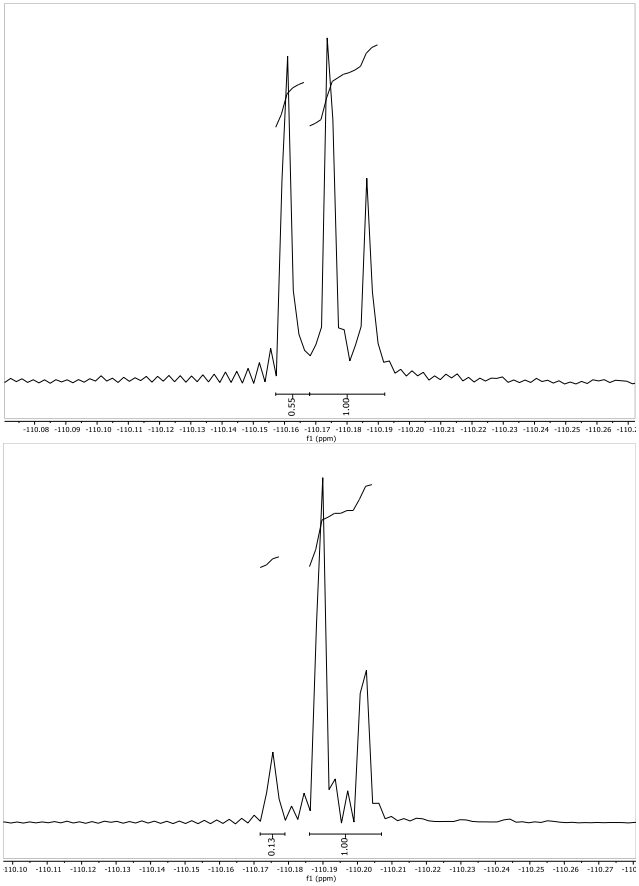

Figure 2: $^{19}F\{^{1}H\}$ NMR of the two LC fractions of **23**. First eluted on the left, second eluted on the right.

The two peaks on the right maintained a constant 1:2 ratio, while the peak on the left changed intensity from one fraction to the other, thus allowing to assign the peak at -110.16 to the *syn* product and the peaks at -110.20 and -110.22 to the *anti* product. From the value of the integrals reported in Figure 1 it was estimated a 1:3 ratio between the *syn* and *anti* isomers, in accordance with a statistical formation of the three acetal units. It is likely to believe that the same product ratio of stereoisomers is present also for the molecule **18**, due to the negligible effect of the substitution of the F atom with H in the aldehyde.

Even though the stereochemistry of these molecule will be lost during the following acetal ring opening steps, it was nevertheless useful and interesting to know more about the reaction stereochemistry, also for possible future applications.

1.4 Synthesis of Hemi-*O*-Alkylated Hexahydroxytriphenylenes

Once the desired triphenylene ketals **18** was obtained, we focused our attention on the procedures aimed at the reductive opening of the ketals in order to get the corresponding hemi-*O*-alkylated hexahydroxytriphenylenes. We initially focused our attention on a contemporary action of a reductive/nucleophilic hydride and a Lewis acid, and later on the use of a more sterically hindered hydride such as diisobutylaluminium hydride (DIBAL-H).

A limited number of examples of nucleophilic ring opening of ketals using hydrides have been reported in the literature, confirming the peculiarity of this moiety as a protecting group under nucleophilic or basic conditions.[15,17] On the other hand, the presence of a Lewis

acid can activate the acetal group, promoting the ring opening with the cleavage of a carbon-oxygen bond. Several combinations of reducing agent and Lewis acid were tested, as reported in Table 1, observing in all cases a mixture of the two possible isomers: the desired ***C*$_3$-26** and the ***C*$_S$-26** symmetric tris-benzyl derivatives that were separated by column chromatography, firstly eluting with DCM until complete recovery of the first less polar isomer, ***C*$_3$-26**, then with ethyl acetate to recover ***C*$_S$-26**.

Entry	Hydride (eq.)	Lewis acid (eq.)	Solvent	Temperature [°C]	Time [h]	Conversion [%][a]	Yield [%][b]	C_3/C_s [a]	C_3-26 Yield [%][b]
1	BH_3·THF (20.2)	$AlCl_3$ (21)	THF	66	15	100	0	-	-
2	$LiAlH_4$ (3.0)	BF_3·OEt_2 (12)	Et_2O / DCM	0 to 60	4.0	50	0	-	-
3	$LiAlH_4$ (14.5)	$AlCl_3$ (12)	DCM	60	0.75	100	0	-	-
4	$LiAlH_4$ (14.5)	$AlCl_3$ (12)	Et_2O / DCM	60	2.5	100	24	1.0:1.2	11
5	$LiAlH_4$ (14.5)	$AlCl_3$ (6)	Et_2O / DCM	60	3.0	100	22	1.0:1.2	10
6	$LiAlH_4$ (14.5)	$AlCl_3$ (3)	Et_2O / DCM	60	1.0	97	19	1.0:1.2	8
7	$LiAlH_4$ (4.0)	$AlCl_3$ (4)	Et_2O / DCM	60	4.5	68	20	1.0:1.2	8

Table 1: Selective cleavage of **18** with different combinations of reducing agent and Lewis acid. [a] Calculated by ^{1}H-NMR. [b] Isolated yield.

When borane in THF with $AlCl_3$ as a Lewis acid was used, it was not possible to isolate any ***C*$_3$-26**, even after complete conversion of the substrate indicating the difficulty in controlling the reaction, observing the formation of further de-benzylation products. Using $LiAlH_4$ as a hydride source, the reaction turned out to be more effective in the presence of $AlCl_3$ as a Lewis acid rather than BF_3 etherate (Table 1, entries 2-7). After optimization of the solvent (use of diethyl ether turned out to be critical, Table 1, entries 3 and 4) and the ratio of $LiAlH_4$ and $AlCl_3$, it was possible to observe the formation of an encouraging 20% yield mixture of ***C*$_3$-26** and ***C*$_S$-26** products in a 1.0:1.2 ratio. Surprisingly, in all cases the ratio of the two isomers was not a statistical 1:3 between ***C*$_3$-26** and ***C*$_S$-26**, suggesting that the three reduction are not independent events. The isolated yield of the desired ***C*$_3$-26** product was never higher than 11%, even when quantitative conversion of reagent **18** was observed. A possible cause was attributed to the high reactivity of $LiAlH_4$ with $AlCl_3$, which is known to provide the formation of alane,[24] a reagent that could lead to complete removal of the benzyl moieties.

To mitigate this over-reactivity and to increase the selectivity of the process, the use of a more hindered alane was considered this time in the absence of Lewis acids. The best results were obtained using commercial diisobutylaluminium hydride (DIBAL-H) in toluene,[15,17] which, conversely to the previous reducing agents, could be added at once. The reaction between substrate **18** and DIBAL-H was further investigated aiming at the optimization of the yield of the ***C*$_3$-26** product, as reported in Table 2.

Entry	DIBAL-H (mol. ratio)	Temp. [°C]	Time [h]	Total Yield [%][b]	C_3/C_s [a]	C_3-26 Yield [%][b]
1	15	0 to r.t.	15.0	45	1.0:1.4	19
2	4	0 to r.t.	0.83	79	1.0:1.0	40
3	4	0	1.0	53	1.0:0.8	30
4	4	0	1.3	76	1.0:0.8	42
5	4	0	4.0	86	1.0:0.9	43
6	5	0	3.0	95	1.0:1.0	47
7	5	-10	8.0	82	1.0:0.8	38
8	6	-10 to 0	5.5	97	1.0:1.0	48

Table 2: Optimization of the selective cleavage of **18** with DIBAL-H in DCM/toluene leading to ***C*$_3$-26**. [a] Calculated by ^{1}H-NMR. [b] Isolated yield.

A large excess of the reducing agent and a prolonged reaction time (Table 2, entries 1 and 2) turned out to be detrimental for the reaction, leading to overreduction of both ***C*$_3$-26** and ***C*$_S$-26** products; moreover, the reaction temperature turned out to influence heavily the yield of the ***C*$_3$-26** product. As reported in Table 2, entries 3-5, the reaction at 0 °C showed a maximum yield for ***C*$_3$-26** after 1.3-4 h and an increase was observed operating with 5 eq. of DIBAL-H with respect to **18** (1.7 eq. per acetal unit) at lower temperature (Table 2, entry 6). The use of 6.0 moles of DIBAL-H per mole of substrate at −10 to 0 °C proved to be the best option (Table 2, entry 8), enabling a favourable lowering of reaction time and the formation of the desired ***C*$_3$-26** product in a 48% isolated yield after purification by flash chromatography. Once again, the ratio of the two isomers was not statistical in every case, showing a remarkable influence of the opening of one acetal to the opening of the surrounding ones. The previously unknown in the literature product ***C*$_S$-26** was isolated and fully characterized.[5] This compound can be conveniently recycled through Pd/C catalyzed hydrogenation and removal of the benzyl moieties, affording quantitatively the starting material **HHTP**. Through this recycling step of ***C*$_S$-26**, the overall yield of ***C*$_3$-26** calculated from veratrole increases up to 53% considering one recycle of ***C*$_S$-26**.[5] To demonstrate the robustness of the synthetic method proposed, the synthesis of ***C*$_3$-26** was scaled up starting from 5.6 g of **HHTP**, obtaining at the end 3.2 g of the desired highly symmetric product with an overall unaltered yield of 48% over two steps.

In Scheme 25 it is reported the final synthetic scheme for the optimized synthesis of 2,6,10-tribenzyloxy-3,7,11-trihydroxytriphenylene, ***C*$_3$-26**.

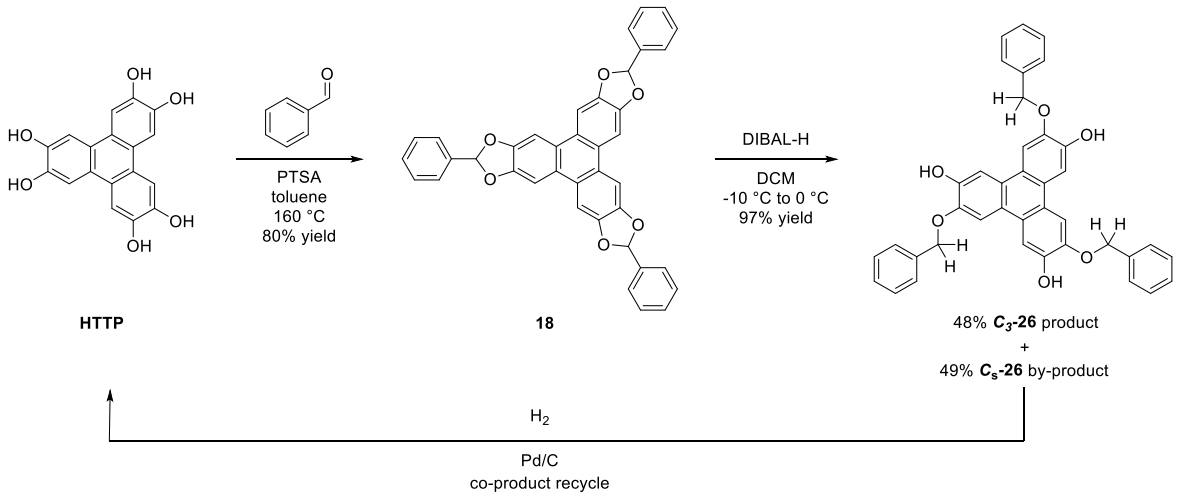

Scheme 24: Complete synthetic scheme for the optimized synthesis of 2,6,10-tribenzyloxy-3,7,11-trihydroxytriphenylene, ***C*$_3$-26**.

This molecule, widely exploited in this work as largely described later in the following chapters, could be also very useful for the synthesis of liquid crystals, due to the possible modification of the free hydroxyl moiety and the feasible removal of the benzyl group, further evidencing its versatility.

1.5 Experimental Section

1.5.1 General Methods

The reactions were followed with TLC Polygram® Sil G/UV254, 0.25 mm thickness. ^{1}H NMR, ^{13}C NMR, and 2D spectra were recorded with a Bruker Avance 300 and Ascend 400 spectrometers, working at 300-400 and 75-100 MHz respectively. Resonance frequencies are referred to tetramethylsilane. IR spectra were recorded with a Perkin Elmer Spectrum One spectrophotometer. Mass spectrometric measurements were performed using a Thermo Scientific LTQ Orbitrap XL equipped with HESI source. The compounds studied were dissolved in methanol or acetonitrile with a concentration of $5 \cdot 10^{-3}$ M. They were injected into the HESI source by direct infusion with the syringe pump integrated in the mass spectrometer at a 5 $mL \cdot min^{-1}$ flow rate. Mass spectra were acquired in positive-polarity mode with the following tuning conditions: Temperature 40 °C, Sheath gas 8 (arbitrary units, arb), Aux gas and Sweep gas 0 arb, Spray Voltage 4.5 kV, Capillary temperature 275 °C, Capillary Voltage -9 V, Tube lence 150 V. In negative polarity the following tuning parameters were employed: Temperature 40 °C, Sheath gas 19 (arbitrary units, arb), Aux gas and Sweep gas 0 arb, Spray Voltage 3.0 kV, Capillary temperature 275 °C, Capillary Voltage 10 V, Tube lence 120 V. Mass spectra were collected in full scan with a resolution of 100000 at m/z 400. The Orbitrap MS was calibrated just before analysis and during the acquisition in order to improve mass accuracy lock masses were employed. Reagents and solvents with high purity degree purchased by the providers were used as given. Otherwise, they were purified following the procedures reported in literature.[25] Anhydrous solvents were prepared by adding activated 3 Å molecular sieves to the solvent under inert atmosphere. Molecular sieves were activated shortly before the use by continuous heating under *vacuum*. Flash chromatography were performed with silica gel Merk 60, 230-400 mesh, following procedures reported in literature.[26]

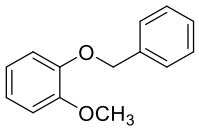

3

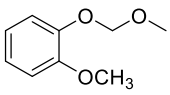

6

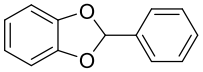

17

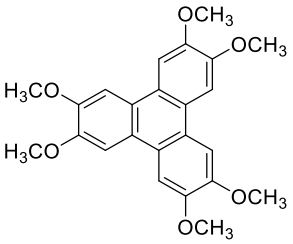

21

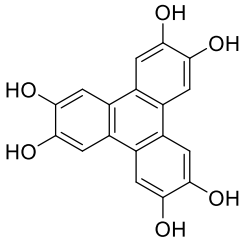

HHTP

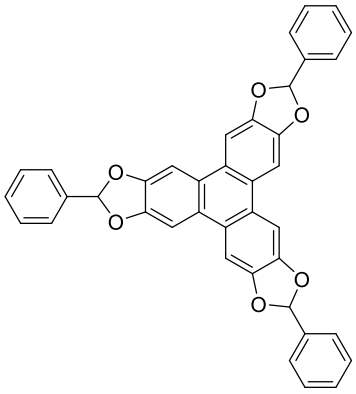

18

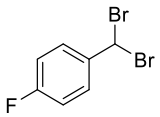

25

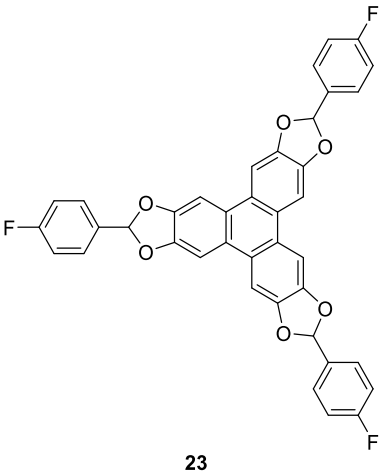

23

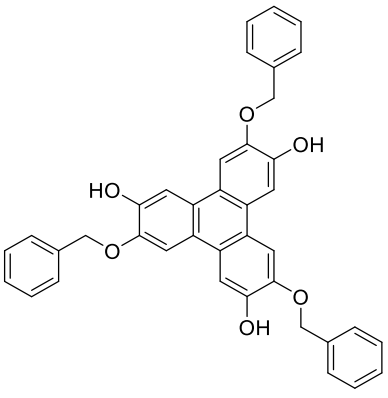

***C*$_3$-26**

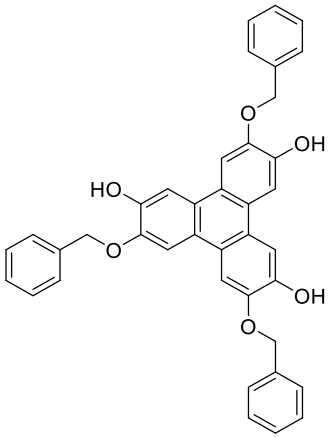

***C*$_s$-26**

1.5.2 Experimental Procedures - Syntheses

1-(Benzyloxy)-2-methoxybenzene (**3**)

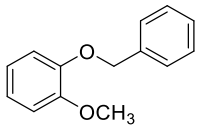

3

A mixture of guaiacol (9.93 g, 80 mmol), K_2CO_3 (12.0 g, 88 mmol) and BnBr (20 g, 120 mmol) in acetone (200 mL), was refluxed under inert atmosphere overnight. The resulting mixture was cooled to room temperature, filtered with Gooch and the solution was concentrated in *vacuum*. The resulting white crystals of product were washed with MeOH (2x15 mL) and dried in *vacuum* (16.0 g, 80 mmol, 100% yield). ^{1}H NMR (300 MHz, $CDCl_3$): δ 7.50-7.30 (5H m), 6.98-6.82 (4H, m), 5.18 (2H, s), 3.91 (3H, s). Further spectroscopic data (^{13}C, MS, IR) are in accordance with the literature.[9]

1-Methoxy-2-(methoxymethoxy)benzene (**6**)

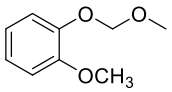

6

A solution of guaiacol (1.5 g, 12 mmol), MOMCl (1.44 g, 18 mmol), and *N,N*-diisopropylethylamine (3.1 g, 27 mmol) in DCM (12 mL) was stirred at 0 °C for 1 hour under inert atmosphere. The solution was allowed to warm to room temperature overnight. Water (14 mL) was added and the layers were separated. The aqueous phase was extracted with Et_2O (3x40 mL). The combined organic phases were washed with 1 M aqueous NaOH (3x30 mL), dried over $MgSO_4$, filtered and concentrated in *vacuum*, to afford the product as an orange oil (1.8 g, 11 mmol, 92% yield). ^{1}H NMR (300 MHz, $CDCl_3$): δ 7.18 (1H, dd, *J* = 8.0 and 1.6 Hz), 7.05-6.88 (3H, m), 5.25 (2H, s), 3.90 (3H, s), 3.54 (3H, s). Further spectroscopic data (^{13}C, MS, IR) are in accordance with the literature. [10]

2-Phenylbenzo[*d*][1,3]dioxole (**17**)

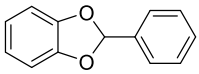

17

A mixture of catechol (12.0 g, 108 mmol), benzaldehyde (11.6 g, 108 mmol) and *PTSA* (0.004 g, 0.020 mmol) in toluene (130 mL) was refluxed in a Dean-Stark apparatus under inert atmosphere for 48 hours. The resulting solution was cooled to room temperature, diluted with diethyl ether (100 mL), washed with 10% aqueous NaOH (3x50 mL), H_2O (50 mL), dried over $MgSO_4$, filtered and concentrated in *vacuum*. Reduced pressure distillation of the crude oil (90 °C at 820 mBar) afforded the product as a white solid (4.3 g, 22 mmol, 20% yield). ^{1}H NMR (300 MHz, $CDCl_3$): δ 7.69-7.61 (2H, m), 7.54-7.47 (3H, m), 7.02 (1H, s), 6.96-6.91 (4H, m). Further spectroscopic data (^{13}C, MS, IR) are in accordance with the literature.[18]

2,3,6,7,10,11-Hexamethoxytriphenylene (**21**)

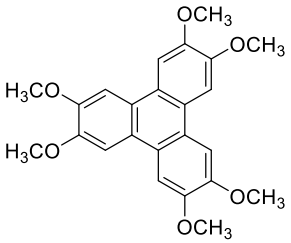

21

To a vigorously stirred mixture of $FeCl_3$ (40 g, 247 mmol) and 0.6 mL of 96% H_2SO_4 in anhydrous DCM (250 mL) under inert atmosphere, a solution of veratrole (11.7 g, 84.4 mmol) in anhydrous DCM (120 mL) was added dropwise in 20 minutes. The mixture was stirred for 3 hours at room temperature. Methanol (330 mL) was added dropwise and the solution was stirred for another 30 minutes. The resulting mixture was filtered with Gooch, washing the precipitate with cold MeOH (3x40 mL), to afford the product as a light brown powder (9.17 g, 22.4 mmol, 80% yield). ^{1}H NMR (300 MHz, $CDCl_3$): δ 7.78 (6H, s), 4.14 (18H, s). Further spectroscopic data (^{13}C, MS, IR) are in accordance with the literature.[8]

2,3,6,7,10,11-Hexahydroxytriphenylene (**HHTP**)

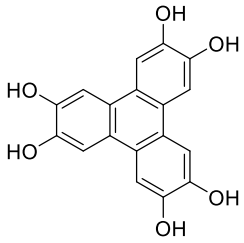

HHTP

A mixture of **21** (9.17 g, 22.4 mmol) in AcOH (310 mL) and 48% aqueous HBr (310 mL) was degassed with argon for 30 minutes and refluxed overnight under inert atmosphere. The resulting solution was cooled to room temperature and the precipitate was filtered off. Recrystallization from a hot 3:2 AcOH/H_2O (500 mL) activated carbon clarified solution afforded the product as white needles, that became purple soon after a brief exposition to air (4.4 g, 13.5 mmol, 60% yield). ^{1}H NMR (300 MHz, DMSO-d_6): δ 9.30 (6H, s), 7.59 (6H, s). Further spectroscopic data (^{13}C, MS, IR) are in accordance with the literature.[8]

2,7,12-Triphenyltriphenyleno[2,3-*d*:6,7-*d*':10,11-*d*'']tris([1,3]dioxole) (**18**)

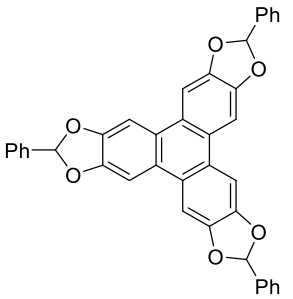

18

A 500 mL round bottomed flask containing a slurry of **HHTP** (4.56 g, 14 mmol), benzaldehyde (100 mL) and PTSA monohydrate (0.106 g, 0.6 mmol) in 130 mL of toluene,

then was topped with a pressure-equalizing dropping funnel filled with activated 3 Å molecular sieves and a reflux condenser. The apparatus was purged with argon and the suspension was refluxed for 96 hours. The resulting solution was cooled to room temperature and washed with saturated $NaHCO_3$ (3×100 mL). The organic phase was diluted with Et_2O (300 mL) and the precipitate was filtered off and recovered. Diethyl ether was removed from the mother liquors with rotavapor, and the residual benzaldehyde was recovered by *vacuum* distillation. The residue of the distillation was diluted in Et_2O (100 mL) and the precipitate was filtered and washed with Et_2O. The product was obtained as a light brown solid (6.6 g, 11.2 mmol, 80% yield). M.P. 244 °C. ^{1}H NMR (400 MHz, $CDCl_3$) δ 7.83 (6H, s), 7.67-7.62 (6H, set of m), 7.49-7.46 (9H, set of m), 7.12 (3H, s). $^{13}C\{^1H\}$ NMR (100 MHz): δ 147.9, 136.2, 136.2, 130.6, 128.9, 126.5, 125.1, 110.8, 101.5. IR (KBr): ν 1638, 1494, 1453, 1396, 1383, 1292, 1240, 1163, 1106, 1033, 1017, 907, 848, 829, 762, 732, 697, 642 cm^{-1}. HRMS (ESI): calcd. for $C_{39}H_{24}O_6$ [M^+] 588.1567; found: 588.1571.

1-(dibromomethyl)-4-fluorobenzene (**25**)

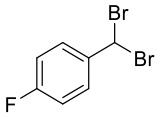

25

In a 50 mL two necked flask, equipped with argon inlet and dropping funnel, triphenylphosphine (2.60 g, 9.9 mmol) and anhydrous ACN (15 mL) were added and the mixture heated until complete dissolution of the solid. The solution was cooled to room temperature and Br_2 (0.51 mL, 9.9 mmol) was added dropwise. *p*-fluorobenzaldehyde (1.03 g, 0.89 mL, 8.24 mmol) was added and the resulting solution was heated at 60 °C for 3.5 hours, it was cooled to room temperature and the precipitate was filtered. Water (50 mL) was added to the filtrated solution and the mixture was extracted with petroleum ether (3×20 mL). The collected organic phases were dried over $MgSO_4$, filtered and concentrated in *vacuum*. Cyclohexane was added to allow the precipitation of some residual triphenylphosphine oxide, that was filtered off. The remaining solution was concentrated in *vacuum* to afford the product as a yellow oil (1.57 g, 5.9 mmol, 71% yield). ^{1}H NMR (300 MHz, $CDCl_3$): δ 7.51-7.61 (2H, set of m), 7.00-7.10 (2H, set of m), 6.66 (1H, s). $^{13}C\{^1H\}$ NMR (100 MHz, $CDCl_3$): δ 163.0 (d, *J* = 250.5 Hz), 138.0 (d, *J* = 3.3 Hz), 128.6 (d, *J* = 8.6 Hz), 115.7 (d, *J* = 22.2 Hz), 39.7. ^{19}F NMR (376 MHz): δ -110.40. Further spectroscopic data (^{13}C, MS, IR) are in accordance with the literature.[23]

2,7,12-tris(4-fluorophenyl)triphenyleno[2,3-*d*:6,7-*d*':10,11-*d*'']tris([1,3]dioxole) (**23**)

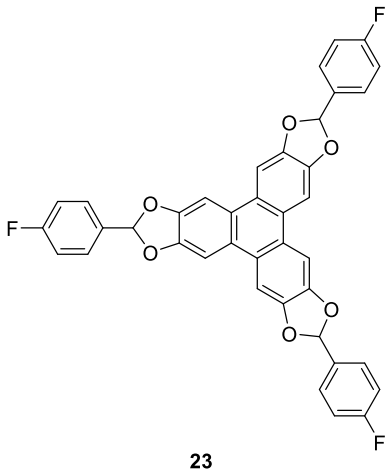

23

A mixture of **25** (0.78 g, 2.9 mmol), **HHTP** (0.20 g, 0.6 mmol) and anhydrous K_2CO_3 (0.85 g, 6.1 mmol) in anhydrous DMF (3.7 mL) was heated at 50 °C for 48 hours. To the cooled mixture H_2O (40 mL) was added and it was extracted with DCM (3×20 mL). The collected organic phases were dried over $MgSO_4$, filtered and concentrated in *vacuum*. The resulting crude oil was filtered over Tonsil® and purified by flash chromatography (eluent cyclohexane/AcOEt 8:2). The product was obtained in two fractions: the first one enriched in the *syn* isomer and the second one prevalently composed by the *anti* product (in total, 0.026 g, 0.041 mmol, 7% yield). ^{1}H NMR (400 MHz, $CDCl_3$): δ 7.82 (6H, s), 7.63 (6H, set of m), 7.16 (6H, t, *J* = 8.23 Hz), 7.09 (3H, s). $^{13}C\{^1H\}$ NMR (100 MHz): δ 165.1, 162.8, 147.7, 132.0, 128.6, 128.6, 125.0, 116.0, 116.0, 110.0, 101.4. $^{19}F\{^1H\}$ NMR (376 MHz): δ -110.2, -110.2, -110.2.

3,7,11-tris(benzyloxy)triphenylene-2,6,10-triol (***C*$_3$-26**) and 3,7,10-tris(benzyloxy)triphenylene-2,6,11-triol (***C*$_s$-26**):

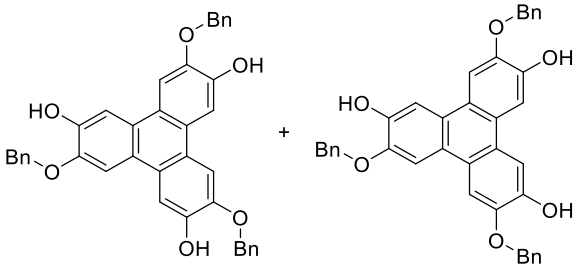

***C*$_3$-26** ***C*$_s$-26**

In a 500 mL two necked flask, equipped with argon inlet and septum, to a -10 °C cooled mixture of **18** (3.44 g, 5.85 mmol) in anhydrous DCM (210 mL) a DIBAL-H solution (1.5 M in toluene, 23.4 mL, 35.1 mmol) was added dropwise with a syringe during 20-25 minutes. The resulting solution was stirred at -10 °C for 2 hours, and finally at 0 °C for 3 hours. The exceeding DIBAL-H was quenched at 0 °C with MeOH (10 mL), 1 M aqueous HCl (135 mL) and the resulting mixture was vigorously stirred at room temperature for 30 minutes. The mixture was decanted, and the organic phase collected. The aqueous layer was extracted with DCM (2×30 mL) and the combined organic phases were dried over $MgSO_4$, filtered and concentrated in *vacuum*. The crude mixture of isomers (C_3 and C_s, 1:1) was purified by flash

chromatography, eluting with DCM until complete recovery of the first isomer, ***C*$_3$-26**, then with AcOEt to recover the ***C*$_s$-26**.

***C*$_3$-26**: 1.68 g, 2.8 mmol, 48% yield. M.P. 222 °C (lit. 221 °C). ^{1}H NMR (400 MHz, DMSO-d_6): δ 9.32 (3H, s), 7.89 (3H, s), 7.88 (3H, s), 7.62 (6H, d, *J* = 7.0 Hz), 7.43 (6H, t, *J* = 7.0 Hz), 7.35 (3H, t, *J* = 7.0 Hz), 5.38 (6H, s). Further spectroscopic data (^{13}C, MS, IR) are in accordance with the literature.[5]

***C*$_s$-26**: 1.70 g, 2.8 mmol, 49% yield. M.P. 208 °C. ^{1}H NMR (400 MHz, DMSO-d_6): δ 9.49 (1H, s), 9.47 (1H, s), 9.29 (1H, s), 7.92 (1H, s), 7.91 (1H, s), 7.88 (1H, s), 7.87 (1H, s), 7.73 (1H, s), 7.72 (1H, s), 7.66-7.58 (6H, set of m), 7.43 (6H t, *J* = 7 Hz), 7.38-7.35 (3H, set of m), 5.39 (2H, s), 5.39 (2H, s), 5.36 (2H, s). $^{13}C\{^1H\}$ NMR (100 MHz): δ 147.3, 147.2, 147.0, 146.9, 137.9, 137.9, 137.8, 128.9, 128.9, 128.4, 128.4, 128.3, 128.2, 123.7, 123.4, 123.2, 122.4, 122.1, 122.0, 109.0, 108.6, 108.6, 107.6, 107.4, 107.2, 70.6, 70.6, 70.3. IR (KBr): ν 1629, 1619, 1596, 1515, 1451, 1434, 1402, 1382, 1312, 1267, 1176, 1151, 1037, 1023, 852, 787, 738, 696 cm^{-1}. HRMS (ESI): calcd. for $C_{39}H_{31}O_6$ [M^+] 593.1970; found: 593.1968.

1.5.3 NMR ad MS Spectra

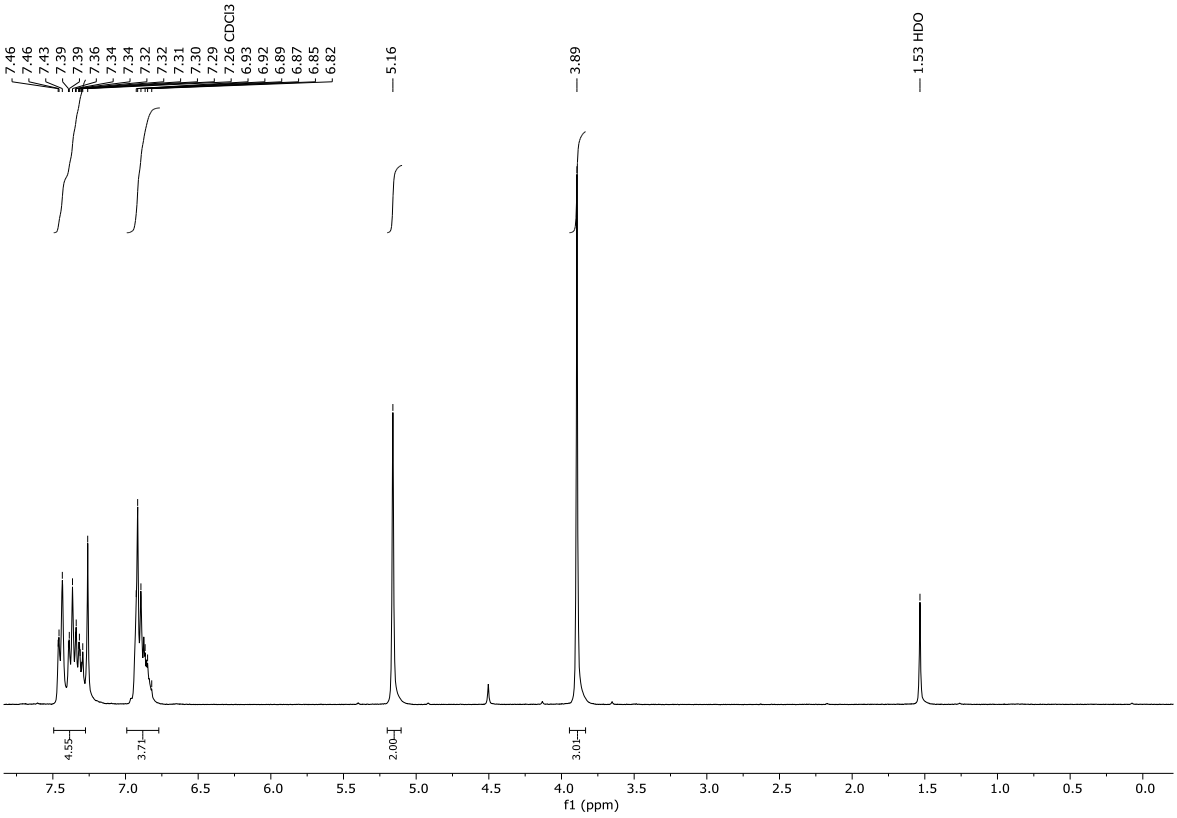

Figure I: ^{1}H NMR of molecule **3**.

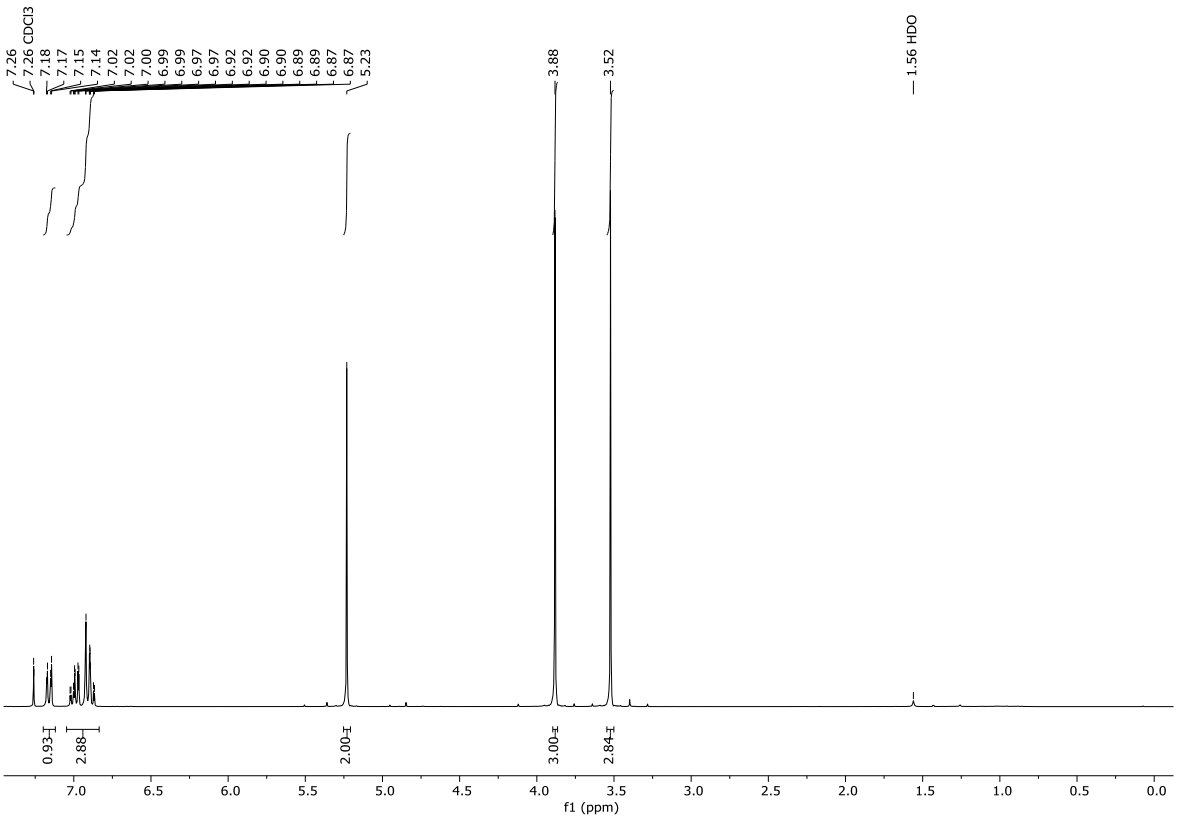

Figure II: ^{1}H NMR of molecule **6**.

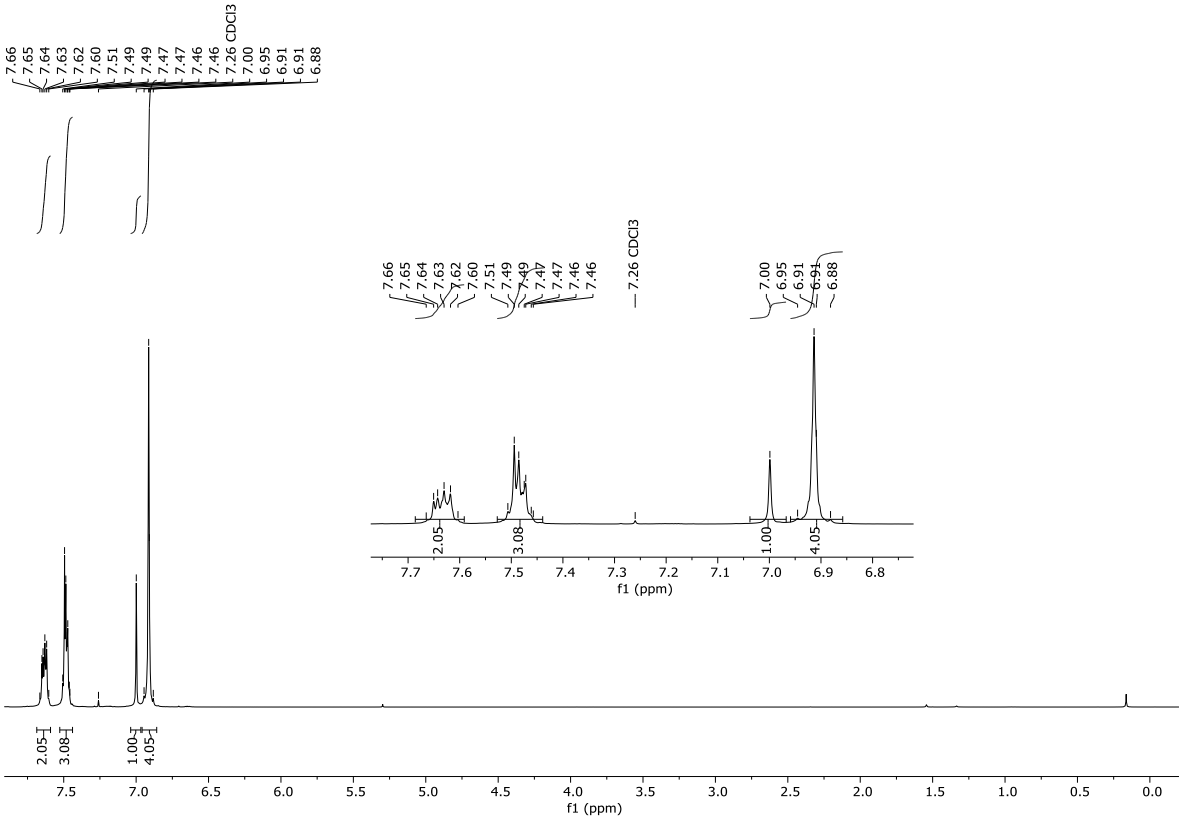

Figure III: ^{1}H NMR of molecule **17**.

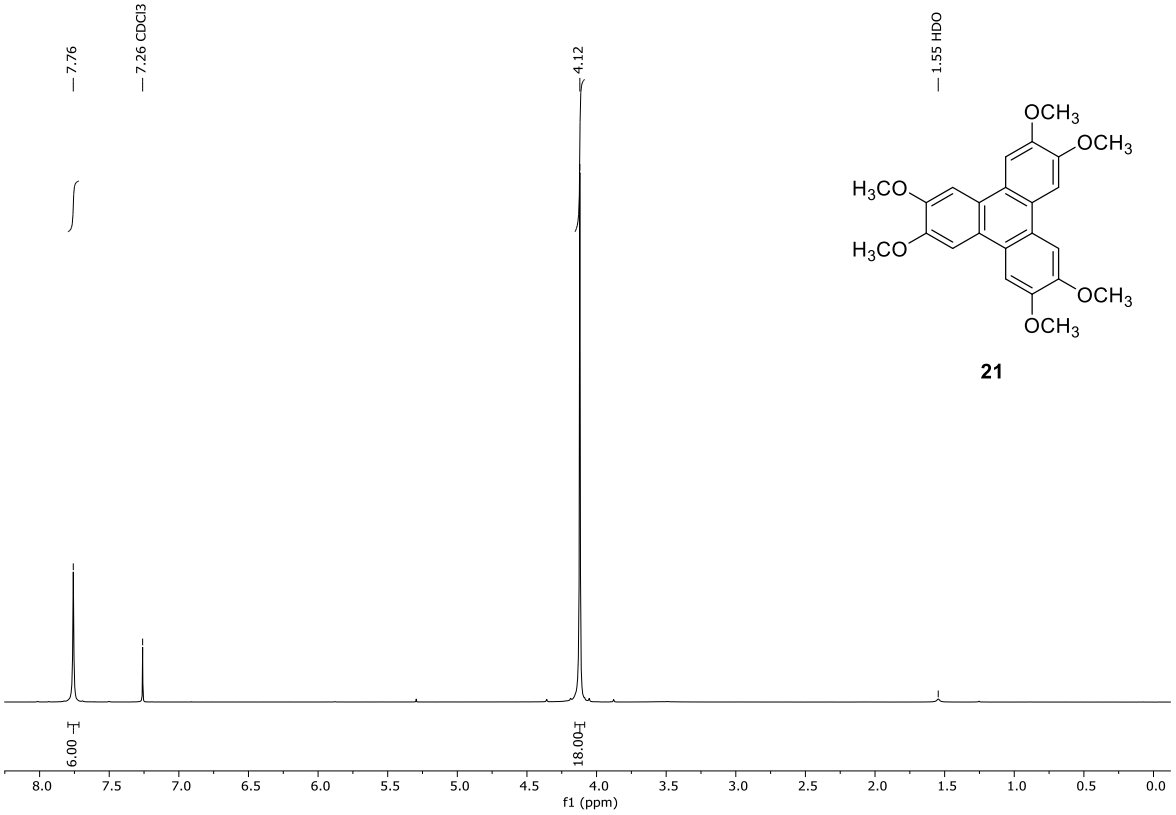

21

Figure IV: ^{1}H NMR of molecule **21**.

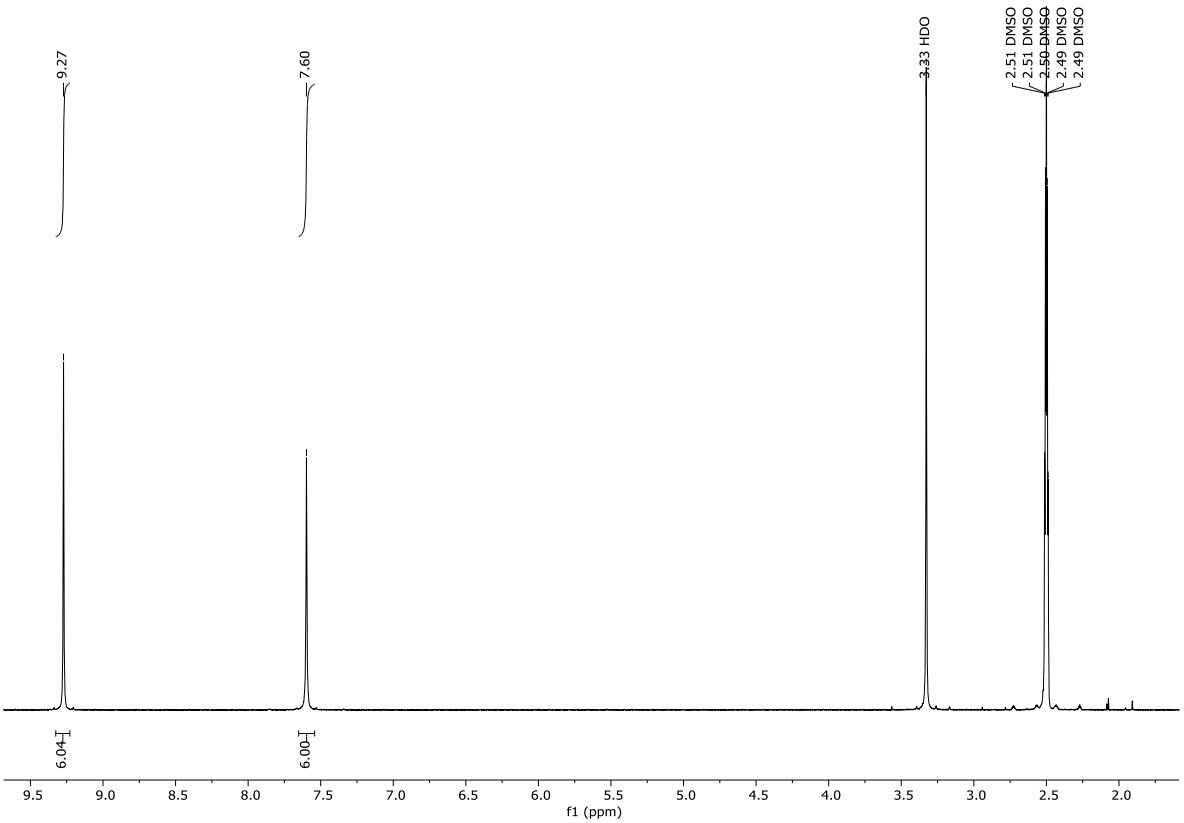

Figure V: ^{1}H NMR of molecule **HHTP**.

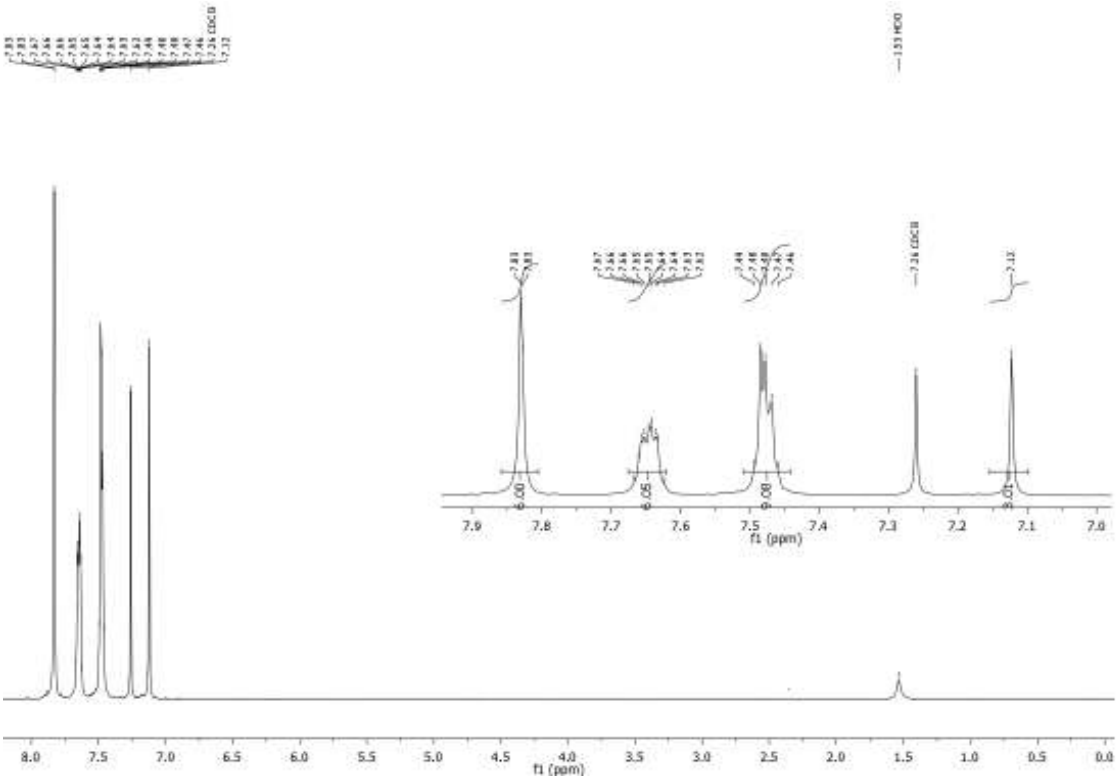

Figure VI: ^{1}H NMR of molecule **18**.

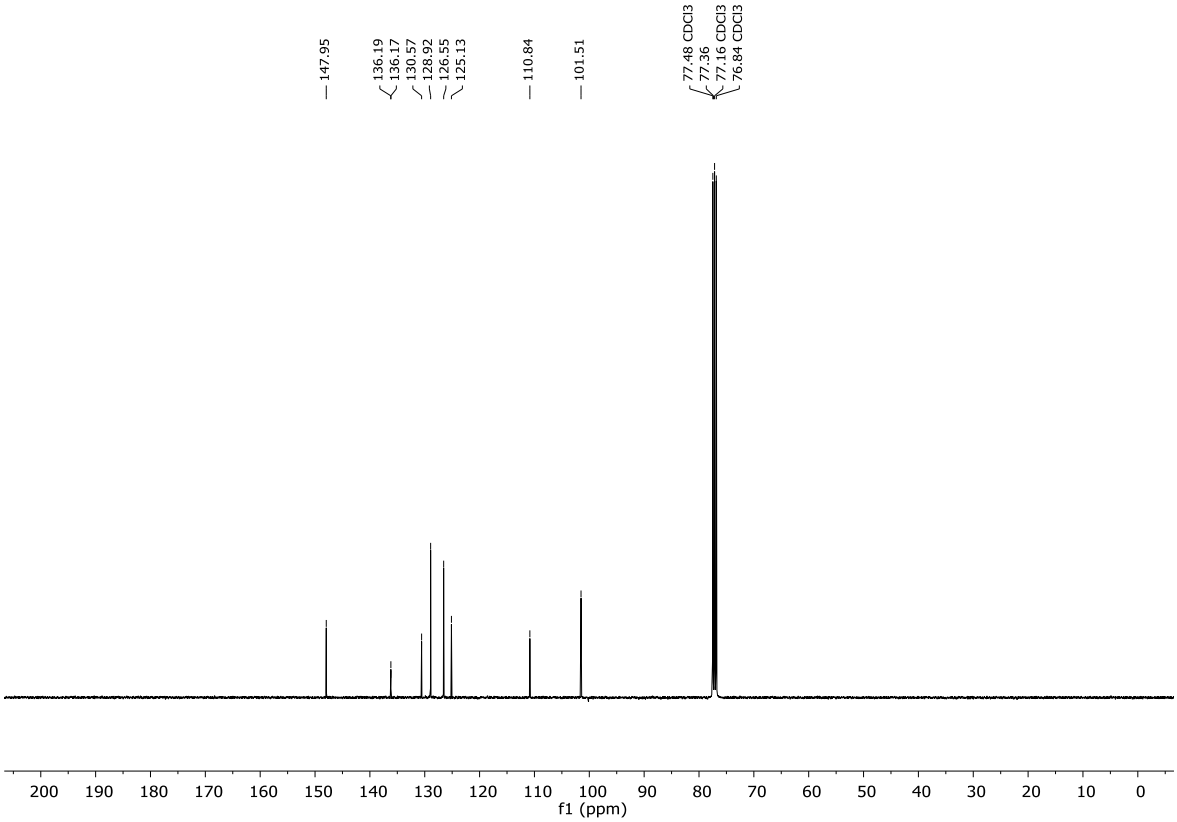

Figure VII: ^{13}C NMR of molecule **18**.

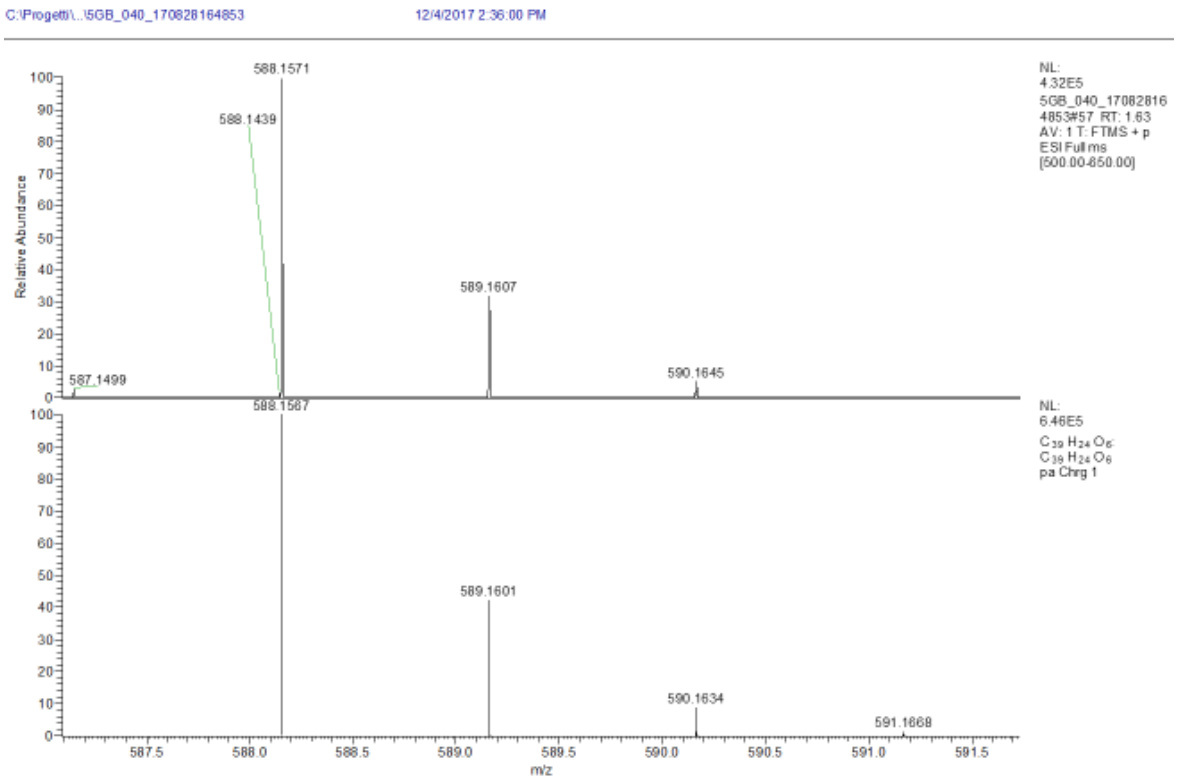

Figure VIII: ESI-HRMS of molecule **18**.

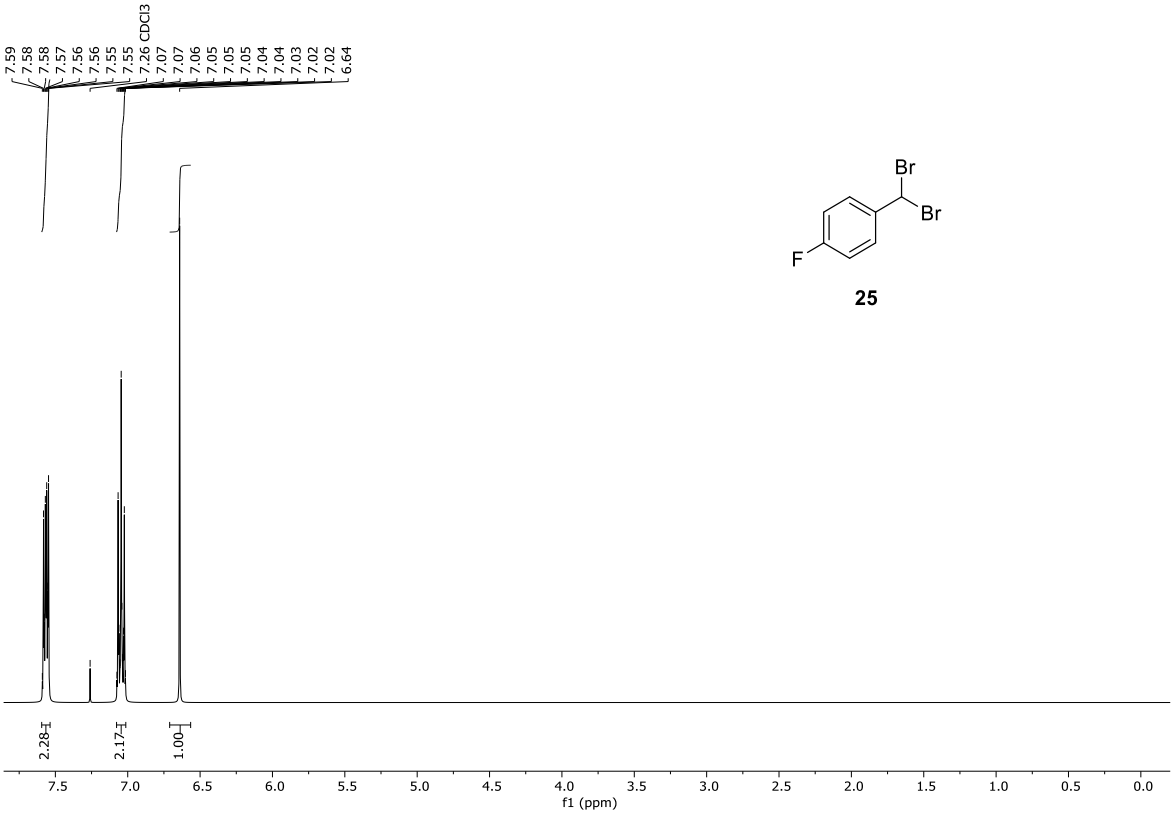

Figure IX: ^{1}H NMR of molecule **25**.

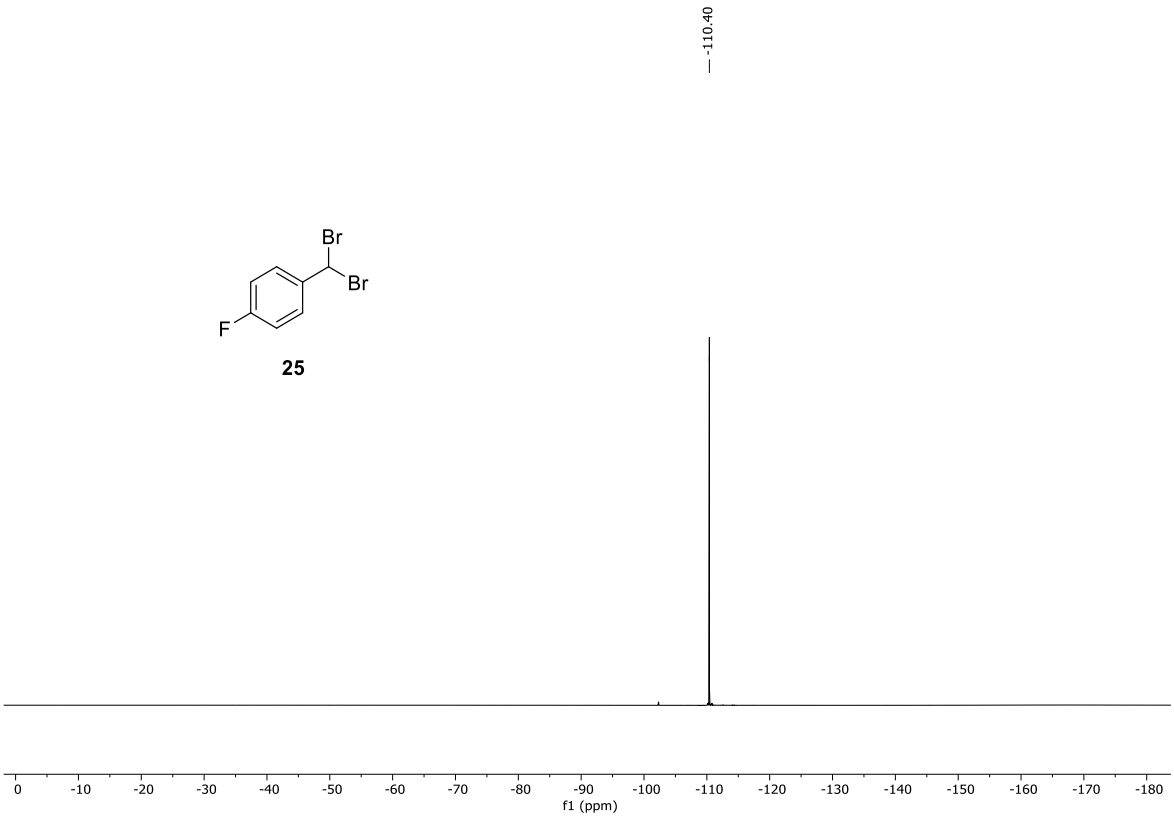

Figure X: ^{19}F NMR of molecule **25**.

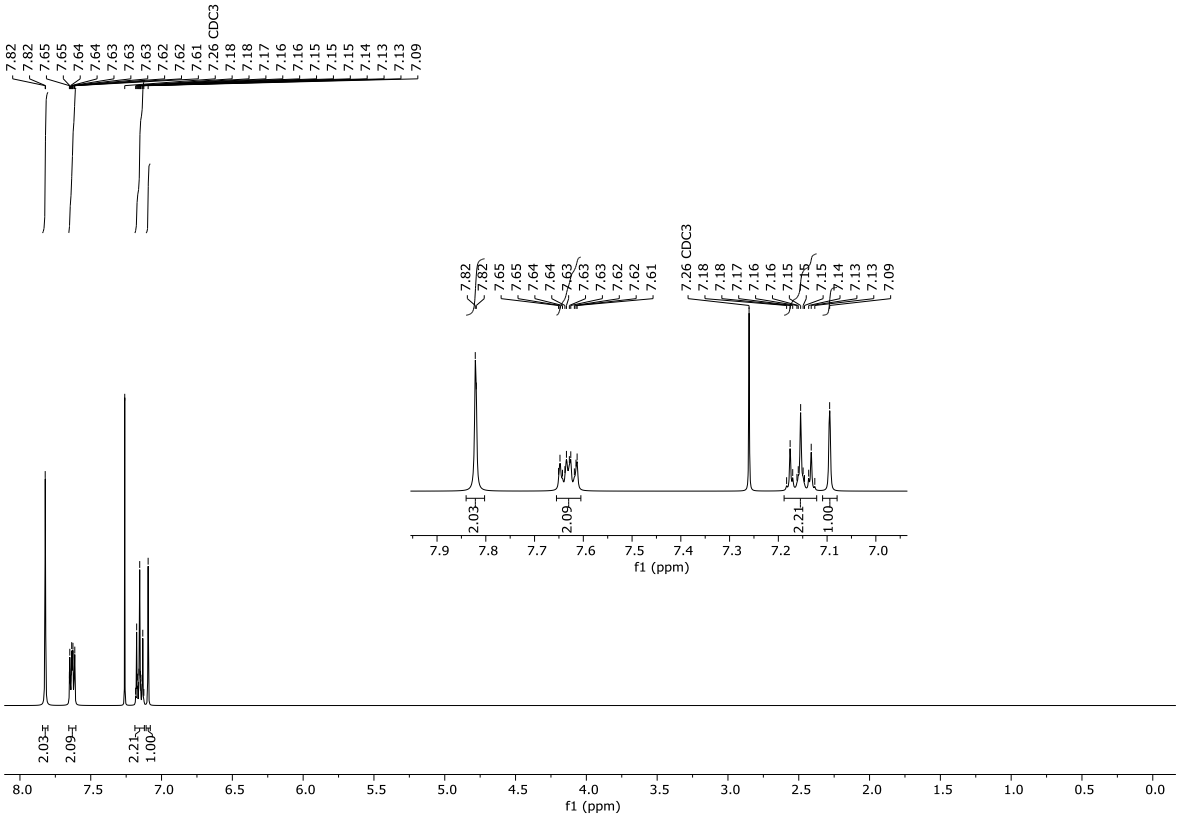

Figure XI: ^{1}H NMR of molecule **23**.

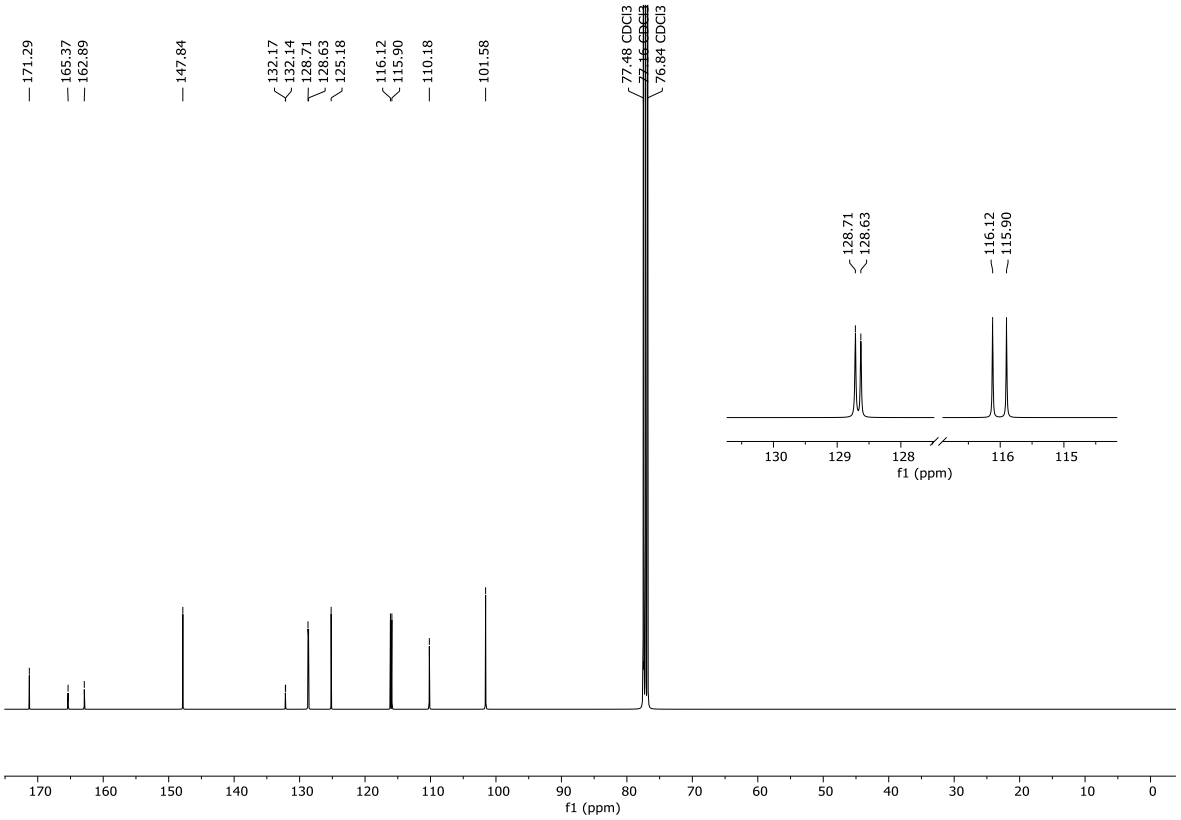

Figure XII: ^{13}C NMR of molecule **23**.

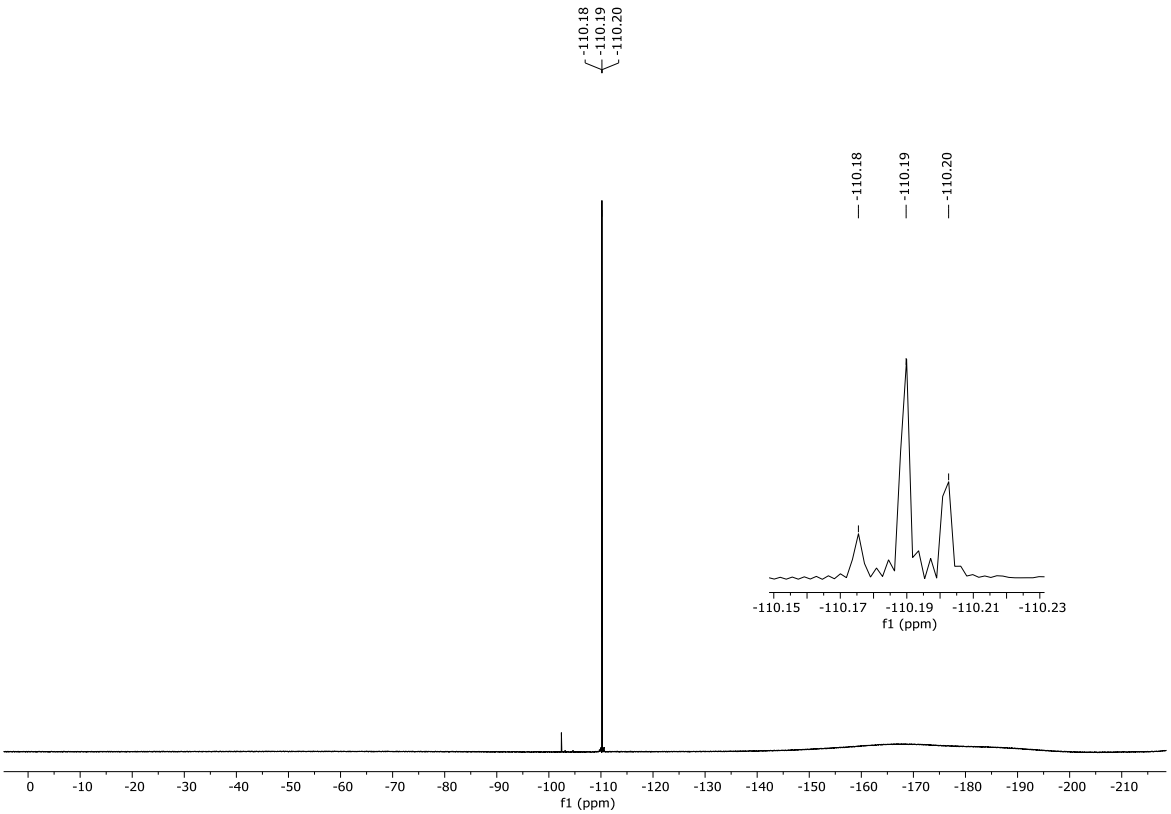

Figure XIII: ^{19}F NMR of molecule **23**.

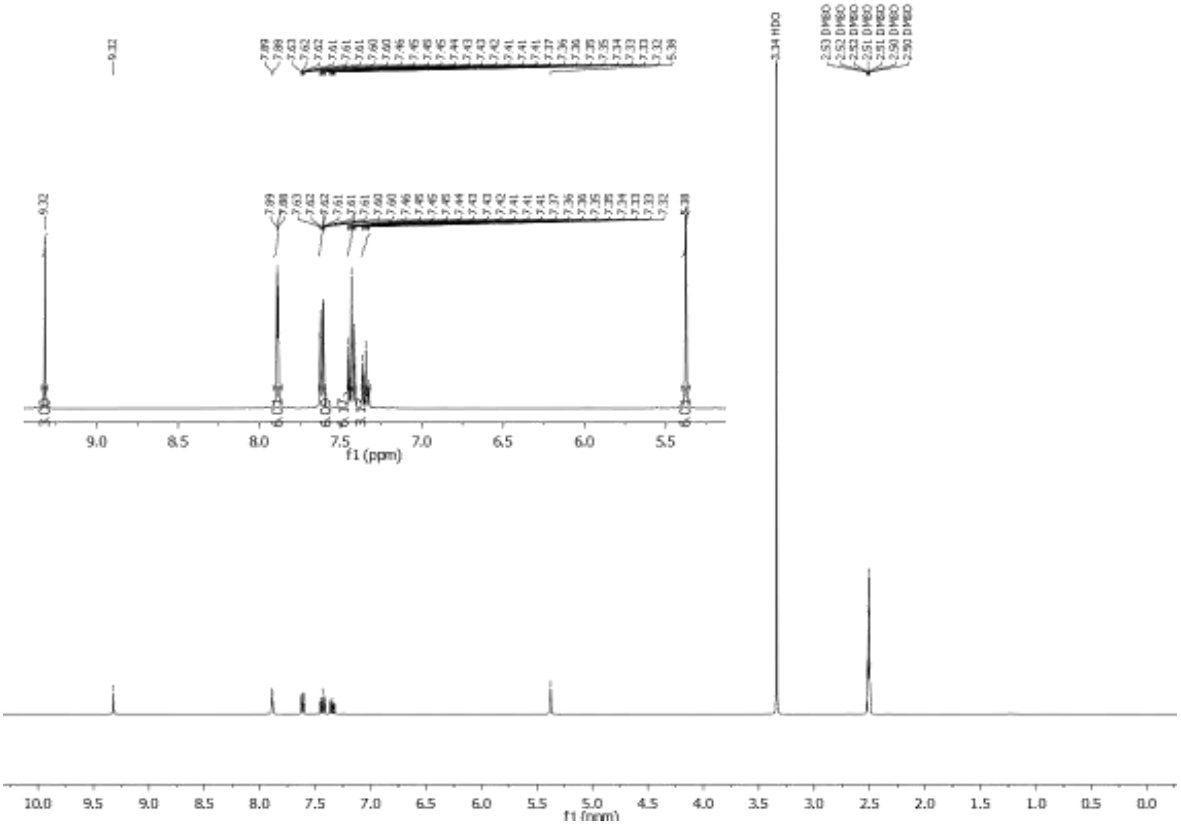

Figure XIV: ^{1}H NMR of molecule ***C*$_3$-26**.

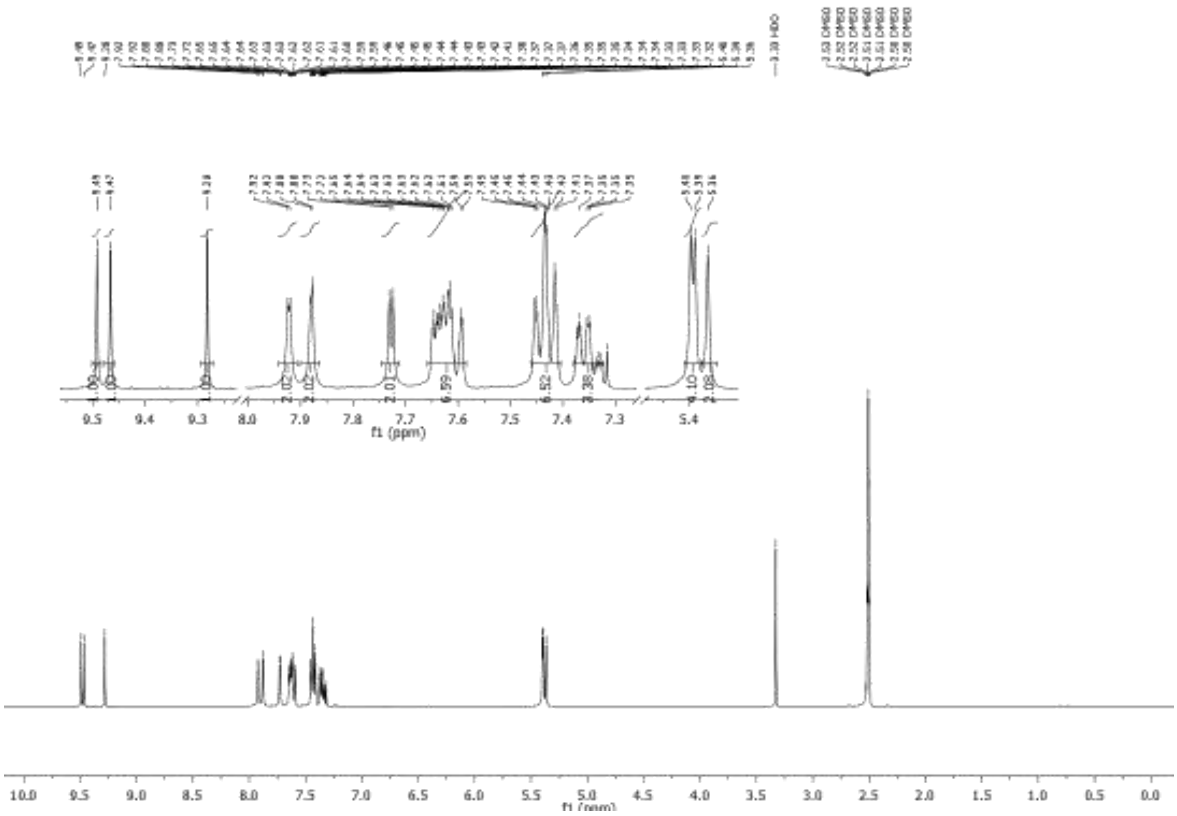

Figure XV: ^{1}H NMR of molecule ***C*$_S$-26**.

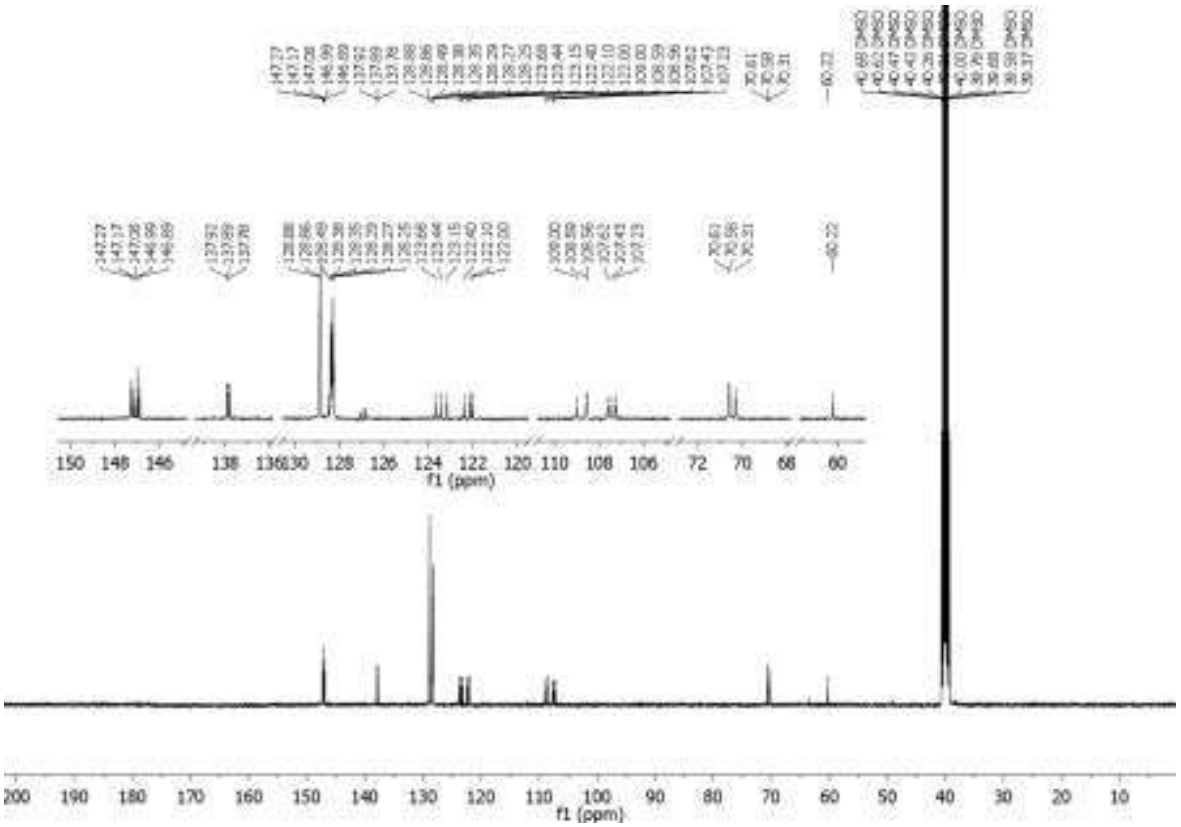

Figure XVI: ^{13}C NMR of molecule ***C*$_S$-26**.

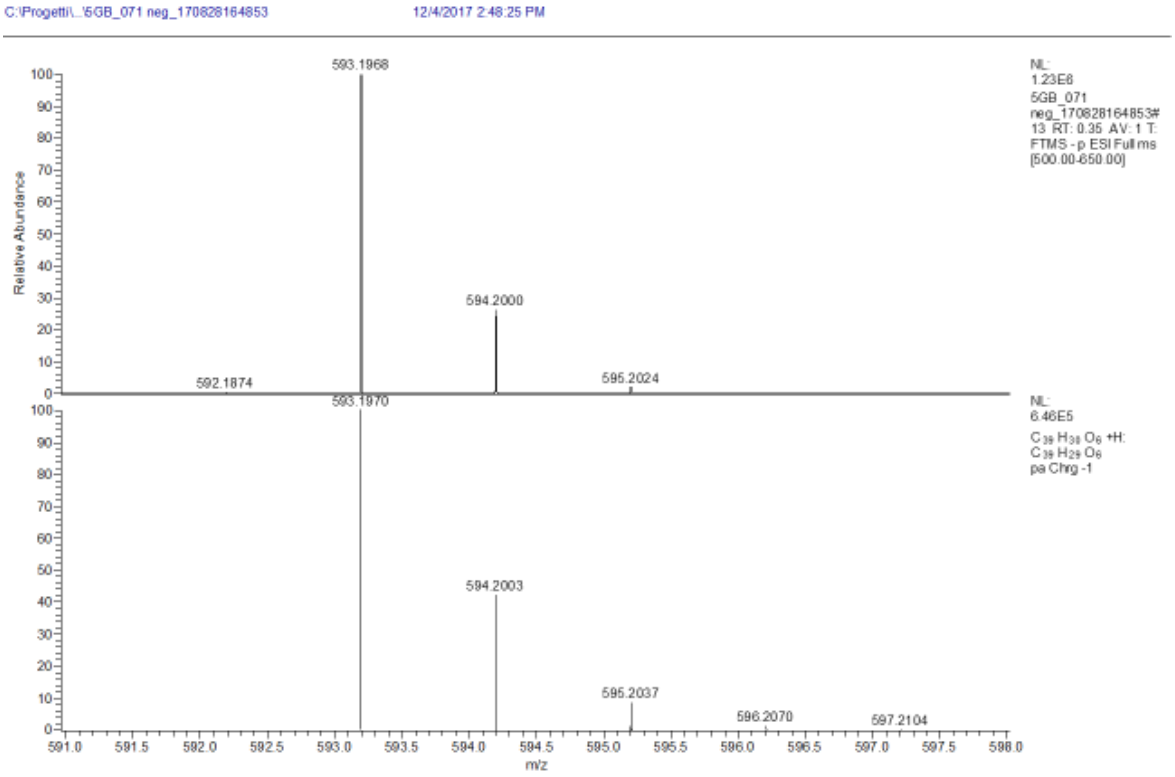

Figure XVII: ESI-HRMS of molecule ***C*$_S$-26**.

1.6 Bibliography

1 M. Iwasaki, S. Iino, Y. Nishihara, *Org. Lett.*, **2013**, *15*, 5326-5329.

2 M. Iwasaki, S. Iino, Y. Araki, Y. Nishihara, *J. Org. Chem.*, **2015**, *80*, 9247-9263.

3 H. S. Kim, S. Gowrisankar, E. S. Kim, J. N. Kim, *Tetrahedron Lett.*, **2008**, *49*, 6569-6572.

4 J-A. García-López, M. F. Greaney, *Org. Lett.*, **2014**, *16*, 2338-2341.

5 P. T. Wright, I. Gillies, J. D. Kilburn, *Synthesis*, **1997**, *9*, 1007-1009.

6 S. Kumar, M. Manickam, *Synthesis*, **1998**, *8*, 1119-1122.

7 K.-Q. Zhao, Y. Gao, W.-H. Yu, P. Hu, B.-Q. Wang, B. Heinrich, B. Donnio, *Eur. J. Org. Chem.*, **2016**, *16*, 2802-2814.

8 V. Percec, M. R. Imam, M. Peterca, D. A. Wilson, R. Graf, H. W. Spiess, V. S. K. Balagurusamy, P. A. Heiney, *J. Am. Chem. Soc.*, **2009**, *131*, 7662-7677.

9 L. Yue, C. Shu-Han, O. Tian-Miao, T. Jia-Heng, L. Ding, G. Lian-Quan, H. Zhi-Shu, *Bioorg. Med. Chem.*, **2011**, *19*, 2074-2083.

10 K. T. Tsang, M. A. Brimble, *Tetrahedron*, **2007**, *63*, 6015-6034.

11 M. Bomkamp, A. Artiukhov, O. Kataeva, S.R. Waldvogel, *Synthesis*, **2007**, *7*, 1107-1114.

12 S. Cardinal, J. Azelmat, D. Grenier, N. Voyer, *Bioorg. Med. Chem. Lett.*, **2016**, *26*, 440-444.

13 M. Watanabe, M. Nishiyama, Y. Koie, *Tetrahedron Lett*., **1999**, *40*, 8837-8840.

14 B. P. Bandgar, S. P. Kasture, *J. Chem. Research (S)*, **2000**, 252-253.

15 S. Takano, A. Kurotaki, Y. Sekiguchi, S. Satho, M. Hirama, K. Ogasawara, *Synthesis*, **1986**, 811-817.

16 B. Classon, P. Garegg, I. Lindh, *Carbohydr. Res.*, **1988**, *179*, 31-35.

17 S. Takano, T. Ohkawa, K. Ogasawara, *Tetrahedron Lett.*, **1988**, *15*, 1823-1824.

18 E. R. Cole, G. Crank, H. T. H. Minh, *Aust. J. Chem.*, **1980**, *33*, 675-680.

19 R. Zniber, R. Achour, M. Z. Cherkaoui, B. Donnio, L. Gehringerb, D. Guillon, *J. Mater. Chem.*, **2002**, *12*, 2208-2213.

20 S. R. Waldvogel, D. Mirk, *Tetrahedron Lett.*, **2000**, *41*, 4769-4772.

21 C. Regenbrecht, S. R. Waldvogel, *Beilstein J. Org. Chem.*, **2012**, *8*, 1721-1724.

22 L. A. Paquette, F. Fabris, F. Gallou, S. Dong, *J. Org. Chem*., **2003**, *68*, 8625-8634.

23 W. A. Sheppard, *Tetrahedron*, **1971**, *27*, 945-951.

24 F. M. Brower, N. E. Matzek, P. F. Reigler, H. W. Rinn, C. B. Roberts, D. L. Schmidt, J. A. Snover and K. Terada, *J. Am. Chem. Soc.*, **1976**, *98*, 242750-242753.

25 W. L. F. Armarego, C. Chai in *Purification of Laboratory Chemicals (Seventh Edition)*, Butterworth-Heinemann, Boston, **2013**.

26 W. C. Still, M. Kahn, A. Mitra, *J. Org. Chem.*, **1978**, *14*, 2923-2925.

2 Mannich Reactions on C_3-triphenylenes

Modified triphenylenes could have very interesting applications in the field of smart materials such as organic photovoltaic devices (OPV),[1] organic field-effect transistors (OFET)[2] and organic light-emitting diodes (OLEDs),[3] where the characteristics of triphenylene have been already widely exploited. Moreover, due to their stacking properties, they could give new classes of liquid crystals. Recently, systems based on C_3-simmetry triphenylenes have also been developed for the detection of explosives[4] or to create trans-membrane molecular devices for chloride transport.[5] For the high potentialities of this class of molecules, we started working on the modification of the triphenylenic scaffold, proposing the application of the Mannich reaction as a reaction that could easily increase the structural complexity of the molecule and, at the same time, include N atoms as important tools for intermolecular interactions (Scheme 1).

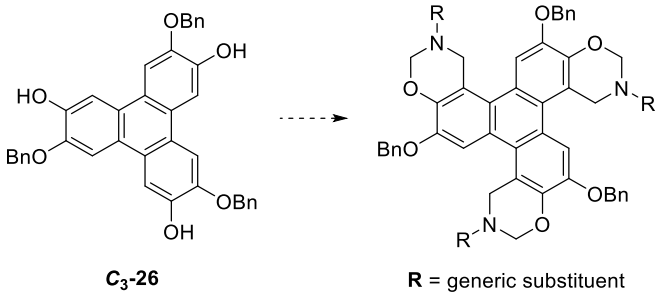

Scheme 1: General idea of triphenylene modification through Mannich reaction.

2.1 First Attempts of Mannich Reaction on C_3-26

For the first trials of the Mannich reaction on ***C*$_3$-26**, we focused our attention on the use of 4-aminopiridine as primary amine, since the pyridinic moiety could open to possible formation of metal-ligand coordination bonds and/or hydrogen bonds.

The first attempt to functionalize the ***C*$_3$-26** substrate was carried out reacting the tris-phenolic substrate directly with the amine and aqueous formaldehyde (37%), stirring at room temperature in ethanol (Scheme 2).[5]

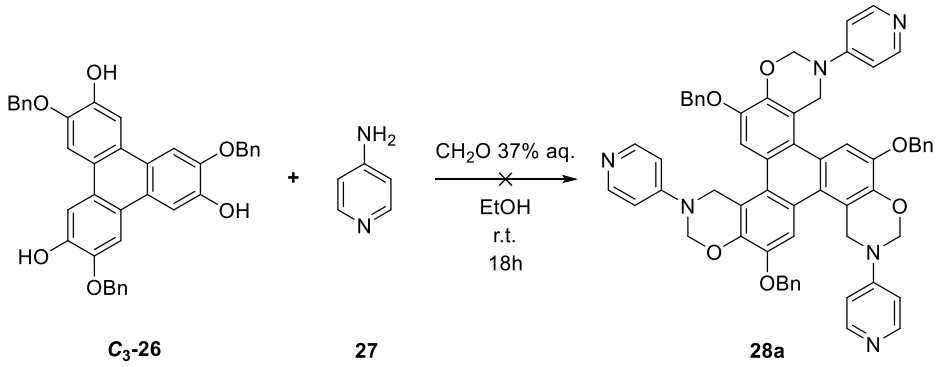

Scheme 2: First attempt of Mannich reaction on molecule ***C*$_3$-26**.

Unfortunately, the reaction did not occur, and the starting material was recovered unaltered. The addition of acetic acid as catalyst to the reaction under the same experimental conditions led to an unchanged result.

Since the first trials failed, we decided to change completely the reaction conditions. Paraformaldehyde was used in place of aqueous formaldehyde in order to limit the amount of water in the system, while ethanol as solvent was replaced by toluene, enabling the use of higher temperatures and a better solubility of the starting material. A mixture of ***C*$_3$-26**, 4-aminopiridine and paraformaldehyde was heated overnight under reflux in toluene, using acetic acid as catalyst (Scheme 3).[6]

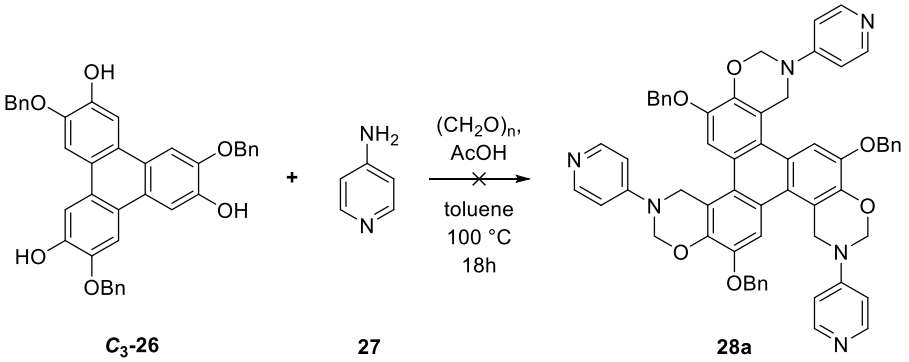

***C*$_3$-26** **27** **28a**

Scheme 3: Second attempt of Mannich reaction on molecule ***C*$_3$-26**.

This time, ^{1}H NMR analysis run on the reaction mixture revealed the presence of several intermediates, with signals in agreement with the formation of new methylene units on the triphenylenic core. Nevertheless, the reaction did not provide sufficient amount of the expected symmetric Mannich product.

2.2 Mannich Reactions on *C*$_3$ Substrates

Even if the first trials failed, from those experiments we gained knowledge on how the desired product could be obtained.

Instead of a single step Mannich reaction, we wondered whether separating the reaction in two steps could help improving the yield of the desired product. We decided to split the reaction in two: i) the formation of an intermediate hemiaminal between the amine, paraformaldehyde and an alcohol and ii) the reaction of the hemiaminal in a subsequent Mannich reaction on ***C*$_3$-26**, using a second amount of paraformaldehyde.

For the first step, 4-aminopiridine was reacted with paraformaldehyde and *n*-butanol, used as solvent, in the presence of acetic acid as a catalyst. The reaction mixture was heated at 90 °C overnight, under inert atmosphere (Scheme 4).

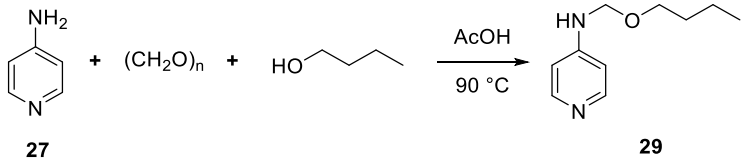

27 **29**

Scheme 4: Synthesis of the intermediate hemiaminal **29.**

^{1}H NMR confirmed the formation of the product **29**, which was not isolated, but used as obtained after removing the excess of butanol under *vacuum*. Once obtained, **29** was reacted together with ***C*$_3$-26** and a second amount of paraformaldehyde in toluene, stirring

overnight at 100 °C under inert atmosphere (Scheme 5). For this reaction, a closed reaction vessel (a vial with screw cap) was used instead of a classical flask with condenser, in order to contain the sublimation of paraformaldehyde. The importance of this method will be discussed in Chapter 5.

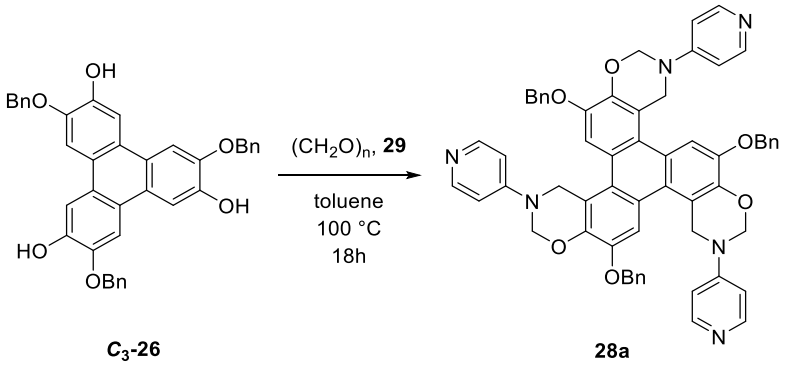

Scheme 5: Mannich reaction on ***C*$_3$-26** to obtain the product **28a**.

The product was obtained by simple precipitation from ethanol, with a 75% yield. The presence of the two new methylene was testify by the ^{1}H NMR spectrum, with signals at 4.61 ppm and 5.64 ppm, respectively for Ar-CH_2-NH and O-CH_2-NH.

Once product **28a** was obtained, we extended the reaction to other amines aiming at investigating the scope of the reaction. For this purpose, two electron rich aliphatic amines (butil and hexylamine) and one aromatic electron poor amine (3,5-*bis*(trifluoromethyl)aniline) were employed. This time, the two steps synthesis was not required, since revealed itself necessary just for aminopyridines. Thus, the reactions were carried out as described in Scheme 6.

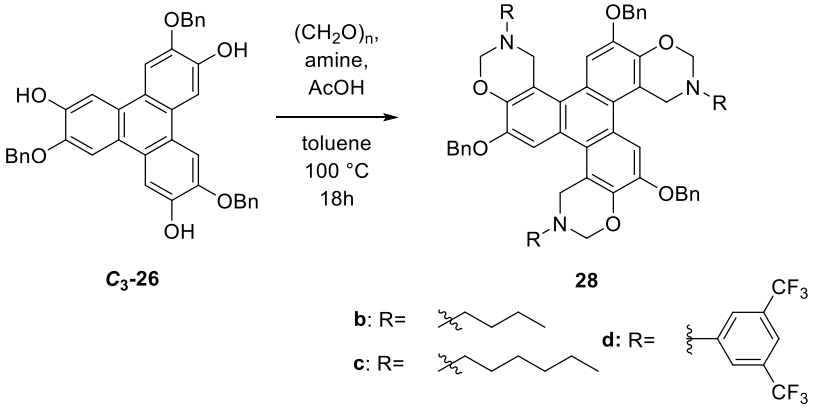

Scheme 6: Synthesis of the other Mannich derivative of ***C*$_3$-24**.

Products **28b**, **28c** and **28d** were obtained by simple precipitation from ethanol in good to moderate yield, respectively 83%, 69% and 52%, proving that the reaction works nicely for both electron-poor and electron-rich amines.

2.3 *C*$_3$ Substrate Modifications and Mannich Reactions

The presence of the benzylic moieties on ***C*$_3$-26** enabled the preparation of another class of *C*$_3$-symmetric triphenylenes which were obtained by a first alkylation of the free phenol

units, followed by de-benzylation through hydrogenolysis with Pd/C to afford the three phenolic groups that can undergo further functionalization. Through this approach it was possible to obtain C_3 symmetry Mannich products either with benzyl, alkyl or acetyl ester units on alternating catechol like units, thus obtaining a small library of C_3-symmetric Mannich triphenylenes derivatives (Scheme 7).

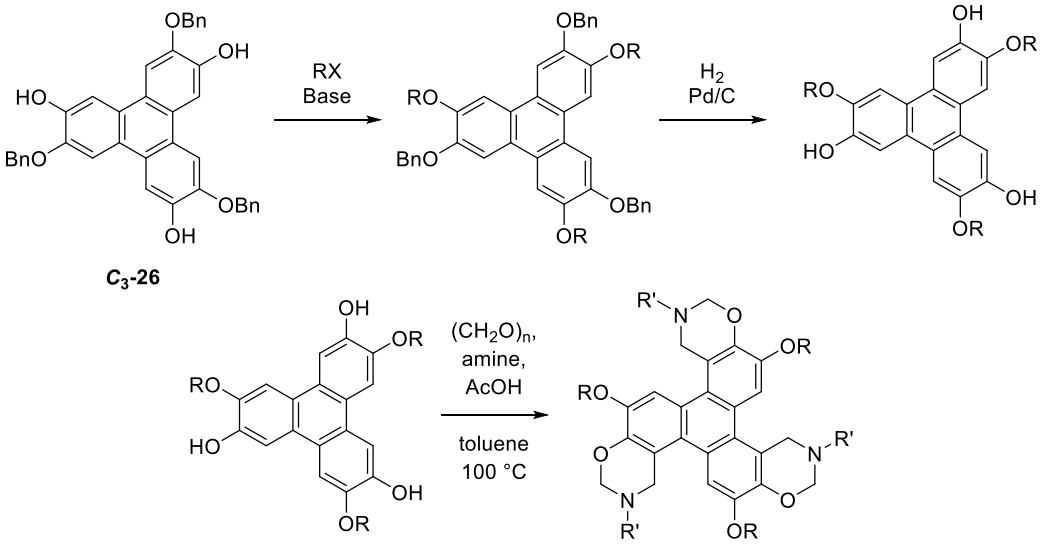

Scheme 7: Alkylation, de-benzylation and further Mannich functionalization of ***C*$_3$-26**.

***C*$_3$-26** was firstly alkylated through a simple protocol, using octyl bromide or bromoacetyl-*t*-butyl ester in the presence of K_2CO_3, stirring in DMF at room temperature for 72 hours (Scheme 8).[7]

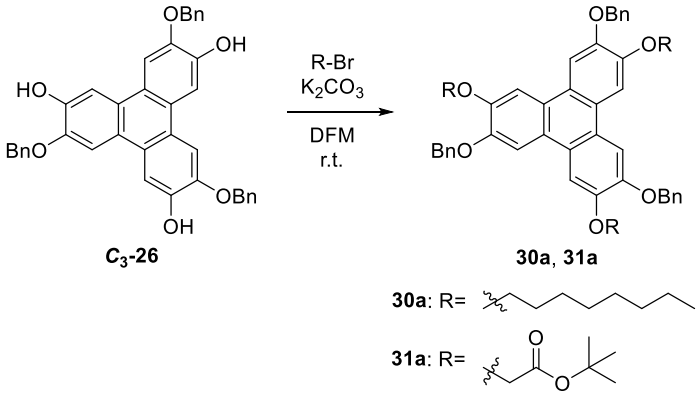

Scheme 8: Alkylation of molecule ***C*$_3$-26**.

After work-up, the crude was purified through recrystallization from ethanol, affording products **30a** and **31a** respectively with 84% and 79% yield.

De-benzylation of **30a** and **31a** was carried out using 5% Pd/C in methanol, stirring overnight at room temperature under H_2 atmosphere (1 bar) (Scheme 9).

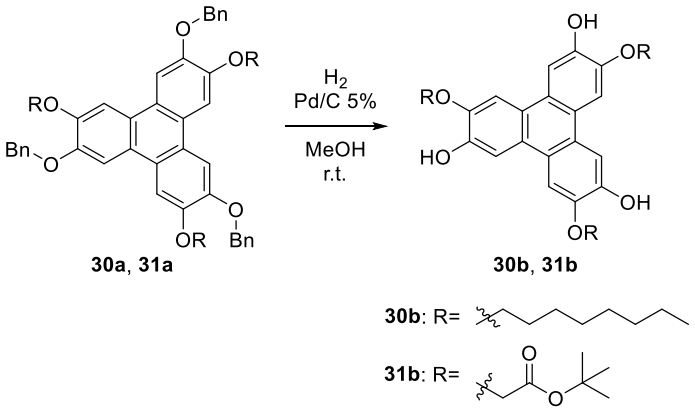

Scheme 9: De-benzylation of molecules **30a** and **31a** through hydrogenation.

The products **30b** and **31b** were recovered after filtration of the catalyst and solvent removal in *vacuum* of the resulting solution, respectively with 95% and 91% yield.

Products **30b** and **31b** were further functionalized through the described Mannich reaction, using butylamine, hexylamine, 4-pyridil aniline and 3,5-*bis*-trifluoromethylaniline (Schemes 10 and 11).

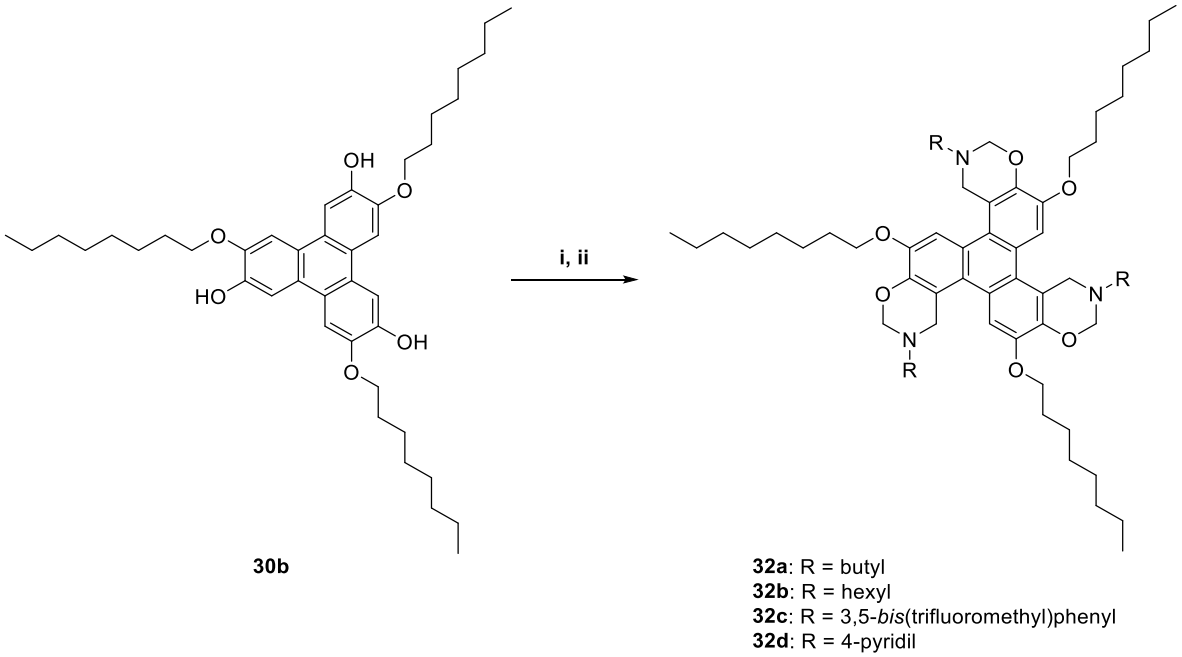

Scheme 10: Mannich reaction on product **30b**. i) butylamine, hexylamine or 3,5-bis(trifluoromethyl)aniline, paraformaldehyde and acetic acid, overnight in toluene at 100 °C. ii) 4-aminopyridine, paraformaldehyde and acetic acid in butanol, refluxing overnight, then **29** and paraformaldehyde, overnight in toluene at 100 °C

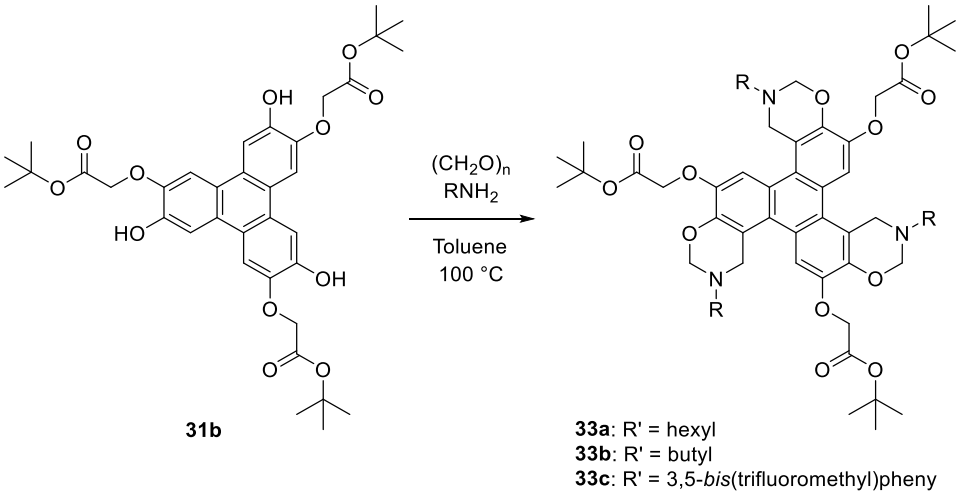

Scheme 11: Mannich reaction on product **31b**.

The corresponding products **32a**, **32b**, **32c**, **33a**, **33b** and **33c** were obtained in good yields after flash chromatography (respectively 98%, 98%, 52%, 35%, 50%, 52%), while product **32d** was obtained in pure form by simple precipitation from diethyl ether with an 83% yield. Unfortunately, the reaction between **31b** and 4-aminopiridine did not provide the desired product but led to a mixture of by-products, probably due to the 4-aminopiridine moiety acting as promoter for nucleophilic attack on the *t*-butyl ester moiety, similarly to the well-known action of 4-dimethylaminopyridine (DMAP).

Functionalization of ***C*$_3$-26** and derivatives through Mannich reactions brought to the synthesis of a small library of overall eleven new molecules, endowed with additional six membered ring units containing N atoms. Attempts were made to repeat the reactions with other primary amines like propargyl and vinyl amine, unfortunately without success. It is likely that the stability of the amines plays an important role in this reaction.

2.4 Investigation on Chirality and Aggregation Properties in Solution and in the Solid State

On the basis of the structure of the Mannich derivatives, we investigated the possible chirality of such molecules due to steric interactions between the benzyl methylene unit bound to the N atom and the neighbouring aromatic C-H. The ^{1}H NMR spectra at room temperature of all derivatives showed singlets for those methylene units indicative of a rapid exchange on the NMR timescale, therefore we decided to run low temperature NMR experiments in CD_2Cl_2 on **28a** (Figure 1).

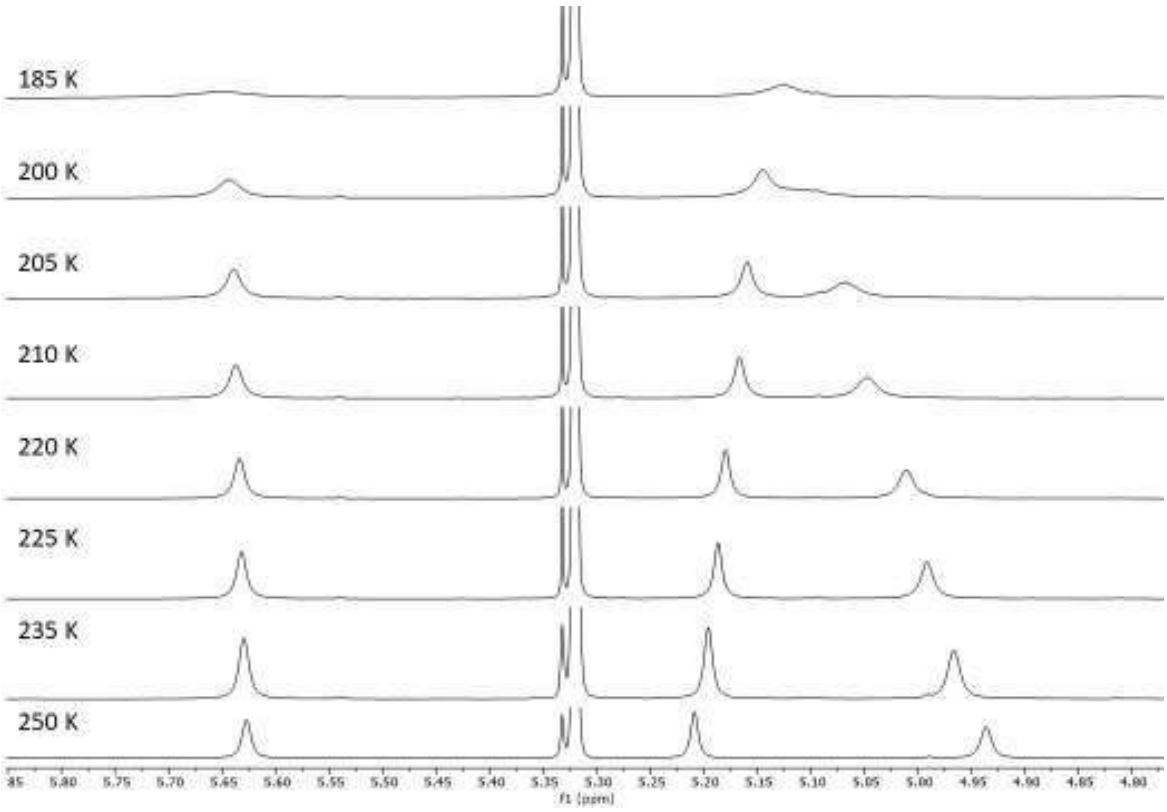

Figure 1: ^{1}H NMR at variable low temperature of **28a** in CD_2Cl_2. Detail of the methylene unit's region.

As reported in Figure 1, the spectra did not show the splitting of the resonances of the methylene units of the benzoxazine moiety, ruling out possible chirality of the molecule.

To further investigate this point, we performed some chiral HPLC analyses on selected **28c** and **32a** derivatives, but in all cases the presence of only one peak suggested the absence of enantiomers, therefore the absence of chirality probably due to rapid slippage of the neighbouring H atoms.

Studies on the solid state properties of the synthesized molecules were carried out right after the synthesis, seeking for possible liquid crystals properties. DSC analyses of the solid samples (**28a**, **28b**, **28c**, **28d**, **32c**, **32d** and **33c**) were carried out in the temperature range between 200-180°C. Unfortunately, just one of the synthesized molecules showed possible liquid crystal behaviour, while all the others demonstrated typical crystalline properties, and in some cases thermal decomposition occurred. In Figure 2 is reported the DSC curve recorded for compound **32c**.

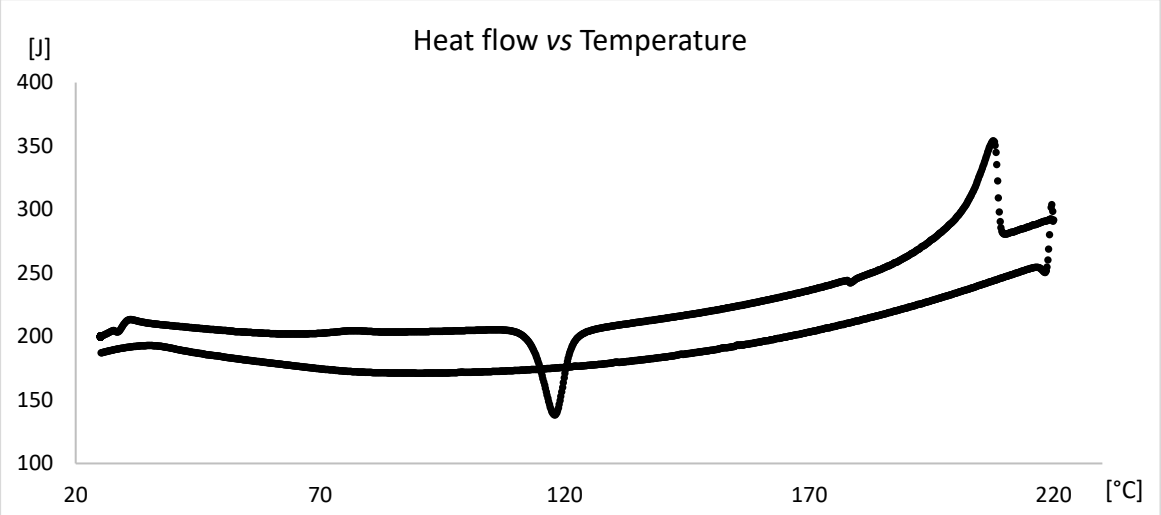

Figure 2: DSC curve of compound **32c**.

As can be noticed in Figure 2, an exergonic peak at 118 °C is present corresponding to a crystallization phenomenon, and another small transition peak is observed at 179 °C, before the melting point. Even though this is not proving a liquid crystal behaviour, we further analysed the compound using a Polarized Optical Microscope (POM) while heating and cooling the sample. The recorded pictures are reported in Figure 3.

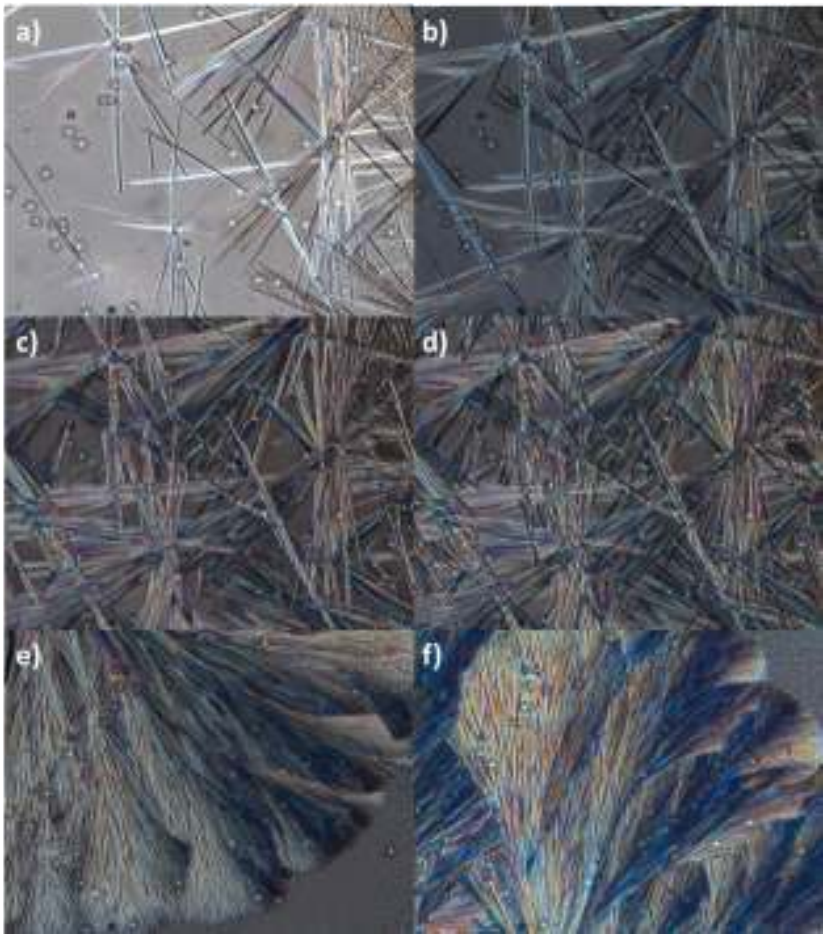

Figure 3: POM pictures of **32c**. a-d) forming crystals under different positions of the polarized light, 180-190 °C. e-f) spherulitic phase, 150 °C.

In Figure 3a-d are reported the pictures of the crystals observed under different positions of the polarized light at a temperature of 180-190 °C, while in Figure 3e-f are reported images of the spherulitic phase at 150 °C. Since the crystals obtained before the spherulitic phase behaved differently under polarized light while moving the sample, which is a typical behaviour of liquid crystals, we submitted the sample for variable temperature X-Ray analysis, but the response confirmed a profile compatible to a classic crystal.

However, observing that the melting point of the products decreases as a function of the increasing content of aliphatic chains on the triphenylenes structure, we understood that the obtainment of one of these triphenylenic derivatives possessing a true liquid crystal behaviour is a matter of a delicate balance between aliphatic and aromatic moieties, that can be easily attached to the triphenylene core throughout the method efficiently developed and herein described.

The results reported in this Chapter, together with the results in Chapter 1, where submitted and published on *Frontiers in Organic Chemistry* (IF 5.076), confirming the general interest on this topic.[8]

With the work of Mannich reaction on C_3-symmetric triphenylenes we achieved an unprecedent derivatization on this class of compounds. Indeed, reactions involving the inner CH position of the triphenylene are rarely encountered in literature, with just one example of nitration of a total symmetric 2,3,6,7,10,11-hexaalkyloxytriphenylene to achieve a C_3-symmetric triazacoronene derivative.[9]

2.5 Experimental Section

2.5.1 General Methods

The reactions were followed with TLC Polygram® Sil G/UV254, 0.25 mm thickness. ^{1}H NMR, ^{13}C NMR, and 2D spectra were recorded with a Bruker Avance 300 and Ascend 400 spectrometers, working at 300-400 and 75-100 MHz respectively. Resonance frequencies are referred to tetramethylsilane. IR spectra were recorded with a Perkin Elmer Spectrum One spectrophotometer. Mass spectrometric measurements were performed using a Thermo Scientific LTQ Orbitrap XL equipped with HESI source. The compounds studied were dissolved in methanol or acetonitrile with a concentration of $5 \cdot 10^{-3}$ M. They were injected into the HESI source by direct infusion with the syringe pump integrated in the mass spectrometer at a 5 mL·min^{-1} flow rate. Mass spectra were acquired in positive-polarity mode with the following tuning conditions: Temperature 40 °C, Sheath gas 8 (arbitrary units, arb), Aux gas and Sweep gas 0 arb, Spray Voltage 4.5 kV, Capillary temperature 275 °C, Capillary Voltage -9 V, Tube lence 150 V. In negative polarity the following tuning parameters were employed: Temperature 40 °C, Sheath gas 19 (arbitrary units, arb), Aux gas and Sweep gas 0 arb, Spray Voltage 3.0 kV, Capillary temperature 275 °C, Capillary Voltage 10 V, Tube lence 120 V. Mass spectra were collected in full scan with a resolution of 100000 at m/z 400. The Orbitrap MS was calibrated just before analysis and during the acquisition in order to improve mass accuracy lock masses were employed. HPLC analysis were performed with a Hewlett Packard Series 1100 G1311A Quat-Pump with a 20 µL injection loop using 1 ml/min flow of eluent with a composition hexane/iPrOH from 97:3 to 90:10 on an Amylose-2 chiral 25 cm column. Reagents and solvents with high purity degree purchased by the providers were used as given. Otherwise, they were purified following the procedures reported in literature.[10] Anhydrous solvents were prepared by adding activated 3 Å molecular sieves to the solvent under inert atmosphere. Molecular sieves were activated shortly before the use by continuous heating under *vacuum*. Flash chromatography were performed with silica gel Merk 60, 230-400 mesh, following procedures reported in literature.[11]

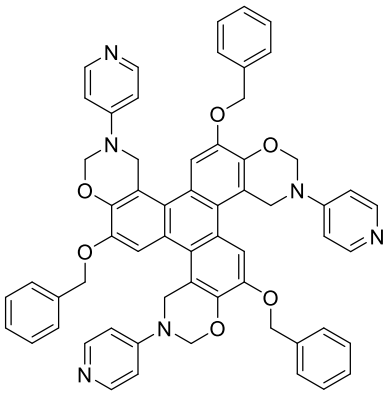

28a

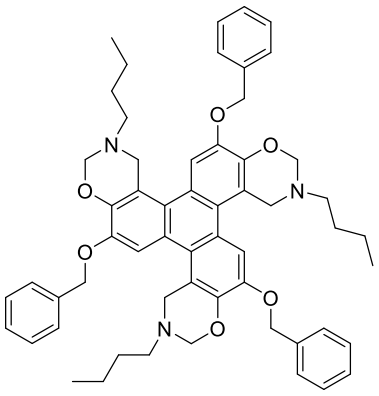

28b

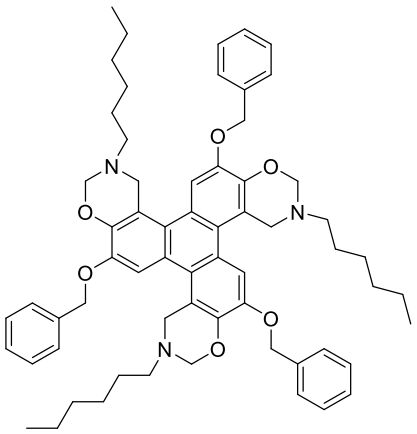

28c

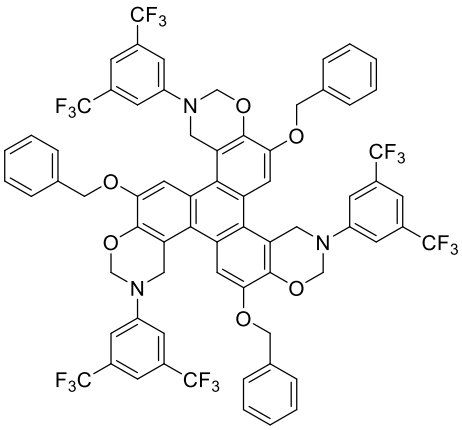

28d

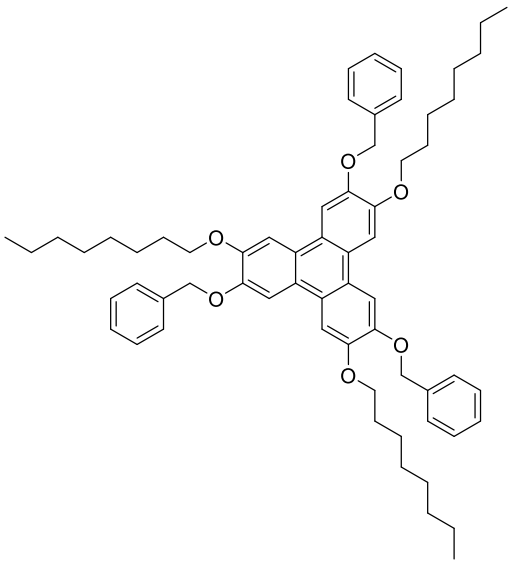

30a

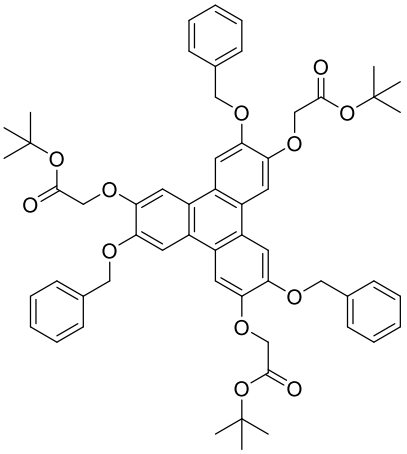

31a

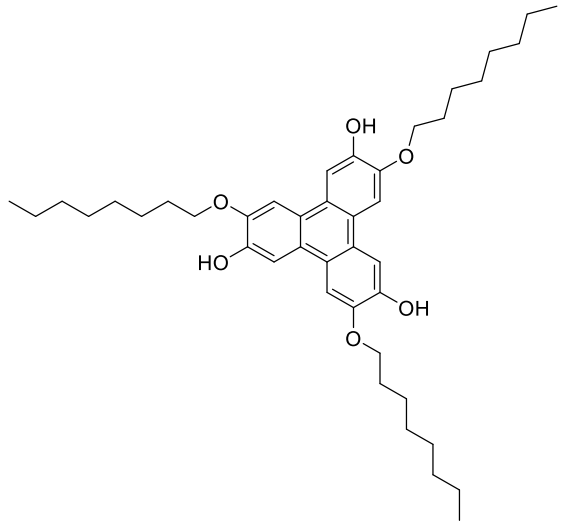

30b

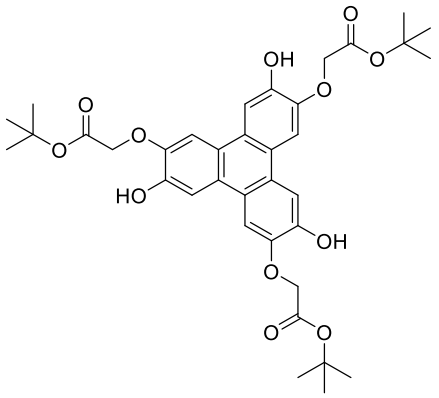

31b

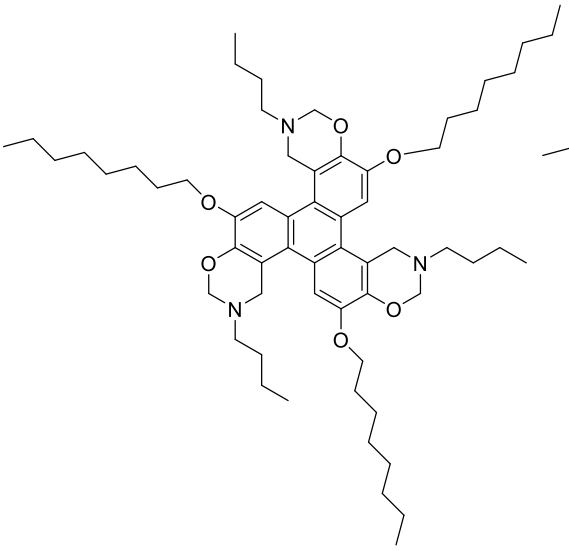

32a

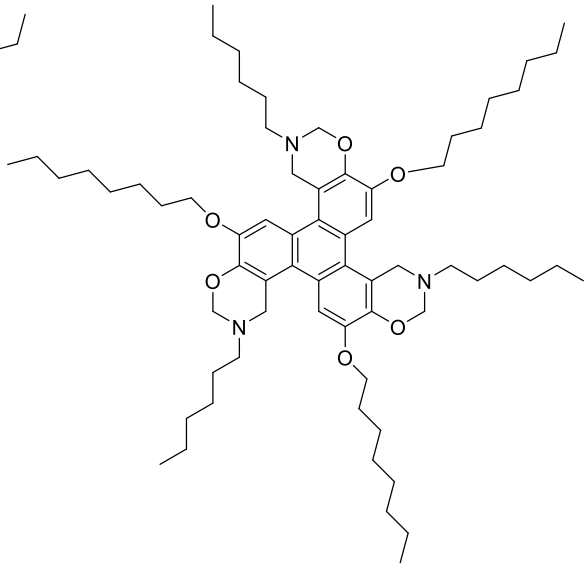

32b

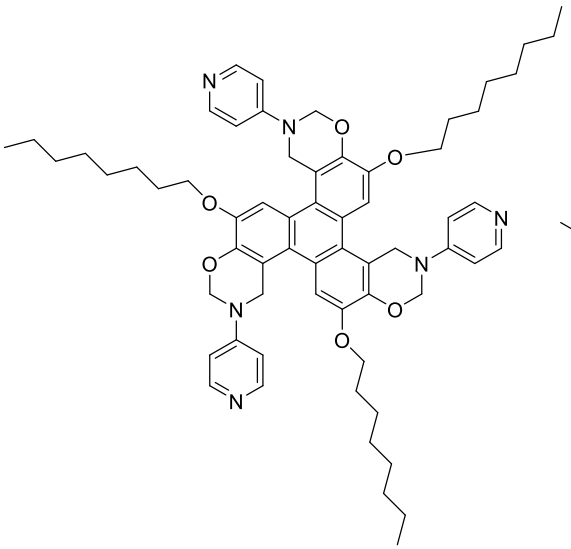

32d

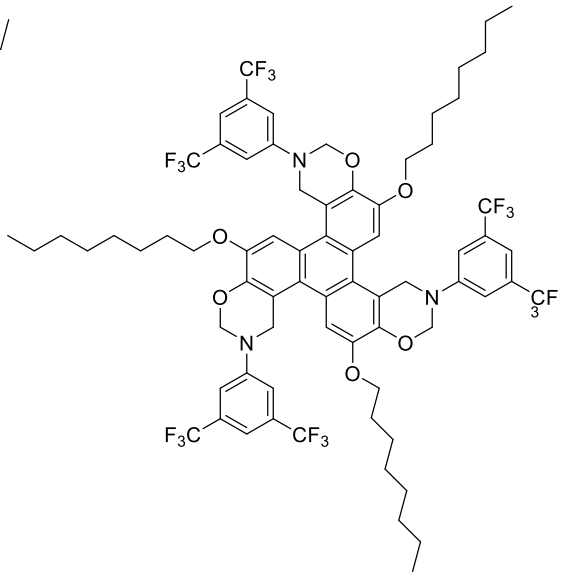

32c

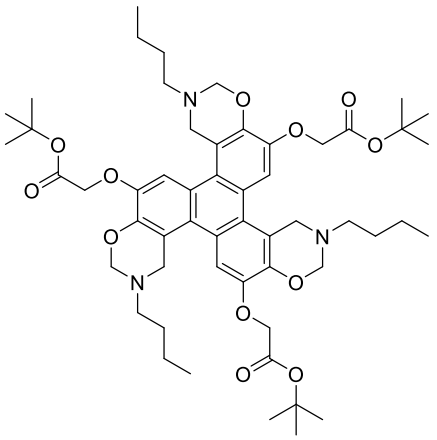

33a

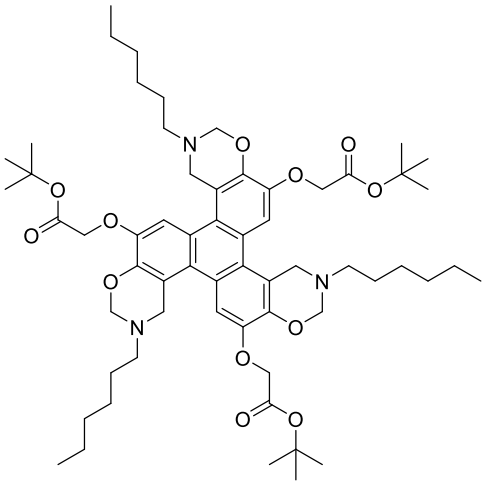

33b

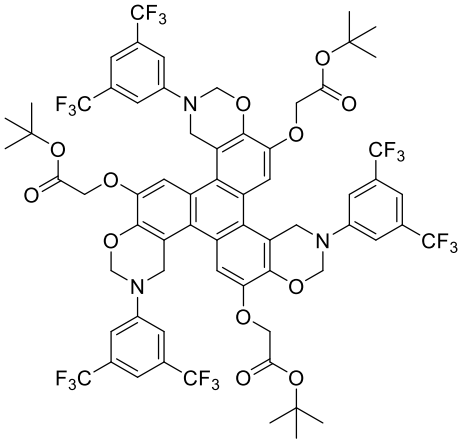

33c

2.5.2 Experimental Procedures - Syntheses

General Procedure 1 (GP1): General procedure for the alkylation and debenzylation of ***C*$_3$-26**.

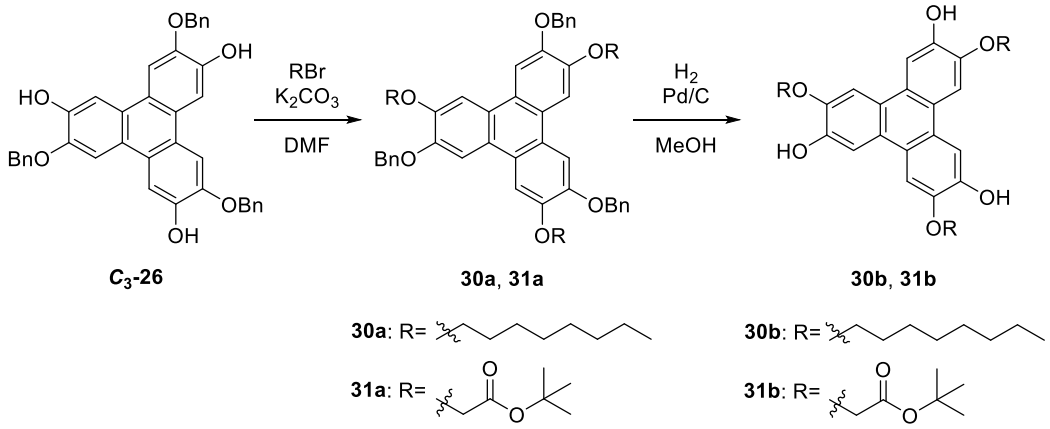

In a pear-shaped two necked 25 mL flask, equipped with argon inlet ad septum, a solution of ***C*$_3$-26** (0.30 g, 0.5 mmol)**,** K_2CO_3 (0.63 g, 4.5 mmol) and alkyl bromide (2.3 mmol) in anhydrous DMF (6 mL) was stirred at room temperature for 72 hours. The mixture was poured into a 1 M aqueous HCl (30 mL) solution and it was extracted with DCM (3×10 mL). The collected organic phases were washed with water (2 × 10 mL), dried over $MgSO_4$, filtered and concentrated in *vacuum*. The crude product was crystallized from absolute EtOH, to afford the product as white crystals. A suspended mixture of alkylated compound, **30a** or **31b,** and 5% Pd/C (0.088 g) in MeOH (20 mL) was stirred under H_2 atmosphere (1 Bar, balloon) at room temperature for 18 h. The resulting mixture was filtered on a celite plug and washed with DCM. The resulting solution was concentrated in *vacuum*, to afford the product as a waxy solid.

2,6,10-tris(benzyloxy)-3,7,11-tris(octyloxy)triphenylene (**30a**): **GP1** was applied to ***C*$_3$-26** and octylbromide. 84% yield. M.P.: 125 °C. ^{1}H NMR (400 MHz, $CDCl_3$): δ 7.82 (3H, s), 7.64 (3H, s), 7.59-7.52 (6H, set of m), 7.40 (6H, set of m), 7.36-7.29 (3H, set of m), 5.34 (6H, s), 4.19 (6H, t, *J* = 6.4 Hz), 2.01-1.91 (6H, set of m), 1.64-1.27 (30H, set of m) 0.90 (9H, t, *J* = 6.9 Hz). $^{13}C\{^1H\}$ NMR (100 MHz): δ 149.4, 148.3, 137.8, 128.7, 128.0, 127.5, 124.3, 123.2, 109.3, 106.6, 72.3, 69.4, 32.0, 29.6, 29.6, 29.5, 26.4, 22.9, 14.3. IR (KBr): ν 1618, 1574, 1519, 1437, 1386, 1261, 1198, 1165, 1038, 858, 822, 798, 749, 701 cm^{-1}. HRMS (ESI): calcd. for $C_{63}H_{79}O_6$ [M$^+$] 931.5871; found: 931.5845.

tri-*tert*-butyl 2,2',2''-((3,7,11-tris(benzyloxy)triphenylene-2,6,10-triyl)tris(oxy))triacetate (**31a**): **GP1** was applied to ***C*$_3$-26** and *tert*-butyl bromoacetate. 79% yield. M.P. 104 °C (lit. 104-103 °C). ^{1}H NMR (400 MHz, $CDCl_3$): δ 7.81 (3H, s), 7.66 (3H, s), 7.60 (6H, d, *J* = 7.5 Hz), 7.43 (6H, t, *J* = 7.5 Hz), 7.34 (3H, t, *J* = 7.4 Hz), 5.36 (6H, s), 4.74 (6H, s), 1.51 (27H, s). Further spectroscopic data (^{13}C, MS, IR) are in accordance with the literature.[7]

3,7,11-tris(octyloxy)triphenylene-2,6,10-triol (**30b**): **GP1** was continued on **30a**. 95% yield. Waxy solid. ^{1}H NMR (400 MHz, DMSO-d_6): δ 9.09 (3H, s), 7.88 (3H, s), 7.75 (3H, s), 4.19 (6H, t, *J* = 5.6 Hz), 1.89-1.78 (6H, set of m), 1.57-1.21 (30H set of m), 0.87 (9H, t, *J* = 6.7 Hz). $^{13}C\{^1H\}$ NMR (100 MHz): δ 146.9, 146.4, 123.2, 121.3, 108.1, 105.6, 68.2, 28.9, 28.9, 28.7, 25.6, 22.10, 13.9. IR (KBr): ν 1632, 1596, 1516, 1454, 1390, 1360, 1303, 1270, 1223, 1179,

1164, 1028, 1006, 853, 801, 576 cm^{-1}. HRMS (ESI): calcd. for $C_{42}H_{59}O_6$ [M^-] 659.4317; found: 659.4305.

tri-*tert*-butyl 2,2',2''-((3,7,11-trihydroxytriphenylene-2,6,10-triyl)tris(oxy))triacetate (**31b**): **GP1** was continued on **31a**. 91% yield. Waxy solid. ^{1}H NMR (300 MHz, DMSO-d_6): δ 7.84 (3H, s), 7.72 (3H, s), 4.89 (6H, s), 1.46 (27H, s). Further spectroscopic data (^{13}C, MS, IR) are in accordance with the literature.[7]

General Procedure 2 (GP2): General procedure for the Mannich reaction of 3,7,11-tris(alkyloxy)triphenylene-2,6,10-triol with butylamine, hexylamine or 3,5-bis(trifluoromethyl)aniline.

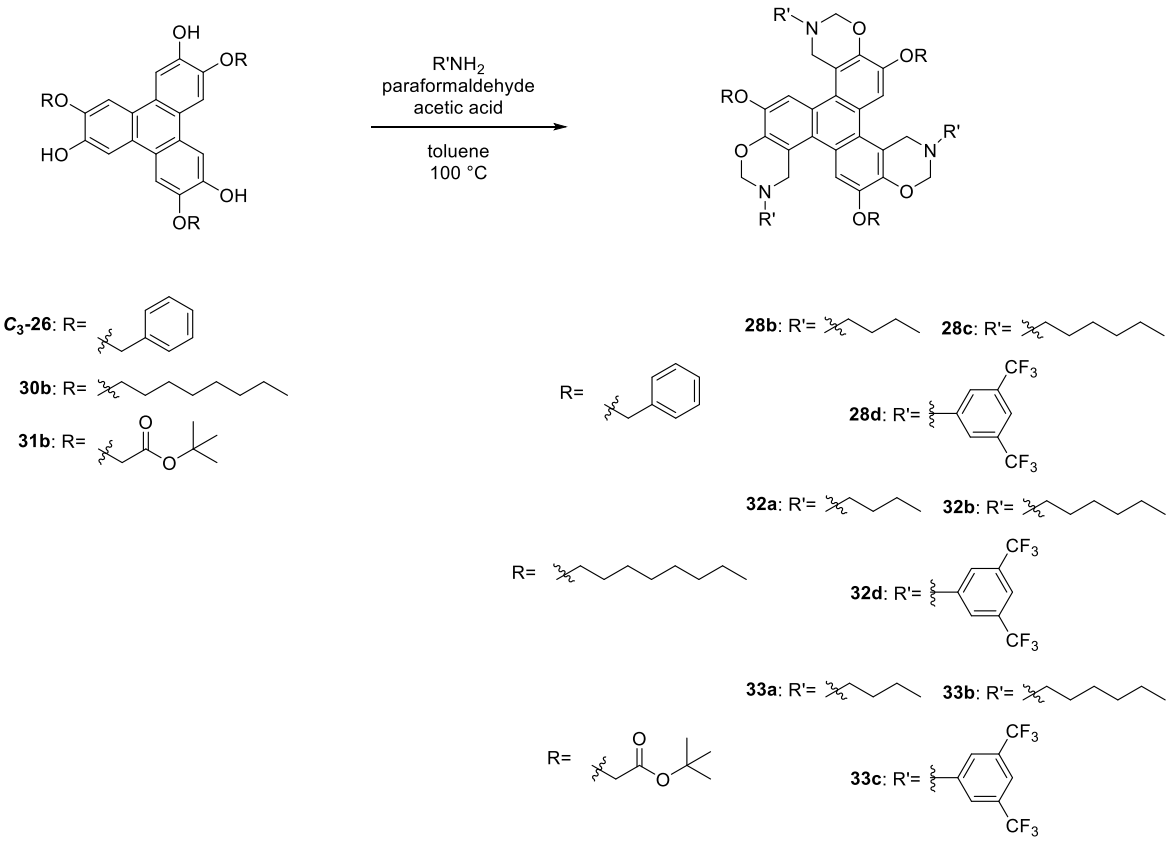

In a 10 mL screw-caped Pyrex test tube, a mixture of 3,7,11-tris(alkyloxy)triphenylene-2,6,10-triol (0.08 mmol), paraformaldehyde (0.087 g, 2.88 mmol), AcOH (0.021 g, 0.35 mmol), and amine (1.44 mmol) in anhydrous toluene (2 mL) was purged with argon and stirred overnight at 100 °C. The resulting red solution was then cooled to room temperature and dried in *vacuum*. The product was obtained after precipitation with absolute EtOH (**28b**,**c**,**d**) or after flash chromatography (**32a**-**c**, **33a**-**c**).

6,12,18-tris(benzyloxy)-3,9,15-tributyl-3,4,9,10,15,16-hexahydro-2H,8H,14H-triphenyleno[1,2-*e*:5,6-*e'*:9,10-*e''*]tris([1,3]oxazine) (**28b**): **GP2** was applied on ***C*$_3$-26** and butylamine, 83% yield. M.P. 112 °C. ^{1}H NMR (400 MHz, $CDCl_3$): δ 7.53-7.43 (6H, set of m), 7.37 (6H, t, *J* = 7.4 Hz), 7.33-7.28 (3H, set of m), 7.25 (3H, s), 5.31 (6H, s), 5.10(6H, s), 4.30(6H, s), 2.43 (6H, t, *J* = 7.2 Hz), 1.44-1.30 (6H, set of m), 1.30-1.15 (6H, set of m), 0.84 (6H, t, *J* = 6.8 Hz). $^{13}C\{^1H\}$ NMR (100 MHz): δ 144.2, 143.7, 137.2, 128.8, 128.1, 127.0, 126.3, 123.2, 115.9, 111.1, 81.9, 71.4, 53.5, 50.2, 30.4, 20.4, 14.1. IR (KBr): ν 1668, 1592, 1484, 1420,

1374, 1313, 1274, 1240, 1148, 1088, 1028, 955, 912, 857, 785, 732, 696 cm^{-1}. HRMS (ESI): calcd. for $C_{57}H_{64}N_3O_6$ [M^+] 886.4790; found: 886.4791.

6,12,18-tris(benzyloxy)-3,9,15-trihexyl-3,4,9,10,15,16-hexahydro-2H,8H,14H-triphenyleno[1,2-*e*:5,6-*e'*:9,10-*e''*]tris([1,3]oxazine) (**28c**): **GP2** was applied on ***C*$_3$-26** and hexylamine, 69% yield. M.P. 98 °C. ^{1}H NMR (400 MHz, $CDCl_3$): δ 7.50-7.45 (6H, m), 7.37 (6H, t, *J* = 7.7 Hz), 7.32-7.28 (3H, m), 7.24 (3H, s), 5.31 (6H, s), 5.10 (6H, s), 4.31 (6H, s), 2.42 (6H, t, *J* = 7.3 Hz), 1.45-1.11 (24H, m), 0.84 (9H, t, *J* = 7.1 Hz). $^{13}C\{^1H\}$ NMR (100 MHz): δ 144.3, 143.7, 137.2, 128.8, 128.1, 127.0, 126.2, 123.2, 115.9, 111.1, 81.9, 71.4, 53.5, 50.5, 31.8, 28.3, 26.9, 22.7, 14.2. IR (KBr): ν 1592, 1483, 1420, 1374, 1313, 1274, 1242, 1163, 1147, 1089, 1028, 1012, 953, 919, 857, 785, 731, 696 cm^{-1}. HRMS (ESI): calcd. for $C_{63}H_{76}N_3O_6$ [M^+] 970.5729; found: 970.5734.

6,12,18-tris(benzyloxy)-3,9,15-tris(3,5-bis(trifluoromethyl)phenyl)-3,4,9,10,15,16-hexahydro-2H,8H,14H-triphenyleno[1,2-*e*:5,6-*e'*:9,10-*e''*]tris([1,3]oxazine) (**28d**): **GP2** was applied on ***C*$_3$-26** and 3,5-bis(trifluoromethyl)aniline, 52% yield. M.P. 202 °C. ^{1}H NMR (400 MHz, $CDCl_3$): δ 7.47-7.43 (6H, set of m), 7.37 (6H, t, *J* = 7.6 Hz), 7.27 (3H, s), 7.25-7.20 (3H, set of m), 7.12 (6H, s), 7.02 (3H, s), 5.59 (6H, s), 5.35 (6H, s), 4.50 (6H, s). $^{13}C\{^1H\}$ NMR (100 MHz): δ 148.4, 144.5, 143.3, 136.9, 132.5 (q, *J* = 34.0 Hz), 129.1, 128.3, 126.4, 125.3, 123.2 (q, *J* = 272.9 Hz) 123.2, 118.2, 116.1, 115.1, 111.1, 78.0, 70.9, 53.4; IR (KBr): ν 1539, 1476, 1423, 1404, 1346, 1278, 1186, 1131, 1073, 1001, 963, 872, 735, 698, 682 cm^{-1}. HRMS (ESI): calcd. for $C_{69}H_{45}F_{18}N_3O_6$ [M^+] 1353.3015; found: 1353.3064.

3,9,15-tributyl-6,12,18-tris(octyloxy)-3,4,9,10,15,16-hexahydro-2H,8H,14H-triphenyleno[1,2-*e*:5,6-*e'*:9,10-*e''*]tris([1,3]oxazine) (**32a**): **GP2** was applied on **30b** and butylamine. Eluent cyclohexane/AcOEt, 9:1, 98% yield. Oil. ^{1}H NMR (400 MHz, $CDCl_3$): δ 7.27 (3H, s), 5.08 (6H, s), 4.59 (6H, s), 4.08 (6H, t, *J* = 6.9 Hz), 2.44 (6H, t, *J* = 7.3 Hz), 1.90-1.77 (6H, set of m), 1.46-1.10 (42H, set of m), 0.83 (9H, t, *J* = 7.4 Hz), 0.75 (9H, t, *J* = 7.4 Hz). $^{13}C\{^1H\}$ NMR (100 MHz): δ 144.7, 143.4, 125.7, 123.4, 115.4, 109.7, 81.7, 69.4, 53.7, 50.1, 48.7, 31.8, 30.3, 29.4, 29.2, 26.1, 22.7, 20.2, 14.1, 13.9. IR (KBr): ν 1724, 1593, 1488, 1469, 1423, 1376, 1314, 1274, 1242, 1192, 1148, 1101, 1089, 951, 924, 785, 723 cm^{-1}. HRMS (ESI): calcd. for $C_{60}H_{94}N_3O_6$ [M^+] 952.7137; found: 952.7154.

3,9,15-trihexyl-6,12,18-tris(octyloxy)-3,4,9,10,15,16-hexahydro-2H,8H,14H-triphenyleno[1,2-*e*:5,6-*e'*:9,10-*e''*]tris([1,3]oxazine) (**32b**): **GP2** was applied on **30b** and hexylamine. Eluent cyclohexane/AcOEt, 9:1, 98% yield. Waxy solid. ^{1}H NMR (400 MHz, $CDCl_3$): δ 7.34 (3H, s), 5.14 (6H, s), 4.65 (6H, s), 4.15 (6H, t, *J* = Hz), 2.50 (6H, t, *J* = Hz), 1.96-1.86 (6H, set of m) 1.62-1.10 (54H, set of m), 0.88 (9H, t, *J* = Hz), 0.81 (9H, t, *J* = Hz). $^{13}C\{^1H\}$ NMR (100 MHz): 144.9, 143.5, 125.9, 123.5, 115.6, 109.9, 81.8, 77.5, 77.4, 77.2, 76.8, 69.5, 53.9, 50.6, 32.0, 31.8, 29.6, 29.4, 28.3, 26.9, 26.2, 22.8, 22.7, 14.2, 14.1, 14.1. IR (KBr): ν 1720, 1593, 1488, 1468, 1422, 1377, 1314, 1273, 1237, 1148, 1091, 950, 728 cm^{-1}. HRMS (ESI): calcd. for $C_{66}H_{106}N_3O_6$ [M^+] 1036.8092; found: 1036.8092.

3,9,15-tris(3,5-bis(trifluoromethyl)phenyl)-6,12,18-tris(octyloxy)-3,4,9,10,15,16-hexahydro-2H,8H,14H-triphenyleno[1,2-*e*:5,6-*e'*:9,10-*e''*]tris([1,3]oxazine) (**32c**): **GP2** was applied on **30b** and 3,5-bis(trifluoromethyl)aniline. Eluent cyclohexane/AcOEt, 9:1, 52% yield. M.P. 162 °C. ^{1}H NMR (400 MHz, $CDCl_3$): δ 7.32 (3H, s), 7.30 (6H, s), 7.29 (3H, s), 5.68 (6H, s), 5.26 (6H, s), 4.16 (6H, t, *J* = 6.7 Hz), 1.98-1.87 (6H, set of m), 1.62-1.23 (30H, set of

m), 0.87 (9H, t, *J* = 7.3 Hz). $^{13}C\{^{1}H\}$ NMR (100 MHz): δ 148.6, 145.8, 143.6, 132.7 (q, *J* = 33.1 Hz), 125.3, 123.8, 123.2 (q, *J* = 273.0 Hz), 118.1, 115.9, 115.2, 110.3, 78.4, 69.9, 53.8, 31.9, 29.5, 29.4, 29.3, 26.2, 22.8, 14.2. IR (KBr): ν 1618, 1591, 1475, 1423, 1404, 1347, 1275, 1183, 1133, 1080, 1001, 965, 875, 682 cm^{-1}. HRMS (ESI): calcd. for $C_{72}H_{75}F_{18}N_3O_6$ $[M^+]$1419.5363; found: 1419.5430.

tri-*tert*-butyl 2,2',2''-((3,9,15-tributyl-3,4,9,10,15,16-hexahydro-2*H*,8*H*,14*H*-triphenyleno[1,2-*e*:5,6-*e'*:9,10-*e''*]tris([1,3]oxazine)-6,12,18-triyl)tris(oxy))triacetate (**33a**): **GP2** was applied on **31b** and butylamine. Eluent cyclohexane/AcOEt, 7:3, 35% yield. Waxy solid. ^{1}H NMR (400 MHz, $CDCl_3$): δ 7.28 (3H, s), 5.14 (6H, s), 4.68 (6H, s), 4.60 (6H, s), 2.49 (6H, t, *J* = 7.6 Hz), 1.50 (27H, s), 1.45-1.32 (6H, set of m), 1.29-1.17 (6H, set of m), 0.82 (9H, t, *J* = 7.3 Hz). $^{13}C\{^{1}H\}$ NMR (100 MHz): δ 168.0, 143.8, 143.6, 127.0, 123.2, 116.1, 110.5, 82.7, 81.8, 66.8, 53.8, 50.2, 30.4, 28.3, 20.3, 14.0. IR (KBr): ν 1753, 1728, 1594, 1487, 1451, 1419, 1368, 1316, 1278, 1245, 1225, 1151, 1111, 1017, 959, 916, 848, 785, 719 cm^{-1}. HRMS (ESI): calcd. for $C_{54}H_{76}N_3O_{12}$ $[M^+]$ 958.5424; found: 958.5420.

tri-*tert*-butyl 2,2',2''-((3,9,15-trihexyl-3,4,9,10,15,16-hexahydro-2*H*,8*H*,14*H*-triphenyleno[1,2-*e*:5,6-*e'*:9,10-*e''*]tris([1,3]oxazine)-6,12,18-triyl)tris(oxy))triacetate (**33b**): **GP2** was applied on **31b** and hexylamine. Eluent cyclohexane/AcOEt, 7:3, 50% yield. Oil. ^{1}H NMR (400 MHz, $CDCl_3$): δ 7.28 (3H, s), 5.14 (6H, s), 4.68 (6H, s), 4.60 (6H, s), 2.39 (6H, t, *J* = 7.4 Hz), 1.50 (27H, s), 1.47-1.38 (6H, set of m), 1.36- 1.24 (18H, set of m), 0.88 (9H, t, *J* = 6.9 Hz). $^{13}C\{^{1}H\}$ NMR (100 MHz): δ 168.0, 143.8, 143.6, 127.0, 123.2, 116.1, 110.5, 81.8, 74.9, 66.8, 53.8, 53.1, 31.9, 28.3, 28.2, 27.4, 22.8, 14.2. IR (KBr): ν 1753, 1728, 1626, 1593, 1574, 1486, 1465, 1415, 1371, 1314, 1229, 1151, 1108, 957, 924, 875, 716 cm^{-1}. HRMS (ESI): calcd. for $C_{60}H_{88}N_3O_{12}$ $[M^+]$ 1042.6363; found: 1042.6389.

tri-*tert*-butyl 2,2',2''-((3,9,15-tris(3,5-bis(trifluoromethyl)phenyl)-3,4,9,10,15,16-hexahydro-2H,8H,14H-triphenyleno[1,2-*e*:5,6-*e'*:9,10-*e''*]tris([1,3]oxazine)-6,12,18-triyl)tris(oxy))triacetate (**33c**): **GP2** was applied on **31b** and 3,5-bis(trifluoromethyl)aniline. Eluent cyclohexane/AcOEt, gradient from 85:15 to 80:20, 52% yield. M.P. 213 °C. ^{1}H NMR (400 MHz, $CDCl_3$): δ 7.36 (3H, s), 7.33 (6H, s), 7.28 (3H, s), 5.69 (6H, s), 5.23 (6H, s), 4.68 (6H, s), 1.45 (27H, s); $^{13}C\{^{1}H\}$ NMR (100 MHz): 168.2, 148.5, 144.7, 143.8, 132.7 (q, *J* = 33 Hz), 126.5, 123.3, 123.1 (q, *J* = 273 Hz) ,118.1, 116.6, 115.2, 112.1, 82.9, 78.3, 67.5, 53.6, 28.1. IR (KBr): ν 1747, 1621, 1577, 1541, 1477, 1415, 1347, 1275, 1231, 1176, 1130, 1091, 1001, 954, 875, 842, 682 cm^{-1}. HRMS (ESI): calcd. for $C_{66}H_{57}F_{18}N_3O_{12}$ $[M^+]$ 1425.3649; found: 1425.3636.

General Procedure 3 (GP3): General procedure for the Mannich reaction on 3,7,11-tris(alkyloxy)triphenylene-2,6,10-triol with 4-aminopyridine.

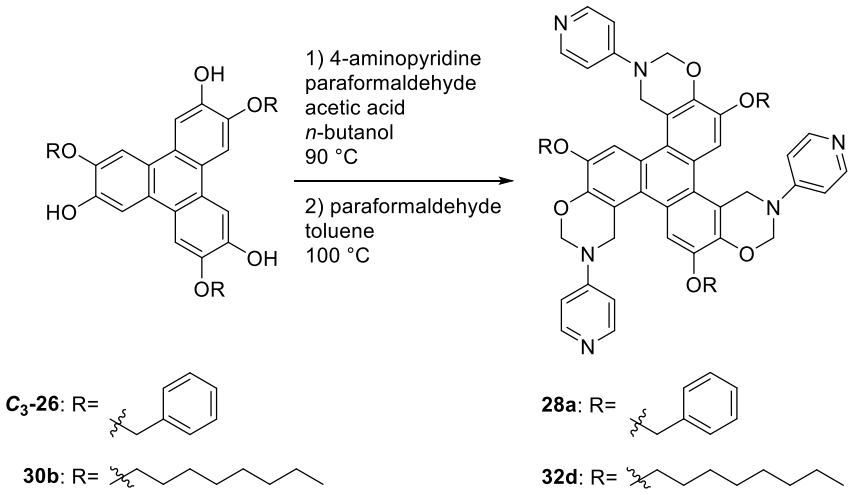

In a pear-shaped 25 mL round bottomed flask, a mixture of 4-aminopyridine (0.112 g, 1.2 mmol), paraformaldehyde (0.04 g, 1.33 mmol), and AcOH (0.08 g, 1.2 mmol) in *n*-BuOH (2 mL) was stirred at 90 °C overnight under argon atmosphere. The resulting solution was cooled to room temperature and concentrated in *vacuum*. The residue was transferred in a 10 mL screw-capped Pyrex test tube and 3,7,11-tris(alkyloxy)triphenylene-2,6,10-triol (0.08 mmol), paraformaldehyde (0.04 g, 1.33 mmol), and anhydrous toluene (2 mL) were added. The mixture was purged with argon and stirred overnight at 100 °C. The resulting mixture was cooled to room temperature and concentrated in *vacuum*. The obtained crude oil was suspended with EtOH (in the case of **28a**) or Et_2O (in the case of **32d**) and the resulting precipitate was filtered, washed with EtOH or Et_2O and dried in *vacuum*, to afford the product as a pale yellow solid.

6,12,18-tris(benzyloxy)-3,9,15-tri(pyridin-4-yl)-3,4,9,10,15,16-hexahydro-2*H*,8*H*,14*H*-triphenyleno[1,2-*e*:5,6-*e'*:9,10-*e''*]tris([1,3]oxazine) (**28a**): **GP3** was applied on ***C*$_3$-26**, 75% yield. M.P. 170-171 °C. ^{1}H NMR (400 MHz, $CDCl_3$): δ 8.21 (6H, dd, *J* = 5.0, 1.6 Hz), 7.46-7.41 (6H, set of m), 7.34 (6H, t, *J* = 7.8 Hz), 7.24-7.19 (3H, set of m), 7.12 (3H, s), 6.56 (6H, dd, *J* = 5.0, 1.6 Hz), 5.64 (6H, s), 5.31 (6H, s), 4.61 (6H, s). $^{13}C\{^1H\}$ NMR (100 MHz): δ 152.8, 149.7, 144.8, 143.5, 136.8, 128.9, 128.2, 126.5, 125.4, 123.1, 116.5, 111.2, 111.0, 76.6, 71.2, 50.3. IR (KBr): ν 1643, 1593, 1552, 1511, 1483, 1459, 1421, 1383, 1319, 1278, 1245, 1159, 1111, 1072, 1034, 997, 960, 874, 799, 782, 740, 697 cm^{-1}; HRMS (ESI): calcd. for $C_{60}H_{49}N_6O_6$ [M^+] 949.3708; found: 949.3744.

6,12,18-tris(octyloxy)-3,9,15-tri(pyridin-4-yl)-3,4,9,10,15,16-hexahydro-2H,8H,14H-triphenyleno[1,2-*e*:5,6-*e'*:9,10-*e''*]tris([1,3]oxazine) (**32d**): **GP3** was applied on **30b**, 83% yield. M.P. 191-192 °C. ^{1}H NMR (400 MHz, $CDCl_3$): δ 8.22 (6H, d, *J* = 5.2 Hz), 7.34 (3H, s), 6.70 (6H, d, *J* = 5.2 Hz), 5.73 (6H, s), 5.26 (6H, s), 4.14 (6H, t, *J* = 6.5 Hz), 1.99 - 1.85 (6H, set of m), 1.61 - 1.18 (36H, set of m), 0.87 (9H, t, *J* = 6.6 Hz). $^{13}C\{^1H\}$ NMR (100 MHz): δ 152.9, 150.7, 145.9, 143.7, 125.4, 123.7, 116.4, 111.3, 110.1, 69.7, 51.1, 31.9, 29.5, 29.4, 26.2, 22.8, 14.2. IR (KBr): ν 1594, 1553, 1484, 1422, 1380, 1318, 1246, 1163, 1112, 1080, 995, 965, 818, 725 cm^{-1}. HRMS (ESI): calcd. for $C_{63}H_{79}N_6O_6$ [M^+] 1015.6056; found: 1015.6050.

2.5.3 NMR and MS Spectra

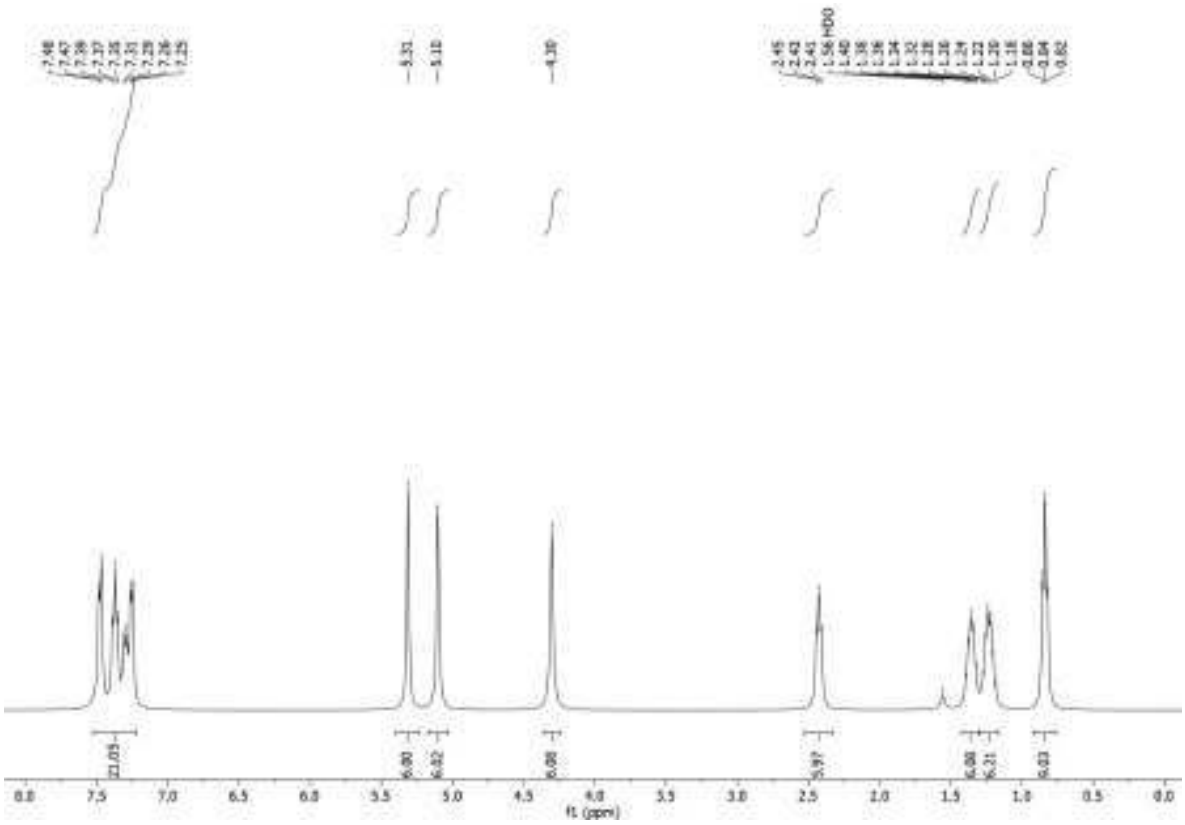

Figure I: ^{1}H NMR of molecule **28b**.

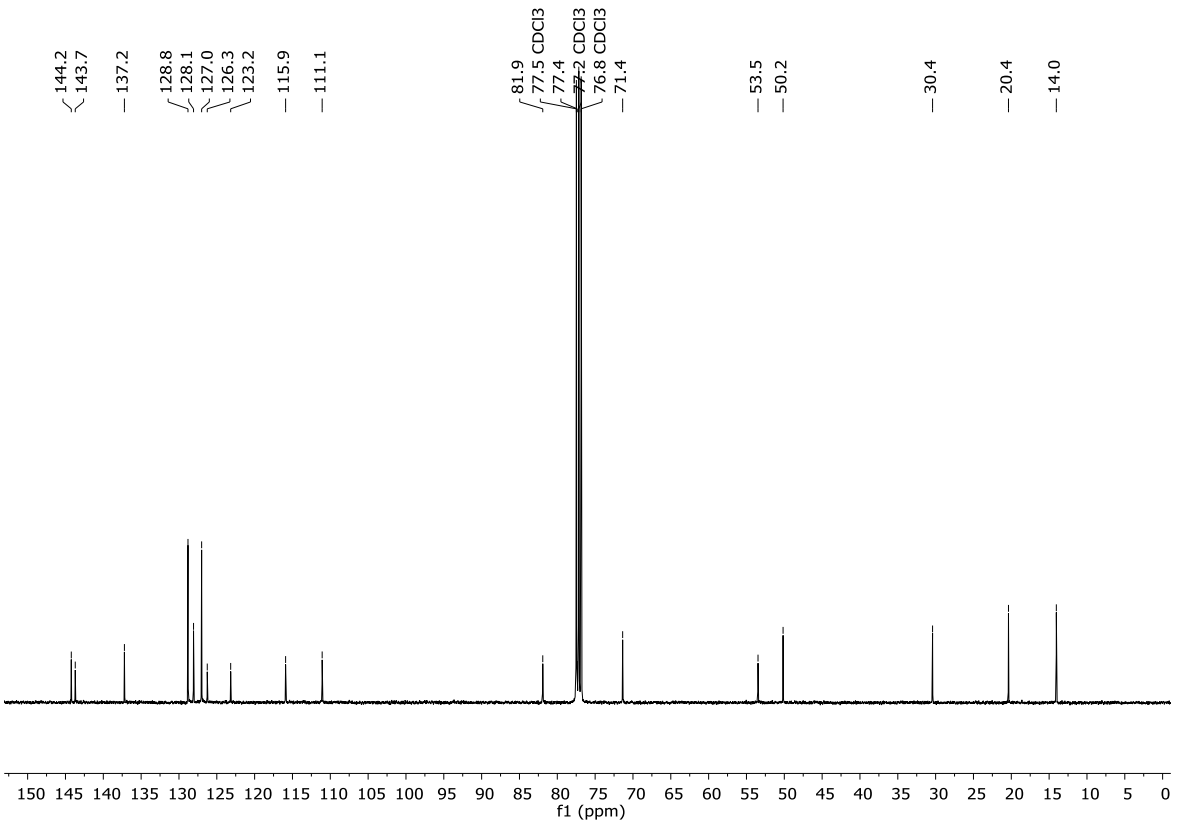

Figure II: ^{13}C NMR of molecule **28b**.

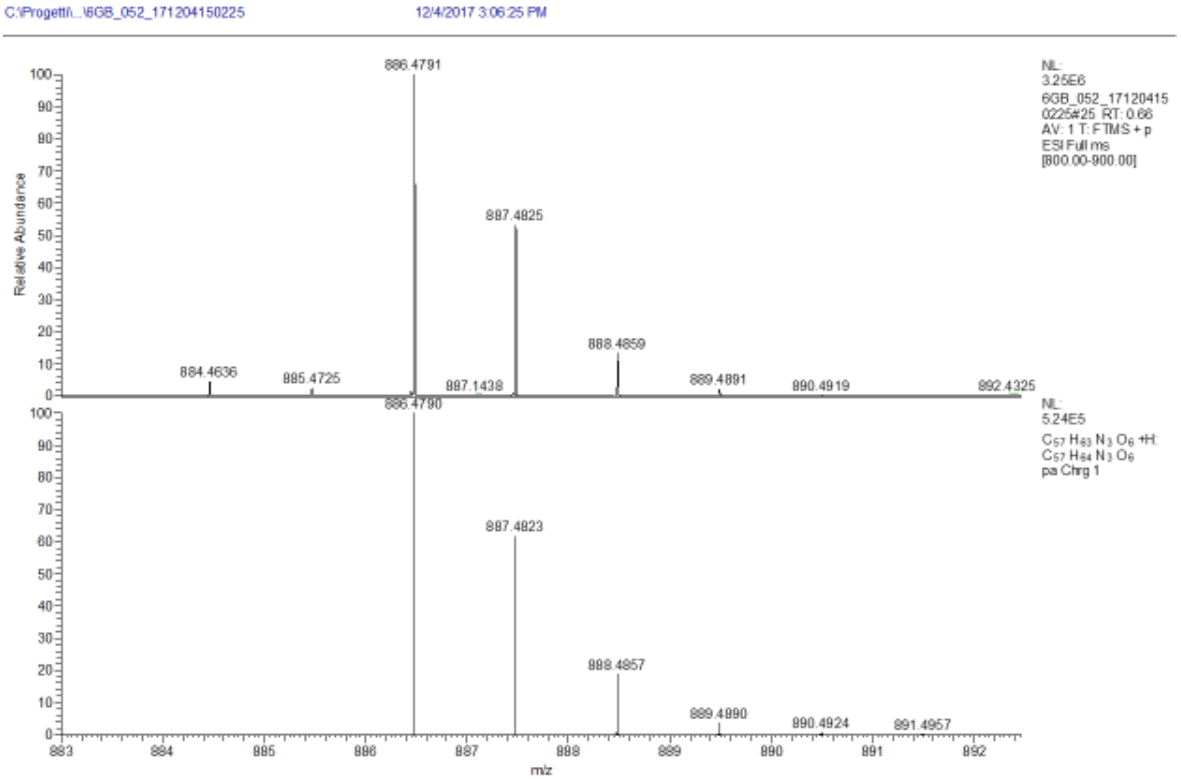

Figure III: ESI-HRMS of molecule **28b**.

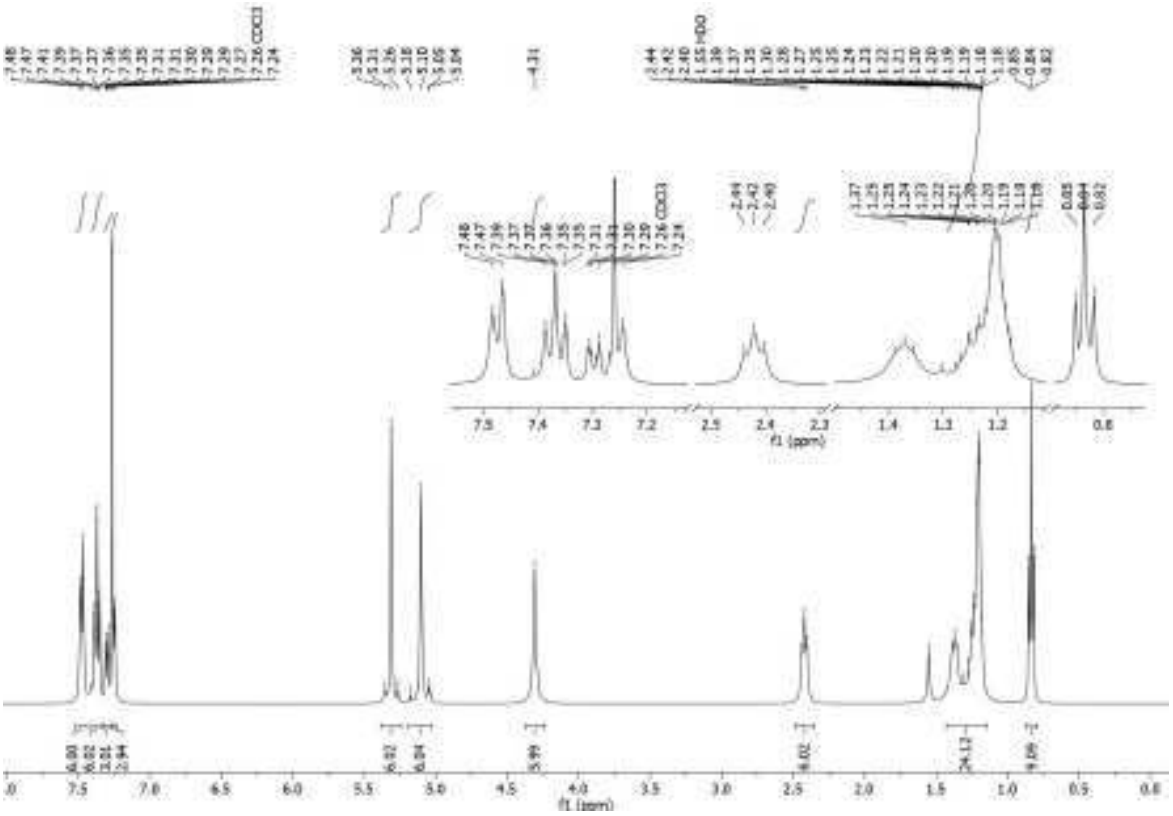

Figure IV: ^{1}H NMR of molecule **28c**.

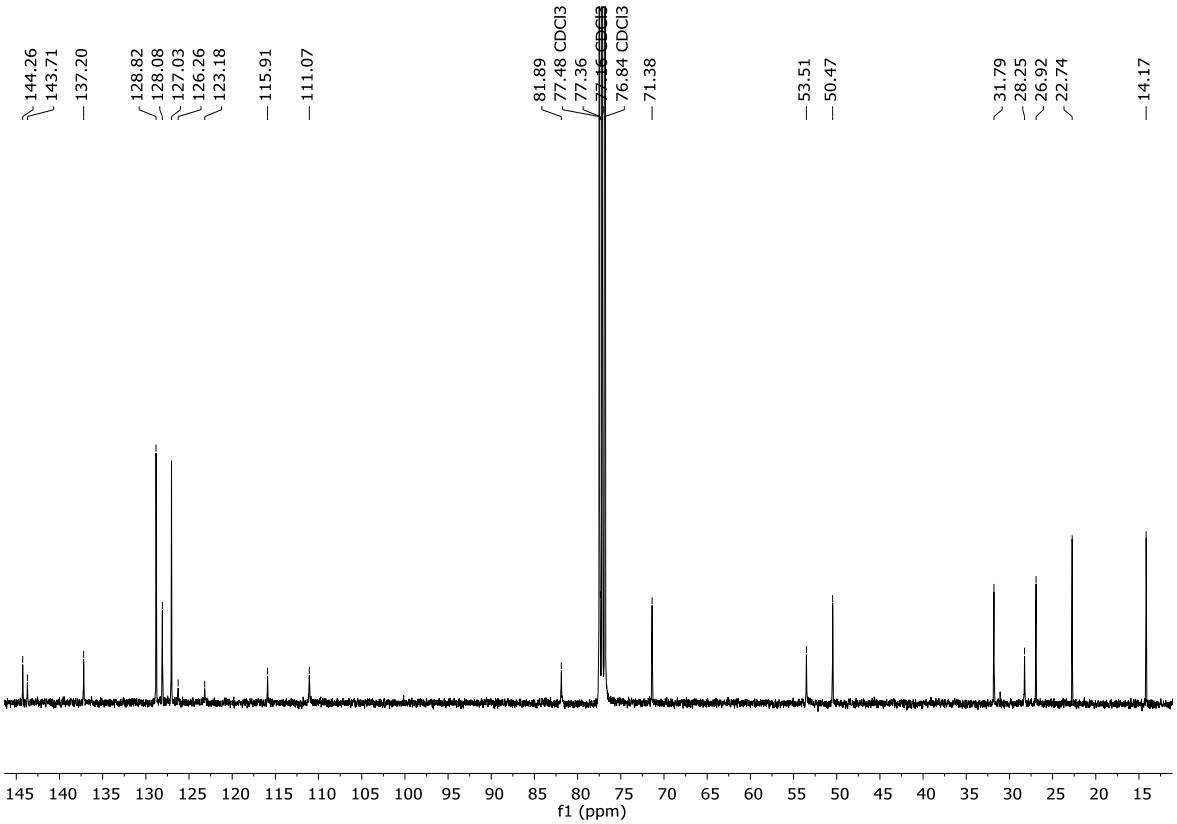

Figure V: ^{13}C NMR of molecule **28c**.

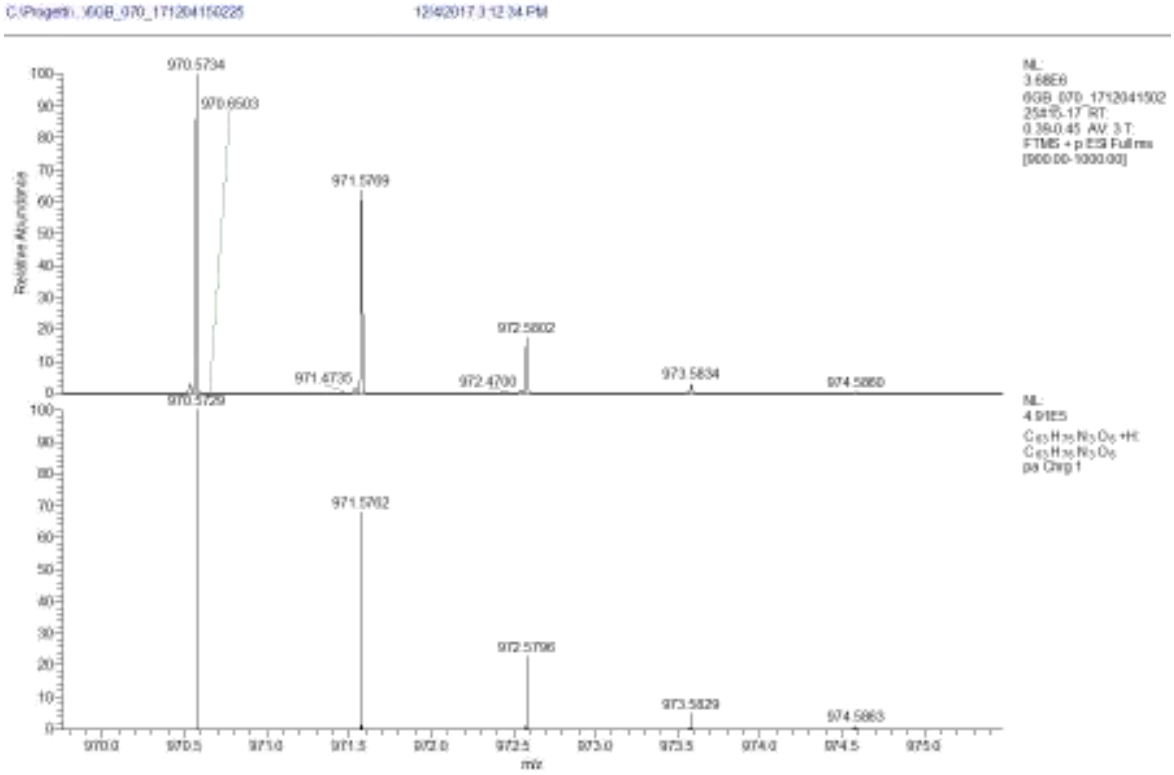

Figure VI: ESI-HRMS of molecule **28c**.

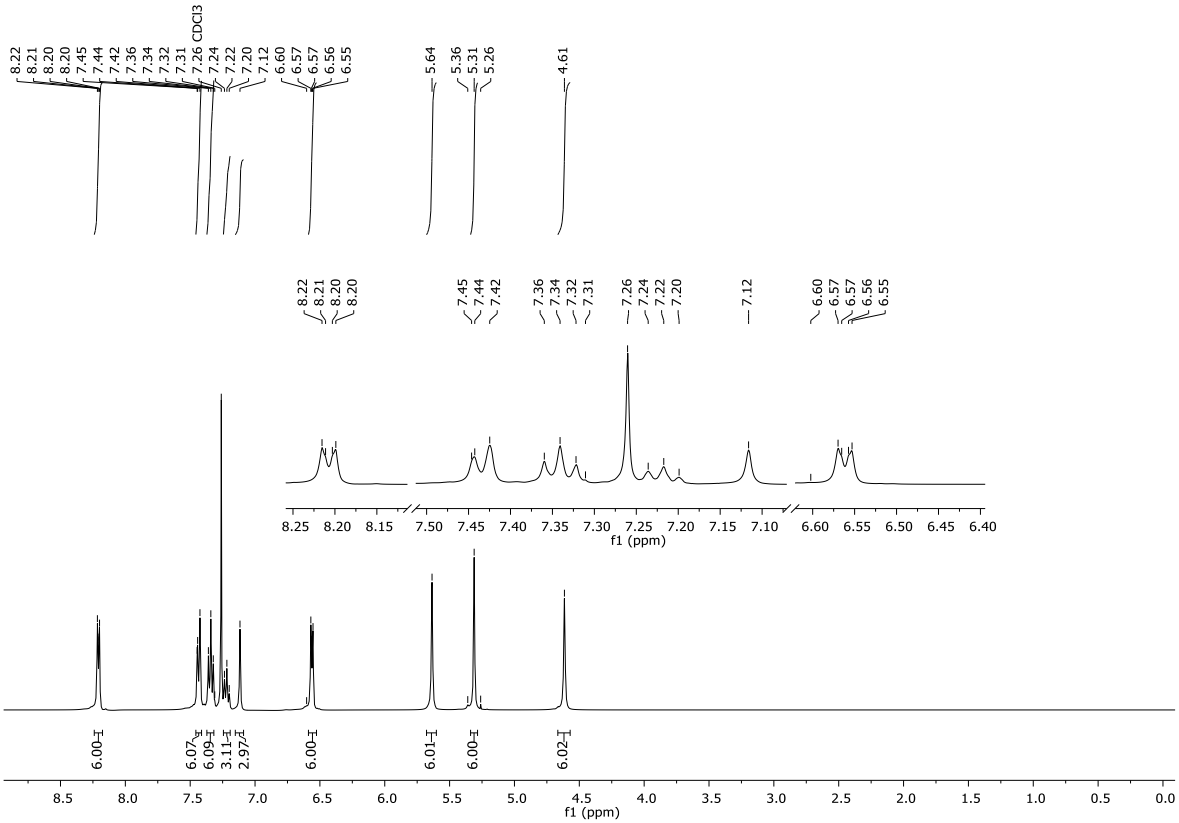

Figure VII: ^{1}H NMR of molecule **28a**.

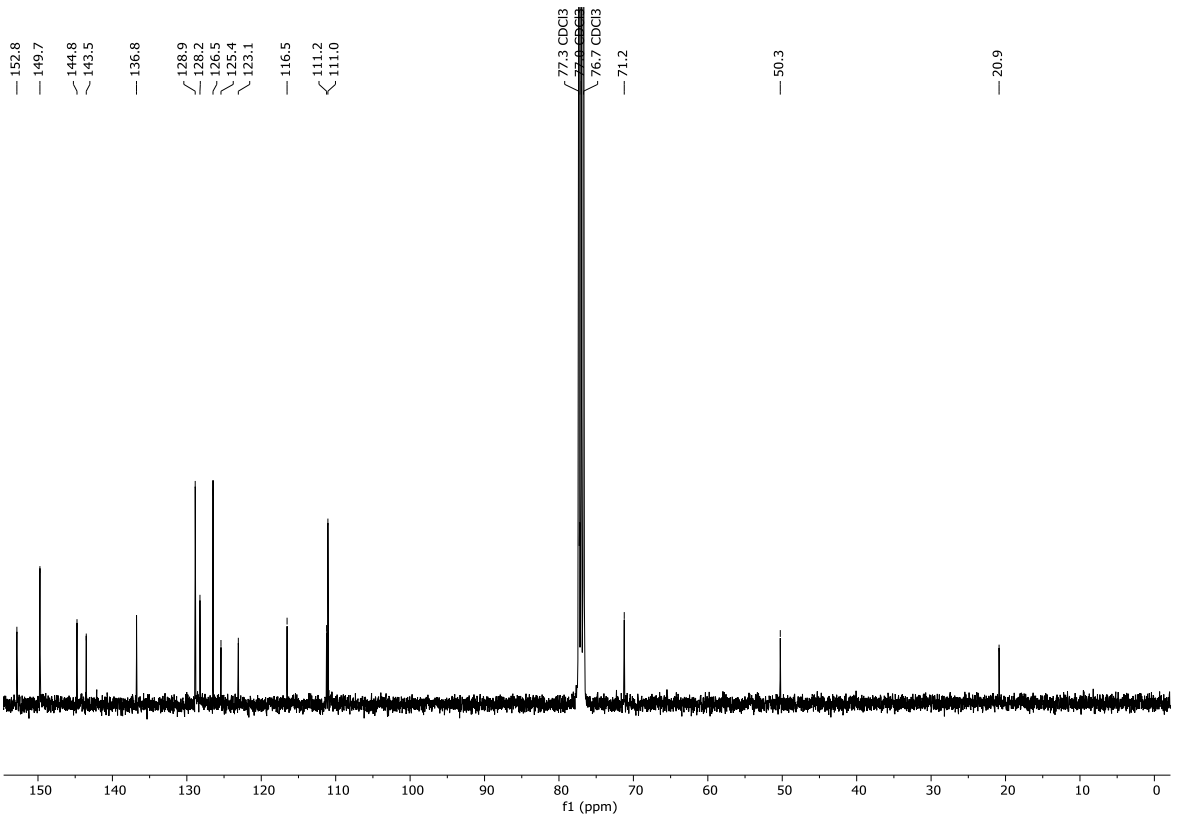

Figure VIII: ^{13}C NMR of molecule **28a**.

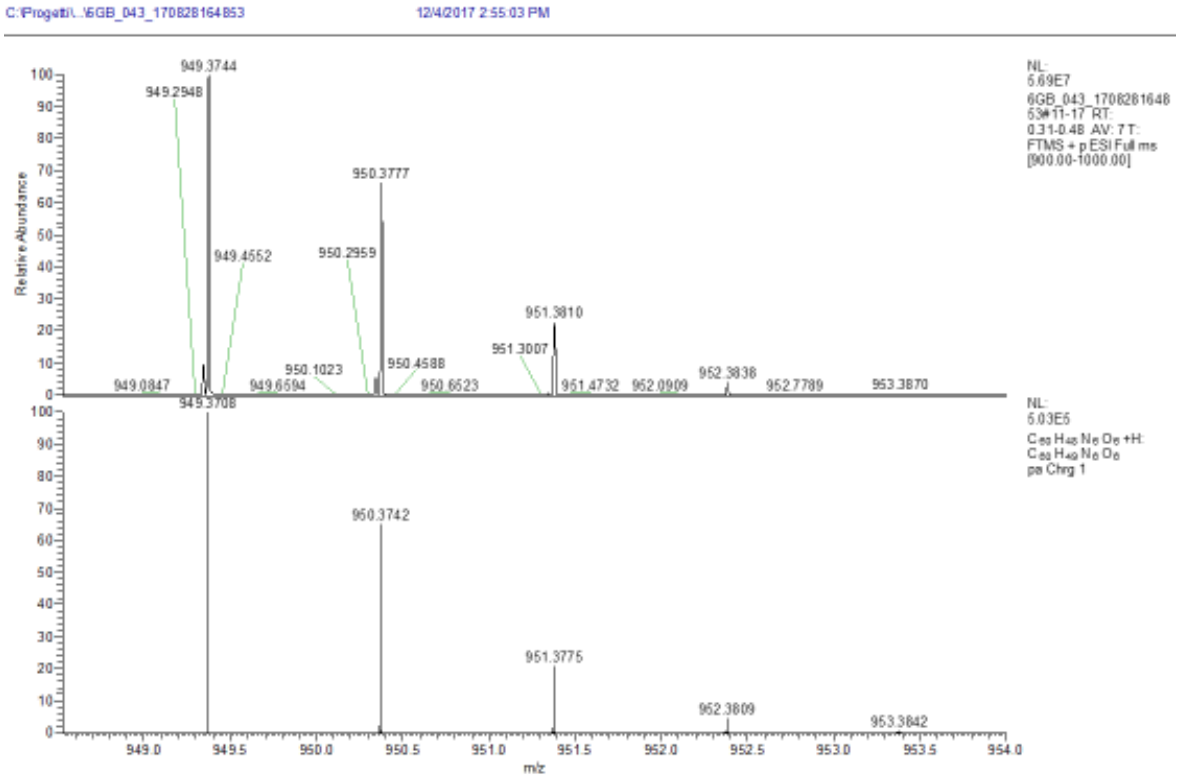

Figure IX: ESI-HRMS of molecule **28a**.

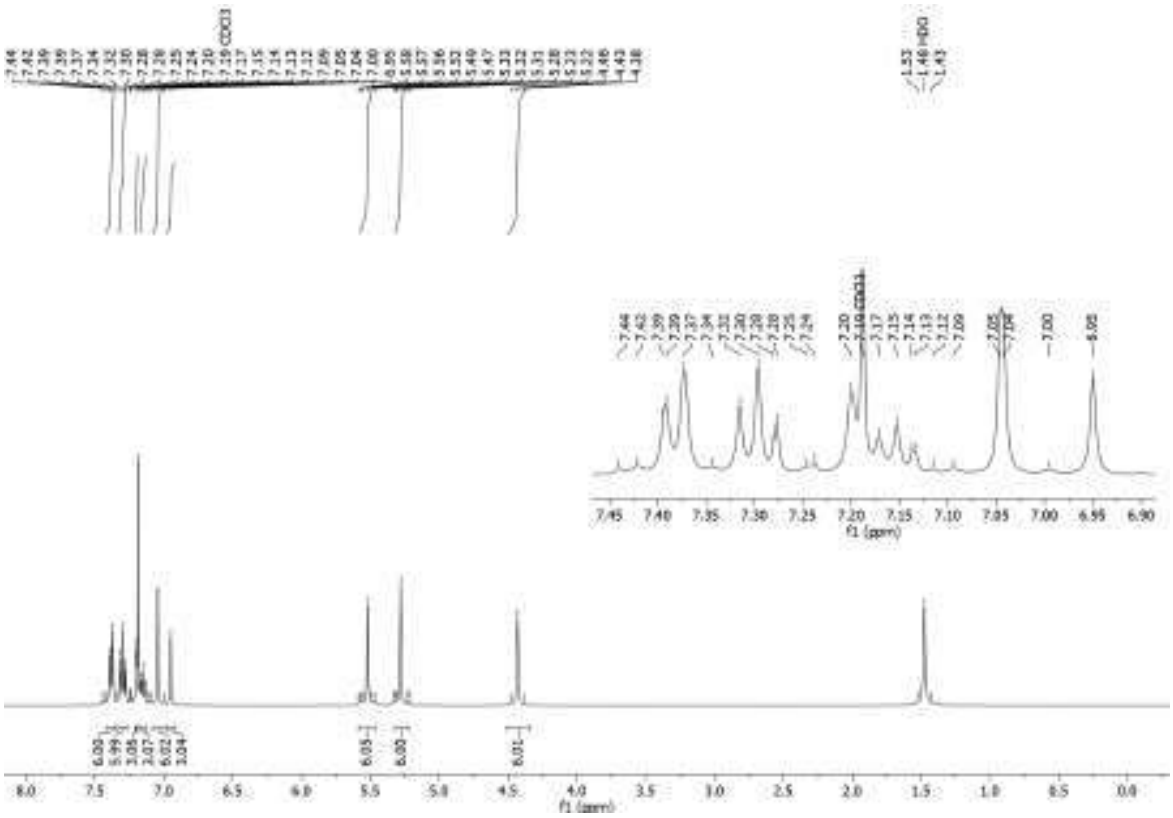

Figure X: ^{1}H NMR of molecule **28d**.

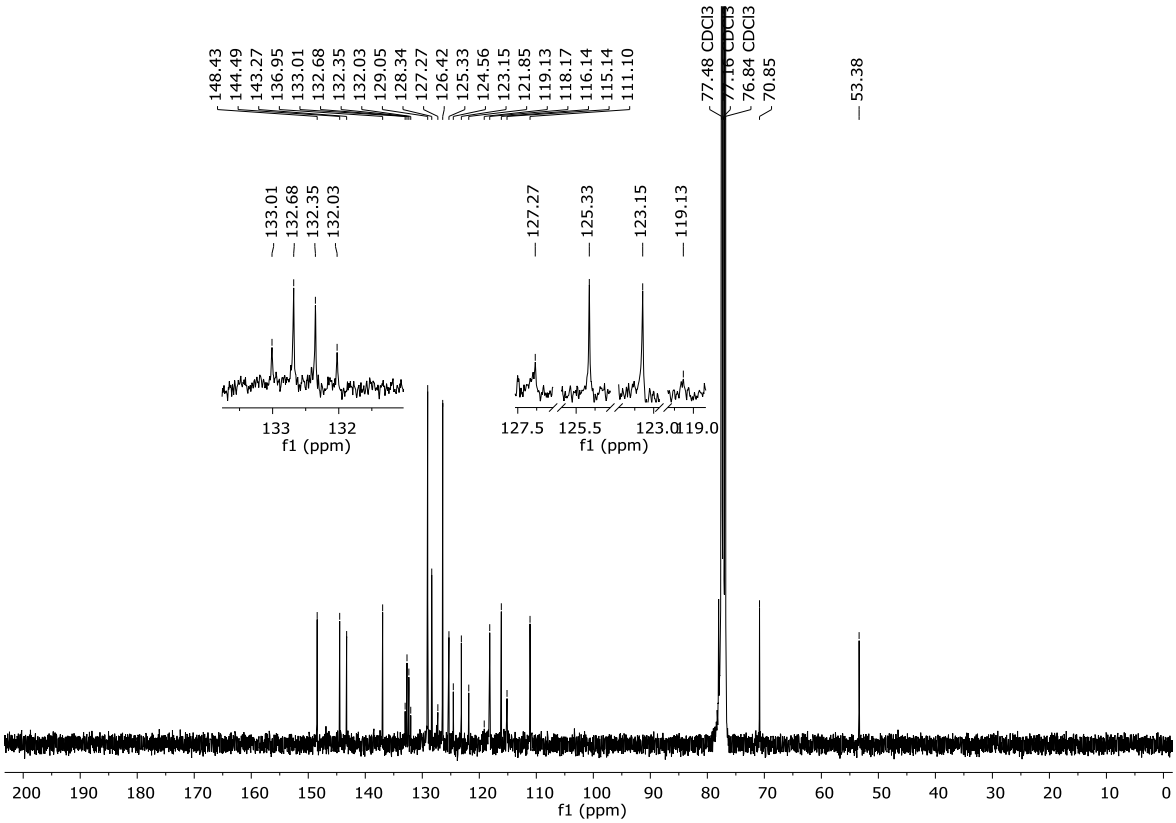

Figure XI: ^{13}C NMR of molecule **28d**.

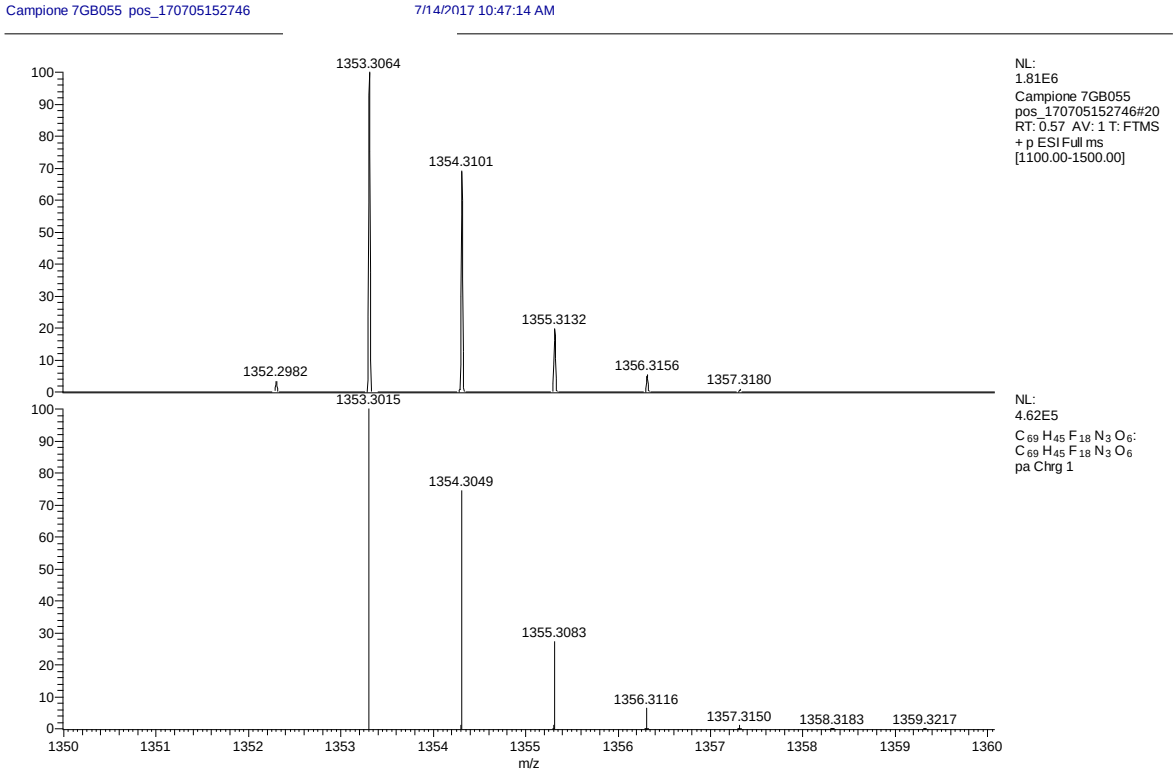

Figure XII: ESI-HRMS of molecule **28d**.

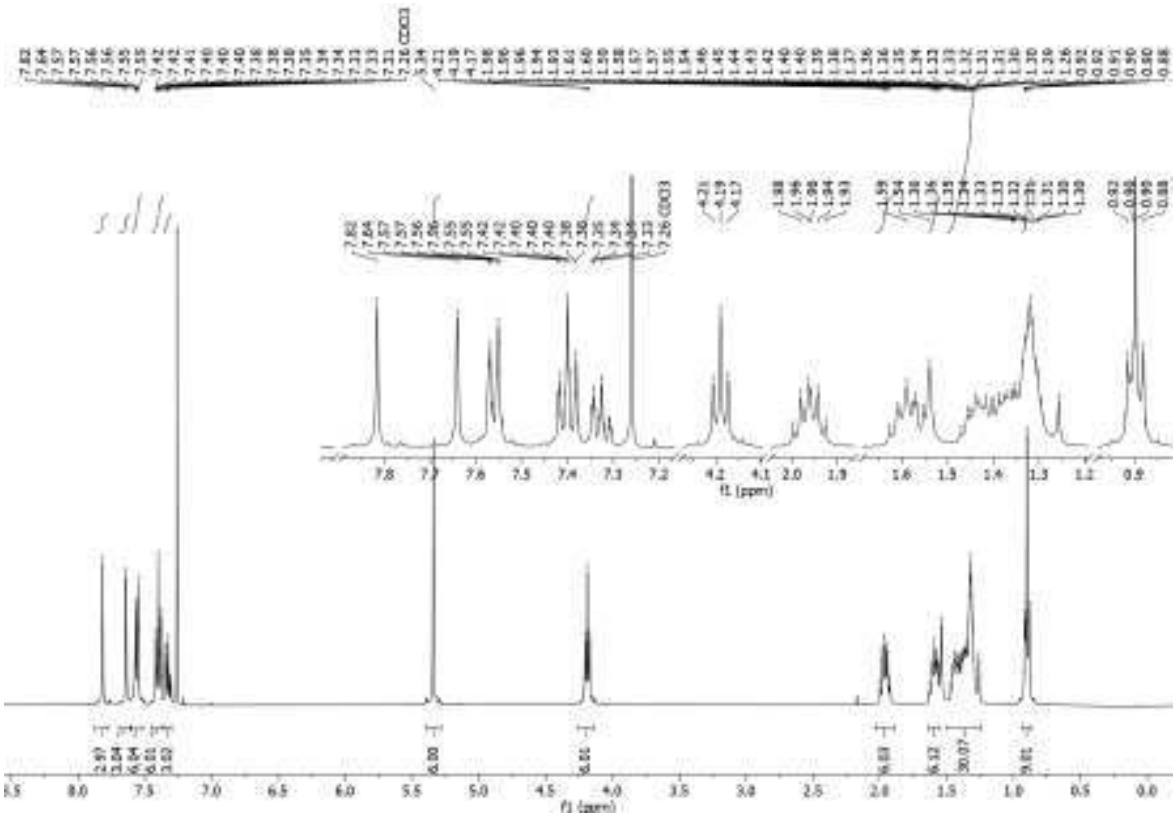

Figure XIII: ^{1}H NMR of molecule **30a**.

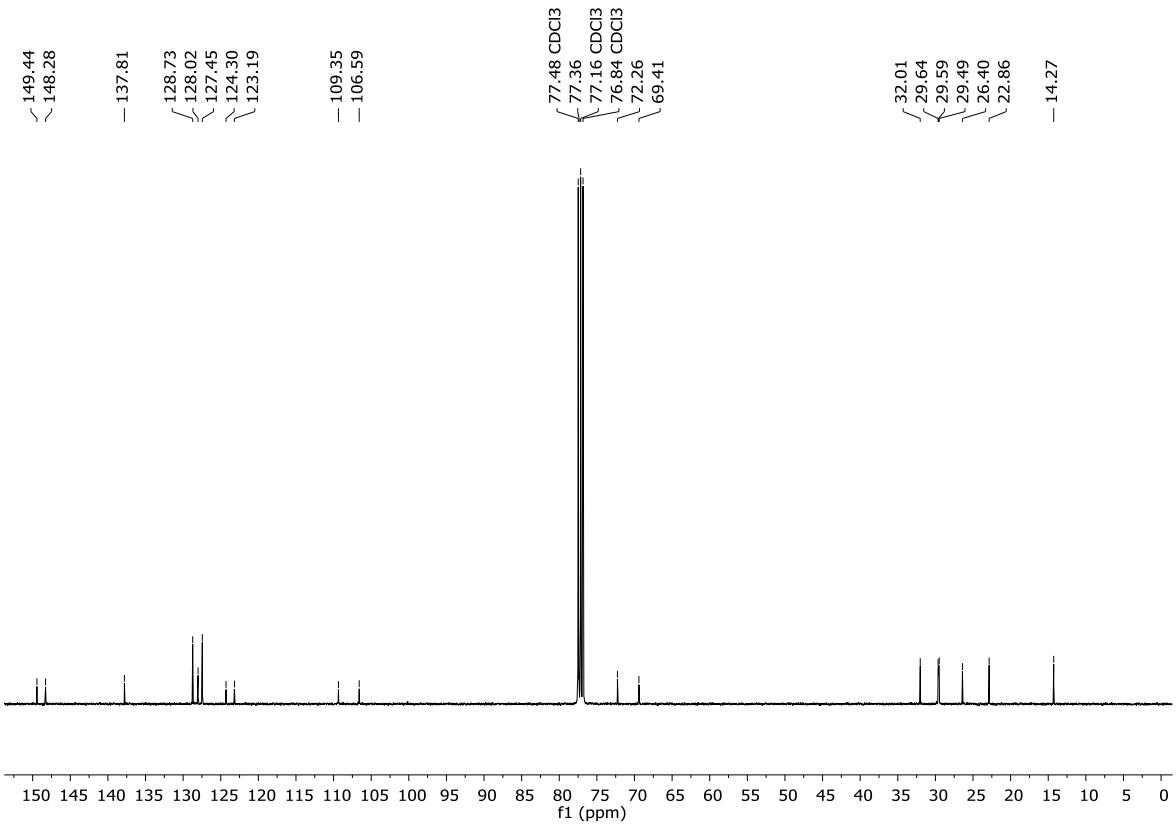

Figure XIV: ^{13}C NMR of molecule **30a**.

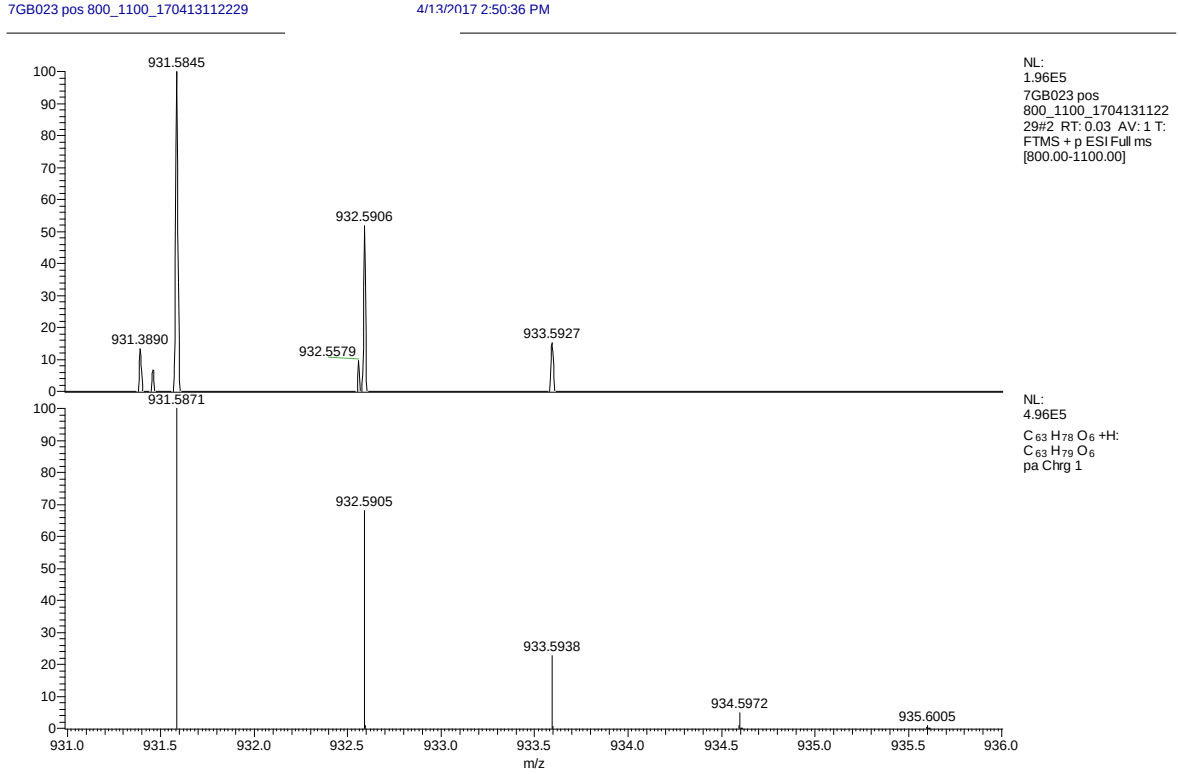

Figure XV: ESI-HRMS of molecule **30a**.

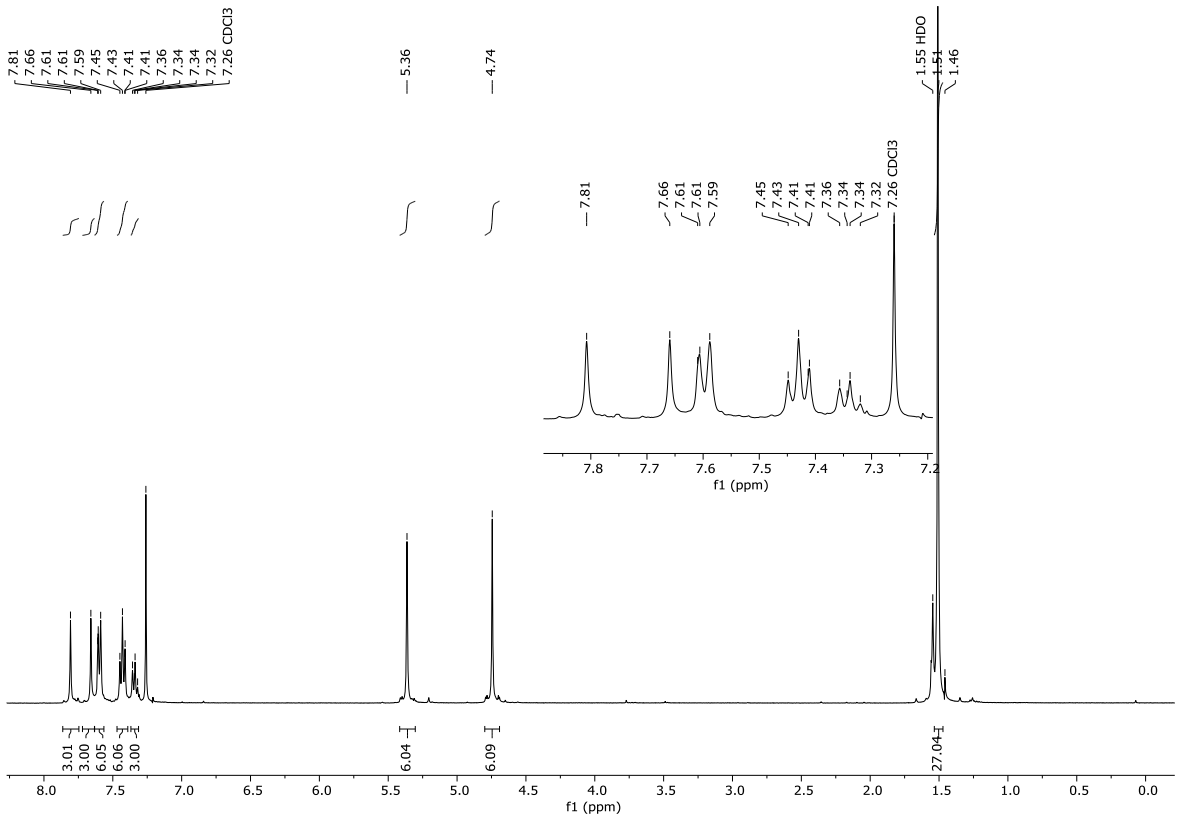

Figure XVI: ^{1}H NMR of molecule **31a**.

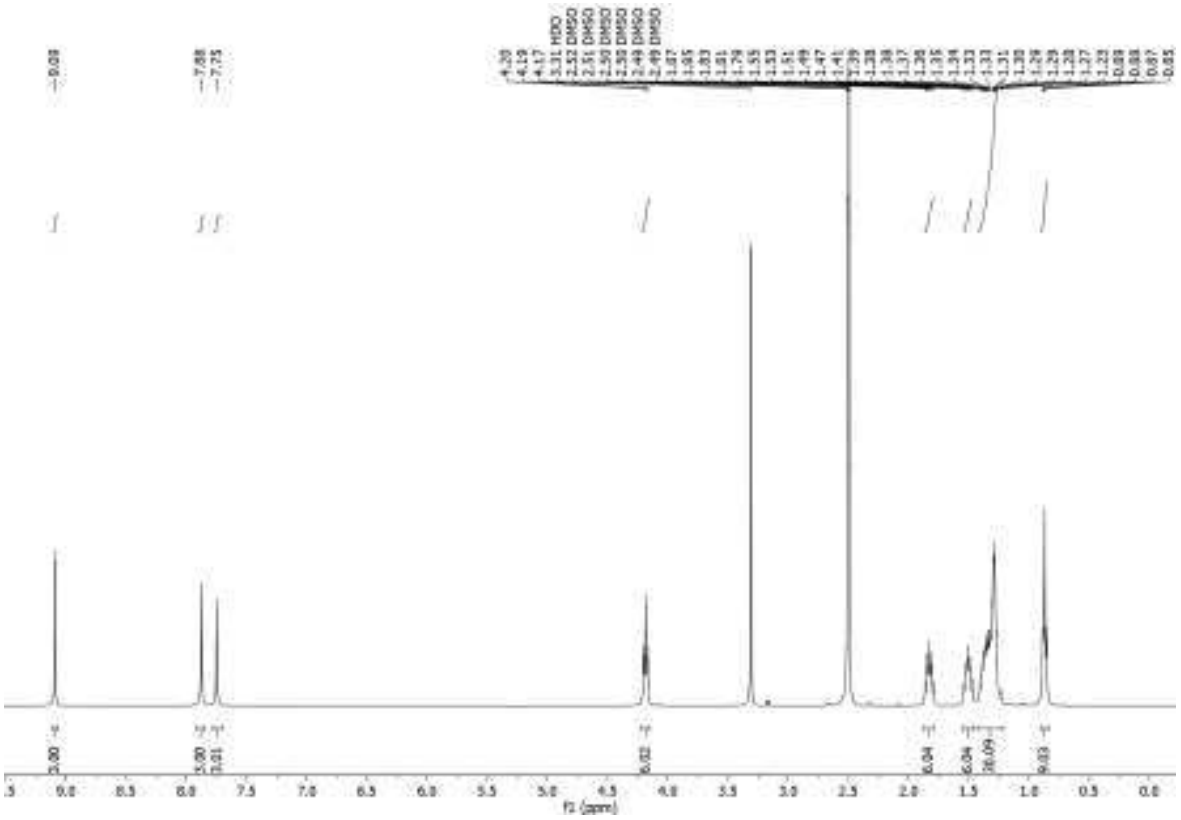

Figure XVII: ^{1}H NMR of molecule **30b**.

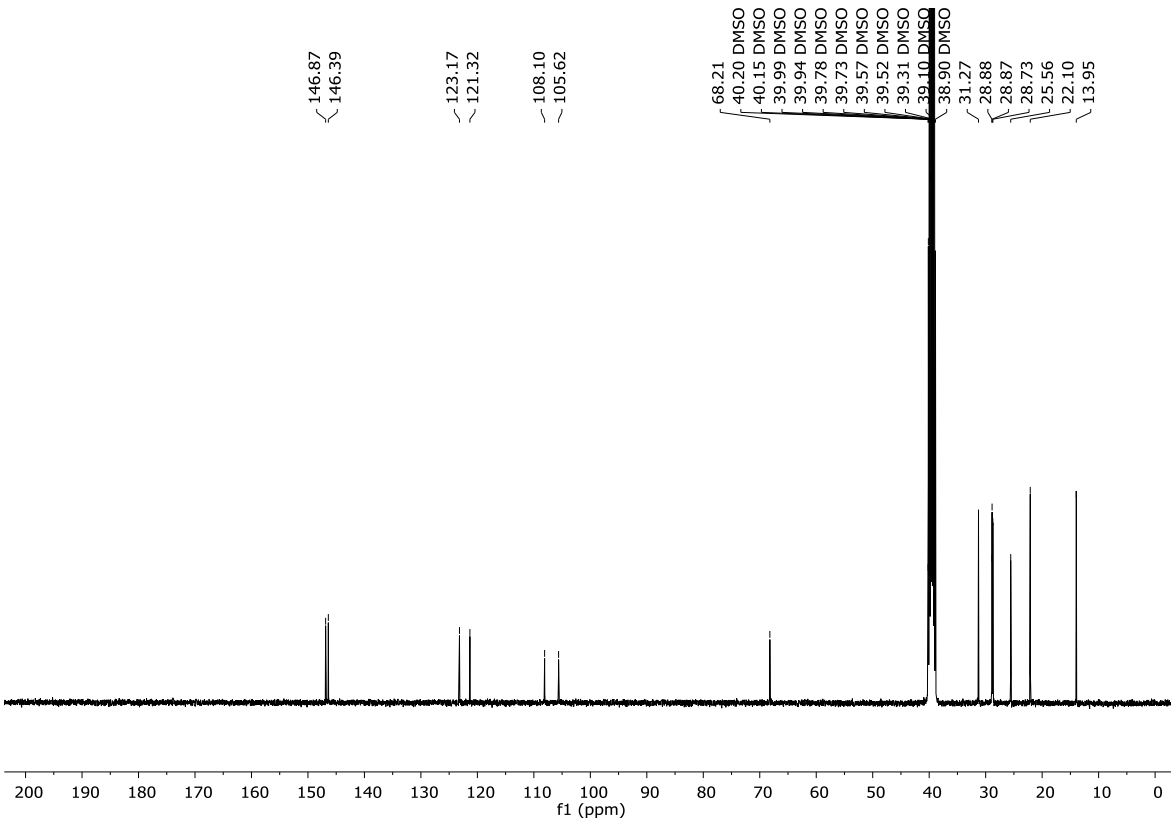

Figure XVIII: ^{13}C NMR of molecule **30b**.

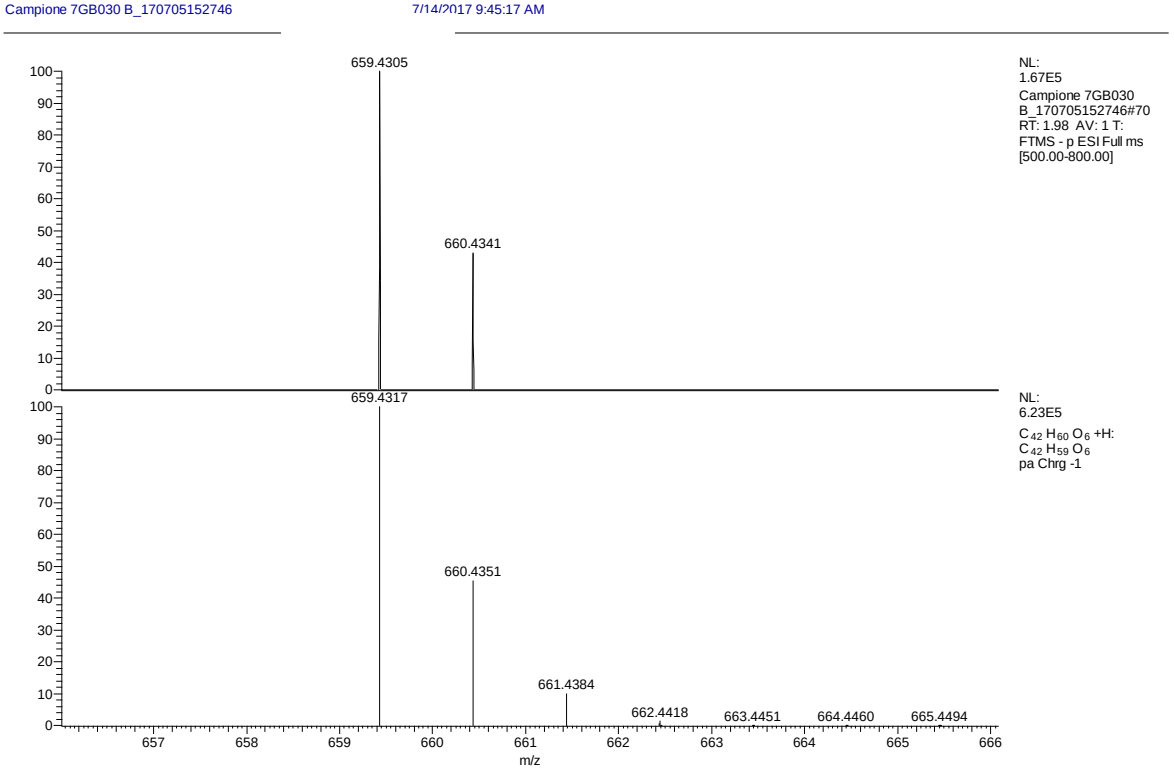

Figure XIX: ESI-HRMS of molecule **30b**.

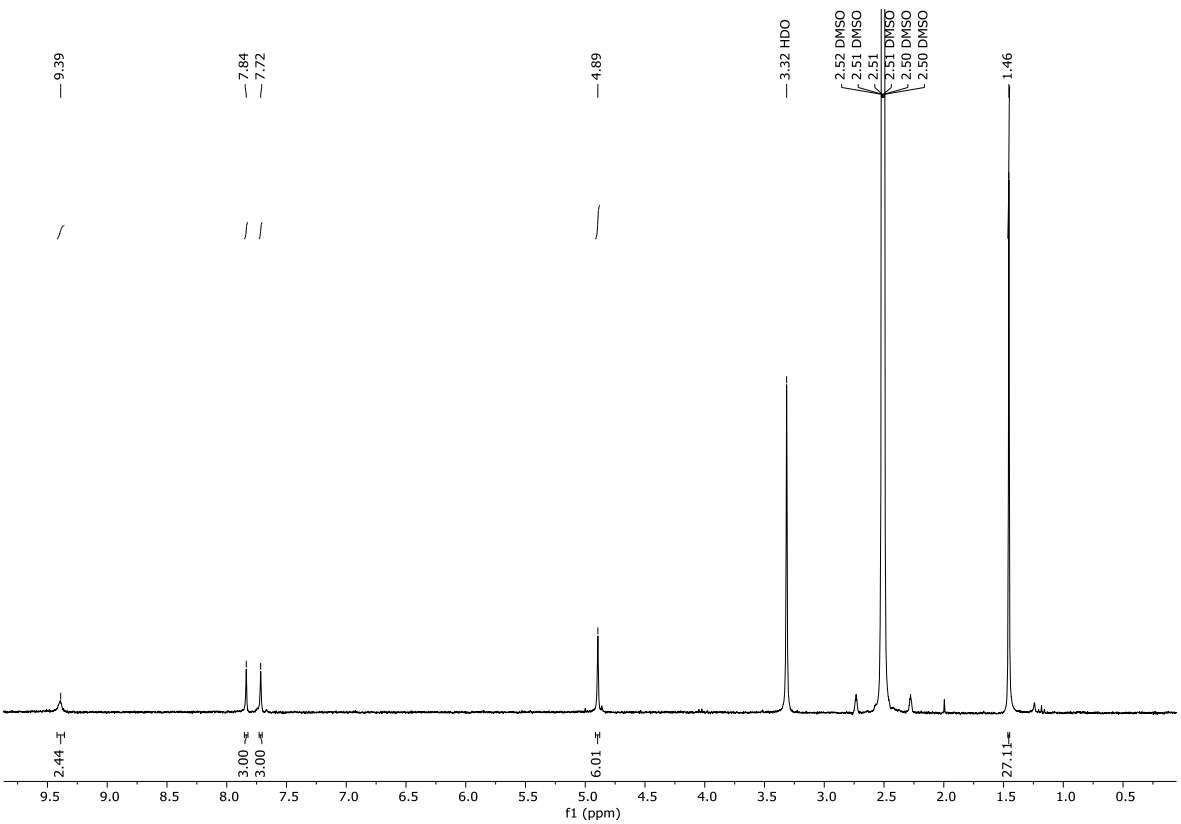

Figure XX: ^{1}H NMR of molecule **31b**.

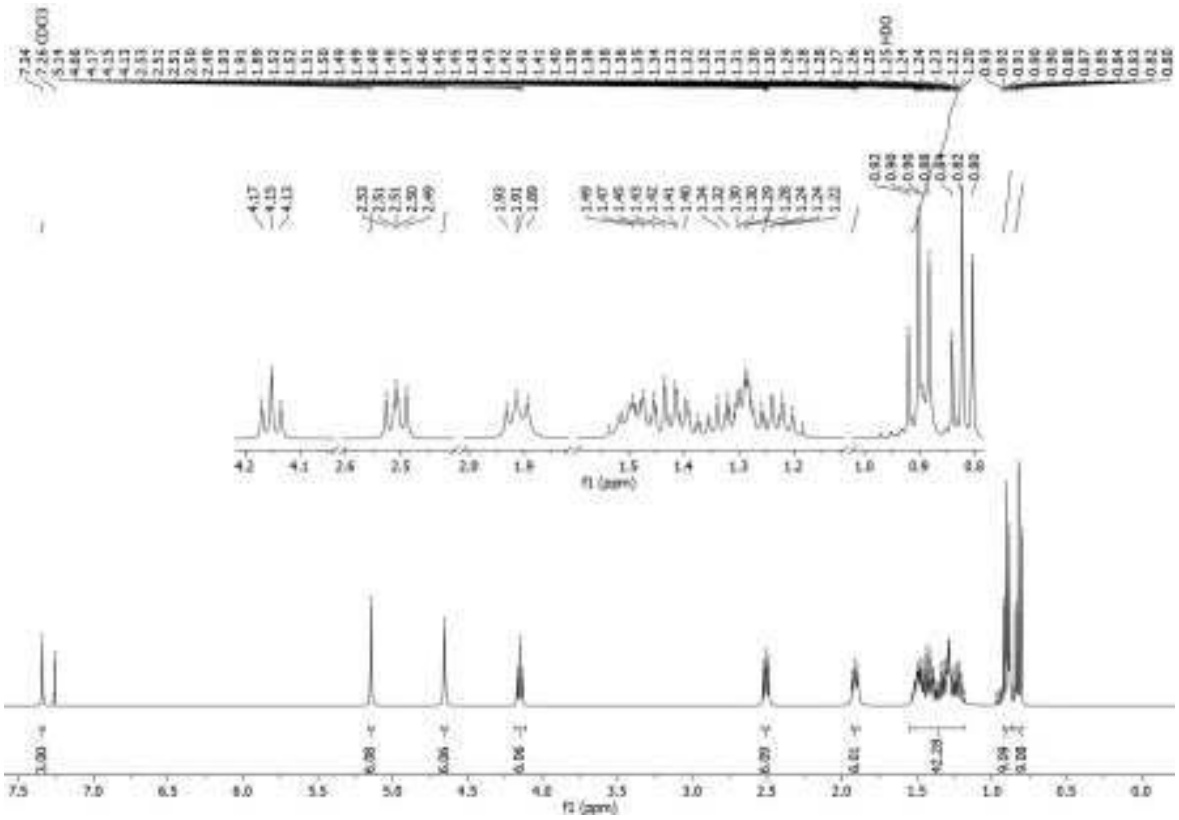

Figure XXI: ^{1}H NMR of molecule **32a**.

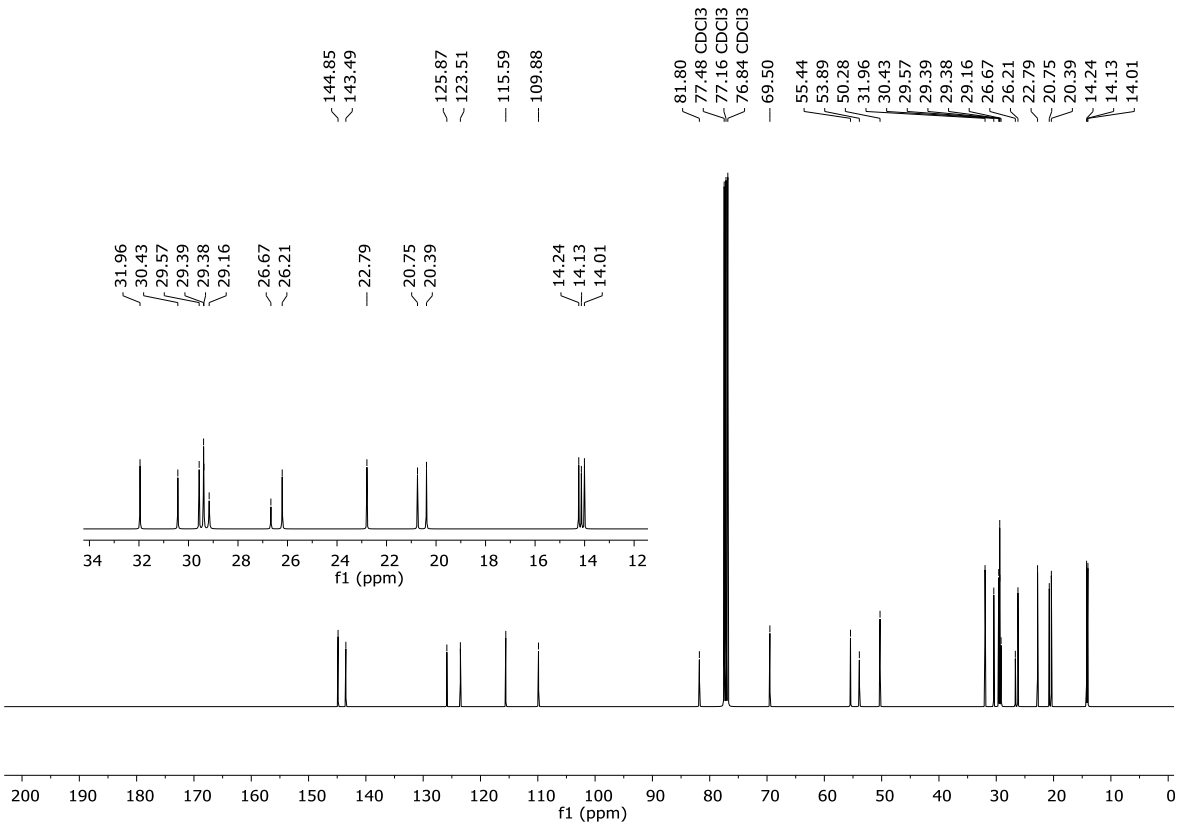

Figure XXII: ^{13}C NMR of molecule **32a**.

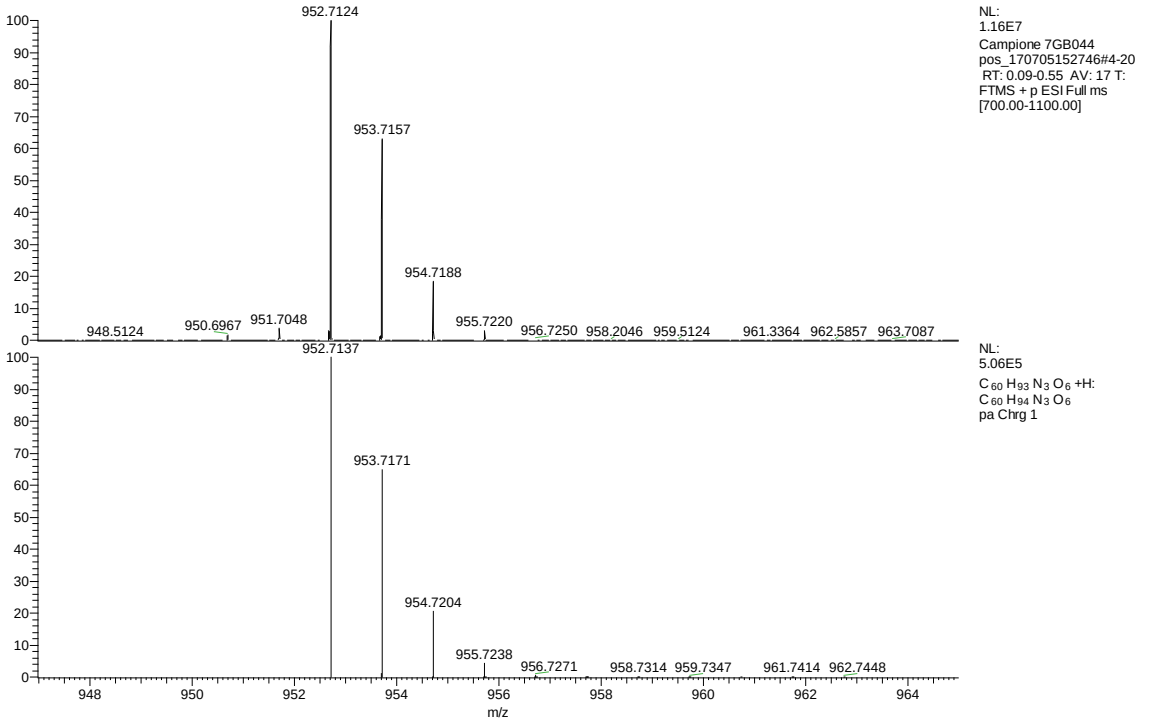

Figure XXIII: ESI-HRMS of molecule **32a**.

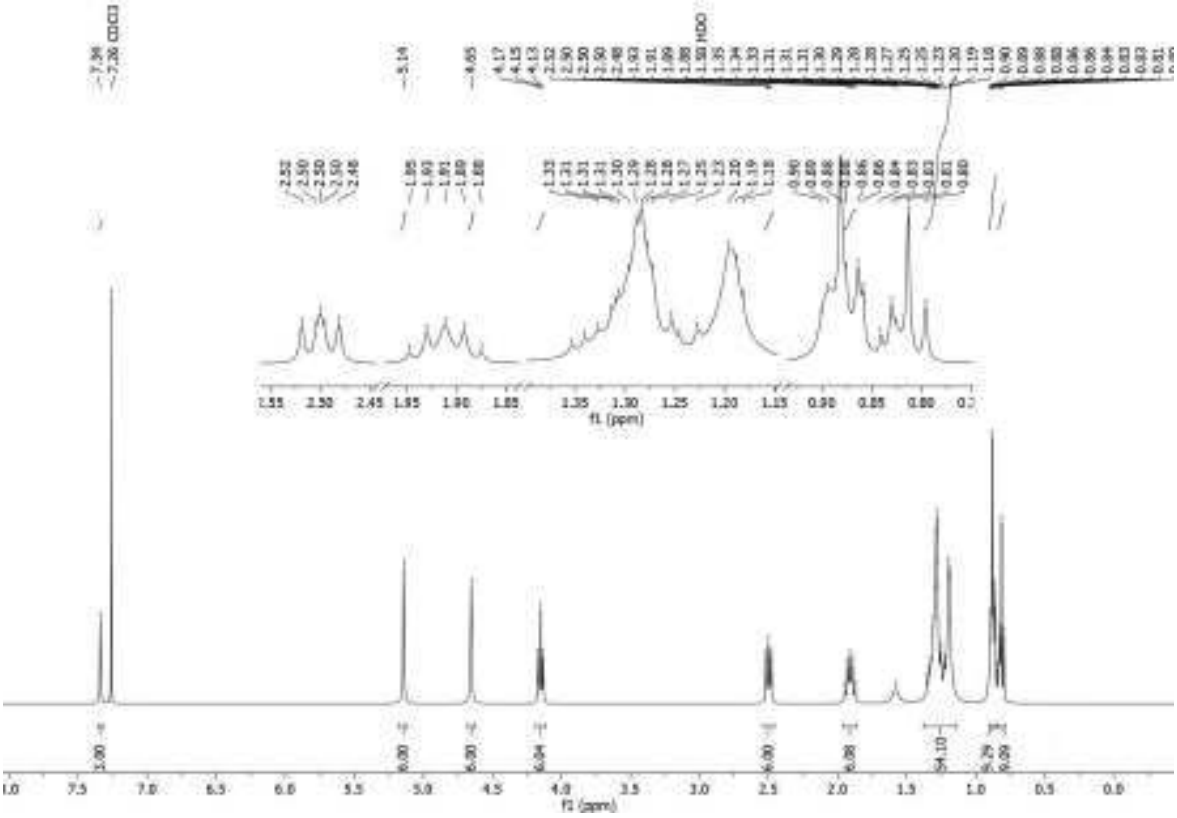

Figure XXIV: ^{1}H NMR of molecule **32b**.

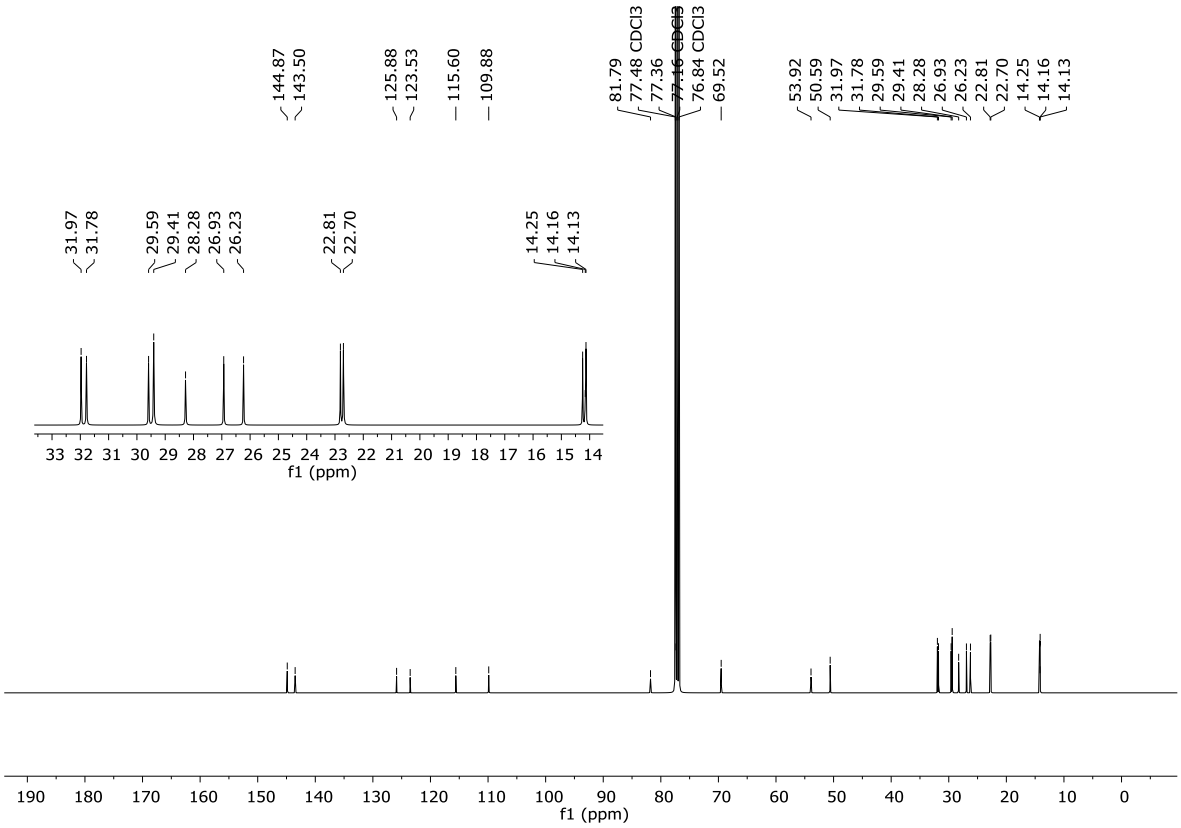

Figure XXV: ^{13}C NMR of molecule **32b**.

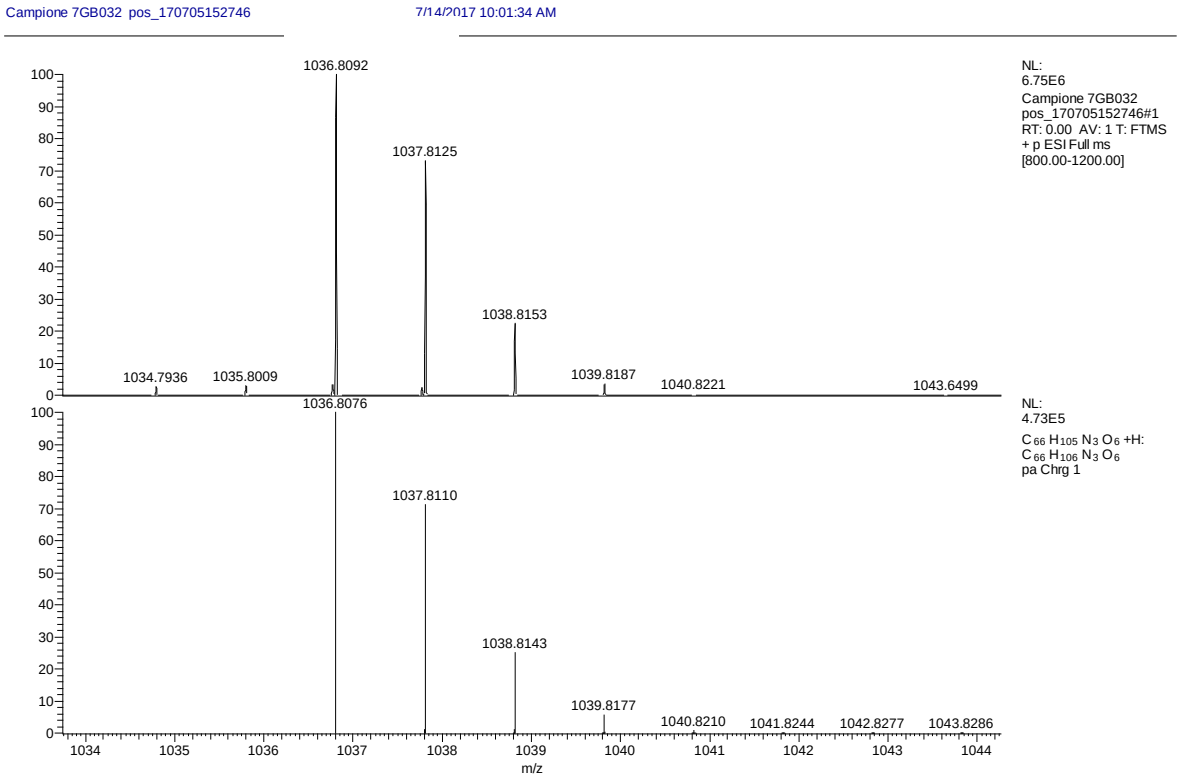

Figure XXVI: ESI-HRMS of molecule **32b**.

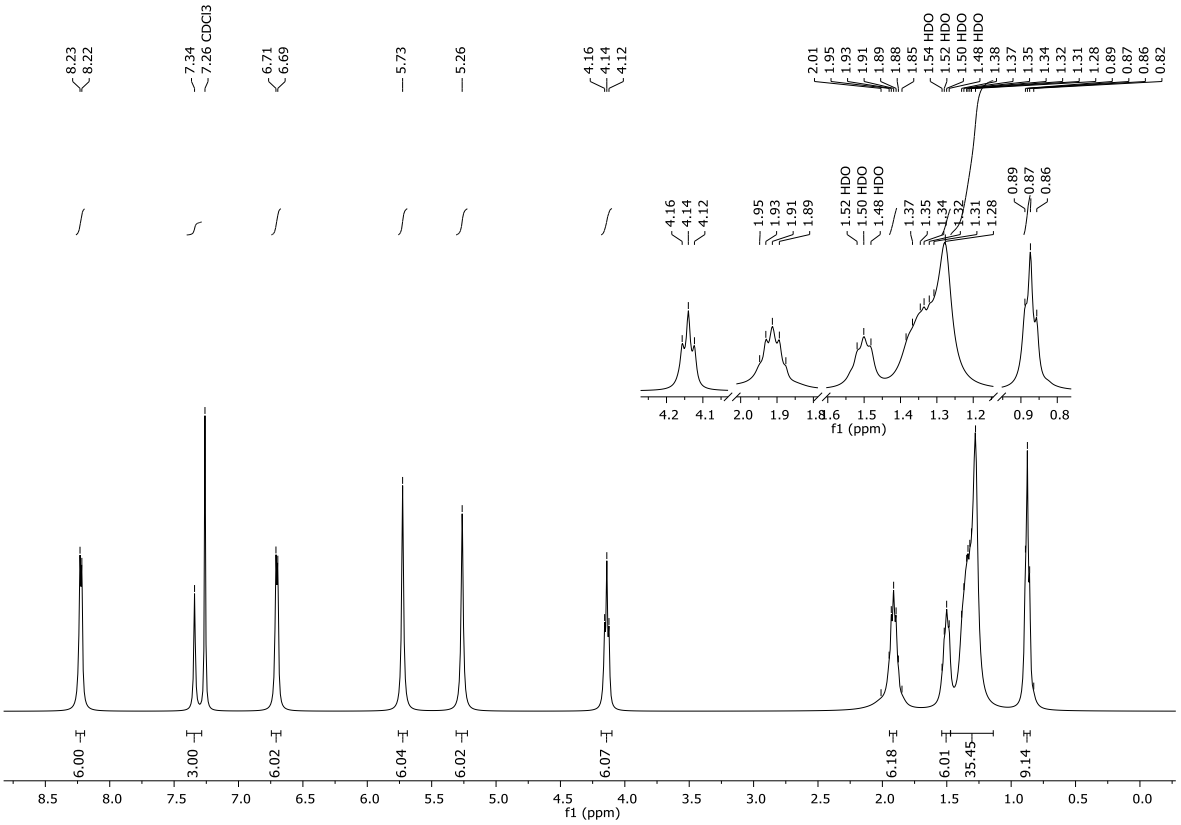

Figure XXVII: ^{1}H NMR of molecule **32d**.

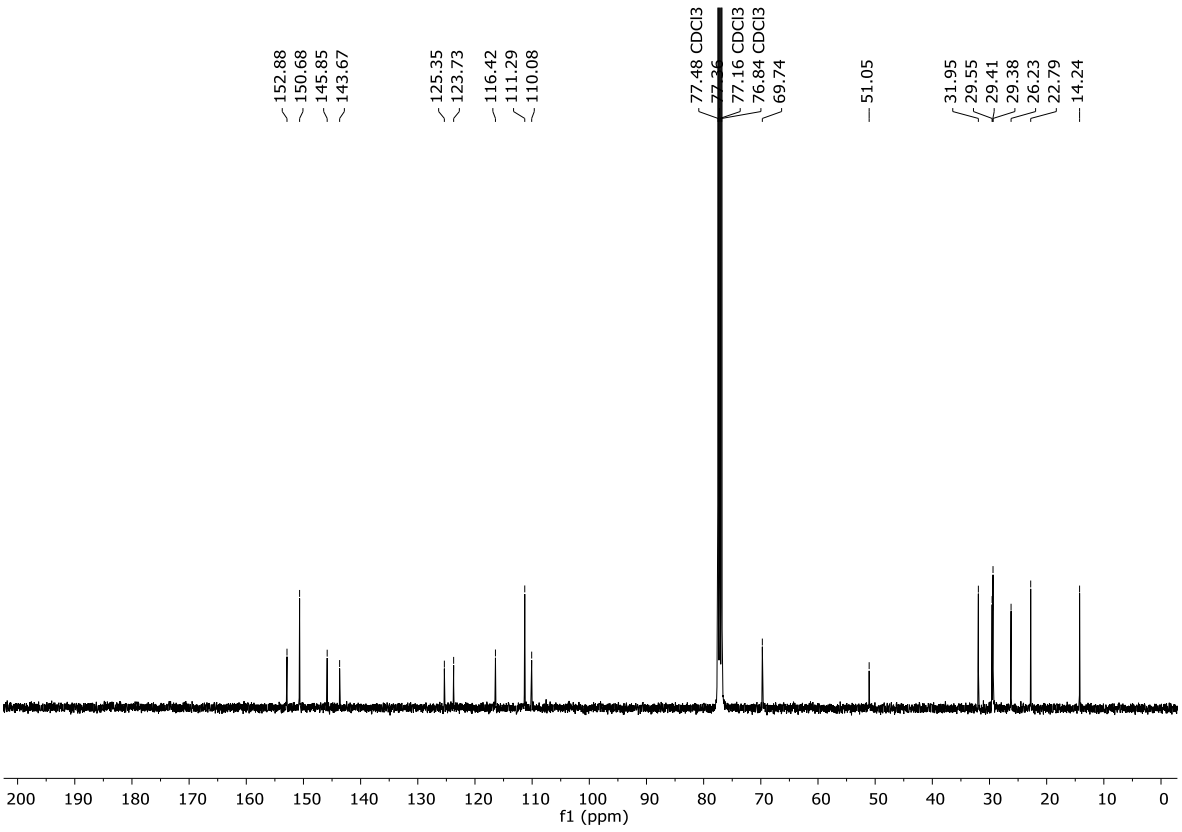

Figure XXVIII: ^{13}C NMR of molecule **32d**.

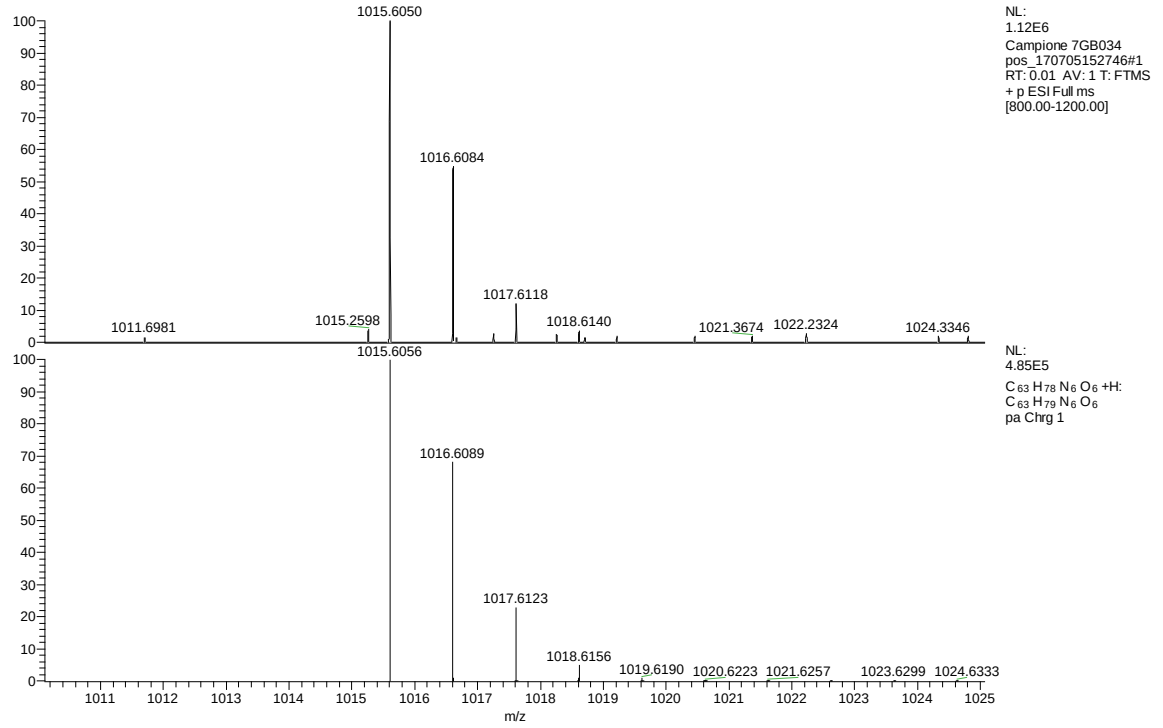

Figure XXIX: ESI-HRMS of molecule **32d**.

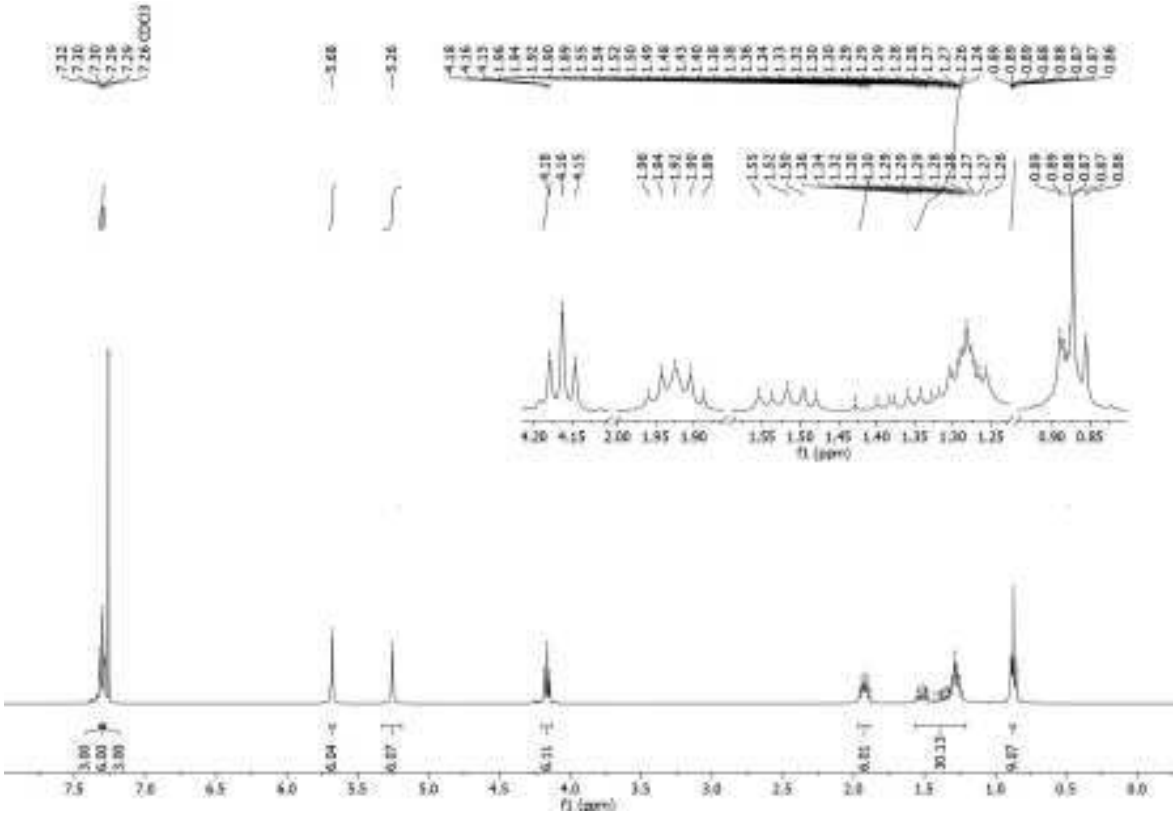

Figure XXX: ^{1}H NMR of molecule **32c**.

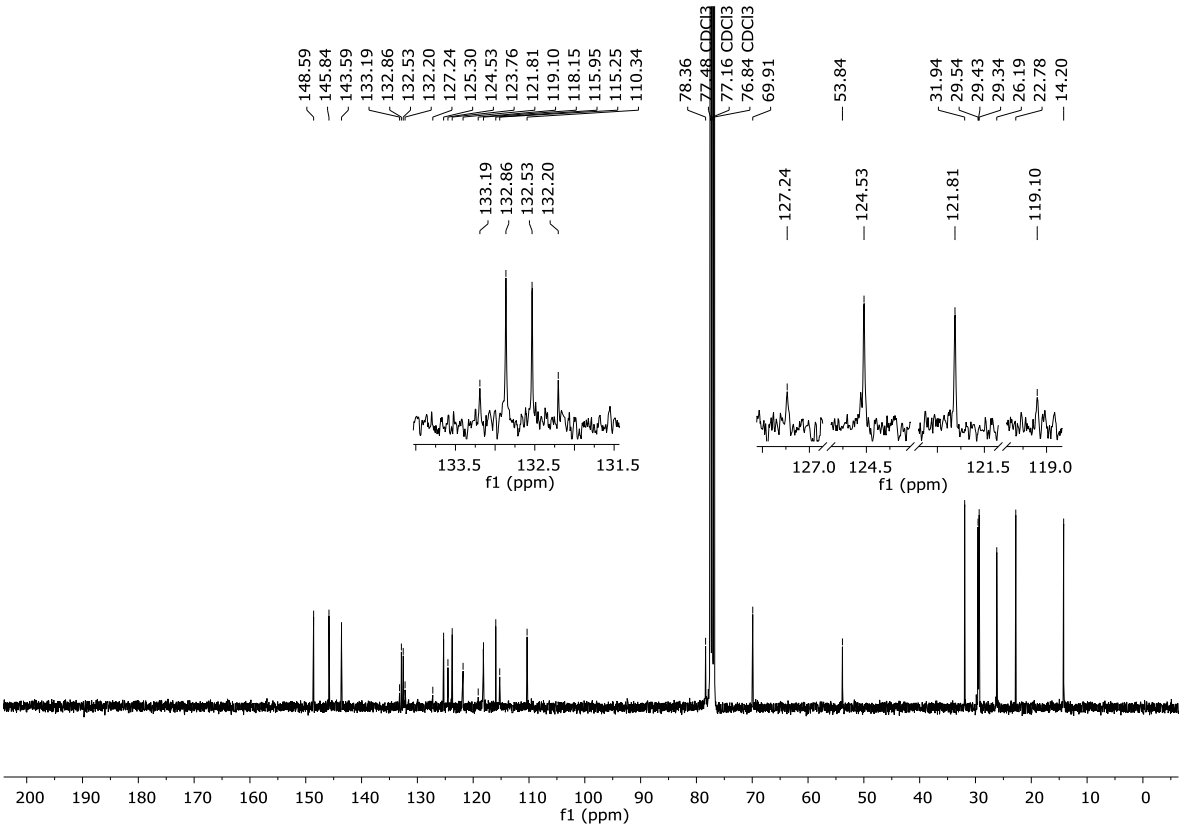

Figure XXXI: ^{13}C NMR of molecule **32c**.

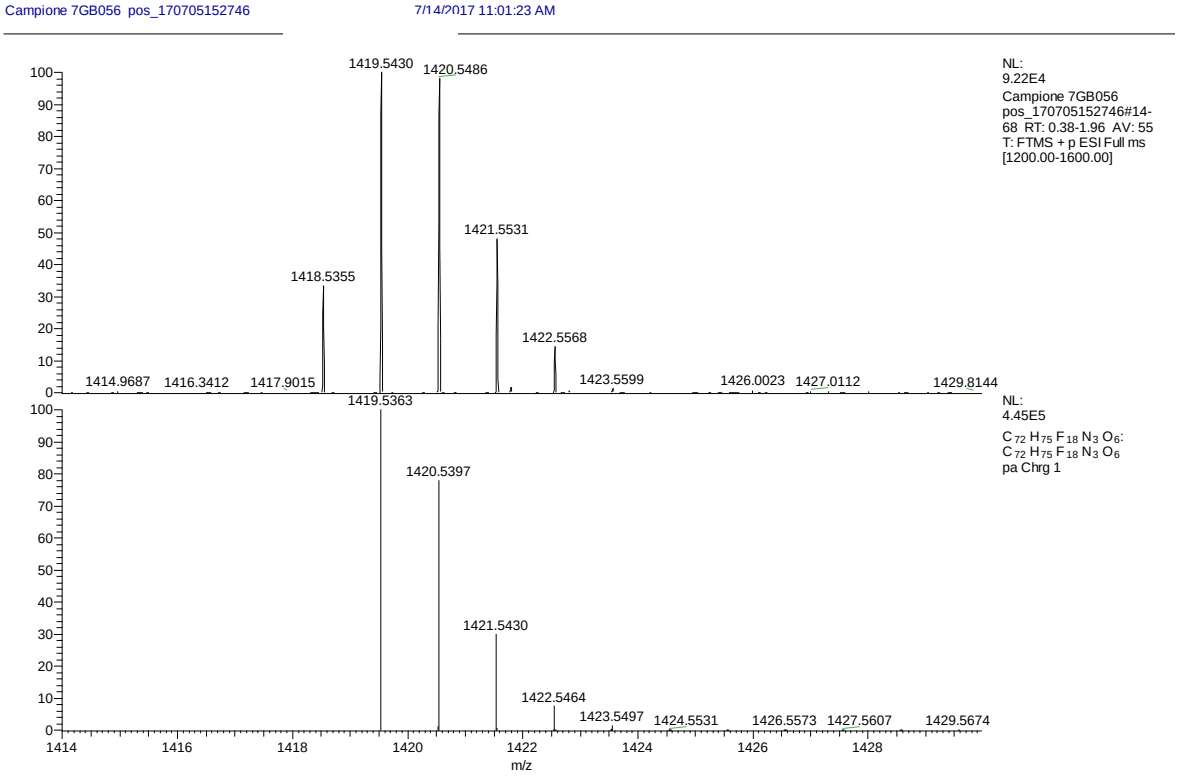

Figure XXXII: ESI-HRMS of molecule **32c**.

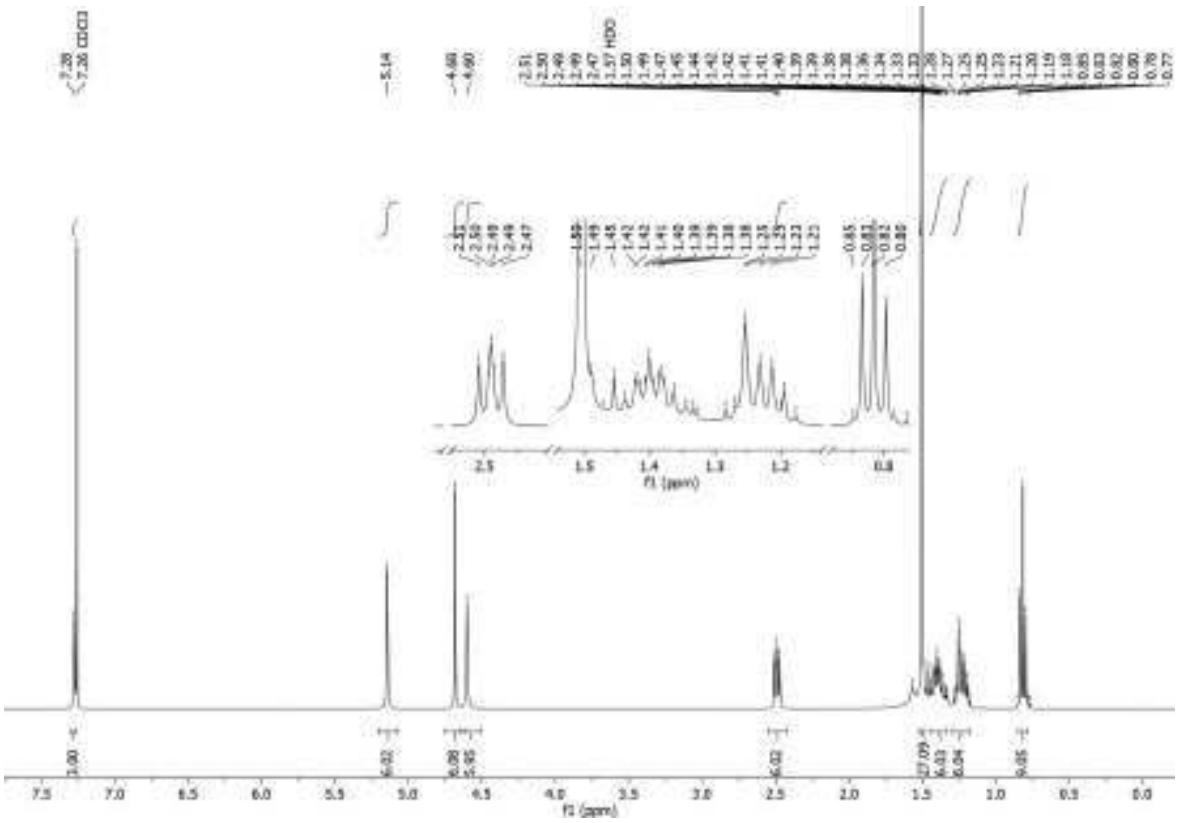

Figure XXXIII: ^{1}H NMR of molecule **33a**.

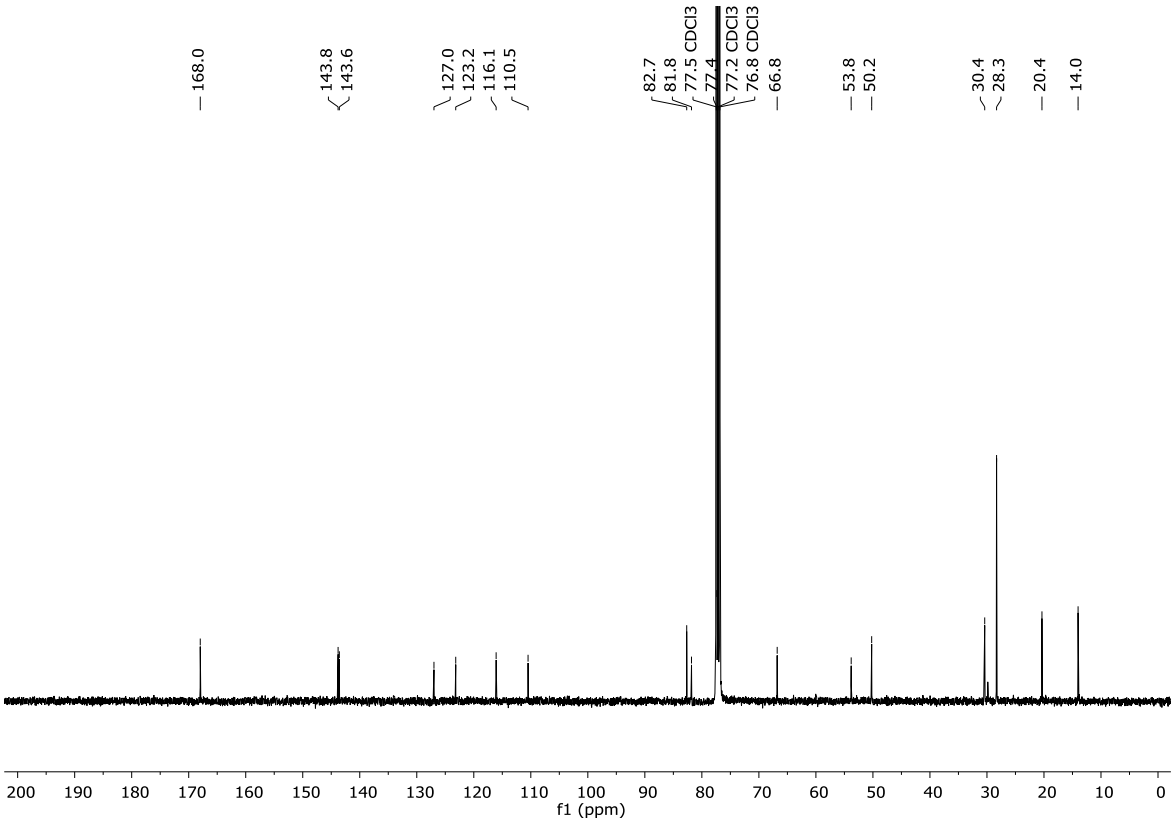

Figure XXXIV: ^{13}C NMR of molecule **33a**.

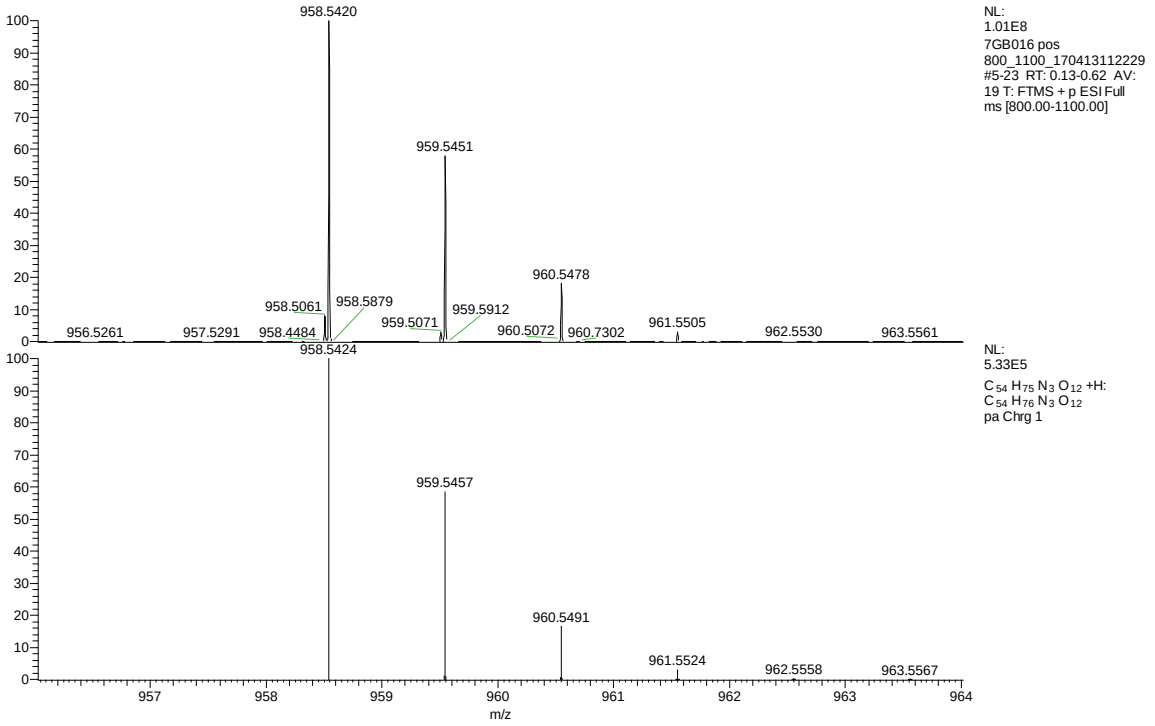

Figure XXXV: ESI-HRMS of molecule **33a**.

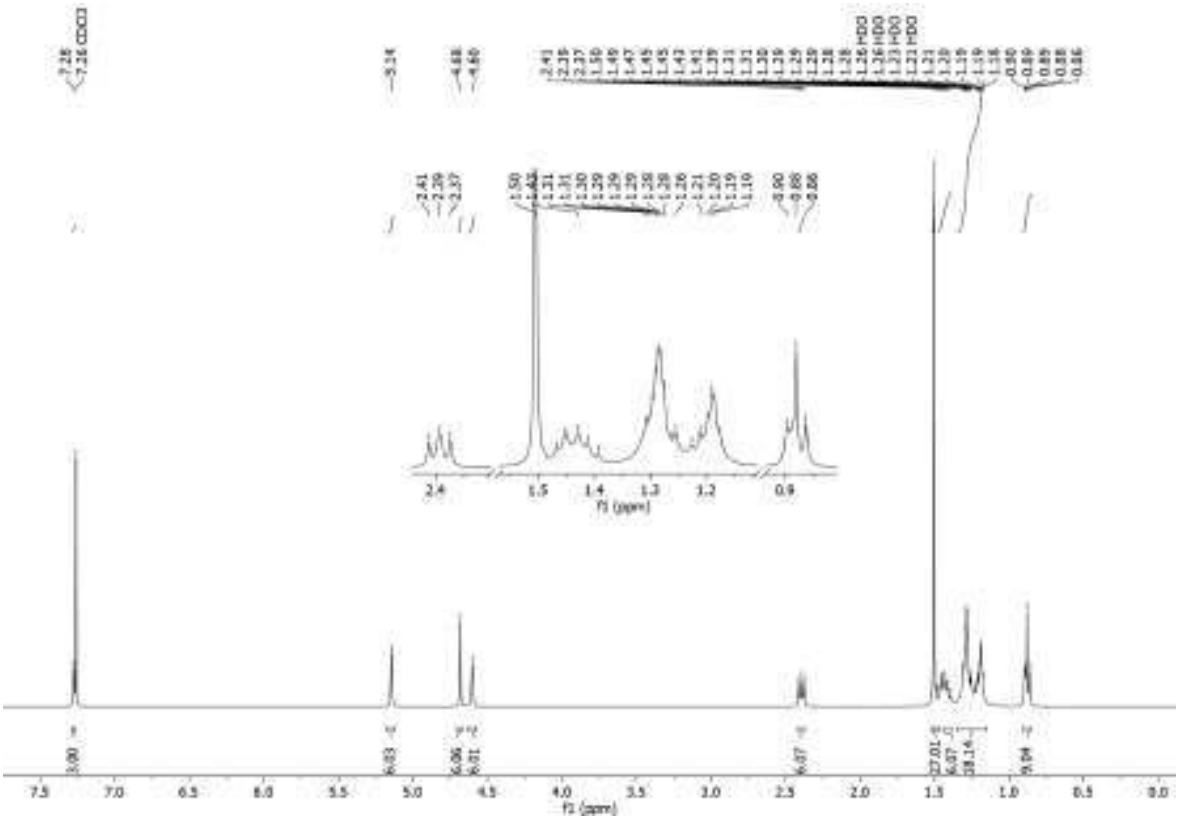

Figure XXXVI: ^{1}H NMR of molecule **33b**.

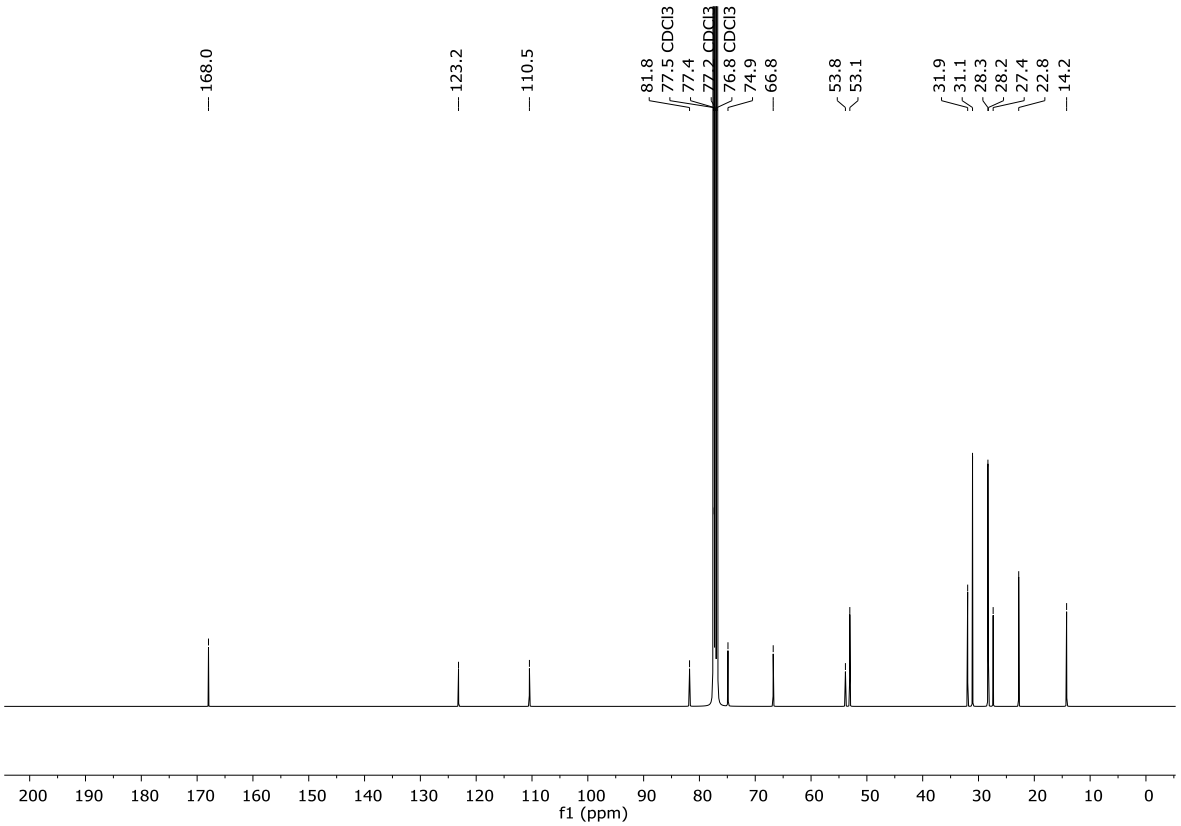

Figure XXXVII: ^{13}C NMR of molecule **33b**.

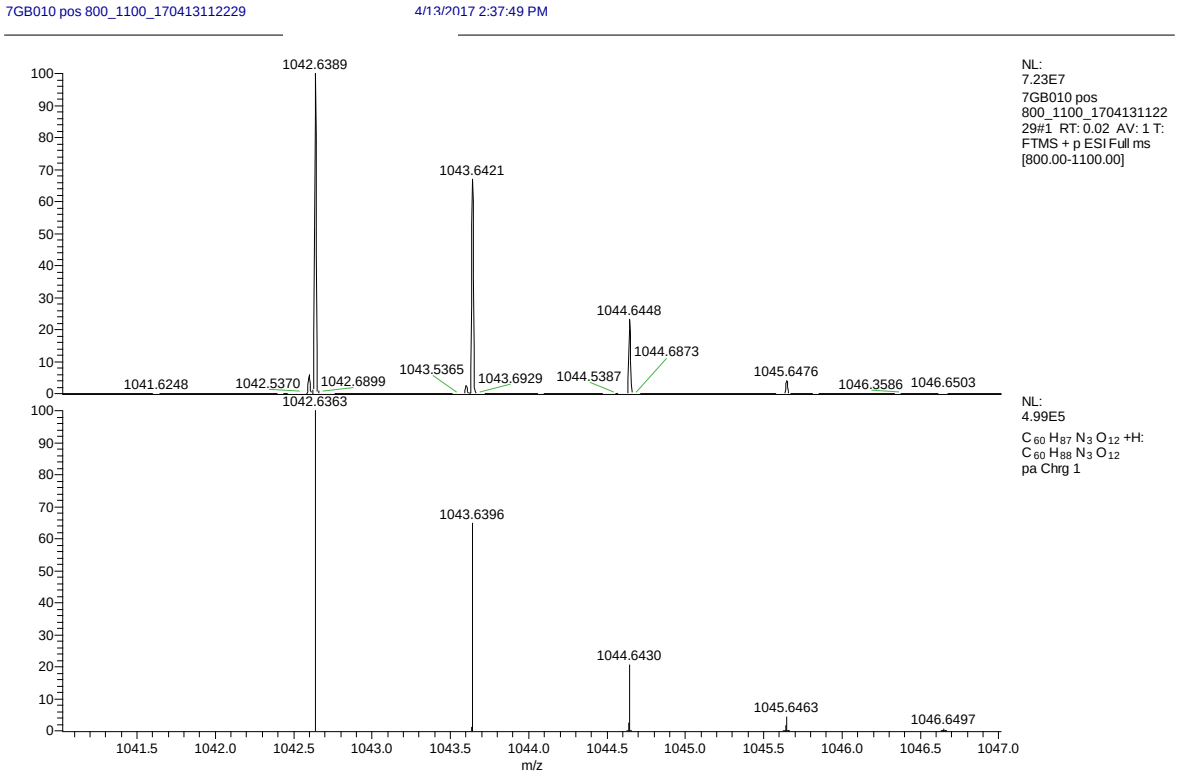

Figure XXXVIII: ESI-HRMS of molecule **33b**.

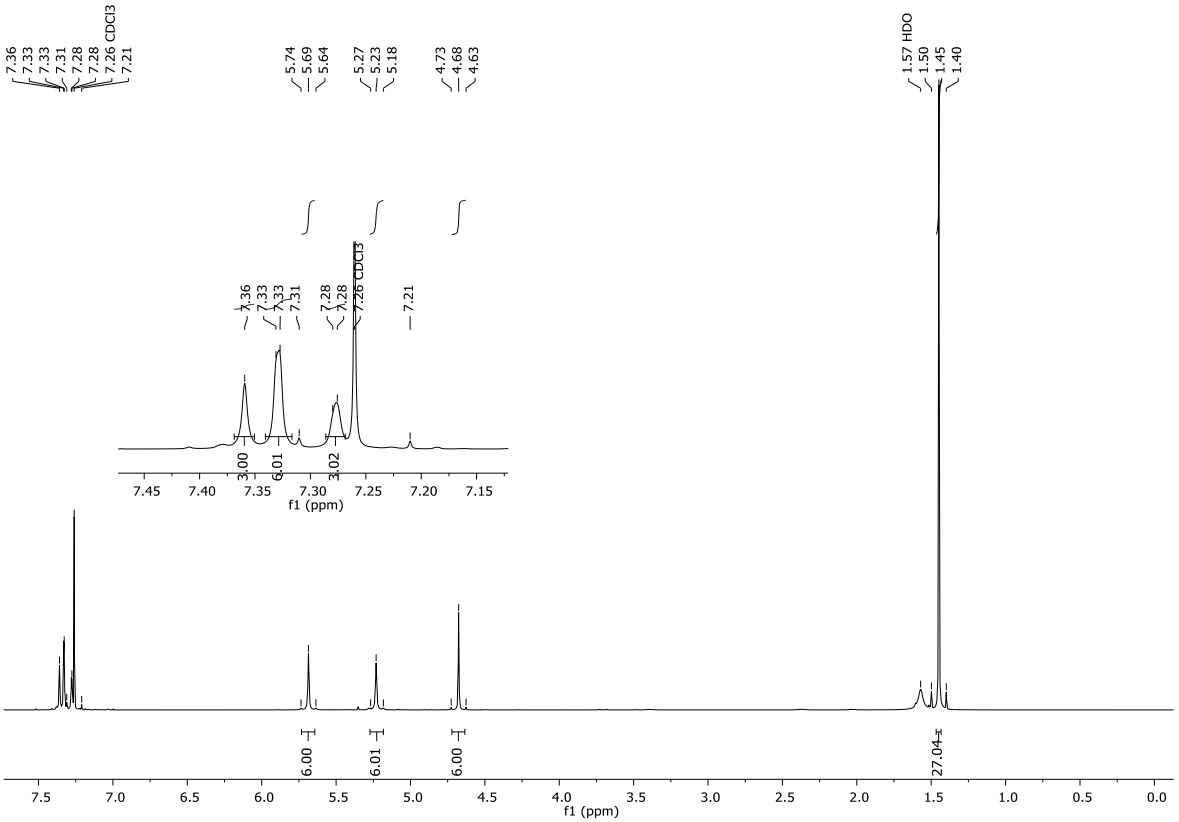

Figure XXXIX: ^{1}H NMR of molecule **33c**.

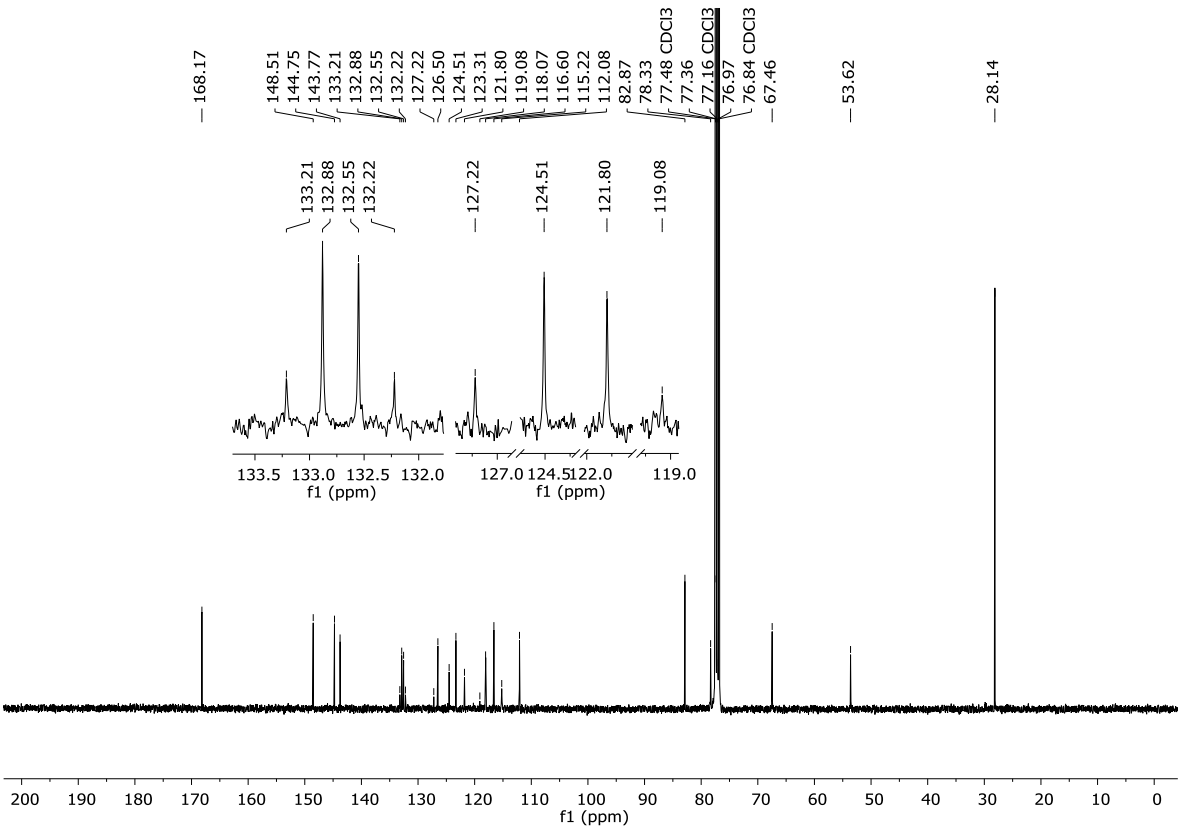

Figure XL: ^{13}C NMR of molecule **33c**.

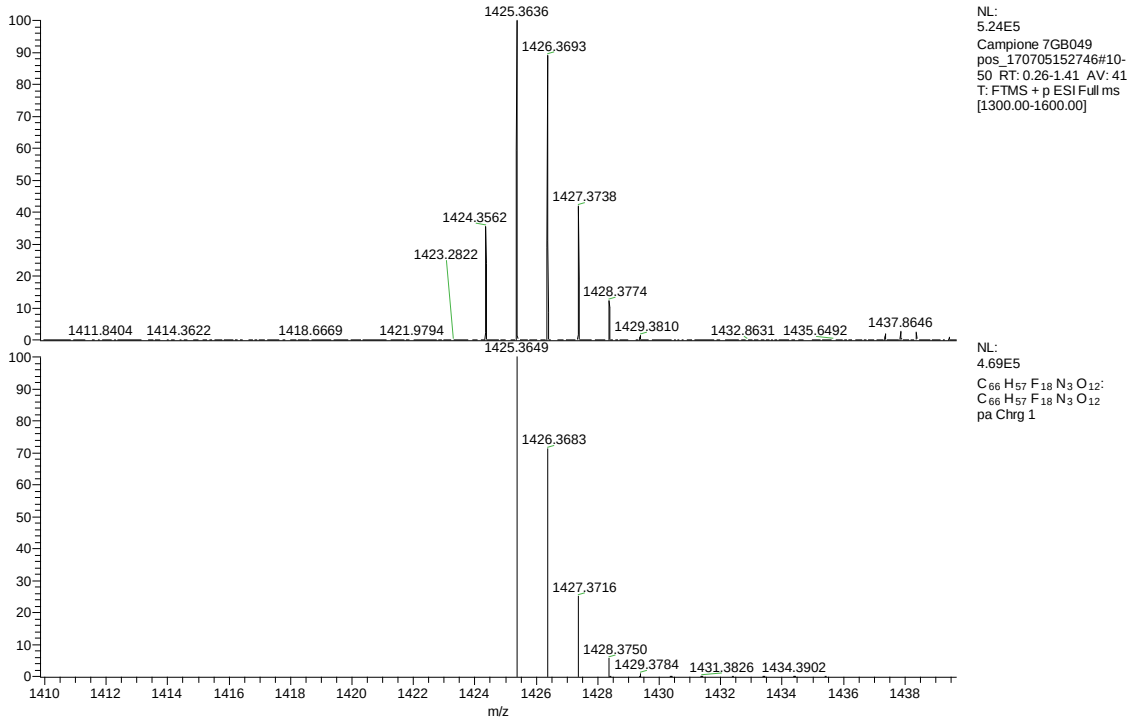

Figure XLI: ESI-HRMS of molecule **33c**.

2.6 Bibliography

1 L. Schmidt-Mende, A. Fechtenkotter, K. Mullen, E. Moons, R. H. Friend, J. D. MacKenzie, *Science*, **2001**, *293*, 1119-1122.

2 Y. Shimizu, K. Oikawa, K. Nakayama, D. Guillon, *J. Mater. Chem.*, **2007**, *17*, 4223–4229.

3 T. Hassheider, S. A. Benning, H. S. Kitzerow, M. F. Achard, H. Bock, *Angew. Chem. Int. Ed.* **2001**, *40*, 2060-2063; *Angew. Chem*., **2001**, *113*, 2119-2122.

4 L. Mosca, J. Ĉejka, B. Dolenský, M. Havlĵk, M. Jakubek, R. Kaplánek, V. Král, P. Anzenbacher, *Chem. Commun.*, **2016**, *52*, 10664-10667.

5 A. Roy, D. Saha, A. Mukherjee, P. Talukdar, *Org. Lett.*, **2016**, *18*, 5864-5867.

6 A. W. Kawaguchi, A. Sudo, T. Endo, *Polymer Chemistry*, **2014**, *52*, 10, 1448-1457.

7 P. T. Wright, I. Gillies, J. D. Kilburn, *Synthesis*, **1997**, *9*, 1007-1009.

8 G. Berton, G. Borsato, R. Zangrando, A. Gambaro, F. Fabris, A. Scarso, *Org. Chem. Front.*, **2018**, *5*, 2458-2462.

9 B. Liu, D. Shi, Y. Yang, D. Liu, M. Li, E. Liu, X. Wang, Q. Zhang, M. Yang, J. Li, X. Shi, W. Wang, J. Wei *Eur. J. Org. Chem.*, **2018**, 869-873.

10 W. L. F. Armarego, C. Chai in *Purification of Laboratory Chemicals (Seventh Edition)*, Butterworth-Heinemann, Boston, **2013**.

11 W. C. Still, M. Kahn, A. Mitra, *J. Org. Chem.*, **1978**, *14*, 2923-2925.

3 Other Derivatizations on the Triphenylenic Core

Since new methods of derivatizations could lead to molecules with interesting properties, we decided to continue the work on triphenylenic CH derivatization, focusing our efforts on formylation and aminomethylation reactions, aiming at the obtainment of a chiral *O*-alkyl substituted sumanene, a class of molecule never reported before in the literature so far (Scheme 1).

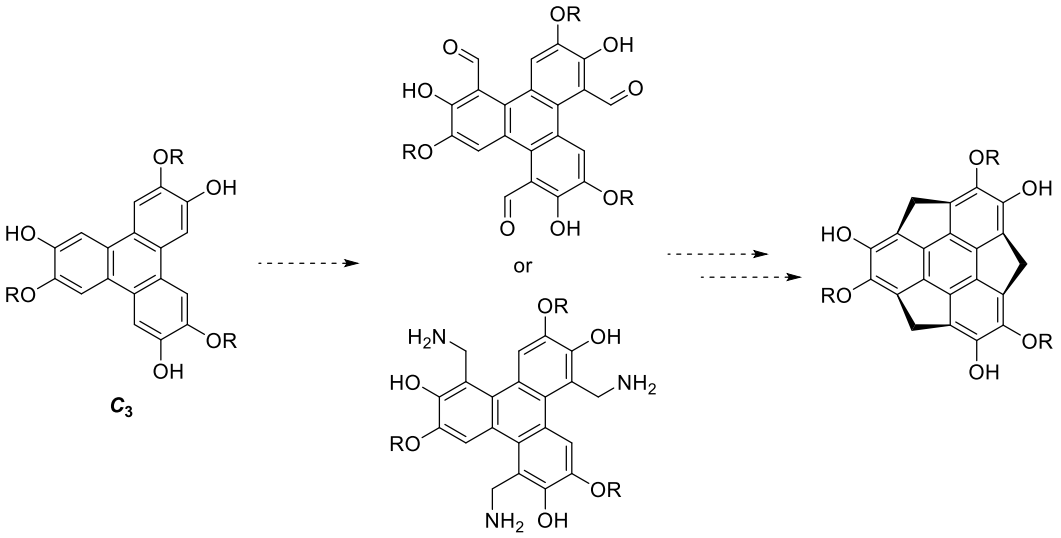

Scheme 1: Proposed synthetic pathway for *O*-alkyl substituted sumanenes.

Sumanene is a highly desirable synthetic target, since this molecule is the smallest curved unit of C_{60} fullerene, and its actual synthesis is rather complicated (Scheme 2).[1]

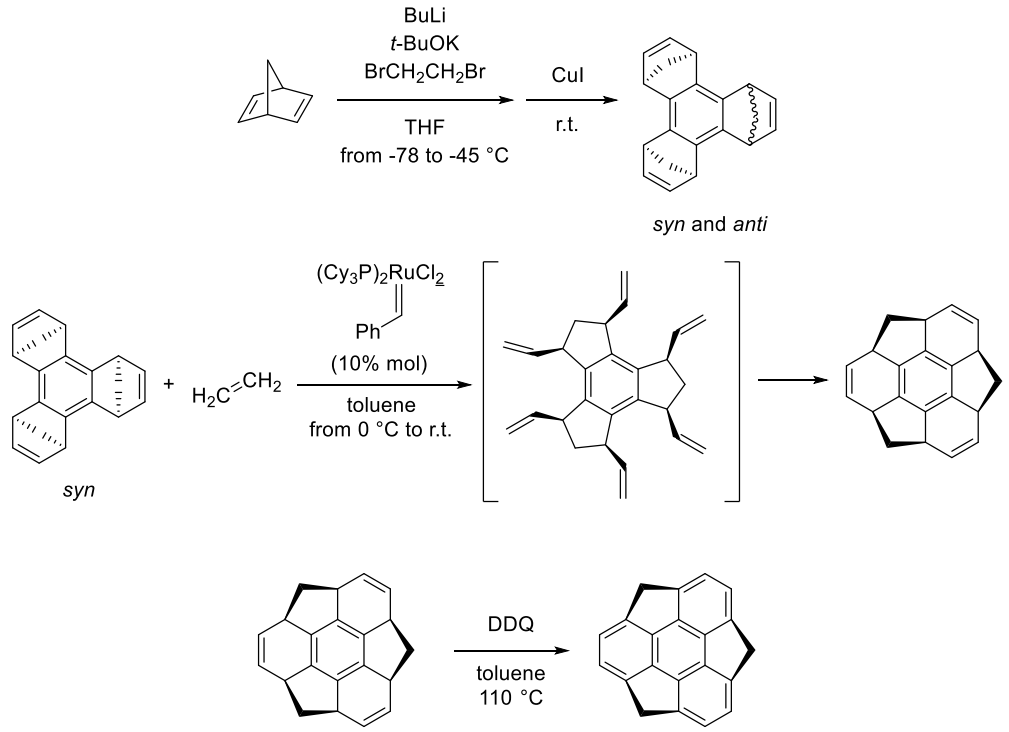

Scheme 2: Actual synthesis of sumanene.

Sumanene can stabilize reactive species such as radicals, carbenes and ions,[2] and its X-ray structure shows how the molecule are assembled in pillars in the solid phase,[2] with the

convex part matching with the concave, making the crystals feasible as charge carriers. This molecule has also been used as ligand for ferrocene,[2] but for what concerns us, it can be interesting just for its concave shape, useful for the synthesis of supramolecular capsules and cages.

3.1 Formylation of the C_3 Compound

The first strategy for the obtainment of *O*-alkyl substituted sumanene was the formylation of one of the obtained C_3-symmetric triphenylene in the *ortho* position with respect of the phenolic group, in order to obtain a formyl unit to be used in a ring closure reaction, having the other side of the triphenylene nucleophilically attaching the carbonyl in an intermolecular Friedel-Craft like reaction (Scheme 3).

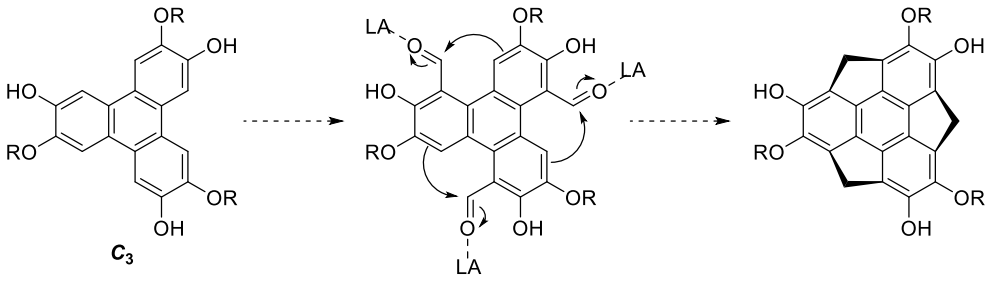

Scheme 3: Generic synthetic route to *O*-alkyl substituted using formylated compounds.

Several trials with different strategies were carried out in order to achieve this objective.

3.1.1 Direct formylation reactions

For the first formylation attempts, a Duff reaction was performed treating the substrate ***C*$_3$-26** with 1,3,5,7-tetraazaadamantane in a 1:1 mixture of acetic and trifluoroacetic acid, at 130 °C for 3 hours (Scheme 4).[3]

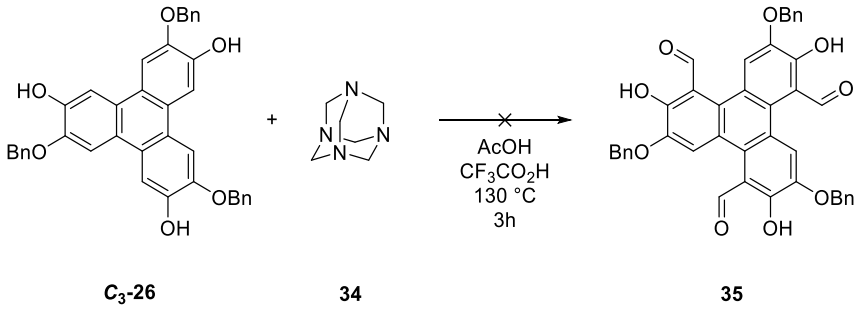

Scheme 4: Duff reaction on compound ***C*$_3$-26**.

The reaction did not provide the desired product, and further trials with different solvent systems such as acetic acid/toluene[4] or acetic acid/DMF,[5] trying also with the addition of paraformaldehyde,[6] did not work. Since the liability of the benzylic unit could be the problem, we decided to move to a more resilient substrate, **8**, obtained by methylation and de-benzylation of ***C*$_3$-26**, as seen in the previous Chapter 2 (Scheme 5).

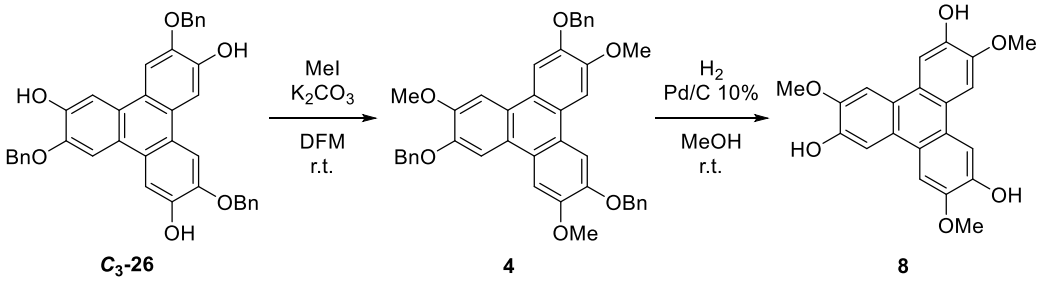

Scheme 5: Alkylation of ***C*$_3$-26** with methyl iodide and de-benzylation of **4** to obtain **8**.

While methylation reaction afforded the desired product **4** with an 89% yield, for the de-benzylation the yield was lower due to the low solubility of the product, that was recovered after a week by solid-liquid extraction with AcOEt in a 74% yield.

The obtained molecule **8** was subjected to the same Duff reaction conditions used for ***C*$_3$-26**, but without a positive response.

We then moved to another reaction, treating **8** with paraformaldehyde, magnesium(II) chloride and triethylamine, in THF, under reflux (Scheme 6).[7]

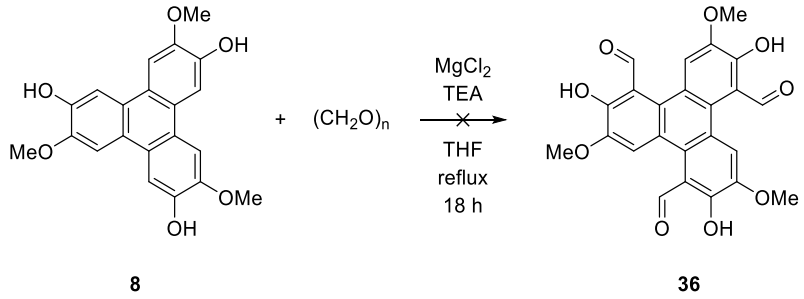

Scheme 6: Formylation reaction of **8** with paraformaldehyde, $MgCl_2$ and TEA.

Even after refluxing overnight, the reaction did not take place, allowing only to recover **8** untamed. Other two attempts for the reaction were carried out using toluene or ACN as solvents, but the result was always the same.

Due to solubility problems of **8**, we decided to synthesize another C_3 compound, more resilient than ***C*$_3$-26** but at the same time more soluble than **8**. ***C*$_3$-26** was treated with dodecyl bromide and debenzylated, following the usual procedure (Scheme 7).

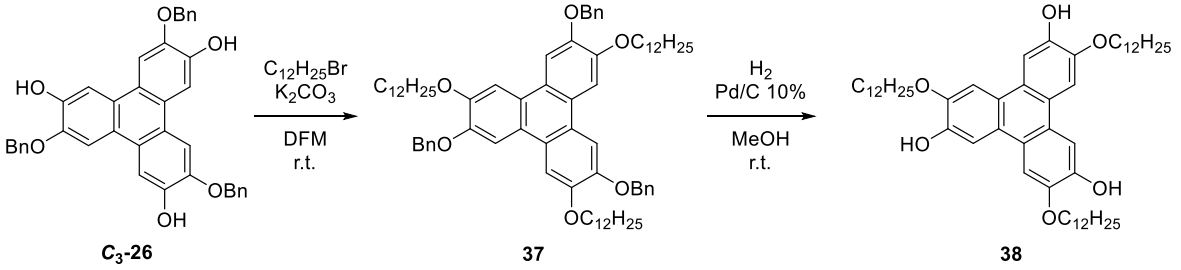

Scheme 7: Alkylation of ***C*$_3$-26** with dodecyl bromide and de-benzylation of **37** to obtain **38**.

Molecule **37** was obtained with a 90% yield, while **38** with a 93% yield. Subsequently, a Rieche reaction was performed on **38**, treating with dichloro(methoxy)methane and titanium(IV) chloride, in DCM (Scheme 8).[8]

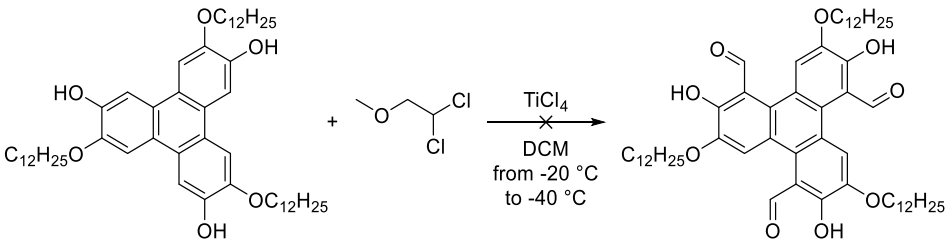

38 39 40

Scheme 8: Rieche reaction on substrate **38**.

The reaction conditions demonstrated to be too harsh for substrate **38**, which was completely converted without affording the desired product.

Last trial was done attempting a Vilsmeier reaction, always on **38**, by treatment with phosphoryl trichloride in DMF, first at 0 °C then at 70 °C for one hour (Scheme 9).[9]

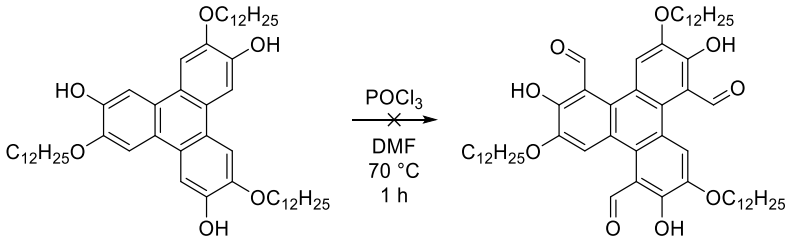

38 40

Scheme 9: Vilsmeier reaction on substrate **38**.

Again, the reaction did not occur, leaving the substrate **38** mostly untouched. Consequently, this synthetic pathway consisting in direct formylation of C_3 triphenylene derivatives was abandoned.

3.1.2 Formylation through rearrangement

With the failure of the direct formylation, we tried a different strategy, using the free hydroxyl units on ***C*$_3$-26** to create a formyl ester that could rearrange in a Fries-like reaction, leading to the migration of thee carbonyl unit in the *ortho* position (Scheme 10).

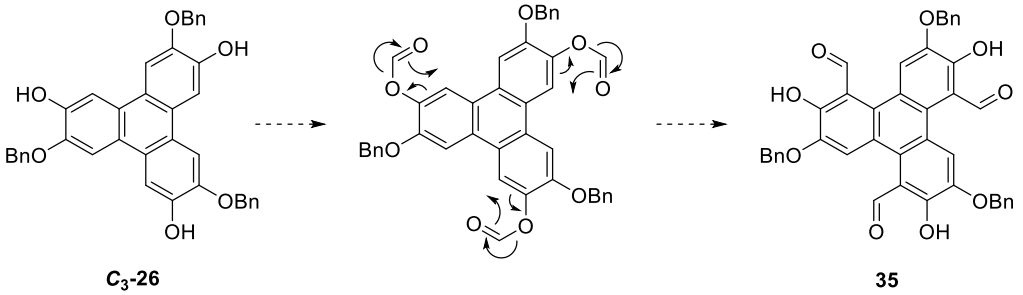

***C*$_3$-26** **35**

Scheme 10: Rearrangement strategy for the obtainment of formylated ***C*$_3$-26**, **35**.

Firstly, the ester was obtained reacting formic acid with acetic anhydride for one hour at 60 °C, in order to obtain the mixed anhydride. The so far obtained anhydride was reacted with ***C*$_3$-26** in DCM, in the presence of pyridine and DMPA at room temperature (Scheme 11).

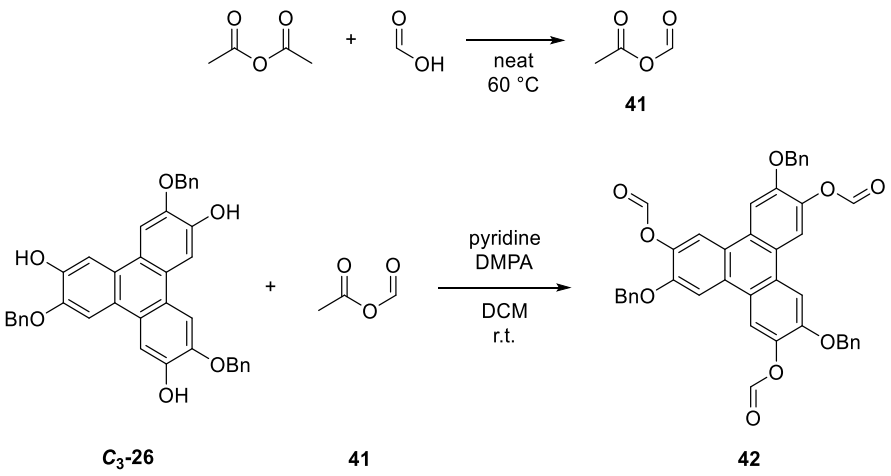

Scheme 11: Synthesis of the formic ester of C_3-**26**, **42**.

After column chromatography, it was possible to isolate the pure **42** in 93% yield.

The rearrangement reactions were all carried out in deuterated chloroform, in order to follow the events directly by ^{1}H NMR spectroscopy. While attempts consisting in heating **42** with or without a Lewis acid like zinc(II) chloride failed, by using methanesulfonic acid as Brønsted acid, we were able to observe the signals of the rearranged product, **35** (Scheme 12).

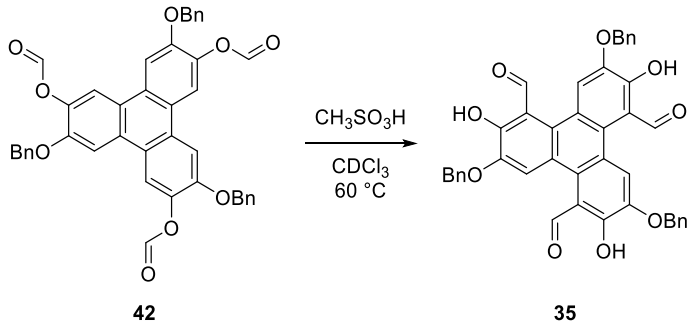

Scheme 12: Fries rearrangement on **42** to obtain the formylated product, **35**.

Unfortunately, any other attempt to continue with this reaction, or to replicate it in a scale larger than an NMR sample, failed and were not reproducible, leading us to abandon this strategy and focus on different methods.

3.2 Aminomethylation of the C_3 Compound

Since the previous attempts of formylation failed, we decided to move forward considering the aminomethylations, that have similar mechanisms to the Mannich reaction, and it works well on this kind of substrates. Once the aminomethylation took place in the *ortho* position with respect of the phenolic group, a reaction with an organo-nitrite could lead to the creation of a good leaving group from the amine, promoting the ring closure with a nucleophilic attack of the other side of triphenylene (Scheme 13).

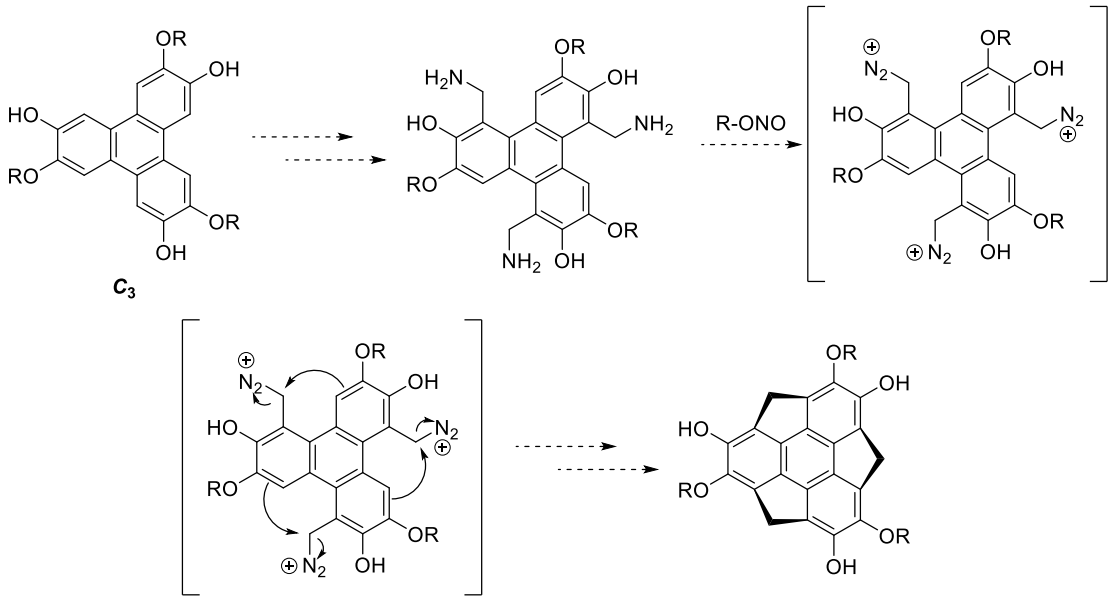

Scheme 13: Generic synthetic route to *O*-alkyl substituted using amino methylated compounds.

3.2.1 Amidomethylation of ***C*$_3$-26**

The easiest way to get an aminomethylation of an aromatic residue is passing through an amide, which can be hydrolysed later on. For this purpose, we employed 2-chloro-*N*-(hydroxymethyl)acetamide, **43**, as amido-methylating agent. At first ***C*$_3$-26** was reacted with 2-chloro-*N*-(hydroxymethyl)acetamide in acetic acid, in the presence of concentrated sulphuric acid as catalyst, overnight at 90 °C (Scheme 14).[10]

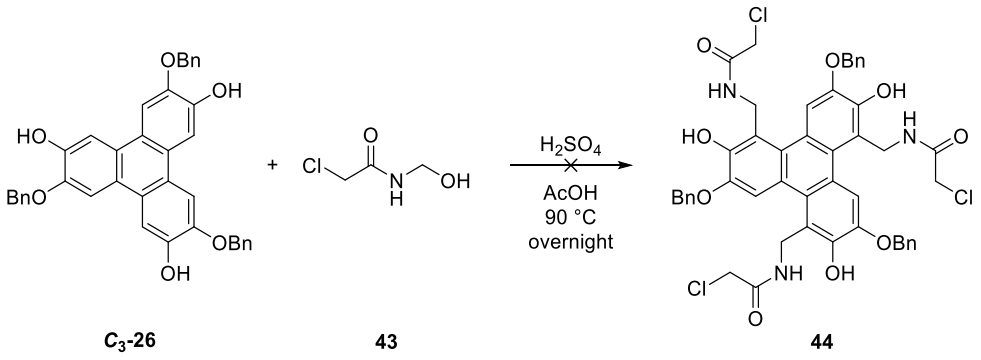

Scheme 14: first trial of amidomethylation of ***C*$_3$-26**.

The reaction conditions were too harsh for the substrate, with loss of the benzylic groups and decomposition of the original substrate, indicating that a change of strategy was needed.

A second reaction was settled, this time using toluene as solvent and *p*-toluensulfonic acid as catalyst, heating overnight at 110 °C. These reaction conditions are very similar to the one reported in Chapter 1 for the synthesis of the benzylidene, ensuring the substrate not to decompose (Scheme 15).[11]

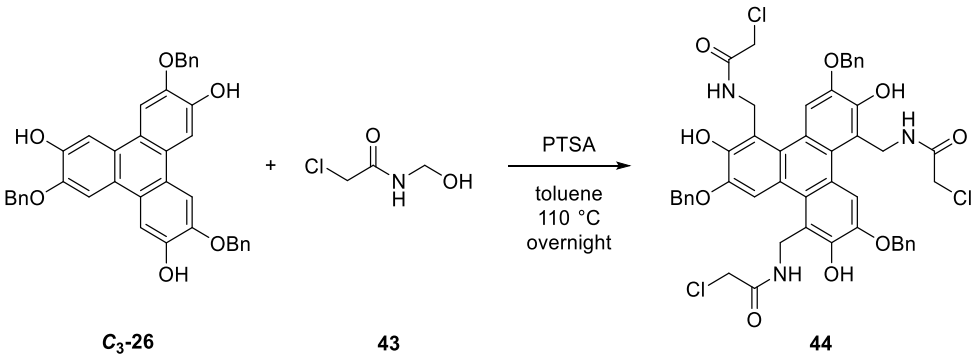

Scheme 15: Amidomethylation of ***C*$_3$-26**.

^{1}H NMR in DMSO-d_6 of the solid precipitated from the solution revealed the absence of one triphenylenic CH and the presence of two new methylenic signals. Filtration and digestions of the solid in absolute EtOH afforded the clean product **44**, in quantitative yield.

3.2.2 Hydrolysis of the Chloroacetamide

The hydrolysis of molecule **44**, which is possible in both basic[12] and acid environment,[10] was tried immediately in basic conditions due to the liability demonstrated by the benzylic group in strong acidic conditions.

A first test of basic hydrolysis was done using potassium hydroxide in DMSO at room temperature overnight (Scheme 16).

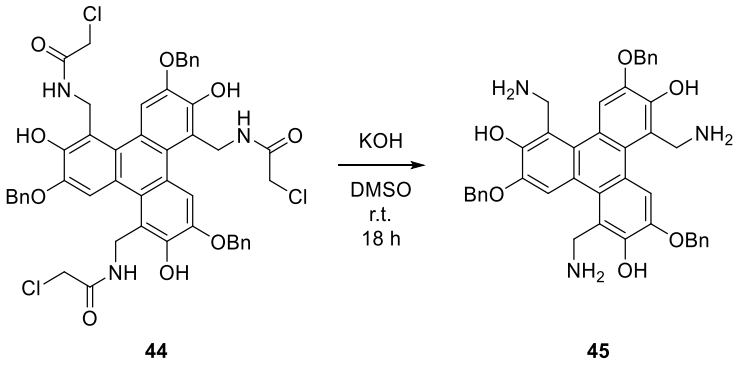

Scheme 16: Basic hydrolysis of **44** using KOH in DMSO.

Once the reaction was elaborated, ^{1}H NMR of the crude revealed the presence of small amount of product and various intermediates. For this reason, we started studying the reaction at different reaction time, temperature and base concentrations. Unfortunately, any of the tried conditions was able to replicate the original result.

Another hydrolysis reaction was tried treating molecule **44** with hydrazine, in the presence of ammonium iodide (Scheme 17).[13]

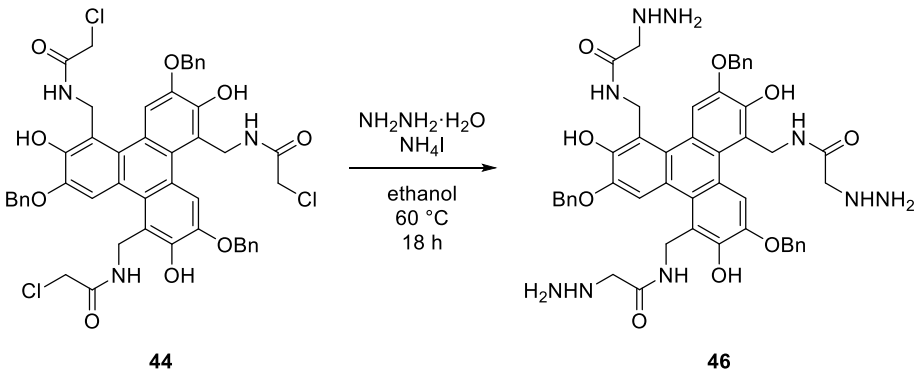

44 **46**

Scheme 17: Reaction between **44** and hydrazine in the presence of ammonium iodide.

Instead of the wanted *tris*-amine, **45**, the reaction gave the *tris*-amide **46**, quantitively, as only product. A second trial was done using 1,4-diossane in place of ethanol, allowing the reaction temperature to rise until 110 °C, without different outcomes. Due to the low interest, product **46** was not isolated.

After this last trial, we decided to suspend the sumanene project. However, the obtainment of product **46** demonstrated the possibility to perform nucleophilic substitutions on the chloride of chloroacetamide moiety, opening the route for the obtainment of novel CH substituted triphenylenes. In particular, we are interest in the reaction of substrate **44** with amines, also chiral, in order to sterically lock the triphenylene in a *P* or *M* helicity and isolate it in an enantiomerically pure form.

3.3 Experimental Section

3.3.1 General Methods

The reactions were followed with TLC Polygram® Sil G/UV254, 0.25 mm thickness. ^{1}H NMR, ^{13}C NMR, and 2D spectra were recorded with a Bruker Avance II 400, Ascend 400 and Ascend 500 spectrometers, working at 400-500 and 100-126 MHz respectively. Resonance frequencies are referred to tetramethylsilane. IR spectra were recorded with a Perkin Elmer Spectrum One spectrophotometer. Mass spectrometric measurements were performed using a Bruker HPLC-TOF (MicroTOF Focus). Reagents and solvents with high purity degree purchased by the providers were used as given. Otherwise, they were purified following the procedures reported in literature.[14] Anhydrous solvents were prepared by adding activated 3 Å molecular sieves to the solvent under inert atmosphere. Molecular sieves were activated shortly before the use by continuous heating under *vacuum*. Flash chromatography were performed with silica gel Merk 60, 230-400 mesh, following procedures reported in literature.[15]

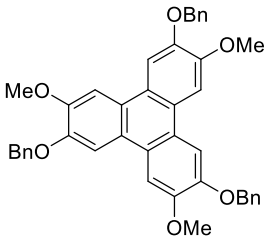
OBn
OMe
MeO
BnO
OBn
OMe

4

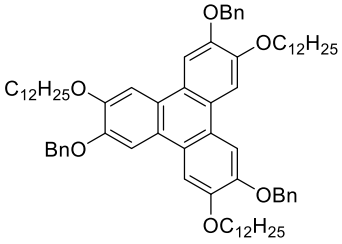
OBn
OC12H25
C12H25O
BnO
OBn
OC12H25

37

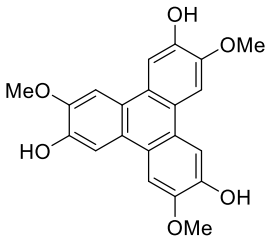
OH
OMe
MeO
HO
OH
OMe

8

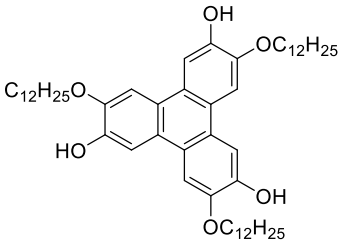
OH
OC12H25
C12H25O
HO
OH
OC12H25

38

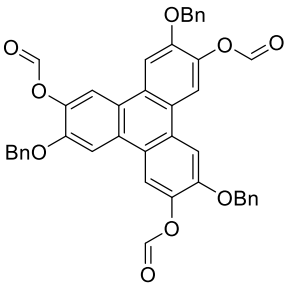
OBn
O
O
O
BnO
OBn
O
O

42

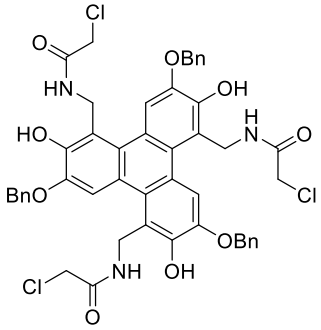
Cl
O
OBn
HN
OH
H
N
O
HO
BnO
Cl
OBn
NH
OH
Cl
O

44

3.3.2 Experimental Procedures – Syntheses

General Procedure 1 (GP1): General procedure for the alkylation and de-benzylation of ***C*$_3$-26**.

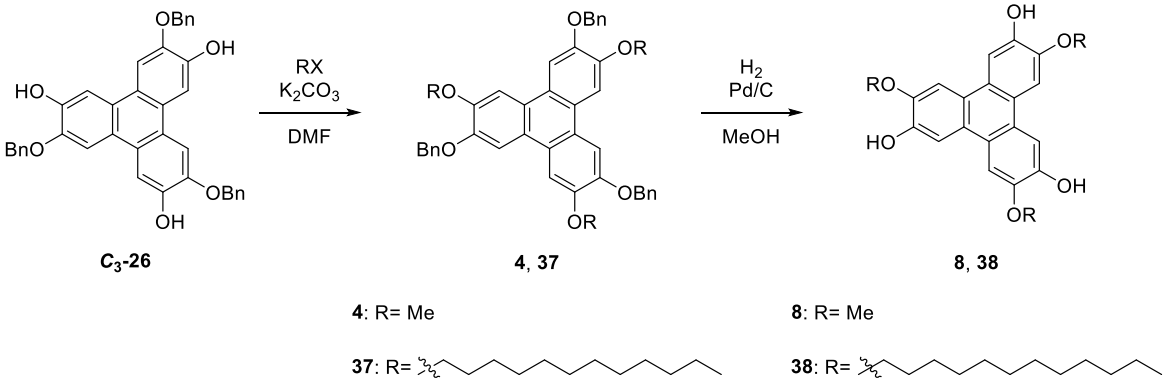

In a pear-shaped two necked 25 mL flask, equipped with argon inlet and septum, a solution of ***C*$_3$-26** (0.30 g, 0.5 mmol)**,** K_2CO_3 (0.63 g, 4.5 mmol) and alkyl halide (2.3 mmol) in anhydrous DMF (6 mL) was stirred at room temperature for 72 hours. The mixture was poured into a 1 M aqueous HCl (30 mL) solution and extracted with DCM (3×10 mL). The organic phase was washed with water (2×10 mL), dried over $MgSO_4$, filtered and concentrated in *vacuum*. The crude product was crystallized from absolute EtOH, to afford the product as white crystals. A suspended mixture of alkylated compound **n** and 10% Pd/C (0.044 g) in MeOH (20 mL) was stirred under H_2 atmosphere (1 Bar, balloon) at room temperature for 18 hours. The resulting mixture was filtered through a celite plug and washed with DCM.

2,6,10-tris(benzyloxy)-3,7,11-trimethoxytriphenylene (**4**): **GP1** was applied to ***C*$_3$-26** and methyl iodide. 89% yield. M.P.: 201 °C. ^{1}H NMR (500 MHz, $CDCl_3$): δ 7.77 (3H, s), 7.59-7.55 (6H, m), 7.54 (3H, s), 7.43-7.37 (6H, m), 7.36-7.30 (3H, m), 5.38 (6H, m), 4.05 (9H, s). $^{13}C\{^1H\}$ NMR (126 MHz): δ 149.5, 147.9, 137.6, 128.9, 128.2, 127.4, 123.8, 123.1, 108.1, 104.6, 77.4, 77.2, 76.9, 71.9, 56.1. IR (KBr): ν 1631, 1617, 1600, 1510, 1445, 1436, 1411, 1390, 1302, 1274, 1182, 1145, 1039, 1020, 851, 791, 735, 701 cm^{-1}. HRMS (ESI): calcd. for $C_{42}H_{35}O_6$ [M$^-$] 635.2428; found: 635.2412.

2,6,10-tris(benzyloxy)-3,7,11-tris(dodecyloxy)triphenylene (**37**): **GP1** was applied to ***C*$_3$-26** and dodecyl bromide affording **37**. 90% yield. M.P.: Waxy solid. ^{1}H NMR (400 MHz, $CDCl_3$): δ 7.82 (3H, s), 7.64 (3H, s), 7.60-7.53 (6H, sets of m), 7.43-7.37 (6H, sets of m), 7.36-7.30 (3H, sets of m), 5.34 (6H, s), 4.19 (6H, t, *J* = 6.6 Hz), 2.01-1.92 (6H, sets of m), 1.65-1.54 (6H, sets of m), 1.49-1.20 (48H, sets of m), 0.87 (9H, t, *J* = 7.0 Hz). $^{13}C\{^1H\}$ NMR (100 MHz): δ 149.4, 148.3, 137.8, 128.7, 128.0, 127.4, 124.3, 123.2, 109.3, 106.6, 72.3, 69.4, 32.1, 29.9, 29.8, 29.8, 29.7, 29.6, 29.5, 26.4, 22.8, 14.3. IR (KBr): ν 2922, 2851, 1617, 1519, 1497, 1465, 1454, 1437, 1385, 1261, 1199, 1165, 1042, 1028, 859, 821, 749, 701 cm^{-1}. HRMS (MALDI): DCTB, calcd. for $C_{75}H_{102}O_6$ [M$^+$]: 1098.7671; found: 1098.7644.

3,7,11-trimethoxytriphenylene-2,6,10-triol (**8**): **GP1** was continued on **4**. The filtered solution was concentrated in *vacuum*, affording negligible amounts of the product **4**. For this reason, the celite plug was extracted with AcOEt in a Soxhlet apparatus for 1 week. The volatile materials of the extract were removed in *vacuum*, affording **4** as a white solid. 74%

yield. M.P.: >300 °C. ^{1}H NMR (400 MHz, DMSO-d_6) δ 9.24 (3H, s), 7.91 (3H, s), 7.78 (3H, s), 4.00 (9H, s). $^{13}C\{^{1}H\}$ NMR (100 MHz): δ 147.6, 146.2, 123.3, 121.4, 108.2, 104.6, 55.6, 40.2, 40.1, 39.9, 39.7, 39.5, 39.3, 39.1, 38.9. IR (KBr): ν 1630, 1595, 1513, 1474, 1457, 1434, 1384, 1356, 1298, 1270, 1227, 1191, 1154, 1045, 978, 850, 832, 789 cm^{-1}. HRMS (ESI): calcd. for $C_{21}H_{17}O_6$ [M^-] 365.1019; found: 365.1047.

3,7,11-tris(dodecyloxy)triphenylene-2,6,10-triol (**38**): **GP1** was continued on **37**. The filtered solution was concentrated in *vacuum*, affording **38**. 94% yield. M.P.: Waxy solid. ^{1}H NMR (400 MHz, $CDCl_3$): δ 7.92 (3H, s), 7.79 (3H, s), 5.89 (3H, s), 4.26 (6H, t, *J* = 6.6 Hz), 2.00-1.89 (6H, sets of m), 1.61-1.49 (6H, sets of m), 1.46-1.20 (48H, sets of m), 0.87 (9H, t, *J* = 7.1 Hz). $^{13}C\{^{1}H\}$ NMR (100 MHz): δ 145.91, 145.44, 124.04, 122.99, 107.13, 104.74, 69.21, 32.08, 29.84, 29.80, 29.77, 29.77, 29.59, 29.51, 29.43, 26.25, 22.85, 14.27. IR (film): ν 3549, 2922, 2852, 1632, 1596, 1512, 1454, 1392, 1358, 1302, 1270, 1225, 1181, 1162, 1030, 855, 805, 721 cm^{-1}. HRMS (MALDI): DCTB, calcd. for $C_{54}H_{84}O_6$ [M^+]: 828.6262; found: 828.6276.

3,7,11-tris(benzyloxy)triphenylene-2,6,10-triyl triformate (**42**):

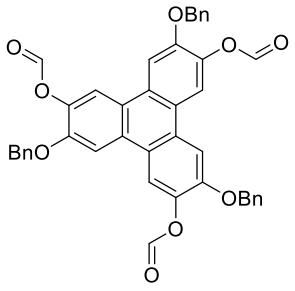

42

In a 10 mL screw-caped Pyrex test tube, a solution of formic acid (0.80 mL, 21.2 mmol) in acetic anhydride (1.35 mL, 14.3 mmol) was purged with argon and heated at 50 °C for 3 hours. The mixed anhydride was obtained in a quantitative yield after *vacuum* concentration.[16]

In a 10 mL two-necked pear-shaped flask, under inert atmosphere, ***C*$_3$-26** (0.05 g, 0.08 mmol), anhydrous DCM (3 mL), the mixed anhydride (0.25 mL, 1.7 mmol) and pyridine (1.0 µL, 0.012 mmol) were stirred at room temperature for 48 hours. The resulting solution was diluted with DCM (30 mL), washed with water (15 mL), saturated aqueous Na_2CO_3 (15 mL), dried over $MgSO_4$, filtered and concentrated in *vacuum*. Flash chromatography of the crude (eluent petroleum ether/AcOEt 75:25) afforded the product as a brown solid (0.052 g, 0.08 mmol, 93% yield). ^{1}H NMR (400 MHz, $CDCl_3$): δ 8,53 (3H, s), 7,85 (3H, s), 7,53 (3H, s), 7,36-7,40 (6H, m), 7,27-7,32 (9H, m), 5,20 (6H, s). $^{13}C\{^{1}H\}$ NMR (100 MHz): δ 159.5, 149.0, 138.6, 136.7, 128.6, 128.5, 128.0, 127.4, 122.3, 117.8, 106.7, 70.3.

N,*N*',*N*''-((3,7,11-tris(benzyloxy)-2,6,10-trihydroxytriphenylene-1,5,9-triyl)tris(methylene))tris(2-chloroacetamide) (**44**):

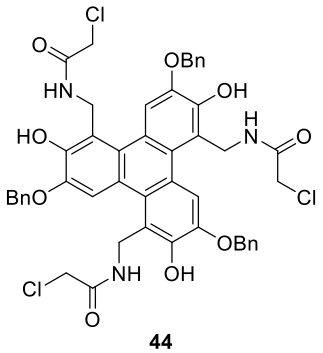

44

In a 10 mL screw-caped Pyrex test tube, a mixture of ***C*$_3$-26** (0.05 g, 0.08 mmol), 2-chloro-*N*-(hydroxymethyl)acetamide (0.093 g, 0.75 mmol) and PTSA (0.8 mg, 0.004 mmol, 5% mol with respect of ***C*$_3$-26**) in anhydrous toluene (2 mL), was heated overnight at 110 °C. The resulting precipitate was centrifuged and separated from the liquid phase. The crude product was digested in absolute EtOH (3 mL), affording the product as a white solid (0.073 g, 0.08 mmol, quantitative yield). ^{1}H NMR (400 MHz, $CDCl_3$): δ 9.28 (3H, s), 8.88 (3H, t, *J* = 3.9 Hz), 7.71 (3H, s), 7.57-7.52 (6H, m), 7.44-7.36 (6H, m), 7.35-7.26 (3H, m), 5.18 (6H, s), 4.66 (6H, d, *J* = 3.8 Hz), 4.16 (6H, s). $^{13}C\{^1H\}$ NMR (100 MHz): δ 166.3, 146.2, 144.3, 136.6, 128.30, 127.8, 127.7, 126.4, 122.2, 117.6, 110.1, 69.9, 42.5, 40.1, 39.9, 39.7, 39.5, 39.3, 39.1, 38.9.

3.3.3 NMR and MS Spectra

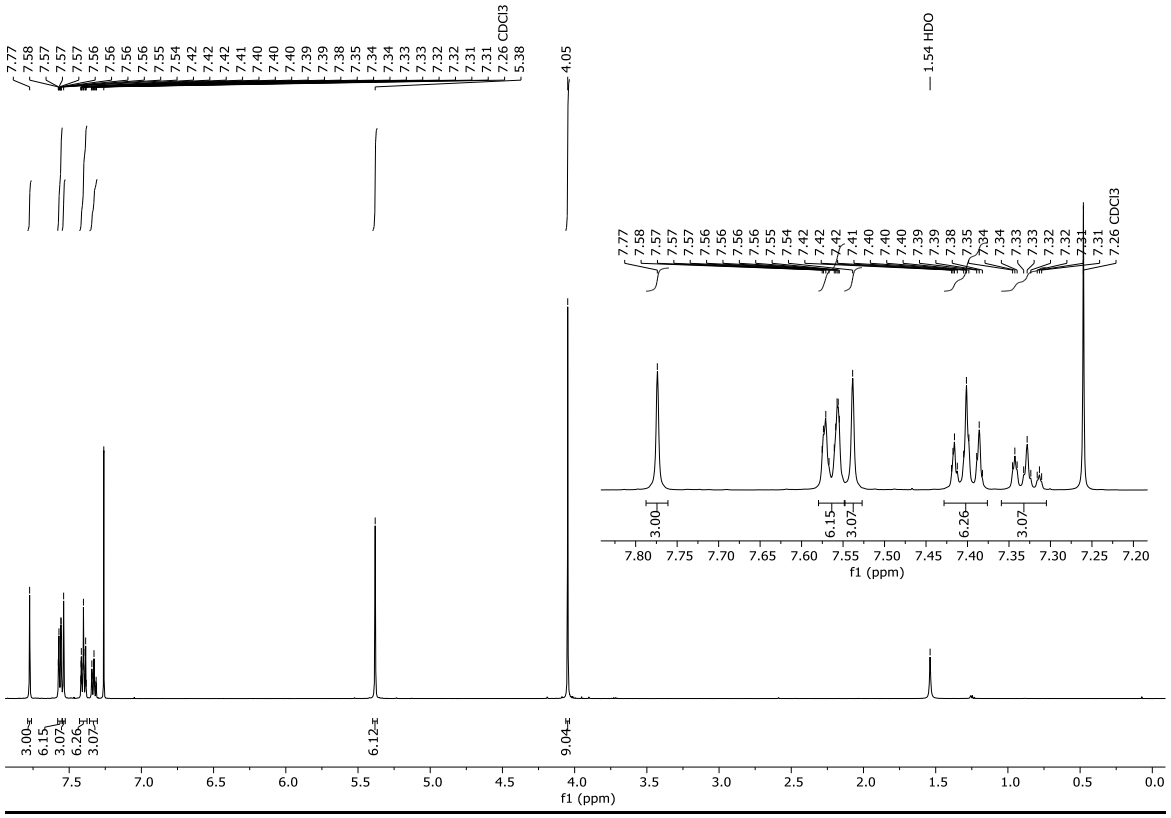

Figure I: ^{1}H NMR of molecule **4**.

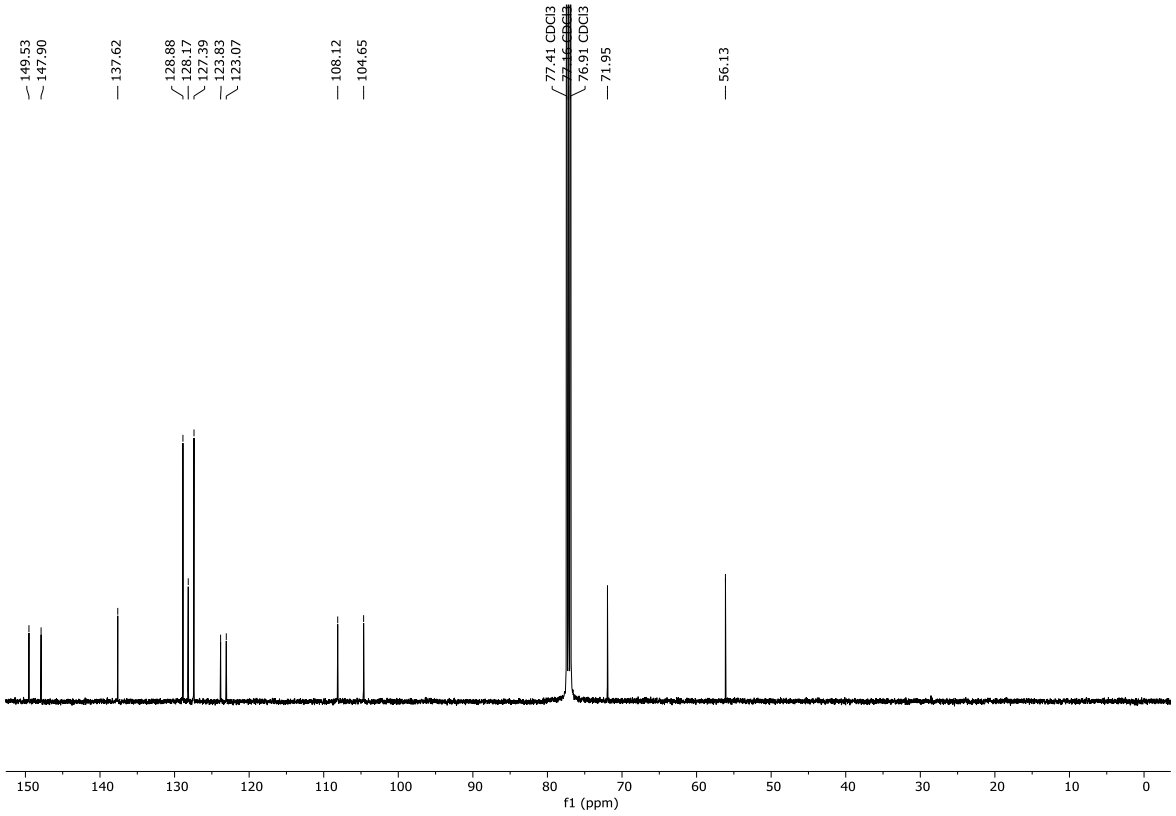

Figure II: ^{13}C NMR of molecule **4**.

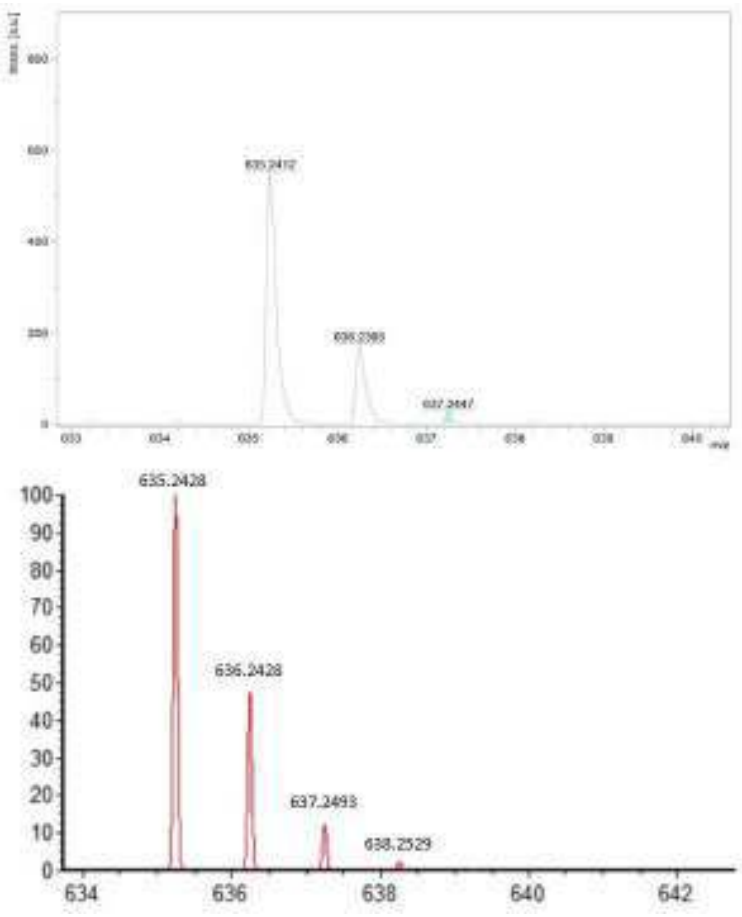

Figure III: ESI-HRMS of molecule **4**.

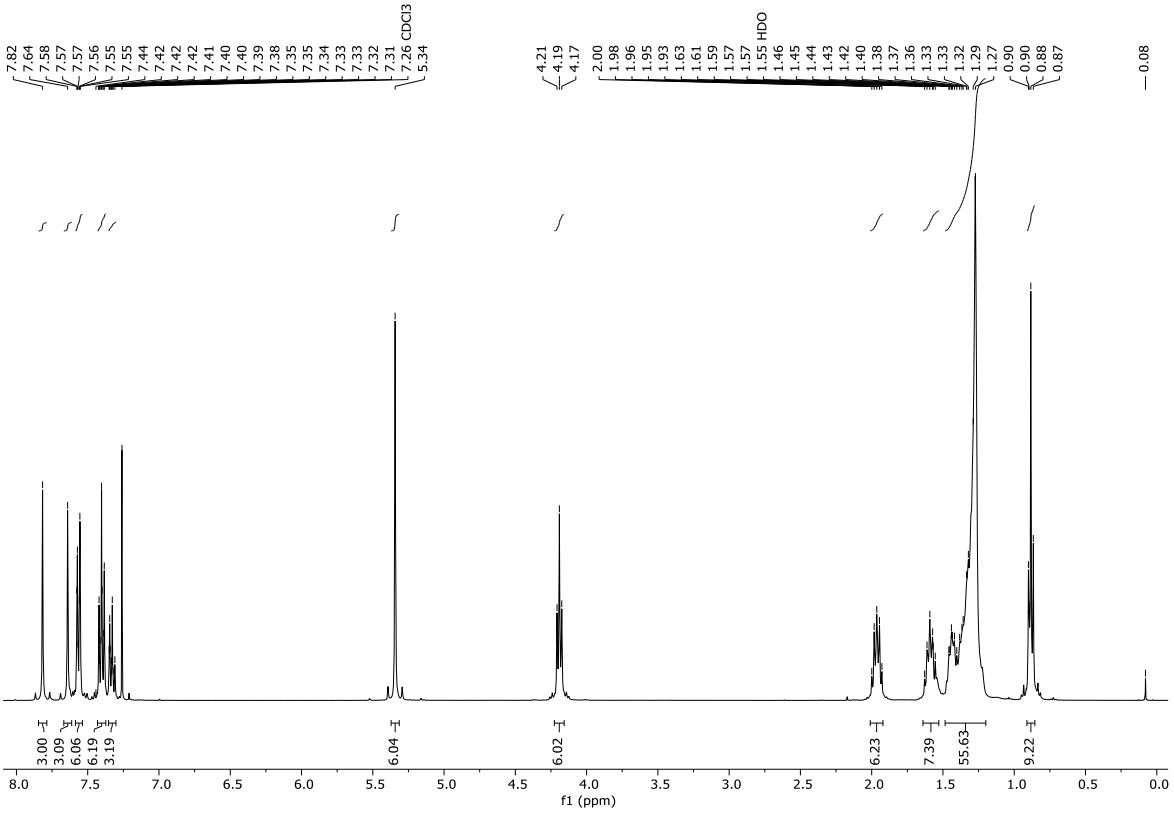

Figure IV: ^{1}H NMR of molecule **37**.

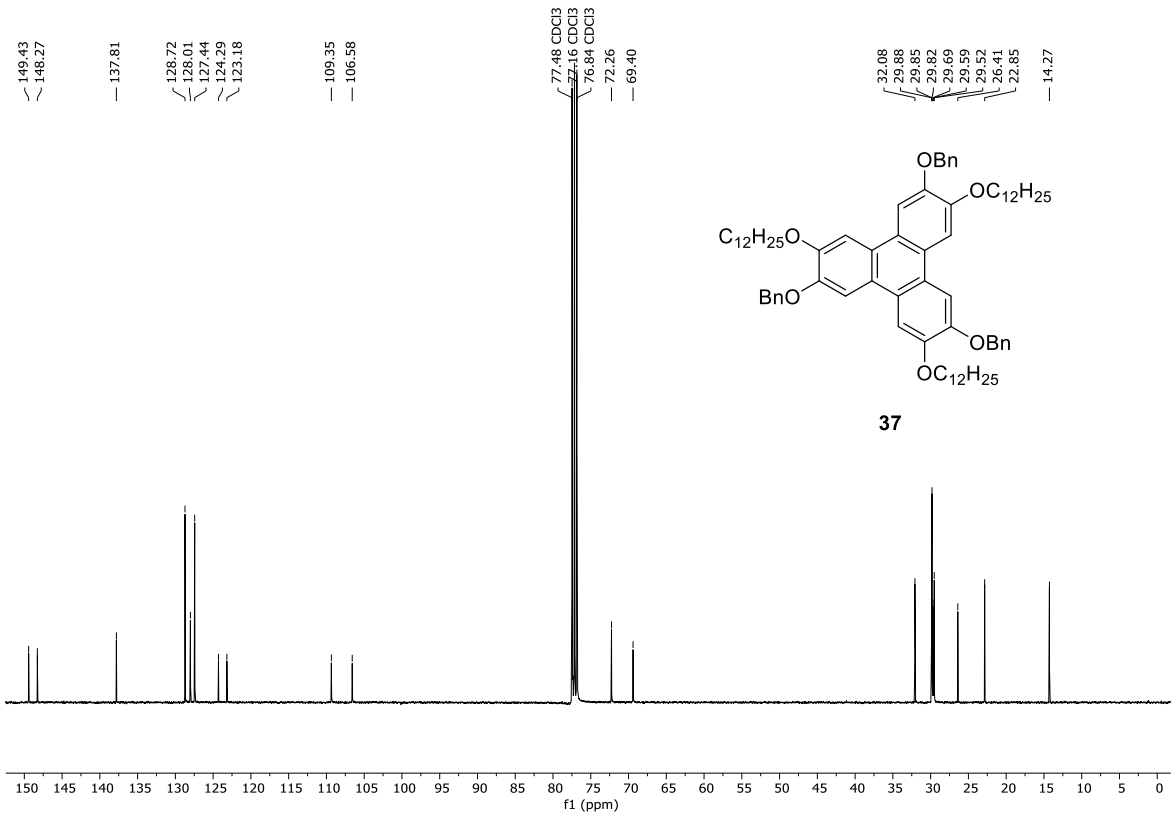

Figure V: ^{13}C NMR of molecule **37**.

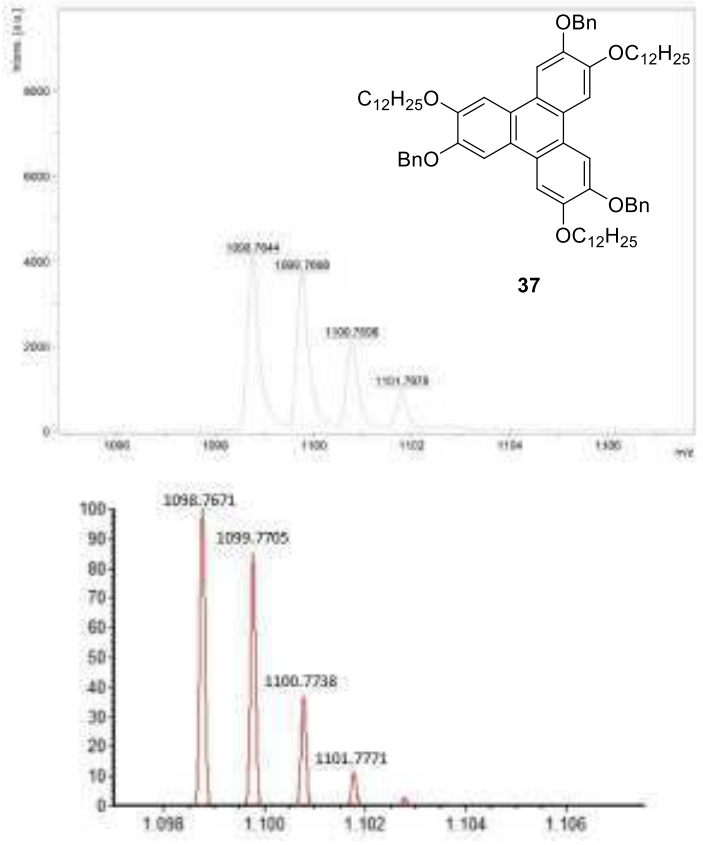

Figure VI: MALDI-HRMS of molecule **37**.

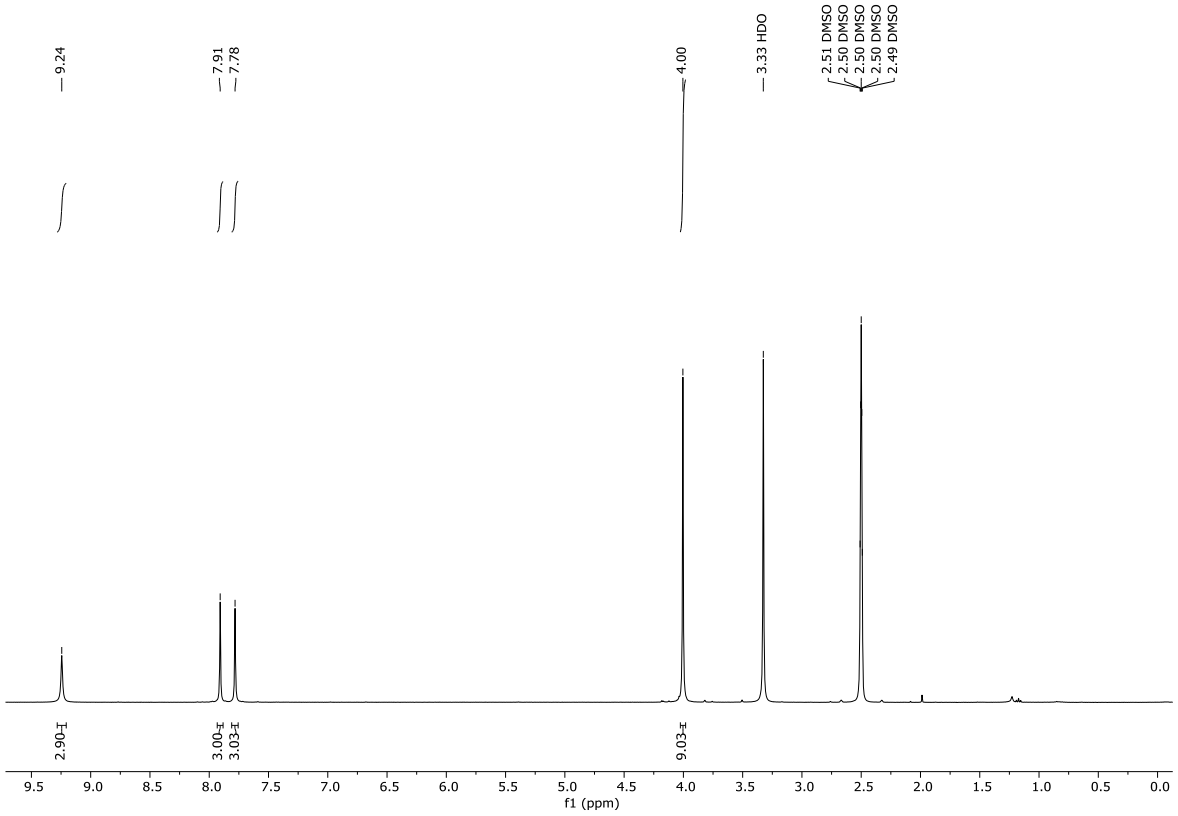

Figure VII: ^{1}H NMR of molecule **8**.

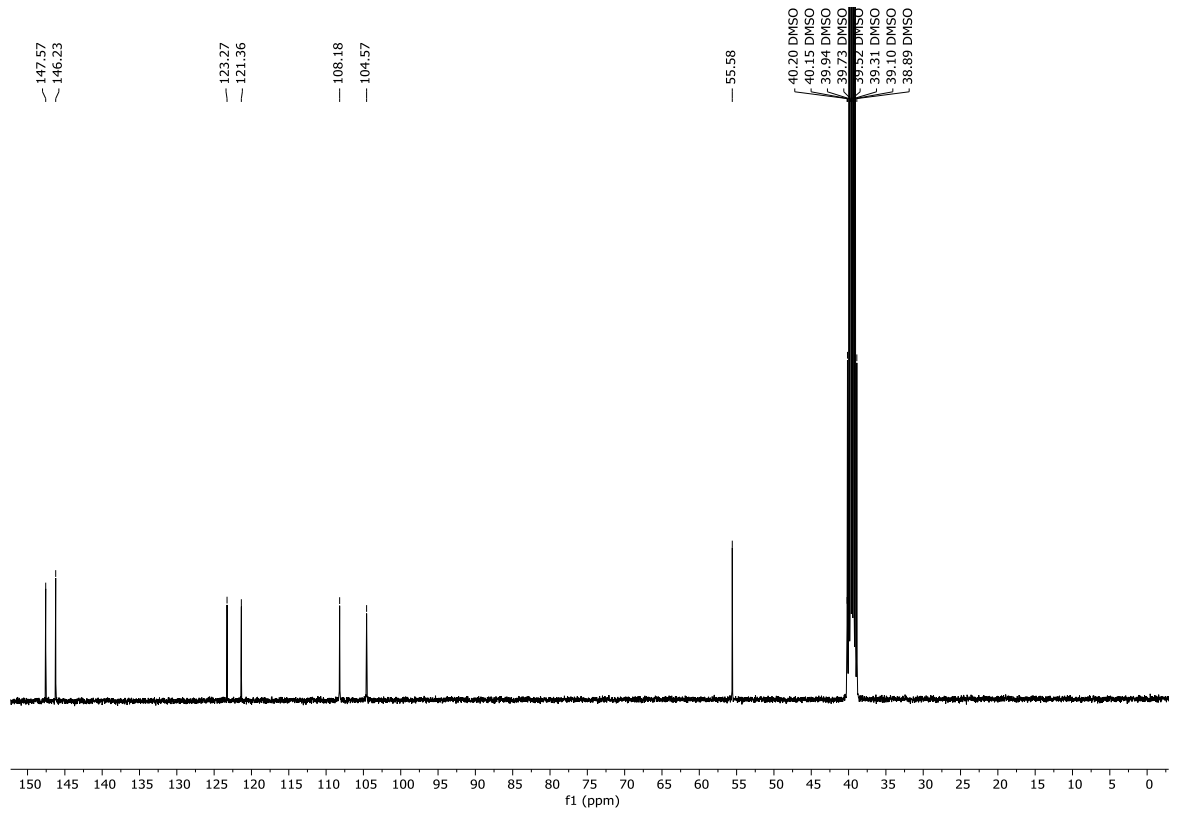

Figure VIII: ^{13}C NMR of molecule **8**.

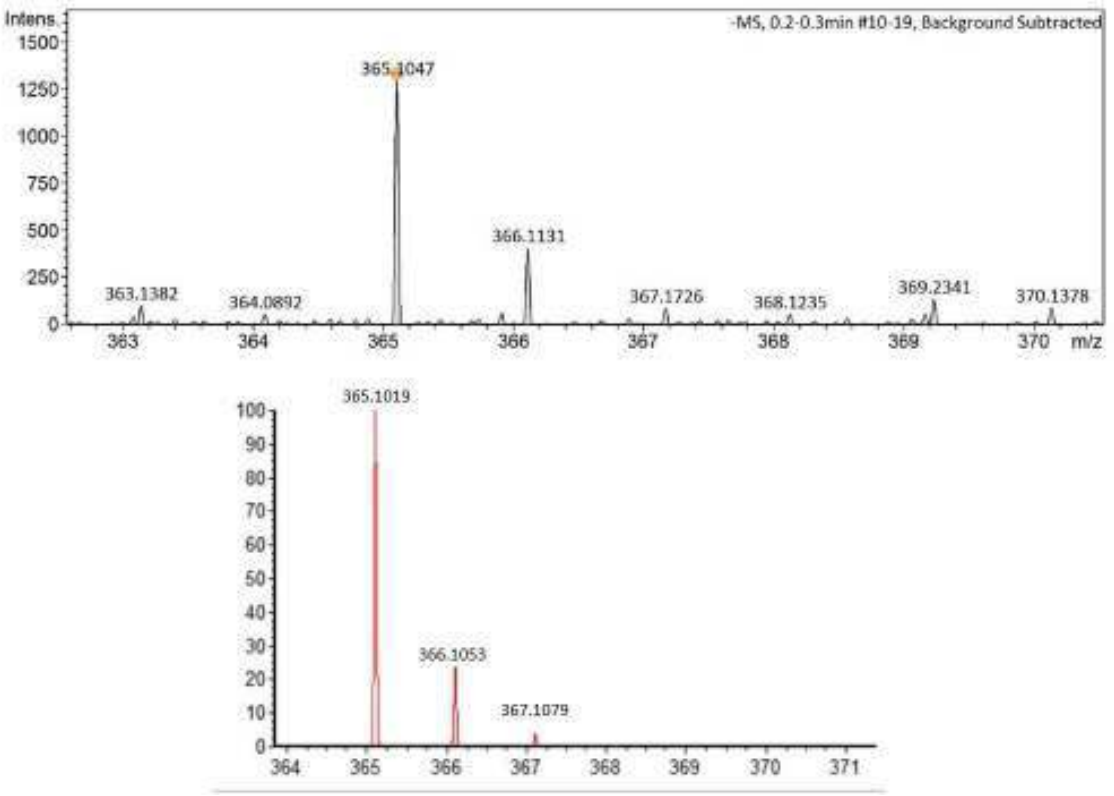

Figure IX: ESI-HRMS of molecule **8**.

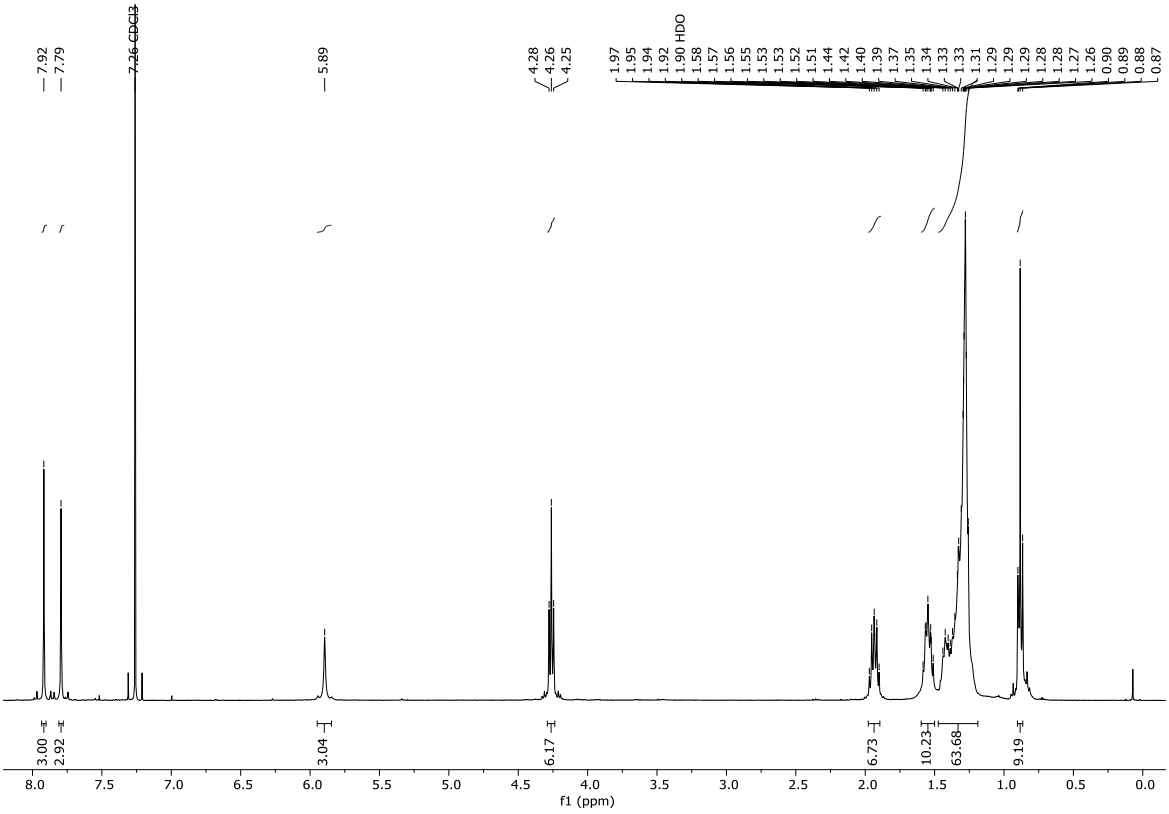

Figure X: ^{1}H NMR of molecule **38**.

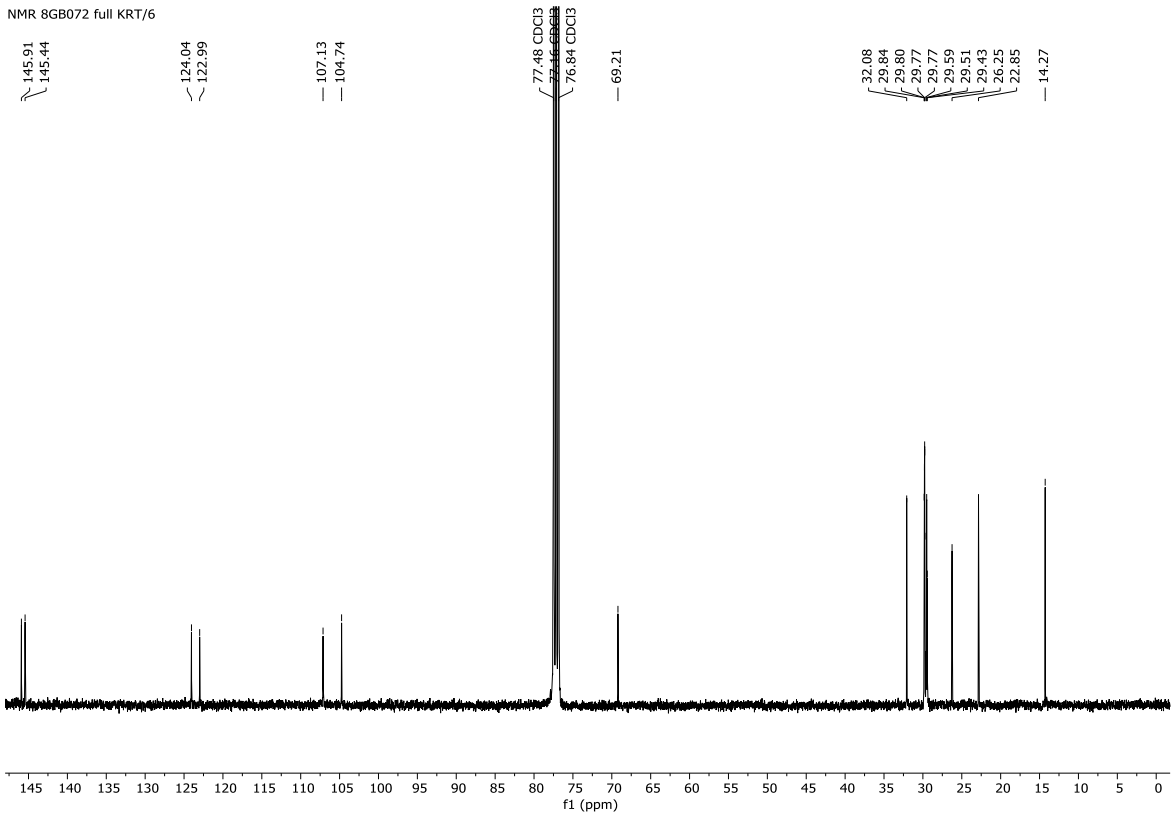

Figure XI: ^{13}C NMR of molecule **38**.

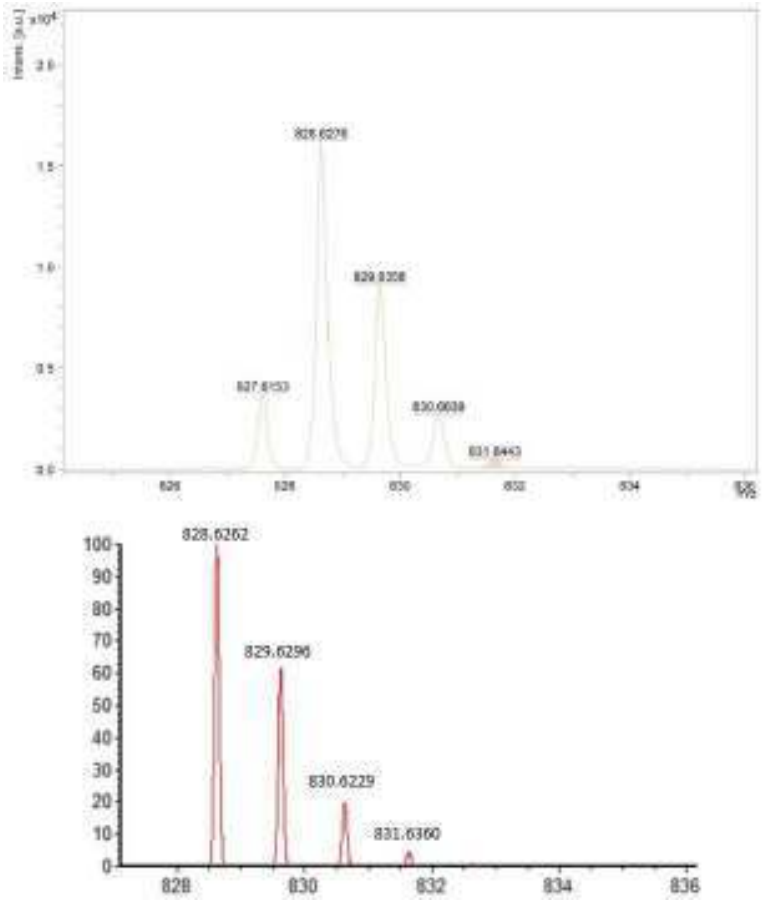

Figure XII: MALDI-HRMS of molecule **38**.

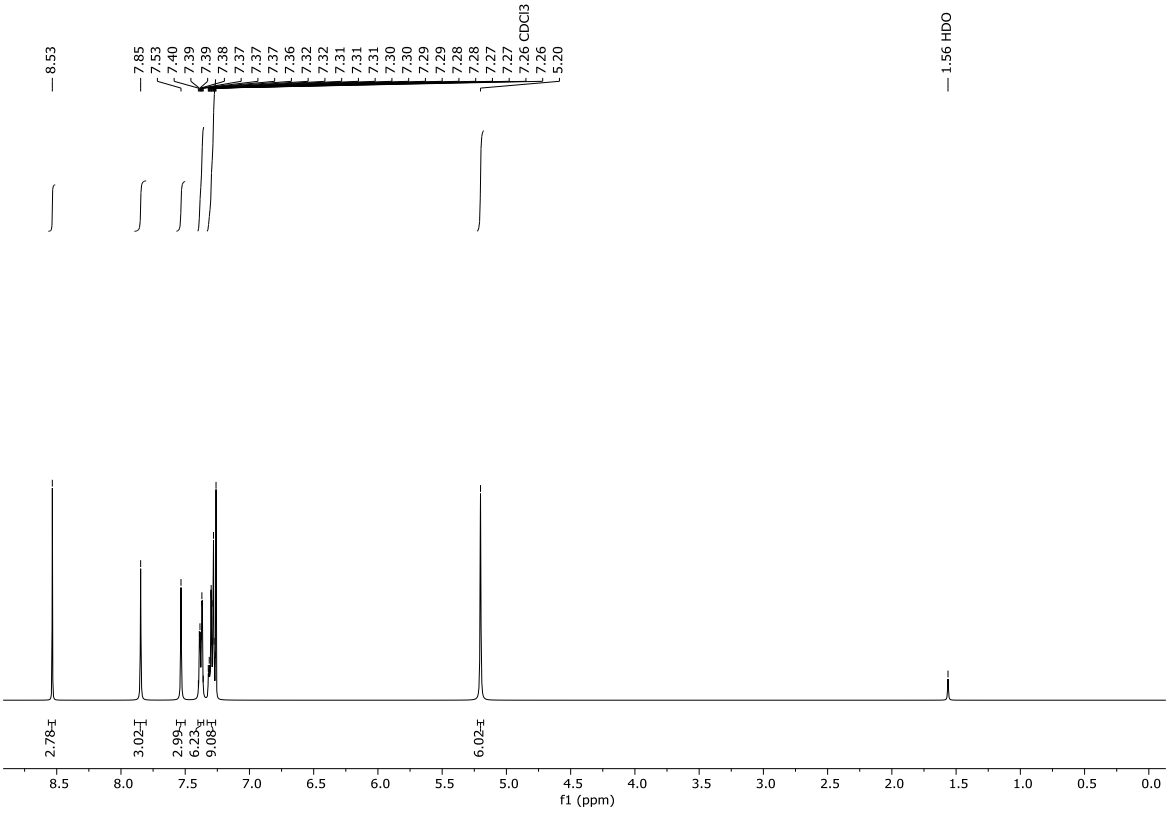

Figure XIII: ^{1}H NMR of molecule **42**.

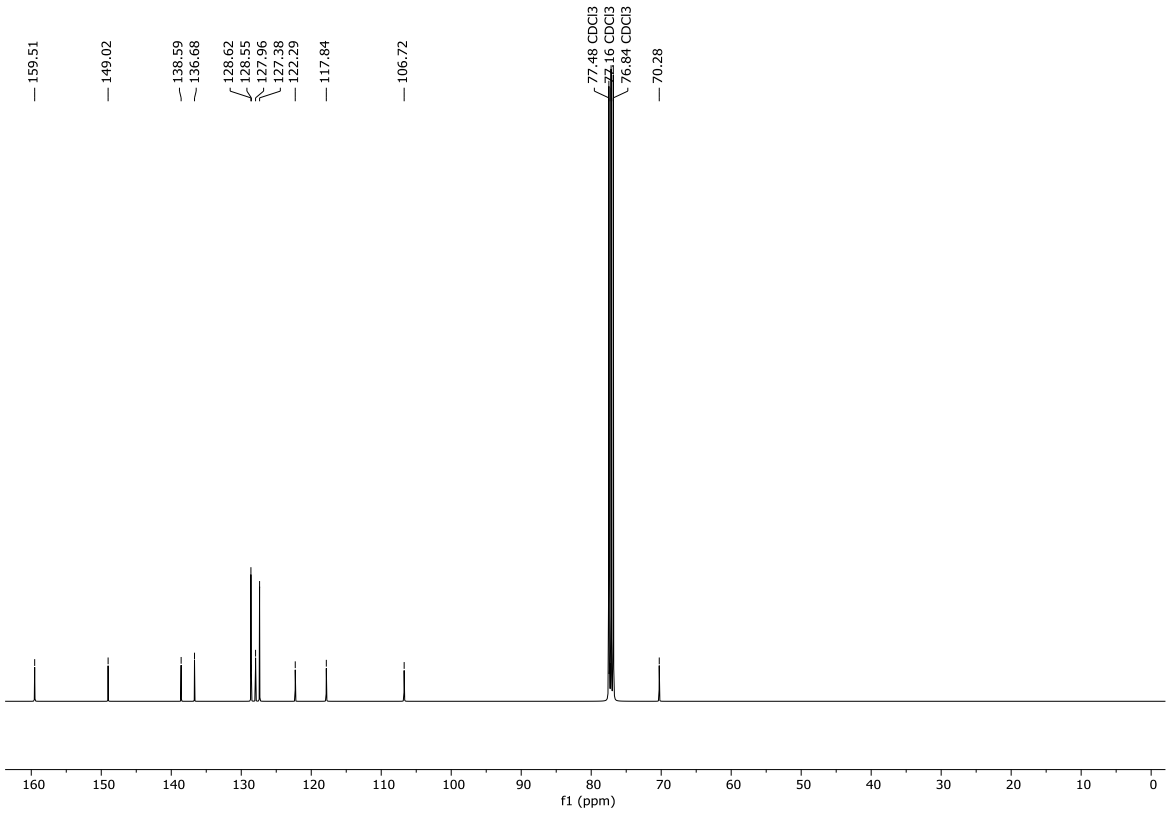

Figure XIV: ^{13}C NMR of molecule **42**.

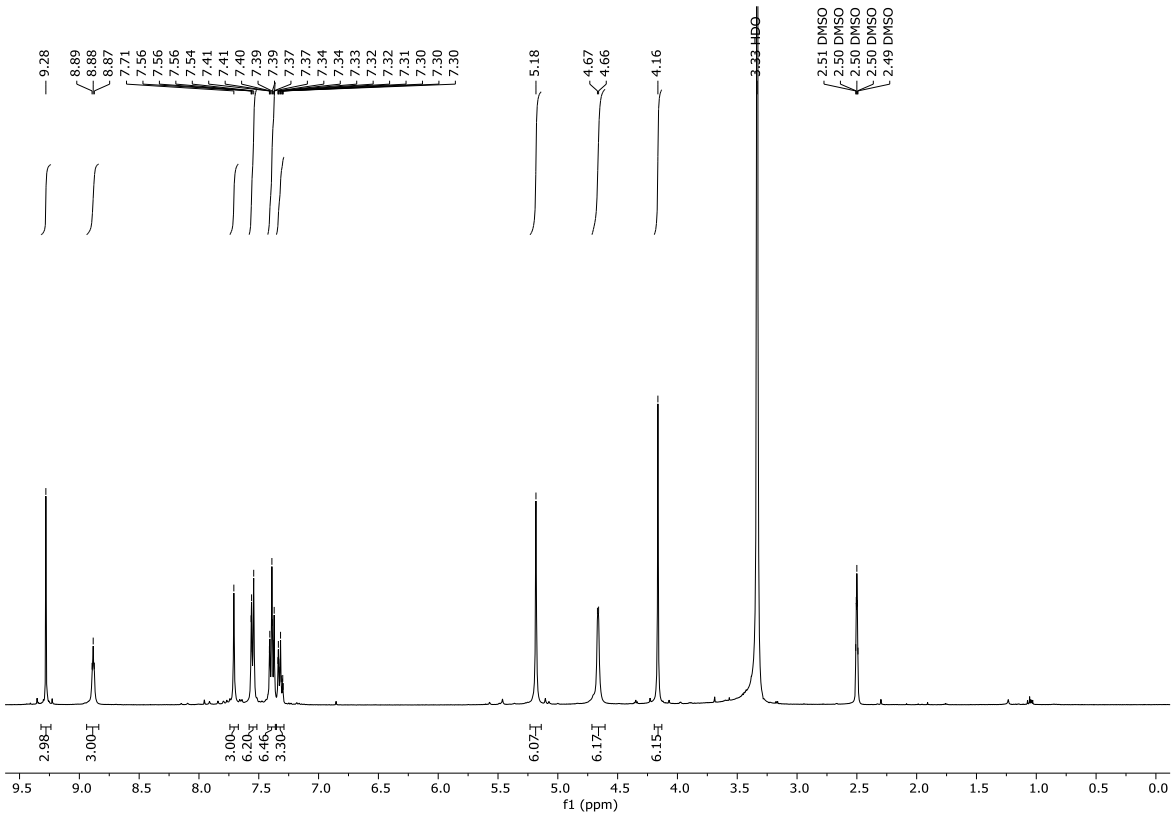

Figure XV: ^{1}H NMR of molecule **44**.

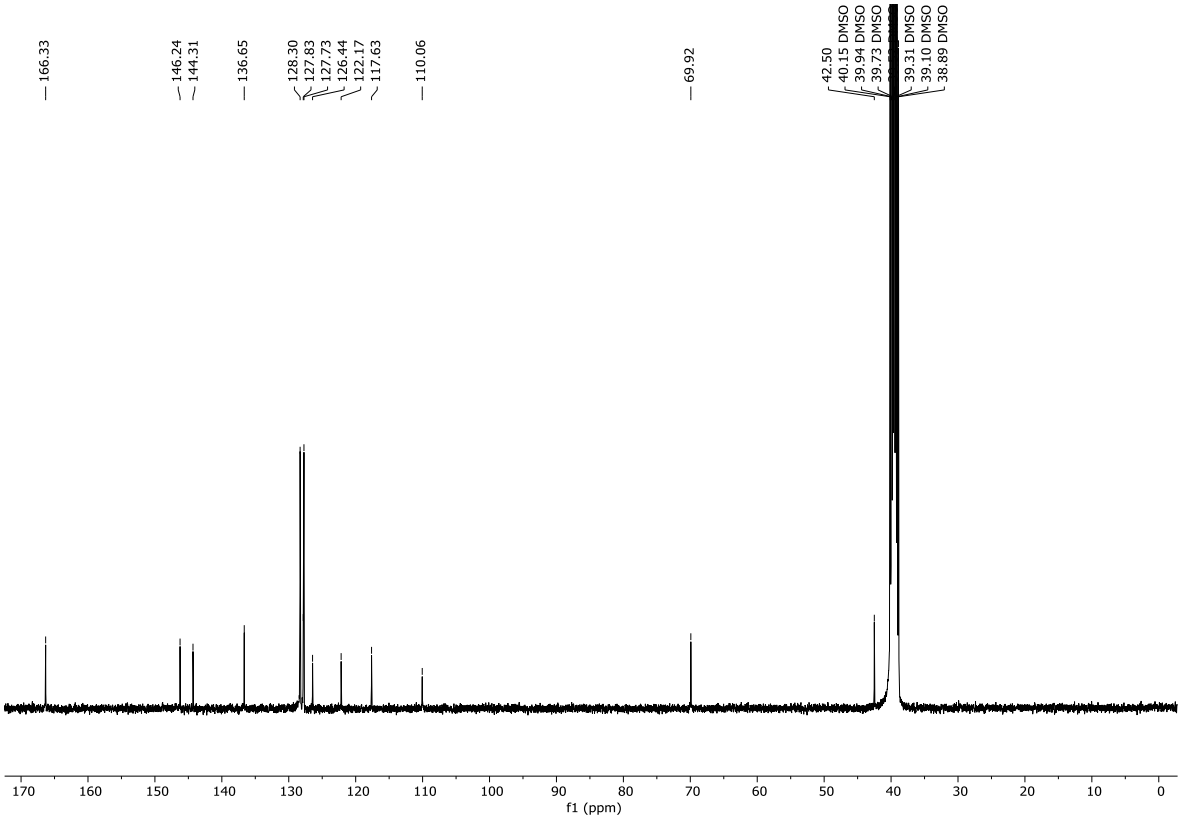

Figure XVI: ^{13}C NMR of molecule **44**.

3.4 Bibliography

1 H. Sakurai, T. Daiko, T. Hirao *Science*, **2003**, *301*, 1878.

2 T. Amaya, T. Hirao *Chem. Rec.*, **2015**, *15*, 310-321.

3 K. V. Sashidhara, A. Kumar, M. Kumar, A Srivastava, A. Puri, *Bioorg. Med. Chem. Lett.* **2010**, *20*, 6504-6507.

4 S. Goswami, A. Manna, S. Paul, A. Kumar Maity, P. Saha, C. K. Quahc, H.-K. Fun *RSC Adv.*, **2014**, *4*, 34572-34576

5 S. Kumar, H.-Y. Lee, J.-P. Liou, *J. Nat. Prod.*, **2017**, *80*, 1294-1301.

6 A. Hens, K. K. Rajak, *RSC Adv.*, **2015**, *5*, 4219-4232

7 K. Alsabil, G. Viault, S. Suor-Cherer a, J.-J. Helesbeux, J. Merza, V. Dumontet, L. M. Peña-Rodriguez, P. Richomme, D. Seraphin, *Tetrahedron* **2017**, *73*, 6863-6870.

8 C. Peschko, C. Winklhofer, A. Terpin, W. Steglich, *Synthesis,* **2006**, *18*, 3048-3057.

9 H. S. Jung, J. Han, J.-H. Lee, J. H. Lee, J.-M. Choi, H.-S. Kweon, J. H. Han, J.-H. Kim, K. M. Byun, J. H. Jung, C. Kang, J. S. Kim, *J. Am. Chem. Soc.*, **2015**, *137*, 3017-3023.

10 Merch & Co. Inc., US4159279, **1979**.

11 L. M. Oh, H. Wang, S. C. Shilcrat, R. E. Herrmann, D. B. Patience, P. G. Spoors, J. Sisko, *Org. Process Res. Dev.*, **2007**, *11*, 1032-1042.

12 a) T. E. Campano, I. Iriarte, O. Olaizola, J. Etxabe, A. Mielgo, I. Ganboa, J. M. Odriozola, J. M. Garcìa, M. Oiarbide, C. Palomo, *Chem. Eur. J.*, **2019**, *25*, 4390- 4397; b) F. King, R. Rathore, J. Y. L. Lam, Z. R. Guo, D. F. Klassen, *J. Am. Chem. Soc.*, **1992**, *114*, 3028-3033.

13 Y. Shimizu, M. Noshita, Y. Mukai, H. Morimoto, T. Ohshima, *Chem. Commun.,* **2014**, *50*, 12623-12625.

14 W. L. F. Armarego, C. Chai in *Purification of Laboratory Chemicals (Seventh Edition)*, Butterworth-Heinemann, Boston, **2013**.

15 W. C. Still, M. Kahn, A. Mitra, *J. Org. Chem.*, **1978**, *14*, 2923-2925.

16 C. Spry, A. L. Sewell, Y. Hering, M. V.J. Villa, J. Weber, S. J. Hobson, S. J. Harnor, S.Gul, R. Marquez, K. J. Saliba, *Eur. J. Med. Chem.*, **2018**, *143*, 1139-1147.

4 Sulphide and Disulphide Cages

In the literature, sulphide and disulphide bonds have been used for the creation of a wide number of molecular objects. Sulphide bridges have been often exploited to synthesize cyclophane, *bis*- or *tris*-bridged structures,[1,2,3] and recently the synthesis of this kind of covalent linkage has been proposed establishing at first a disulphide bond and eventually converting it into a sulphide, increasing the overall yield like in the example reported in Scheme 1.[4]

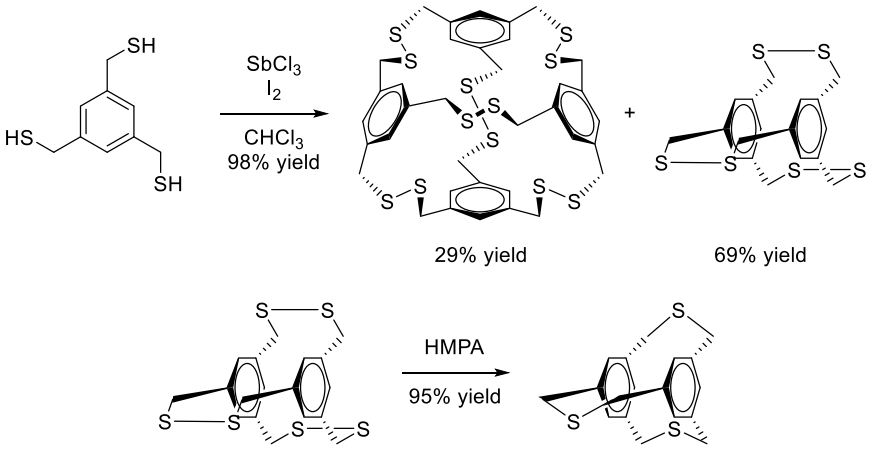

Scheme 1: Synthesis of disulphide and sulphide based cyclophane. Adapted from [4].

Disulphide bonds have also been used for the formation of covalent cages, characterized by several shapes and dimensions, often relying on the use of mesitylene derivatives to create the branching central unit.[5,6,7] Usually, these cages are too small to display a host-guest chemistry, and the few with a reported host-guest activity can host rather small molecules, like methyl iodide or methane (Scheme 2).[8,9]

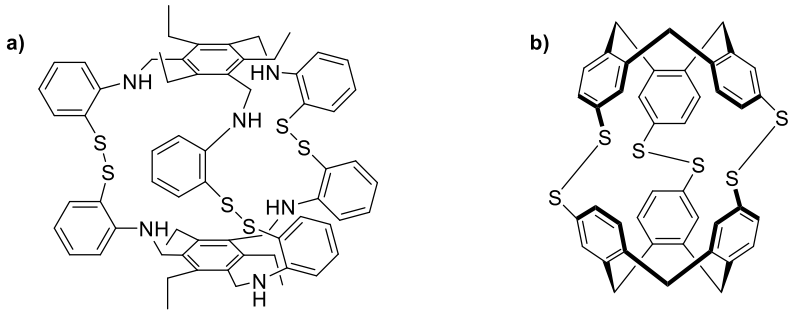

Scheme 2: Disulphide cages for the encapsulation of a) methyl iodide and b) methane. Adapted from [8] and [9] respectively.

While sulphide linkages have the advantage to be easy to prepare from thiols and alkyl halide derivatives, disulphide bonds have the advantage to be a reversible bond and, because of this, they have been largely used recently in dynamic covalent chemistry. In fact, their reversible nature allows them to establish an equilibrium, that eventually leads to the formation of the thermodynamic product.[10,11]

So far, among all the covalent cages created and reported in the literature, at the best of our knowledge none exploits the triphenylene as fundamental building block, conversely in

some cases it is considered as an electron-rich guest.[12] For these reasons, we started working on the synthesis of triphenylene thiol derivatives, in order to achieve the formation of new supramolecular cages, characterized by an electron-rich cavity that could be the optimal environment for electron-poor guests.

Moreover, the synthesized thiols should be useful as ligands for gold surfaces or nanoparticles,[13,14] thus asymmetrical triphenylene thiols will be prepared.

4.1 Synthesis of *tris*-, *bis*- and *mono*-Thiol Triphenylenes

For the creation of a thiol moiety on the triphenylenic core of ***C*$_3$-26**, the undertaken synthetic strategies consisted in the insertion of an alkyl chain with a terminal hydroxylic group, which can be converted into a good leaving group, allowing the nucleophilic insertion of thiourea. Once the thiouronium salt has been formed, it can be hydrolysed to thiol under basic conditions.

To insert the hydroxyalkyl moiety, a nucleophilic substitution was performed on 3-chloro-1-propanol using ***C*$_3$-26** as a nucleophile in the presence of potassium carbonate. The reaction was carried out in anhydrous DMF, stirring the mixture at room temperature for 60 hours (Scheme 3).

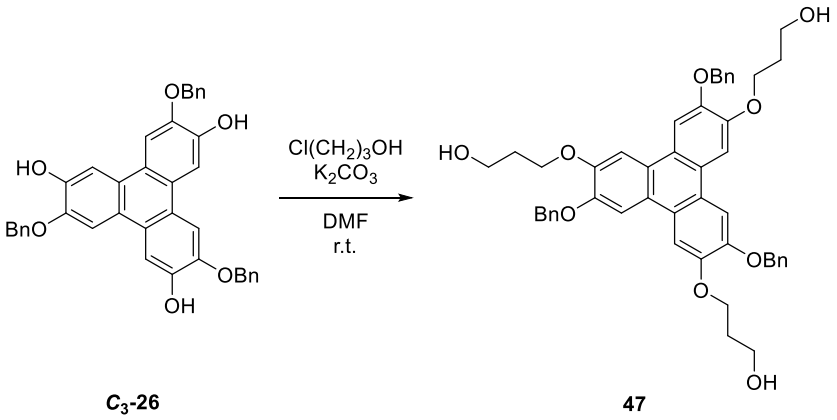

Scheme 3: hydroxy alkylation of ***C*$_3$-26**.

The addition of water to the reaction mixture provided the precipitation of the product **47**, that was isolated with 84% yield.

The next step was the transformation of the primary alcohols into good leaving groups. For this task, an Appel reaction was performed on **47**, treating it with carbon tetrabromide and triphenyl phosphine, in DCM at 0 °C (Scheme 4).[15]

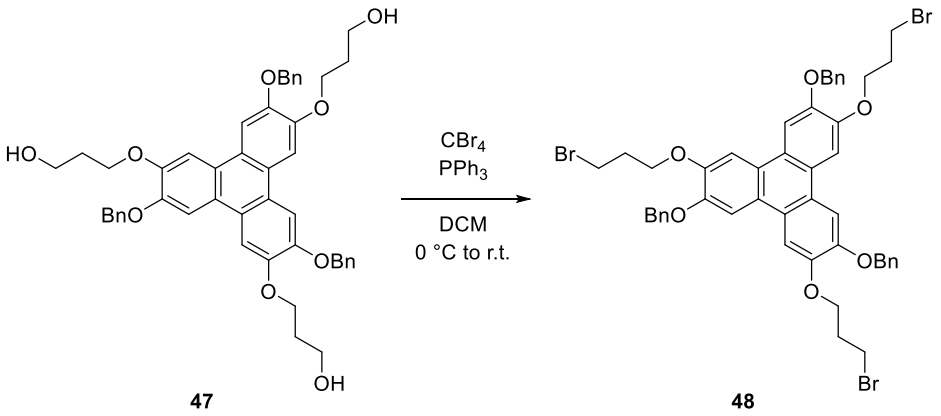

Scheme 4: Appel reaction on substrate **47**.

The reaction was continued overnight, allowing the temperature to rise. The product was obtained after flash chromatography of the crude with a final 72% yield.

Last step for the synthesis of the *tris*-thiol was the creation of the thiouronium salt and the corresponding hydrolysis. Molecule **48** was treated firstly with thiourea, heating the mixture overnight in DMF at 100 °C. After cooling the obtained solution, aqueous 0.4 M NaOH was added and the resulting solution was stirred overnight at room temperature (Scheme 5).[16]

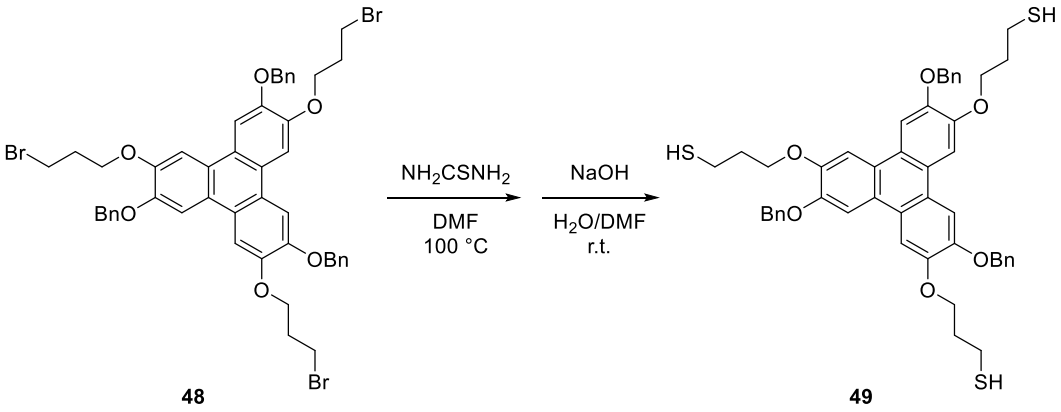

Scheme 5: Synthesis of the *tris*-thiol **49**.

The *tris*-thiol **49** was obtained by simple extraction with DCM from the aqueous solution, with an overall yield of 84% in two steps.

Together with the *tris*-thiol **49**, *mono*- and *bis*-thiol were synthesized by serendipitous methylation of molecule **47** with methyl iodide, under basic conditions, to obtain the corresponding *mono*-, *bis*- and *tris*-methylated products (Scheme 6).

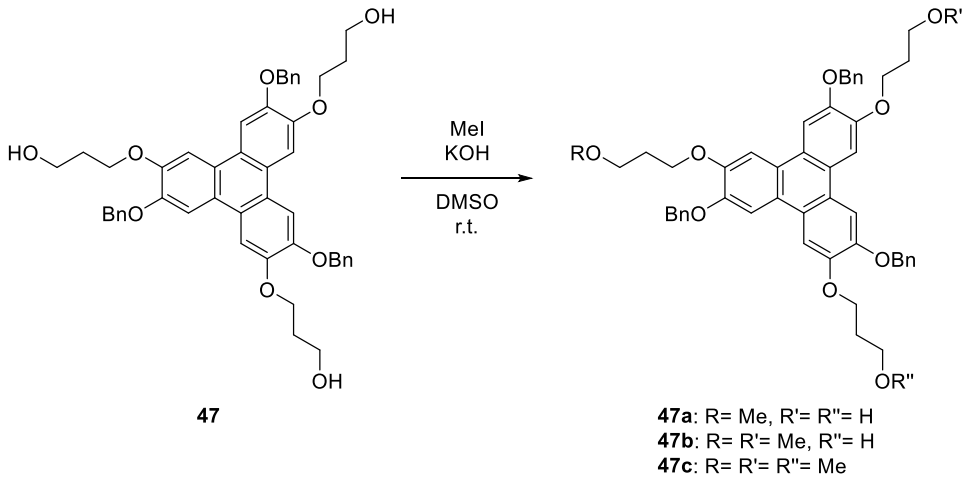

47

47a: R= Me, R'= R"= H
47b: R= R'= Me, R"= H
47c: R= R'= R"= Me

Scheme 6: Synthesis of the *mono*-, *bis*- e *tris*-methylated compound, **47a**, **47b** and **47c**.

The products were isolated from the crude by flash chromatography, with a 28%, 24% and 6% yield for *mono*-, *bis*- and *tris*-methylated compound, respectively.

Products **47a** and **47b** were treated as previously described for molecule **47** via Appel reaction, followed by nucleophilic displacement with thiourea and its hydrolysis, leading to the formation of the corresponding thiols (Scheme 7).

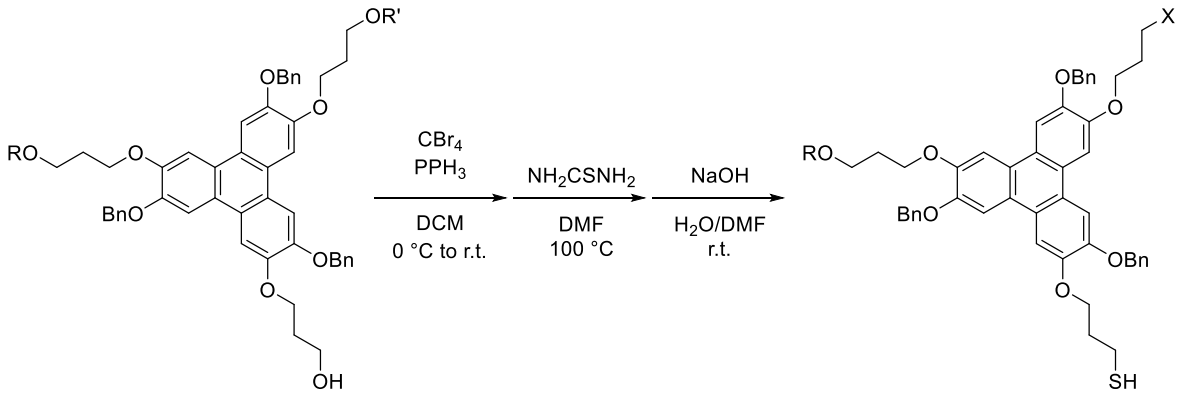

47a: R = Me, R' = H
47b: R = R' = Me

49a: R = Me, X = SH
49b: R = X = Me

Scheme 7: Synthesis of the *mono*- and *bis*-thiol compound **49a** and **49b**.

Thiols **49a** and **49b** were obtained with an 81% and 80% yield, respectively. The obtained molecules will be investigated for the surface functionalization of Au nanoparticles to ascertain the effect of the large triphenylene unit in close proximity with the metal centre.

4.2 Synthesis of Dimeric Disulphide Cages

Aiming at the synthesis of larger disulphide based covalent cages, suitable for hosting bigger molecules compared to methane or methyl iodide, the use of triphenylenes derivatives, in a host-guest perspective, should grant a wider host's cavity, strongly electron-rich, which could be suitable for hosting large electron-poor molecules or cations.

We started taking inspiration from a recent work on the synthesis of sulphide cages from the corresponding disulphide species. More specifically, the work reported about the

synthesis of disulphide cages by oxidation with iodide in the presence of antimony(III) chloride and their conversion into sulphide-based cyclophanes.[4] The role of $SbCl_3$ is to create an equilibrium between the thiol and the newly formed disulphides, favouring the thermodynamic products.

With this idea in mind, iodide and antimuonium(III) chloride were added to a solution of **49** in chloroform and the resulting mixture was stirred for 48 hours at room temperature (Scheme 8).[4]

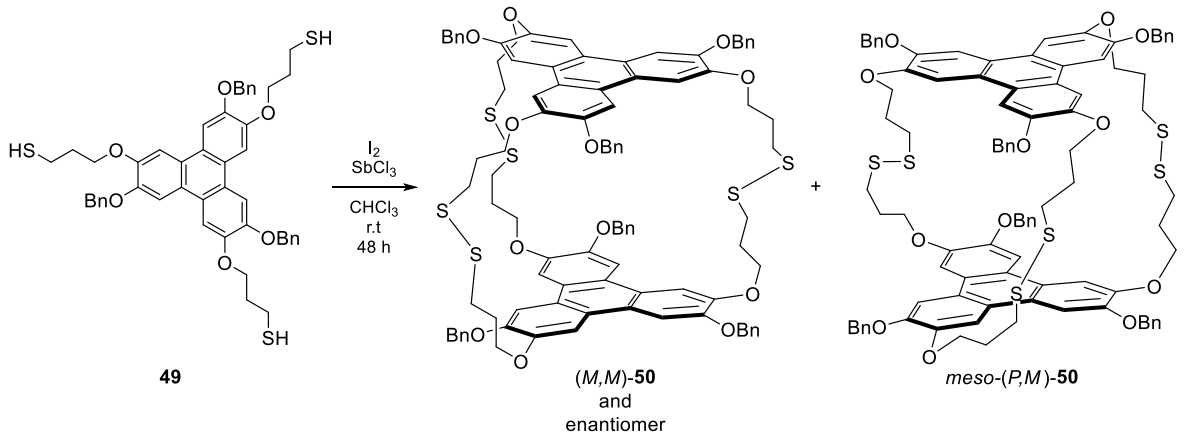

Scheme 8: Oxidation of **49** to achieve disulphide bridges between two **49** molecules.

After treatment with sodium thiosulfate to quench the excess of iodide followed by extraction, two different molecules were obtained, both characterized by very similar ^1H NMR signals. A first important observation was that all the CH_2 signals were splitted in AB systems (Figure 1) which is strongly indicative of the formation of chiral dimeric species or *meso* compounds.

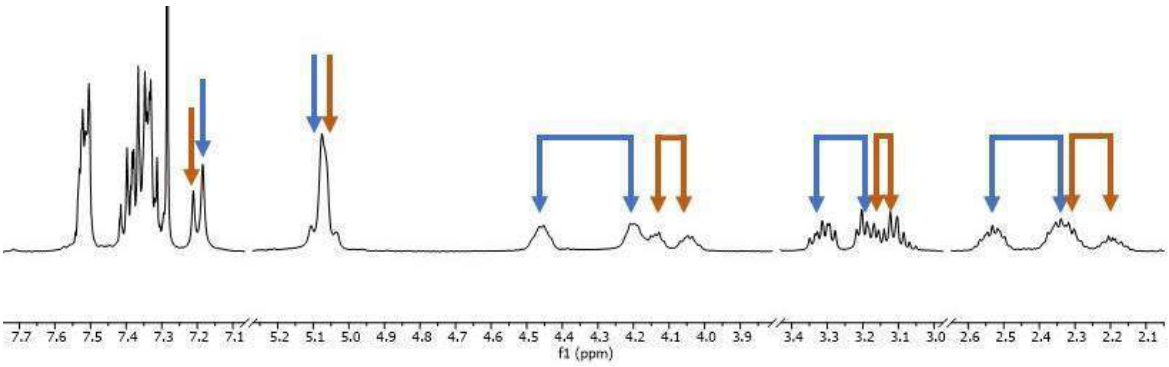

Figure 1: ^1H NMR details of the two disulphides **50**. AB systems belonging to the same molecule are highlighted by the arrow of the same colour.

Flash chromatography of the products did not allow full separation of the two stereoisomers, giving two mixed fractions, each one enriched in one of the two molecules. ESI-MS analysis on these two fractions confirmed the dimeric structure of the products, ruling out the formation of other higher oligomers. Moreover, since the two fractions have exactly the same mass spectra, this means that they were diastereoisomers, obtained with an overall 69% yield.

Thanks to the C_3-symmetry of substrate **49**, it is possible to assign the two capsular diastereoisomeric dimeric structures. Indeed, the intrinsic achirality of the tris-thiol brings to the formation of dimers in which the three thiol moieties of a *pro-P* or *pro-M* unit dimerize with a second unit, also *pro-P* or *pro-M*. Thus, a racemic compound (*P*,*P*)-**50** and (*M*,*M*)-**50** and an achiral *meso*-(*P,M*)-**50**, characterized by a similar abundance due to a comparable thermodynamic stability, are formed (Figure 2).

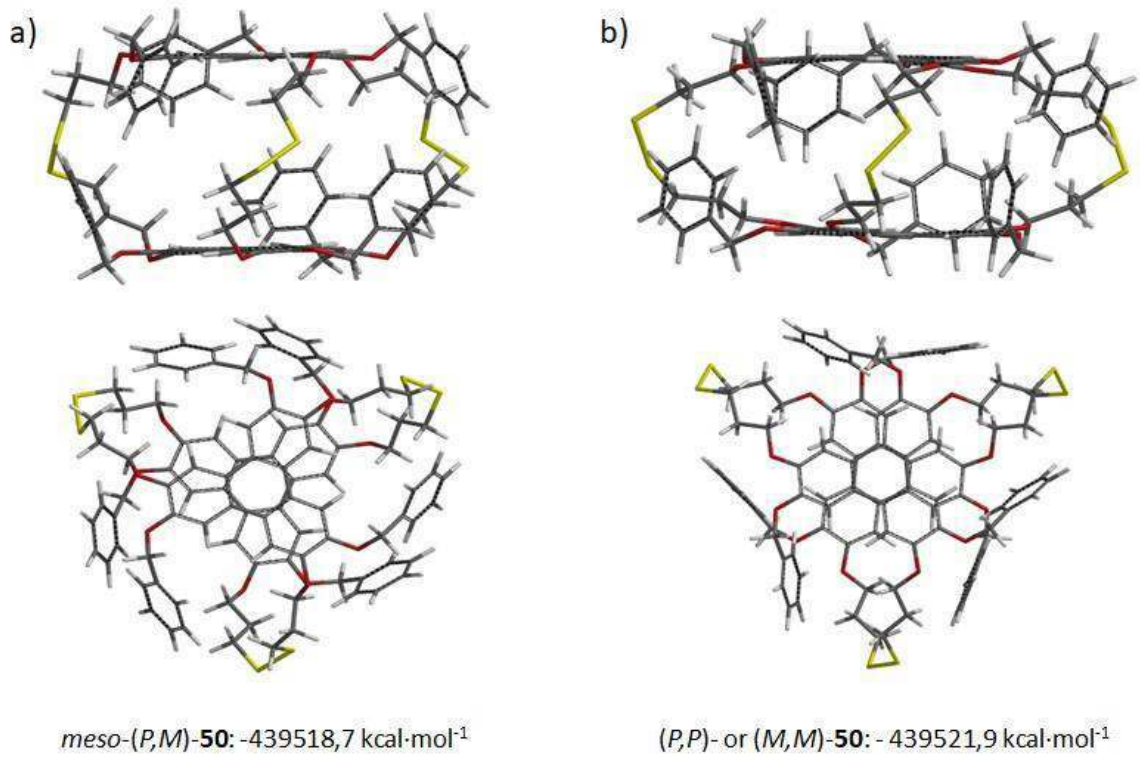

Figure 2: Top and side view of the computational models of a) *meso-(P,M)*-**50** and b) (*M,M*)-**50** and relative formation energies.

To attribute the stereochemistry of the more abundant product, the formation energies of the two compounds were calculated, allowing to point out how the (*M,M*)-**50** and (*P,P,*)-**50** isomers are thermodynamically more stable compared to the *meso*-**50** (Figure 2), thus the more abundant.

From ^{1}H NMR the distribution of the two isomers was 1:0.6, meaning one of the two is more stable than the other. Attempts of separation of the isomers in order to assign the signals were done also with preparative HPLC, unfortunately without success. For this reasons, computational *ab initio* calculations were carried out to obtain the energies of the two diastereoisomeric molecules, supposing that the more thermodynamically stable should also be the more abundant. The calculations showed that the racemic (*M,M*)-**50** and (*P,P,*)-**50** isomer is 3.2 kcal·mol^{-1} more thermodynamically stable, thus we reasonably assign its structure to the more abundant of the two isomers observed in the ^{1}H NMR spectrum.

A low-resolution ESI-MS analysis was run on the sample of **50** mixed isomers, clearly showing the foreseen product, together with sodium and potassium cations (Figure 3).

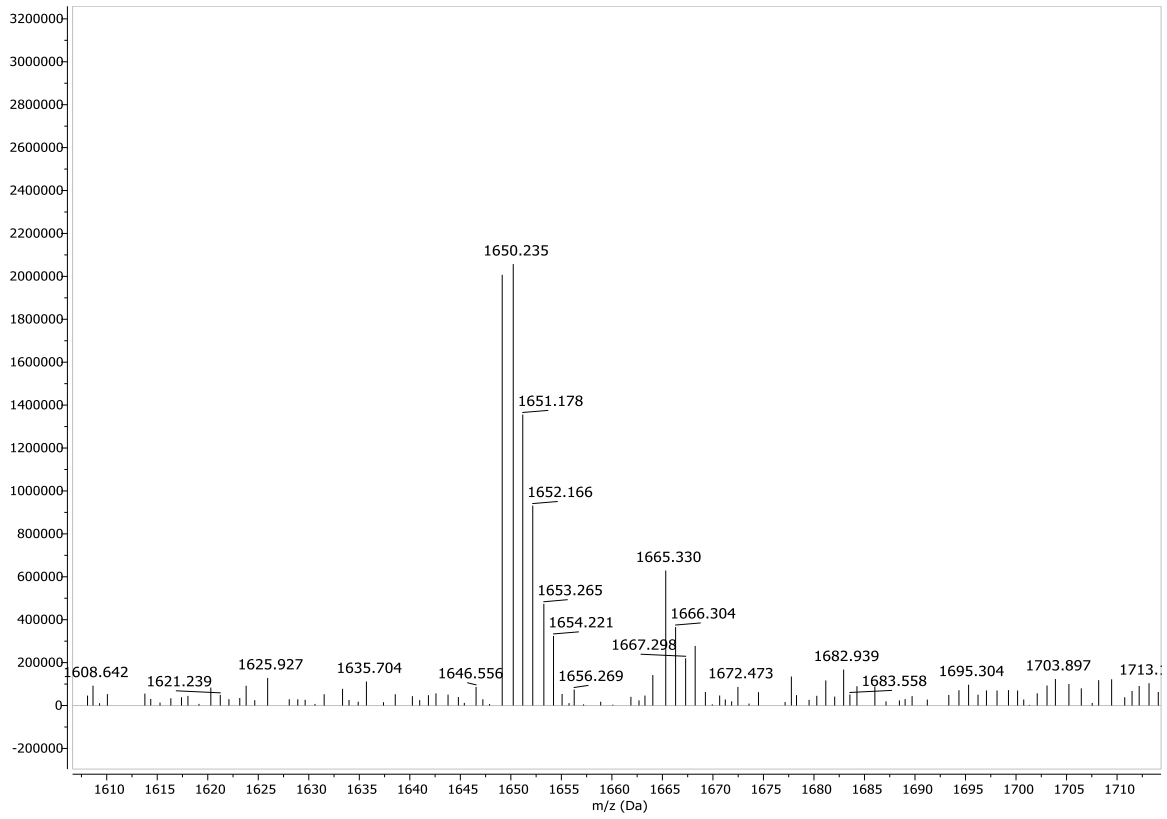

Figure 3: Low-resolution ESI-MS showing the adducts [**50**·Na]$^+$ and [**50**·K]$^+$.

Moreover, the analysis showed just one product, confirming the presence of two molecule sharing the same molecular weight.

The reaction was repeated at -20 °C to improve the diastereoselectivity of the dimerization step, but the ratio between the diastereoisomers was unchanged compared to the reaction run at room temperature.

Due to the reversibility of the disulphide bond, we investigated the stability of the covalent cages obtained and, unfortunately, we observed that the disulphide cages were not very stable over time, even at low temperature. In fact, even in the solid state, at -20 °C, the product showed partial decomposition with formation of the original thiol form after 30 days. This limits a bit the application of this class of capsules for supramolecular applications. The lower stability observed with respect to other disulphide based covalent capsules reported in the literature is likely to be due to the fact that while the latter are based on aromatic disulphide bonds,[8,9] our capsules are based on aliphatic disulphide bonds that probably are more labile.

4.3 Synthesis of the Thioether Cage Bearing a Mesitylene Unit

After the obtainment of the two disulphide cages, we decided to synthesize another cage based on sulphide covalent bonds. Following the literature highlighted at the beginning of this Chapter, we reacted the *tris*-thiol **49** with a *tris*-halogenated mesitylene derivative in order to create a smaller cage compared to the previous disulphide cages, but still larger than the majority of those reported in literature.

For this purpose, a solution of **49** and *tris*-iodomesitylene was slowly added to a mixture of K_2CO_3 in anhydrous DMF. After the addition, the resulting mixture was stirred at room temperature for 96 hours (Scheme 9).[5,6]

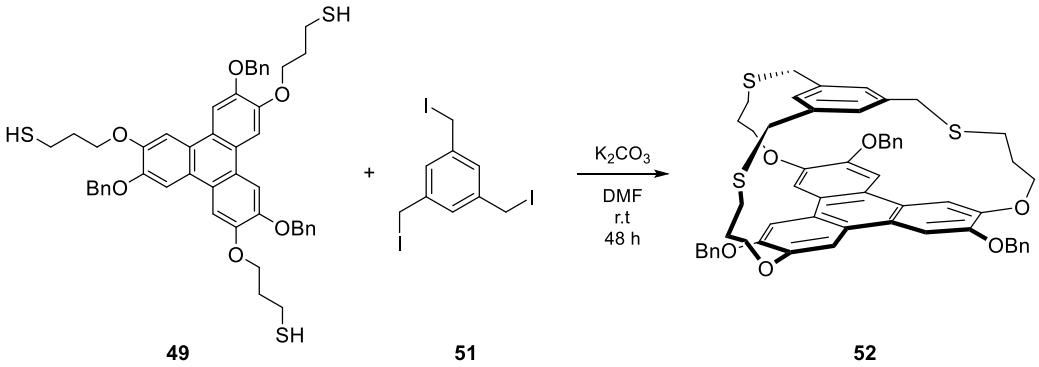

Scheme 9: Synthesis of sulphide cage **52**.

After the work-up, flash chromatography of the crude afforded the cage **52** with only a 3% yield. This very low yield is the consequence of the possible large formation of polymers in the solution, instead of well-defined entities, due to the poly-functional character of both substrates of the reaction.

The computational models of cage **52** are reported in Figure 4.

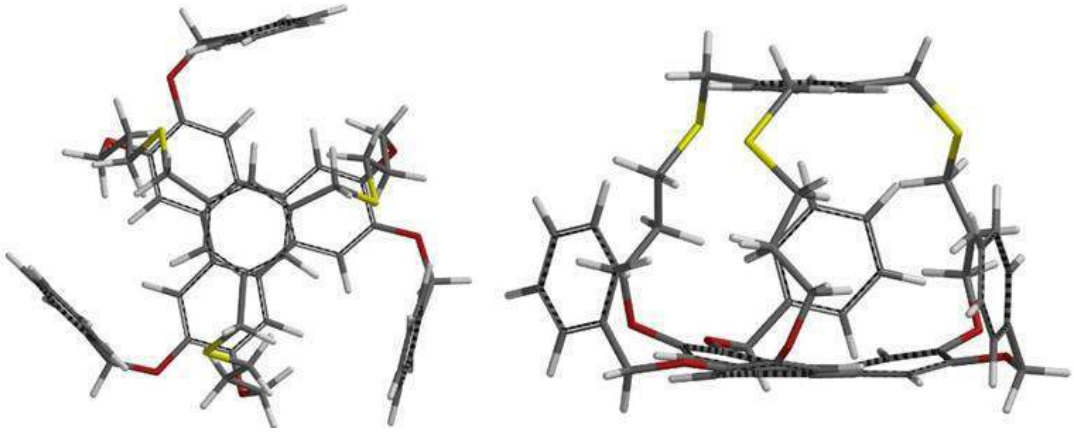

Figure 4: Top and side view of the computational models of sulphide cage **52**.

The signals in the recorded ^1H NMR spectrum of molecule **52** confirmed the foreseen molecular structure. In particular, it is possible to observe the diagnostic splitting into AB systems of all the methylenic signals (Figure 5).

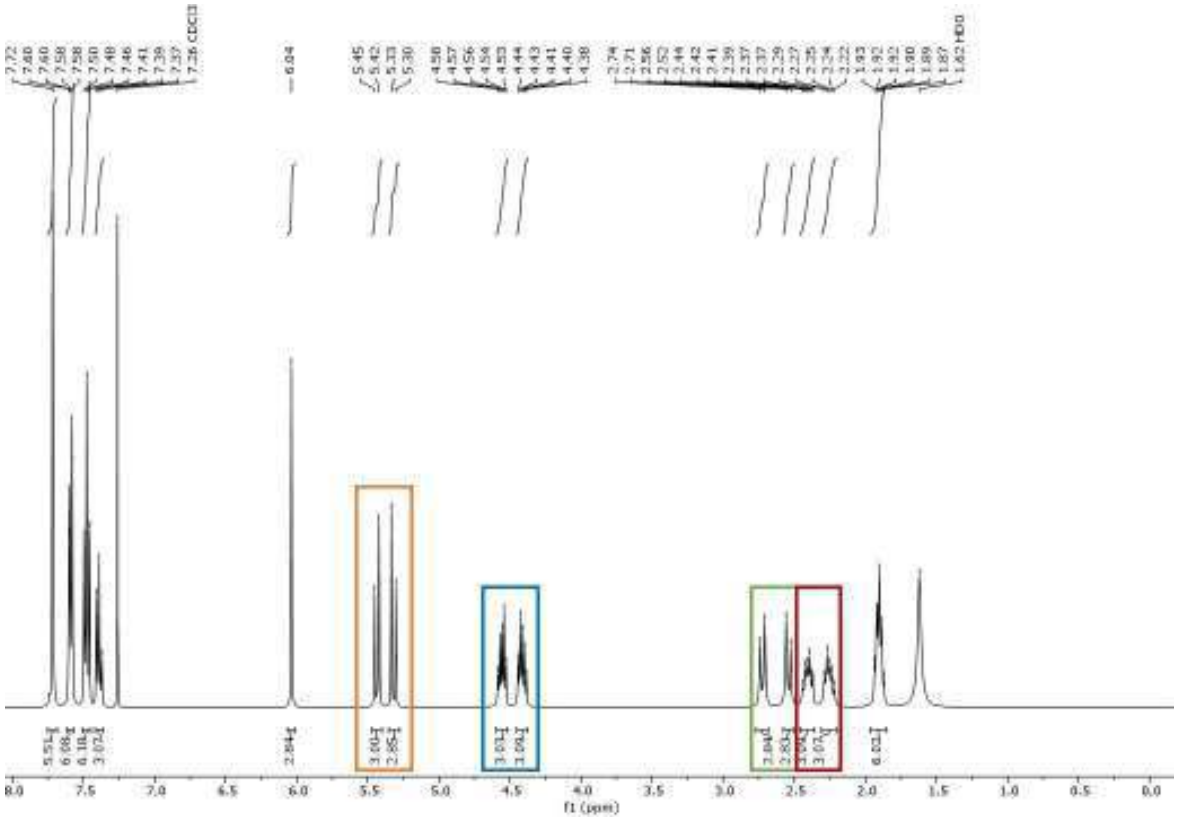

Figure 5: ^{1}H NMR spectrum of the sulphide cage **52**. Diastereotopic signals are highlighted with different colours.

The recorded ^{1}H NMR signals reported in Figure 5 confirm the expected molecular structure, with the newly formed AB systems testifying the formation of **52** as a chiral object. Indeed, even if the two subunits composing the cage are achiral, thanks to the prochirality of C_3-symmetric molecule **49** the product becomes chiral, yielding a racemic mixture. Methylenic protons are influenced by chemical and magnetical non-equivalent surrounding, thus displaying two signals with different chemical shifts, which couple with each other and eventually with other methylenic signals.

To complete the preliminary analysis, a low-resolution ESI-MS analysis was run on a sample of **52**, showing the adduct between product **52**, methanol and a proton (Figure 6).

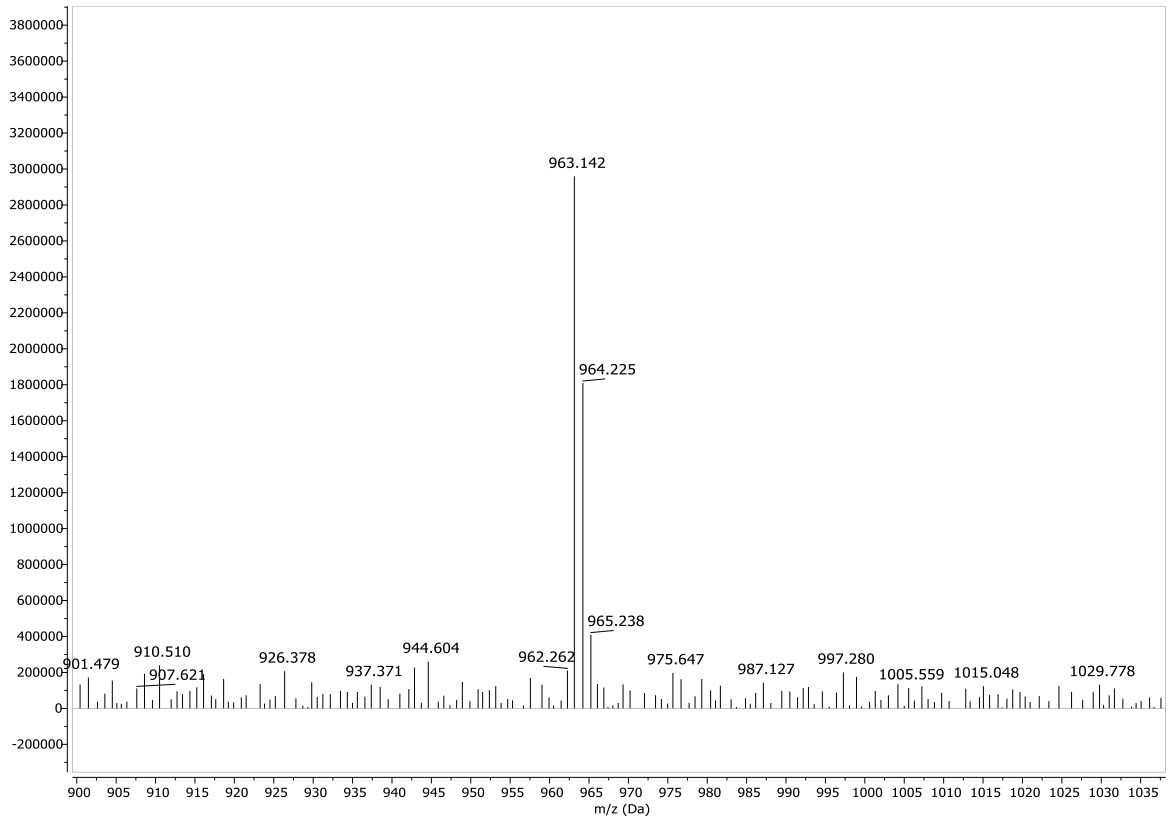

Figure 6: Low-resolution ESI-MS showing the adduct [**52**·MeOH·H]$^+$.

In order to enhance the reaction yield, trials with other halides, longer addition times and higher dilutions were taken into consideration. All the different trials and the corresponding results are reported in Table 1.

Entry	Halide	Conc. 49 [mM]	Conc. Halide [mM]	Addition time [h]	Reaction time [h]	Temperature [°C]	Yield 52[a] %
1	Iodide	12	12	12	96	25	3
2	Iodide	10	10	6	24	25	5
3	Bromide	12	12	12	72	50	4
4	Bromide	6	6	24	72	50	23
5	Bromide	4	4	24	72	50	11

Table 1: Trials at different reaction conditions for the synthesis of sulphide cage **52**. [a]: Isolated yield.

By looking at the data reported in Table 1, the reagents concentrations and the addition time play a fundamental role in the yield of the reaction, even though the formation of polymers always represents the majority of by-products. However, a compromise between dilution and reactivity is necessary since the increase of the dilution causes an unacceptable elongation of the reaction times. The use of mesityl-bromide instead of iodide allowed to obtain very similar results, enabling a better reproducibility of the reaction. In particular, with the tri-bromomesitylene the reaction was optimized under higher dilution conditions, compensating the lower activity with an increase of the reaction temperature.

It was very interesting to notice that, in addition to the expected product **52**, in all these experiments a considerable amount of the dimeric disulphide capsules **50** was present as secondary products. Even more interesting was to realize that the amount of this secondary

product was even higher than the expected mesityl-capsule **52**, obtaining the disulphide **50** as the main product of the reaction (polymers excluded). Even in this case, both *rac*- and *meso*-isomers of the disulphide **50** were obtained, with a slight difference in their relative ratio compared to the precedent synthesis. All the data relative to the disulphide found in the sulphide synthesis trials are reported in Table 2.

Entry	Halide	Conc. 49 [mM]	Conc. Halide [mM]	Addition time [h]	Reaction time [h]	Yield 50[a] %	Ratio rac-50/meso-50[b]
1	Iodide	12	12	12	96	33	1:0.5
2	Iodide	10	10	6	24	6	1:0.4
3	Bromide[c]	12	12	12	72	6	1:0.3
4	Bromide[c]	6	6	24	72	33	1:0.4
5	Bromide[c]	4	4	24	72	21	1:0.4

Table 2: Yields of disulphide cage **50** while attempting the synthesis of sulphide cage **52** at 25 °C, [a]: Isolated yield. [b]: Determined by ^{1}H NMR; [c]: 50 °C.

Table 1 and 2 clearly show that the trend in the amounts of disulphide **50** and sulphide **52** covalent cages tends to be similar, meaning that the disulphide formation and the thiol nucleophilic substitution are intimately related, with comparable reaction rates, even if the two mechanism are different. An explanation for this could be the initial formation of bromide and iodide as released anions in solution and their oxidation to molecular iodine or bromine that could act as oxidant for the thiol, causing the formation of the dimer. This hypothesis was suggested by the purple, or red, colour observed for the reaction mixtures.

In contrast with the previous reactions, pure fractions of the more abundant of the two diastereoisomers of **50**, *rac*-**50**, were isolated, allowing us to perform a full characterization and finally some supramolecular experiments with such cage (Figure 7).

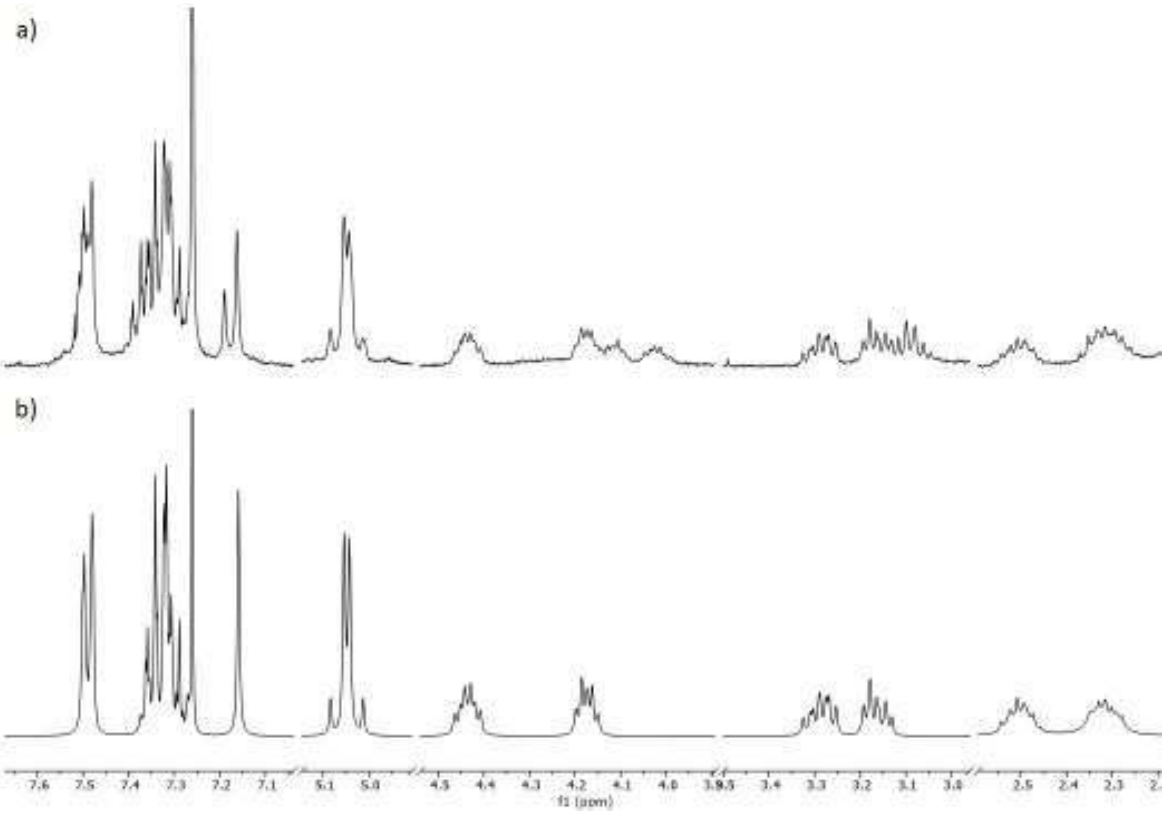

Figure 7: Comparison between ^{1}H NMR spectrum of a) mixture of **50** isomer and b) isolate fractions of the more abundant *rac*-**50**.

4.4 Host Guest Chemistry

Once the synthesis of the sulphide and disulphide cages were completed, trials with different guest were done in order to characterize their supramolecular behaviour.

4.4.1 Host Guest with Dimeric di-Sulphide Cages

Considering the high electronic density in the inside of the disulphuric cages due to two facing triphenylenic systems, cationic compounds or neutral electron-poor molecules, soluble in organic medium, were considered as potential guests.

The choice fell upon salts like NH_4BPh_4, $NaBPh_4$, 1-butyl-3-methylimidazolium chloride (BMIMCl) and, as lone neutral guest, tetracyanoquinodimethane (TCNQ), selected for the presence of four cyanide moieties, strong electron-withdrawing groups (Figure 8).

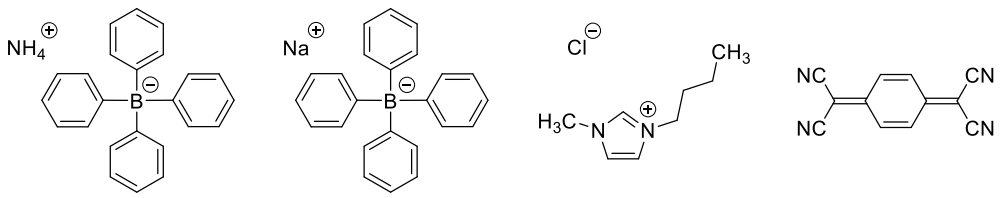

Figure 8: Guests used in the host-guest experiments. From left to right: NH_4BPh_4, $NaBPh_4$, BMIMCl and TCNQ.

The effective positive charge or the electron-deficiency of these substances should be well compensated by the extended π-conjugation of the aromatic triphenylenic systems creating the host cavity, favouring the interaction and the complexation inside the latter.

The host-guest experiments were done adding a concentrated solution of guests in $CDCl_3$ to a 1 mM solution of an isomer mixture of **50** (1:0.6 of *rac* and *meso* stereoisomers) in $CDCl_3$, in order to reach a concentration of guest equal to 5 mM. ^1H NMR spectra were later recorded.

Unfortunately, the host-guests trials done did not provide significative results, also due to a low solubility of the guests in chloroform. No significative chemical shifts variations were observed with NH_4BPh_4, $NaBPh_4$ and BMIMCl, even if preliminary low-resolution ESI-MS analysis highlighted the affinity of the host **50** for sodium cation. It will be necessary to carry on this investigation with more liposoluble ionic species, in order to increase the solubility in chloroform of the guests and allow them to better interact with the host.

The interaction of **50** with TCNQ was rather interesting, since the analysis evidenced how TCNQ brought to the fast decomposition of the disulphide bonds back to the original thiol, **49**. This was peculiar and will be subjected to more investigations, since TCNQ, an oxidizing agent, reduced the disulphide bonds.

4.4.2 Host Guest with Sulphide Cage

Even if the properties of the thioether cage **52** are comparable with those of disulphide cage **50**, its dimensions are sensibly lower. For this reason, guests like BMIMCl and TCNQ were excluded from the beginning, while NH_4BPh_4 and $NaBPh_4$ were tried as reported before for the disulphide cage. Moreover, to evaluate the host-guest properties towards neutral guests, in two different 5 mM solutions of **52** in $CDCl_3$, methane or nitrogen were bubbled for 10 minutes, in order to test their affinity for the cage. On the sample containing methane, further analysis at gradually decreasing temperature were run.

In this case, weak interactions between the host and the cationic guests were observed. Indeed, ^1H NMR spectra show small downfield shifts, about 0.01 ppm, of the aromatic and benzylic signals of **52**. ^1H NMR spectra of pure **52** and with NH_4BPh_4 and $NaBPh_4$ are reported in Figure 9.

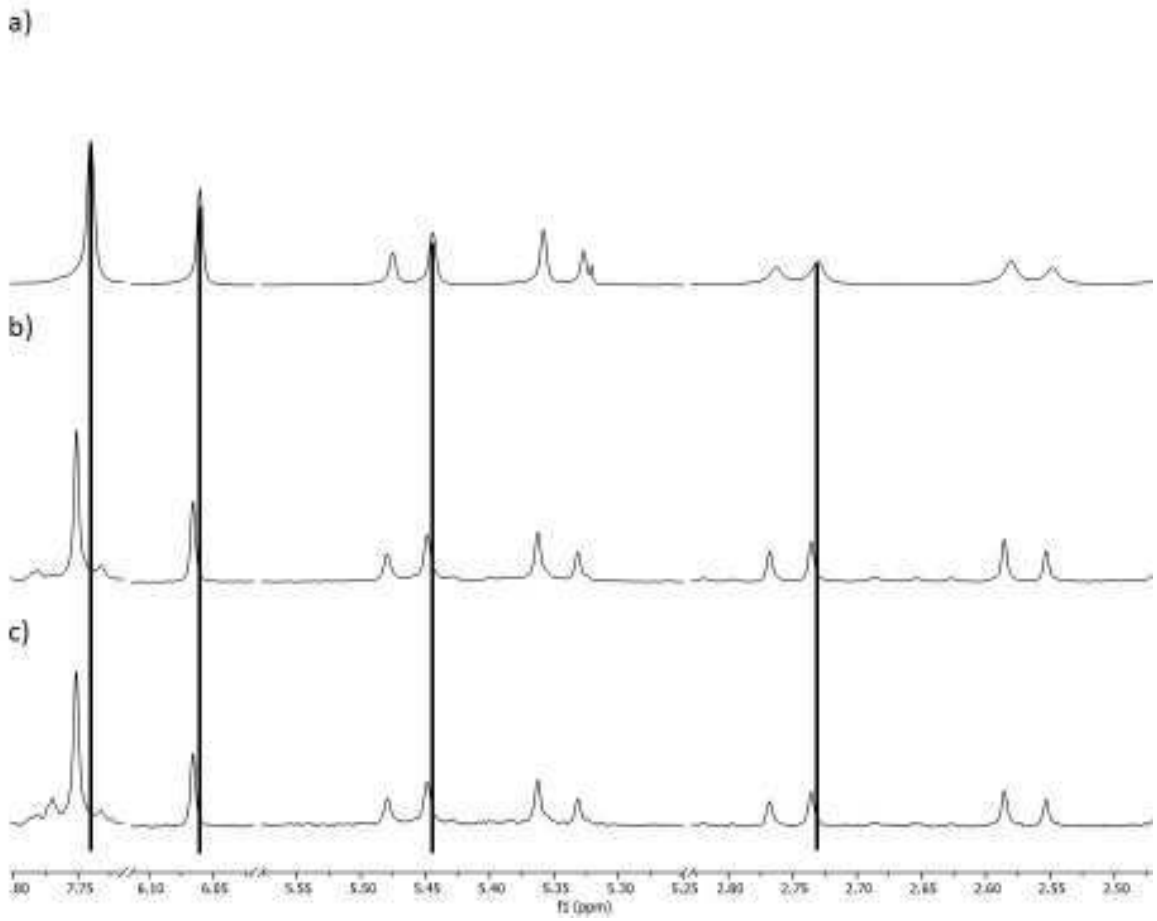

Figure 9: Comparison between ^{1}H NMR spectra details of a) only **52**, b) **52** and NH_4BPh_4 and c) **52** and $NaBPh_4$. Shifts are highlighted with a black line.

In addition to these experiments, the previously reported low-resolution ESI-MS analysis showed how the cage is easily ionized by the addition of a proton together with a methanol molecule, highlighting the affinity of this cage for cations. These results confirm the potential supramolecular properties of cage **52** and give interesting hints about its possible applications.

4.5 Experimental Section

4.5.1 General Methods

The reactions were followed with TLC Polygram® Sil G/UV254, 0.25 mm thickness. ^{1}H NMR, ^{13}C NMR, and 2D spectra were recorded with a Bruker Avance 300 and Ascend 400 spectrometers, working at 300-400 and 75-100 MHz respectively. Resonance frequencies are referred to tetramethylsilane. IR spectra were recorded with a Perkin Elmer Spectrum One spectrophotometer. Mass spectrometric measurements were performed using a Thermo Scientific LTQ Orbitrap XL equipped with HESI source. The compounds studied were dissolved in methanol or acetonitrile with a concentration of $5 \cdot 10^{-3}$ M. They were injected into the HESI source by direct infusion with the syringe pump integrated in the mass spectrometer at a 5 $mL \cdot min^{-1}$ flow rate. Mass spectra were acquired in positive-polarity mode with the following tuning conditions: Temperature 40 °C, Sheath gas 8 (arbitrary units, arb), Aux gas and Sweep gas 0 arb, Spray Voltage 4.5 kV, Capillary temperature 275 °C, Capillary Voltage -9 V, Tube lence 150 V. In negative polarity the following tuning parameters were employed: Temperature 40 °C, Sheath gas 19 (arbitrary units, arb), Aux gas and Sweep gas 0 arb, Spray Voltage 3.0 kV, Capillary temperature 275 °C, Capillary Voltage 10 V, Tube lence 120 V. Mass spectra were collected in full scan with a resolution of 100000 at m/z 400. The Orbitrap MS was calibrated just before analysis and during the acquisition in order to improve mass accuracy lock masses were employed. Low resolution MS of the cages were recorded on a Finningan LCQ Deca XP Max mass spectrometer coupled to electrospray ionisation source (ESI) in positive or negative mode. Reagents and solvents with high purity degree purchased by the providers were used as given. Otherwise, they were purified following the procedures reported in literature.[17] Anhydrous solvents were prepared by adding activated 3 Å molecular sieves to the solvent under inert atmosphere. Molecular sieves were activated shortly before the use by continuous heating under *vacuum*. Flash chromatography were performed with silica gel Merk 60, 230-400 mesh, following procedures reported in literature.[18]

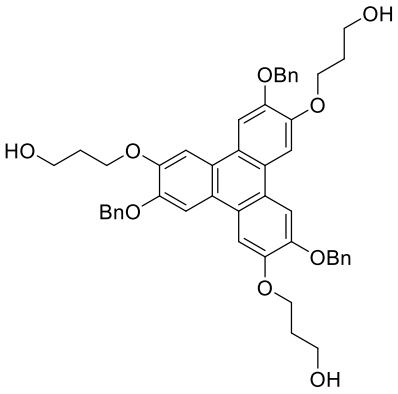

47

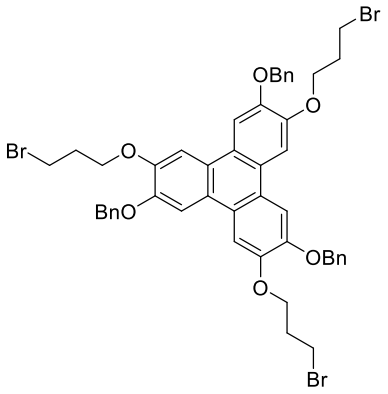

48

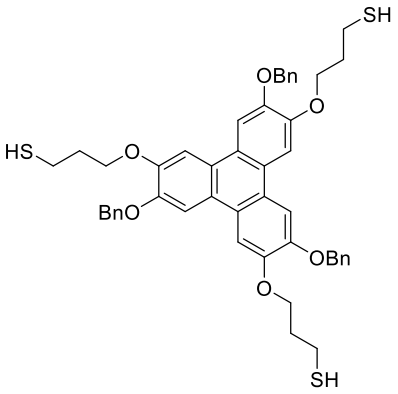

49

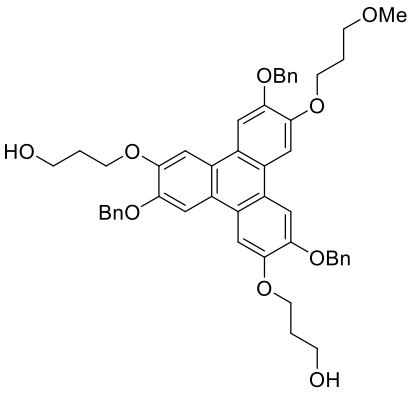

47a

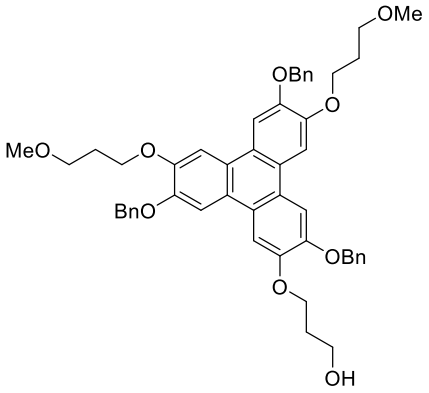

47b

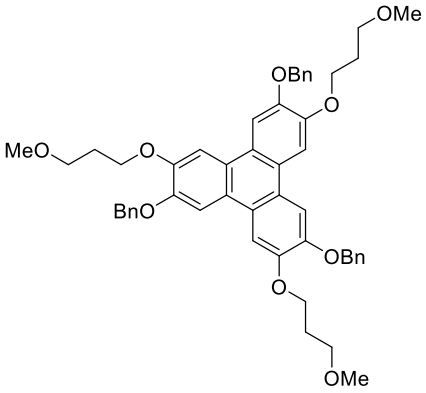

47c

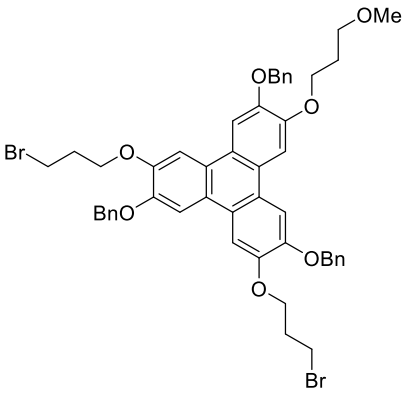

48a

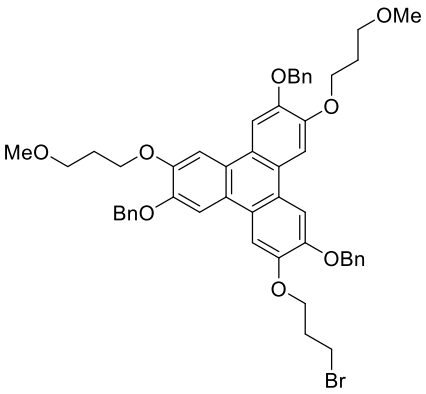

48b

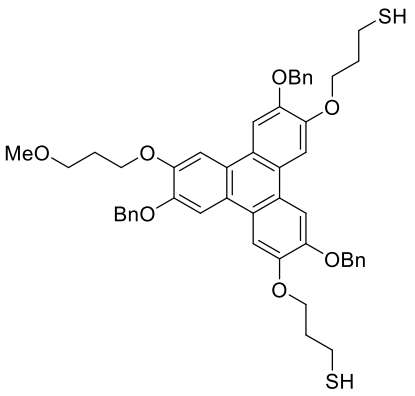

49a

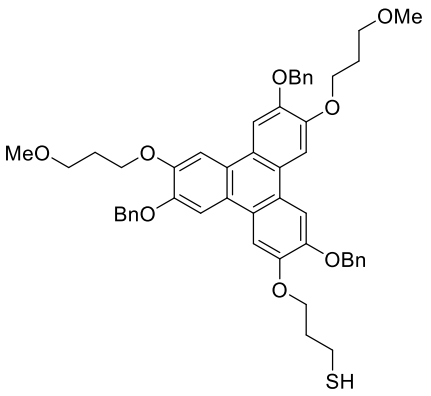

49b

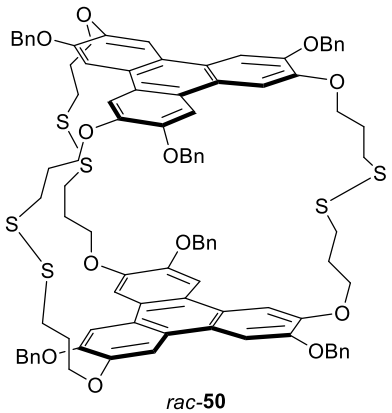

rac-**50**

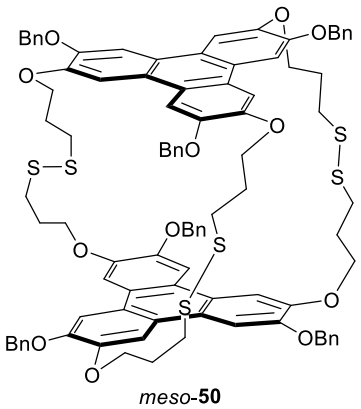

meso-**50**

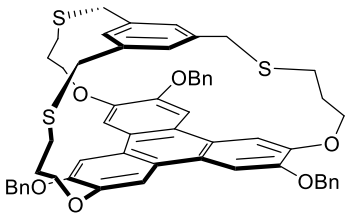

52

4.5.2 Experimental Procedures - Syntheses

3,3',3''-((3,7,11-tris(benzyloxy)triphenylene-2,6,10-triyl)tris(oxy))tris(propan-1-ol) (**47**):

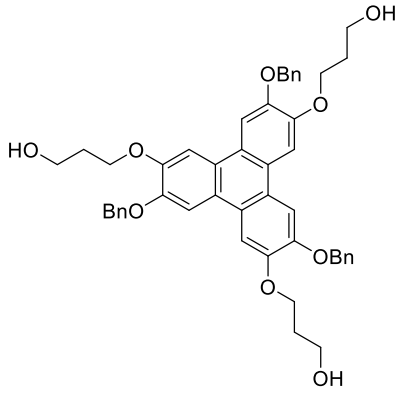

47

In a 25 mL two-necked flask, a mixture of ***C*$_3$-26** (0.25 g, 0.42 mmol), K_2CO_3 (0.522 g, 3.78 mmol) and 3-chloro-1-propanol (0.179 g, 1.89 mmol) in anhydrous DMF (5 mL) was stirred under inert atmosphere at room temperature for 60 hours. Water (25 mL) was added and the resulting precipitate was filtered, washed with water (3×3 mL) and dried in *vacuum*, to afford the product as a grey solid (0.271 g, 0.352 mmol, 84% yield). M.P. 156 °C. ^{1}H NMR (400 MHz, $CDCl_3$): δ 7.79 (3H, s), 7.65 (3H,s), 7.58-7.52 (6H, set of m), 7.42 (6H, t, *J* = 7.4 Hz), 7.38-7.31 (3H, set of m), 5.33 (6H, s), 4.37 (6H, t, *J* = 5.7 Hz), 3.96 (6H, t, *J* = 5.3 Hz), 2.24-2.14 (6H, set of m), 1.76 (3H,s). $^{13}C\{^1H\}$ NMR (100 MHz): δ 148.66, 148.30, 137.27, 128.84, 128.25, 127.56, 123.77, 123.59, 107.76, 106.57, 71.74, 68.44, 61.49, 32.09. IR (KBr): v 3434, 2918, 2846, 1651, 1618, 1518, 1454, 1436, 1382, 1262, 1193, 1045, 1026, 831, 737, 698, 614 cm^{-1}. HRMS (ESI): calcd. for $C_{48}H_{47}O_9$ [M^-] 767.3226; found: 767.3217.

Serendipitous methylation of **47**:

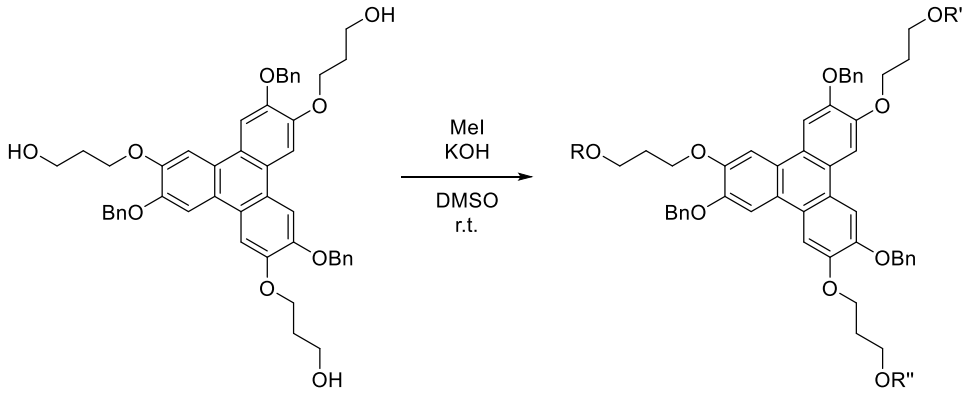

47

47a: R= Me, R'= R''= H
47b: R= R'= Me, R''= H
47c: R= R'= R''= Me

In a 25 mL two-necked flask, a mixture of **47** (0.457 g, 0.6 mmol), freshly grinded KOH (0.131 g, 2.34 mmol) and MeI (0.085 g, 0.6 mmol) in anhydrous DMSO (14 mL) was stirred for 18 hours at room temperature under inert atmosphere. A second aliquot of MeI (0.021 g, 0.15 mmol) was added and the solution was stirred at room temperature for 18 hours. The resulting solution was diluted with 1 M aqueous HCl (100 mL) and extracted with DCM (3×30

mL). The combined organic phases were dried over $MgSO_4$, filtered and concentrated in *vacuum*. The resulting crude mixture (*mono*, *bis*- and *tris*-methylated, plus unreacted substrate) was purified by gradient flash chromatography (eluent AcOEt/CyH, from 4:6 to 6:4) to afford the three products with an overall 58% yield.

3,3'-((3,7,11-tris(benzyloxy)-10-(3-methoxypropoxy)triphenylene-2,6-diyl)bis(oxy))bis(propan-1-ol) (**47a**), 28% yield. M.P. 143 °C. ^{1}H NMR (400 MHz, $CDCl_3$): δ 7.77 (2H, s), 7.74 (1H, s), 7.65 (1H, s), 7.62 (1H, s), 7.61 (1H, s), 7.59- 7.51 (6H, sets of m), 7.45-7.38 (6H, sets of m), 7.37-7.31 (3H, sets of m), 5.32 (4H, s), 5.29 (2H, s), 4.39-4.32 (4H, sets of m), 4.30 (2H, t, *J* = 6.2 Hz), 3.99-3.90 (4H, sets of m), 3.68 (2H, t, *J* = 6.1 Hz), 3.40 (3H, s), 2.27-2.13 (6H, sets of m). $^{13}C\{^1H\}$ NMR (100 MHz): δ 149.2, 148.6, 148.6, 148.3, 148.2, 148.1, 137.7, 137.3, 137.3, 128.8, 128.8, 128.7, 128.2, 128.2, 128.0, 127.6, 127.5, 127.5, 124.0, 123.8, 123.7, 123.6, 123.4, 123.3, 108.8, 107.7, 107.7, 106.6, 106.5, 106.4, 72.1, 71.7, 71.6, 69.5, 68.3, 68.3, 66.3, 61.4, 58.9, 32.1, 29.9. IR (KBr): ν 3528, 3423, 2917, 2846, 1618, 1517, 1454, 1437, 1381, 1263, 1190, 1166, 1038, 1023, 839, 741, 701, 615 cm^{-1}. HRMS (ESI): calcd. for $C_{49}H_{50}O_9$ [M^+] 782.3460; found: 782.3492.

3-((3,7,11-tris(benzyloxy)-6,10-bis(3-methoxypropoxy)triphenylen-2-yl)oxy)propan-1-ol (**47b**), 24% yield. M.P. 110 °C. ^{1}H NMR (400 MHz, $CDCl_3$): δ 7.83 (1H, s), 7.81 (2H, s), 7.68 (2H, s), 7.66 (1H, s), 7.60-7.53 (6H, sets of m), 7.45-7.38 (6H, sets of m), 7.37-7.31 (3H, sets of m), 5.34 (2H, s), 5.33 (4H, s), 4.37 (2H, t, *J* = 5.8 Hz), 4.32 (2H, t, *J* = 6.3 Hz), 4.31 (2H, t, *J* = 6.3 Hz), 3.96 (2H, t, *J* = 5.5 Hz), 3.68 (2H, t, *J* = 6.1 Hz), 3.68 (2H, t, *J* = 6.1 Hz), 3.41 (6H, s), 2.28-2.15 (6H, sets of m). $^{13}C\{^1H\}$ NMR (100 MHz): δ 149.2, 148.6, 148.4, 148.3, 148.3, 148.2, 137.7, 137.7, 137.3, 128.8, 128.8, 128.7, 128.2, 128.1, 128.0, 127.6, 127.5, 127.5, 124.2, 124.1, 123.8, 123.8, 123.6, 123.4, 123.3, 109.0, 107.8, 106.7, 106.6, 72.1, 72.1, 71.7, 69.5, 68.5, 66.3, 66.3, 61.6, 59.0, 32.1, 29.9, 29.8. . IR (KBr): ν 2917, 2846, 1618, 1519, 1470, 1437, 1382, 1262, 1164, 1048, 1031, 1017, 822, 745, 699, 621 cm^{-1}. HRMS (ESI): calcd. for $C_{50}H_{51}O_9$ [M^-] 795.3539; found: 795.3535.

2,6,10-tris(benzyloxy)-3,7,11-tris(3-methoxypropoxy)triphenylene (**47c**), 6% yield. M.P. 111 °C. ^{1}H NMR (400 MHz, $CDCl_3$): δ 7.84 (3H, s), 7.69 (3H, s), 7.59-7.54 (6H, sets of m), 7.44-7.39 (6H, sets of m), 7.36-7.30 (3H, sets of m), 5.34 (6H, s), 4.32 (6H, t, *J* = 6.4 Hz), 3.68 (6H, t, *J* = 6.1 Hz), 3.41 (9H, s), 2.27-2.18 (6H, sets of m). $^{13}C\{^1H\}$ NMR (100 MHz): δ 149.2, 148.3, 137.7, 128.8, 128.1, 127.5, 124.2, 123.3, 109.1, 106.7, 72.1, 69.6, 66.3, 59.0, 30.0. IR (KBr): ν 3060, 3033, 2924, 2868, 1618, 1520, 1437, 1386, 1262, 1165, 1199, 1121, 1093, 1050, 1029, 929, 861, 823, 749, 702, 618 cm^{-1}. HRMS (ESI): calcd. for $C_{51}H_{54}O_9$ [M^+] 810.3762; found: 810.3788.

General Procedure 1 (GP1): General procedure for conversion of alcohols into bromides.

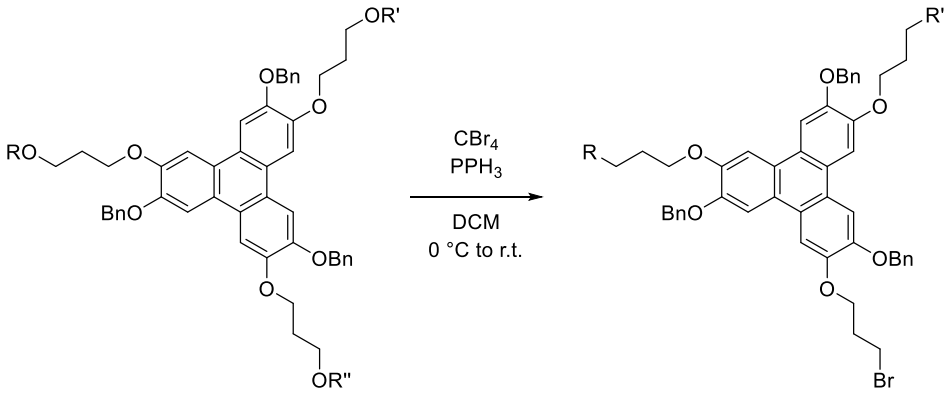

47: R= R'= R''= H
47a: R= Me, R'= R''= H
47b: R= R'= Me, R''= H

48: R= R'= Br
48a: R= OMe, R'= Br
48b: R= R'= OMe

In a 25 mL pear-shaped two-necked flask, a solution of the substrate (0.2 mmol) and CBr_4 (1.25 eq. for each hydroxy group) in anhydrous DCM (4 mL) was cooled to 0 °C under inert atmosphere. Triphenylphosphine (1.8 eq. for each hydroxyl group) was added in small portions, allowing the reaction to warm to room temperature overnight. The resulting solution was concentrated in *vacuum* and subjected to flash chromatography.

2,6,10-tris(benzyloxy)-3,7,11-tris(3-bromopropoxy)triphenylene (**48**): **GP1** was applied on **47**. Eluent DCM, 72% yield. M.P. 133 °C. ^{1}H NMR (400 MHz, $CDCl_3$): δ 7.84 (3H, s), 7.70 (3H, s), 7.58-7.53 (6H, set of m), 7.45-7.39 (6H, set of m), 7.37-7.32 (3H, set of m), 5.34 (6H, s), 4.35 (6 H, t, *J* = 5.9 Hz), 3.72 (6 H, t, *J* = 6.3 Hz), 2.52-2.43 (6 H, set of m). $^{13}C\{^1H\}$ NMR (100 MHz): δ 148.8, 148.6, 137.5, 128.8, 128.2, 127.4, 124.0, 123.7, 108.7, 107.4, 72.0, 67.1, 32.6, 30.5. IR (KBr): ν 3445, 2917, 2846, 1637, 1619, 1577, 1517, 1436, 1382, 1264, 1160, 1045, 1028, 823 cm^{-1}. HRMS (ESI): calcd. for $C_{48}H_{45}Br_3O_6$ [M$^-$] 956.0740; found: 956.0750.

2,6,10-tris(benzyloxy)-3,7-bis(3-bromopropoxy)-11-(3-methoxypropoxy)triphenylene (**48a**): **GP1** was applied on **47a**. Eluent DCM/Et_2O, 99:1, 74% yield. M.P. 136 °C. ^{1}H NMR (400 MHz, $CDCl_3$): δ 7.84 (1H, s), 7.83 (1H, s), 7.83 (1H, s), 7.70 (3H, s), 7.59-7.53 (6H, sets of m), 7.45-7.38 (6H, sets of m), 7.37-7.32 (3H, sets of m), 5.35 (2H, s), 5.34 (4H, s), 4.35 (4H, t, *J* = 5.8 Hz), 4.32 (2H, t, *J* = 6.4 Hz), 3.72 (4H, t, *J* = 6.3 Hz), 3.68 (2H, t, *J* = 6.1 Hz), 3.41 (3H, s), 2.51-2.43 (4H, sets of m), 2.27-2.19 (2H, sets of m). $^{13}C\{^1H\}$ NMR (100 MHz): δ 149.3, 148.8, 148.8, 148.5, 148.5, 148.4, 137.7, 137.5, 128.8, 128.8, 128.2, 128.1, 128.1, 127.5, 127.4, 124.1, 124.0, 123.9, 123.6, 123.4, 108.9, 108.9, 108.8, 107.4, 107.4, 106.8, 72.1, 72.0, 69.5, 67.1, 66.4, 59.0, 32.7, 30.5, 29.9. IR (KBr): ν 2917, 2846, 1617, 1519, 1436, 1385, 1262, 1196, 1164, 1122, 1047, 1026, 823, 746, 699, 617 cm^{-1}.

2,6,10-tris(benzyloxy)-3-(3-bromopropoxy)-7,11-bis(3-methoxypropoxy)triphenylene (**48b**): **GP1** was applied on **47b**. Eluent DCM/Et_2O, 97:3, 61% yield. M.P. 128 °C. ^{1}H NMR (400 MHz, $CDCl_3$): δ 7.84 (1H, s), 7.84 (1H, s), 7.83 (1H, s), 7.70 (3H, s), 7.59-7.54 (6H, sets of m), 7.45-7.38 (6H, sets of m), 7.37-7.30 (3H, sets of m), 5.35 (4H, s), 5.34 (2H, s), 4.35 (2H, t, *J* = 5.9 Hz), 4.32 (4H, t, *J* = 6.3 Hz), 3.72 (2H, t, *J* = 6.3 Hz), 3.68 (4H, t, *J* = 6.1 Hz), 3.41 (6H, s), 2.51-2.43 (2H, sets of m), 2.27-2.19 (4H, sets of m). $^{13}C\{^1H\}$ NMR (100 MHz): δ 149.3, 149.2, 148.8, 148.4, 148.4, 148.3, 137.7, 137.6, 128.8, 128.8, 128.1, 128.1, 128.1, 127.5, 127.4, 124.2, 124.1, 123.7, 123.5, 123.3, 109.0, 109.0, 108.9, 107.4, 106.8, 106.7, 72.1, 72.1,

69.6, 67.1, 66.3, 59.0, 32.7, 30.5, 30.0. IR (KBr): ν 2917, 2862, 2807, 1617, 1250, 1437, 1386, 1262, 1164, 1199, 1164, 1120, 1091, 1047, 1028, 860, 823, 748, 701, 617 cm^{-1}.

General Procedure 2 (GP2): General procedure for conversion of bromides into thiols.

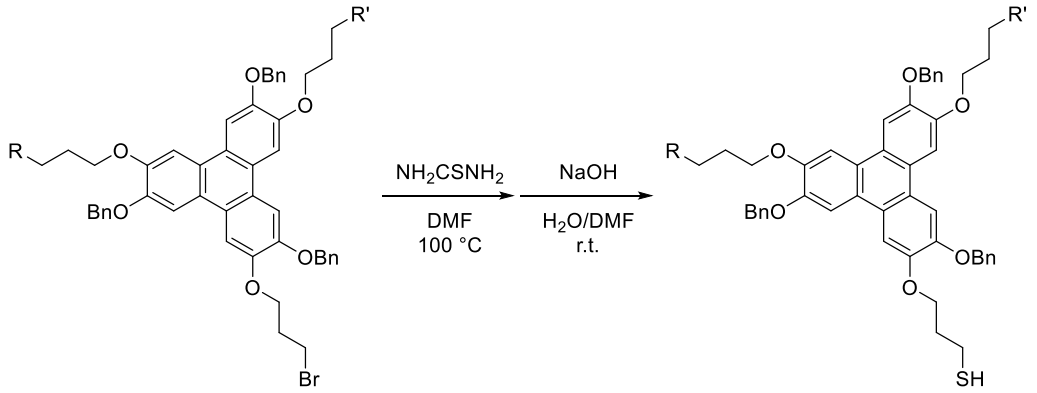

48: R= R'= Br
48a: R= OMe, R'= Br
48b: R= R'= OMe

49: R= R'= SH
49a: R= OMe, R'= SH
49b: R= R'= OMe

In a 25 mL pear-shaped two-necked flask, a suspension of substrate (0.07 mmol) and thiourea (2 eq. for each bromide on the substrate) in anhydrous DFM (4 mL) was heated overnight at 100 °C under inert atmosphere. The resulting solution was cooled to room temperature, transferred in a 50 mL two-necked flask and degassed with argon for 1 hour. Simultaneously, a freshly prepared 0.4 M aqueous NaOH solution (20 mL) was degassed with argon for 1 hour. The NaOH solution was added to the DMF and the resulting solution was stirred overnight at room temperature under inert atmosphere. The resulting mixture was extracted with degassed DCM (3×15 mL) and the combined organic phases were dried over $MgSO_4$, filtered and concentrated in *vacuum*, to afford the products as yellowish solids.

3,3',3''-((3,7,11-tris(benzyloxy)triphenylene-2,6,10-triyl)tris(oxy))tris(propane-1-thiol) (**49**): **GP2** was applied on **48**, 84% yield. M.P. 153 °C. ^{1}H NMR (400 MHz, $CDCl_3$): δ 7.84 (3H, s), 7.69 (3H, s), 7.58-7.53 (6H, set of m), 7.45-7.39 (6H, set of m), 7.38-7.31 (3H, set of m), 5.34 (6H, s), 4.33 (6H, t, *J* = 6.0 Hz), 2.85 (6H, dt, *J* = 8.1 Hz, *J* = 6.8 Hz), 2.28-2.20 (6H, set of m), 1.52 (3H, t, *J* = 8.1 Hz). $^{13}C\{^1H\}$ NMR (100 MHz): δ 149.0, 148.5, 137.5, 128.8, 128.1, 127.5, 124.0, 123.6, 108.8, 107.1, 72.1, 67.3, 33.5, 21.6. IR (KBr): ν 1616, 1591, 1436, 1385, 1259, 1162, 1042, 1027, 823, 750, 701, 614. cm^{-1}. HRMS (ESI): calcd. for $C_{48}H_{48}O_6S_3$ [M^+] 816.2608; found: 816.2638.

3,3'-((3,7,11-tris(benzyloxy)-10-(3-methoxypropoxy)triphenylene-2,6-diyl)bis(oxy))bis(propane-1-thiol) (**49a**): **GP2** was applied on **48a**, 80% yield. M.P. 111 °C. ^{1}H NMR (400 MHz, $CDCl_3$): δ 7.84 (1H, s), 7.83 (2H, s), 7.70 (1H, s), 7.68 (2H, s), 7.62-7.51 (6H, sets of m), 7.48-7.38 (6H, sets of m), 7.39-7.29 (3H, sets of m), 5.35 (2H, s), 5.34 (4H, s), 4.32 (6H, t, *J* = 6.1 Hz), 3.68 (2H, t, *J* = 6.1 Hz), 3.41 (3H, s), 2.85 (4H, dt, *J* = 8.0, 6.8 Hz), 2.32-2.16 (6H, sets of m), 1.52 (2H, t, *J* = 8.1 Hz). $^{13}C\{^1H\}$ NMR (100 MHz): δ 149.3, 149.0, 149.0, 148.5, 148.4, 148.4, 137.7, 137.6, 137.6, 128.8, 128.8, 128.1, 128.1, 128.1, 127.5, 127.5, 127.4, 124.1, 124.1, 124.0, 123.7, 123.5, 123.3 109.0, 108.8, 108.8, 107.1, 107.1, 106.7, 72.1, 72.1, 72.0, 69.5, 67.3, 67.3, 66.3, 59.0, 33.5, 21.6. IR (KBr): 2917, 2846, 1617, 1519, 1437, 1387, 1261, 1199, 1163, 1048, 1029, 860, 823, 750, 702, 619 cm^{-1}.

3-((3,7,11-tris(benzyloxy)-6,10-bis(3-methoxypropoxy)triphenylen-2-yl)oxy)propane-1-thiol (**49b**): **GP2** was applied on **49b**, 81% yield. M.P. 113 °C. ^{1}H NMR (400 MHz, $CDCl_3$): δ 7.84 (2H, s), 7.83 (1H, s), 7.70 (2H, s), 7.69 (1H, s), 7.62-7.51 (6H, sets of m), 7.44-7.39 (6H, sets of m), 7.37-7.31 (3H, sets of m), 5.35 (4H, s), 5.34 (2H, s), 4.34-4.29 (6H, sets of m), 3.68 (4H, t, *J* = 6.1 Hz), 3.41 (6H, s), 2.85 (2H, dt, *J* = 8.1, 6.8 Hz), 2.29-2.17 (6H, sets of m), 1.52 (1H, t, *J* = 8.1 Hz). IR (KBr): ν 2918, 2846, 1618, 1520, 1437, 1386, 1262, 1165, 1119, 1050, 1028, 861, 823, 749, 703, 620 cm^{-1}.

$1^{3,7,11}$,$12^{3,7,11}$-haxabenzyloxy-2,11,13,21,23,32-haxaoxa-6,7,17,18,27,28-haxathia-1,12(2,6,10)-bistriphenylenabicyclo[10.10.10]dotriacontanophane (*rac*-**50** and *meso*-**50**):

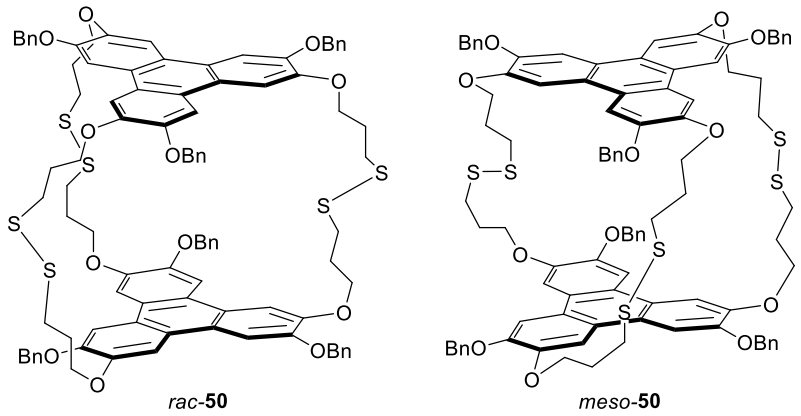

In a 100 mL round-bottomed flask, to a solution of substrate **49** (0.081 g, 0.10 mmol) in dry $CHCl_3$ (24 mL) maintained under argon atmosphere was added dropwise a solution of iodine (0.076 g, 0.30 mmol) and $SbCl_3$ (0.057 g, 0.25 mmol) in anhydrous $CHCl_3$ (24 mL). The resulting purple solution was maintained under stirring overnight. Saturated aqueous $Na_2S_2O_3$ (50 mL) was added, the layers were separated, and the aqueous layer was extracted with $CHCl_3$ (2×20 mL). The combined organic layers were washed with water (2×30 mL), dried over $MgSO_4$, filtered and concentrated in *vacuum*, to afford the two isomers of the product as a yellowish solid (0.056 g, 0.03 mmol, 69% yield, *rac*-**50**/*meso*-**50** ratio 1:0.6).

meso-**50**: ^{1}H NMR (400 MHz, $CDCl_3$): δ 7.52-7.47 (12H, set of m), 7.41-7.27 (24 H, set of m), 7.18 (6H, s), 5.06 (6H, d, *J* = 11.8 Hz), 5.02 (6H, d, *J* = 11.9 Hz), 4.14- 4.07 (6H, set of m), 4.05-3.97 (6H, set of m), 3.14-3.01 (12H, set of m), 2.37-2.24 (6H, set of m), 2.21-2.11 (6H, set of m).

rac-**50**: M.P. 197 °C. ^{1}H NMR (400 MHz, $CDCl_3$): δ 7.53- 7.45 (12H, set of m), 7.39-7.27 (24 H, set of m), 7.16 (6H, s), 5.07 (6H, d, *J* = 12.0 Hz), 5.03 (6H, d, *J* = 12.0 Hz), 4.48-4.39 (6H, set of m), 4.22-4.12 (6H, set of m), 3.36-3.23 (6H, set of m), 3.23- 3.11 (6H, set of m), 2.57-2.45 (6H, set of m), 2.37-2.23 (6H, set of m). $^{13}C\{^{1}H\}$ NMR (100 MHz): δ 147.9, 147.8, 137.8, 128.6, 127.8, 127.3, 123.3, 122.9, 107.1, 106.4, 77.5, 77.2, 76.8, 70.6, 66.9, 37.0, 29.5. IR (KBr): ν 1617, 1517, 1454, 1453, 1377, 1263, 1162, 1048, 738 cm^{-1}.

$8^{3,7,11}$-tribenzyloxy-7,9,20-trioxa-3,13,16-trithia-1(1,3,5)-benzena-8(2,6,10)triphenylenabicyclo[6.6.6]eicosaphane (**52**):

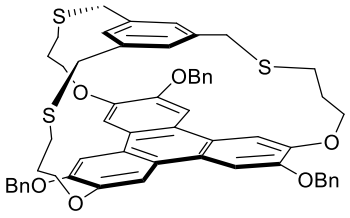

52

In a 100 mL two-necked round-bottomed flask maintained under inert atmosphere, to a slurry of K_2CO_3 (0.114 g, 0.8 mmol) in degassed anhydrous DMF (7.5 mL) was added dropwise in 24 hours, with the help of a syringe-pump a solution of substrate **49** (0.070 g, 0.09 mmol) and mesitylene *tris*-bromide (0.031 g, 0.09 mmol) in degassed anhydrous DMF (7.5 mL), maintaining the mixture at 50 °C. The mixture was further stirred at 50 °C for 72 hours. 1 M aqueous HCl (80 mL) was added and the mixture was extracted with DCM (3×20 mL). The combined organic layers were dried over $MgSO_4$, filtered and concentrated in *vacuum*. The crude product was subjected to gradient column chromatography (eluent from DCM/CyH 9:1 to pure DCM), affording the desired product **52** (0.02 g, 0.02 mmol, 23% yield). M.P. 200 °C (dec.). ^{1}H NMR (400 MHz, $CDCl_3$): δ 7.72 (6H, s), 7.63-7.55 (6H, set of m), 7.51-7.44 (6H, set of m), 7.42-7.35 (3H, set of m), 6.04 (3H, s), 5.44 (3H, d, *J* = 12.4 Hz), 5.32 (3H, d, *J* = 12.5 Hz), 4.56 (3H, dt, *J* = 11.5, 5.6 Hz), 4.41 (3H, dt, *J* = 11.7, 5.7 Hz), 2.72 (3H, d, *J* = 12.9 Hz), 2.54 (3H, d, *J* = 13.0 Hz), 2.45-2.34 (3H, set of m), 2.32-2.21 (3H, set of m), 1.99-1.84 (6H, set of m). $^{13}C\{^1H\}$ NMR (100 MHz): δ 150.0, 146.8, 137.4, 137.2, 129.0, 128.4, 127.6, 126.7, 124.9, 123.5, 114.3, 107.7, 71.2, 69.5, 36.9, 30.1, 29.7. IR (KBr): ν 1613, 1503, 1454, 1425, 1257, 1143, 1030, 729, 700 cm^{-1}.

From the same reaction, product **50** was also isolated (0.023 mg, 0.014 mmol, 33% yield).

4.5.3 NMR and MS Spectra

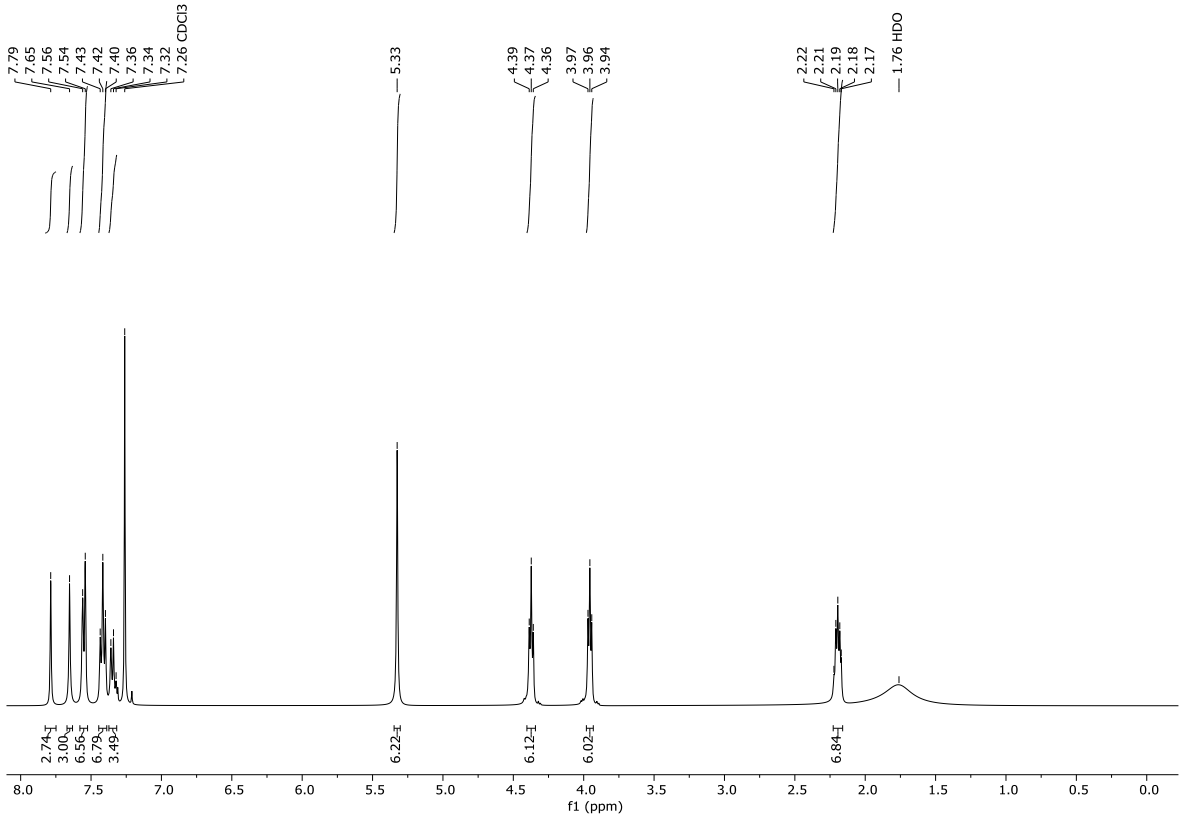

Figure I: ^{1}H NMR of molecule **47**.

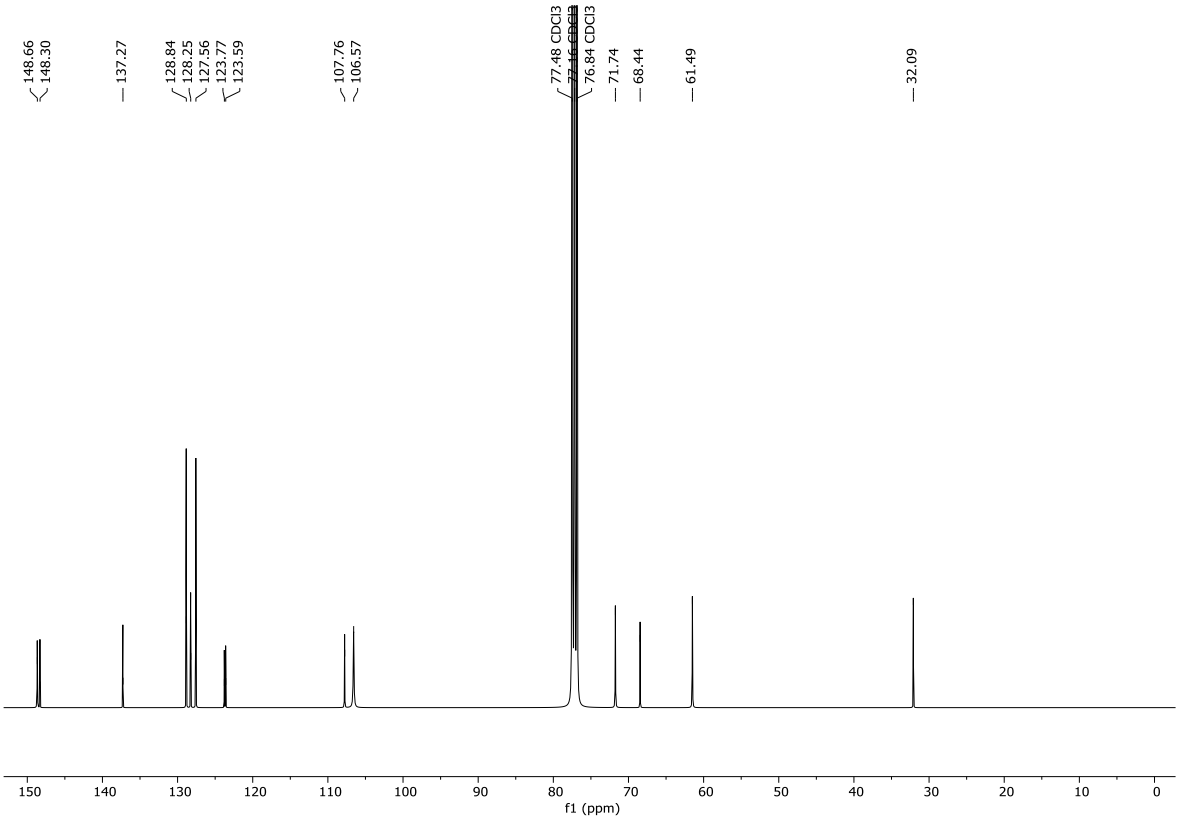

Figure II: ^{13}C NMR of molecule **47**.

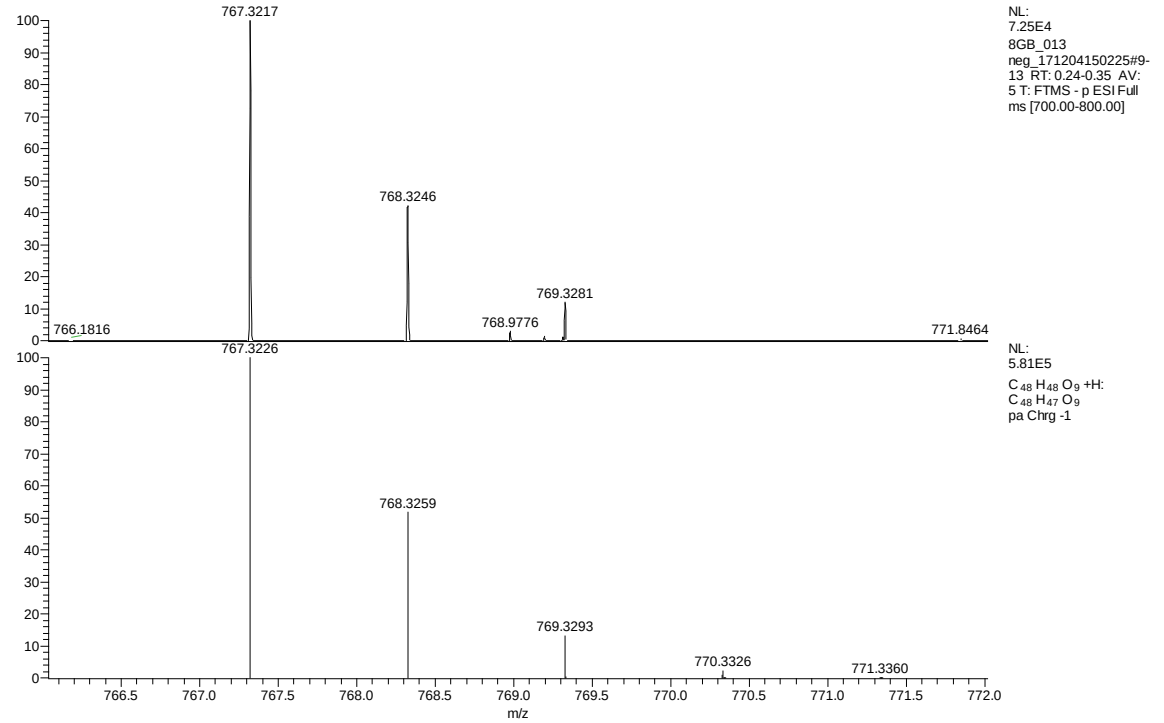

Figure III: ESI-HRMS of molecule **47**.

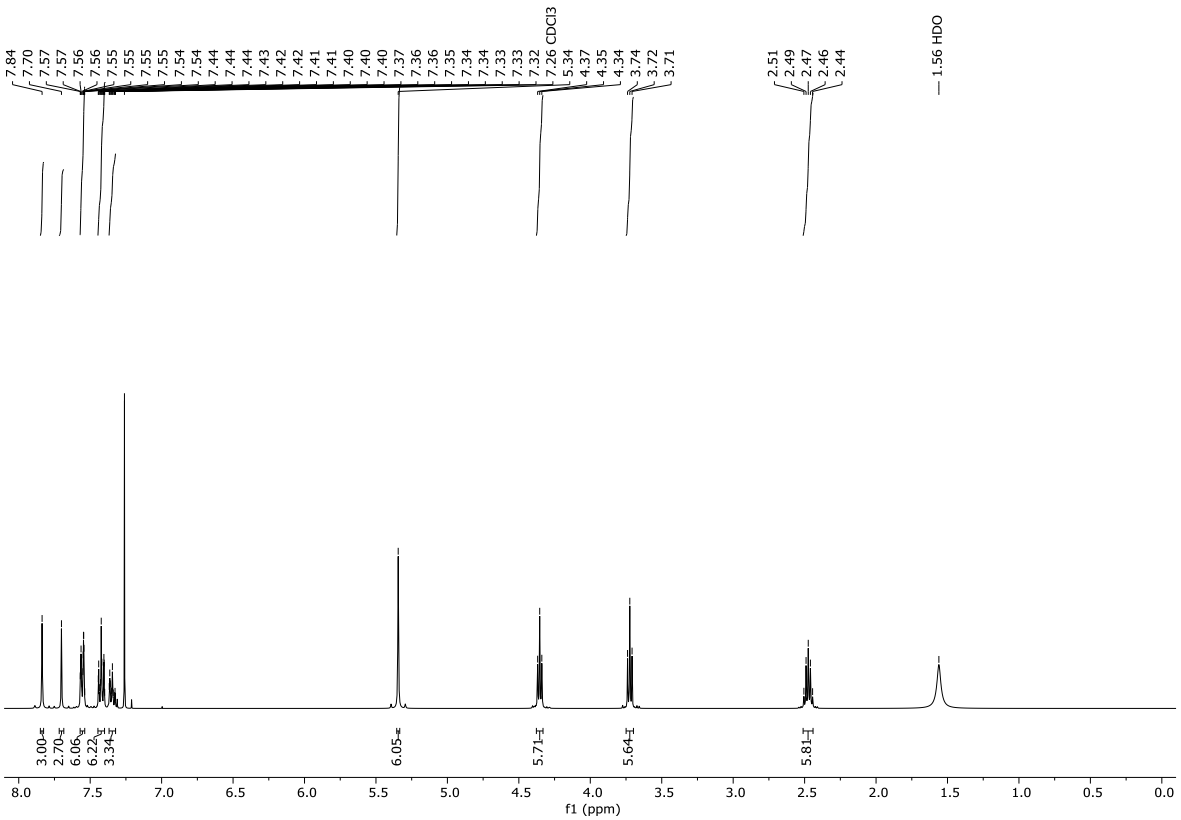

Figure IV: ^{1}H NMR of molecule **48**.

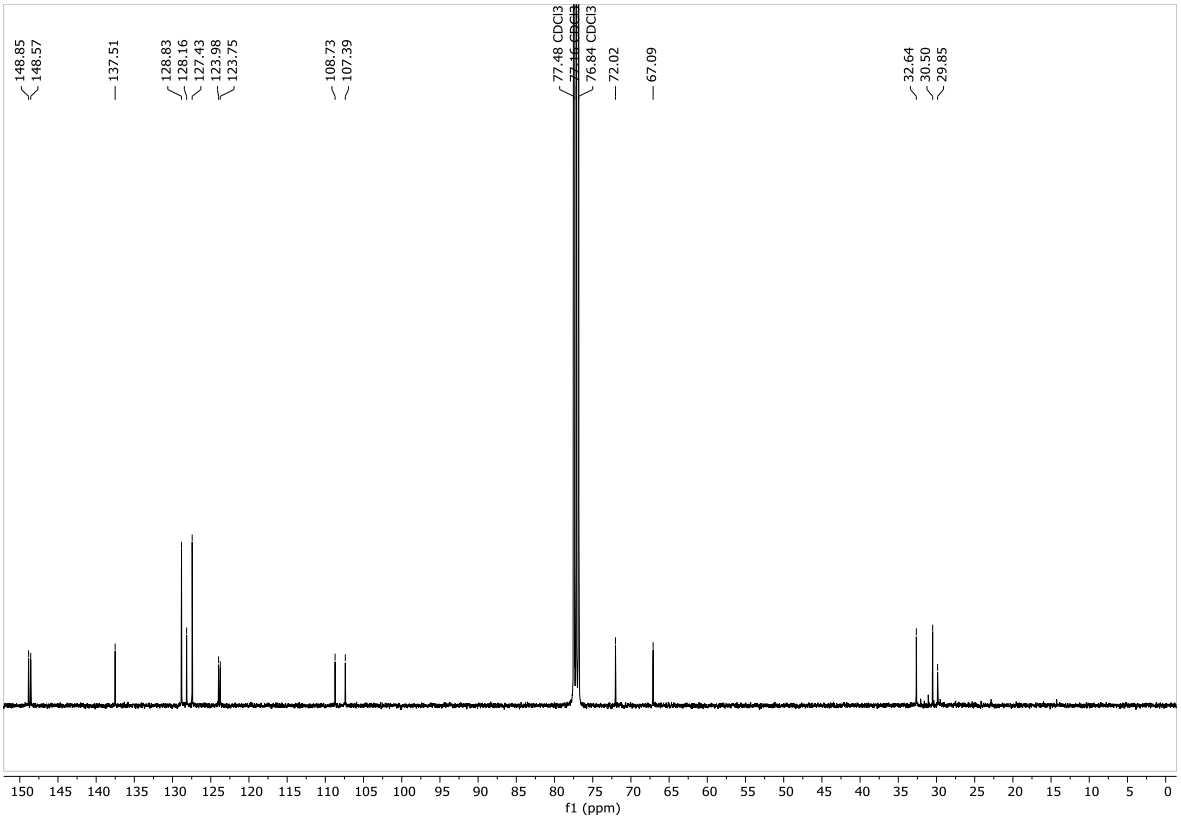

Figure V: ^{13}C NMR of molecule **48**.

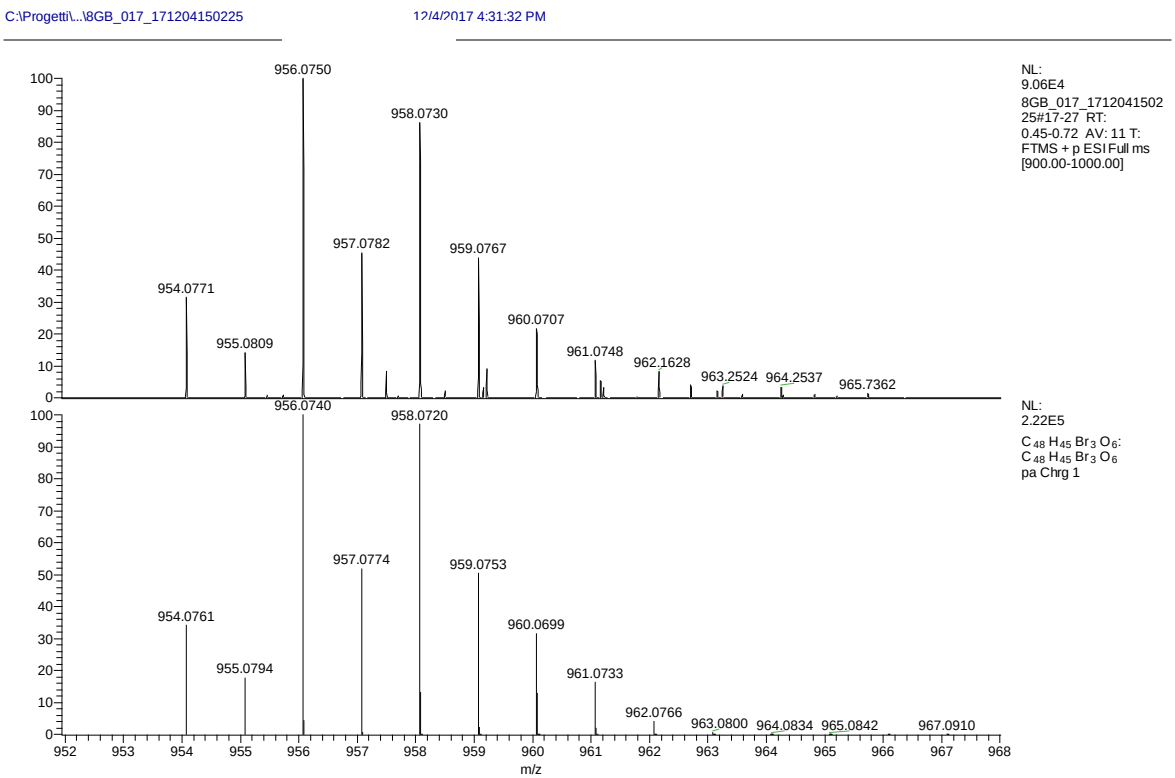

Figure VI: ESI-HRMS of molecule **48**.

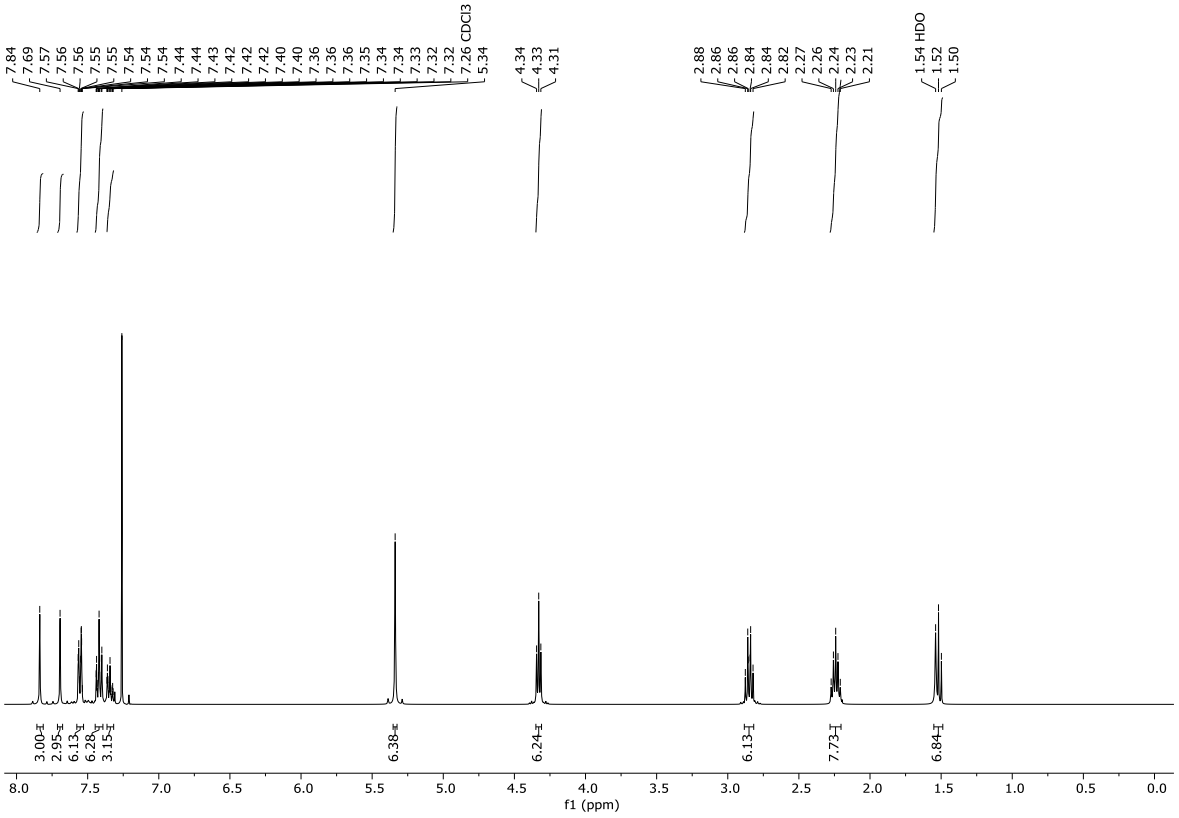

Figure VII: ^{1}H NMR of molecule **49**.

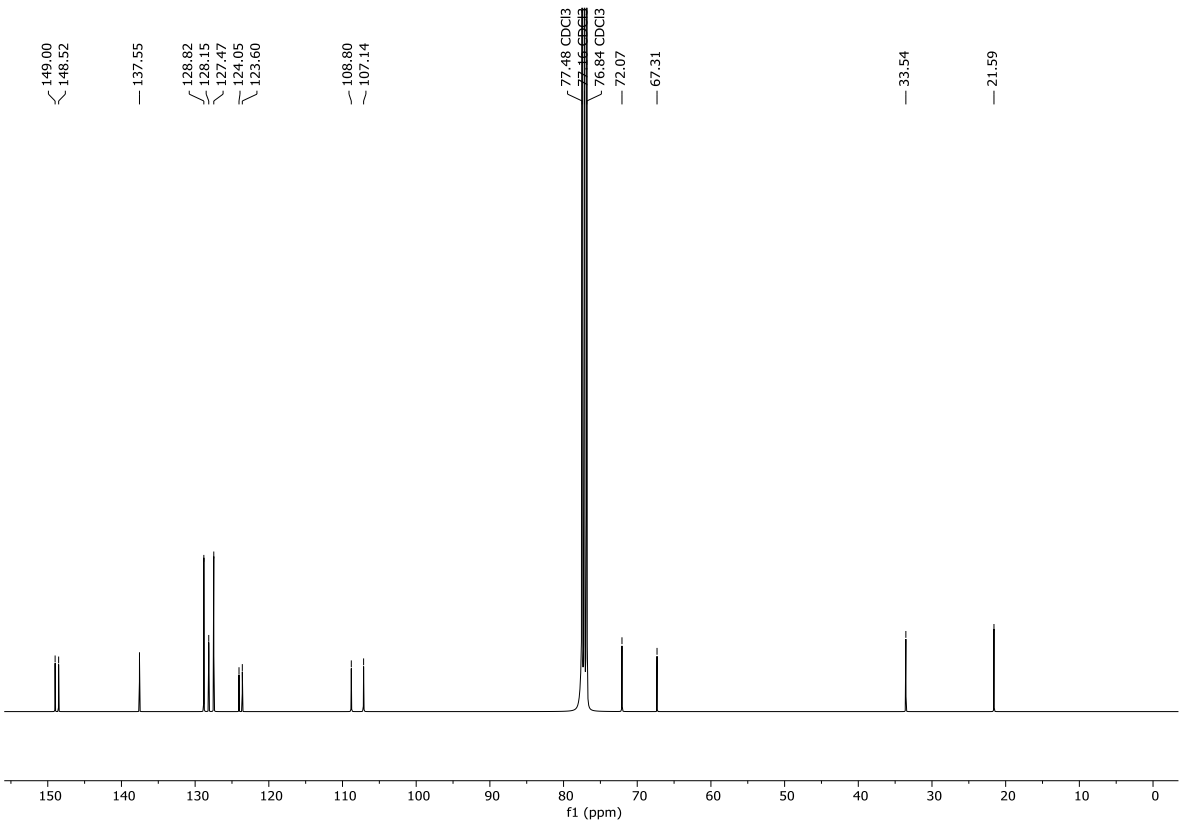

Figure 10: ^{13}C NMR of molecule **49**.

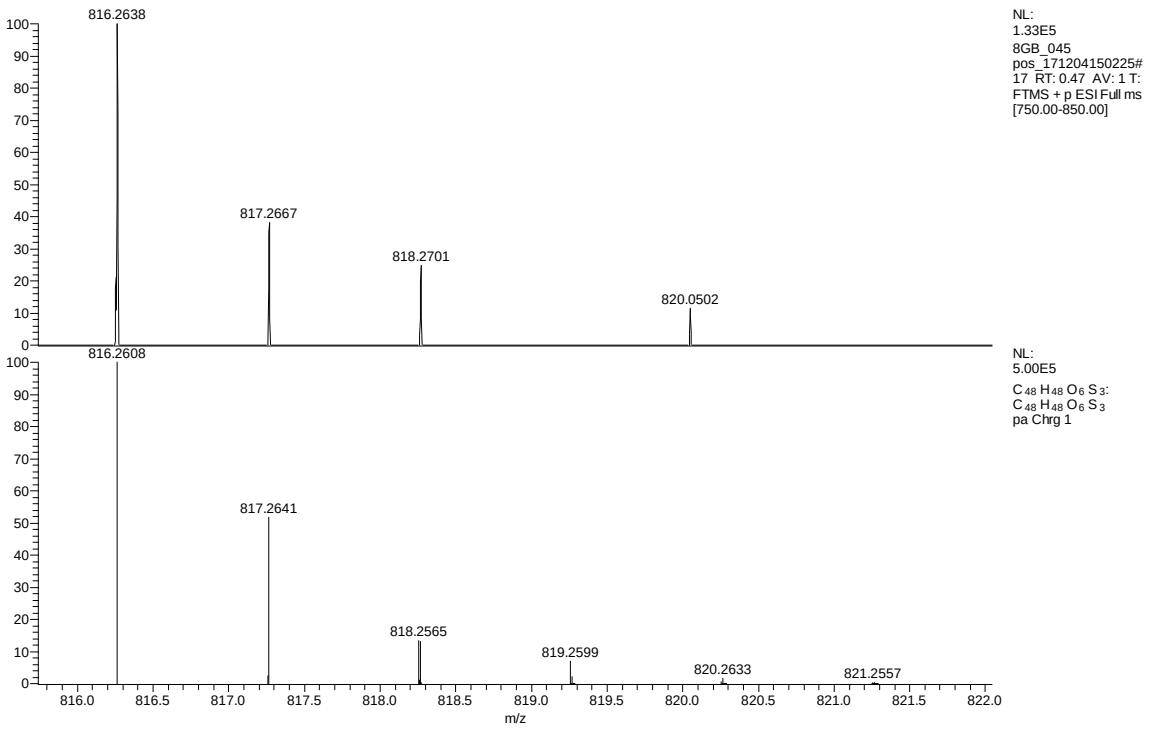

Figure IX: ESI-HRMS of molecule **49**.

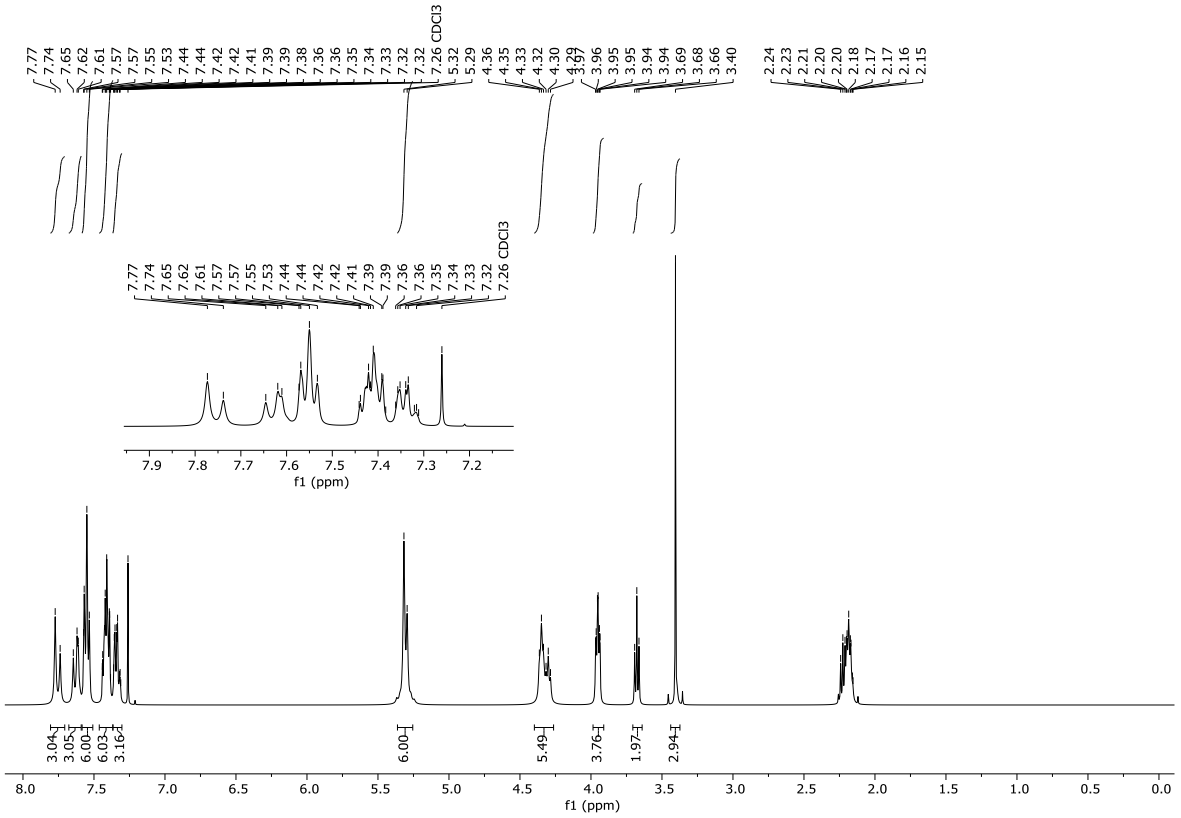

Figure X: ^{1}H NMR of molecule **47a**.

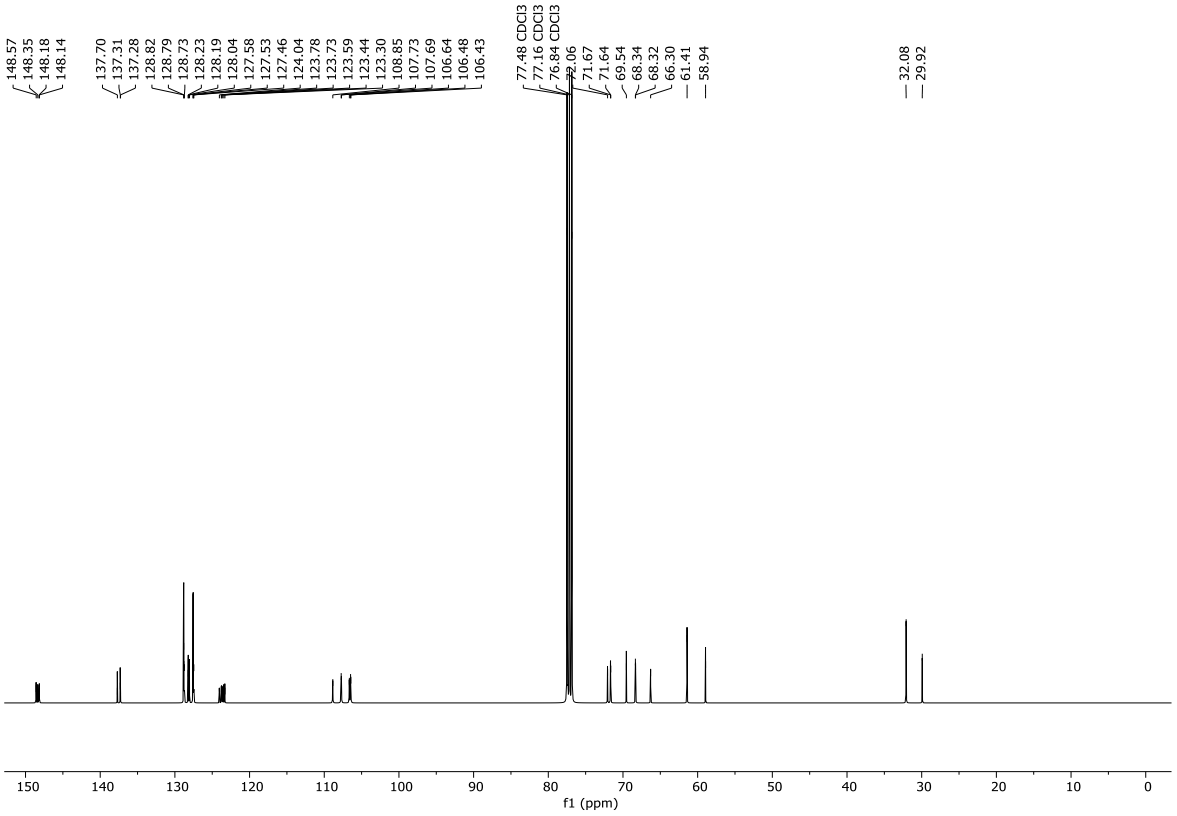

Figure XI: ^{13}C NMR of molecule **47a**.

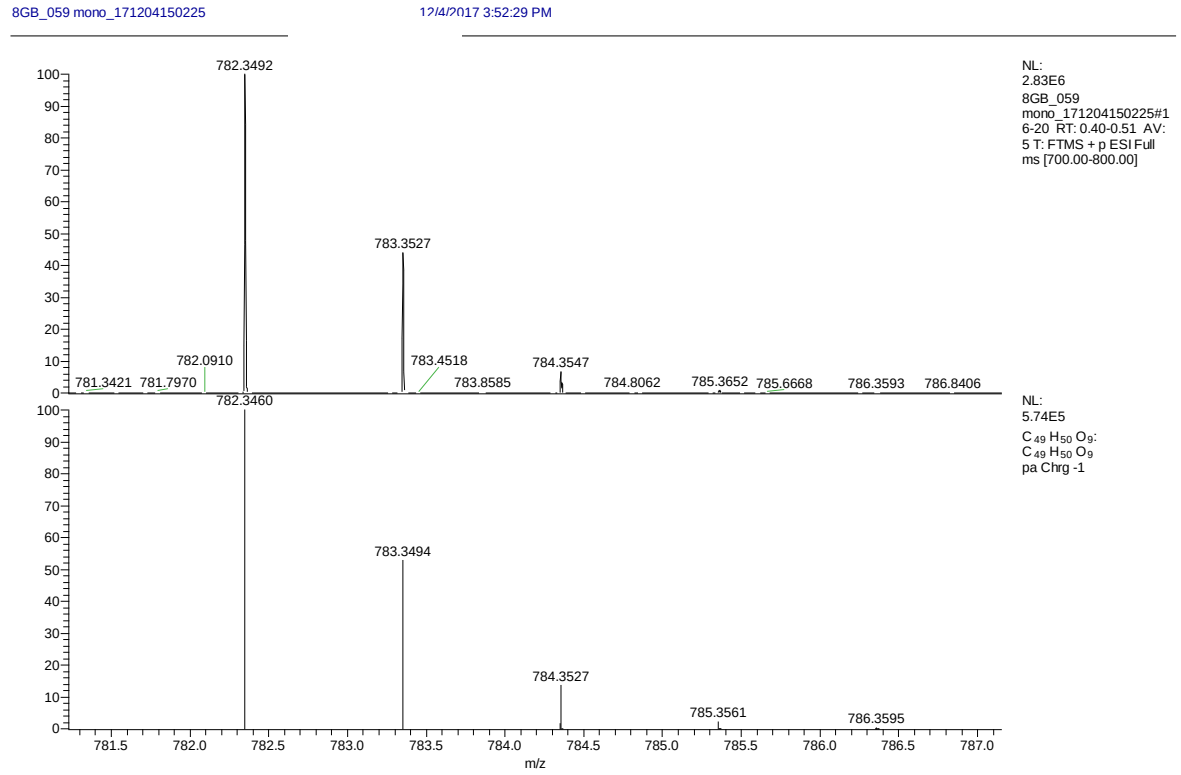

Figure XII: ESI-HRMS of molecule **47a**.

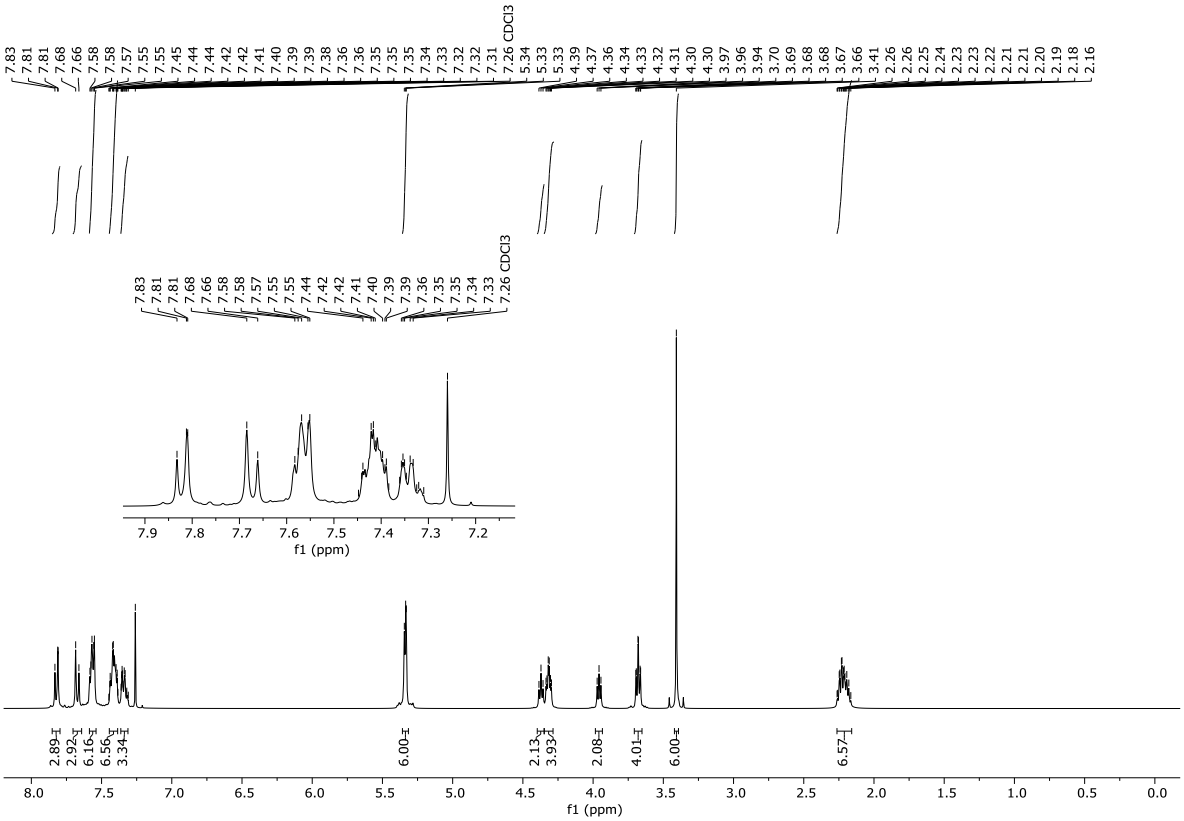

Figure XIII: ^{1}H NMR of molecule **47b**.

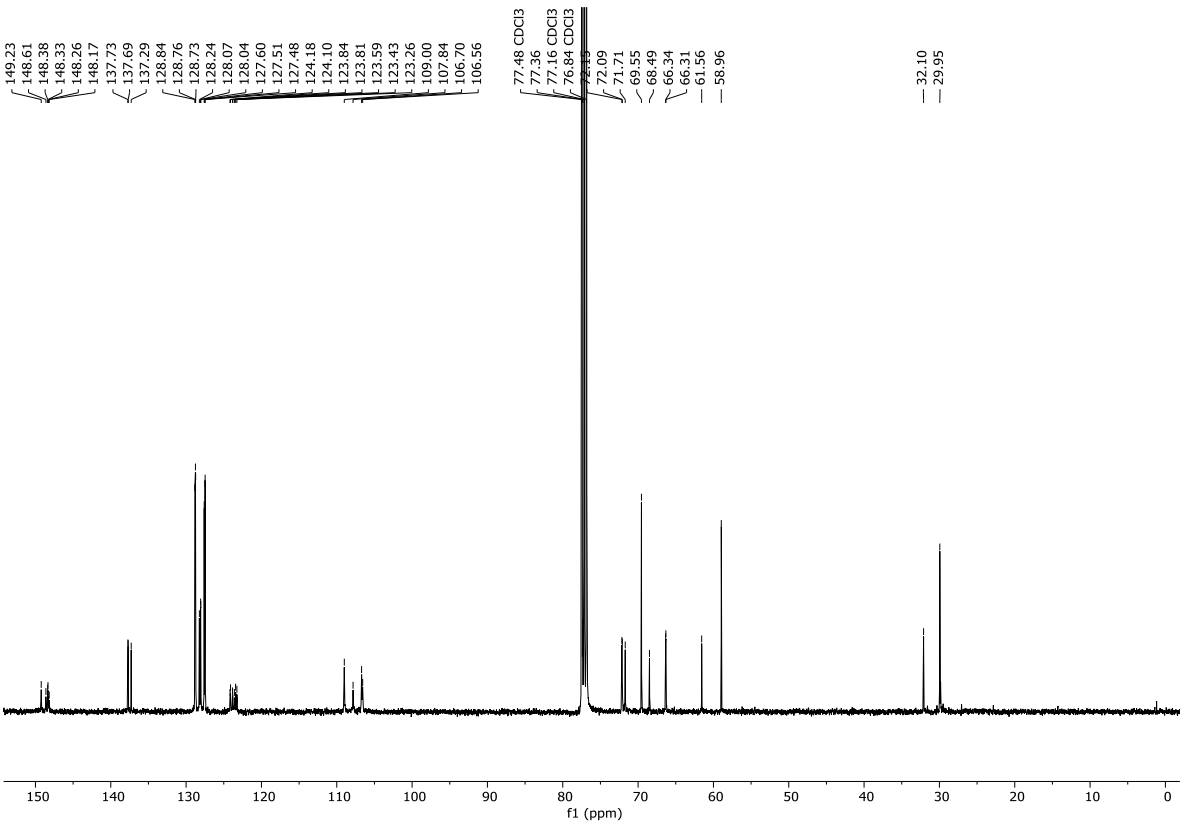

Figure XIV: ^{13}C NMR of molecule **47b**.

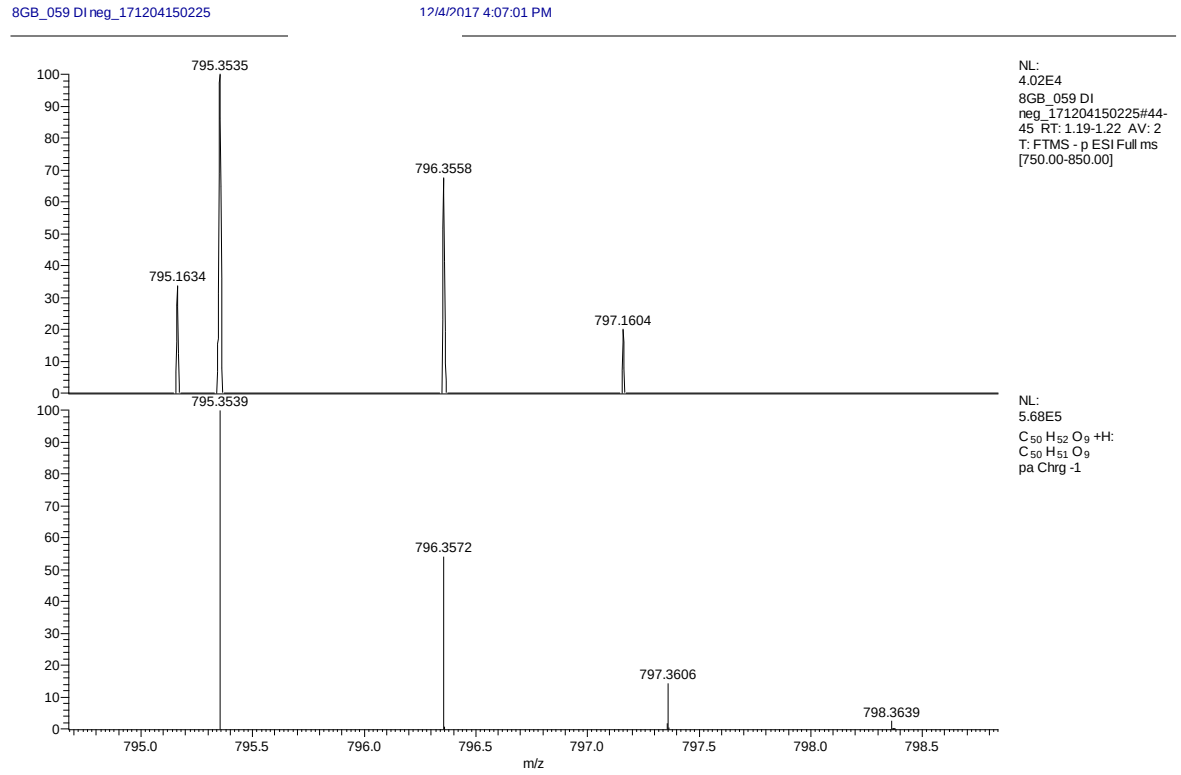

Figure XV: ESI-HRMS of molecule **47b**.

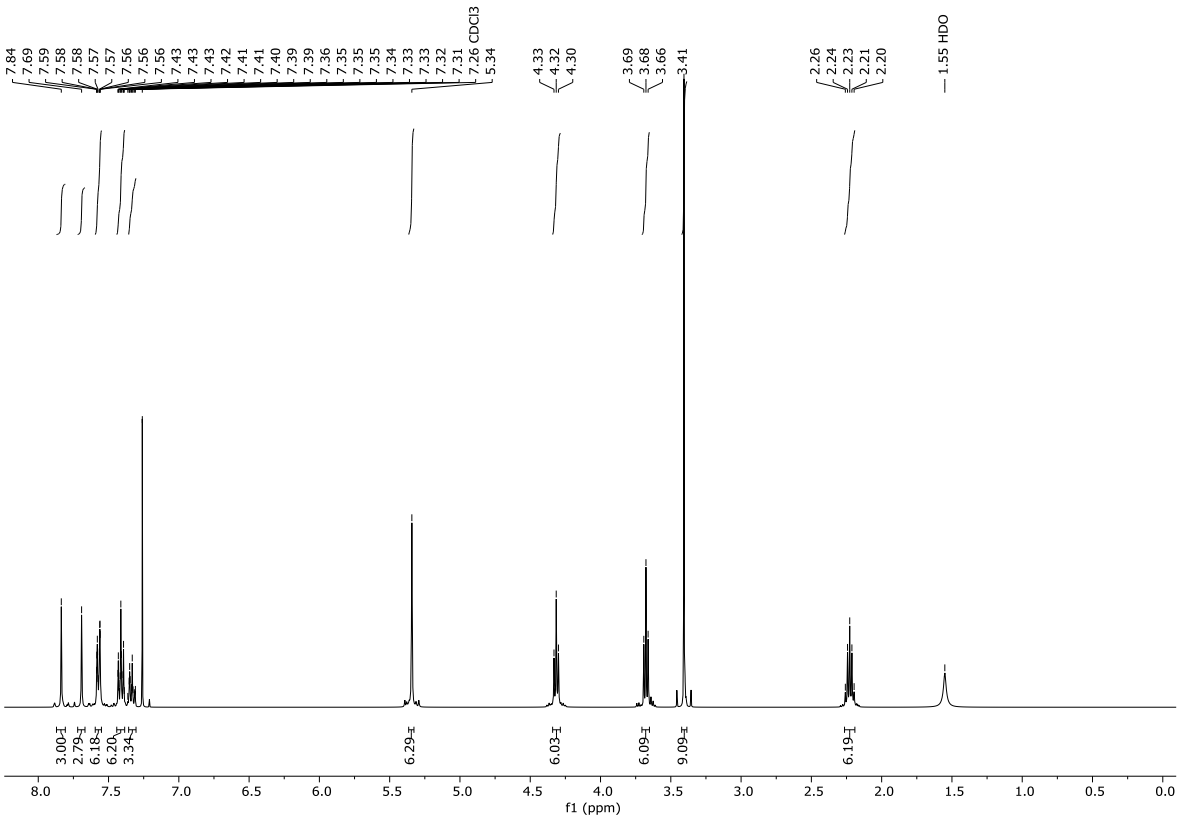

Figure XVI: ^{1}H NMR of molecule **47c**.

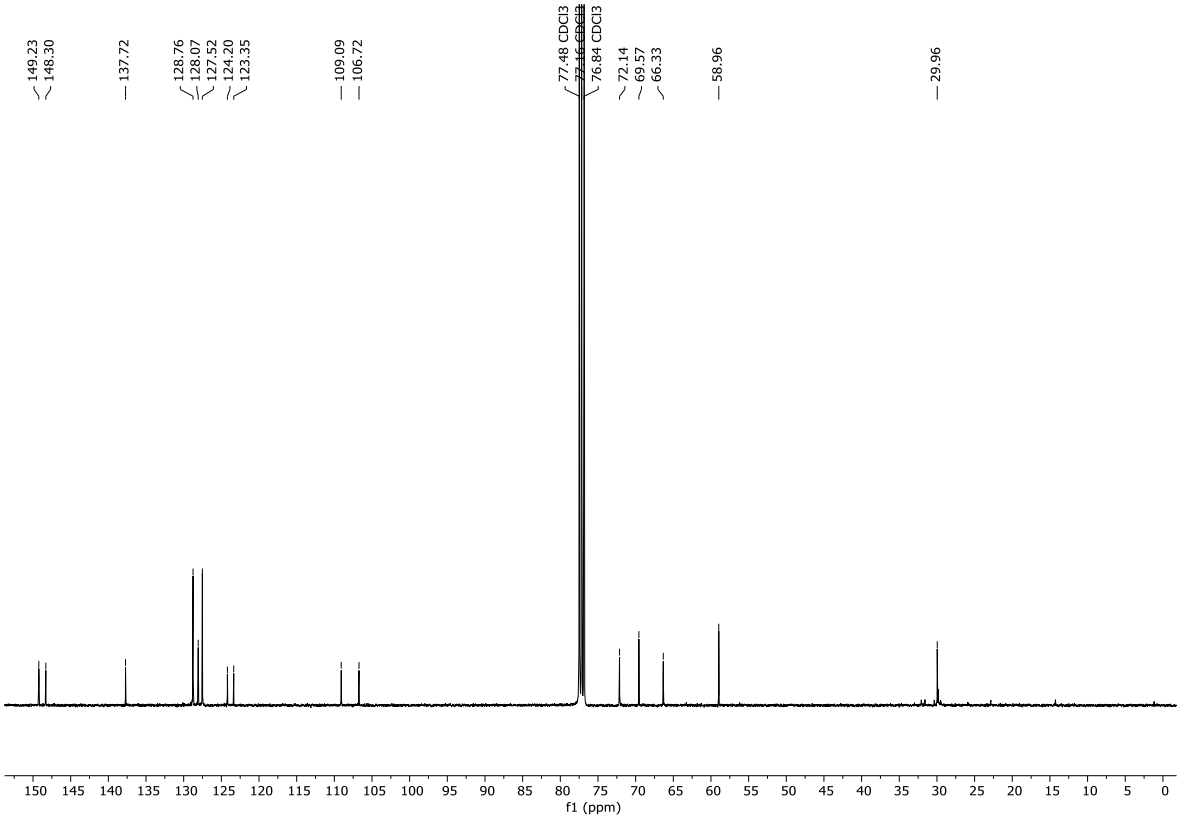

Figure XVII: ^{13}C NMR of molecule **47c**.

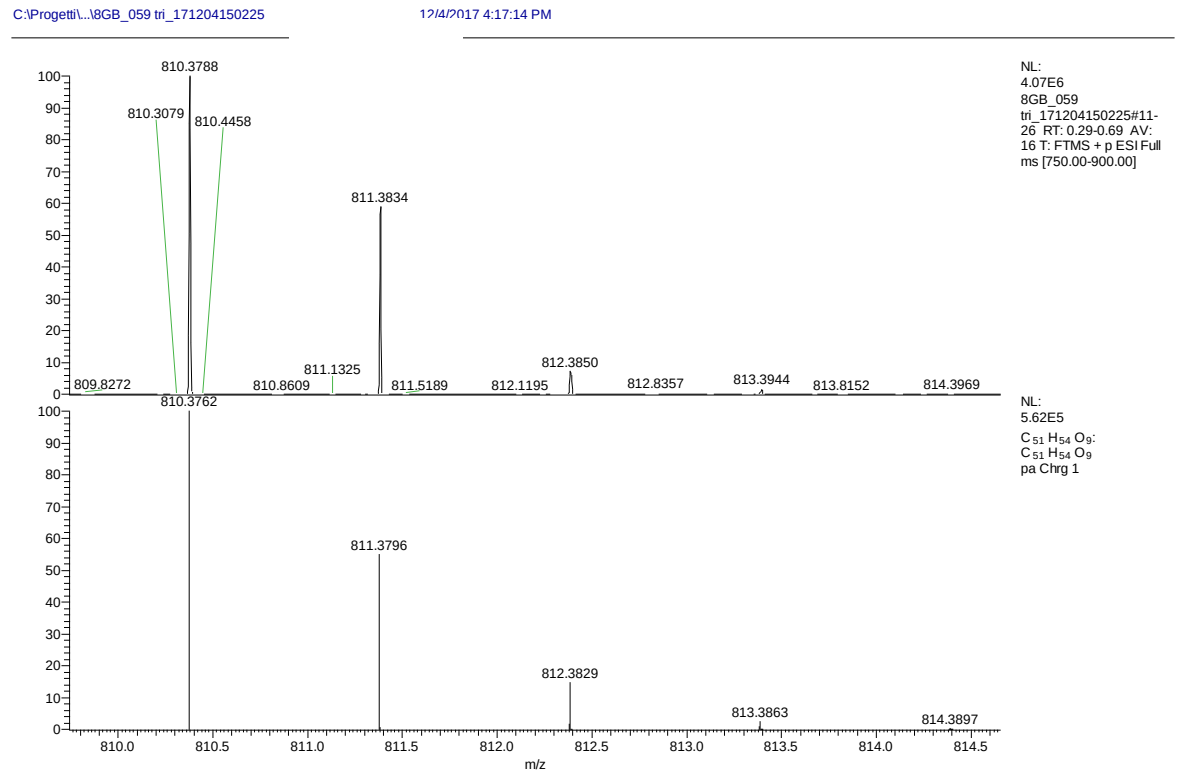

Figure XVIII: ESI-HRMS of molecule **47c**.

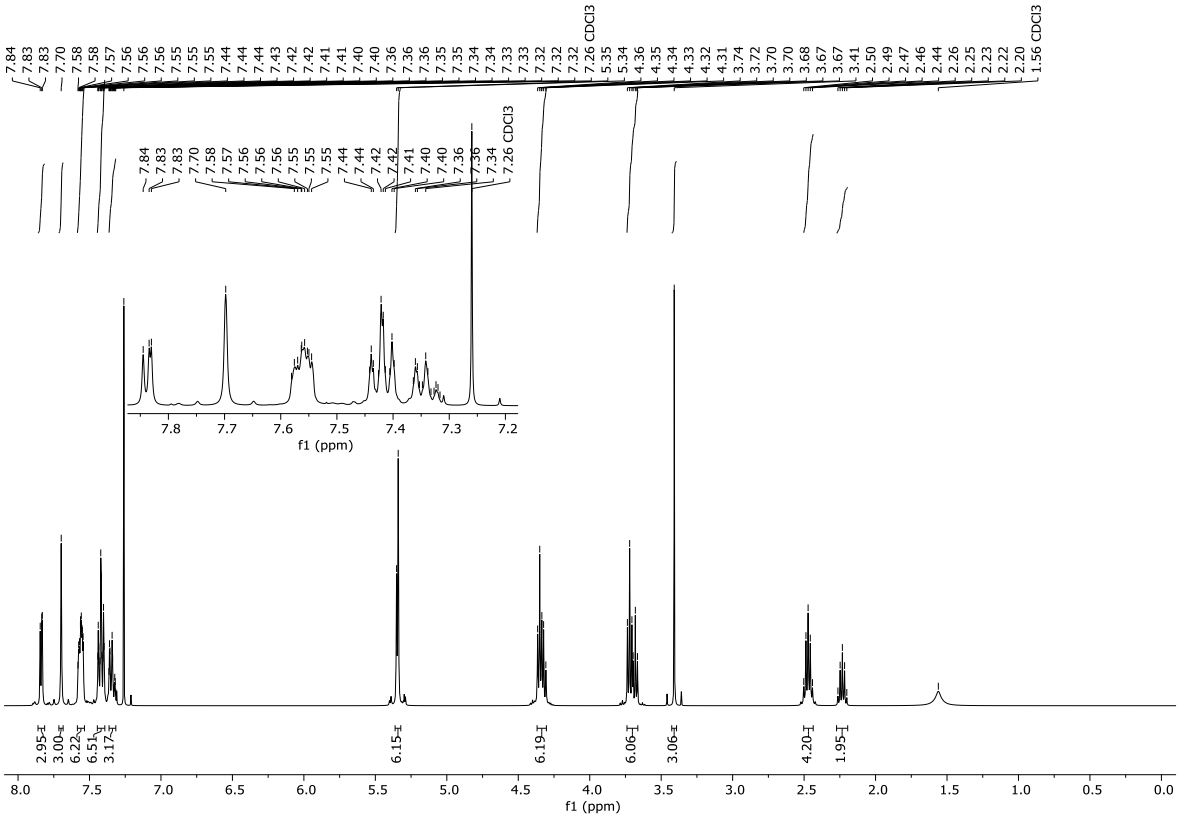

Figure XIX: ^{1}H NMR of molecule **48a**.

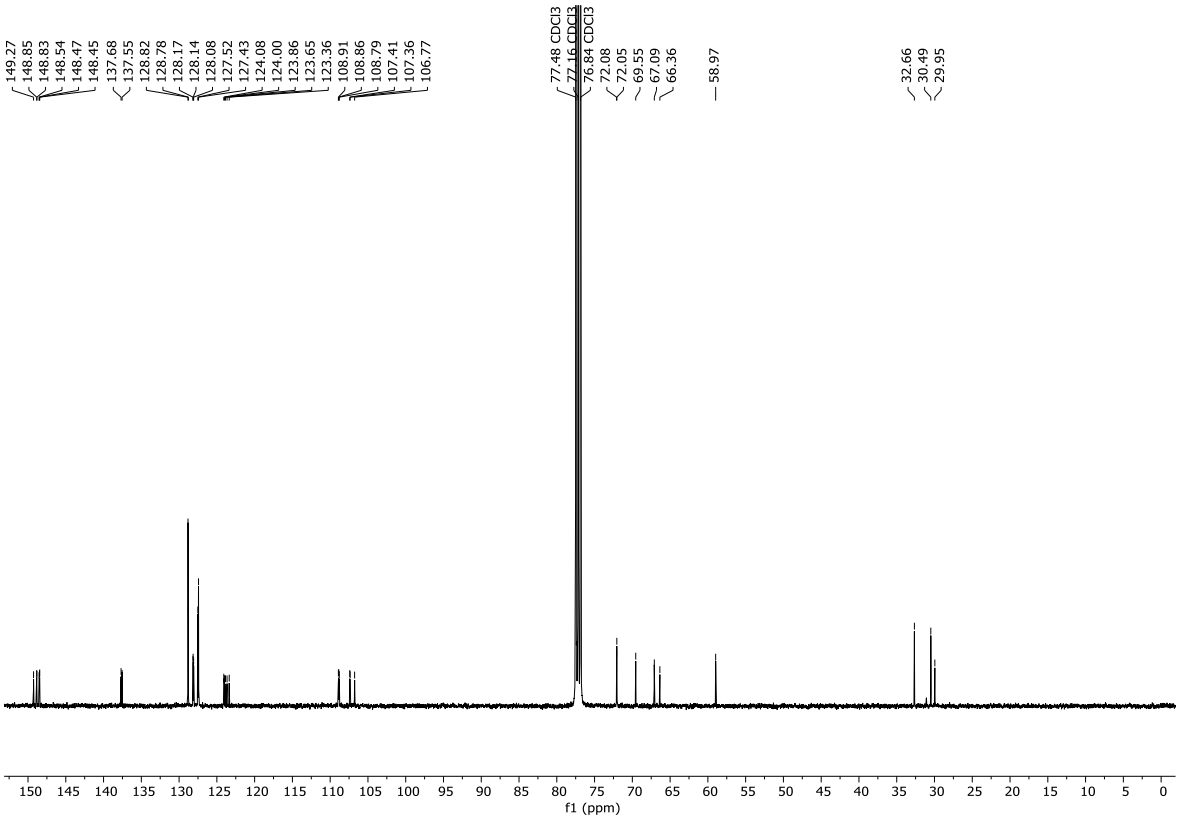

Figure XX: ^{13}C NMR of molecule **48a**.

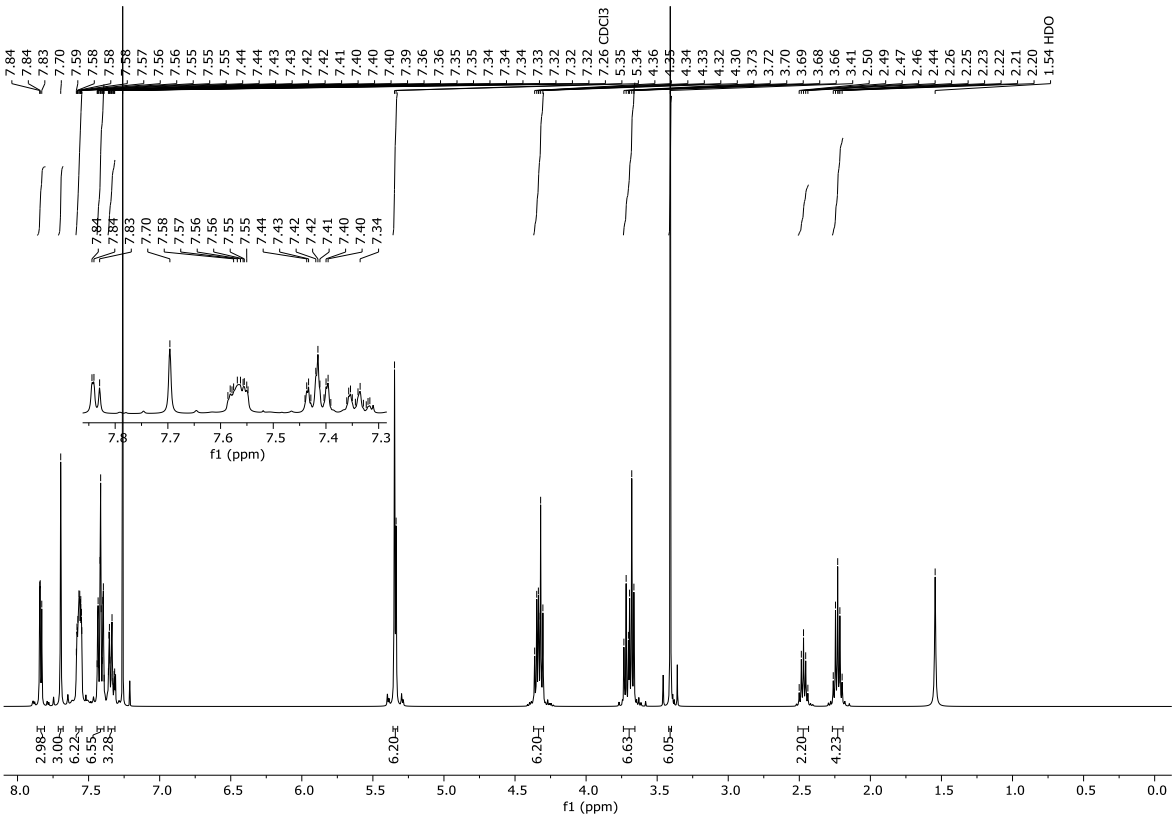

Figure XXI: ^{1}H NMR of molecule **48b**.

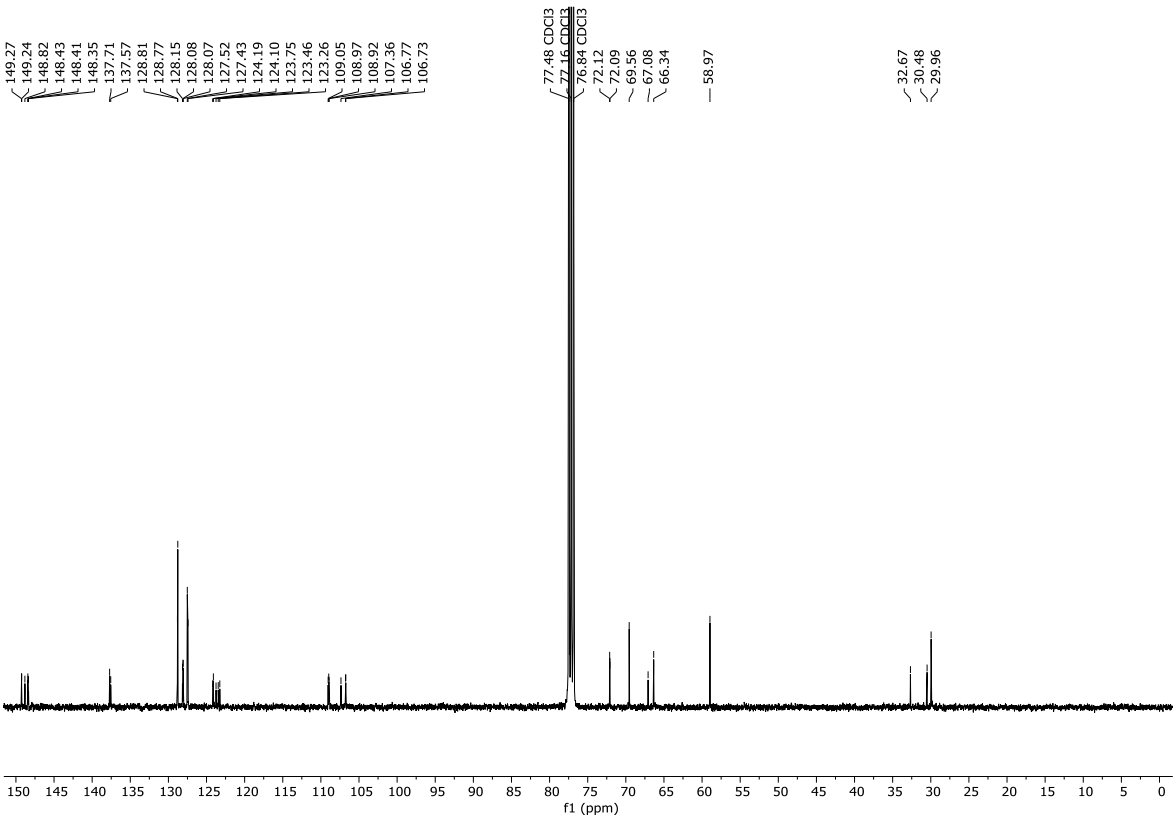

Figure XXII: ^{13}C NMR of molecule **48b**.

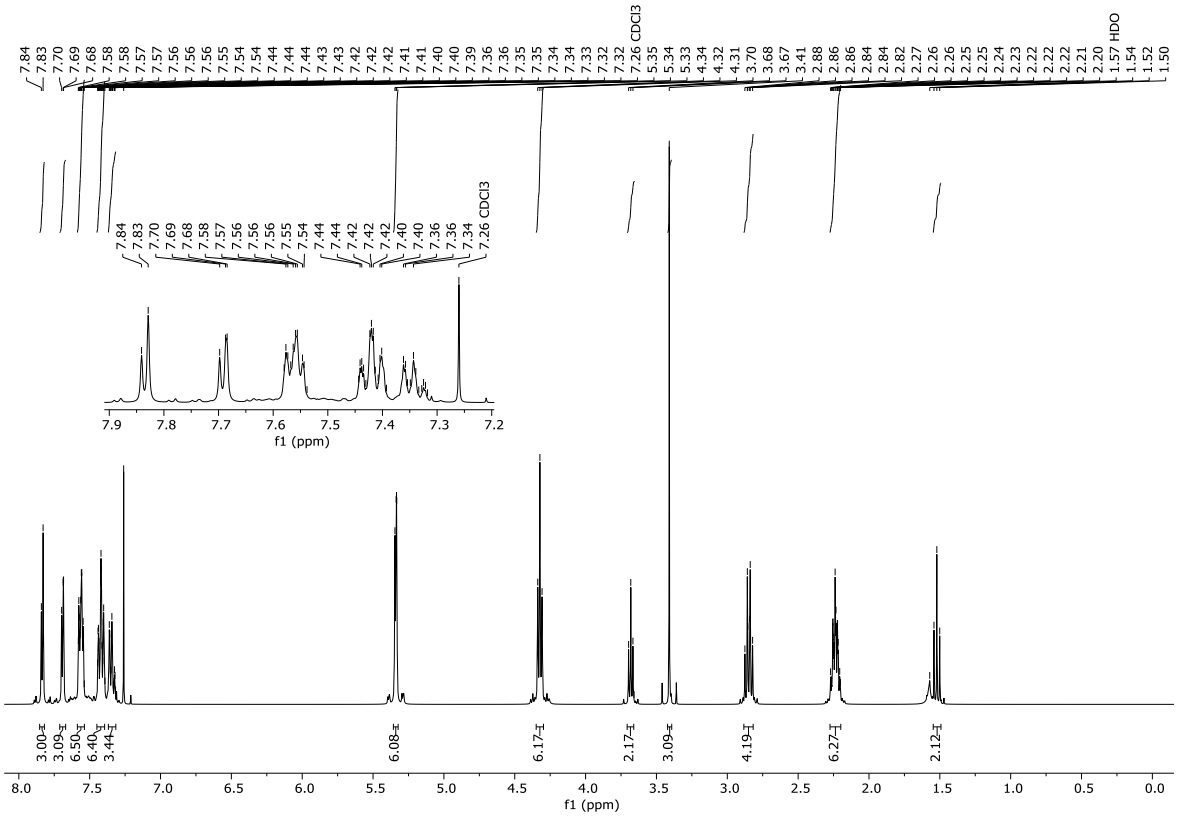

Figure XXIII: ^{1}H NMR of molecule **49a**.

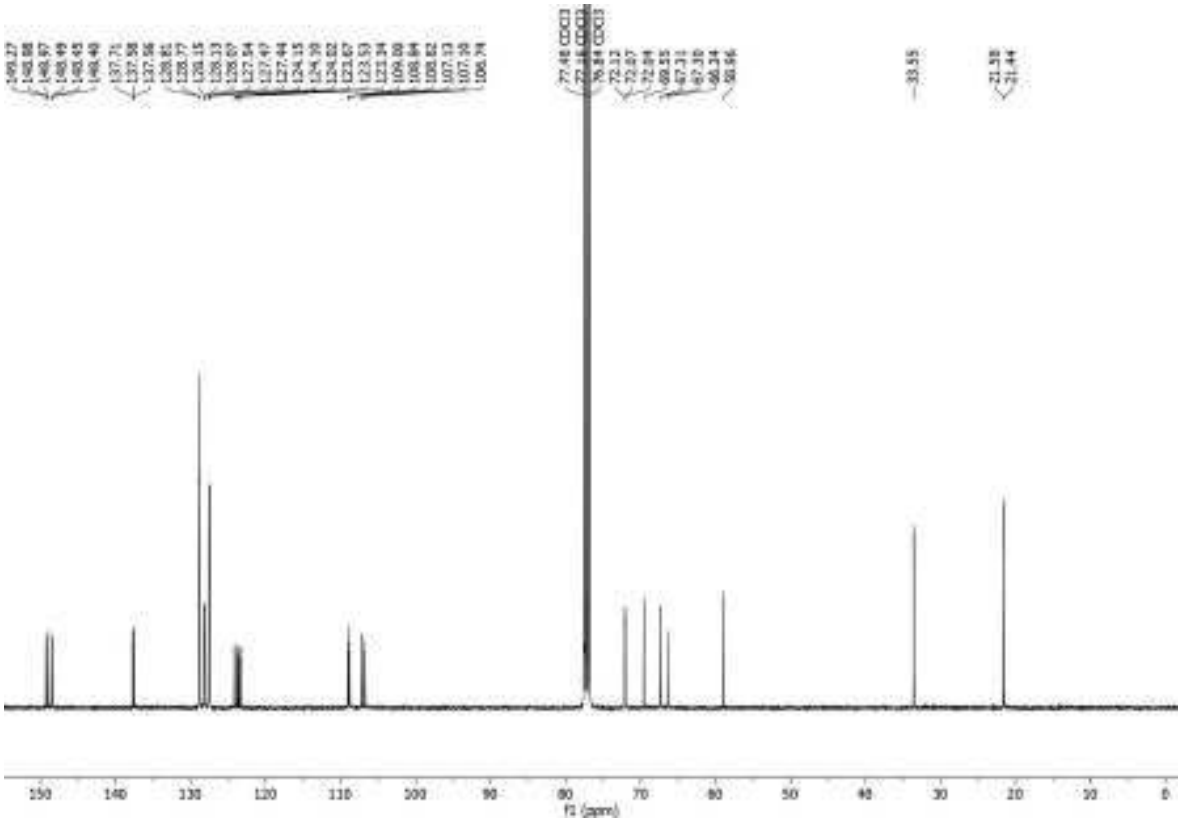

Figure XXIV: ^{13}C NMR of molecule **49a**.

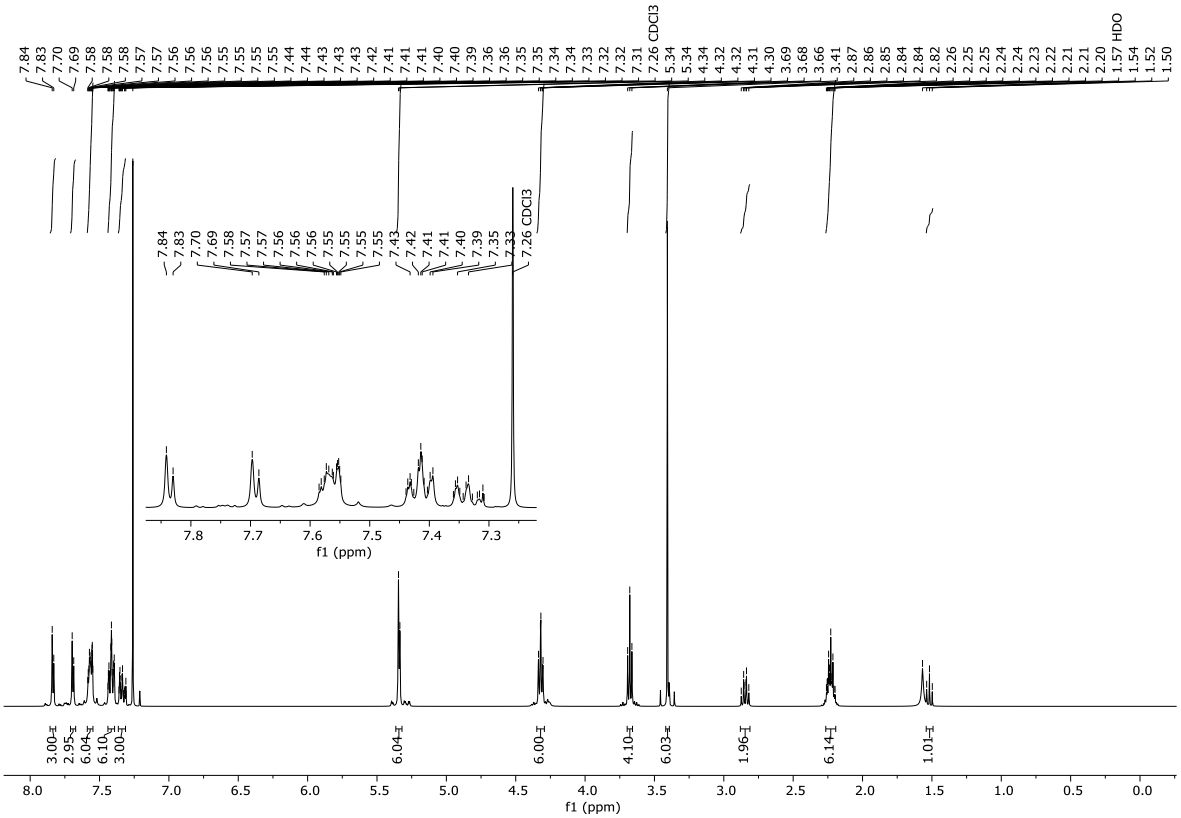

Figure XXV: ^{1}H NMR of molecule **49b**.

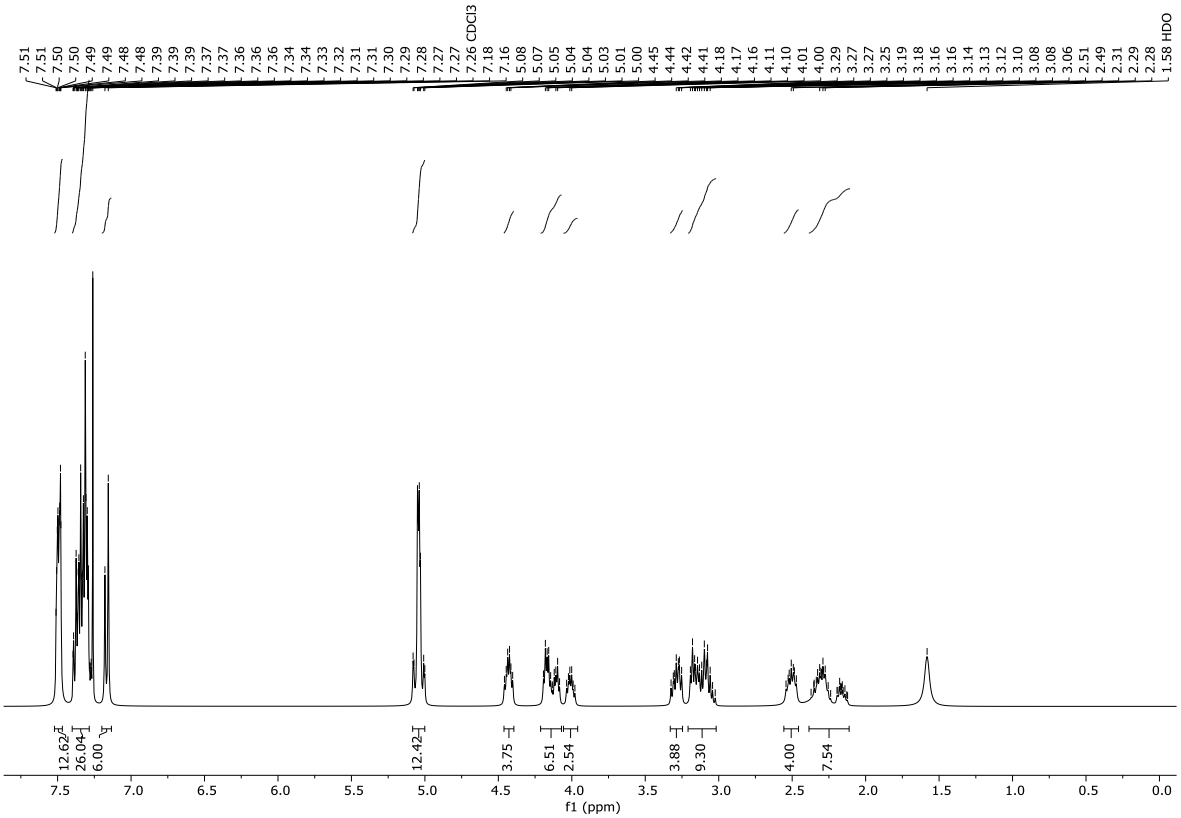

Figure XXVI: ^{1}H NMR of molecules *rac*-**50** and *meso*-**50**.

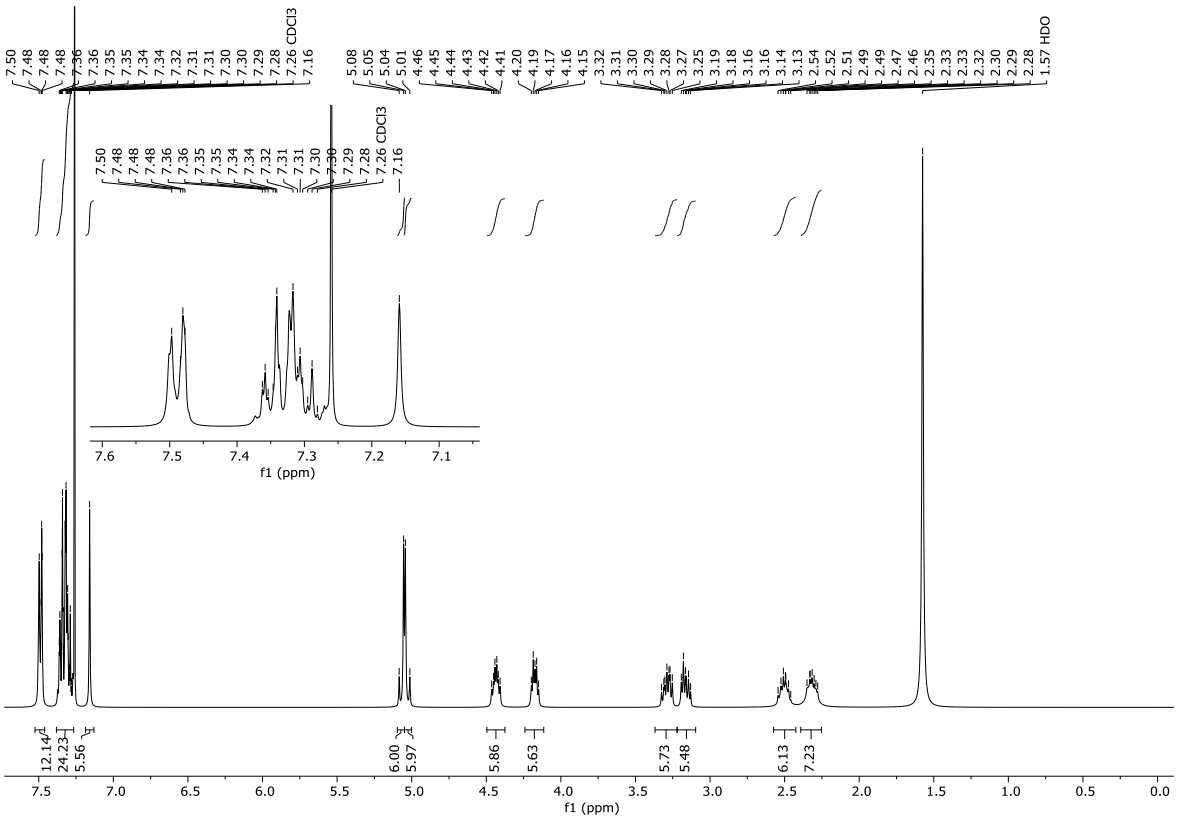

Figure XXVII: ^{1}H NMR of molecule *rac*-**50**.

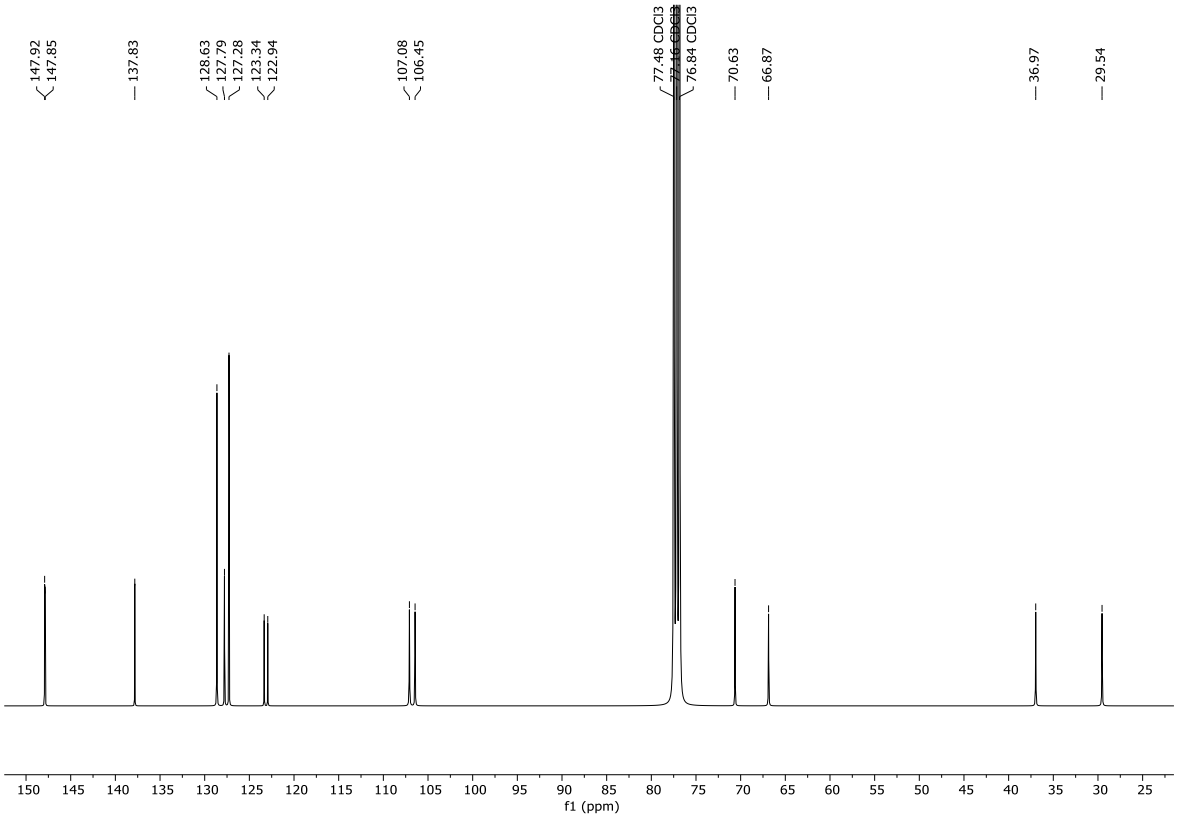

Figure XXVIII: ^{13}C NMR of molecule *rac*-**50**.

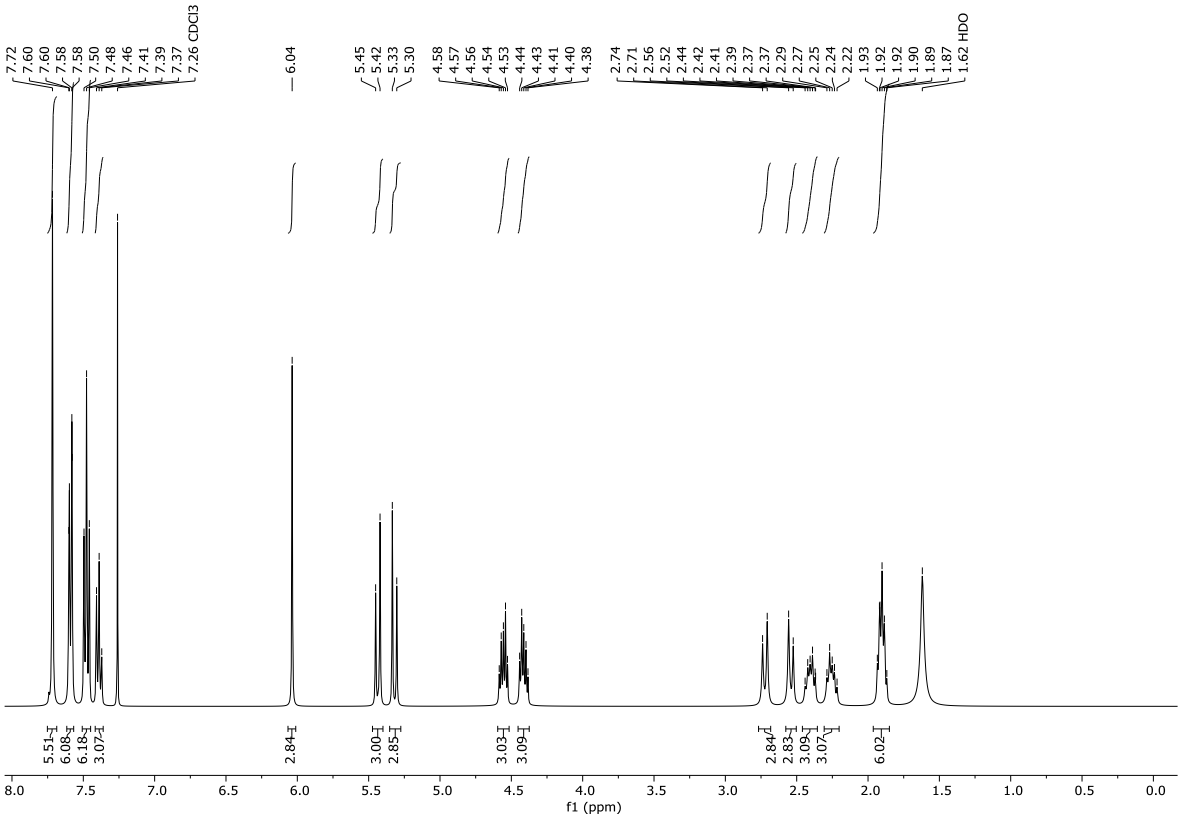

Figure XXIX: ^{1}H NMR of molecule **52**.

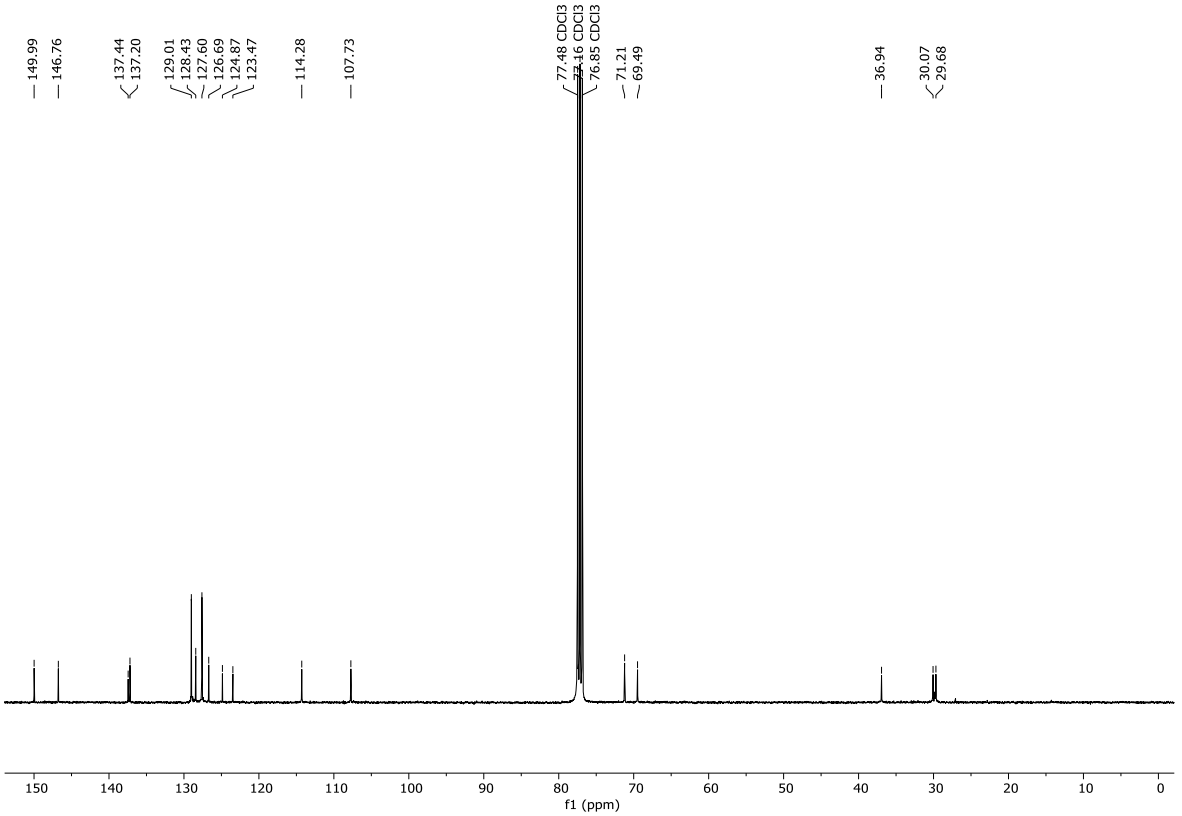

Figure XXX: ^{13}C NMR of molecule **52**.

4.6 Bibliography

1 M. Nakazaki, K. Yamamoto, T. Toya, *J. Org. Chem.*, **1981**, *46*, 1611-1615.

2 R. P. L'Esperance, A. P. West Jr., D. Van Engen, R. A. Pascal Jr., *J. Am. Chem. Soc.*, **1991**, *113*, 2612-2616.

3 S. Sathyamoorthi, J. T. Mague, R. A. Pascal Jr., *Org. Lett.*, **2012**, *14*, 3427-3429.

4 M. S. Collins, M. E. Carnes, B. P. Nell, L. N. Zakharov, D. W. Johnson, *Nat. Commun.*, **2016**, *7*, 11052.

5 L. Wang, J.-C. Chambron, *Org. Lett.,* **2004**, *6*, 747-750.

6 A. Lélias-Vanderperre, J.-C. Chambron, E. Espinosa, P.Terrier, E. Leize-Wagner, *Org. Lett.*, **2007**, *9*, 2961-2964.

7 L. Wang, C., J.-C. Chambron, *Synthesis*, **2009**, *20*, 3419-3426.

8 Y.-C. Horng, P.-S. Huang, C.-C. Hsieh, C.-H. Kuo, T.-S. Kuo, *Chem. Commun.*, **2012**, *48*, 8844-8846.

9 M. A. Little, J. Donkin, J. Fisher, M. A. Halcrow, J. Loder, M. J. Hardie, *Angew. Chem. Int. Ed.*, **2012**, *51*, 764-766.

10 S. J. Rowan, S. J. Cantrill, G. R. L. Cousins, J. K. M. Sanders, J. F. Stoddart, *Angew. Chem. Int. Ed.*, **2002**, *41*, 898-952.

11 Y. Jin, C. Yu, R. J. Denman, W. Zhang, *Chem. Soc. Rev.,* **2013**, *42*, 6634-6654.

12 B. Icli, E. Sheepwash, T. Riis-Johannessen, K. Schenk, Y. Filinchuk, R. Scopelliti, K. Severin, *Chem. Sci.*, **2011**, *2*, 1719-1721.

13 W. M. Pankau, K. Verbist, G. von Kiedrowski, *Chem. Commun.*, **2001**, 519-520.

14 S. Antonello, T. Dainese, M. De Nardi, L. Perotti, F. Maran, *ChemElectroChem*, **2016**, *3*, 1237-1244.

15 C. J. Hawker, J. M. J. Fréchet, *J. Am. Chem. Soc.*, **1990**, *112*, 7638-7647.

16 J. M. Blanco, O. Caamaño, F. Fernández, G. Gómez, C. López, *Tetrahedron Asymmetry*, **1992**, *3*, 749-752.

17 W. L. F. Armarego, C. Chai in *Purification of Laboratory Chemicals (Seventh Edition)*, Butterworth-Heinemann, Boston, **2013**.

18 W. C. Still, M. Kahn, A. Mitra, *J. Org. Chem.*, **1978**, *14*, 2923-2925.

5 Pt and Pd Ligands from C_3-Triphenylenes

Metal-ligand self-assembled cages[1,2,3] are very promising host systems[4] characterized by unique features and properties in the field of supramolecular recognition,[5,6] being able in some cases to stabilize highly reactive molecular structures,[7,8] with future potential biomedical applications.[9,10] As container molecules, they feature internal cavities that can bind multiple guests,[11] acting as supramolecular catalysts or nanoreactors[12,13] and in some cases promoting regio- and stereo-selective transformations.[14] In particular, worth of mention are the tetrahedral capsules developed by the group of Raymond,[15] based on catechol units connected through Ga(III) metal corners, that can stabilize cationic intermediates and have been applied in a series of organic transformations with accelerations up to more than two million-fold with respect to the uncatalyzed reaction (Scheme 1).[16]

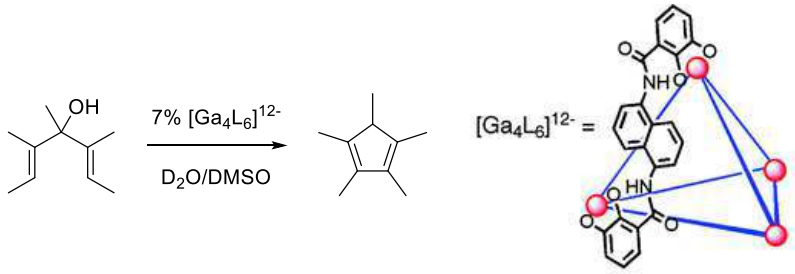

Scheme 1: Enzymelike catalysis of the Nazarov cyclization by tetrahedral capsule. Adapted from [16].

Other landmark examples were reported by the group of Fujita, based on *tris*-pyridyl units connected with Pd(II) corners leading to water soluble cavitand or capsule hosts.[17] Larger supramolecular cages were introduced by Fujita[18] and by Reek[19] as nanoreactors, with the ability to provide multiple catalytic sites within the cavity of the coordination cages. The groups of Nitschke[20] and Ward[21] further extended the field with a series of metal-ligand boxes and tetrahedral assemblies, able to bind multiple guests for a wide range of applications. As long as the organic polydentate units are concerned, the most common units are based on large flat aromatic surfaces, like porphyrins,[22] banana-shaped units,[23] or several other scaffolds often endowed with pyridine terminal units.[24]

With the aim of widening the range of organic scaffolds to be combined with metal corners for the development of new supramolecular host systems, characterized by new shapes, size and molecular recognition properties, inspired by the molecules described in Chapter 2, we decided to synthesize three tridentate pyridine ligands to be tested with different metalorganic complexes.

5.1 Synthesis of the Triphenylenic Ligands

Following the methodology for the Mannich reaction described in Chapter 2, we started synthetizing three tridentate ligands using three different aminopyridine: *o*-, *m*- and *p*-aminopyridine. The reactions were performed on a bigger scale, dividing the synthesis in

two steps, as seen before with the use of aminopyridines: the formation of the hemiaminal between amine, paraformaldehyde and *n*-butanol and the subsequent Mannich reaction.

The hemiaminals ***o*-53**, ***m*-53** and ***p*-53** were obtained by reaction with paraformaldehyde and *n*-butanol, using the latter as solvent in the presence of acetic acid as catalyst, heating overnight at 90 °C (Scheme 2).

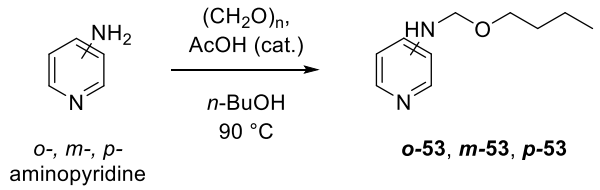

Scheme 2: Synthesis of the hemiaminals ***o*-53**, ***m*-53** and ***p*-53.**

The hemiaminals were obtained in high yield (90-95%), without being isolated, and directly reacted with ***C*$_3$-26** and a second amount of paraformaldehyde, in toluene, heating at 100 °C or 110 °C (Scheme 3).

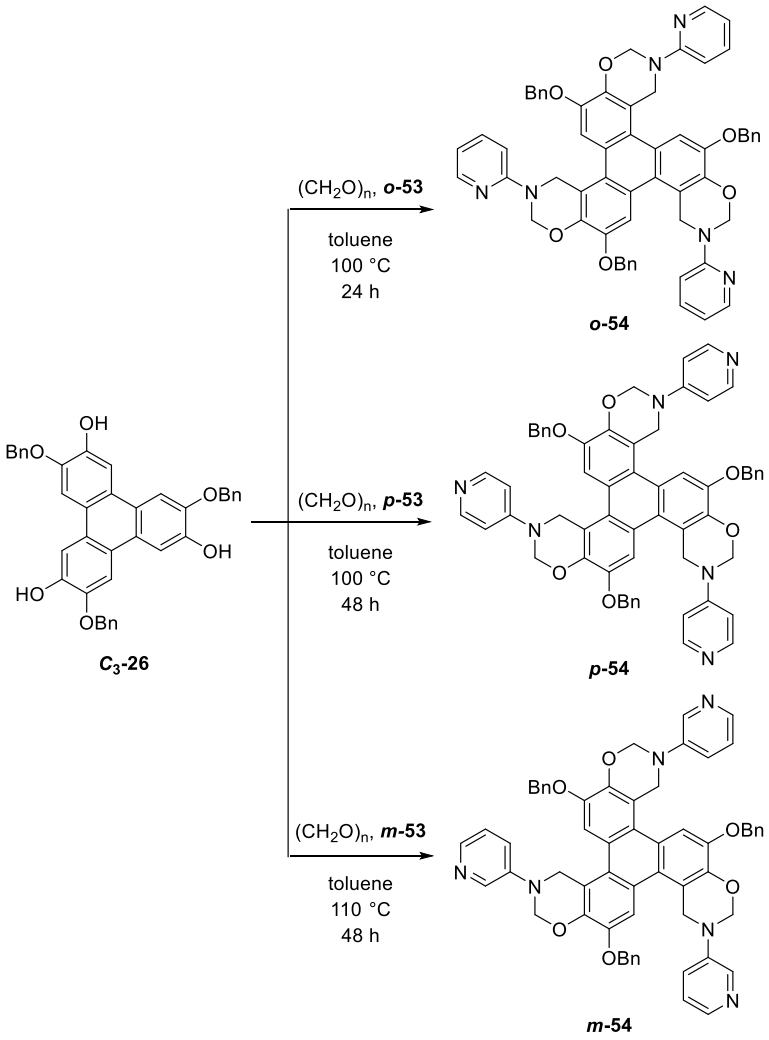

Scheme 3: Synthesis of Mannich products ***o*-54** (90% yield), ***m*-54** (75% yield) and ***p*-54** (86% yield)**.**

In contrast to the previous syntheses reported in Chapter 2, the lower nucleophilicity of the aminopyridine substrates and the larger scale of the reaction (five times larger) led to an increase in the reaction time (from 24 hours for ***o*-54** and ***p*-54**, to 48 hours for ***m*-54**), and

in the case of ***m*-54** it was necessary to further increase also the reaction temperature. After some effort in the optimization of the experimental conditions, the products were obtained by simple precipitation with EtOH (in the case of ***o*-54** and ***m*-54**) or Et_2O (in the case of ***p*-54**), with good yields of 90%, 75% and 86% for ***o*-54***, **m*-54** *and* ***p*-54**, respectively.

5.2 Synthesis of the Pt and Pd Complexes as Metal Corners

Once the C_3-symmetric *tris*-pyridine triphenylene ligands were ready, we proceeded with the synthesis of the metal corners. We selected, among several possible examples in the literature, two *cis*-complexes of palladium(II) and one *cis*-complex of platinum(II) bearing two labile triflate ligands, that can be efficiently displaced by pyridine in solution: $[Pd(dppe)(OTf)_2]$, $[Pt(dppe)(OTf)_2]$ and $[Pd(dppp)(OTf)_2]$. The two different metal centres were chosen to investigate the effect of the well-known lower exchange rate of ligands that characterizes Pt(II) complexes with respect to Pd(II) analogues. The three complexes were prepared adapting procedures reported in the literature. A further advantage related to the selected metal corners is the possibility to monitor the coordination by the tris-pyridine triphenylene ligands not only following the ^1H NMR resonances of the latter, but also with the ^{31}P resonances of the ligand on the metal and the ^{19}F resonances of the counter-anions, that are going to be displaced by the incoming ligand.

The first to be synthetized was $[Pd(dppe)(OTf)_2]$, **57**. First, palladium(II) chloride was reacted with 1,5-cyclooctadiene (COD), then the resulting complex **55** was treated with 1,2-diphenylphosphinoethane (dppe) to form the corresponding $[Pd(dppe)(Cl)_2]$, with subsequent halide exchange using silver triflate (Scheme 4).[25,26]

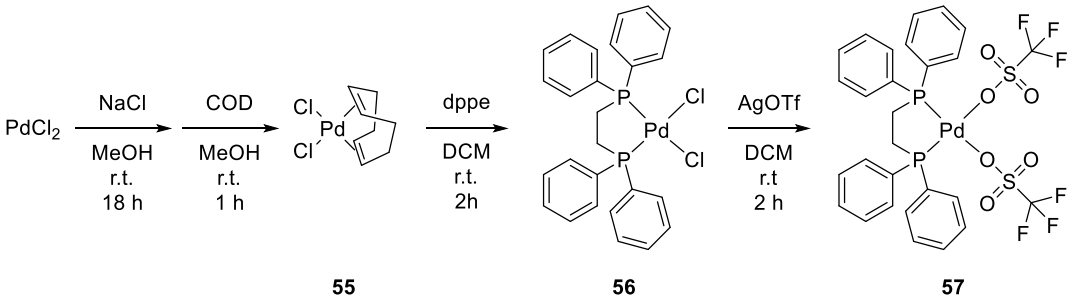

Scheme 4: Synthetic route to $[Pd(dppe)(OTf)_2]$, **57**.

The final product **57** was obtained after precipitation with Et_2O, with an overall 81% yield in three steps.

$[Pd(dppp)(OTf)_2]$, **59**, was obtained using the same synthetic pathway used for **57**, treating the precursor with 1,3-diphenylphosphino propane (dppp) (Scheme 6).[25,26]

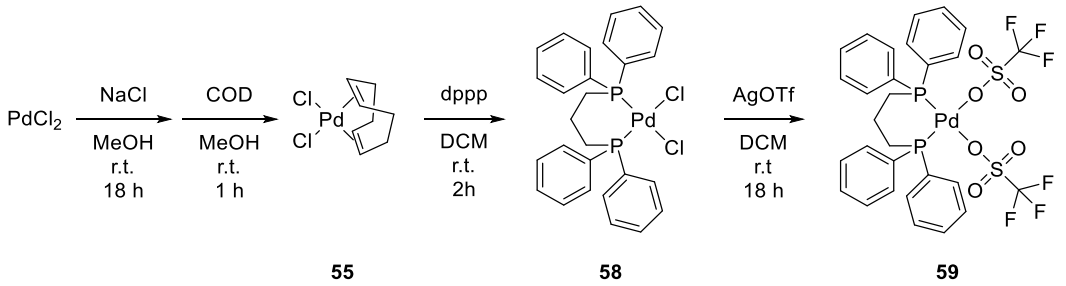

Scheme 5: Synthetic route to [Pd(dppp)(OTf)$_2$], **59**.

Complex **59** was obtained after precipitation with Et_2O, with an overall 82% yield in three steps.

[Pt(dppe)(OTf)$_2$], **62**, was obtained with a similar procedure, starting directly from [PtCODCl$_2$] and treating it with dppe, followed by chloride substitution with silver triflate (Scheme 5).[27]

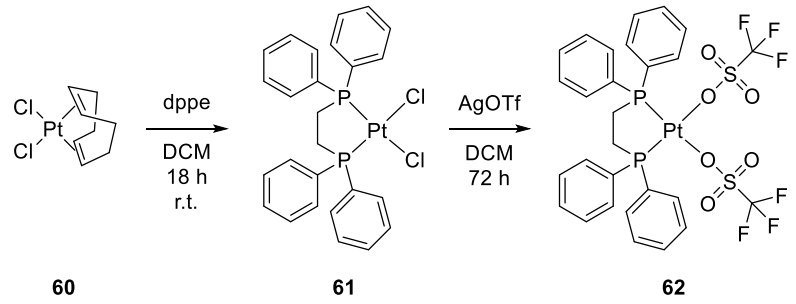

Scheme 6: Synthetic route to [Pt(dppe)(OTf)$_2$], **62**.

The final platinum complex, **62**, was obtained after precipitation with Et_2O, with an overall 85% yield in two steps.

5.3 NMR Titrations

The interaction between the polydentate ligands and the metal complexes was investigated undertaking a series of NMR titration experiment on a 5 mM solution of **54** in CD_2Cl_2, using a 25 mM (**57**) or 12.5 mM solution (**59** and **62**) of the metal complex in the same solvent to monitor the formation of the coordination complexes. In particular ^{1}H, ^{31}P and ^{19}F NMR spectra were recorded, following the resonances of **54** with ^{1}H NMR, the resonances of the diphosphino ligands directly coordinated to the metal with ^{31}P NMR and of the triflate anions that are displaced by the incoming pyridine units with ^{19}F NMR. .

The titration experiment between ***o*-54** and the Pd complex **57** showed, even after 0.2 equivalents of metal complex with respect to the triphenylene ligand, the broadening of the resonances of the aromatic scaffold and a certain down-field shift, especially for the resonances of the pyridine residues (Figure 1).

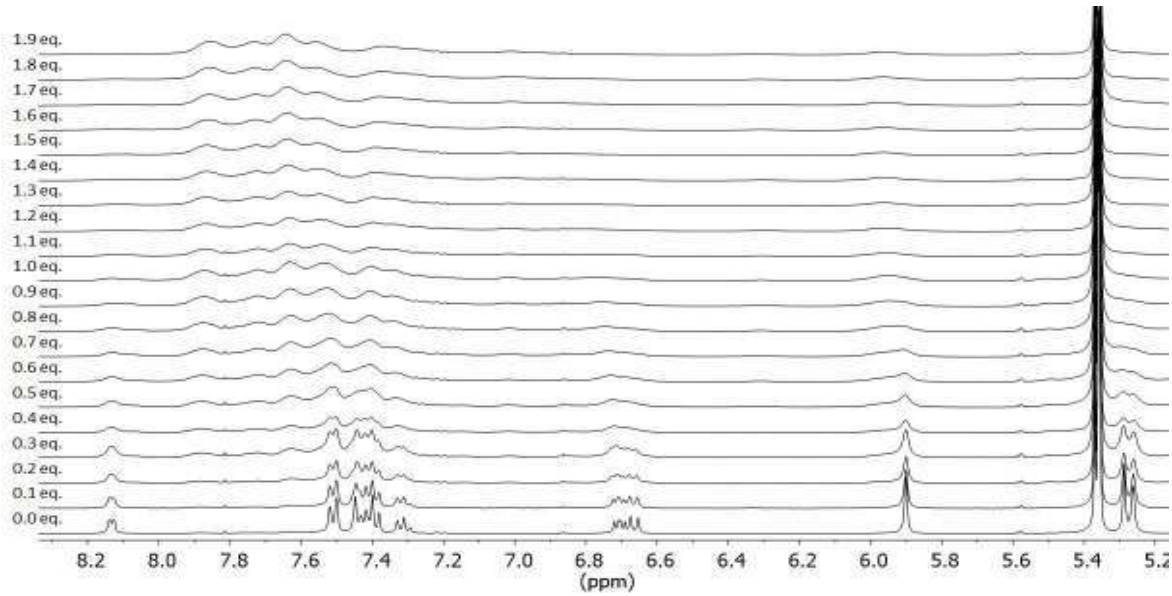

Figure 1: ^{1}H NMR of the titration of a 5 mM solution of ***o*-54** in CD_2Cl_2 with a 25 mM solution of [Pd(dppe)(OTf)$_2$], **57**, in CD_2Cl_2.

After reaching a 1:1 ratio between metal and ligand, the resonances were too broad to be unequivocally assigned. No new resonances were observed ascribable to new species in slow exchange on the NMR timescale or decompositions pathways, indicating the high stability of the triphenylene ligand in the presence of the metal centre. The broadening of the resonances is likely to be due to some exchange process, occurring between different metal centres and the coordinating pyridine units. Even the ^{31}P NMR spectra recorded during the titration were not useful to better follow the process (see Experimental Section, Titration 1), while the ^{19}F NMR spectra turned out to be more sensitive, observing the gradual de-shielding of the resonance of the triflate anion during the titration, until a maximum value corresponding to a molar fraction of 0.4 (Figure 2), which corresponds to a 2:3 ligand-to-metal ratio, coherent with the formation of metal-ligand cages with a L_2M_3 stoichiometry between ***o*-54** and **57**.

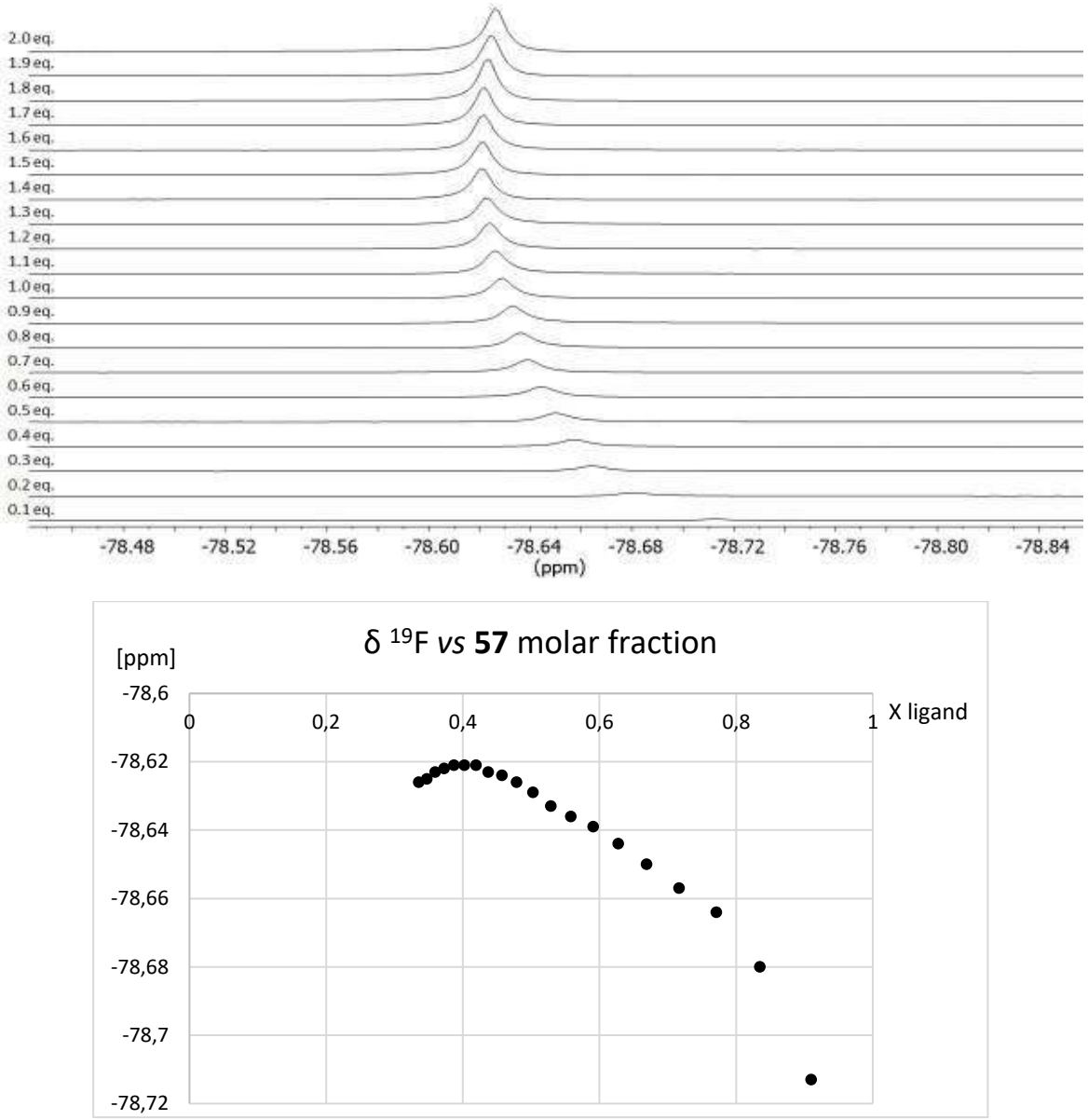

Figure 2: ^{19}F NMR spectra during the titration of ***o*-54** with increasing amounts of **57** (each spectrum after 0.1 eq. of metal complex) (top); plot of the ^{19}F NMR chemical shift of the triflate anion *vs* the molar fraction of ligand (bottom).

A similar behaviour of the NMR spectra was observed for the titration between ***p*-54** and **57**, with a rapid broadening of the ^{1}H NMR resonances and the down-field shifting of the ^{19}F resonances of the triflate anion. Moreover, after the addition of 1.0 eq. of **57** with respect to the triphenylene ligand, precipitation was observed, which hampered the continuation of the titration experiments due to the formation of poorly soluble metal-ligand aggregates, likely to be attributed to some coordination polymers (see Experimental Section, Titration 2).

The titration experiment with the ***m*-54** ligand turned out to be the clearer one, since no precipitation was observed. Similarly, the ^{1}H NMR spectra showed the rapid broadening of the resonances (Figure 3), while the ^{19}F NMR showed a clear-cut change of chemical shift for the triflate anion, corresponding to a molar ratio 0.4 between ligand and metal (Figure 4), in accordance with the formation in solution of a well-defined M_3L_2 coordination species.

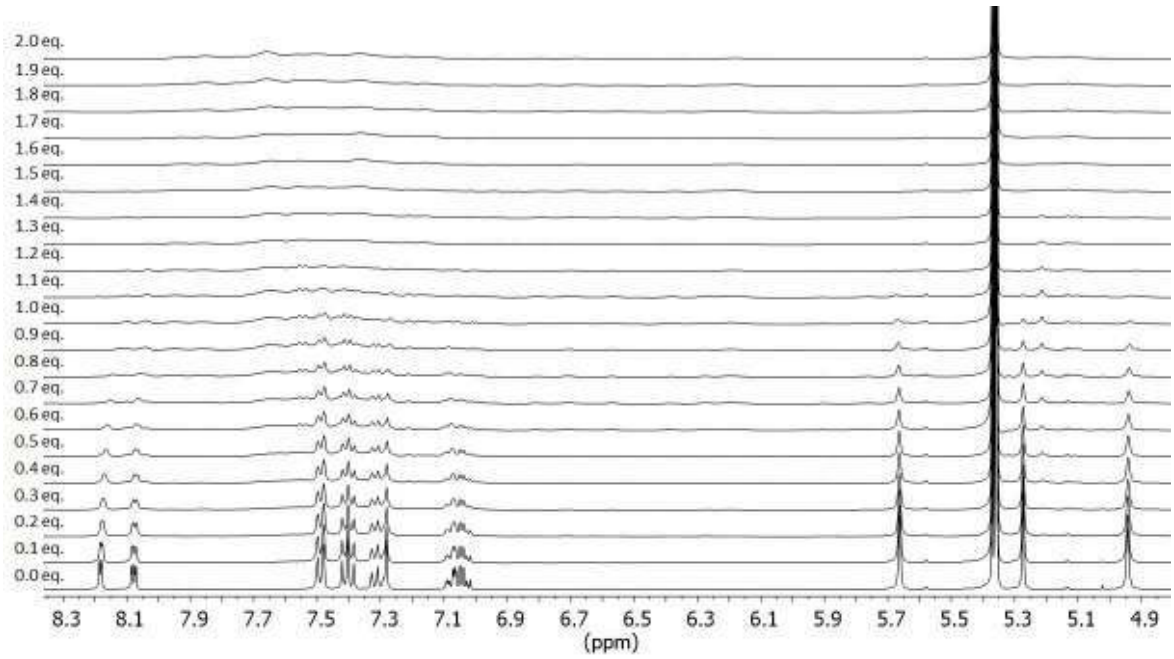

Figure 3: ^{1}H NMR spectra for the titration of the triphenylene polydentate ligand ***m*-54** with **57** (from bottom to top each spectrum corresponds to 0.1 eq. of metal with respect to the ligand).

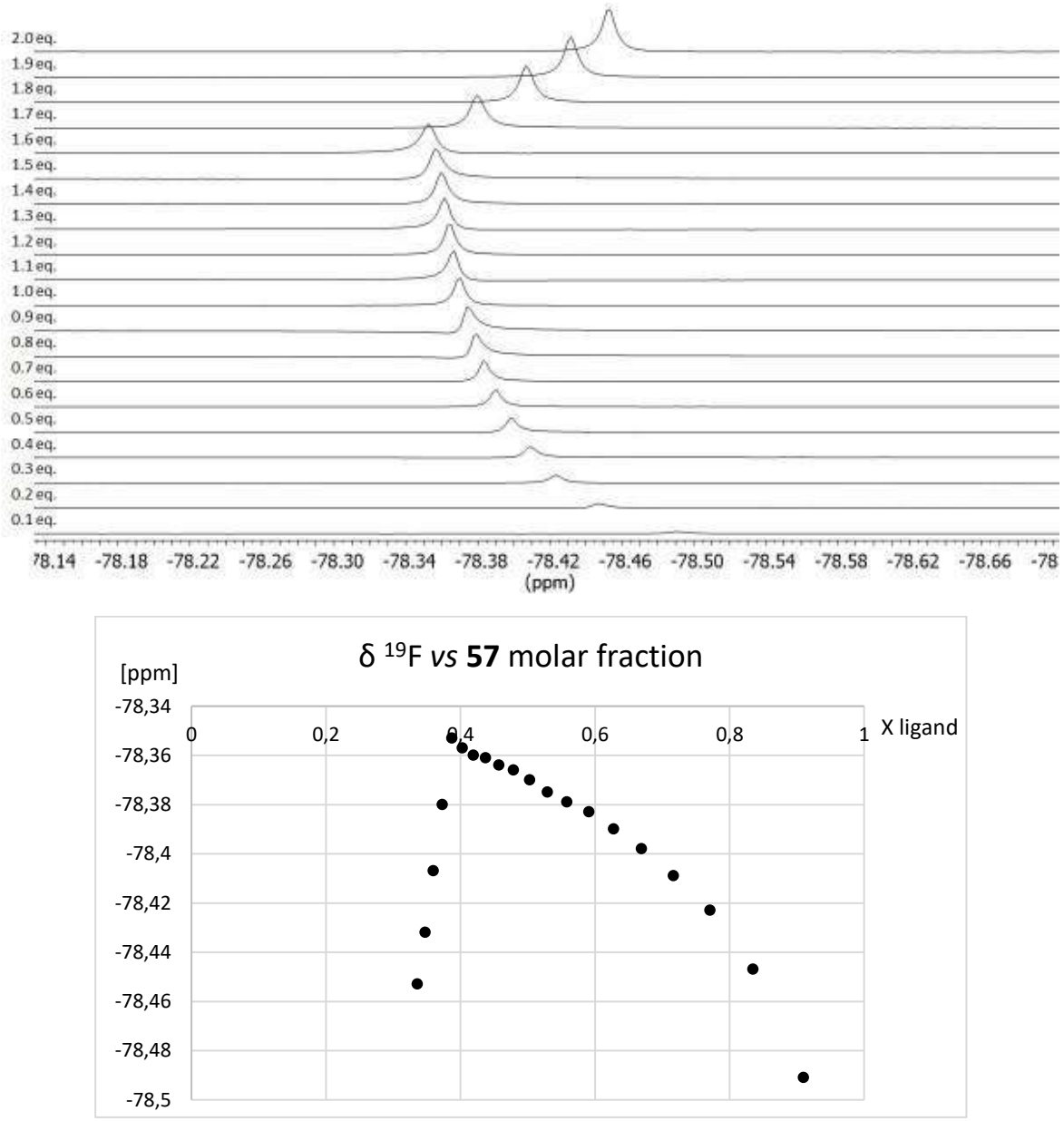

Figure 4: ^{19}F NMR spectra during the titration of ***m*-54** with increasing amounts of **57** (each spectrum after 0.1 eq. of metal complex) (top); plot of the ^{19}F NMR chemical shift of the triflate anion *vs* the molar fraction of ligand (bottom).

In order to try to observe more clear resonances in the ^{1}H NMR for the interaction between ***m*-54** and **57**, we recorder the spectra in CD_3CN for the M_3L_2 assembly at the correct stoichiometric ratio at 302 K, 332 K e 347 K (Figure 5).

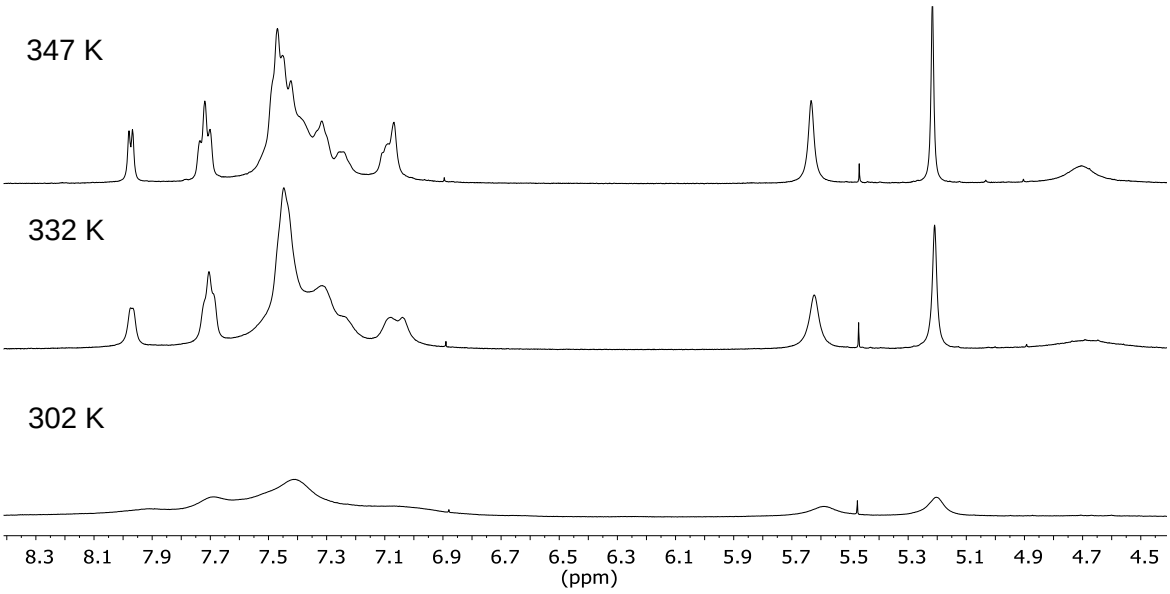

Figure 5: ^{1}H NMR spectra of **57** with ***m*-54** in a M_3L_2 ratio in CD_3CN at 347 K, 332 K and 302 K (from top to bottom).

The spectrum at 302 K was really broad and an increase of the temperature to 332 K led to the observation of some resonances, that further sharpened at 347 K, revealing the doublet attributed to the aromatic proton in the *ortho* position with respect to the N atom of the pyridine units. Furthermore, the observation of only one resonance for the benzyl methylene units indicated the presence of a major species in solution. The spectrum recorded again at room temperature corresponded to the original one, indicating that the system was stable and reversible in the range of investigated temperatures.

The exchange process that involves the metal-ligand assemblies in solution could also be explained considering that, when two molecules of **54** face each other through coordination with the metal, two diastereomeric M_3L_2 assemblies are possible due to the combination of the two enantiotopic faces of the triphenylene **54**. Specifically, such diastereoisomers are the C_3-symmetric homochiral coordination cage (racemate due to combination of *P-P* and *M-M* ligands) and the C_{3h}-symmetric *meso* cage (with heterochiral ligands *P-M*), thus causing the doubling of all resonances that at room temperature provide a rather broad NMR spectrum (Scheme 7).

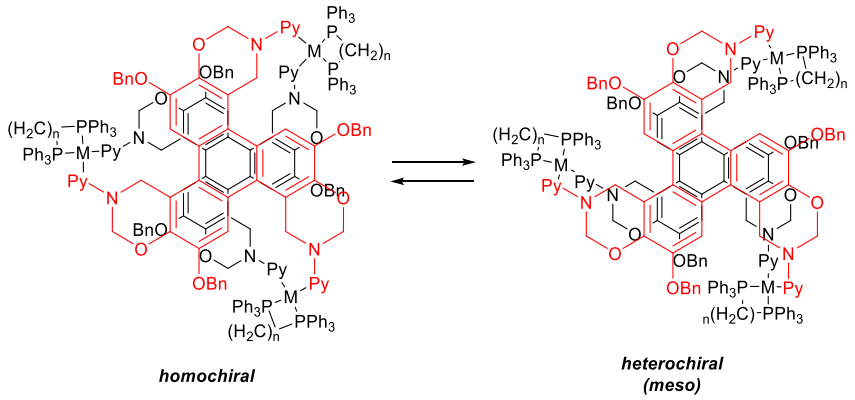

Scheme 7: Heterochiral meso and homochiral racemic M_3L_2 assemblies obtained from the achiral **54** triphenylene pyridine ligands.

To further investigate the formation of the coordination cages in solution, a series of pseudo 2D-DOSY NMR spectra were recorded for the free ligand ***m*-54**, the free complex **57** and the M_3L_2 assembly in CD_2Cl_2 solution at 300 K (Figure 6).

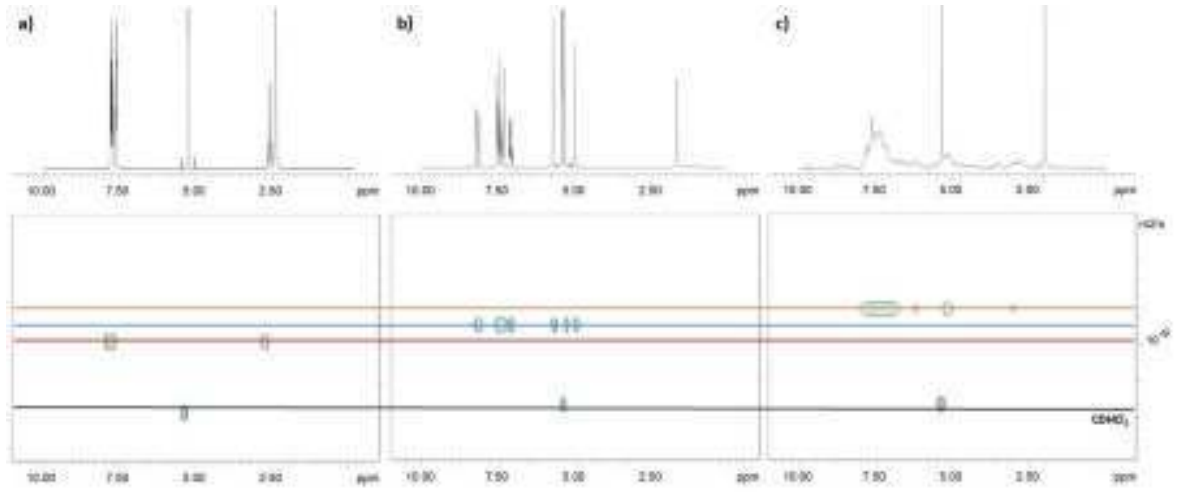

Figure 6: Pseudo-2D DOSY NMR spectra of a) **57**, b) tris-pyridine triphenylene ligand ***m*-54** and c) a M_3L_2 combination of **57** and ***m*-54** in CD_2Cl_2 at 300 K.

The comparison between the experiments showed that the diffusion coefficient in solution of the metal complex **57** is larger than that one of free triphenylene ***m*-54**, which is an expected result, considering the smaller size of the former and its more spherical shape. When **57** and ***m*-54** were both present in a 3:2 molar ratio, two effects can be highlighted: i) the diffusion coefficients of both species are identical, ii) the common diffusion coefficient is lower than both the two corresponding free species, which is a strong indication of the formation of a new coordination species. Based on the flat non-spherical shape of the ligand, and the similar but thicker shape of the expected M_3L_2 assembly, the decrease of the diffusion coefficient observed agrees with the possible formation of a trigonal bipyramidal cage. Considering the broadening of the resonances of the coordination species, which is an indication of an ongoing exchange process, it was not possible to extrapolate an indication of the MW of the aggregate in solution.[28] Nevertheless, the value of the diffusion coefficient is not drastically different with respect to that of the single triphenylene ligand ***m*-54** in solution, thus excluding the formation of polymeric assemblies and of very large aggregates characterized by the same M_3L_2 stoichiometry but eventually composed of multiple of these units.

The triphenylene ligand ***m*-54** was also investigated with other metal corners, such as $[Pt(dppe)(OTf)_2]$, **62**, in order to investigate the effect of the different metal centre characterized by a generally lower rate of exchange of the ligands. The titration of ***m*-54** with **62** was monitored by multinuclear NMR experiments, showing a series of spectra very similar to those observed previously for the metal complex **57**. The ^{19}F NMR was again the most efficient experiment to determine the stoichiometry of the assembly, observing a drastic change in chemical shift for the triflate anion when a 0.4 ligand molar fraction was reached, corresponding to the formation of a cage with M_3L_2 stoichiometry (see Experimental Section, Titration 4). We also investigated the effect of the temperature on the NMR spectra, either in CD_3CN at 300 K, 348 K as well as in CD_2Cl_2 at 193 K and 233 K, observing in all cases rather complicated spectra (see Experimental Section). In particular,

only at high temperature in CD_3CN the resonances of the assembly turned out to be a little bit sharper, even though the number of resonances was really very high. The pseudo 2D-DOSY NMR spectra of the M_3L_2 assembly in CD_3CN at 348 K, reported in Figure 7, shows how the signals of ligand and ***m*-54** and **57** have the same diffusion coefficient also at high temperature.

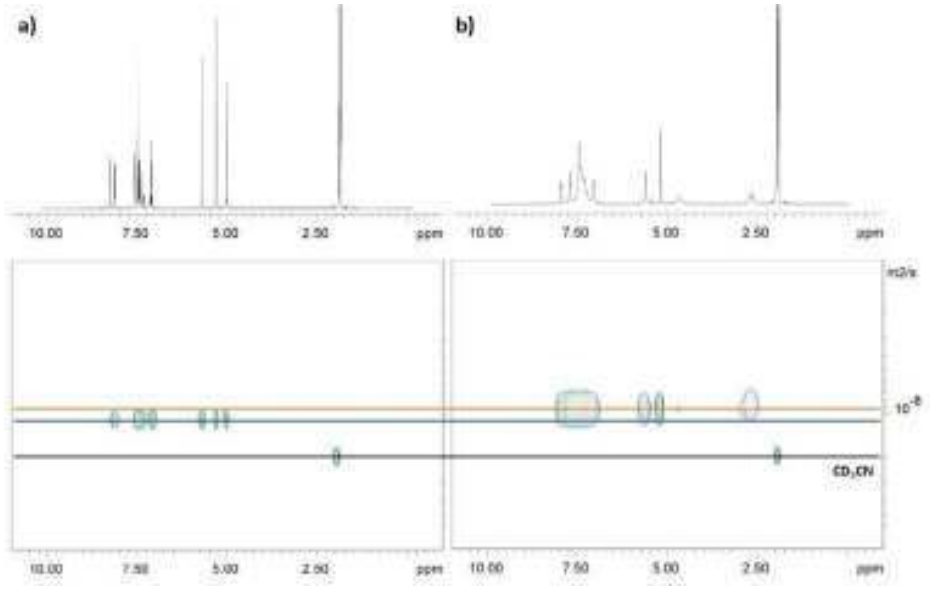

Figure 7: Pseudo-2D DOSY NMR spectra of a) ***m*-54** and b) a M_3L_2 combination of **57** and ***m*-54** in CD_3CN at 348 K.

The interaction between ***m*-54** and the [Pd(dppp)$(OTf)_2$], **59**, was considered to investigate the effect of a larger bite angle on the Pd(II) corners. The results of the titration are reported in the experimental part (Titration 5), from which in this case the ^{19}F NMR experiments suggest a 1:1 ratio between the tridentate ligand and the metal. The pseudo-2D-DOSY experiments with this combination of metal complex and ligand supported the formation of polymeric aggregates in solution rather than a discrete M_3L_2 cage, due to the observation of very broad cross-peaks in the DOSY spectrum, corresponding to a rather small and uncertain diffusion coefficient for the 1:1 mixture of **59** and ***m*-57**. A rapid comparison of this diffusion coefficient with that of the free triphenylene ligand ***m*-57** suggested the formation of aggregates that were about 100 times larger than the single triphenylene unit ***m*-57**. The 1:1 metal-to-ligand stoichiometry, and the observation of these large aggregates, suggested the formation of coordination polymers in solution. The latter experiments clearly demonstrated that the use of a larger bite angle of the diphosphine ligands, when using dppp instead of dppe, causes higher steric hindrance between the diphosphine ligand and the pyridine units of the triphenylene ligand, that eventually drives to the formation of completely different assemblies. When less hindered ligated palladium(II) corners are used with ***m*-54**, the expected triangular prism-shaped multiple complex is presumably obtained.

5.4 Investigation of the Metal-Ligand Aggregation in Solution

In order to prove this hypothesis, attempts to grow crystals from dichloromethane solutions of ***m*-54** with **57** and **62** in a M_3L_2 molar ratio were made. Unfortunately, the obtained crystals were not suitable for X-ray diffraction. Hence, several ESI-MS analyses were carried out both with dichloromethane and acetonitrile solutions, but no evidence of the formation

stable polycationic cages in solution was observed. The main detected peaks corresponded to a Pd(II) metal centre bearing the diphosphine, one triflate anion and one ***m*-54** ligand coordinated through one pyridine unit (*m/z* 1600.93 and 1614.91, corresponding to $[Pd(dppe)(\mathbf{m\text{-}54})(OTf)]^+$ and $[Pd(dppp)(\mathbf{m\text{-}54})(OTf)]^+$ fragments). None of such peaks were detected with the Pt(II) metal corners. It is likely that the M_3L_2 assembly, because of the presence of several exchange equilibria in solution, due to the multiple chirality of the triphenylene and to steric interactions arising by the proximity of the two triphenylene units, cannot survive the de-solvation process in the ESI analysis. This could explain the fact that mainly the $[M_1L_1OTf]^+$ species was detected by mass spectrometry (see Experimental Section).

As a final investigation on the formation of a M_3L_2 coordination cage, we studied the coordination of the three *tris*-pyridine ligands ***o*-**, ***m*-** and ***p*-54** with a *cis*-square planar palladium(II) *in silico.*[29] The modelling process initially started considering simplified structures, in which the flexible benzyl moieties were removed to reduce the number of possible conformers, focusing on M_3L_2 aggregates with *cis*-square planar palladium(II) with chloride in place of the diphosphine ligands (see Experimental Section). Through this approach, we determined the relative energies of the C_3-symmetric homo-chiral racemic cages and the C_{3h}-symmetric hetero-chiral *meso* cages (confirming that the latter are characterized by higher energy), as well as different combination of axial and equatorial conformations of the pyridine units in the di-hydro-oxazolinic moieties. This analysis confirmed that for the homo-chiral M_3L_2 cages many isomeric structures with comparable energies could be possible in equilibrium (see Experimental Section). Finally, the dppe ligand (in both helical conformations) was substituted to the chloride ligands in the lower energy obtained structures for the more stable homo-chiral M_3L_2 assemblies (Table 1 and Figure 8). According to these calculations, the more stable complex was observed with ligand ***m*-54** (in particular with *M* helicity of the dppe ligands and *ax-eq* conformation of the amine pyridine units).

Cage	Enantio-topic faces	Amine-pyridine conformer	Helicity of dppe	Rel. Energy [Kcal/mol]
cis-[5$_3$(***o*-54**)$_2$],	*RR/SS*	*ax-ax*	*P*	140.4
cis-[5$_3$(***o*-54**)$_2$],	*RR/SS*	*eq-eq*	*M*	131.4
cis-[5$_3$(***m*-54**)$_2$]	*RR/SS*	*ax-ax*	*P*	66.2
cis-[5$_3$(***m*-54**)$_2$]	*RR/SS*	*ax-eq*	*M*	0.0
cis-[5$_3$(***p*-54**)$_2$]	*RR/SS*	*ax-ax*	*P*	36.4
cis-[5$_3$(***p*-54**)$_2$]	*RR/SS*	*eq-eq*	*M*	32.6

Table 1: Minimized energies (semi-empirical level PM6) for the simplified complexes of ***o***,***m***,***p*-54** (benzyl units omitted) and **57** (see Experimental Section for details).

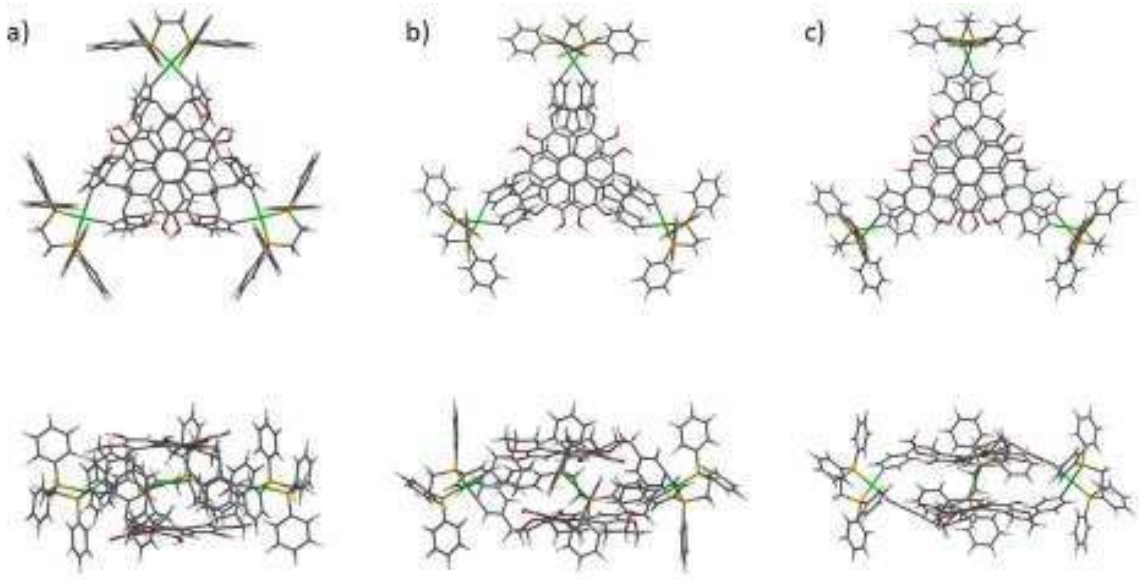

Figure 8: Top and side view for the minimized (benzyl-omitted) M_3L_2 cages for a) *cis*-[**5**$_3$(***o*-54**)$_2$], b) *cis*-[**5**$_3$(***m*-54**)$_2$] and c) *cis*-[**5**$_3$(***p*-54**)$_2$].

These computational results agreed with the experimental observations for the coordination of ***m*-54** with **57** of a clear solution and a well-defined M_3L_2 stoichiometry in different solvents, as well as pseudo 2D-DOSY experiments with a diffusion coefficient for the cage that was lower but still comparable to that of the free ligand. The calculations further supported the experimental observation of the broadening of the resonances observed on the ^{1}H NMR, likely caused by exchange processes between the different conformers of the pyridine and the diphosphane units.

Among the three ligands considered, ***m*-54** turned out to provide in solution the formation of a M_3L_2 cage both with Pd(II) or Pt(II) metal centres when using dppe as ligand for the metal. Differently, the ***o*-54** ligand led to more unstable assemblies and ***p*-54** ligands led only to the formation of coordination polymers that eventually precipitated from the solution, regardless the use of Pd(II) or Pt(II) metal centres. As long as the ***m*-54** ligand is concerned, ^{1}H NMR pseudo-2D-DOSY experiments and ^{19}F NMR titrations demonstrated the formation of clear M_2L_3 aggregates in solution, even though ^{31}P NMR and ^{1}H NMR were not informative due to some exchange processes. The latter were attributed to the formation of diastereoisomeric cages, derived by the prochiral nature of the *tris*-pyridine triphenylene ligand once coordinated forming the trigonal bipyramidal unit, and conformational equilibria of the ligand itself and of the diphosphane, as supported by quanto-mechanical calculations. No clear-cut evidence of guest binding was observed due to the dynamic properties of the assemblies, although it cannot be excluded that in the narrow cavity, in particular for the cages formed with ***o*-54** and ***m*-54**, binding of solvent molecules or more probably of counter-anions could occur.

The results reported in this Chapter where submitted and published on *Tetrahedron Letters* (IF 2.26).[30]

5.5 Experimental Section

5.5.1 General Methods

The reactions were followed with TLC Polygram® Sil G/UV254, 0.25 mm thickness. ^{1}H NMR, ^{13}C NMR, and 2D spectra were recorded with a Bruker Avance 300 and Ascend 400 spectrometers, working at 300-400 and 75-100 MHz respectively. Resonance frequencies are referred to tetramethylsilane. ^{31}P NMR and ^{19}F NMR were recorded with a Bruker Ascend 400, working at 162 e 376 MHz respectively. DOSY experiments were performed the BPLED sequence, calibrating the diffusion time (Δ) in order to obtain a signal ratio of 20 between *gpz* = 2 and *gpz* = 95, and elaborated with Bruker Topspin and Dynamics Center. IR spectra were recorded with a Perkin Elmer Spectrum One spectrophotometer. Mass spectrometric measurements were performed using a Thermo Scientific LTQ Orbitrap XL equipped with HESI source. The compounds studied were dissolved in methanol or acetonitrile with a concentration of $5 \cdot 10^{-3}$ M. They were injected into the HESI source by direct infusion with the syringe pump integrated in the mass spectrometer at a 5 mL·min^{-1} flow rate. Mass spectra were acquired in positive-polarity mode with the following tuning conditions: Temperature 40 °C, Sheath gas 8 (arbitrary units, arb), Aux gas and Sweep gas 0 arb, Spray Voltage 4.5 kV, Capillary temperature 275 °C, Capillary Voltage -9 V, Tube lence 150 V. In negative polarity the following tuning parameters were employed: Temperature 40 °C, Sheath gas 19 (arbitrary units, arb), Aux gas and Sweep gas 0 arb, Spray Voltage 3.0 kV, Capillary temperature 275 °C, Capillary Voltage 10 V, Tube lence 120 V. Mass spectra were collected in full scan with a resolution of 100000 at m/z 400. The Orbitrap MS was calibrated just before analysis and during the acquisition in order to improve mass accuracy lock masses were employed. MS of the metal-pyridine ligand adducts were recorded on a Finningan LCQ Deca XP Max mass spectrometer coupled to electrospray ionisation source (ESI) in positive or negative mode. Reagents and solvents with high purity degree purchased by the providers were used as given. Otherwise, they were purified following the procedures reported in literature.[31] Anhydrous solvents were prepared by adding activated 3 Å molecular sieves to the solvent under inert atmosphere. Molecular sieves were activated shortly before the use by continuous heating under *vacuum*. Flash chromatography were performed with silica gel Merk 60, 230-400 mesh, following procedures reported in literature.[32] Titrations were performed using a 10 µL Transferpettor™ with glass capillary. The structures were minimized at semi-empirical level (PM6) with MOPAC2016, Version: 19.179W, James J. P. Stewart, Stewart Computational Chemistry.

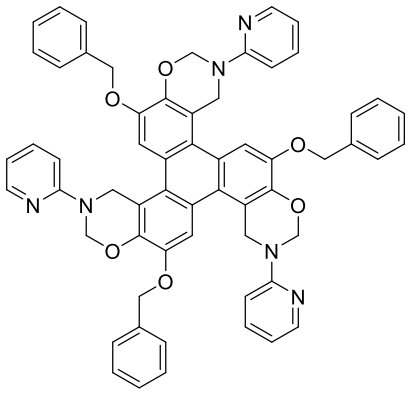

***o*-54**

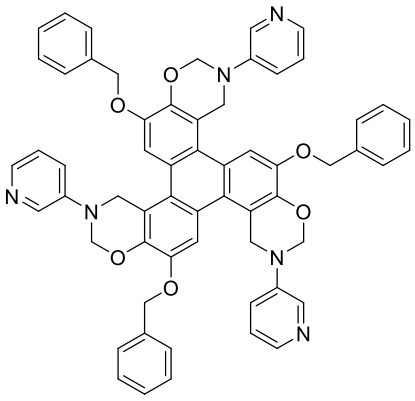

***m*-54**

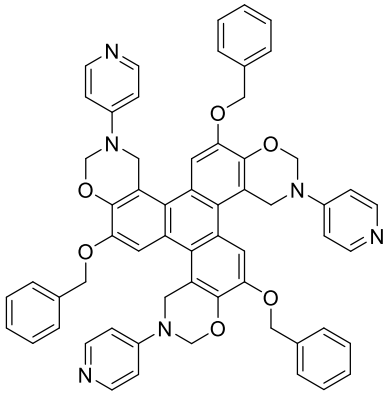

***p*-54**

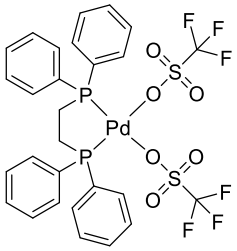

57

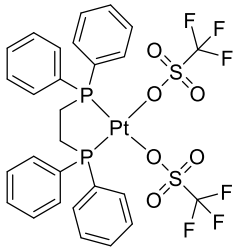

62

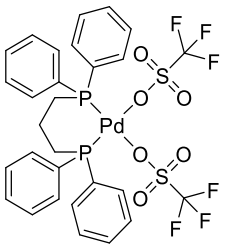

59

5.5.2 Experimental Procedures - Syntheses

General Procedure 1 (GP1): General procedure for the Mannich reaction of 3,7,11-tris(benzyloxy)triphenylene-2,6,10-triol with aminopyridine.

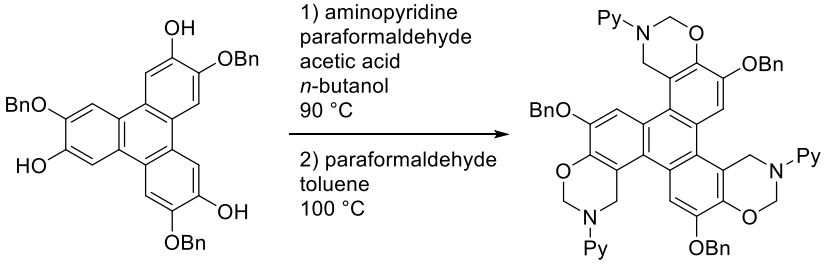

***C*$_3$-26**

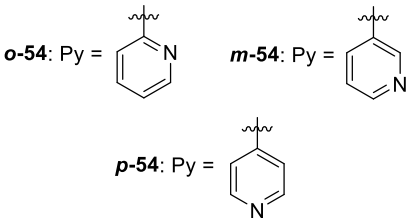

In a 25 mL round bottomed flask, a mixture of *o*-, *m*- or *p*-aminopyridine (0.56 g, 5.9 mmol), paraformaldehyde (0.20 g, 6.7 mmol), and acetic acid (0.04 g, 0.7 mmol) in *n*-butanol (10 mL) was stirred at 90 °C overnight under argon atmosphere. The resulting solution was cooled to room temperature and concentrated in *vacuum*, to obtain the corresponding hemiaminal (***o*-53**, **m-53** or ***p*-53**). The residue was transferred in a 25 mL screw capped Schott Duran® bottle and 3,7,11-tris(benzyloxy)triphenylene-2,6,10-triol (***C*$_3$-26**) (0.25 g, 0.42 mmol), paraformaldehyde (0.20 g. 6.7 mmol), and anhydrous toluene (10 mL) were added. The mixture was purged with argon and stirred at 100 or 110 °C for 24 or 48 hours. The resulting mixture was cooled to room temperature and concentrated in *vacuum*. The resulting crude oil was suspended with EtOH (in the case of ***o*-54** and ***m*-54**) or Et_2O (in the case of ***p*-54**) and the resulting precipitate was filtered, washed with EtOH or Et_2O and dried in *vacuum*, to afford the product as a pale-yellow solid.

6,12,18-tris(benzyloxy)-3,9,15-tri(pyridin-2-yl)-3,4,9,10,15,16-hexahydro-2*H*,8*H*,14*H*-triphenyleno[1,2-*e*:5,6-*e'*:9,10-*e''*]tris([1,3]oxazine) (***o*-54**): **GP1** was applied on ***C*$_3$-26**. 100 °C for 24 hours. 90% yield. M.P. 191 °C. ^{1}H NMR (400 MHz, $CDCl_3$): δ 8.14 (3H, ddd, *J* = 4.9 Hz, *J* = 2.0 Hz, *J* = 0.8 Hz), 7.47-7.42 (6H, set of m), 7.38-7.28 (12H, set of m), 7.23-7.16 (3H, set of m), 6.66 (3H, ddd, *J* = 7.3 Hz, *J* = 4.9 Hz, *J* = 0.8 Hz), 6.50 (3H, d, *J* = 8.3 Hz), 5.85 (6H, s), 5.31 (6H, s), 5.01 (6H, s). $^{13}C\{^1H\}$ NMR (100 MHz) δ 157.1, 148.3, 145.0, 144.0, 138.0, 137.2, 128.8, 128.1, 127.0, 125.9, 123.4, 117.3, 115.5, 111.4, 108.9, 76.1, 71.5, 48.8. IR (KBr): ν 1593, 1566, 1476, 1435, 1421, 1377, 1313, 1275, 1244, 1160, 1122, 1072, 953, 772, 732, 695 cm^{-1}. HRMS (ESI): calcd. for $C_{60}H_{49}N_6O_6$ [M^+] 949.3708; found: 949.3713.

6,12,18-tris(benzyloxy)-3,9,15-tri(pyridin-3-yl)-3,4,9,10,15,16-hexahydro-2*H*,8*H*,14*H*-triphenyleno[1,2-*e*:5,6-*e'*:9,10-*e''*]tris([1,3]oxazine) (***m*-54**): **GP1** was applied on ***C*$_3$-26**. 110 °C for 48 hours. 86% yield. M.P. 58-60 °C. ^{1}H NMR (400 MHz, $CDCl_3$): δ 8.17-8.13 (3H, set of m), 8.09-8.06 (3H, set of m), 7.46-7.41 (6H, set of m), 7.34 (6H, t, *J* = 7.6 Hz), 7.23 (3H, t, *J* = 7.4 Hz), 7.11 (3H, s), 7.00-6.94 (6H, set of m), 5.58 (6H, s), 5.29 (6H, s), 4.63 (6H, s). $^{13}C\{^1H\}$ NMR (100 MHz): δ 144.6, 143.7, 143.5, 142.9, 141.4, 137.0, 128.9, 128.2, 126.8, 125.6,

125.6, 123.6, 123.2, 116.3, 111.5, 79.2, 71.4, 52.3. IR (KBr): ν 3027, 2917, 2846, 1635, 1583, 1481, 1423, 1376, 1317, 1279, 1242, 1156, 1107, 1073, 949, 913, 803, 736, 698, 621 cm^{-1}. HRMS (ESI): calcd. for $C_{60}H_{49}N_6O_6$ [M^+] 949.3708; found: 949.3734.

6,12,18-tris(benzyloxy)-3,9,15-tri(pyridin-4-yl)-3,4,9,10,15,16-hexahydro-2*H*,8*H*,14*H*-triphenyleno[1,2-*e*:5,6-*e'*:9,10-*e''*]tris([1,3]oxazine) (***p*-54**): **GP1** was applied on ***C*$_3$-26**. 100 °C for 48 hours. 75% yield. M.P. 170-171 °C. ^{1}H NMR (400 MHz, $CDCl_3$): δ 8.21 (6H, dd, *J* = 5.0, 1.6 Hz), 7.46-7.41 (6H, set of m), 7.34 (6H, t, *J* = 7.8 Hz), 7.24-7.19 (3H, set of m), 7.12 (3H, s), 6.56 (6H, dd, *J* = 5.0, 1.6 Hz), 5.64 (6H, s), 5.31 (6H, s), 4.61 (6H, s). $^{13}C\{^1H\}$ NMR (100 MHz): δ 152.8, 149.7, 144.8, 143.5, 136.8, 128.9, 128.2, 126.5, 125.4, 123.1, 116.5, 111.2, 111.0, 76.6, 71.2, 50.3. IR (KBr): ν 1643, 1593, 1552, 1511, 1483, 1459, 1421, 1383, 1319, 1278, 1245, 1159, 1111, 1072, 1034, 997, 960, 874, 799, 782, 740, 697 cm^{-1}; HRMS (ESI): calcd. for $C_{60}H_{49}N_6O_6$ [M^+] 949.3708; found: 949.3744.

Dichloride(1,5-cyclooctadiene)palladium(II) (**55**):

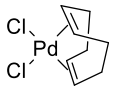

55

In a 250 mL round-bottomed flask, $PdCl_2$ (2.00 g, 11.3 mmol) was added to a solution of NaCl (1.32 g, 22.7 mmol) in MeOH (150 mL). The resulting suspension was stirred for 18 hours, filtered, and cyclooctadiene (3.64 g, 33.7 mmol) was added to the resulting solution. The resulting suspension was stirred for 1 hour. The formed precipitate was filtered washed with MeOH (3×10 mL) and dried in *vacuum*, affording the product as a yellow solid (2.99 g, 10.5 mmol, 93% yield). ^{1}H NMR (400 MHz, $CDCl_3$), δ 6.31 (4H, s), 2.91 (4H, s), 2.57 (4H, set of m). Further spectroscopic data (^{13}C, MS, IR) are in accordance with the literature.[25]

[1,2-Bis(diphenylphosphino)ethane]dichloridepalladium(II) (**56**):

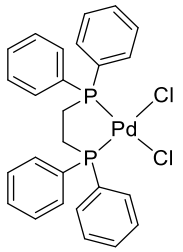

56

In a 100 mL two-necked round-bottomed flask, under inert atmosphere, **55** (0.49 g, 1.72 mmol) was dissolved in anhydrous DCM (20 mL). A solution of 1,2-bis(diphenylphosphino)ethane (0.72 g, 1.8 mmol) in anhydrous DCM (15 mL) was injected in the flask and the resulting mixture was stirred for 2 hours and concentrated in *vacuum*. The resulting solid was dispersed in anhydrous toluene (70 mL) and refluxed, under inert atmosphere, for 4 hours. The formed precipitate was filtered, washed with EtOH (2×6 mL) and dried in *vacuum*, affording the product as a pale-yellow solid (0.95 g, 1.65 mmol, 96% yield). ^{1}H NMR (400 MHz, $CDCl_3$) δ 7.87 (8H, set of m), 7.54 (4H, set of m), 7.47 (8H, set of m), 2.44 (4H, set of m). $^{31}P\{^1H\}$ NMR (162 MHz): δ 63.68. Further spectroscopic data (^{13}C, MS, IR) are in accordance with the literature.[25]

[1,2-Bis(diphenylphosphino)ethane]palladium(II) triflate (**57**):

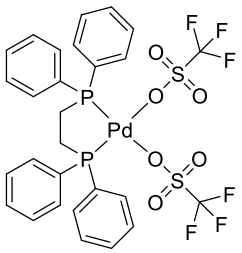

57

In a 100 mL two-necked round-bottomed flask, under inert atmosphere, anhydrous DCM (17 mL), **56** (0.30 g, 0.52 mmol) and AgOTf (0.27 g, 1.04 mmol) were added in sequence. The resulting suspension was stirred for 2 hours, protected from light. The suspension was filtered, and the mother liquor concentrated in *vacuum*. The crude was dispersed in anhydrous Et_2O, filtered and dried in *vacuum*, affording the product as a pale-yellow solid (0.38 g, 0.35 mmol, 91% yield). ^1H NMR (400 MHz, CD_2Cl_2) δ 7.85-7.73 (12H, set of m), 7.65 (8H, set of m), 2.74 (4H, set of m). $^{31}P\{^1H\}$ NMR (162 MHz): δ 72.22. $^{19}F\{^1H\}$ NMR (376 MHz): δ -78.94. Further spectroscopic data (^{13}C, MS, IR) are in accordance with the literature.[26]

[1,2-Bis(diphenylphosphino)ethane]dichlorideplatinum(II) (**61**):

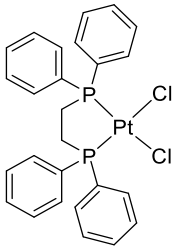

10

In a 250 mL two-necked round-bottomed flask, under inert atmosphere, [$PtCODCl_2$], (0.15 g, 0.4 mmol) was dissolved in anhydrous DCM (90 mL). A solution of 1,2-bis(diphenylphosphino)ethane (0.159 g, 0.4 mmol) in anhydrous DCM (60 mL) was injected in the flask during 2.5 hours and the resulting mixture was stirred for 18 hours and concentrated in *vacuum*. Anhydrous Et_2O was added to the residue and the resulting precipitate was filtered, washed with EtOH (2×6 mL) and dried in *vacuum*, affording the product as a pale-yellow solid (0.247 g, 0.37 mmol, 93% yield). ^1H NMR (300 MHz, CD_2Cl_2): δ 7.96-7.83 (8H, m), 7.67-7.51 (12H, m), 2.53-2.26 (4H, m). $^{31}P\{^1H\}$ NMR (122 MHz): δ 41.95. Further spectroscopic data (^{13}C, MS, IR) are in accordance with the literature.[27]

[1,2-Bis(diphenylphosphino)ethane]platinum(II) triflate (**62**):

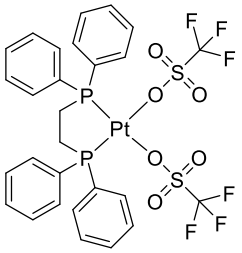

62

In a 100 mL two-necked round-bottomed flask, under inert atmosphere, anhydrous DCM (30 mL), **61** (0.226 g, 0.34 mmol) and AgOTf (0.173 g, 0.64 mmol) were added in sequence. The resulting suspension was stirred for 72 hours, protected from light. The suspension was filtered, and the mother liquor concentrated in *vacuum*. The crude was dispersed in anhydrous Et_2O, filtered and dried in *vacuum*, affording the product as a pale-yellow solid (0.275 g, 0.31 mmol, 91% yield). ^1H NMR (400 MHz): δ (CD_2Cl_2) 7.86-7.53 (20H, set of m), 2.55 (4H, set of m), 2.44-2.25 (2H, set of m). $^{31}P\{^1H\}$ NMR (162 MHz): δ 36.16. $^{19}F\{^1H\}$ NMR (376 MHz): δ -78.80. Further spectroscopic data (^{13}C, MS, IR) are in accordance with the literature.[27]

[1,3-Bis(diphenylphosphino)propane]dichloridepalladium(II) (**58**):

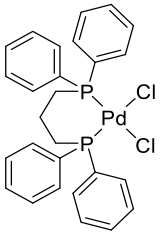

58

In a 100 mL two-necked round-bottomed flask, under inert atmosphere, **55** (0.30 g, 1.05 mmol) was dissolved in anhydrous DCM (17 mL). A solution of 1,3-bis(diphenylphosphino)propane (0.455 g, 1.1 mmol) in anhydrous DCM (5 mL) was injected in the flask and the resulting mixture was stirred for 2 hours and concentrated in *vacuum*. The crude product solid was recrystallized in anhydrous toluene (70 mL), filtered, washed with EtOH (2×6 mL) and dried in *vacuum*, affording the product as a pale-yellow solid (0.611 g, 1.04 mmol, 99% yield). ^1H NMR (300 MHz, CD_2Cl_2): δ 7.88-7.74 (8H, set of m), 7.60-7.45 (12H, set of m), 2.51-2.40 (4H, set of m), 2.58-1.92 (2H, set of m). $^{31}P\{^1H\}$ NMR (122 MHz): δ 11.49. Further spectroscopic data (^{13}C, MS, IR) are in accordance with the literature.[33]

[1,3-Bis(diphenylphosphino)propane]palladium(II) triflate (**59**):

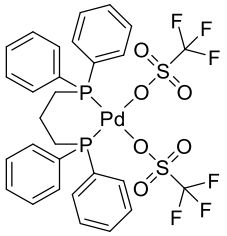

59

In a 100 mL two-necked round-bottomed flask, under inert atmosphere, anhydrous DCM (30 mL), **58** (0.20 g, 0.34 mmol) and AgOTf (0.186 g, 0.72 mmol) were added in sequence. The resulting suspension was stirred for 18 hours, protected from light. The suspension was filtered, and the mother liquor concentrated in *vacuum*. The crude was dispersed in anhydrous Et_2O, filtered and dried in *vacuum*, affording the product as a pale-yellow solid (0.247 g, 0.30 mmol, 89% yield). ^{1}H NMR (400 MHz, CD_2Cl_2): δ 7.74-7.58 (12H, m), 7.54-7.46 (8H, m), 2.82-2.74 (4H, m). $^{31}P\{^{1}H\}$ NMR (162 MHz, CD_2Cl_2): δ 17.28. $^{19}F\{^{1}H\}$ NMR (376 MHz, CD_2Cl_2): δ -78.63. Further spectroscopic data (^{13}C, MS, IR) are in accordance with the literature.[33]

5.5.3 NMR and MS Spectra

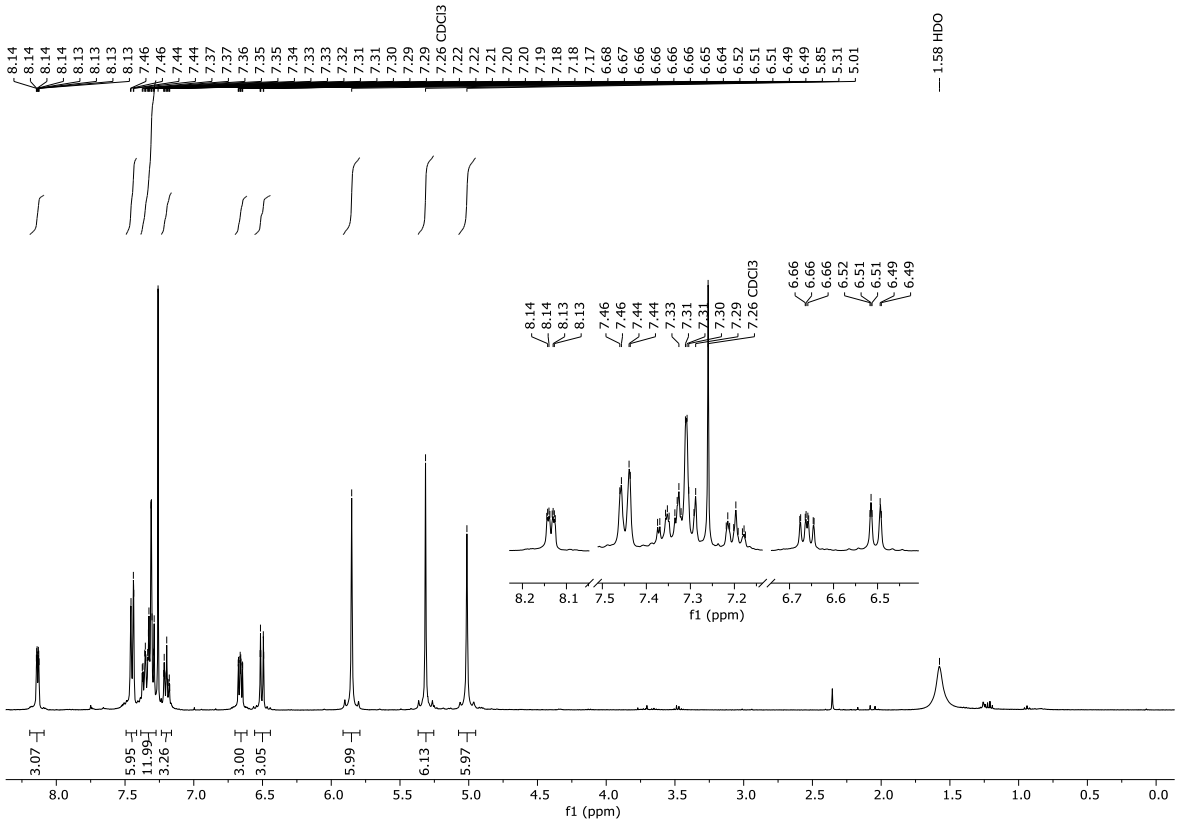

Figure I: ^{1}H NMR of molecule ***o*-54**.

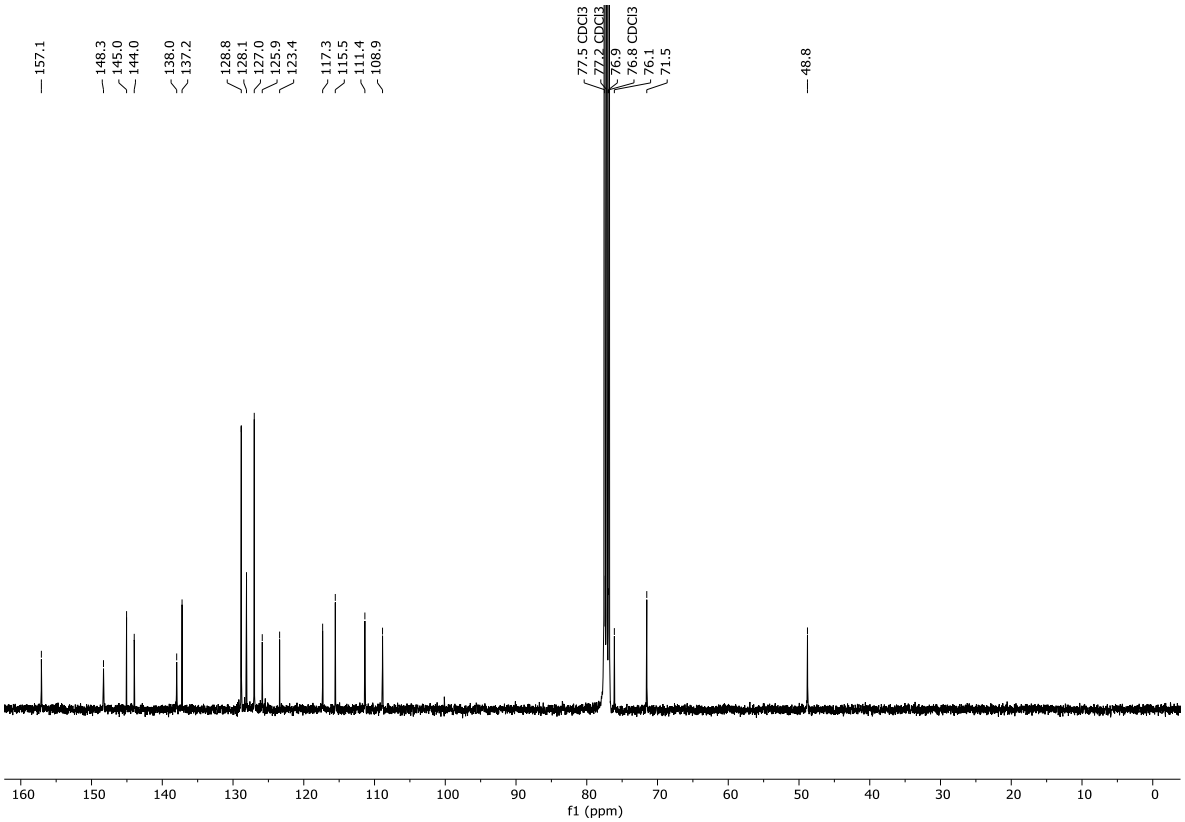

Figure II: ^{13}C NMR of molecule ***o*-54**.

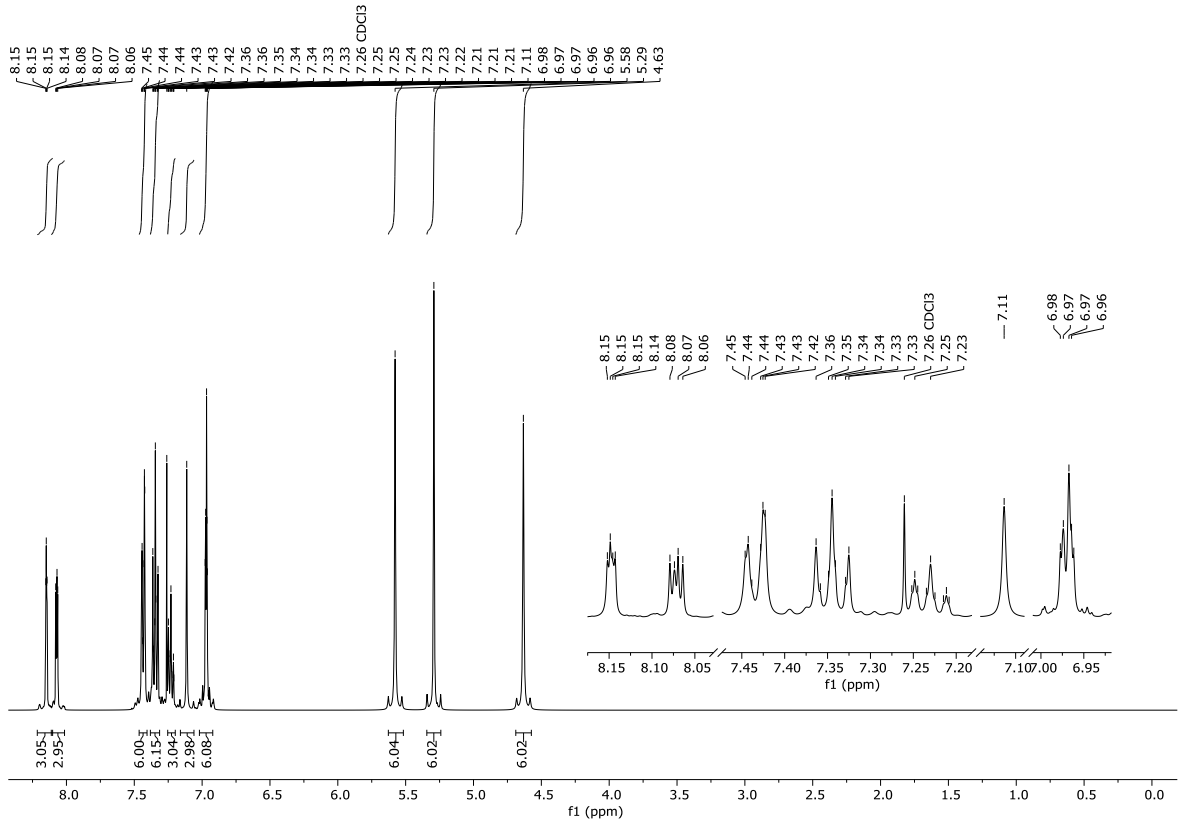

Figure III: ^{1}H NMR of molecule ***m*-54**.

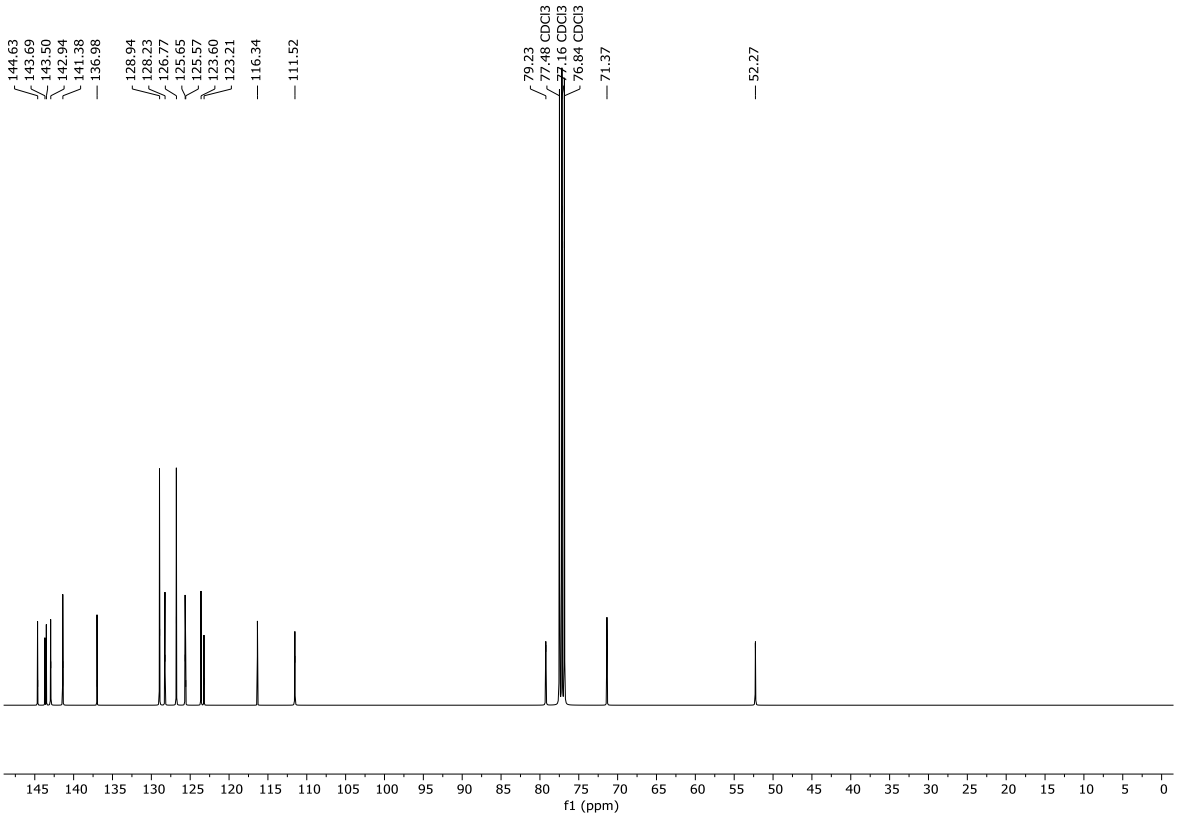

Figure IV: ^{13}C NMR of molecule ***m*-54**.

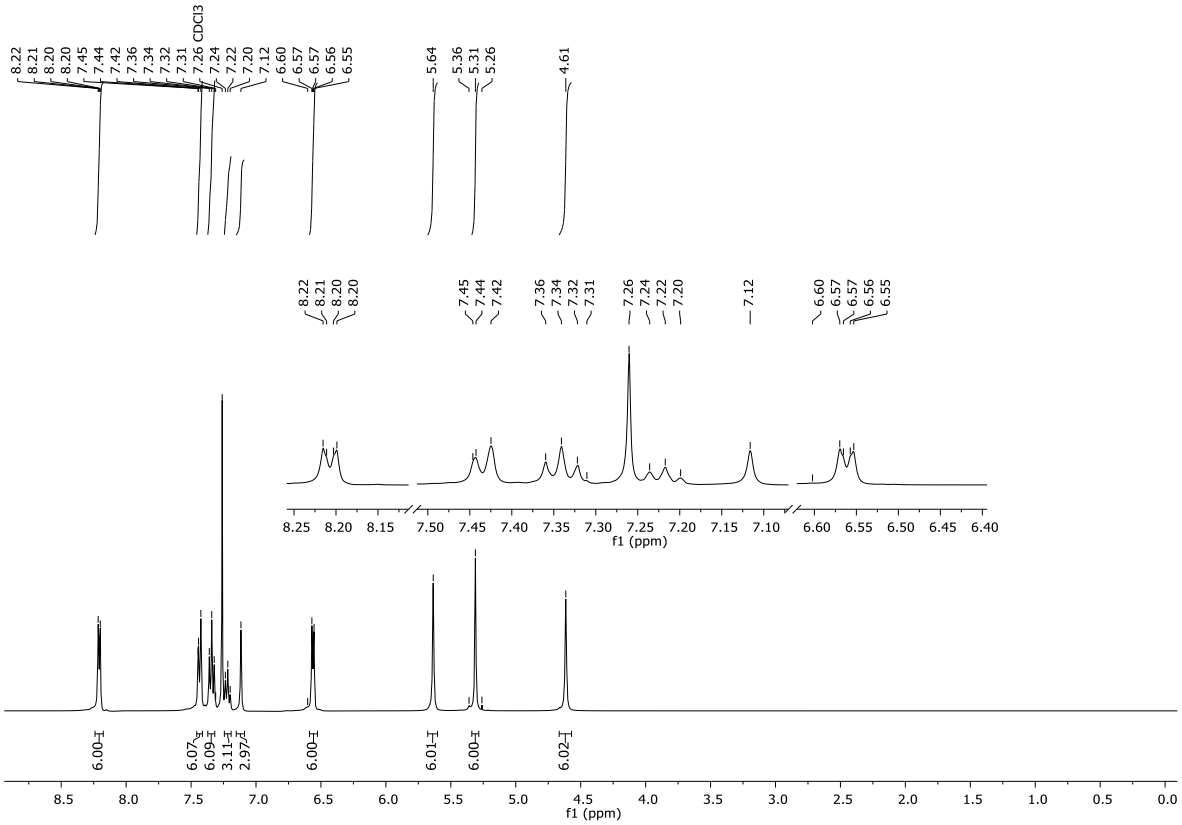

Figure V: ^{1}H NMR of molecule ***p*-54**.

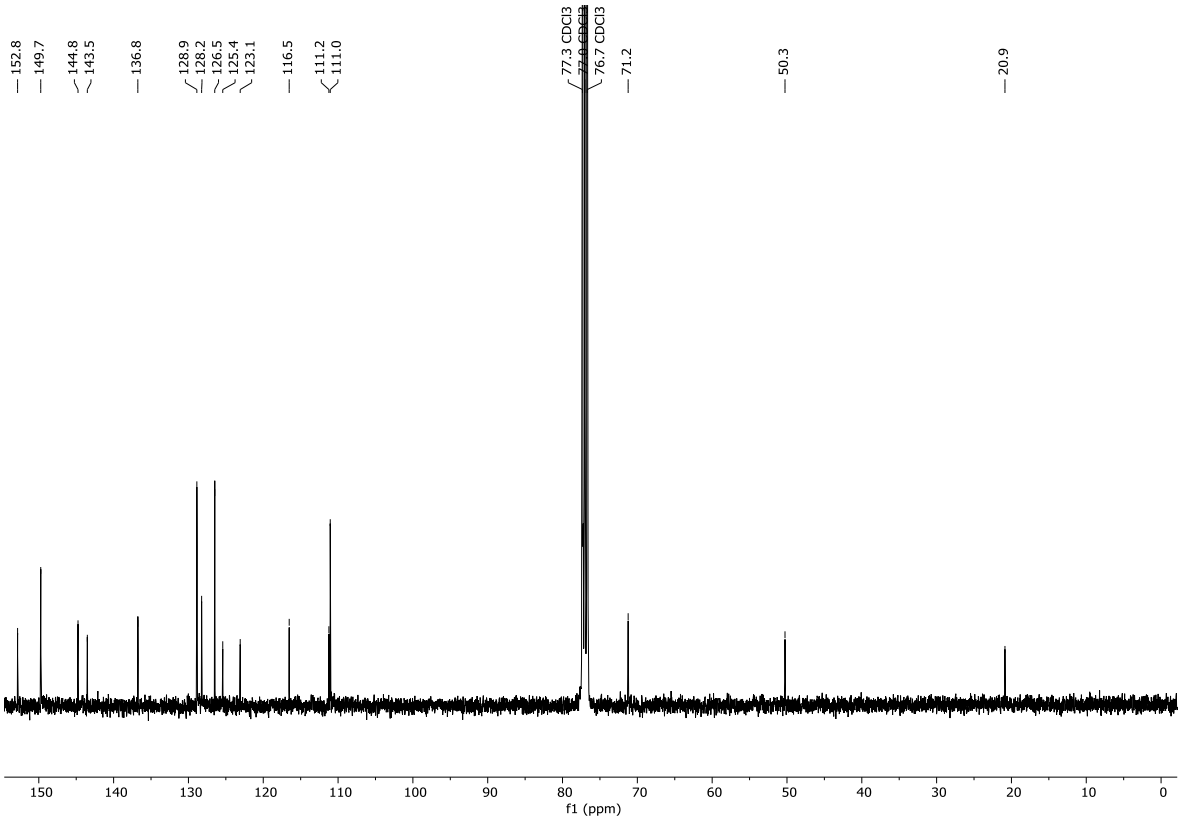

Figure VI: ^{13}C NMR of molecule ***p*-54**.

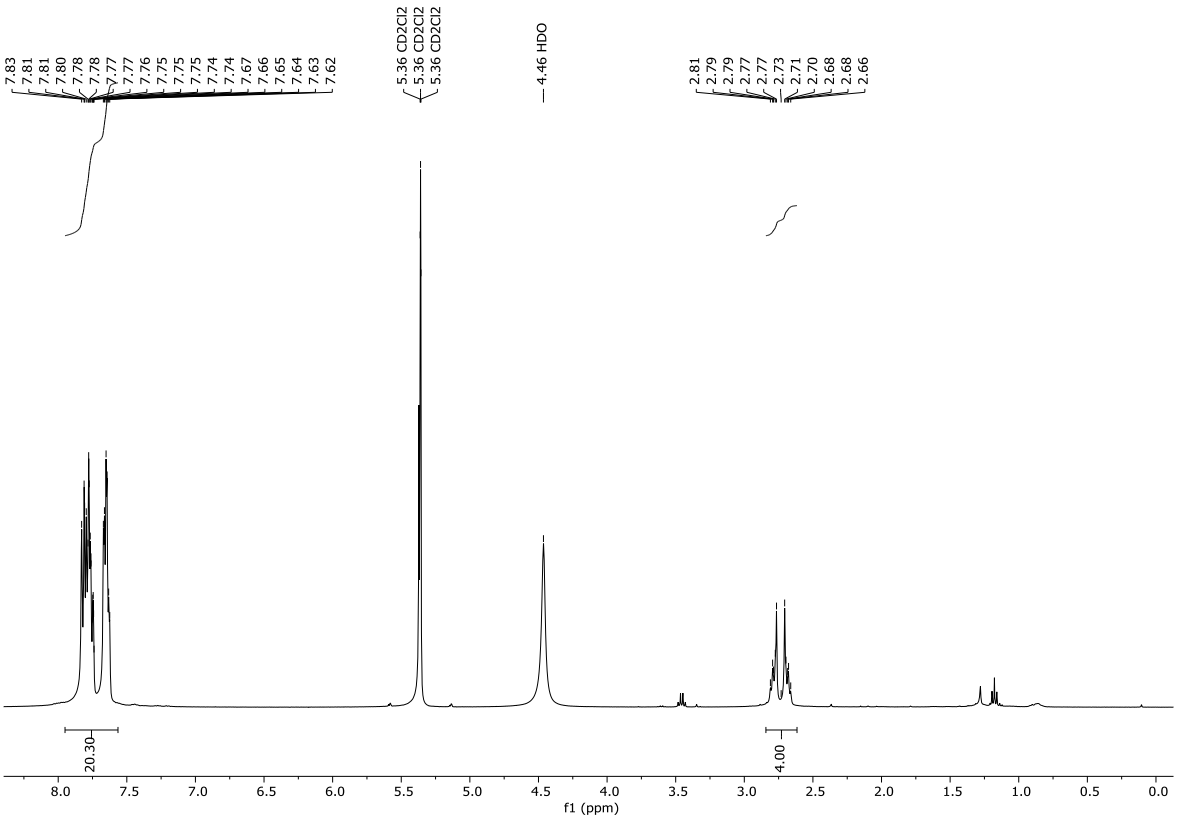

Figure VII: ^{1}H NMR of molecule **57**.

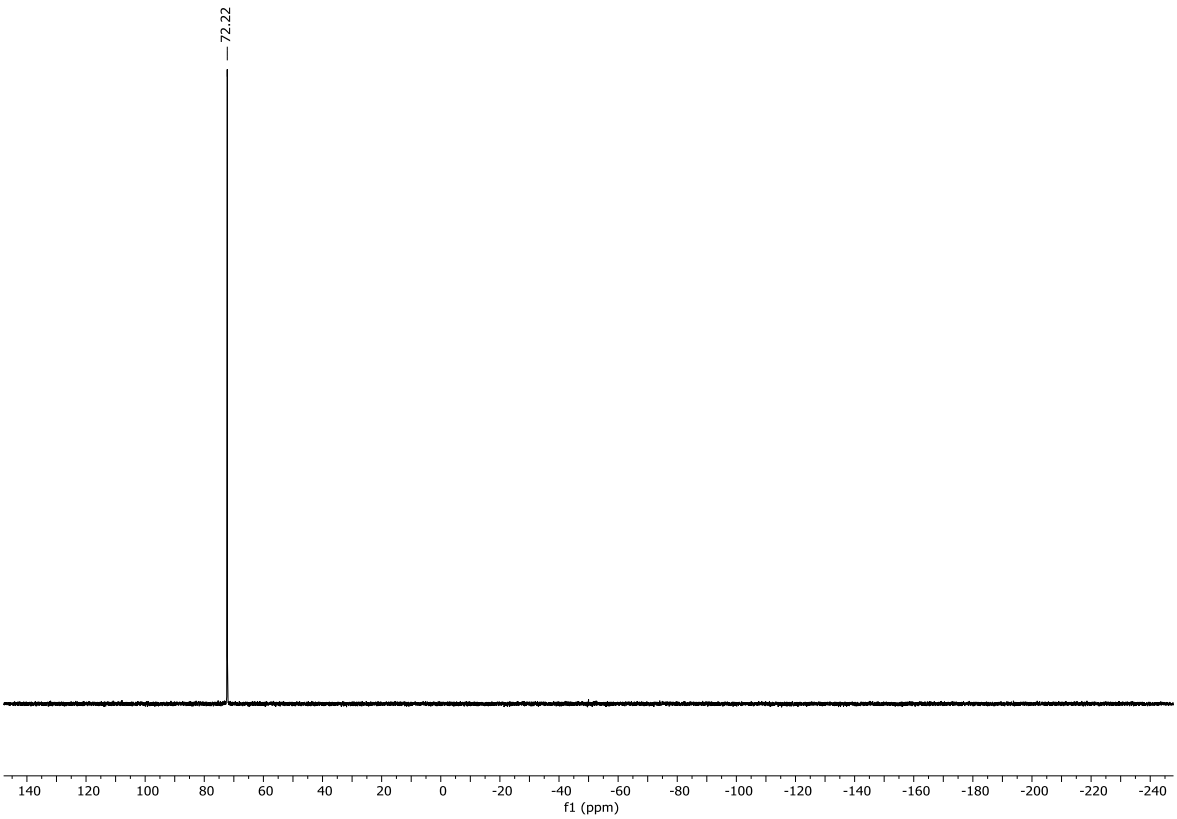

Figure VIII: ^{31}P NMR of molecule **57**.

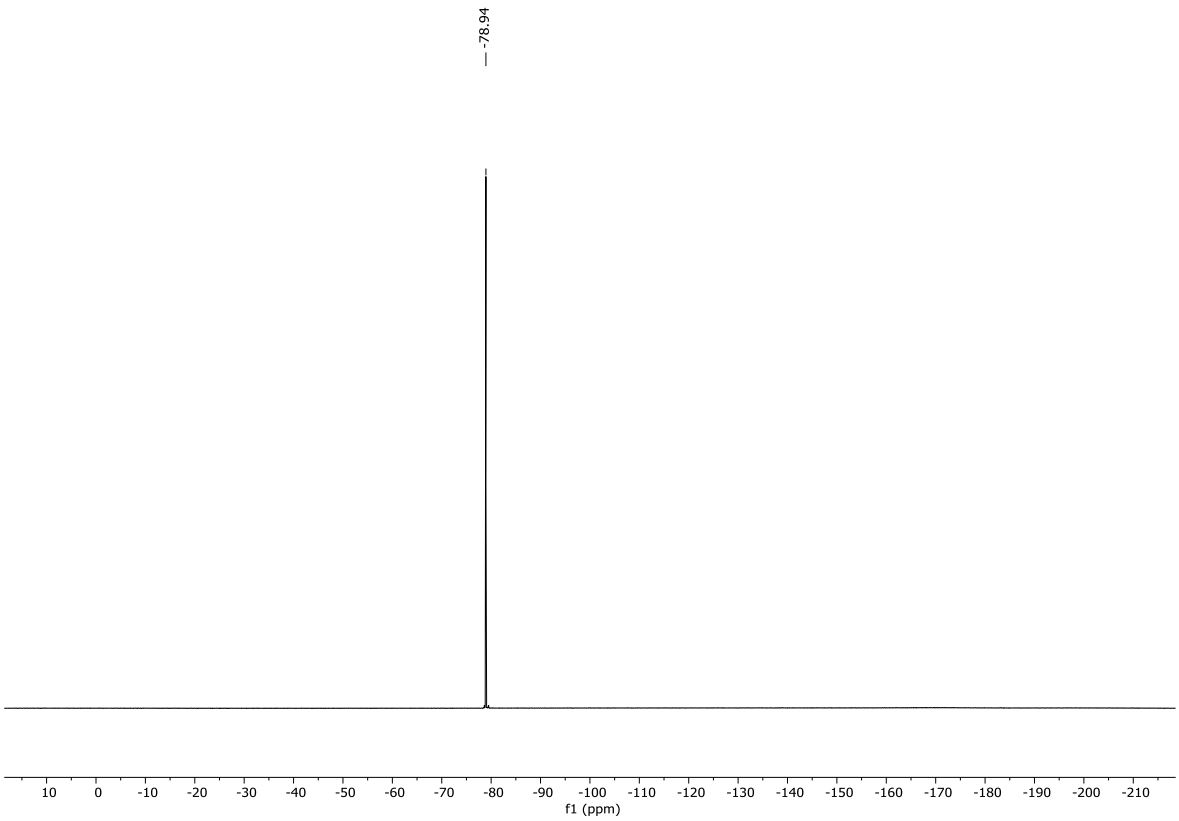

Figure IX: ^{19}F NMR of molecule **57**.

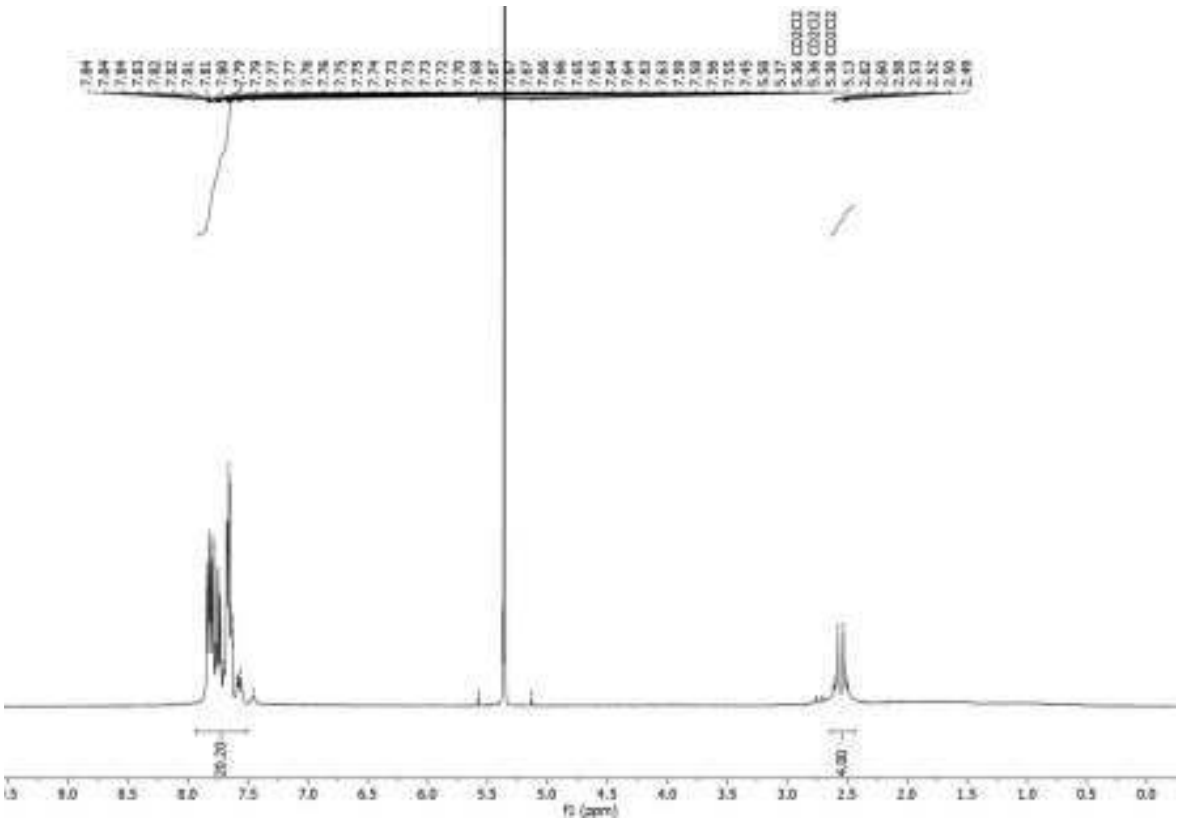

Figure X: ^{1}H NMR of molecule **62**.

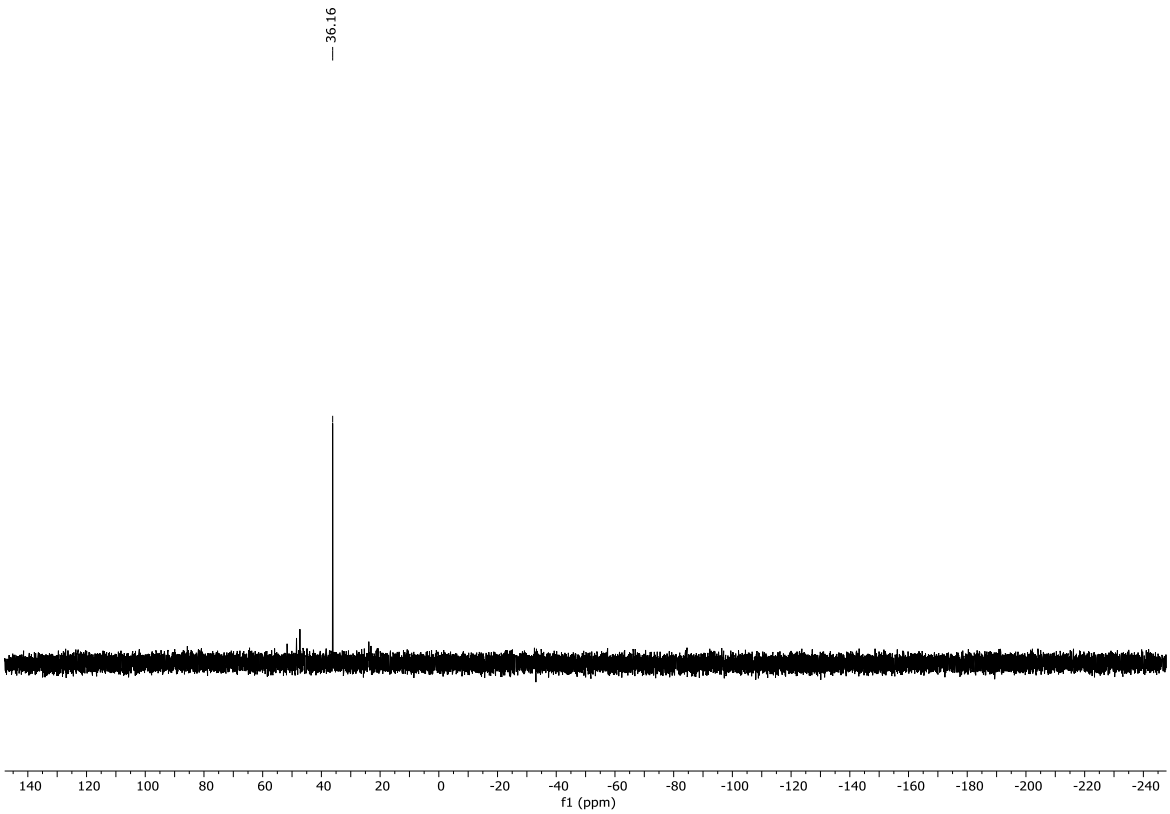

Figure XI: ^{31}P NMR of molecule **62**.

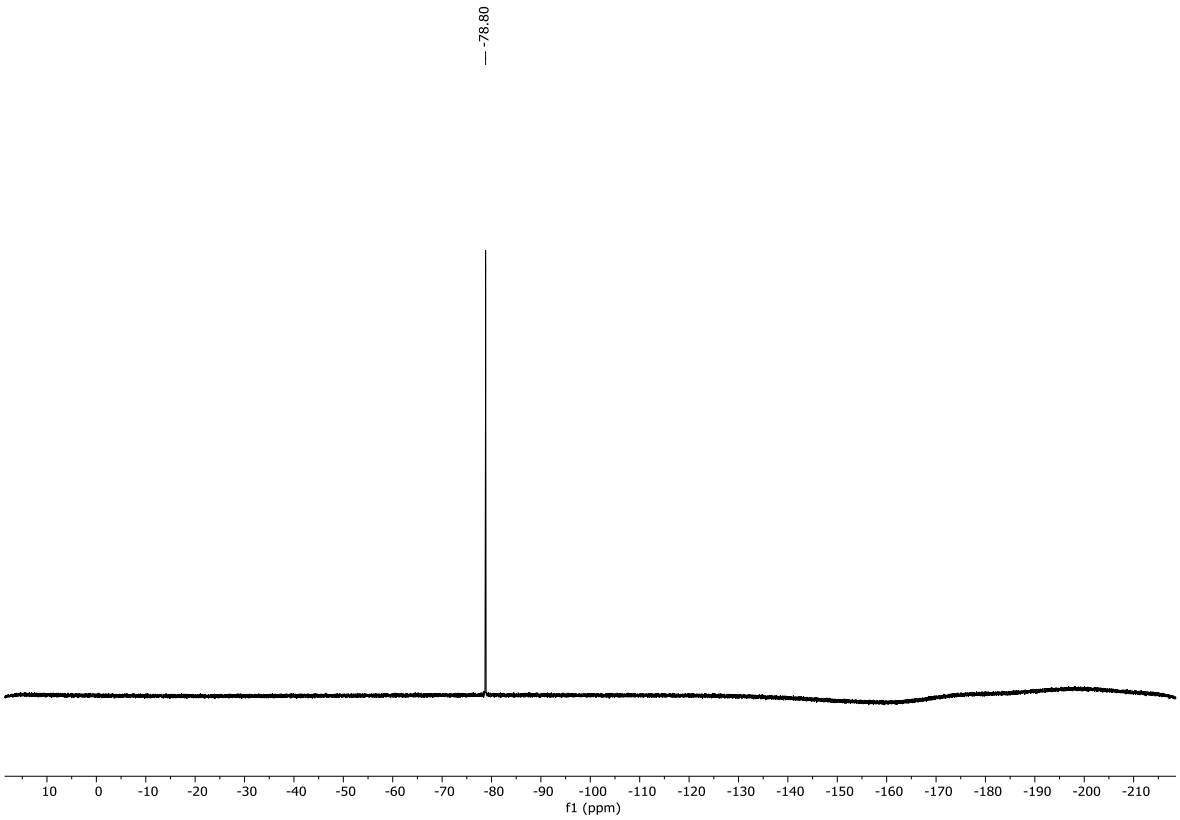

Figure XII: ^{19}F NMR of molecule **62**.

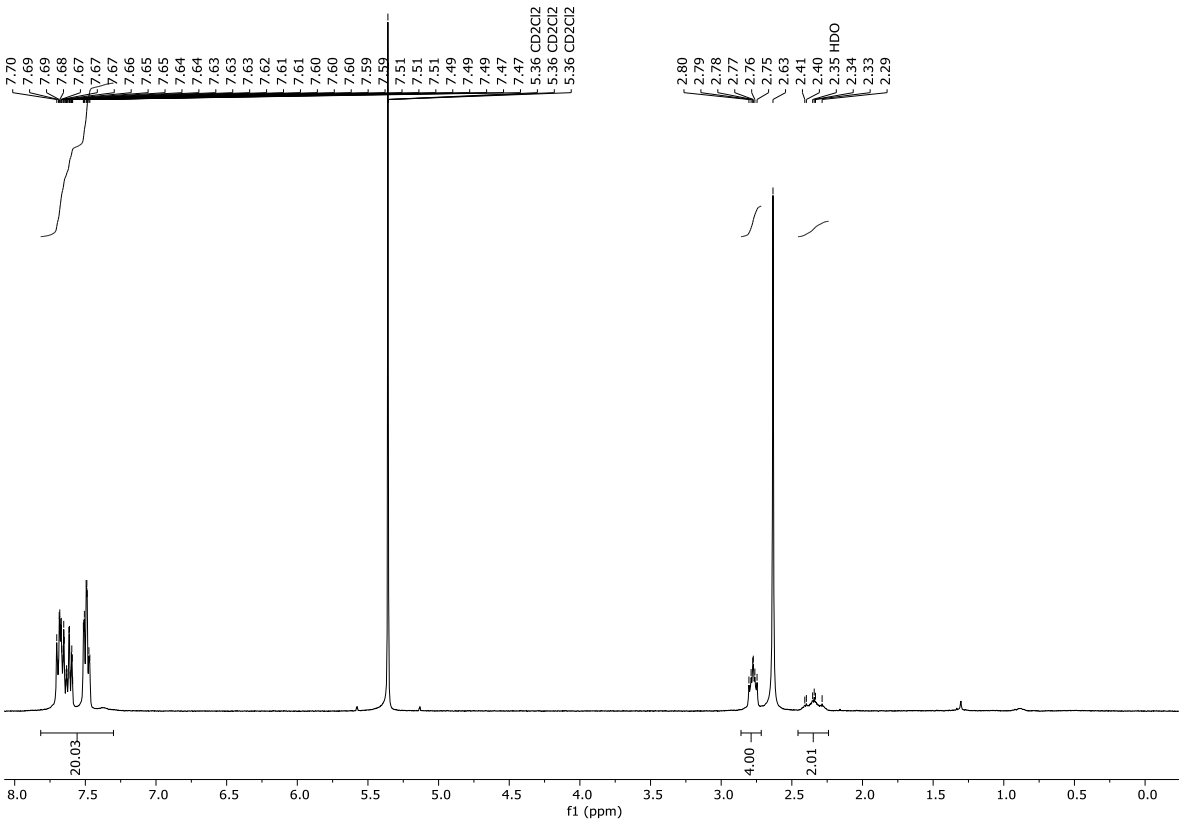

Figure XIII: ^{1}H NMR of molecule **59**.

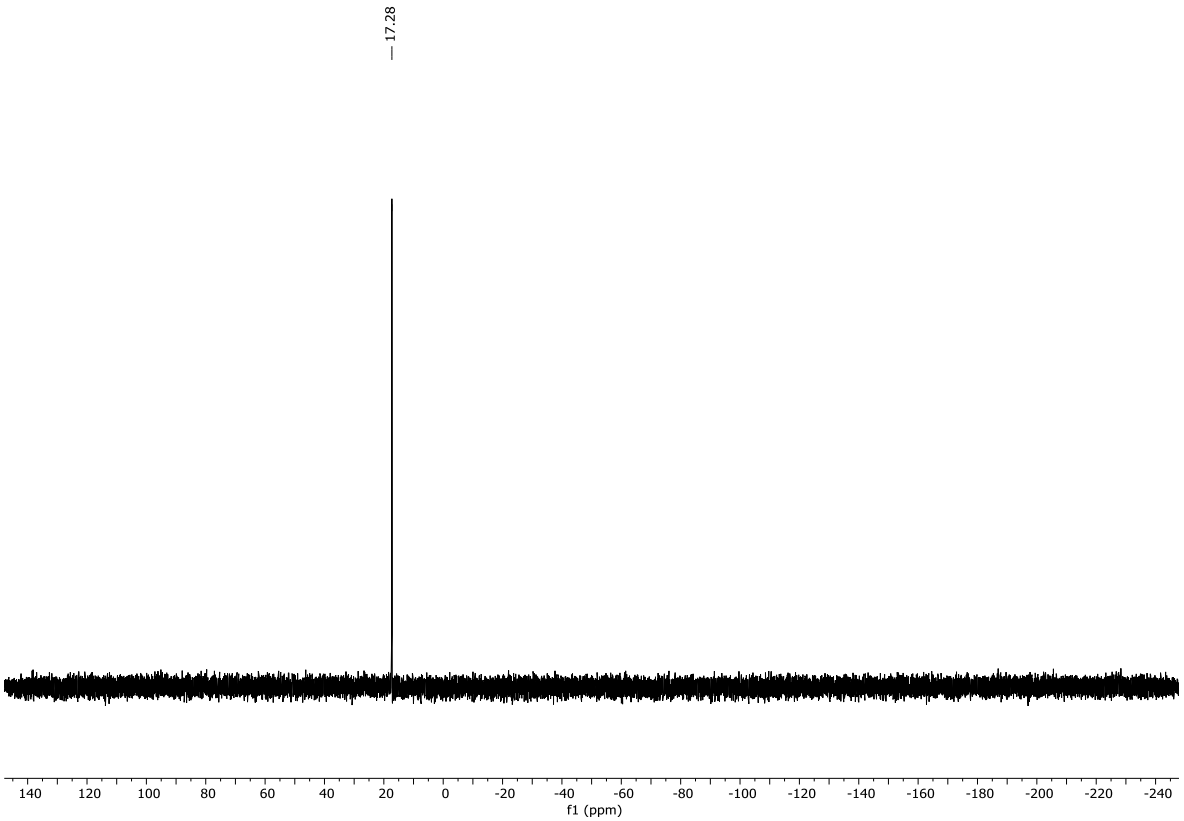

Figure 9: ^{31}P NMR of molecule **59**.

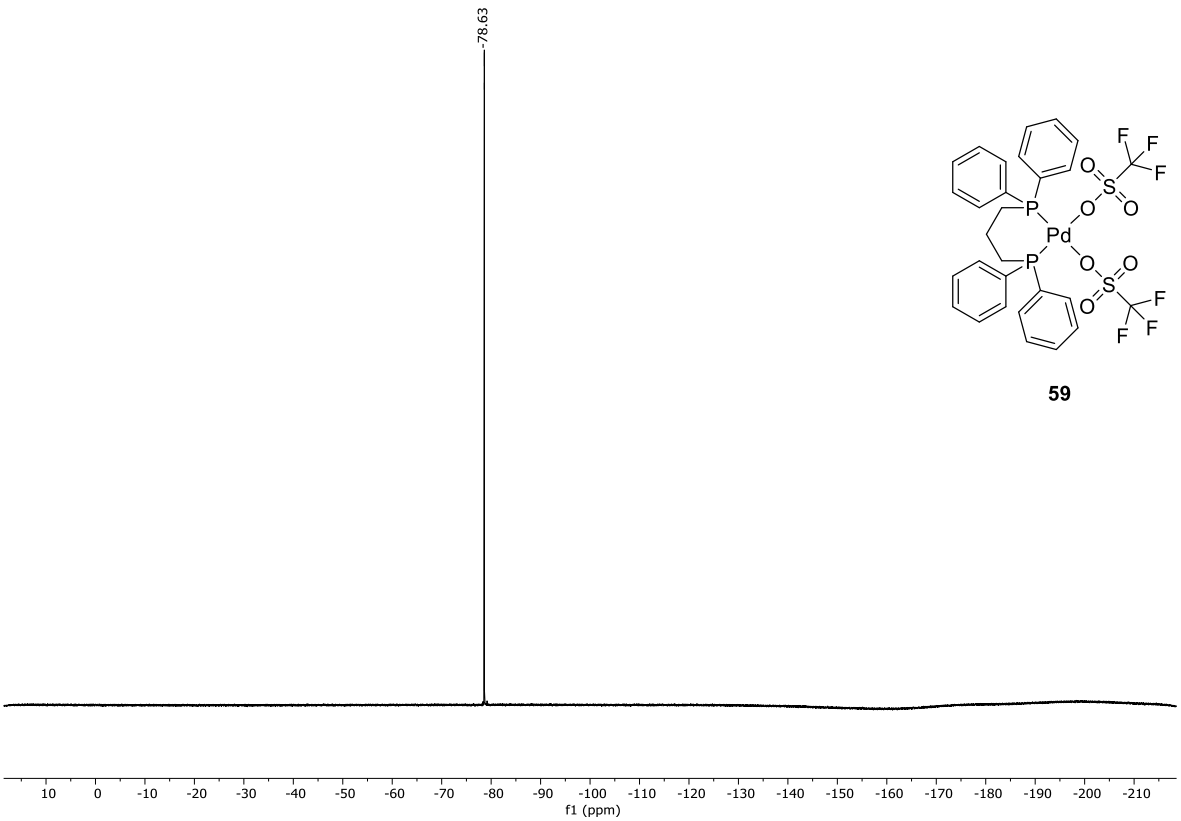

Figure XV: ^{19}F NMR of molecule **59**.

5.5.4 NMR Titration

Titration 1: Titration of a 5 mM solution of ***o*-54** in CD_2Cl_2 with a 25 mM solution of [Pd(dppe)(OTf)$_2$] (**57**) in CD_2Cl_2. 10 µL of titrating solution were added for each step.

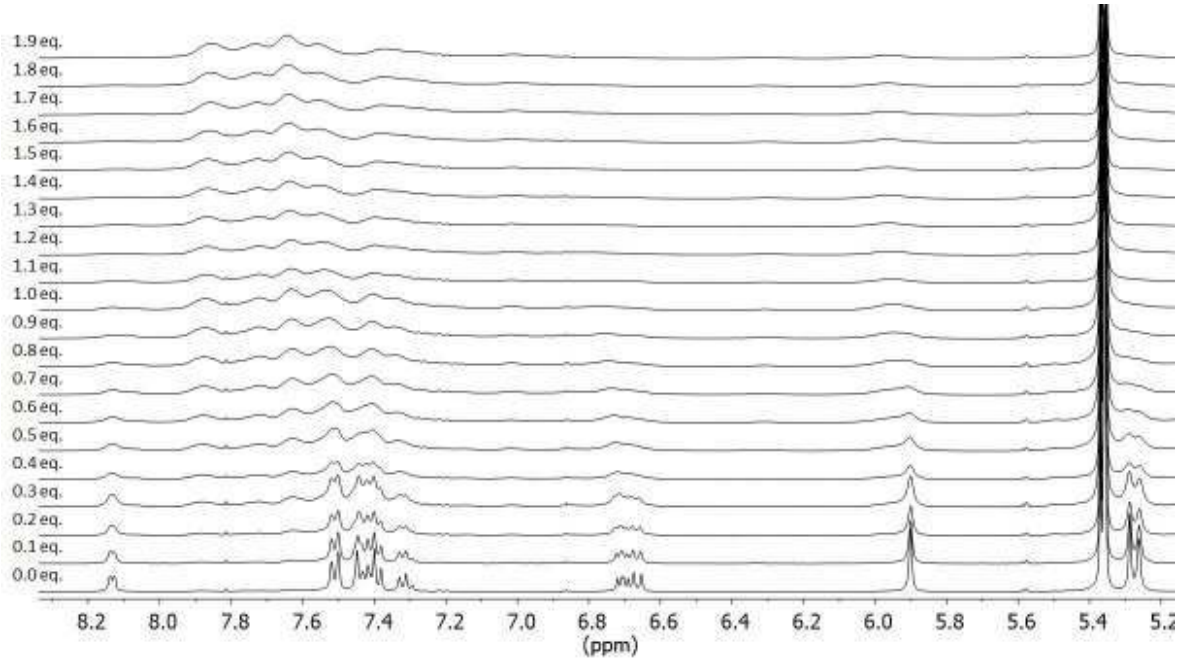

Figure XVI: Titration 1, ^{1}H NMR.

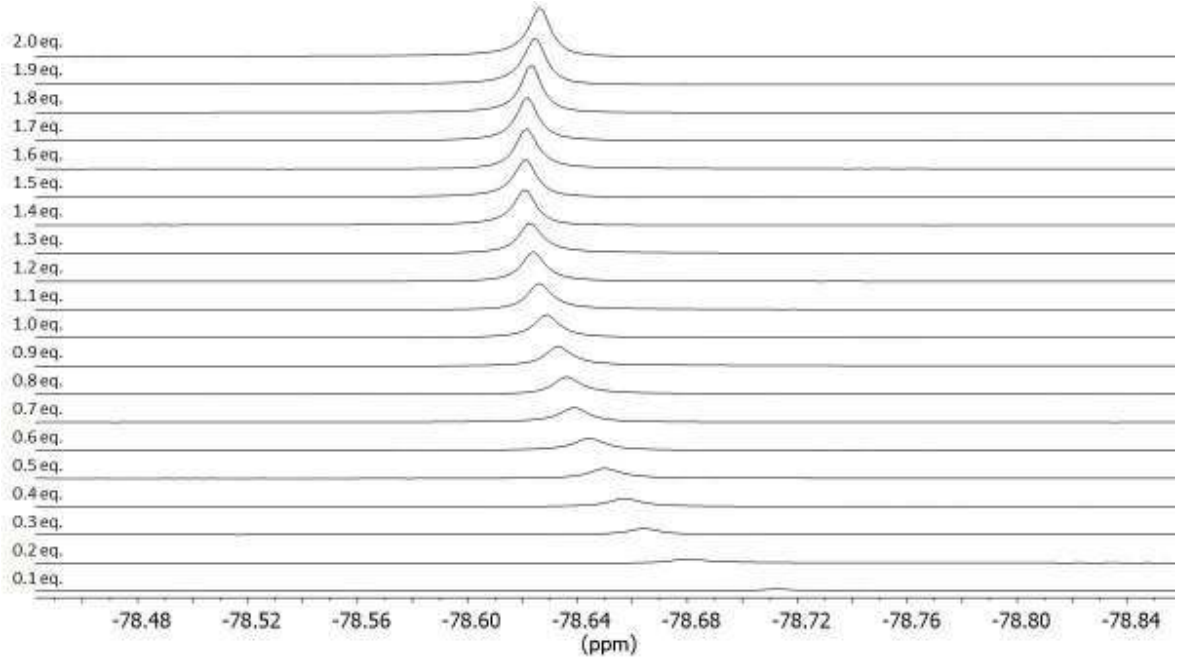

Figure XVII: Titration 1, ^{19}F NMR.

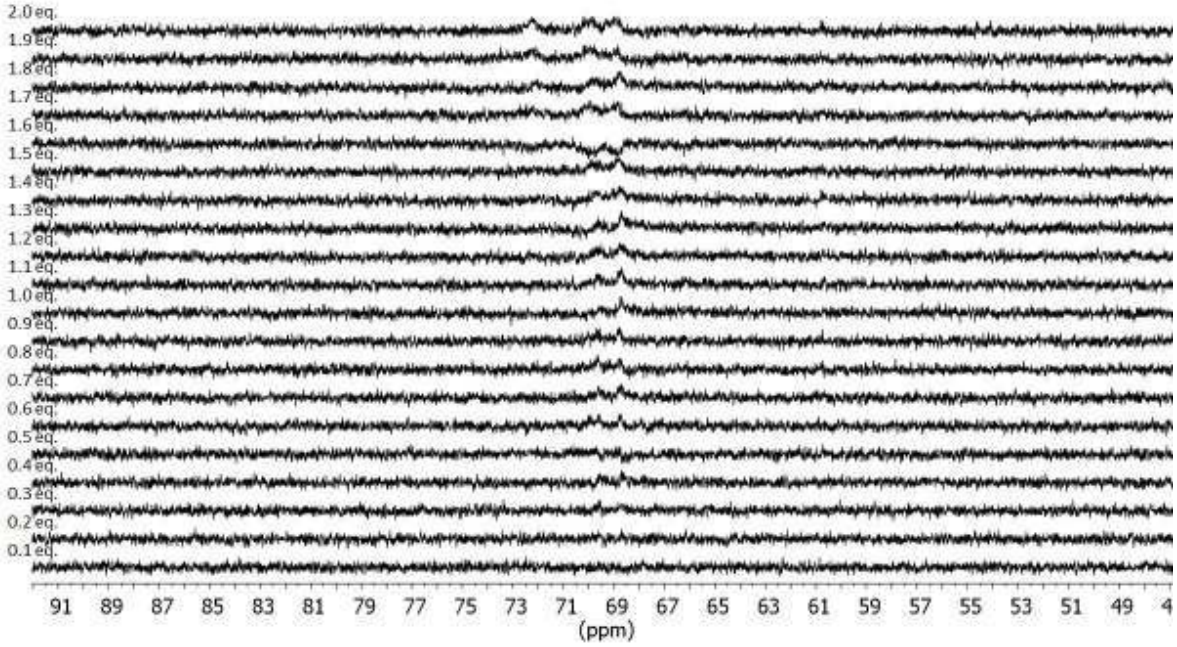

Figure XVIII: Titration 1, ^{31}P NMR.

Titration 2: Titration of a 5 mM solution of ***p*-54** in CD_2Cl_2 with a 25 mM solution of [Pd(dppe)(OTf)$_2$] (**57**) in CD_2Cl_2. 10 µL of titrating solution were added for each step.

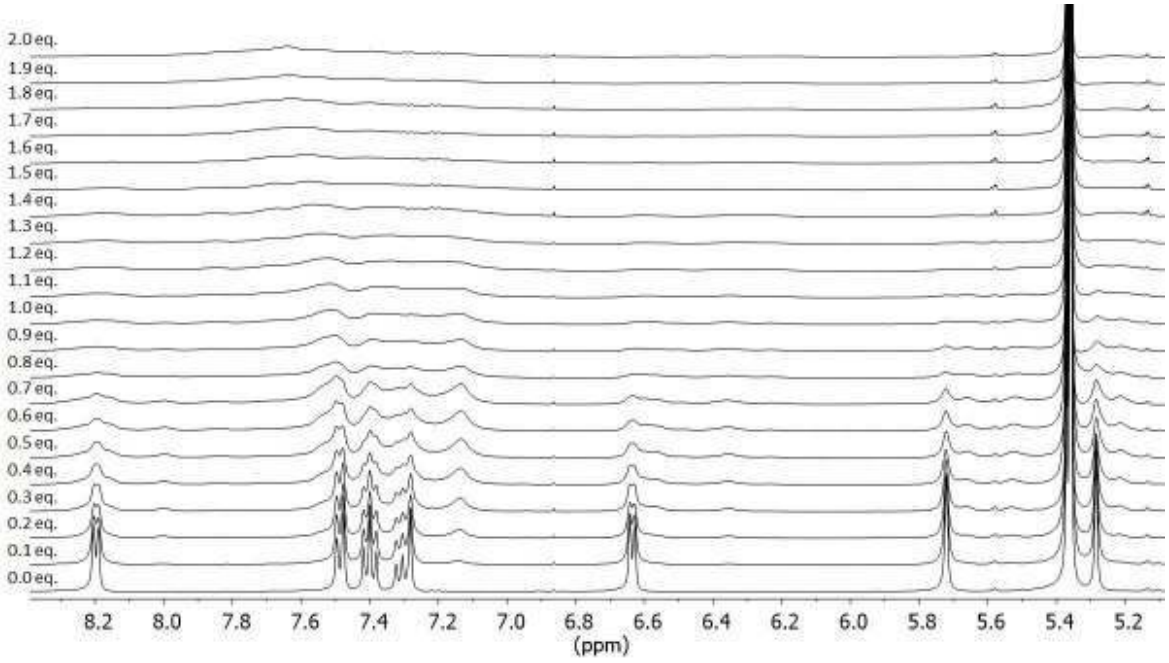

Figure XIX: Titration 2, ^{1}H NMR.

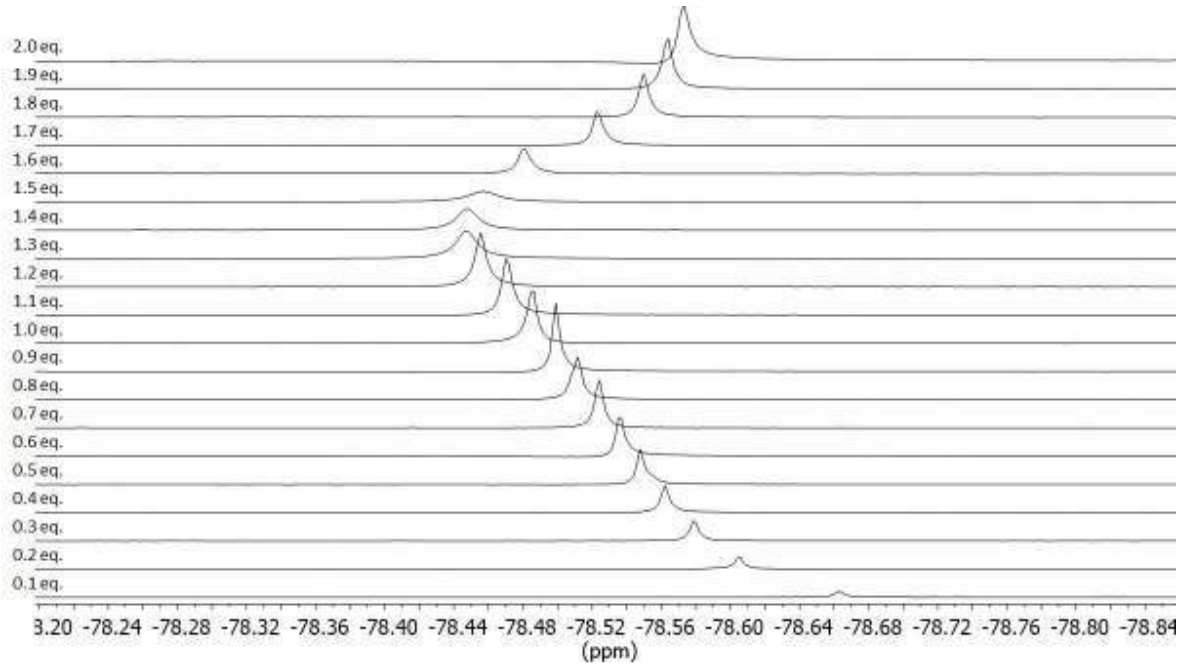

Figure XX: Titration 2, ^{19}F NMR.

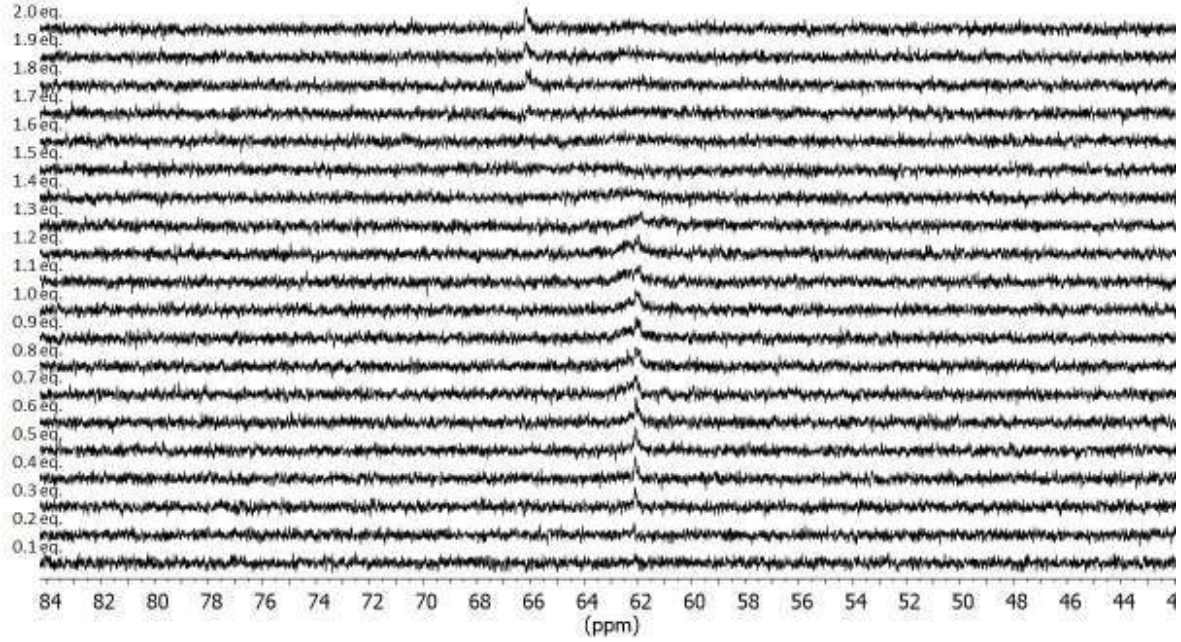

Figure XXI: Titration 2, ^{31}P NMR.

Titration 3: Titration of a 5 mM solution of ***m*-54** in CD_2Cl_2 with a 25 mM solution of [Pd(dppe)$(OTf)_2$] (**57**) in CD_2Cl_2. 10 µL of titrating solution were added for each step.

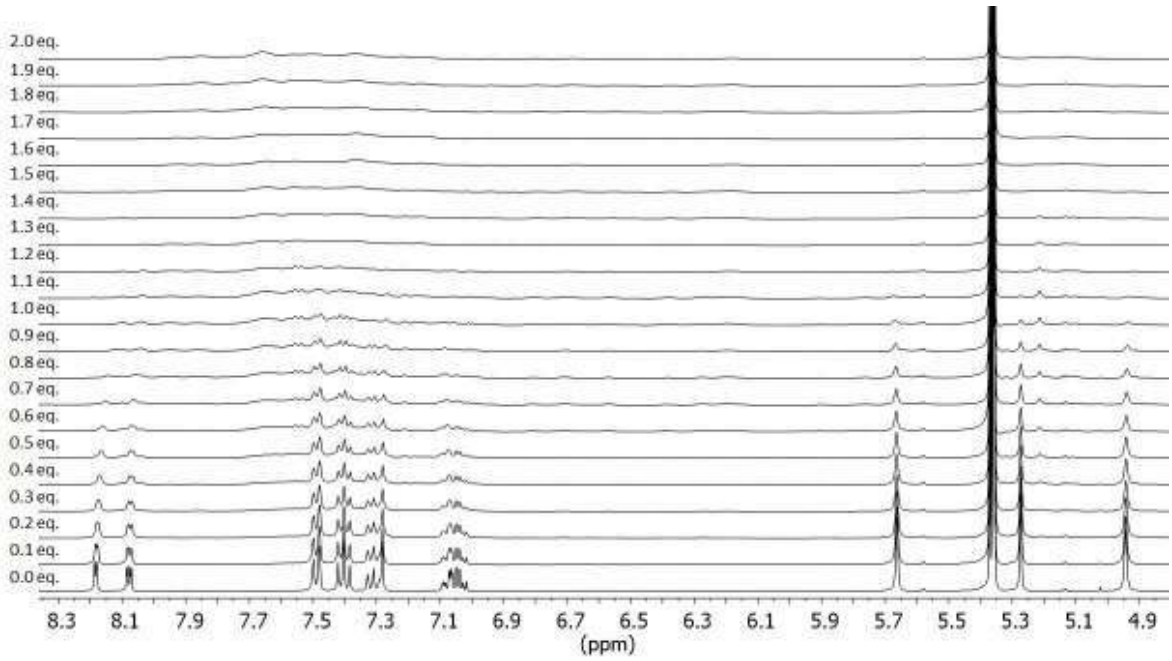

Figure XXII: Titration 3, ^{1}H NMR.

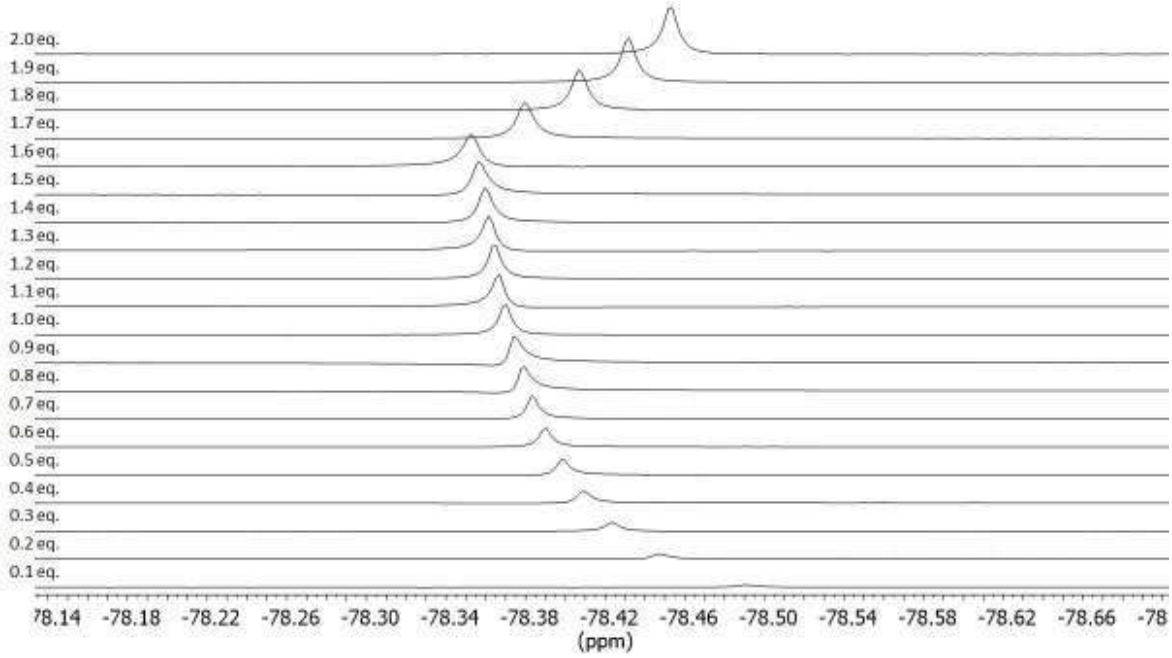

Figure XXIII: Titration 3, ^{19}F NMR.

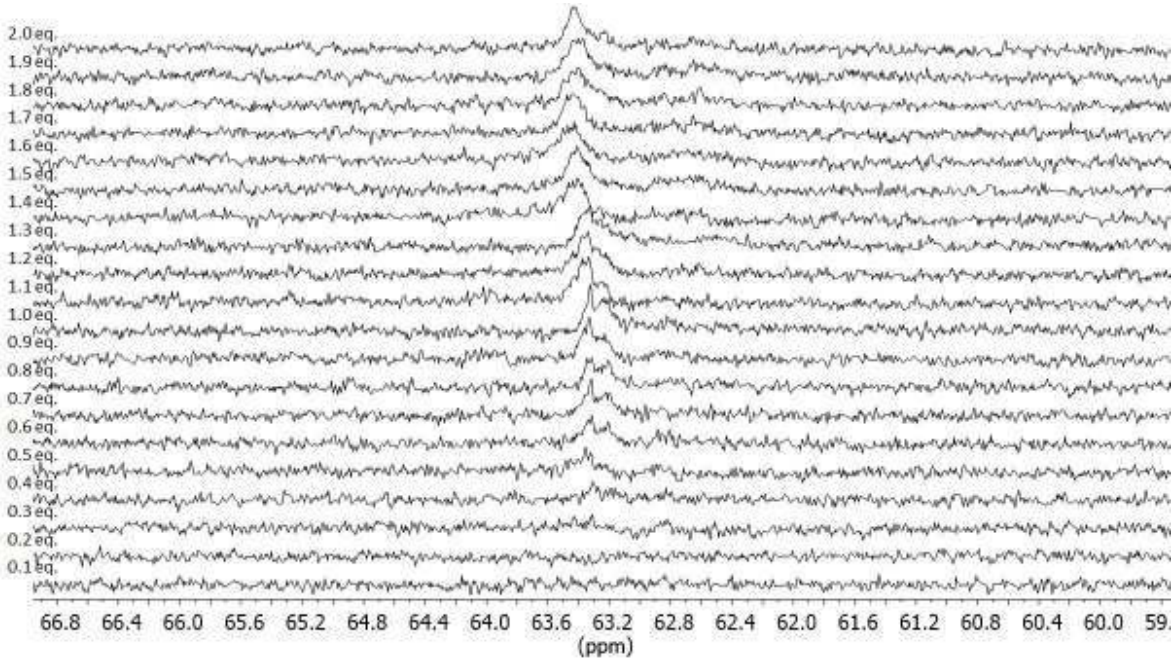

Figure XXIV: Titration 3, ^{31}P NMR.

Titration 4: Titration of a 5 mM solution of ***m*-54** in CD_2Cl_2 with a 12.5 mM solution of [Pt(dppe)(OTf)$_2$] (**62**) in CD_2Cl_2. 20 µL of titrating solution were added for each step.

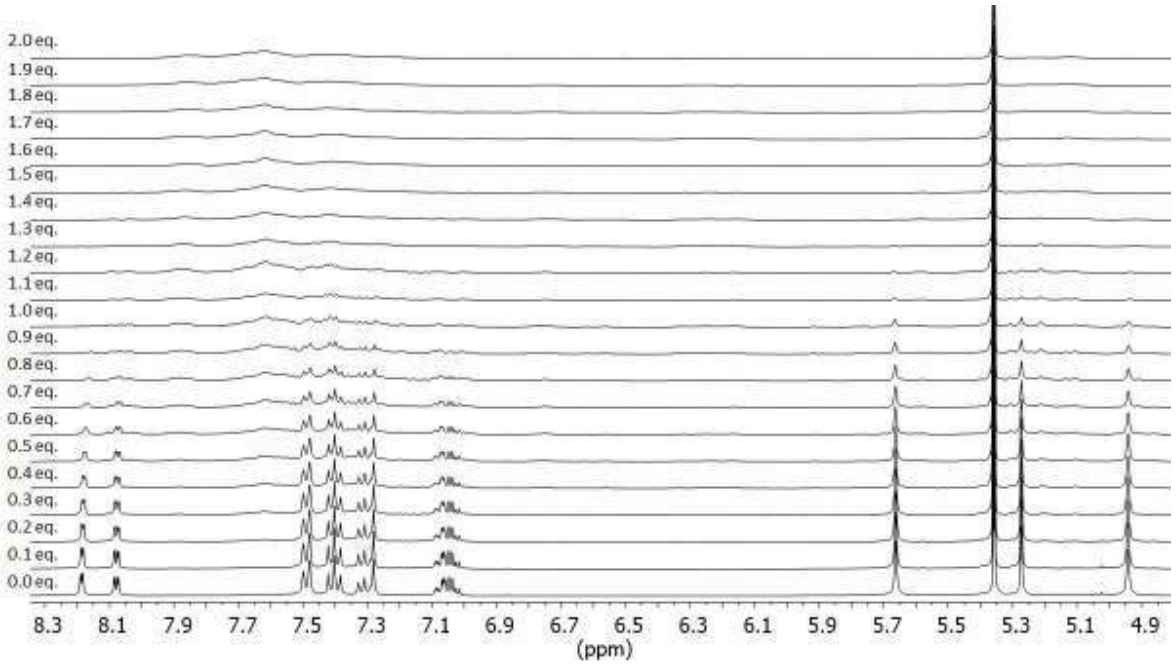

Figure XXV: Titration 4, ^{1}H NMR.

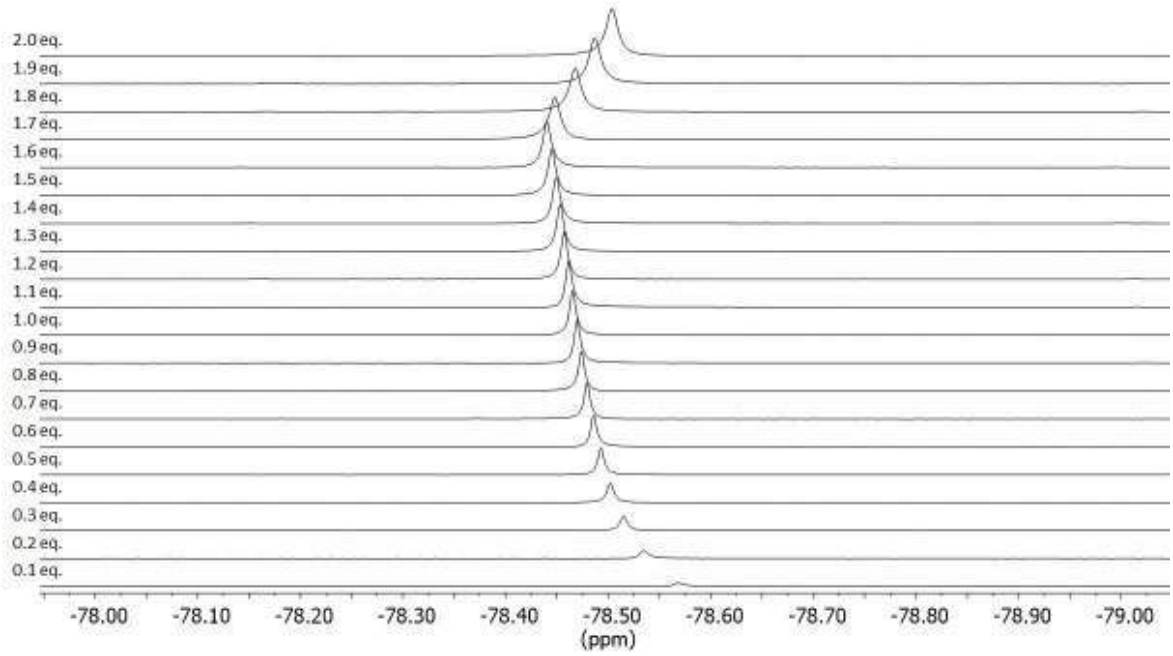

***Figure XXVI**:* Titration 4, *^{19}F NMR.*

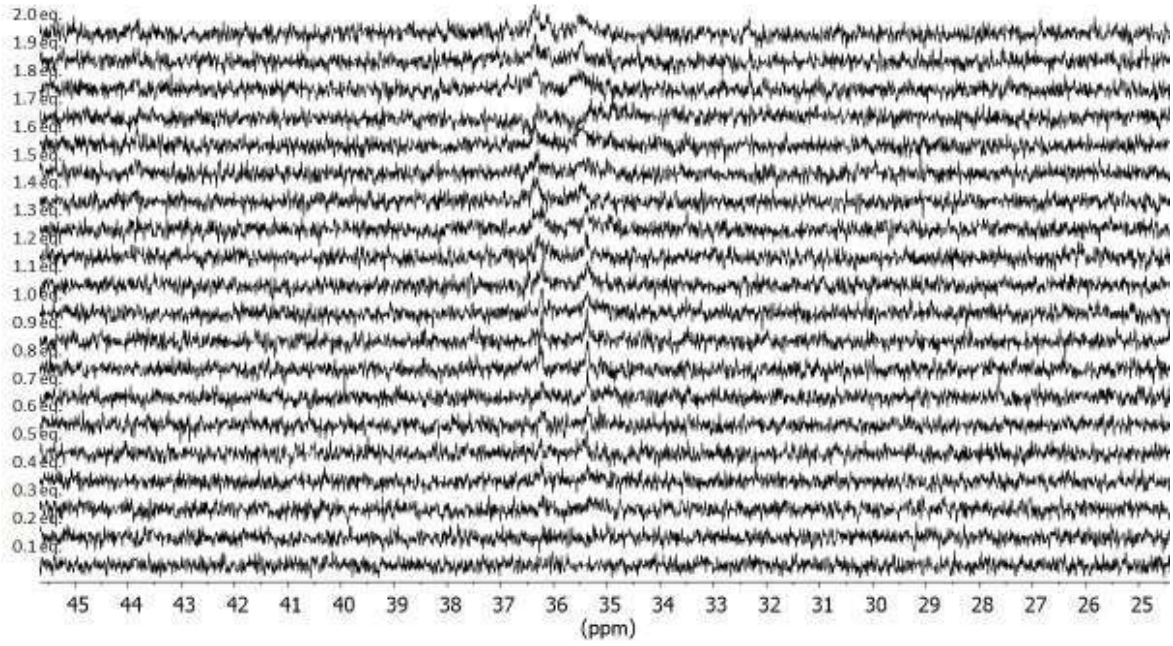

Figure XXVII: Titration 4, ^{31}P NMR.

Titration 5: Titration of a 5 mM solution of ***m*-54** in CD_2Cl_2 with a 12.5 mM solution of [Pd(dppp)$(OTf)_2$] (**59**) in CD_2Cl_2. 20 µL of titrating solution were added for each step.

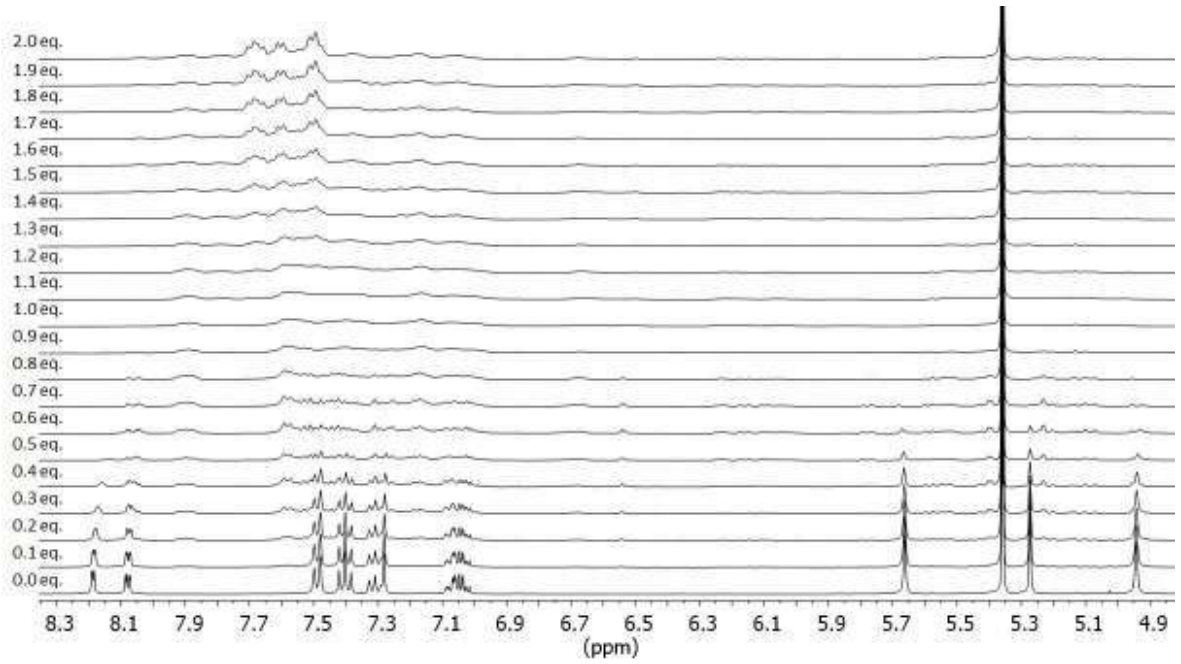

Figure XXVIII: Titration 5, ^{1}H NMR.

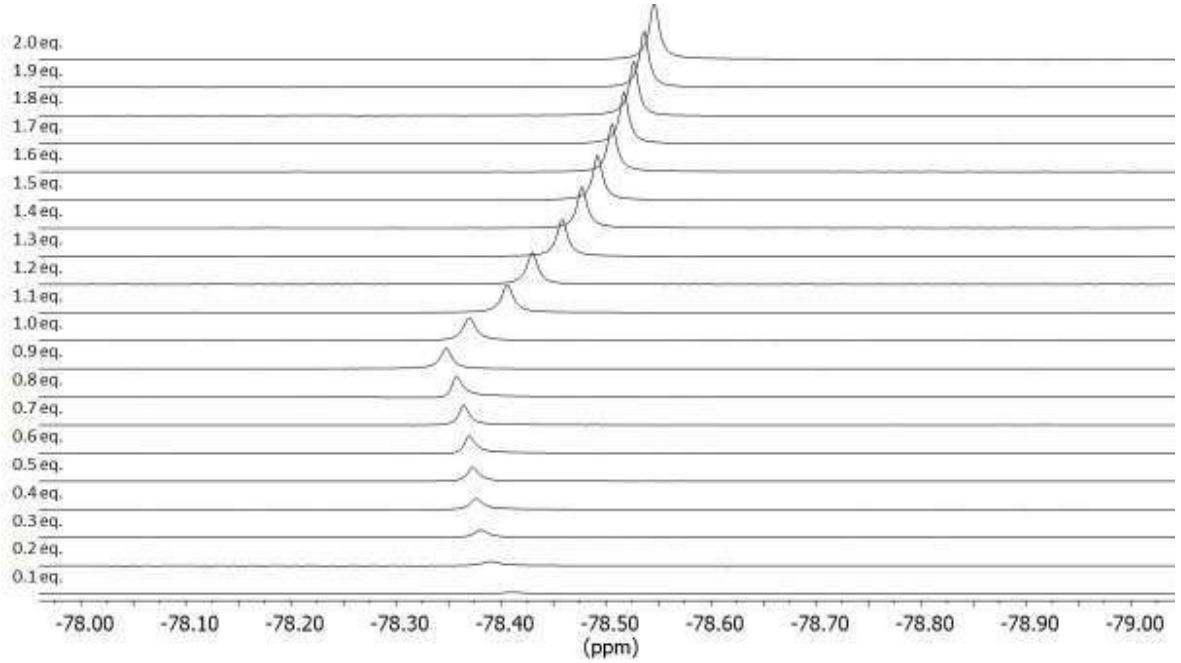

Figure XXIX: Titration 5, ^{19}F NMR.

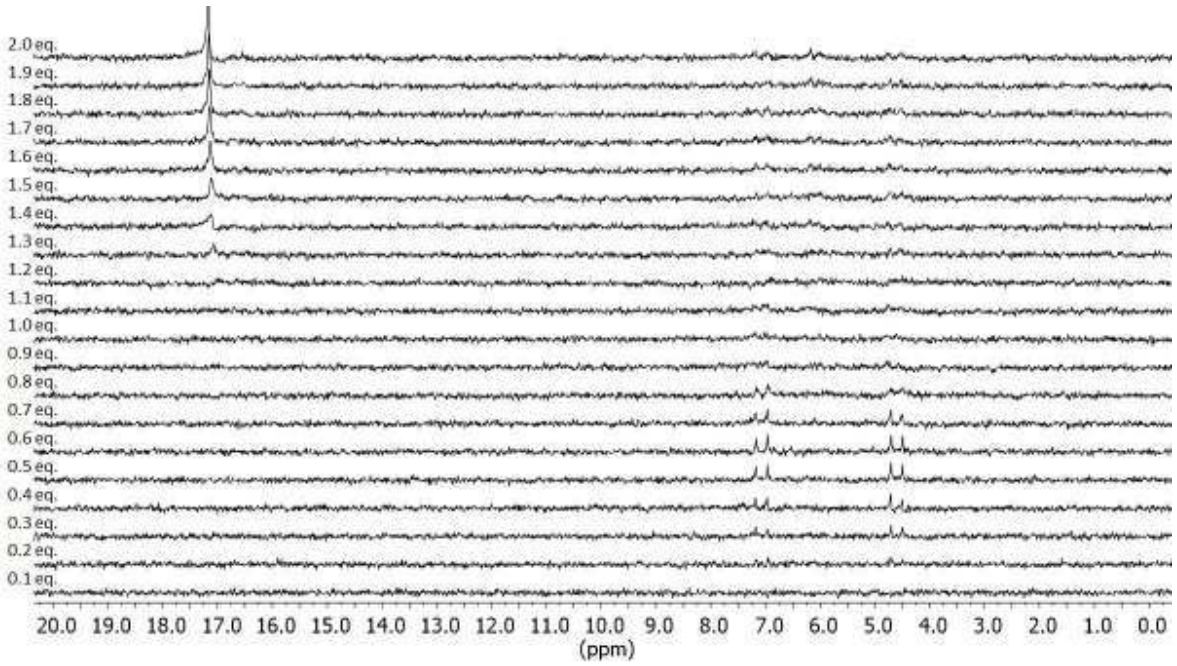

Figure XXX: Titration 5, ^{31}P NMR.

5.5.5 Variable Temperature NMR

Variable temperature NMR 1: Variable temperature NMR of a 3:2 solution of [Pd(dppe)(OTf)$_2$] (**57**) and ***m*-54** in CD_3CN.

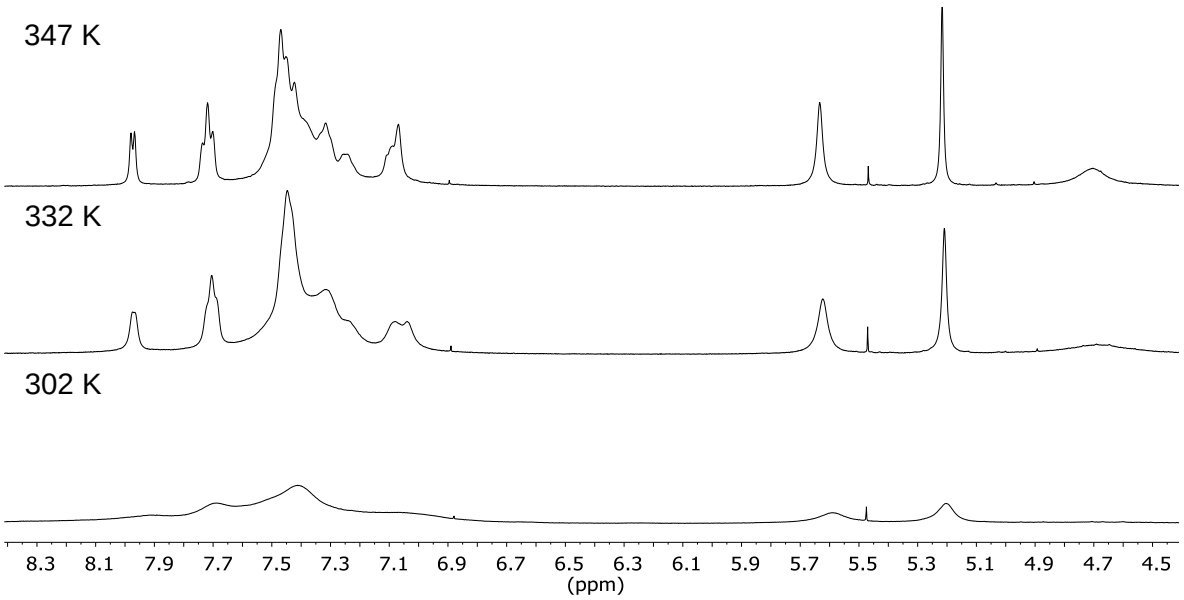

***Figure XXXI**: Variable temperature NMR 1, ^1H NM*R.

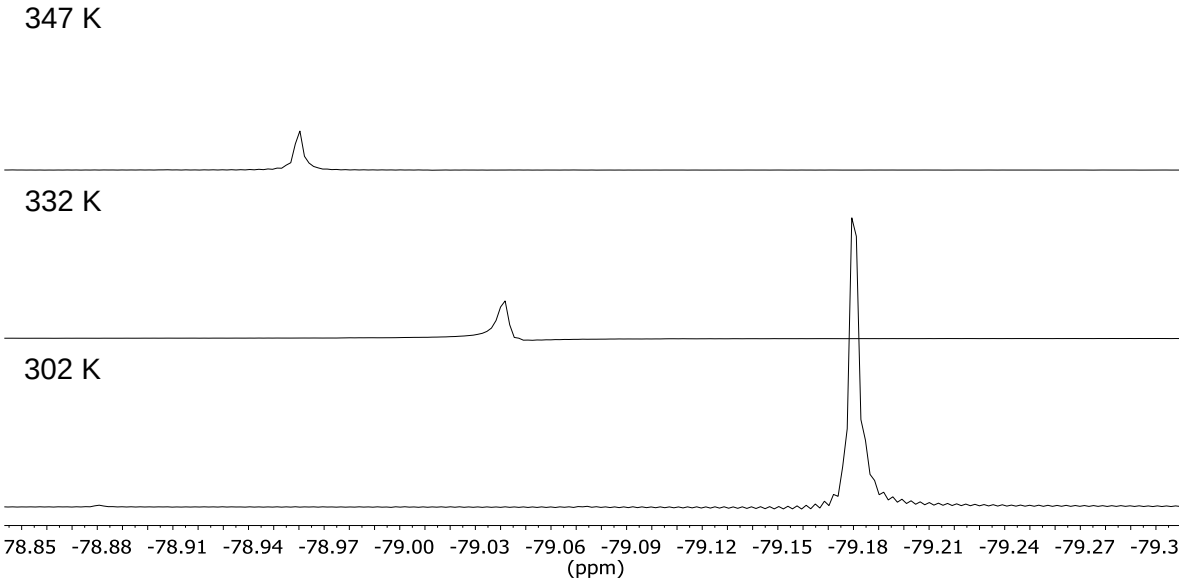

Figure XXXII: Variable temperature NMR 1, ^{19}F NMR.

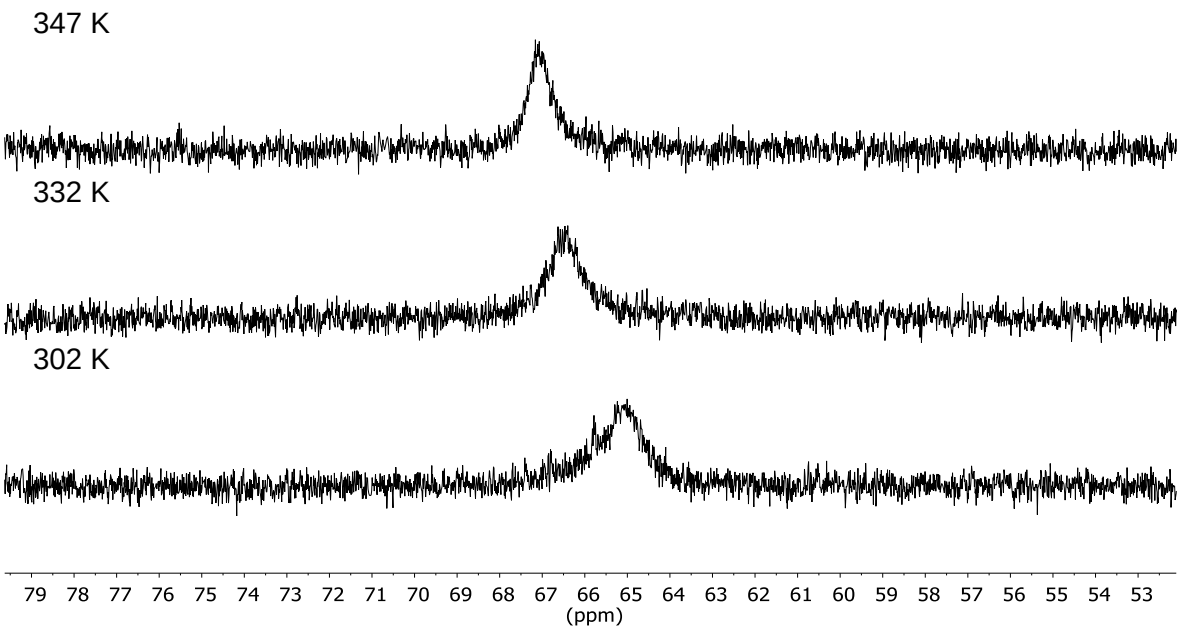

Figure XXXIII: Variable temperature NMR 1, ^{31}P NMR.

Variable temperature NMR 2: Variable temperature NMR of a 3:2 solution of [Pd(dppp)(OTf)$_2$] (**59**) and ***m*-54** in CD_3CN.

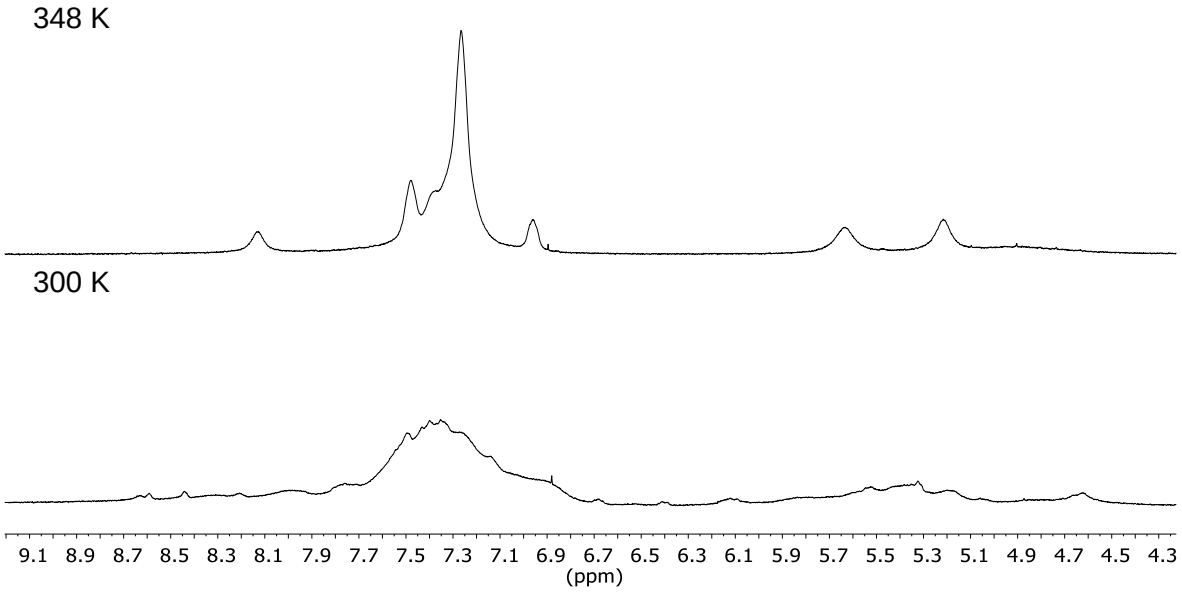

Figure XXXIV: Variable temperature NMR 2, ^{1}H NMR.

Variable temperature NMR 3: Variable temperature NMR of a 3:2 solution of [Pd(dppp)(OTf)$_2$] (**59**) and ***m*-54** in CD_2Cl_2.

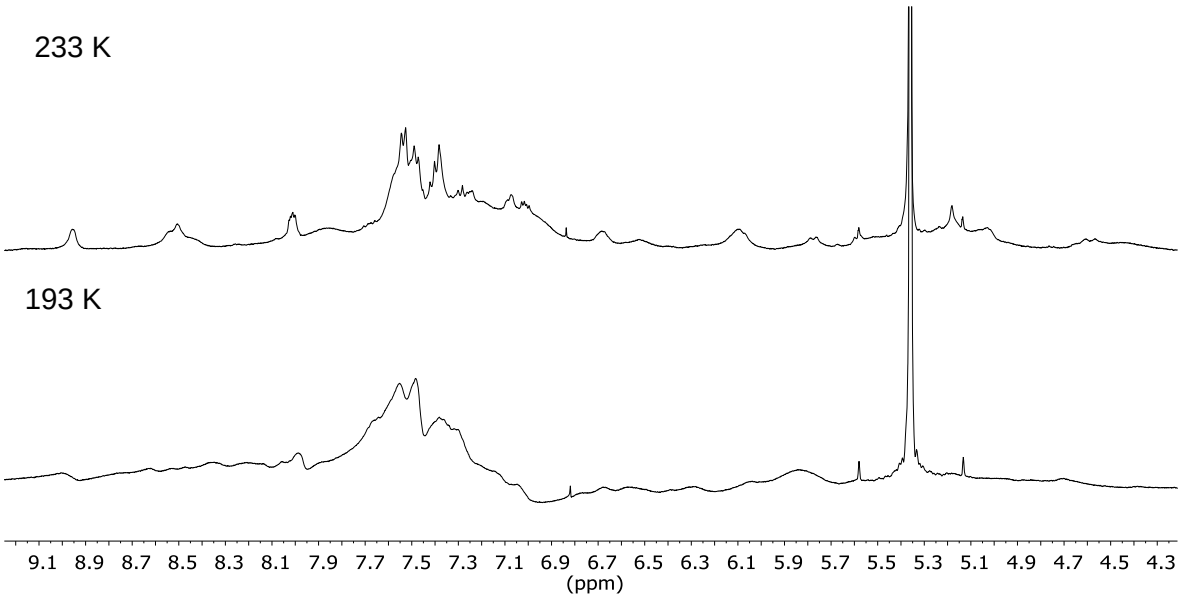

Figure XXXV: Variable temperature NMR 3, ^{1}H NMR.

Variable temperature NMR 4: Variable temperature NMR of a 3:2 solution of [Pt(dppe)(OTf)$_2$] (**62**) and ***m*-54** in CD_3CN.

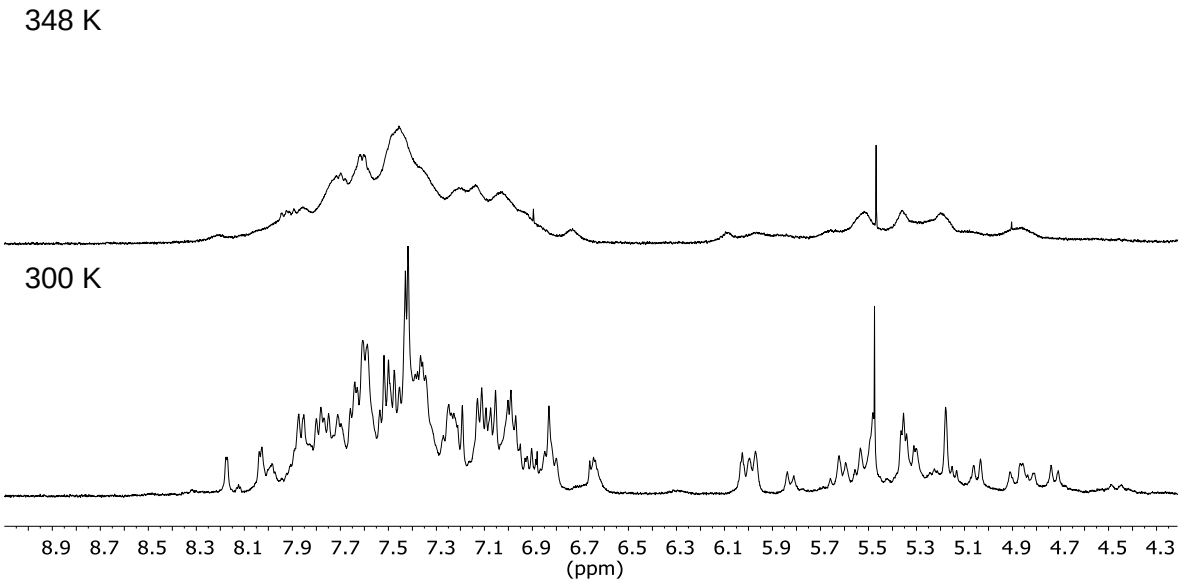

Figure XXXVI: Variable temperature NMR 4, ^{1}H NMR.

Variable temperature NMR 5: Variable temperature NMR of a 3:2 solution of [Pt(dppe)(OTf)$_2$] (**62**) and ***m*-54** in $C_2D_2Cl_4$.

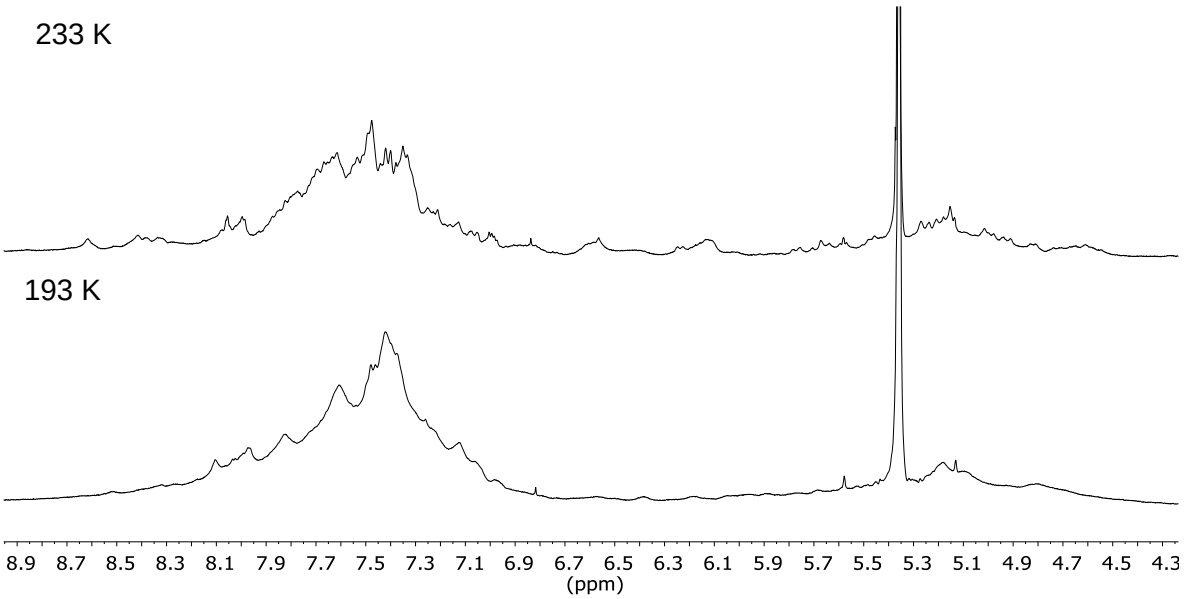

Figure* XXXVII:* Variable temperature NMR 5, ^{1}H NMR.

5.5.6 DOSY NMR

DOSY NMR 1: **57** 5 mM in CD_2Cl_2 at 300 K.

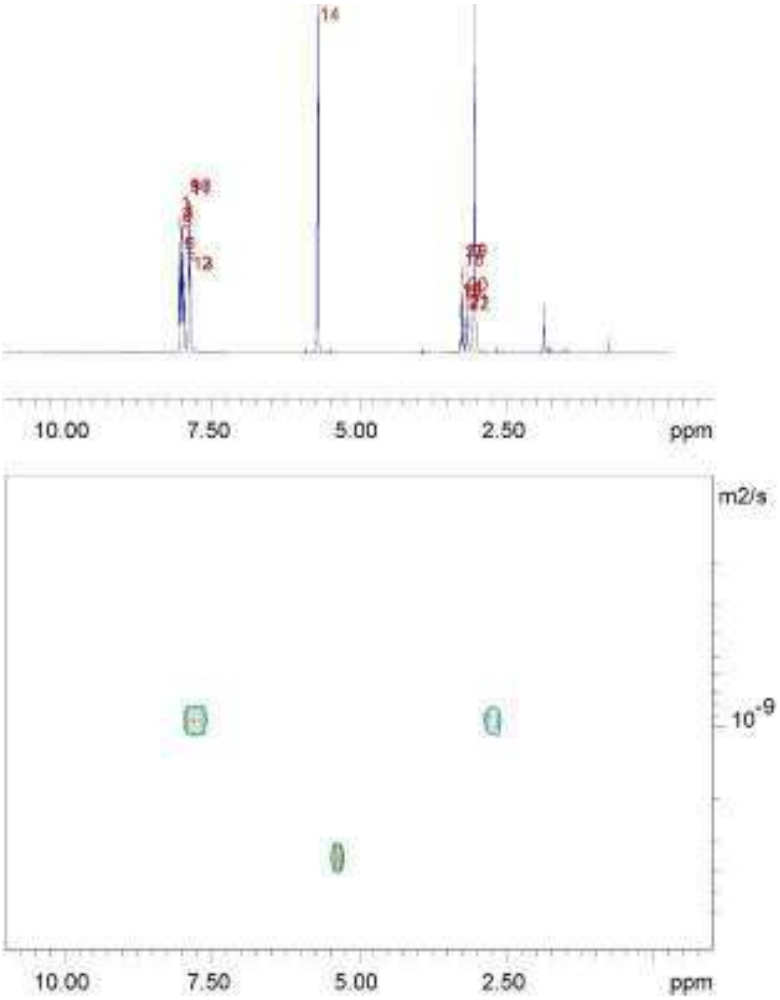

Figure XXXVIII: DOSY NMR 1, pseudo 2D-DOSY NMR.

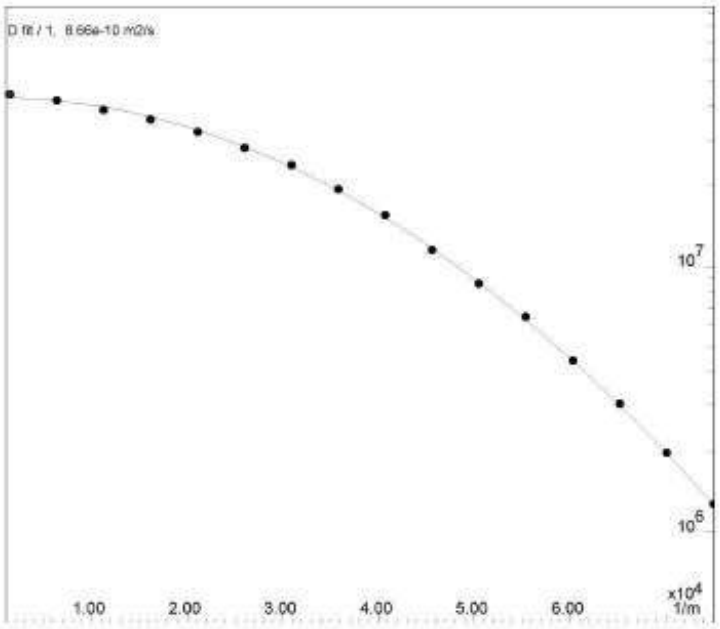

Figure XXXIX: DOSY NMR 1, monoexponential signal decay.

DOSY NMR 2: ***m*-54** 5 mM in CD_2Cl_2 at 300 K.

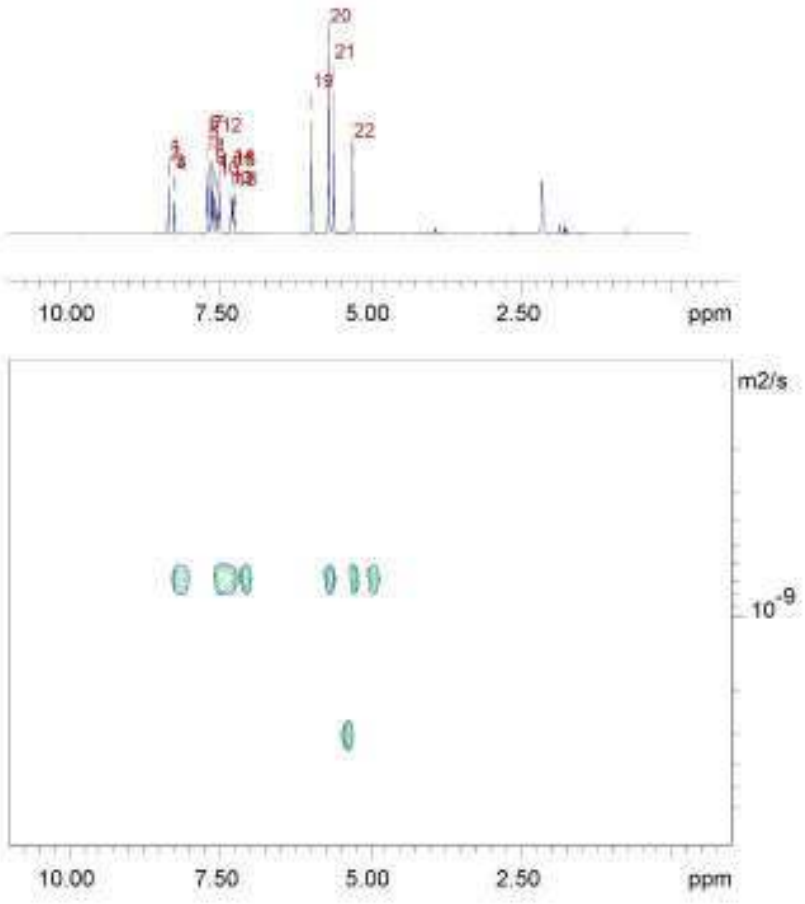

Figure XL: DOSY NMR 2, pseudo 2D-DOSY NMR.

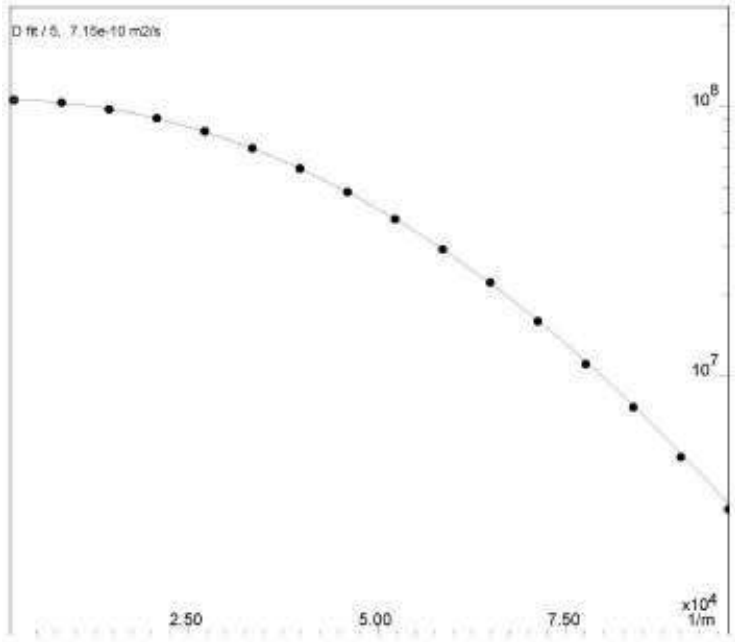

Figure XLI: DOSY NMR 2, monoexponential signal decay.

DOSY NMR 3: ***m*-54** and **57** 5 mM in CD_2Cl_2 at 300 K.

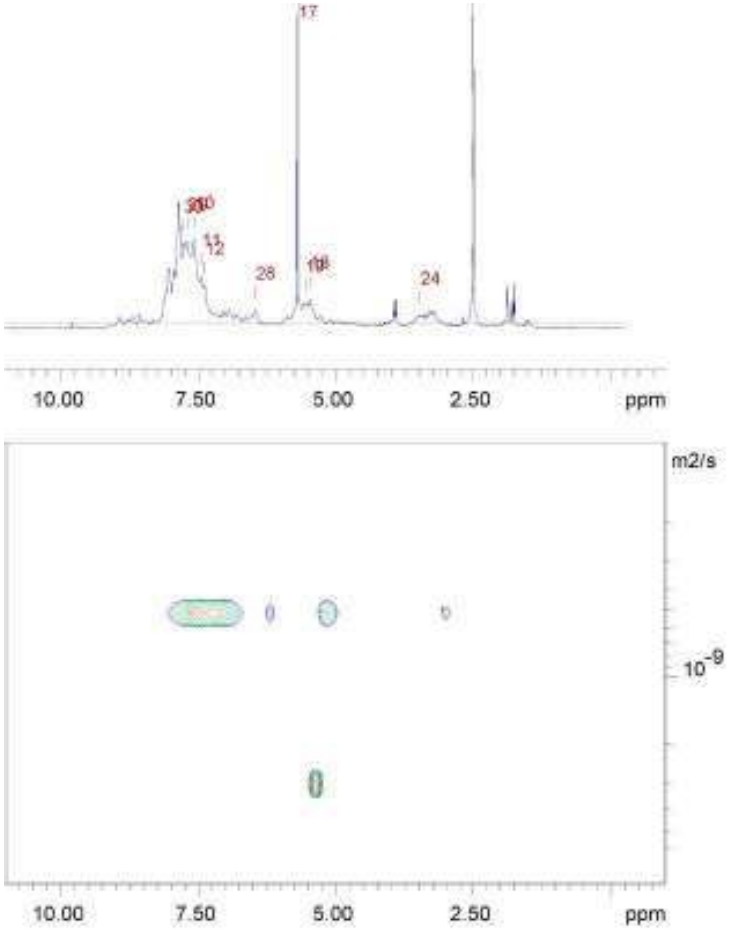

Figure XLII: DOSY NMR 3, pseudo 2D-DOSY NMR.

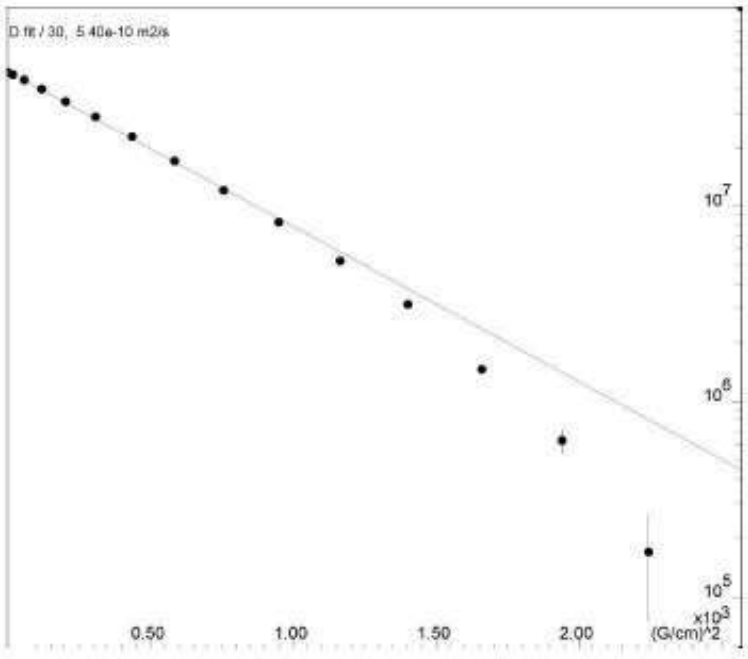

Figure XLIII: DOSY NMR 3, monoexponential signal decay.

DOSY NMR 4: ***m*-54** 5 mM in CD_3CN at 348 K.

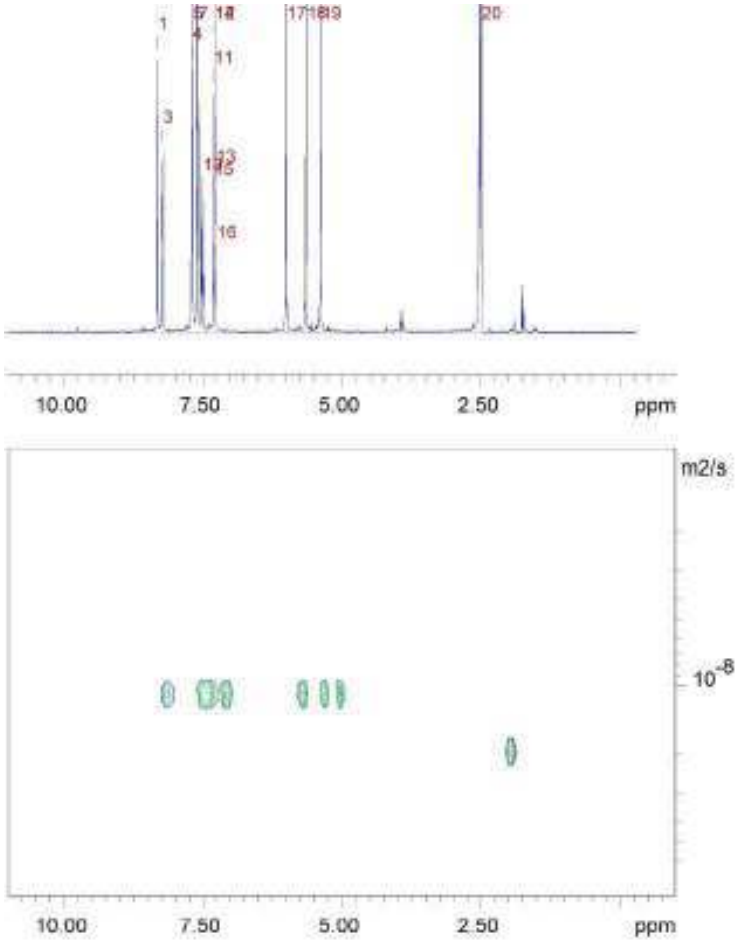

Figure XLIV: DOSY NMR 4, pseudo 2D-DOSY NMR.

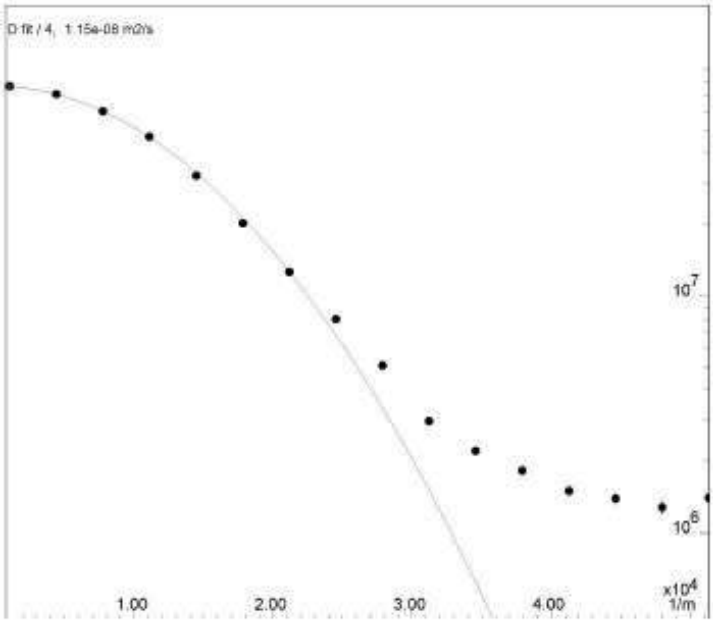

Figure XLV: DOSY NMR 4, monoexponential signal decay.

DOSY NMR 5: ***m*-54** and **57** 5 mM in CD_3CN at 348 K.

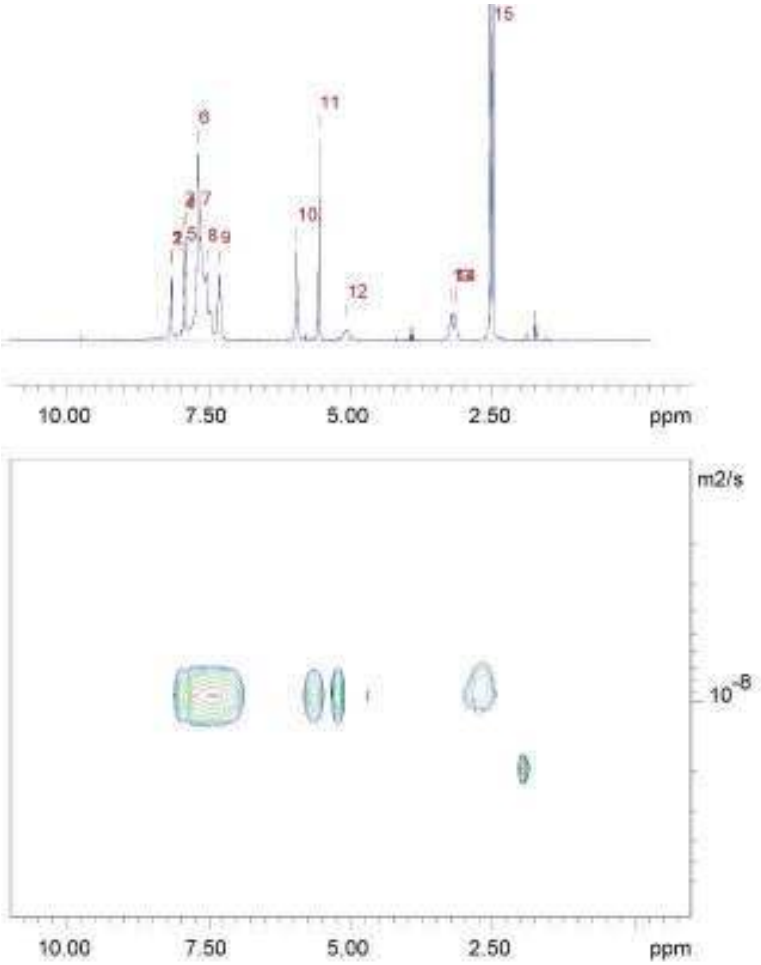

Figure XLVI: DOSY NMR 5, pseudo 2D-DOSY NMR.

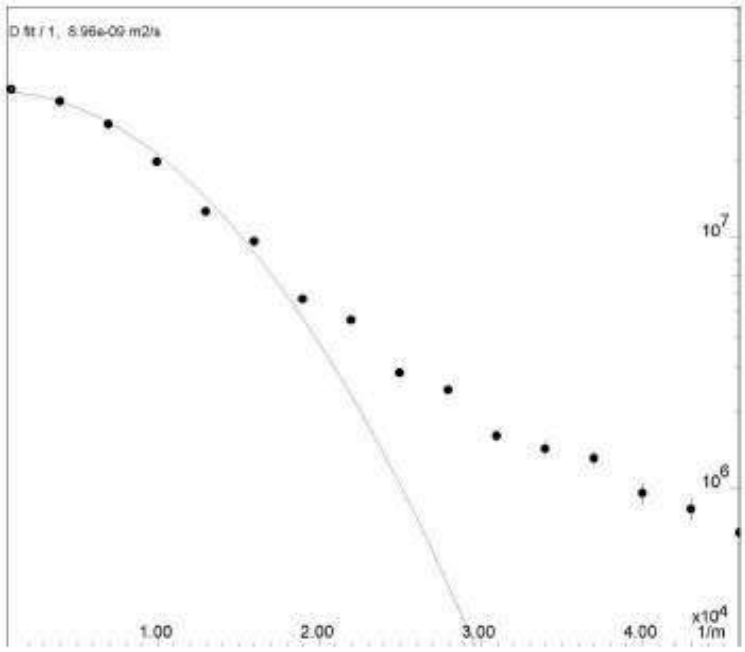

Figure XLVII: DOSY NMR 5, monoexponential signal decay.

5.5.7 MS of the metal-pyridine ligand complexes

MS 1: Mass spectrum (ESI) of a 3:2 solution of [Pd(dppe)(OTf)$_2$] (**57**) and ***m*-54** in methanol.

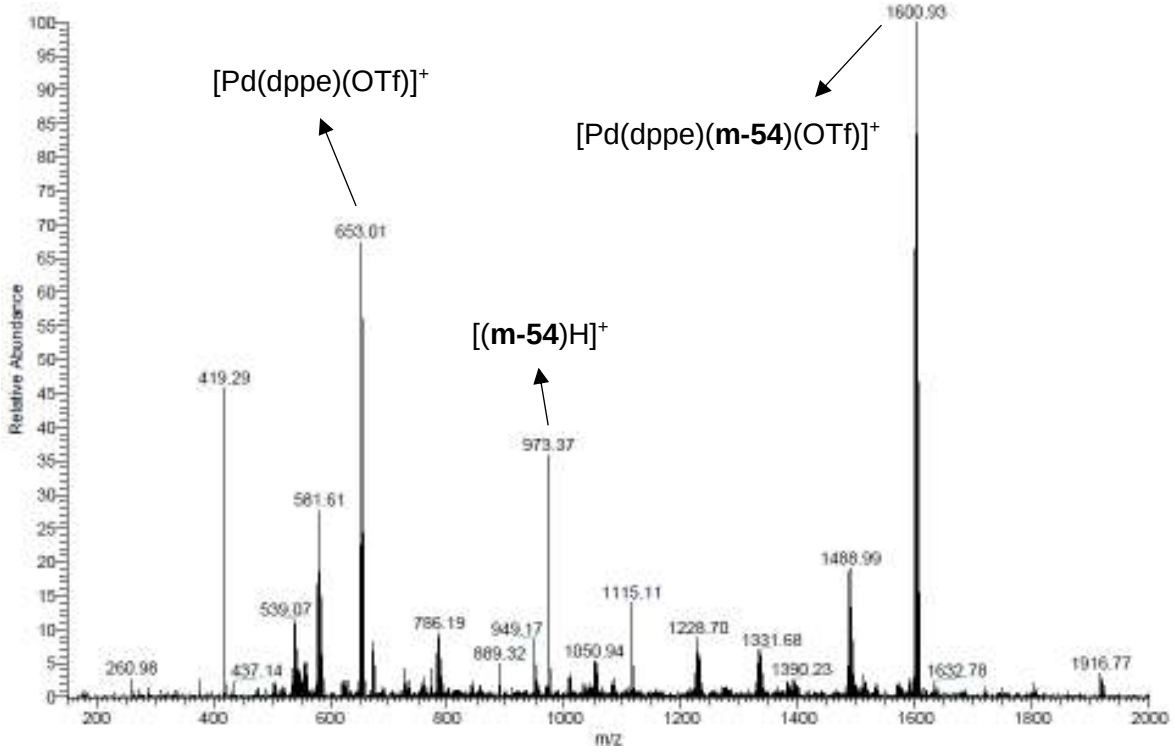

Figure XLVIII: ESI-MS 1.

MS 2: Mass spectrum (ESI) of a 3:2 solution of [Pd(dppp)(OTf)$_2$] (**59**) and ***m*-54** in methanol.

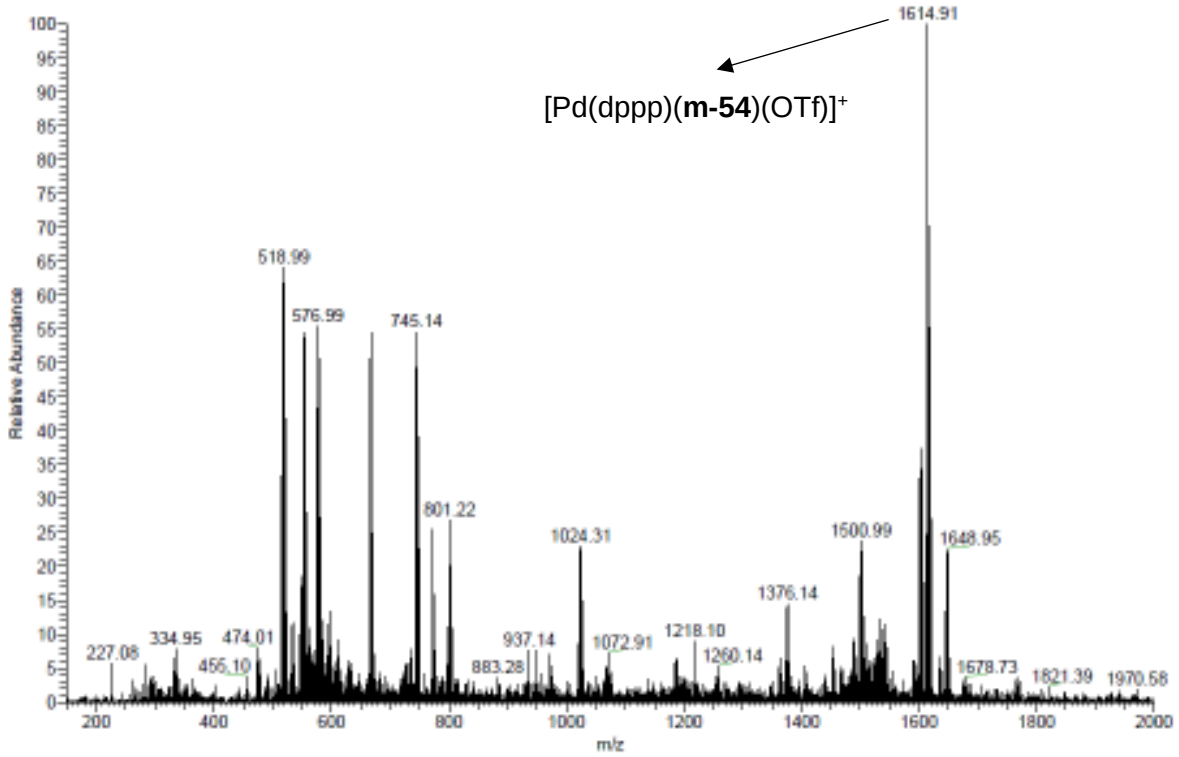

Figure XLIX: ESI-MS 2.

MS 3: Mass spectrum (ESI) of a 3:2 solution of [Pt(dppe)(OTf)$_2$] (**62**) and ***m*-54** in methanol.

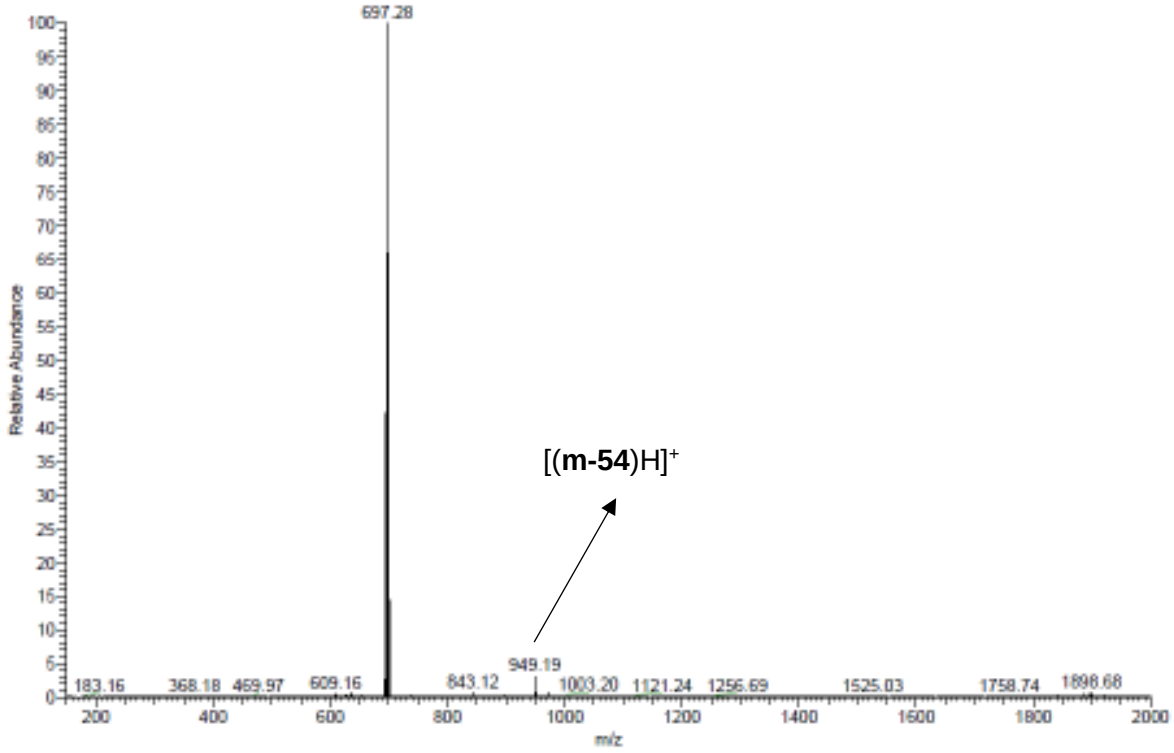

Figure L: ESI-MS 3.

5.5.8 Minimized structures

The structures were minimized at semi-empirical level (PM6) with MOPAC2016, Version: 19.179W, James J. P. Stewart, Stewart Computational Chemistry, web: http://OpenMOPAC.net.[29]

In a first stage, a set of simplified models of the complexes were prepared and minimized:

1) Benzyl moieties were removed to neglect conformational considerations and to have a clearer visualization of the complexes.

2) The complexes *cis*-Pd_3Cl_6***o***,***m***,***p***-**54**$_2$ were considered versus hexa-cationic *cis*-[Pd_3***o***,***m***,***p***-**54**$_2L_3$]: a) to minimize neutral trinuclear complexes, b) to neglect conformational considerations regarding the diphosphane ligands, c) to have a clearer visualization of the complexes.

3) The first stereochemical consideration regarded the helical conformation of the quasi-planar triphenylene moiety. The two enantiomers are in rapid equilibrium (Figure 9).

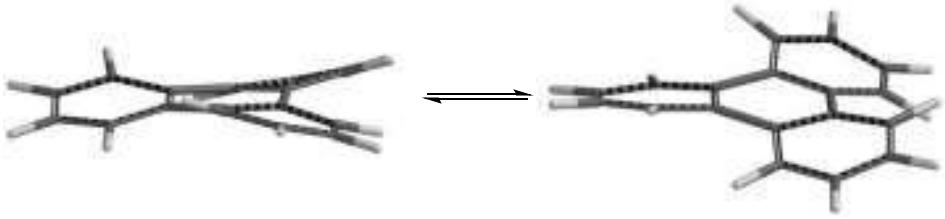

Figure LI: *M* and *P* helicity of a triphenylene unit in equilibrium

The sole homo-helical conformation diastereomer was considered as starting point for the construction of the various trinuclear complexes, considering that in this situation the distances between the three pyridines are equal, leading to a higher level of symmetry and a minimum of energy (Figure 10).

Figure LII: *M,M*-homo-helical diasteromer (left) and *P,M*-etero-helical diasteromer (right).

4) Minimization were performed starting from tridentate ligand with pyridines in axial or in equatorial conformation: a) both ligands all-axial [*ax-ax*], b) both ligands all-equatorial [*eq-eq*], c) eventually considering the mixed situation with one ligand all-axial and the other all equatorial [*ax-eq*] (Figure 11).

Figure LIII: Axial displacement of pyridines (named *ax*, left) and Equatorial displacement of pyridines (named *eq*, right).

All these configurational or conformational isomers can generate different diastereomers, which can interconvert each other without any bond rupture.

5) Trinuclear complexes in which different enantiotopic faces of the substituted triphenylenes are facing generate different diastereoisomers: one C_3-symmetric couple of enantiomers (named *RR/SS*) and one C_{3h}-symmetric *meso* compound (named *meso*). Both diastereomers were considered for calculation. These diastereomers can convert each other in the trinuclear complexes only by synchronous rupture of at least two metal-Py bonds (Figure 12).

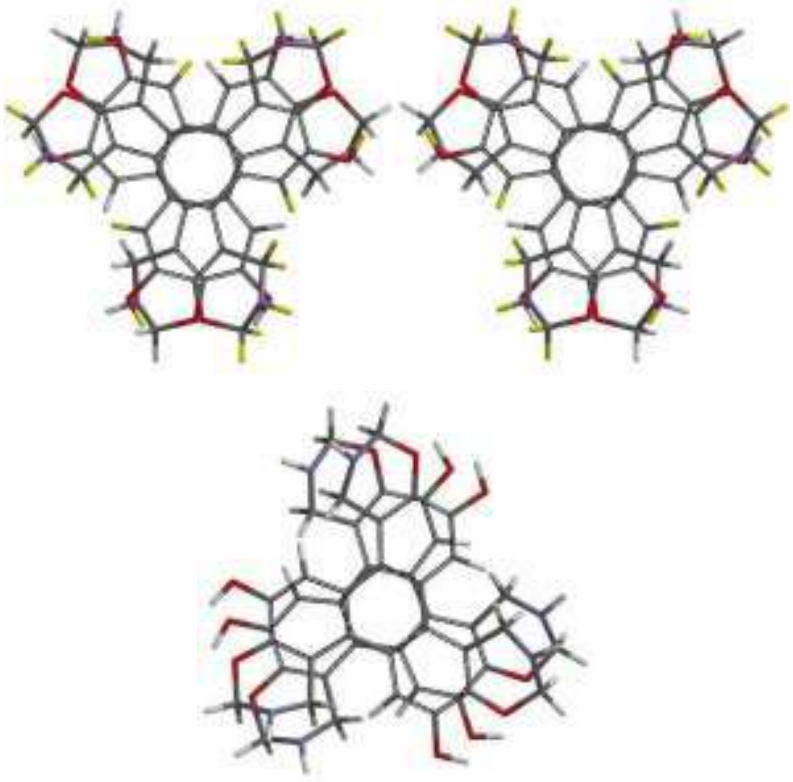

Figure LIV: C_3-symmetric homo-chiral compound and its enantiomer (named *RR*/*SS*, left and centre), and C_{3h}-symmetric hetero-chiral (named meso, right).

6) Calculation were performed on those stereomers with *o*-, *m*-, *p*-pyridines attached to the six nitrogens, searching the best conformers of the metal complexes and minimizing the geometry of the structure (Figure 13-22). Results are reported in Table 2.

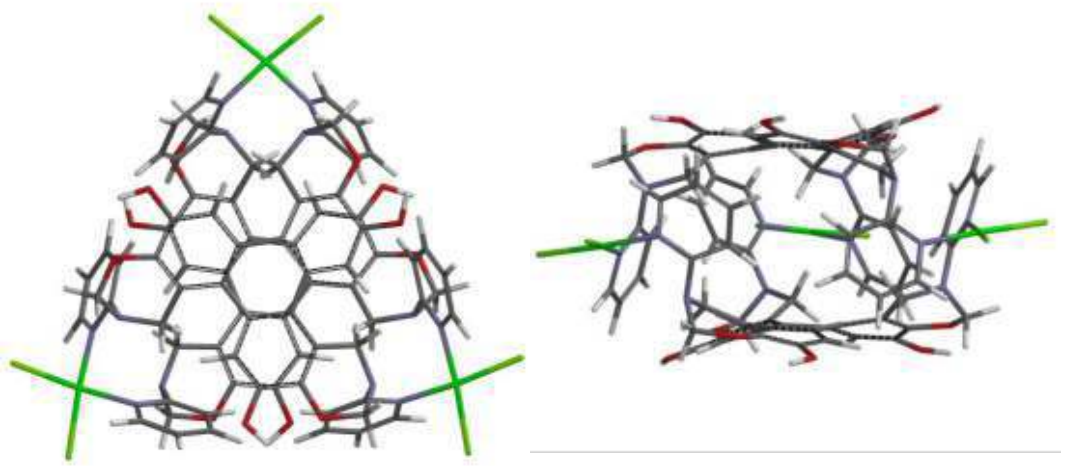

Figure LV: Top and side view of the cis-[Pd_3Cl_6***o*-54**$_2$] named *orto_RR/SS_ax-ax*.

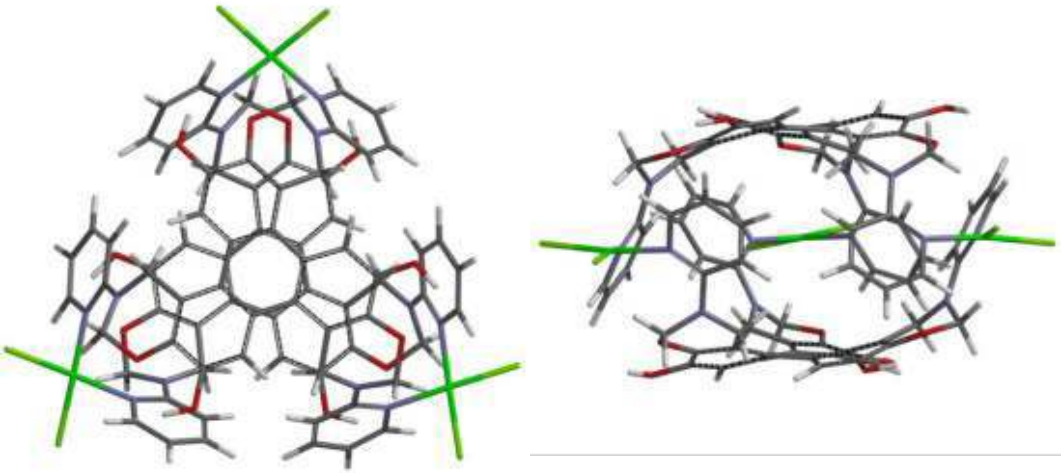

Figure LVI: Top and side view of the cis-[Pd_3Cl_6***o*-54**$_2$] named *orto_RR/SS_eq-eq*.

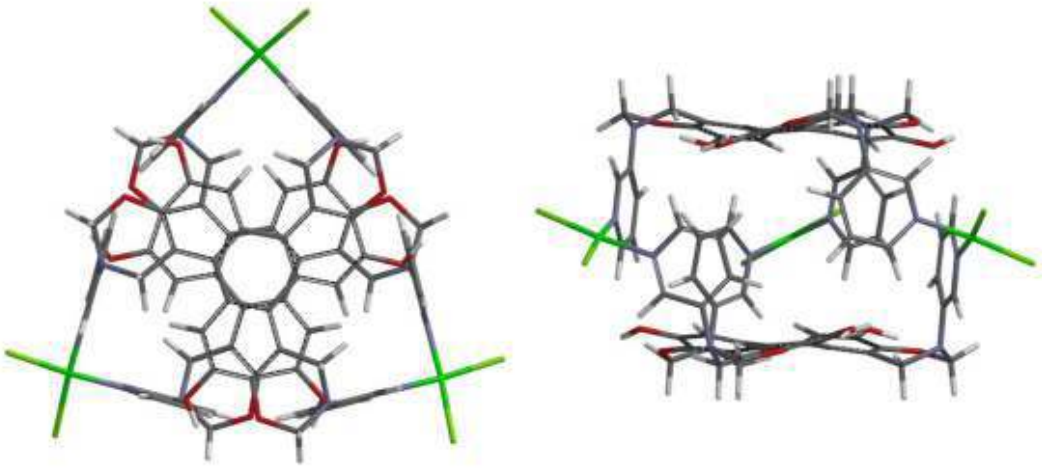

Figure LVII: Top and side view of the cis-[Pd_3Cl_6***m*-54**$_2$] named *meta_RR/SS_ax-ax.*

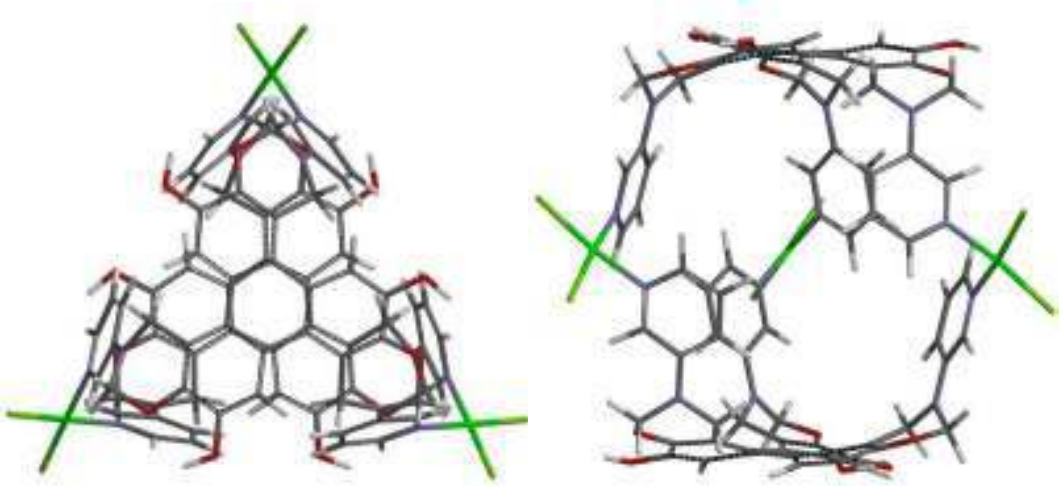

Figure LVIII: Top and side view of the cis-[Pd_3Cl_6***m***-**54**$_2$] named *meta_RR/SS_ax-eq.*

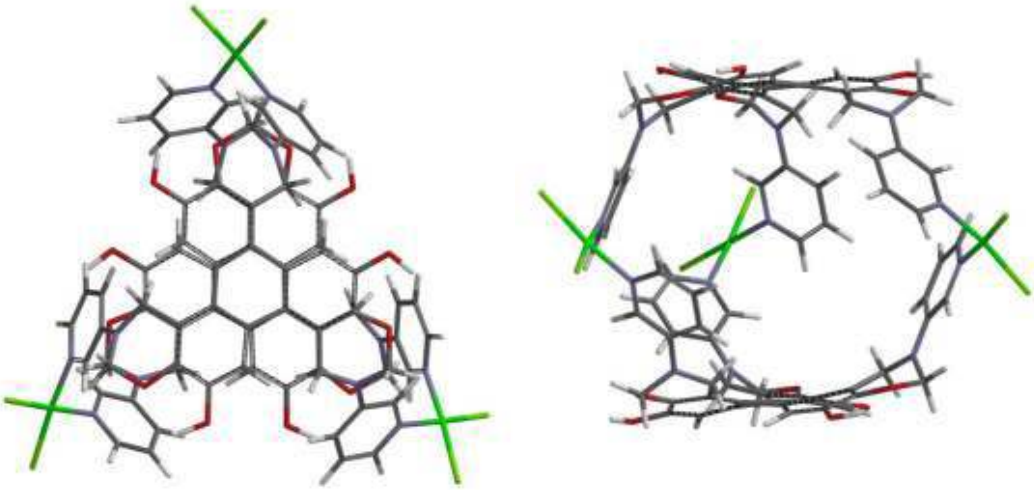

Figure LIX: Top and side view of the cis-[Pd_3Cl_6***m***-**54**$_2$] named *meta_RR/SS_eq-eq*.

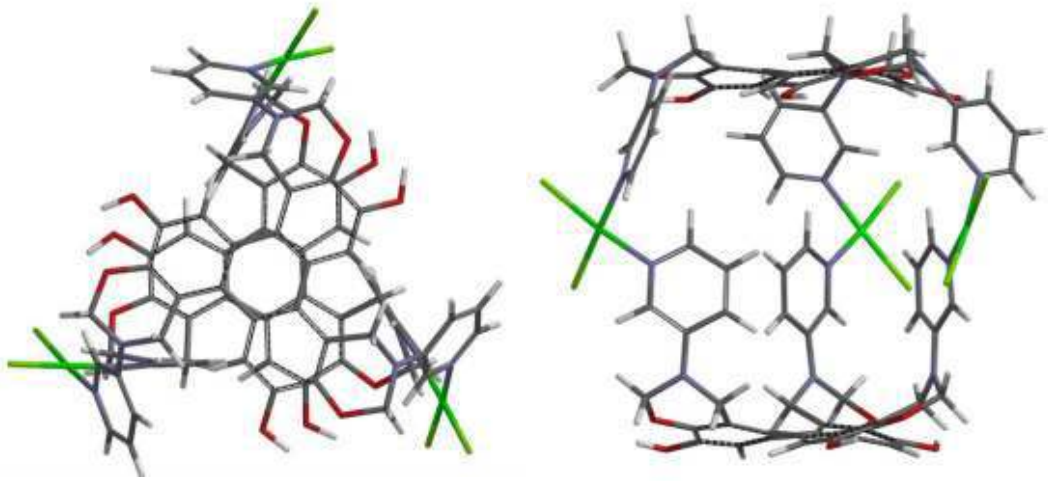

Figure LX: Top and side view of the cis-[Pd_3Cl_6***m***-**54**$_2$] named *meta_meso_ax-ax*.

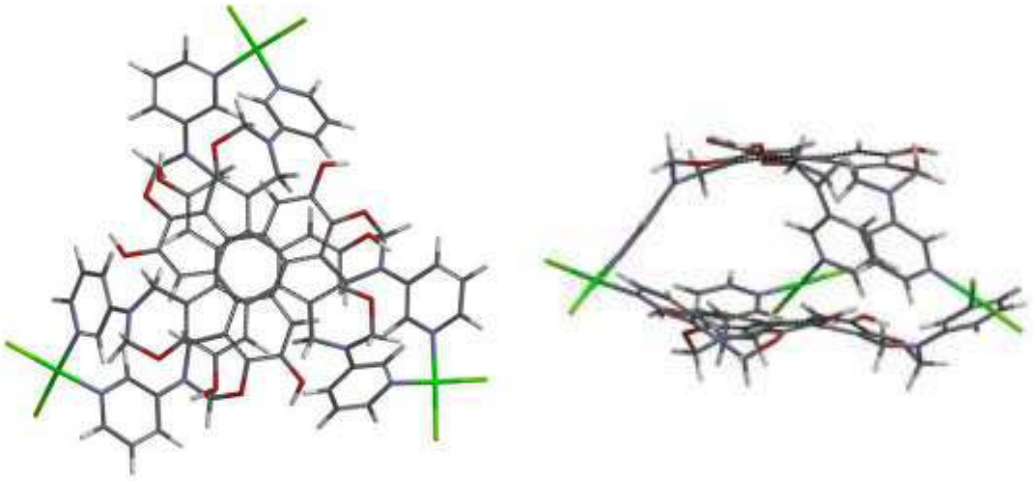

Figure LXI: Top and side view of the cis-[Pd_3Cl_6***m***-**54**$_2$] named *meta_meso_ax-eq.*

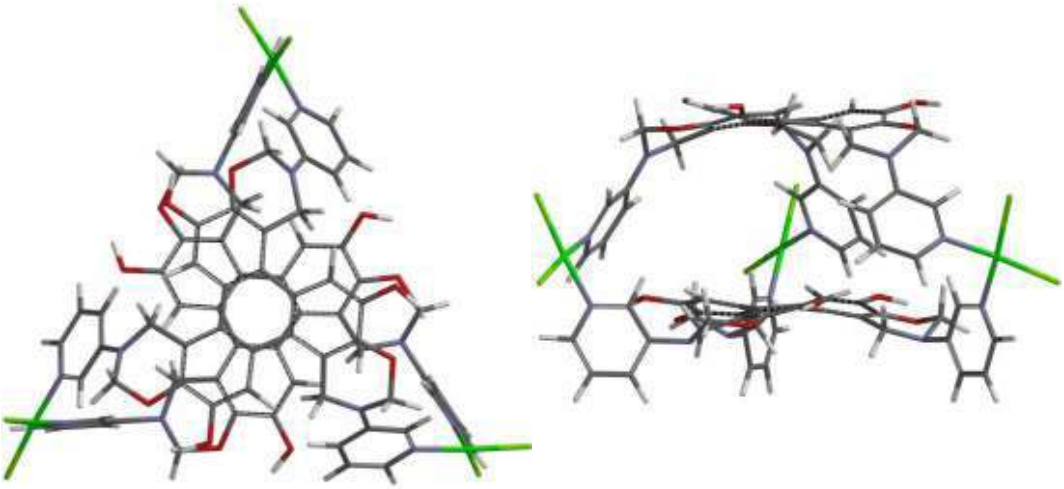

Figure LXII: Top and side view of the cis-[Pd_3Cl_6***m***-**54**$_2$] named *meta_meso_eq-eq.*

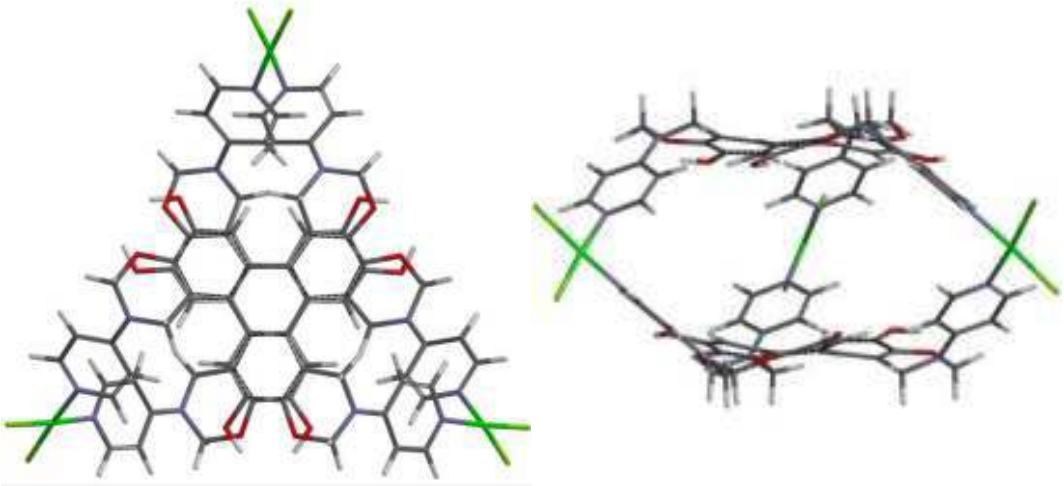

Figure LXIII: Top and side view of the cis-[Pd_3Cl_6***p***-**54**$_2$] named *para_RR/SS_ax-ax*.

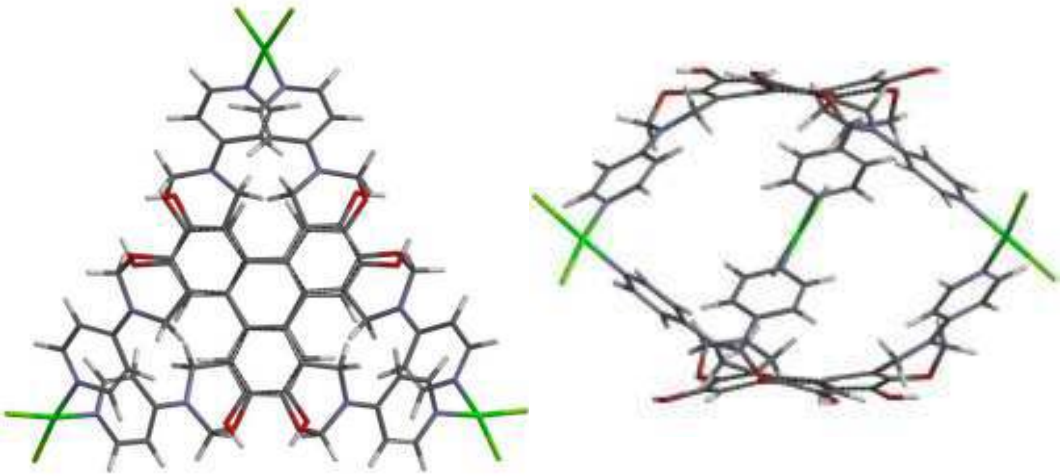

Figure LXIV: Top and side view of the cis-[Pd_3Cl_6***p*-**54**$_2$] named *para_RR/SS_eq-eq*.

Pyridine	Facial topology	Conformations of pyridines	Obtained energy [kJ/mol]	Obtained energy [kcal/mol]	Relative energy [kcal/mol]
orto	*RR/SS*	*ax-ax*	-680	-162.3	37.3
orto	*RR/SS*	*eq-eq*	-711	-169.8	29.9
meta	*RR/SS*	*ax-ax*	-722	-172.3	27.3
meta	*RR/SS*	*ax-eq*	-796	-190.2	9.5
meta	*RR/SS*	*eq-eq*	-801	-191.3	8.3
meta	*meso*	*ax-ax*	-800	-191.0	8.7
meta	*meso*	*ax-eq*	-755	-180.2	19.4
meta	*meso*	*eq-eq*	-702	-167.7	32.0
para	*RR/SS*	*ax-ax*	-815	-194.5	5.1
para	*RR/SS*	*eq-eq*	-836	-199.7	0.0

Table I: Energy of the resulting minimized structures of the *cis*-Pd_3 Cl_6 ***o***,***m***,***p*-54$_2$ complexes.

According to these calculations the minima between the isomers were used for the preparation of the model with the dppe ligand, which was considered in the two possible enantiomeric conformers (Figure 23 to 26). Results are reported in Table 3.

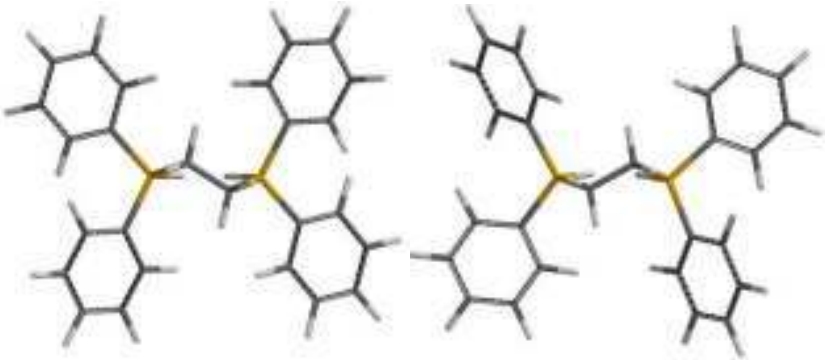

Figure LXV: The two possible enantiomeric conformation of dppe ligand P (left) and M (right), that were used to complete the structure of possible complexes *cis*-Pd_3dppe_3***o***,***m***,***p*-54$_2$.

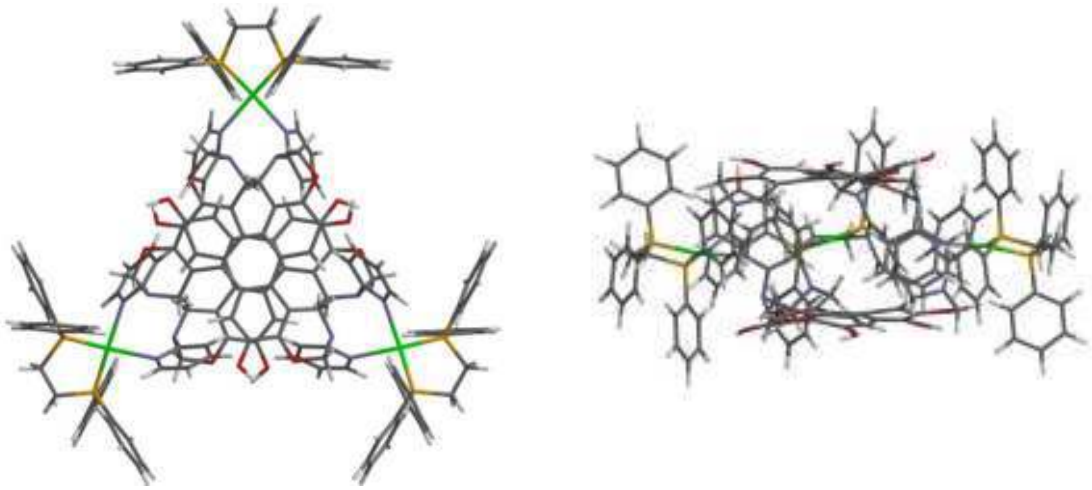

Figure LXVI: Top and side view of the *cis*-[Pd_3dppe_3***o*-54**$_2$] named *orto_RR/SS_eq-eq_M* (benzyl moieties omitted for clarity).

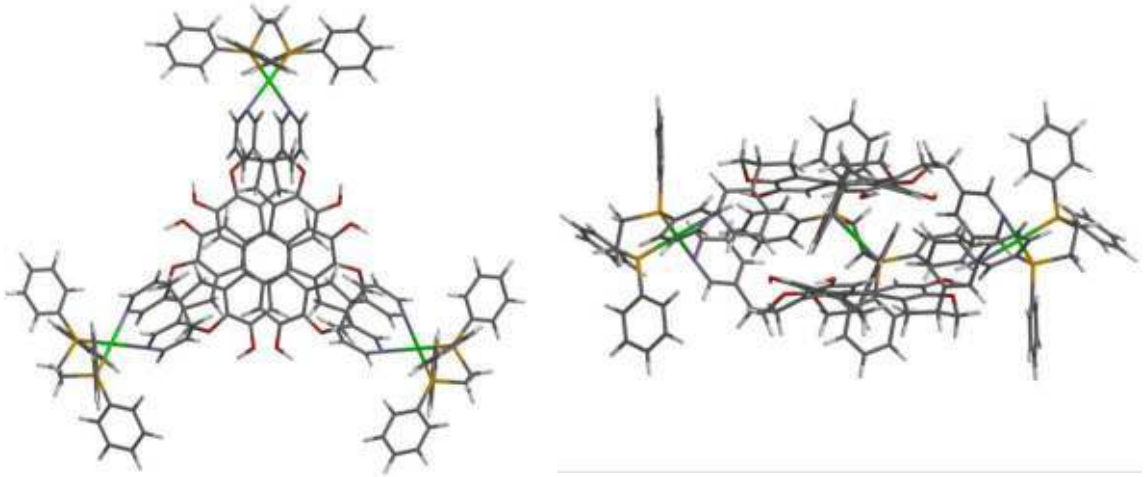

Figure LXVII: Top and side view of the *cis*-[Pd_3dppe_3***m*-54**$_2$] named *meta_RR/SS_eq-eq_M* (benzyl moieties omitted for clarity).

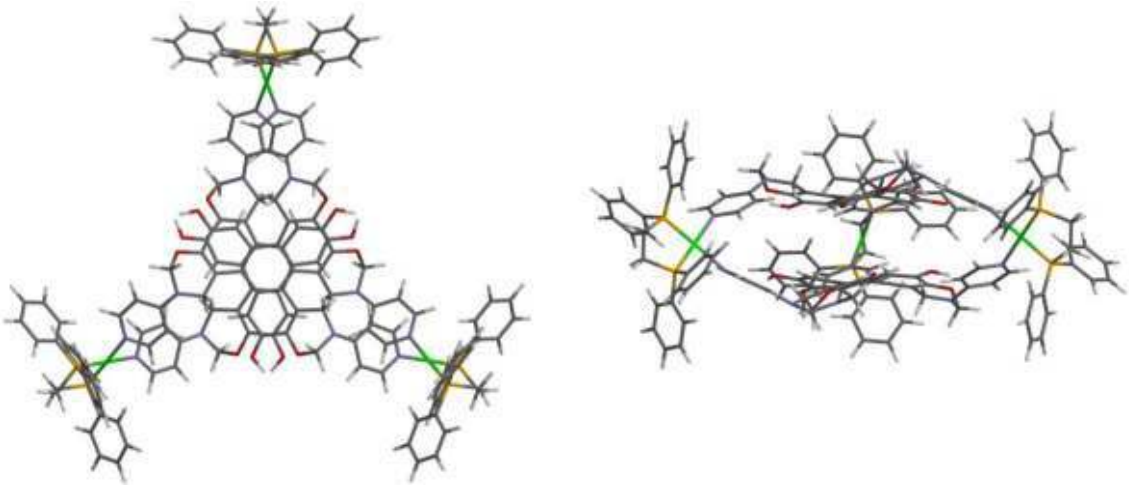

Figure LXVIII: Top and side view of the *cis*-[Pd_3dppe_3***p*-54**$_2$] named *para_RR/SS_eq-eq_P* (benzyl moieties omitted for clarity).

Pyridine	Facial topology	Conformations of pyridines	Helicity of dppe	Obtained energy [kJ/mol]	Obtained energy [kcal/mol]	Relative energy [kcal/mol]
orto	*RR/SS*	*ax-ax****	*P*	5743	1371.4	140.4
orto	***RR/SS***	***ax-ax****	***M***	**5705**	**1362.4**	**131.4**
meta	*RR/SS*	*ax-ax*	*P*	5432	1297.2	66.2
meta	***RR/SS***	***ax-ax***	***M***	**5155**	**1231.0**	**0.0**
para	***RR/SS***	***ax-ax***	***P***	**5307**	**1267.4**	**36.4**
para	*RR/SS*	*ax-ax*	*M*	5292	1263.6	32.6

Table II*:* Energy of the resulting minimized structures of the best cis-Pd_3 $dppe_3$***o***,***m***,***p***-**3**$_2$ complexes.

*: the *eq-eq* isomers employed for the minimization of the phosphane complexes "decomposed" abstracting a palladium atom.

5.6 Bibliography

1 R. Chakrabarty, P.S. Mukherjee, P.J Stang., *Chem. Rev.* **2011**, *111*, 6810-6918.

2 A. Schmidt, A. Casini, F.E. Kühn, *Coord. Chem. Rev.* **2014**, *275*, 19-36.

3 L. Chen, Q. Chen, M. Wu, F. Jiang, M. Hong, *Acc. Chem. Res.* **2015**, *48,* 201-210.

4 a) L.-J. Chen, H.-B. Yang, M. Shionoya, *Chem. Soc. Rev*., **2017**, *46*, 2555; b) W. M. Bloch, G. H. Clever, *Chem. Commun*., **2017**, *53*, 8506; c) M. D. Ward, C. A. Hunter, N. H. Williams, *Chem. Lett*., **2017**, *46*, 2; d) R. A. S. Vasdev, D. Preston, J. D. Crowley, *Chem. Asian J.*, **2017**, *12*, 2513; e) J. J. Henkelis,M. J. Hardie, *Chem. Commun.*, **2015**, *51*, 11929; f) S. Zarra, D. M. Wood, D. A. Roberts, J. NitschkeR., *Chem. Soc. Rev.*, **2015**, *44*, 419; g) T. R. Cook, Y.-R. Zheng, P. J. Stang, *Chem. Rev.*, **2013**, *113*, 734.

5 A. J. Metherell, M.D. Ward, *Dalton Trans.*, **2016**, *45*, 16096–16111.

6 L. R. Holloway, P. M. Bogie, R. J. Hooley, *Dalton Trans*., **2017**, *46*, 14719-14723.

7 A. Galana, P. Ballester, *Chem. Soc. Rev.,* **2016**, *45*, 1720-1737.

8 a) S. Horiuchi, T. Murase, M. Fujita, *J. Am. Chem. Soc.*, **2011**, 133, 12445-12447; b) P. Mal,B. Breiner, K. Rissanen, J. R. Nitschke, *Science*, **2009**, 324, 1697-1699; c) J. L. Brumaghim, M. Michels, D. Pagliero, K. N. Raymond, *Eur. J. Org. Chem.*, **2004**, 5115-5118; d) J. L. Brumaghim, M. Michels, K. N. Raymond, *Eur. J. Org. Chem.*, **2004**, 4552-4559; e) M. Yamashina, Y. Sei, M. Akita,M. Yoshizawa, *Nature Commun.*, **2014**, 5, 5179.

9 N. Ahmad, H.A. Younus, A.H. Chughtai, F. Verpoort, *Chem. Soc. Rev.,* **2015**, *44*, 9-25.

10 A. Ahmedova, *Front. Chem.* **2018**, *6*, 620.

11 F. J. Rizzuto, L. K. S. von Krbek, J. R. Nitschke, *Nature Rev. Chem.,* **2019***, 3*, 204-222.

12 M. D. Ward, C. A. Hunter, N. H. Williams, *Chem. Lett.* **2017**, *46*, 2-9.

13 W.-X. Gao, H.-N. Zhang, G.-X. Jin, *Coord. Chem. Rev.* **2019**, *386*, 69-84.

14 C. Tan, D. Chu, X. Tang, Y. Liu, W. Xuan, Y. Cui, *Chem. Eur. J.* **2019**, *25*, 662-672.

15 C. M. Hong, R. G. Bergman, K. N. Raymond, F. D. Toste, *Acc. Chem. Res.*, **2018**, *51*, 2447-2455.

16 C. J. Hastings, R. G. Bergman, K. N. Raymond, *J. Am. Chem. Soc.*, **2010**, *132*, 6938-6940.

17 M. Yoshizawa, J. K. Klosterman, M. Fujita, *Angew. Chem. Int. Ed.* **2009**, *48*, 3418-3438.

18 Y. Ueda, H. Ito, D. Fujita, M. Fujita, *J. Am. Chem. Soc.*, **2017**, *139*, 6090-6093.

19 a) S. Gonell, X. Caumes, N. Orth, I. Ivanović-Burmazović, J. N. H. Reek, *Chem. Sci.* **2019,** *10*, 1316-1321, b) S. Gonell, J. N. H. Reek, *ChemCatChem*, **2019**, *11*, 1458-1464.

20 a) D. Zhang, T.K. Ronson, J. R. Nitschke, *Acc. Chem. Res.*, **2018**, *51*, 2423-2436; b) E. G. Percástegui, J. Mosquera, T. K. Ronson, A. J. Plajer, M. Kieffer, J. R. Nitschke, *Chem. Sci.* **2019**, *10*, 2006-2018.

21 M. D. Ward, C. A. Hunter, N. H. Williams, *Acc. Chem. Res.*, **2018**, *51*, 2073-2082.

22 S. Durot, J. Taesch, V. Heitz, *Chem. Rev*. **2014**, *114*, 8542−8578.

23 M. Han, D. M. Engelhard, G. H. Clever, *Chem. Soc. Rev.,* **2014**, *43*, 1848-1860.

24 R. Custelcean, *Chem. Soc. Rev.* **2014**, *43*, 1813-1824.

25 G. T. L. Broadwood-Strong, P. A. Chaloner, P. B. Mitchcock, *Polyhedron*, **1993***, 12*, 721-729.

26 S. J. Sabounchei, M. Ahmadi, Z. Nasri, E. Shams; S. J. Sabounchei; M. Ahmadi; Z. Nasri; E. Shams, *C. R. Chimie,* **2013**, *16*, 159-175.

27 P. J. Stang, D. H. Cao, S. Saito, A. M. Arif, *J. Am. Chem. Soc.*, **1995**, *117*, 6273-6283

28 A. Macchioni, G. Ciancaleoni, C. Zuccaccia, D. Zuccaccia, *Chem. Soc. Rev.*, **2007**, 37, 479-489.

29 Structures minimized at semi-empirical level (PM6) with MOPAC2016, Version: 19.179W, J. J. P. Stewart, Stewart Computational Chemistry, http://OpenMOPAC.net. J. J. P. Stewart, *J. Mol. Mod.* **2007**, *13*, 1173-1213.

30 G. Berton, T. Lorenzetto, G. Borsato, P. Sgarbossa, C. Santo, F. Visentin, F. Fabris, A. Scarso, *Tetrahedron Lett*., **2019**, 60, 151202.

31 W. L. F. Armarego, C. Chai in *Purification of Laboratory Chemicals (Seventh Edition)*, Butterworth-Heinemann, Boston, **2013**.

32 W. C. Still, M. Kahn, A. Mitra, *J. Org. Chem.*, **1978**, *14*, 2923-2925.

33 J. DePriest, G.Y. Zheng, C. Woods, D.P. Riilema, N.A. Mikirova, M.E. Zandler, *Inorganica Chimica Acta*, **1997**, *264*, 287-296.

6. Hydrogen Bonded Capsules

As extensively reported in the Introduction, the use of hydrogen bonding interactions for the preparation of self-assembled nano-containers represents one of the most successful method for the development of recognition hosts, even for neutral guests and for the rise of supramolecular catalysis, with impressive examples in the recent literature.

As long as triphenylene based closed self-assembled systems are concerned, in the literature only one example from Rebek and collaborators showed the synthesis of a triphenylene adorned with three glycoluril units, forming a dimeric capsule characterized by a highly electron rich cavity, known as "jelly doughnut".[1]

Our idea to exploit the ***C*$_3$-26** substrate for the formation of hydrogen bonding capsule consisted in the introduction of three carboxylic acid moieties, connected to the main triphenylenic core by phenyl ether linkages (Figure 1).

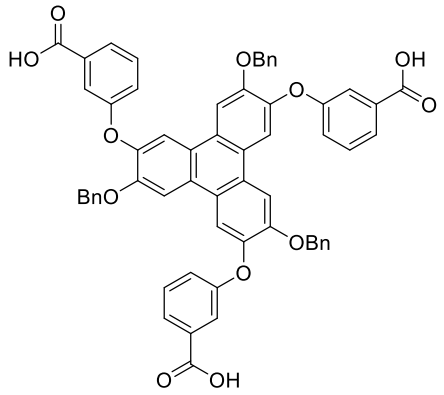

63

Figure 1: Structure of target triacid **63**.

The presence of the carboxylic acids, in the proper solvent, should allow the formation of six classical hydrogen bonds between two carboxylic acid moieties. The feasibility of the dimeric assembly was investigated by molecular modelling, confirming that the derivative bearing the carboxylic moiety in *meta* position should be the best choice for the stable formation of a dimer (Figure 2). Computer modelling allowed to calculate the size of the cavity of the possible dimer (about 540 Å^3), which should be able to bind guests in the range of 270-325 Å^3 (a volume of about half of the one of the cavity) (Figure 2).[2]

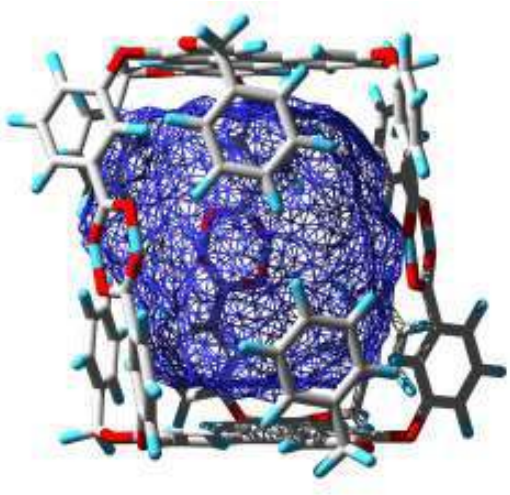

Figure 2: Molecular modelling of dimer composed by two molecules of **63**, connected by six hydrogen bonds, forming a cavity of about 540 Å^3.

It is important to note that Figure 2 represents just one of the two possible combinations of dimeric capsules, since, as seen in Chapter 4, the prochiral faces of a C_3 molecule once a dimer is formed can combine in a homochiral or heterochiral fashion giving rise to two diastereoisomeric species: one racemate comprising *P-P* and *M-M* stereoisomers and one *meso*-capsule *M-P*.

Whit this idea in mind, we started the synthesis and the supramolecular characterization of the triacid **63**.

6.1 Synthesis of the *tris*-carboxylic Triphenylenes

To synthesize the hemisphere of the hydrogen bonded capsule starting from the common building block C_3-symmetric molecule ***C*$_3$-26**, two different reactions were considered: a Buchwald C-O coupling and an aromatic nucleophilic substitution.

The Buchwald coupling was our first choice, because it could afford in just two steps the final product, **63**, starting from relatively inexpensive reagents. ***C*$_3$-26** was reacted with methyl 3-bromobenzoate, using palladium(II) acetate as catalyst and di-*tert*-BuXPhos as ligand for the palladium, as reported by Buchwald (Scheme 1).[3]

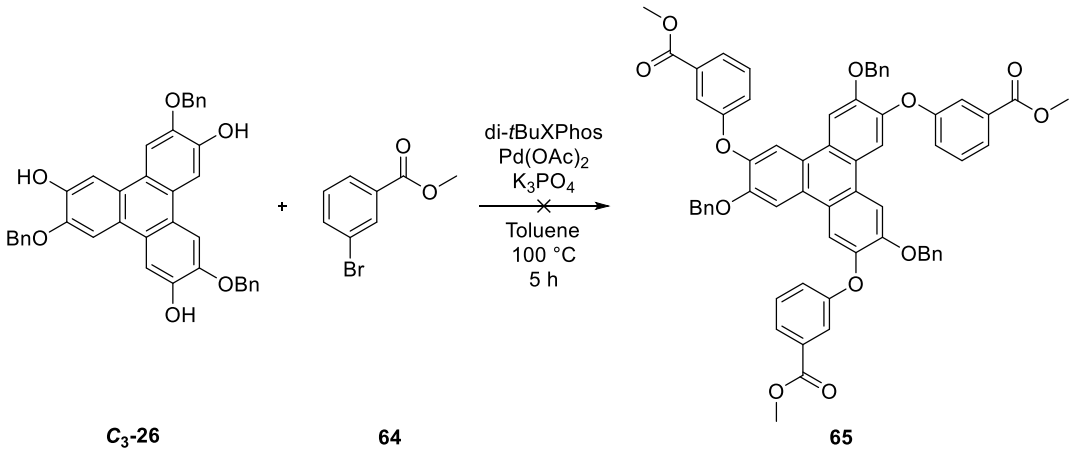

Scheme 1: Synthesis of product **65** through Buchwald coupling.

The first reaction was carried out with a 3 mol% of Pd/substrate ratio and it did not provide any product, leaving the starting material untamed. A second attempt using a 30 mol% of catalyst led to the same result. For this reason, we decided to move to a different strategy.

The second synthetic strategy involved an aromatic nucleophilic substitution using methyl 3-fluoro-4-nitrobenzenecarboxylate as electrophile. With this procedure, the resulting product contains also a nitro group, that could be removed through reduction and deamination reactions. ***C*$_3$-26** was reacted with methyl 3-fluoro-4-nitrobenzenecarboxylate, in the presence of K_2CO_3, heating at 90 °C in anhydrous DMF (Scheme 2).[4]

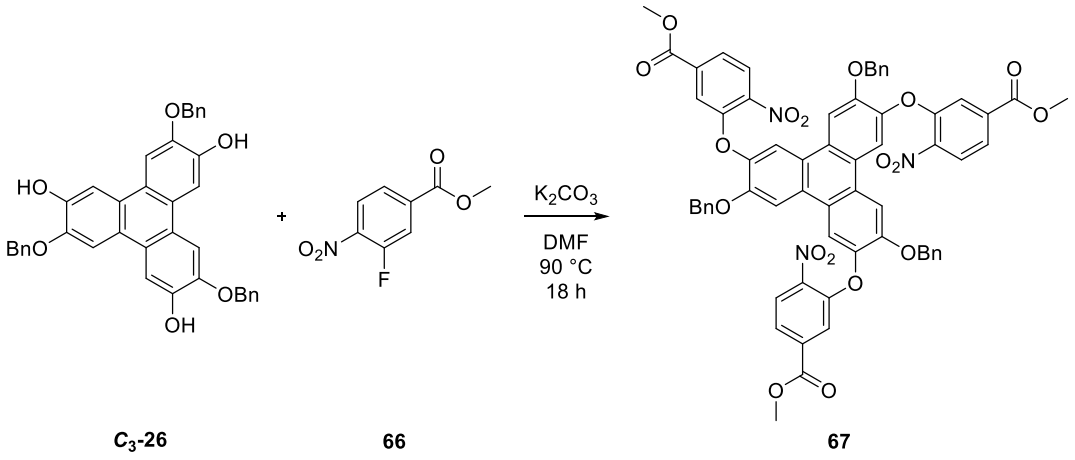

***C*$_3$-26** **66** **67**

Scheme 2: Synthesis of product **67** through nucleophilic aromatic substitution.

The reaction was very clean, and the product was obtained after flash chromatography in 90% yield.

For the reduction of the nitro group in molecule **67**, the possible methods were limited by the presence of the benzyl moiety, since the latter residue is sensible to most of the reagents able to promote the reduction of the nitro group. For this reason, we selected tin(II) chloride as reducing agent, due to its high selectivity toward the nitro group. Methyl ester **67** was then treated with tin(II) chloride using absolute ethanol as solvent (Scheme 3).[5]

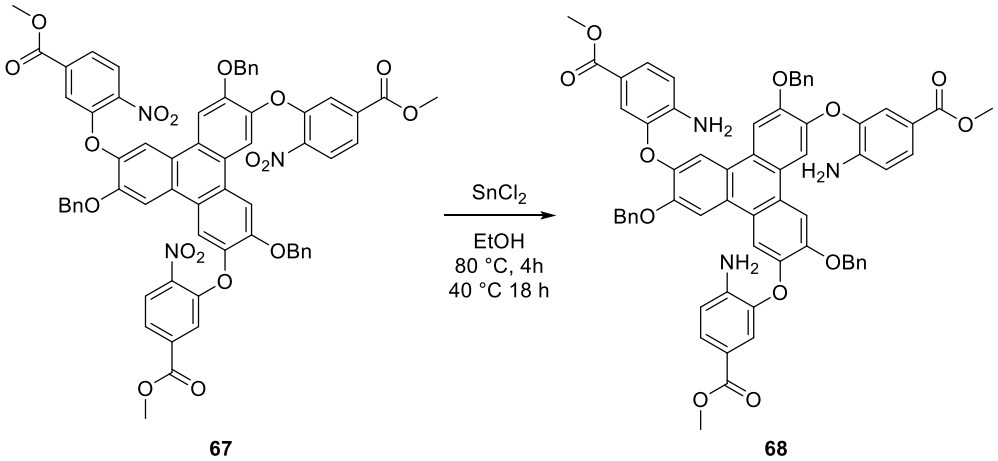

67 **68**

Scheme 3: Reduction of the nitro group of substrate **67** to achieve the *tris*-amine **68**.

After the purification of the reaction crude by flash chromatography, the desired *tris*-amine **68** was obtained in 61% yield.

Last step of the synthetic route was the removal of the amine groups. For this purpose, the *tris*-amine **68** was treated with *tert*-butyl nitrite in the presence of DMSO as mild reducing agent (Scheme 4).[6]

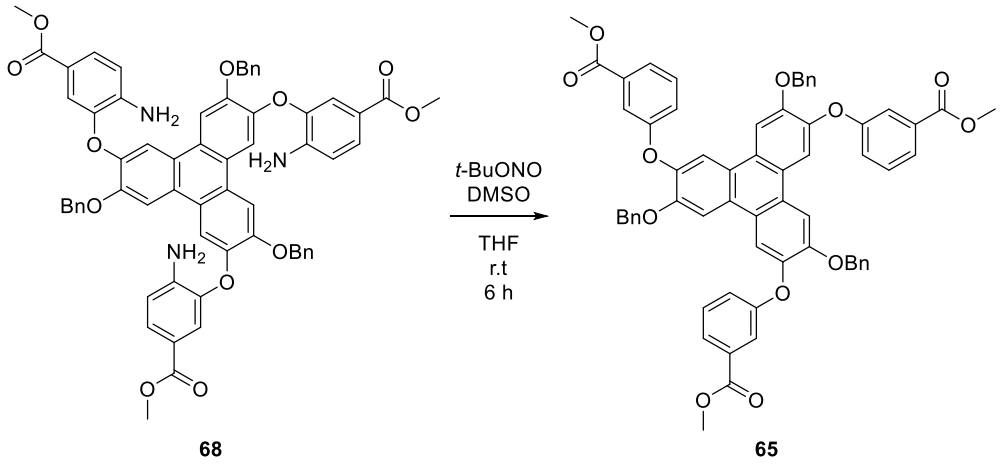

68 **65**

Scheme 4: Removal of the amine groups on **68** to achieve the methyl ester **65**.

After chromatography of the reaction crude the methyl ester **65** was obtained in 36% yield.

The last step for the synthesis of the triacid **63** was the hydrolysis of the methyl ester moiety of **65**, that was achieved by reaction of hydroxide ion in THF (Scheme 5).[7]

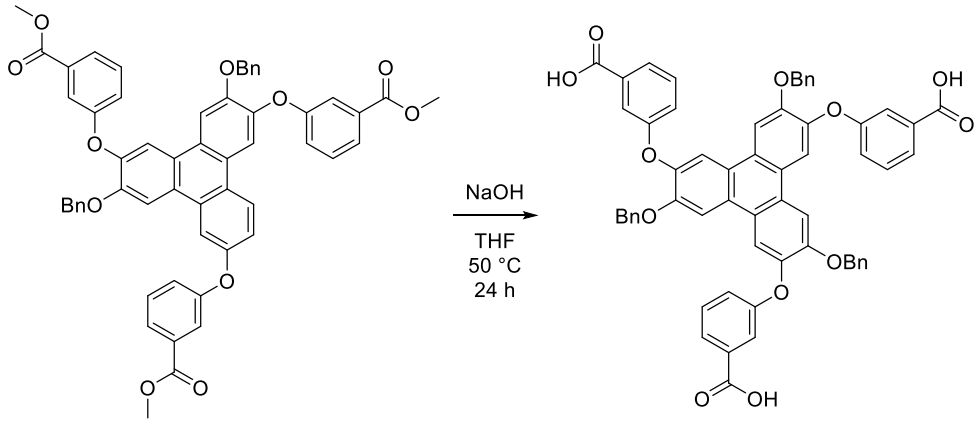

65 **63**

Scheme 5: Hydrolysis of ester **65** to obtain the triacid **63**.

The target triacid was obtained in 52% yield, after acidification and extraction , without the need of further purifications.

As a comparison, we decided to hydrolyse also the methyl ester **67**, in order to obtain a triacid with different substitutions, applying the same saponification procedure to ester **65**, for a shorter reaction time in agreement with the higher electrophilicity due to the presence of the nitro moieties (Scheme 6).[7]

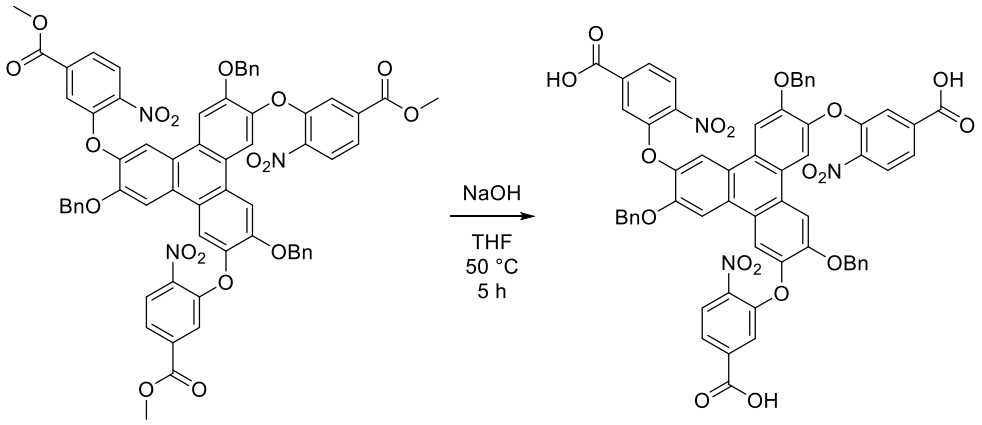

67 69

Scheme 6: Hydrolysis of ester **67** to obtain the nitro triacid **69**.

The nitro-triacid **69** was obtained in nearly quantitative yield after the previously described purification procedure.

6.2 Aggregation Studies

As anticipated in the introduction of this Chapter, when working with hydrogen bonded capsule, the choice of the solvent plays a fundamental role on the aggregation properties and on the dynamic effects of the assemblies. Indeed, a too polar solvent could compete in the formation of H-bonding with the two hemi-capsules, preventing the formation of the desired supramolecular aggregate. On the other side, in apolar solvents the H-bonding species could be not sufficiently soluble, preventing the possibility of equilibria leading to the formation of well-defined soluble aggregates.

Once accomplished the synthesis of the triacid **63** and the nitro triacid **69**, we carried out a series of studies in order to investigate their aggregation properties. Unfortunately, and despite our expectations, triacid **63** proved to be sufficiently soluble only in DMSO, resulting only sparingly soluble in different solvents like methanol, chloroform and DCM, in which **63** provided too diluted solutions not suitable for NMR studies. For this reason, only its structural characterization was possible by NMR in DMSO-d_6, but no investigation of the aggregation properties in solution was carried out.

As long as the nitro triacid **69** is concerned, it turned out not to be sufficiently soluble in chloroform or DCM. On the other hand, methanol proved to be a good solvent for this triacid. Despite the polar nature of this solvent, which could hamper the possible aggregation of the triacid **69**, we carried out a series of ^{1}H NMR studies on the molecule in methanol-d_4. In particular, it was possible to notice the broad resonance of the signals attributed to the benzylic CH_2, resulting as a set of two resonances (Figure 3).

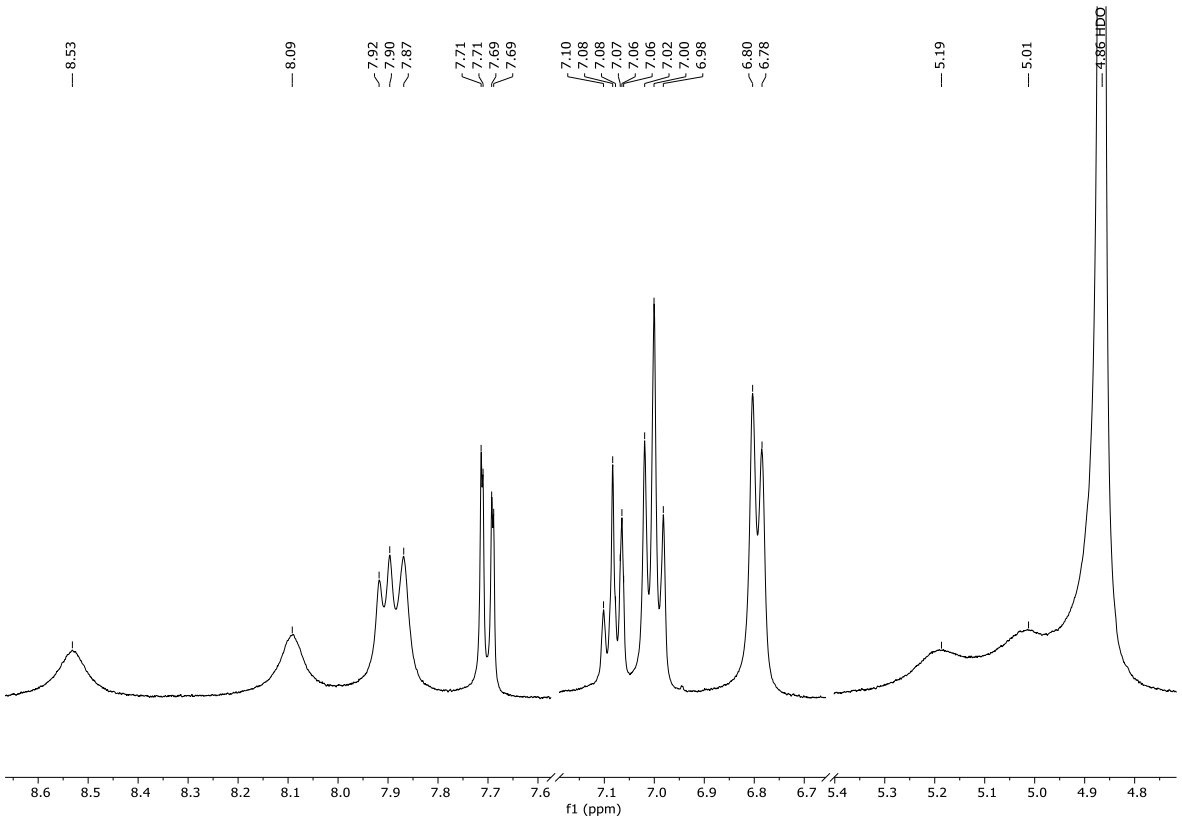

Figure 3: ^{1}H NMR detail of the benzylic and aromatic regions of **69**. Broad benzylic signals are present at 5.19 and 5.01 ppm.

This phenomenon resembles what already observed in Chapter 4 concerning the formation of sulphide and disulphide covalent cages, for which the prochirality of C_3-symmetric tris-thiol containing triphenylene molecules led to the formation of diastereomers. To better understand this behaviour, we decided to acquire a series of ^{1}H NMR spectra in methanol-d_4 at low temperatures, at which the H-bonds between the acids are less contrasted by the statistically more favoured interactions with the protic polar solvent, enabling to see the effect on the pseudo-AB system (Figure 4).

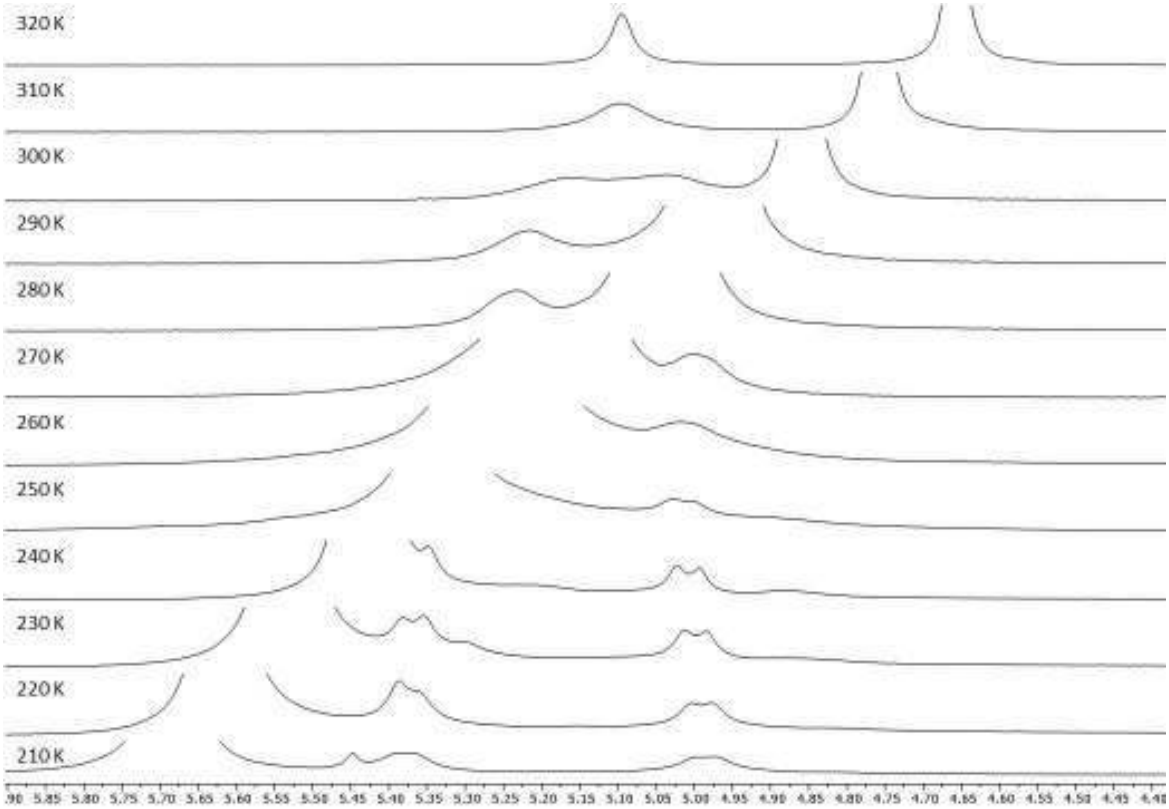

Figure 4: ^{1}H NMR detail of the benzylic region of **69** at variable temperature (indicated on the pictures).

As can be seen in the figure above reported, the broad pseudo-AB system observed at 300 K turned into a singlet at 320 K, while decreasing the temperature lower than 260 K the AB system turned out clearly into two doublets. Since the only way to observe the benzylic CH_2 splitting into an AB system is the formation of a dimer, it is licit to suppose the presence of a dimer of some sort in solution, despite the polarity of the solvent. Moreover, due to the observation of only two doublets, it is likely that only one dimeric species in solution is present, which could possibly be the homochiral racemic *P-P* and *M-M* stereoisomers, since these are usually more stable than the heterochiral *meso* derivative *M-P*.

Therefore, a series of ^{1}H NMR of **69** in methanol-d_4 at different concentrations were recorded in the range of 8.9-0.9 mM (10 mM was the maximum solubility in methanol-d_4), observing how neither the aromatic or methylenic residues of the benzyl, nor the protons of the benzoic acid residue and the triphenylenic C-H had a variation with the change of concentration (Figure 5).

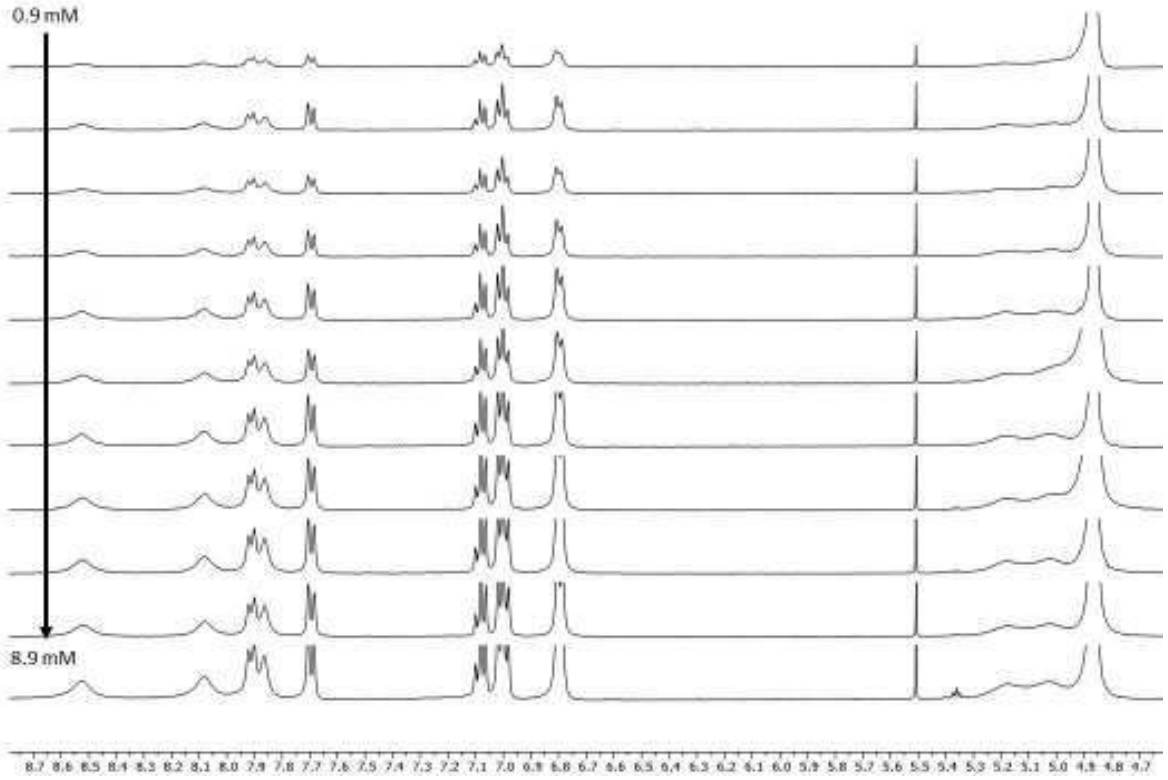

Figure 5*:* Detail of the aromatic and benzylic region of *^{1}H NMR* of **69** in *methanol-d_4* in the concentration range of 8.9-0.9 mM.

Pseudo 2D DOSY NMR spectra at 8.9 mM and 0.9 mM showed the same values of diffusion coefficient, meaning that molecule **69** exists always as a monomer or, on the opposite side, always as an aggregate. Considering that in DMSO-d_6 the benzylic methylene is present as a sharp singlet, it is likely that in DMSO **69** is not able to aggregate, due to the solvating effect of this solvent on the hydrogen bonds, while in methanol the acid can aggregate to generate, probably, a dimer.

In order to better understand the aggregation process, we decided to titrate with $CDCl_3$ a 5 mM solution of **69** in methanol-d_4. In this way, by increasing the amount of the apolar solvent in solution, it is expected that the molecule of triacid should more likely interact through H-bonding due to the decreased polarity and the decreased amount of methanol in solution. A detail of the ^{1}H NMR titration is reported in Figure 6.

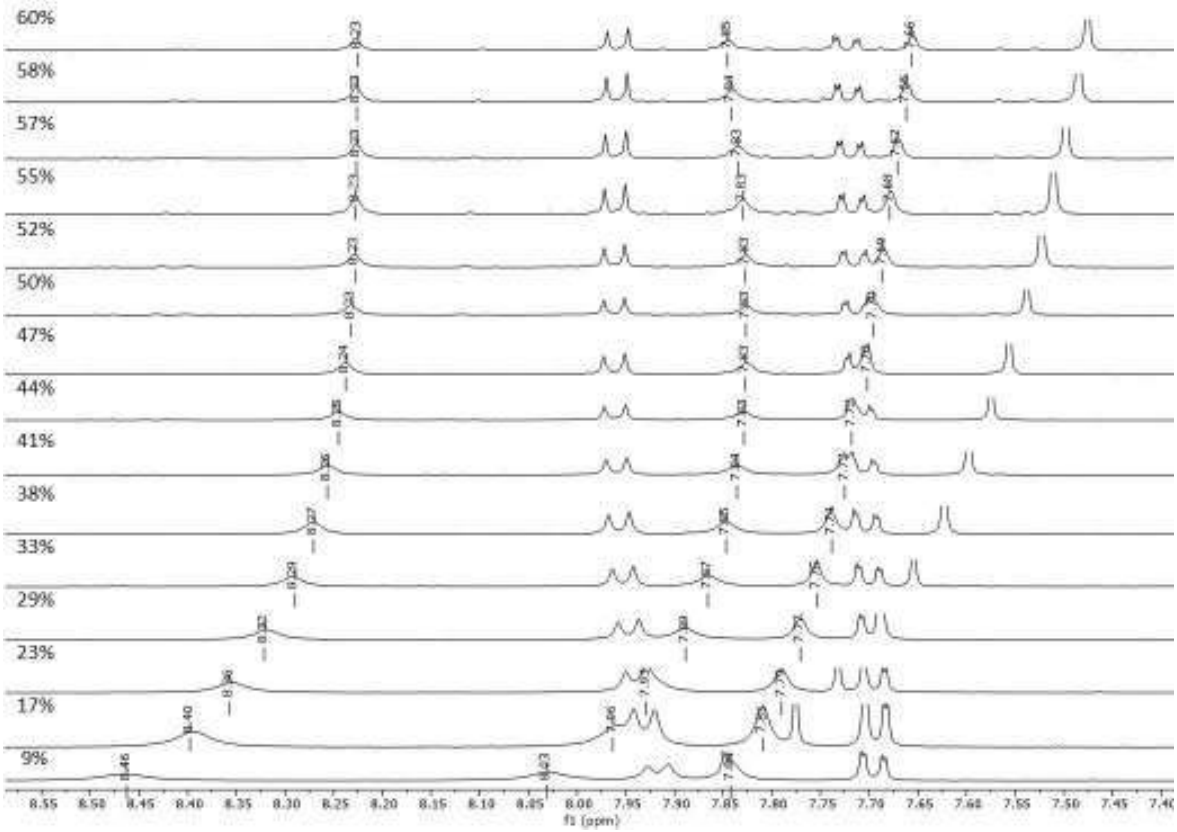

Figure 6: ^{1}H NMR titration of a solution of **69** in methanol-d_4 with $CDCl_3$. $CDCl_3$ percentual increases from the bottom to the top.

As can be seen in Figure 6, during the titration all the peaks start shifting for effect of both the dilution and the change of polarity of the medium. In particular, the resonances of the triphenylenic CH and the CH between the carboxylic and the aryl ether moiety started to move upfield with a Δδ up to -0.4 ppm, until they reached a constant value once the ration between $CDCl_3$ and methanol-d_4 was 1:1. In Figure 7 are reported the chemical shifts of the three signals cited against the addition of $CDCl_3$. On the contrary, all the other resonances of **69** showed much smaller down-filed shift, with Δδ up to a maximum of 0.1 ppm.

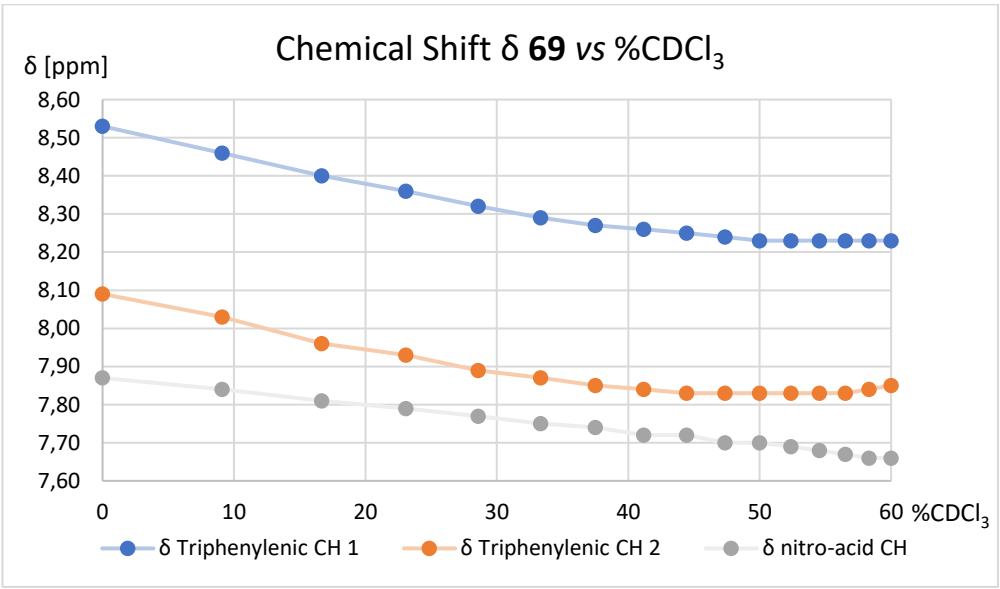

Figure 7: ^{1}H NMR chemical shifts of the titration of a solution of **69** in methanol-d_4 with $CDCl_3$. Three different signals are followed.

The plot of Figure 7 shows that after a $CDCl_3$/methanol-d_4 ratio of 1:1 a plateau is reached; therefore, the system is no longer influenced by the addition of apolar solvent. This could mean that, if dimeric aggregates are formed, a 1:1 ratio between polar and apolar is a good compromise between solubility and H-bond interactions without interference from the polar solvent. The formation of a dimeric capsule is further supported by the fact that the three most influenced signals by the addition of $CDCl_3$ are the two triphenylenic protons and the inner proton of the nitro-acid aryl moiety. In fact, with the formation of the dimer, the triphenylenic protons are shielded due to their reciprocal proximity and the nitro-aromatic C-H pointing inward in the cavity, experiencing a strong shielding effect due to the presence of several aromatic units on the surface of the dimeric capsule and their anisotropic effect (Figures 6 and 7). Interestingly, benzylic signals sharpen with the addition of $CDCl_3$ (see Experimental Section) due to their position on the external surface of the capsule, not being affected by the formation of the dimeric assembly

To add more evidences to our interpretations of the experimental data, pseudo-2D-DOSY NMR were run on samples of the triacid **69** and ester **67**, using the 1:1 $CDCl_3$/methanol-d_4 mixture as solvent. By not having the possibility to establish hydrogen bonds, ester **67**, which has the same molecular size of triacid **69**, can be used as a standard for a molecule not interacting with others. It is therefore expected that under identical solvent conditions the diffusion coefficient of the acid should be lower than that of the ester due to aggregation phenomena. Unfortunately, neither in 1:1 $CDCl_3$/methanol-d_4 nor in methanol-d_4 the triester **67** was only sparingly soluble, hampering a correct determination of the diffusion coefficient in solution.

However, pseudo-2D DOSY NMR spectra of **69** in DMSO-d_6 were recorded, a solvent where the molecule is present as a monomer, and the results were compared to those done in methanol-d_4, solvent in which the possible dimeric capsule was observed. Through the Stokes-Einstein equation, the two diffusion coefficient gave the hydrodynamic radius of the species in solution, showing how the hydrodynamic radius of **69** in methanol-d_4 is ca. 20% bigger than the hydrodynamic radius in DMSO-d_6. This increment is further indicative of the formation of a dimeric capsule in solution.

Due to the lack of time, it was not possible to investigate the host-guest properties of such capsule, which, once determined, will confirm the dimeric structure of the nitro tri-acid **69** in methanol-d_4.

6.3 Experimental Section

6.3.1 General Methods

The reactions were followed with TLC Polygram® Sil G/UV254, 0.25 mm thickness. ^{1}H NMR, ^{13}C NMR, and 2D spectra were recorded with a Bruker Avance 300 and Ascend 400 spectrometers, working at 300-400 and 75-100 MHz respectively. Resonance frequencies are referred to tetramethylsilane. ^{31}P NMR and ^{19}F NMR were recorded with a Bruker Ascend 400, working at 162 e 376 MHz respectively. DOSY experiments were performed the BPLED sequence, calibrating the diffusion time (Δ) in order to obtain a signal ratio of 20 between *gpz* = 2 and *gpz* = 95, and elaborated with Bruker Topspin and Dynamics Center. IR spectra were recorded with a Perkin Elmer Spectrum One spectrophotometer. Mass spectrometric measurements were performed using a Finningan LCQ Deca XP Max mass spectrometer coupled to electrospray ionisation source (ESI) in positive or negative mode. Reagents and solvents with high purity degree purchased by the providers were used as given. Otherwise, they were purified following the procedures reported in literature.[8] Anhydrous solvents were prepared by adding activated 3 Å molecular sieves to the solvent under inert atmosphere. Molecular sieves were activated shortly before the use by continuous heating under *vacuum*. Flash chromatography were performed with silica gel Merk 60, 230-400 mesh, following procedures reported in literature.[9]

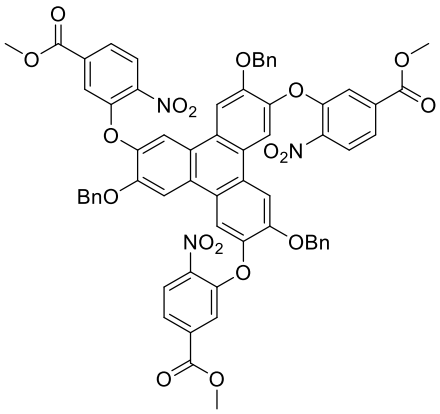

67

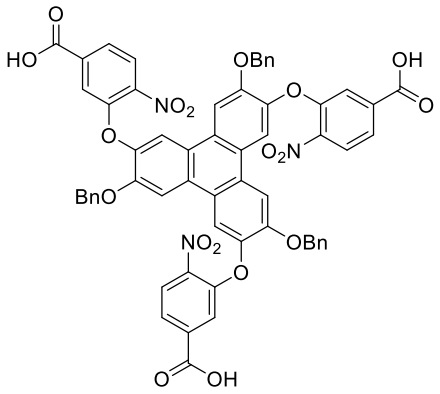

69

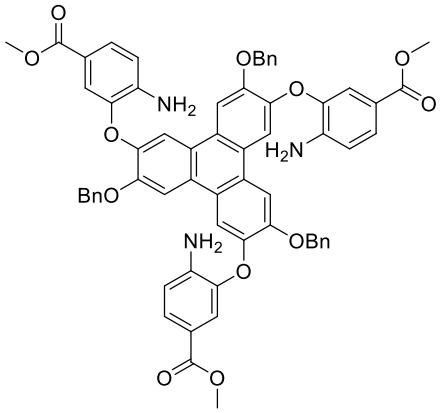

68

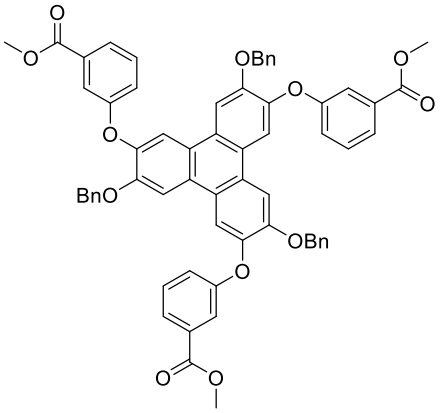

65

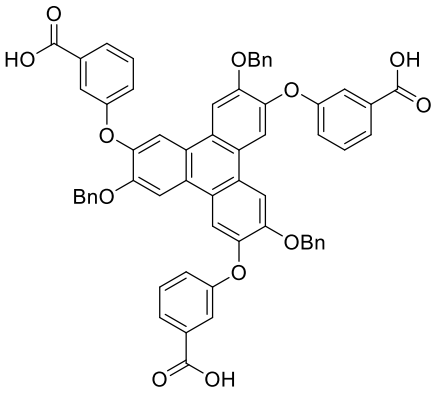

63

6.3.2 Experimental Procedures - Syntheses

Trimethyl 3,3',3''-((3,7,11-tris(benzyloxy)triphenylene-2,6,10-triyl)tris(oxy))tris(4-nitrobenzoate) (**67**):

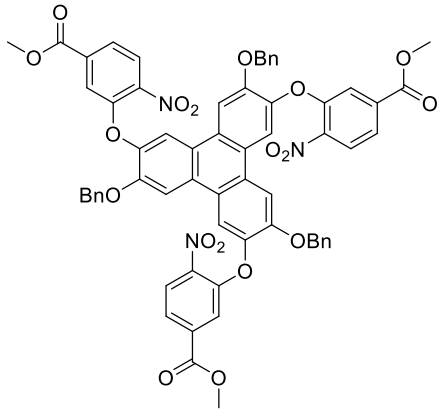

67

In a 10 mL screw-caped Pyrex test tube, a mixture of ***C*$_3$-26** (0.21 g, 0.35 mmol), methyl 3-fluoro-4-nitrobenzenecarboxylate (0.21 g, 1.0 mmol) and anhydrous K_2CO_3 (0.28 g, 2.0 mmol) in dry DMF (5 mL) was heated at 90 °C for 24 hours. The reaction was poured in water (100 mL) and extracted with DCM (3×30 mL). The combined organic layers were dried over $MgSO_4$, filtered and concentrated in *vacuum*. The crude of the reaction was purified by gradient flash chromatography (eluent from DCM/CyH 8:2 to pure DCM), affording the product as a yellow solid (0.36 g, 0.32 mmol, 90% yield). M.P. 276 °C. ^{1}H NMR (400 MHz, $CDCl_3$): δ 8.17 (3H, s), 7.94 (3H, d, *J* = 8.5 Hz), 7.81 (3H, s), 7.70 (3H, dd, *J* = 8.5, 1.6 Hz), 7.62 (3H, d, *J* = 1.6 Hz), 7.19-7.06 (9H, set of m), 6.95 (6H, d, *J* = 6.7 Hz), 5.30 (6H, s), 5.09 (9H, s). $^{13}C\{^1H\}$ NMR (101 MHz): δ 165.0, 151.9, 149.8, 142.4, 142.2, 135.9, 134.9, 128.5, 128.32, 127.9, 126.9, 125.8, 123.1, 122.9, 118.8, 117.2, 107.6, 70.7, 60.5, 53.6, 53.0. IR (KBr): ν 3027, 2951, 1726, 1621, 1592, 1529, 1507, 1429, 1412, 1353, 1288, 1267, 1219, 1135, 1079, 1025, 987, 838, 770, 742, 700 cm^{-1}.

3,3',3''-((3,7,11-tris(benzyloxy)triphenylene-2,6,10-triyl)tris(oxy))tris(4-nitrobenzoic acid) (**69**):

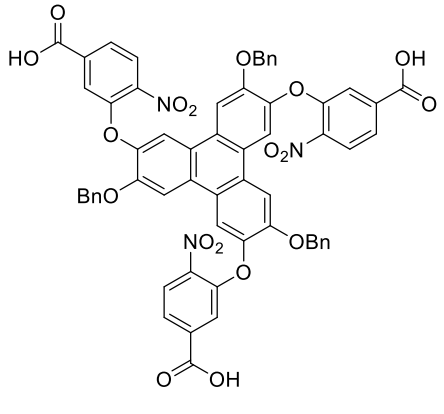

69

In a 10 mL screw-caped Pyrex test tube, a mixture of **67** (0.025 g, 0.02 mmol) and aqueous NaOH (0.15 mL, 2.5 M) in THF (1 mL) was heated at 50 °C for 5 hours. Aqueous HCl (1 M) was added until acidic pH and the resulting mixture was extracted with DCM (3×10 mL).

Combined organic layers were dried over $MgSO_4$, filtered and concentrated in *vacuum*. The product was obtained as a yellow solid, without the need of further purifications (0.024 g, 0.02 mmol, 98% yield). M.P. 270 °C. ^{1}H NMR (400 MHz, DMSO-d_6): δ 8.95 (3H s), 8.50 (3H, s), 8.15 (3H, d, *J* = 8.4 Hz), 7.76 (3H, dd, *J* = 8.4, 1.6 Hz), 7.39 (3H, d, *J* = 1.7 Hz), 7.30-7.16 (9H, m), 7.15-7.02 (6H, set of m), 5.37 (6H, s). $^{13}C\{^1H\}$ NMR (100 MHz): δ 186.2, 165.3, 150.9, 149.6, 141.9, 141.5, 136.3, 128.5, 128.2, 127.7, 126.9, 125.8, 123.0, 122.8, 118.6, 117.1, 108.7, 70.1. IR (KBr): ν 2963, 1700, 1589, 1525, 1507, 1428, 1262, 1098, 1027, 839, 803, 746 cm^{-1}.

Trimethyl 3,3',3''-((3,7,11-tris(benzyloxy)triphenylene-2,6,10-triyl)tris(oxy))tris(4-aminobenzoate) (**68**):

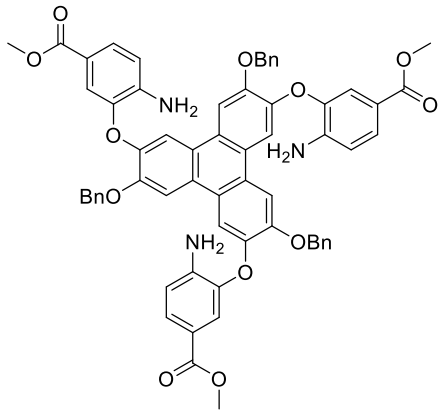

68

In a 25 mL two-necked round-bottomed flask, equipped with condenser, a mixture of $SnCl_2$ (0.94 g, 5 mmol) in absolute EtOH (41 mL) was heated at 80 °C under inert atmosphere. A solution of **67** (0.230 g, 0.21 mmol) in DCM (5 mL) was added dropwise to the boiling solution and heating was maintained for further 4 hours. A second aliquot of $SnCl_2$ (0.47 g, 2.5 mmol) was added and the system heated at 40 °C for 16 hours. The cooled reaction mixture was poured on ice and saturated aqueous Na_2CO_3 was added until basic pH. The resulting mixture was extracted with AcOEt (3×30 mL) and the combined organic layers were dried over $MgSO_4$, filtered and concentrated in *vacuum*. The reaction crude was purified by flash chromatography (eluent CyH/AcOEt 1:1), affording the product as a yellowish solid (0.14 g, 0.13 mmol, 61% yield). M.P. 231 °C. ^{1}H NMR (400 MHz, DMSO-d_6): δ 8.64 (3H, s), 8.30 (3H, s), 7.52 (3H, dd, *J* = 8.4, 1.9 Hz), 7.30-7.12 (18H, set of m), 7.05 (3H, d, *J* = 1.9 Hz), 6.85 (3H, d, *J* = 8.3 Hz), 5.37 (6H, s), 3.62 (9H, s). $^{13}C\{^1H\}$ NMR (100 MHz): δ 166.1, 150.1, 144.3, 143.8, 143.6, 136.8, 128.2, 127.6, 127.2, 127.0, 125.4, 122.8, 117.6, 115.9, 114.6, 113.5, 108.2, 69.7, 51.3. IR (KBr): ν 3653, 3351, 2946, 1701, 1621, 1506, 1428, 1289, 1262, 1199, 1145, 1096, 1026, 907, 766, 700 cm^{-1}.

Trimethyl 3,3',3''-((3,7,11-tris(benzyloxy)triphenylene-2,6,10-triyl)tris(oxy))tribenzoate (**65**):

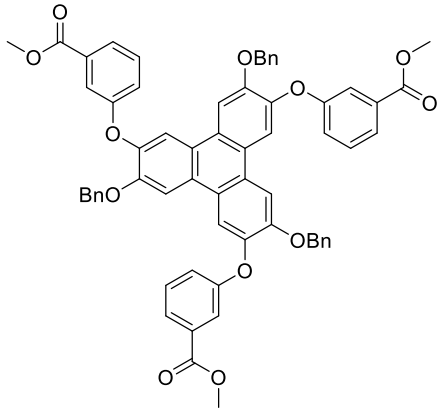

65

In a 25 mL two-necked round-bottomed flask, , to a solution of *t*-BuONO (0.64 g, 5.2 mmol, 620 µL) and DMSO (0.04 g, 0.44 mmol, 30 µL) in THF (28.5 mL), a solution of **67** (0.116 g, 0.11 mmol) in THF (1 mL) was added dropwise under inert atmosphere at room temperature. After 5 hours volatile materials were removed in *vacuum*, and the residue was purified by gradient flash chromatography (eluent from DCM/CyH 8:2 to pure DCM), affording the product as a white solid (0.04 g, 0.04 mmol, 36% yield). M.P. 198 °C. ^{1}H NMR (400 MHz, $CDCl_3$): δ 8.12 (3H, s), 7.89 (3H, s), 7.78 (3H, dt, *J* = 7.7, 1.3 Hz), 7.66 (3H, dd, *J* = 2.6, 1.5 Hz), 7.40 (3H, t, *J* = 8.0 Hz), 7.-7.19 (12H, set of m), 7.11 (6H, dt, *J* = 4.8, 3.6 Hz), 5.19 (6H, s), 3.86 (9H, s). $^{13}C\{^{1}H\}$ NMR (100 MHz): δ 166.8, 158.9, 150.5, 144.3, 136.3, 131.9, 129.7, 128.6, 128.0, 127.6, 127.2, 123.7, 123.5, 121.3, 117.3, 116.8, 107.9, 70.9, 52.3. IR (KBr): ν 3663, 2951, 1728, 1622, 1606, 1586, 1507, 1484, 1447, 1429, 1379, 1273, 1208, 1186, 1145, 1093, 1079, 1027, 1000, 896, 872, 844, 804, 756, 700, 676, 470 cm^{-1}.

3,3',3''-((3,7,11-tris(benzyloxy)triphenylene-2,6,10-triyl)tris(oxy))tribenzoic acid (**63**):

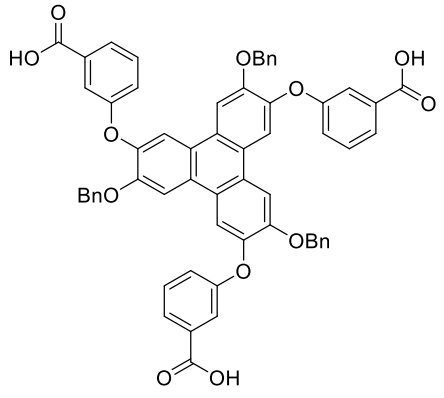

63

In a 25 mL two-necked round-bottomed flask, equipped with condenser, a mixture of **65** (0.03 g, 0.03 mmol) and aqueous NaOH (2.6 mL, 2.5 M) in THF (17.4 mL) was heated at 50 °C for 24 hours. Aqueous HCl (1 M) was added until acidic pH and the resulting slurry was extracted with AcOEt (3×10 mL). Combined organic layers were dried over $MgSO_4$, filtered and concentrated in *vacuum*. The product was obtained as a white solid, without the need of further purifications (0.016 g, 0.017 mmol, 55% yield). M.P. 303 °C. ^{1}H NMR (400 MHz,

DMSO-d_6) δ 8.77 (3H, s), 8.41 (3H, s), 7.67 (3H, d, *J* = 7.7 Hz), 7.50 (3H, t, *J* = 8.0 Hz), 7.41 (3H, t, *J* = 2.1 Hz), 7.29 (3H, dd, *J* = 8.2, 2.7 Hz), 7.23-7.18 (9H, set of m), 7.10-7.60 (6H, set of m), 5.35 (6H, s). $^{13}C\{^1H\}$ NMR (100 MHz) δ 166.9, 158.7, 150.4, 143.0, 136.7, 132.4, 130.0, 128.2 (2C), 127.8, 127.7, 127.0 (2C), 122.9, 120.4, 118.3, 115.6, 69.9. IR (KBr): ν 3649, 2917, 2846, 1689, 1587, 1507, 1425, 1264, 1222, 1142, 1023, 926, 754, 698 cm^{-1}.

6.3.3 NMR and MS Spectra

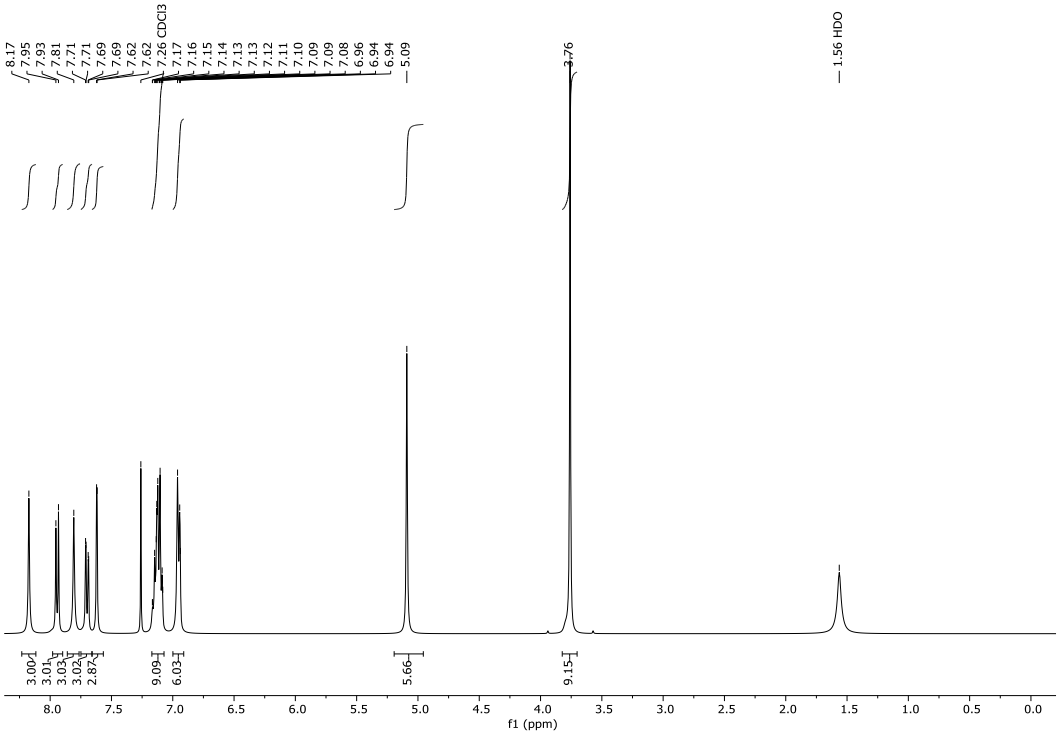

Figure I: ^{1}H NMR of molecule **67**.

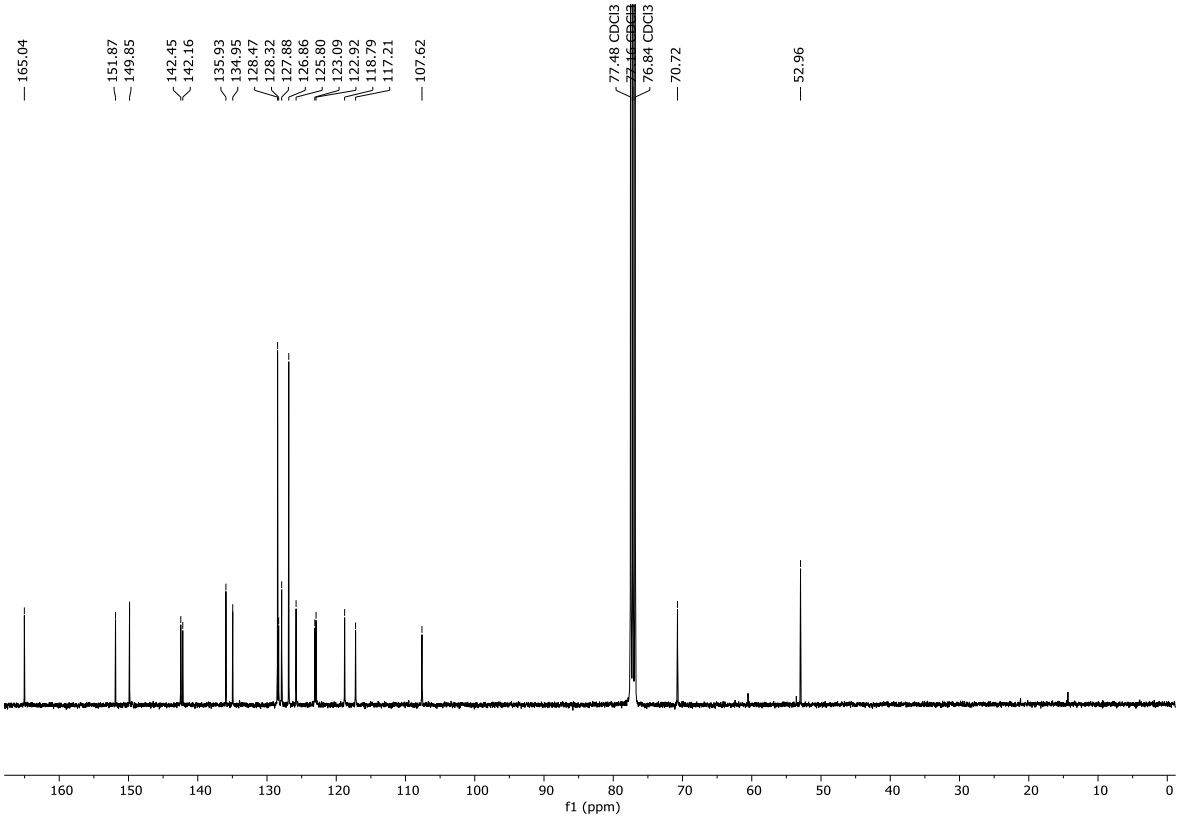

Figure II: ^{13}C NMR of molecule **67**.

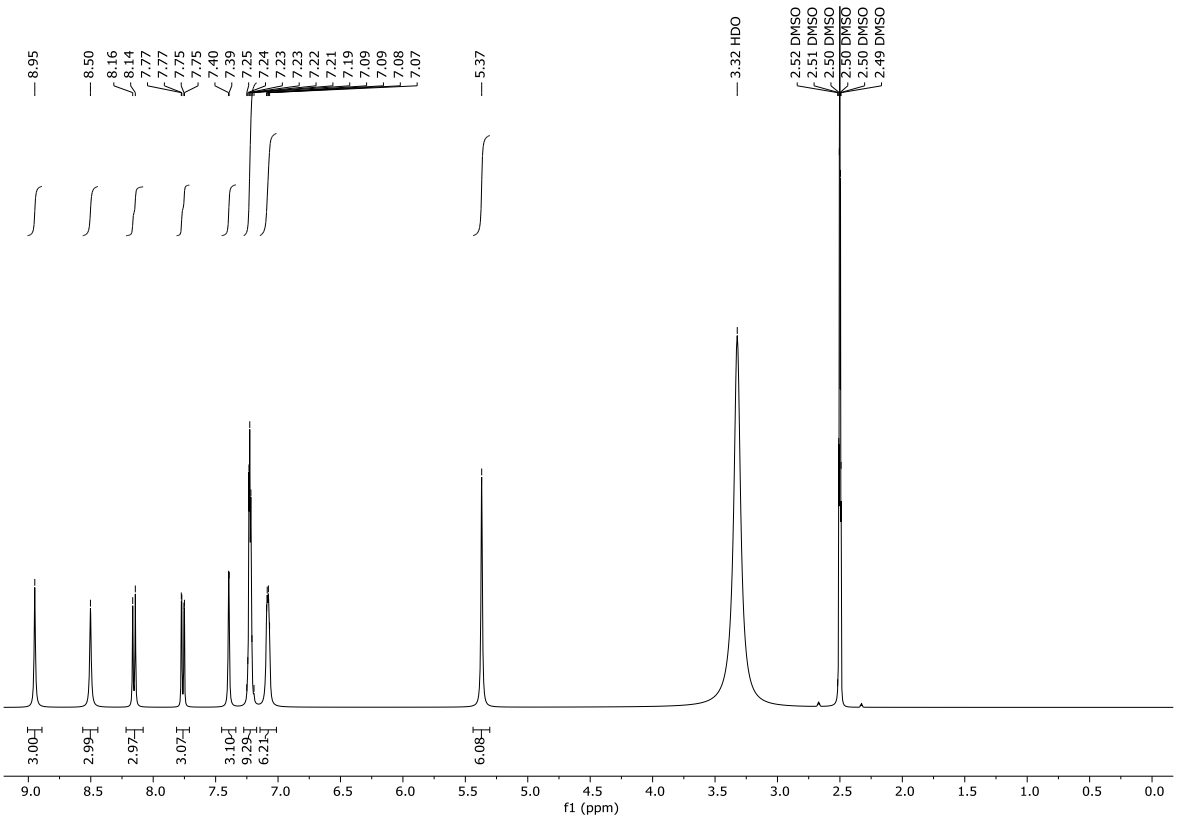

Figure III: ^{1}H NMR of molecule **69**.

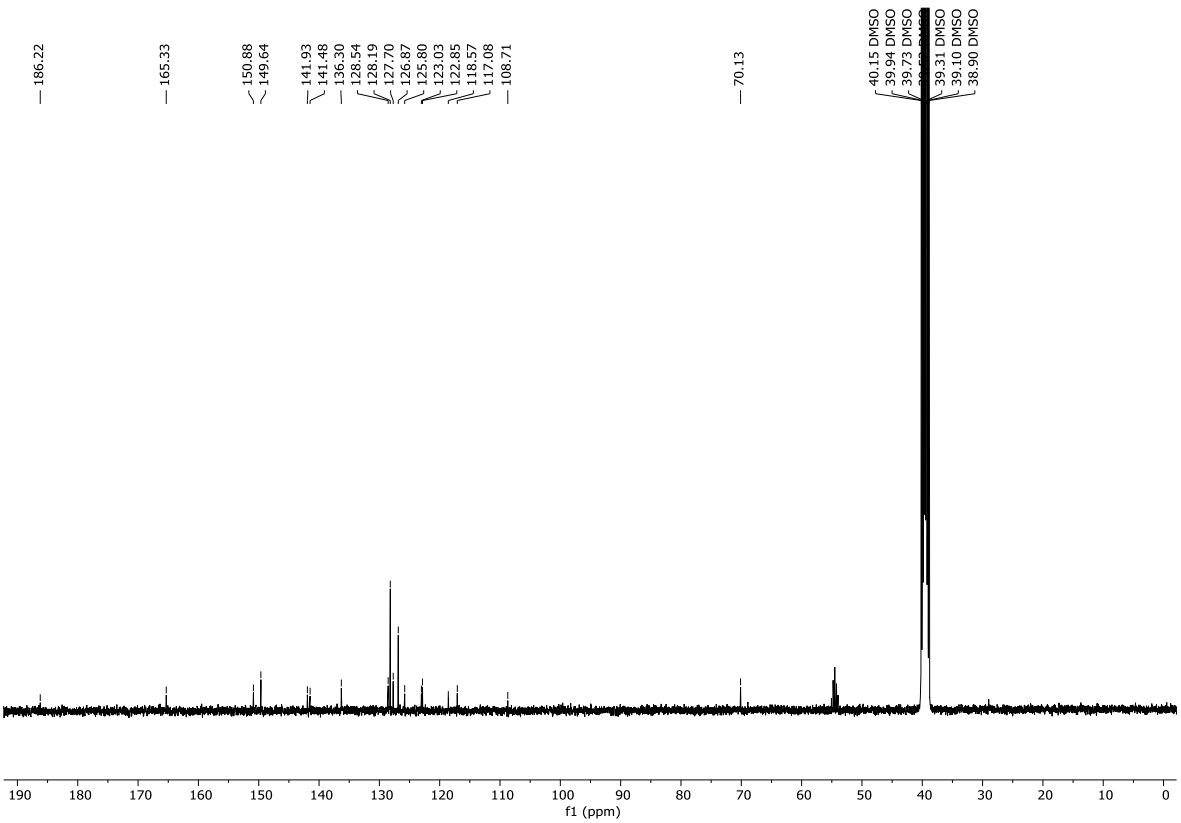

Figure IV: ^{13}C NMR of molecule **69**.

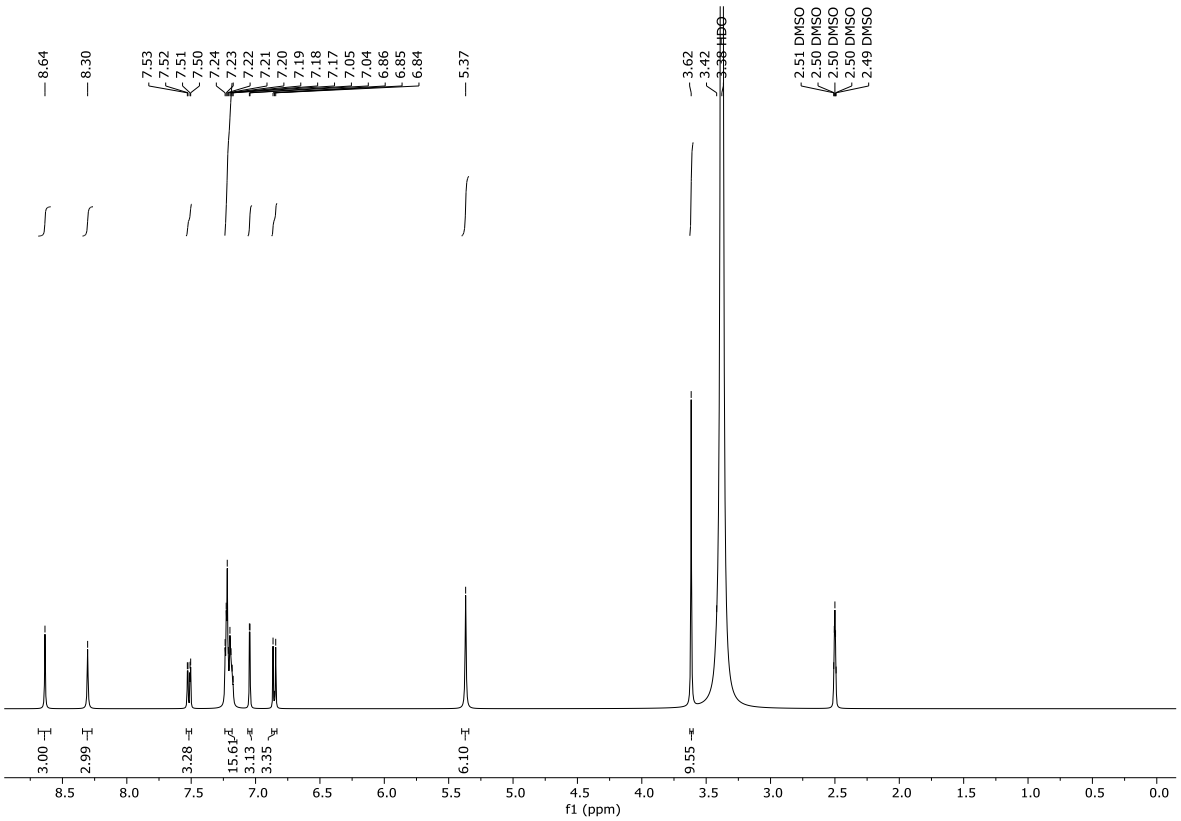

Figure V: ^{1}H NMR of molecule **68**.

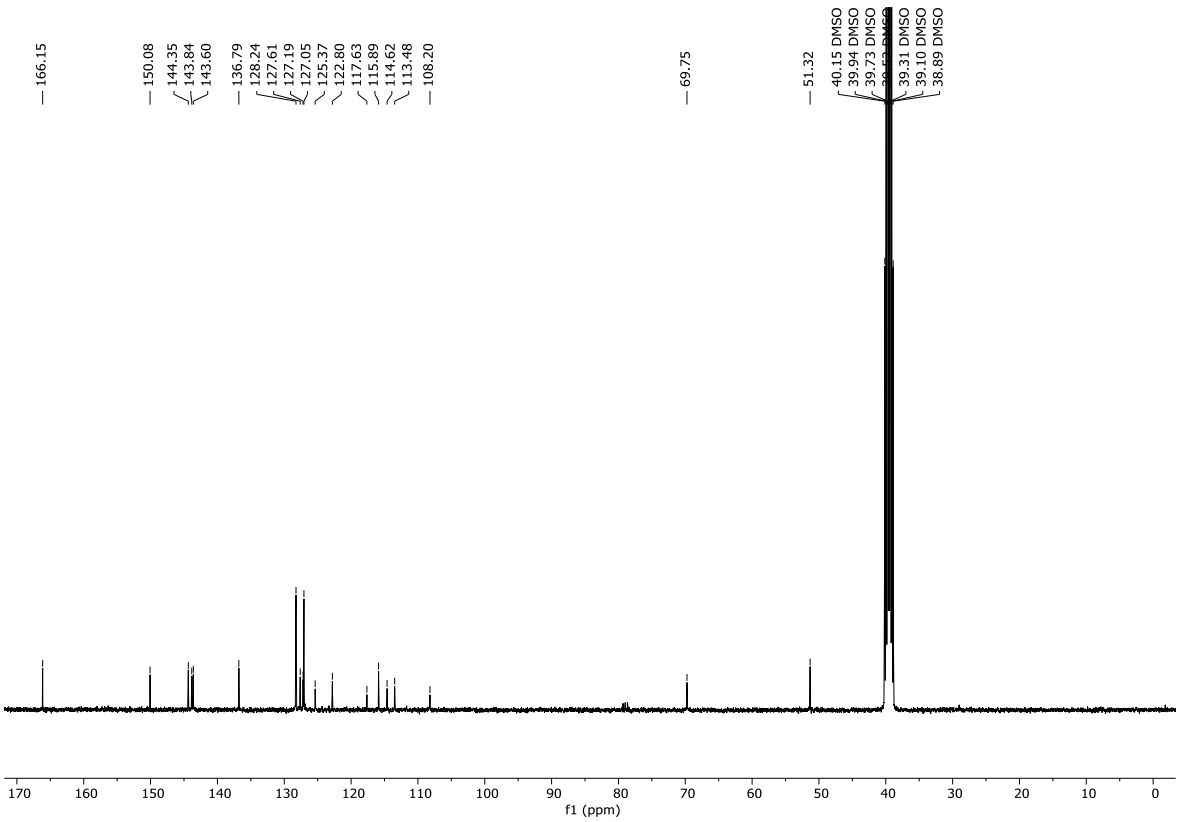

Figure VI: ^{13}C NMR of molecule **68**.

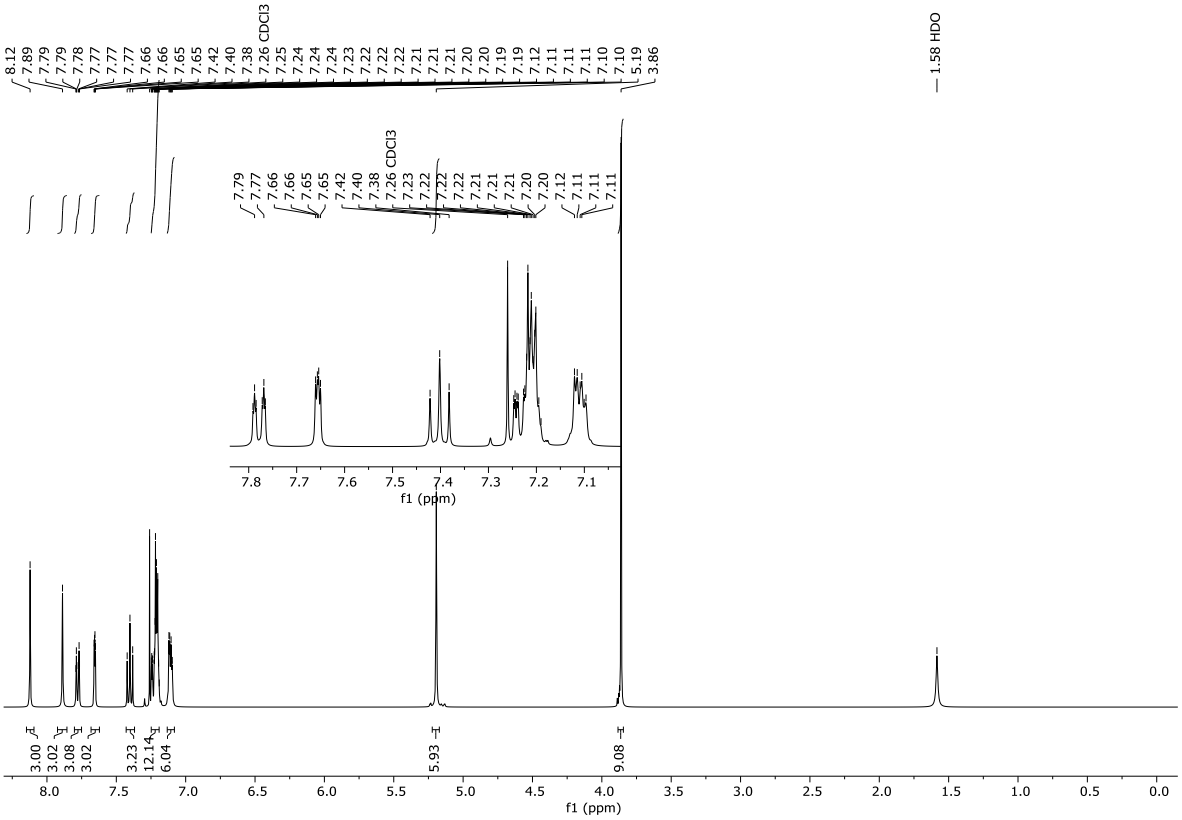

Figure VII: ^{1}H NMR of molecule **65**.

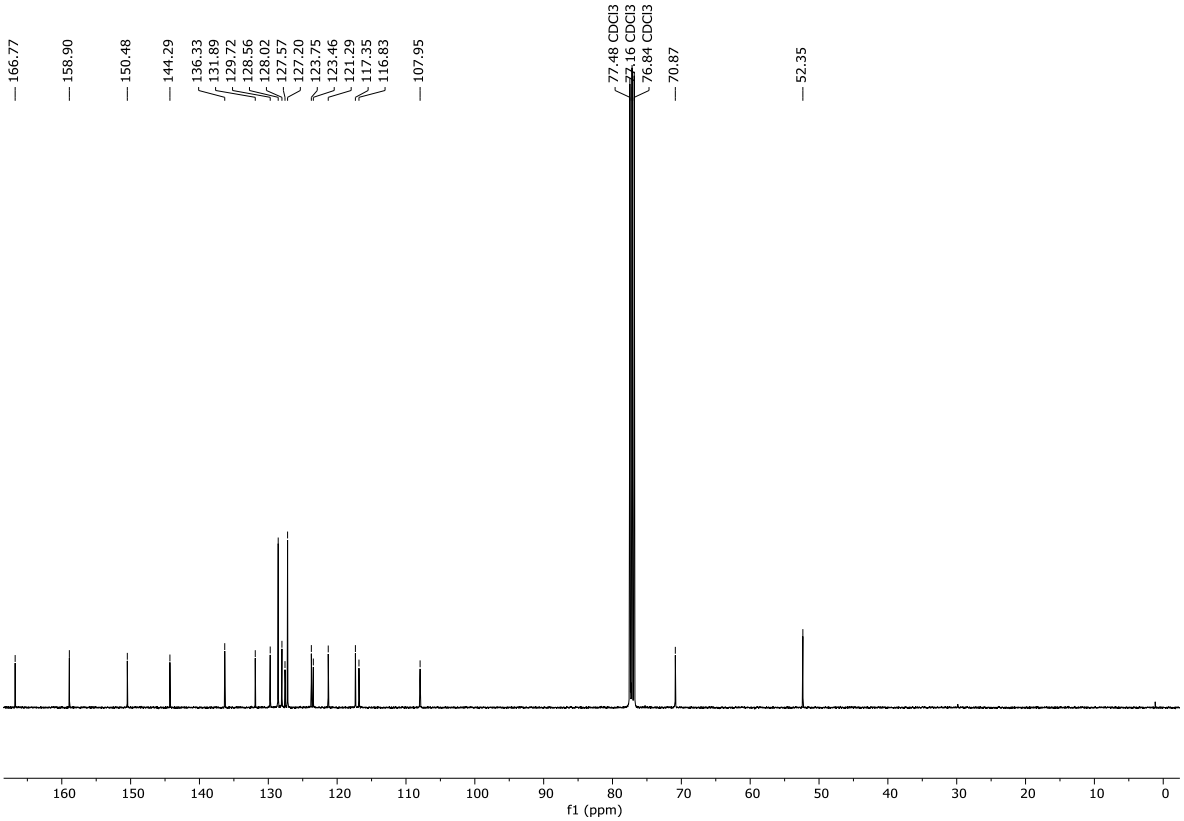

Figure VIII: ^{13}C NMR of molecule **65**.

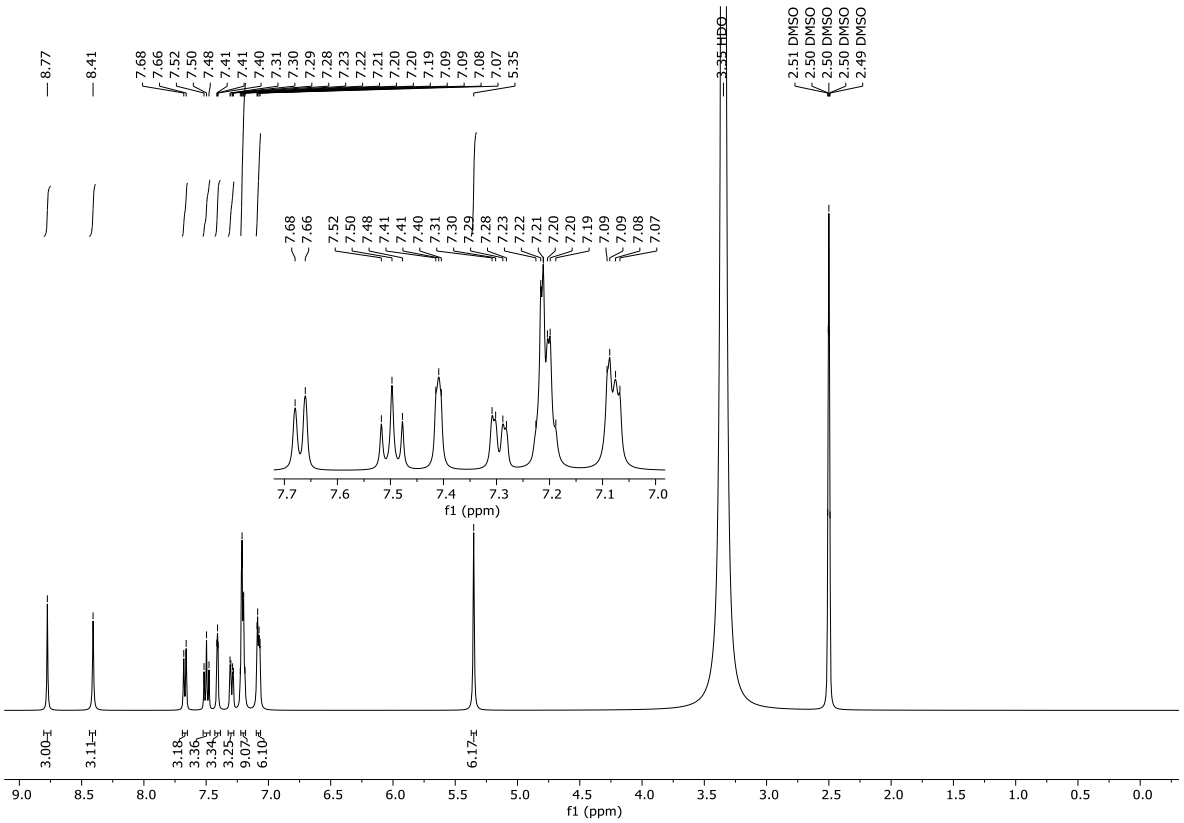

Figure IX: ^{1}H NMR of molecule **63**.

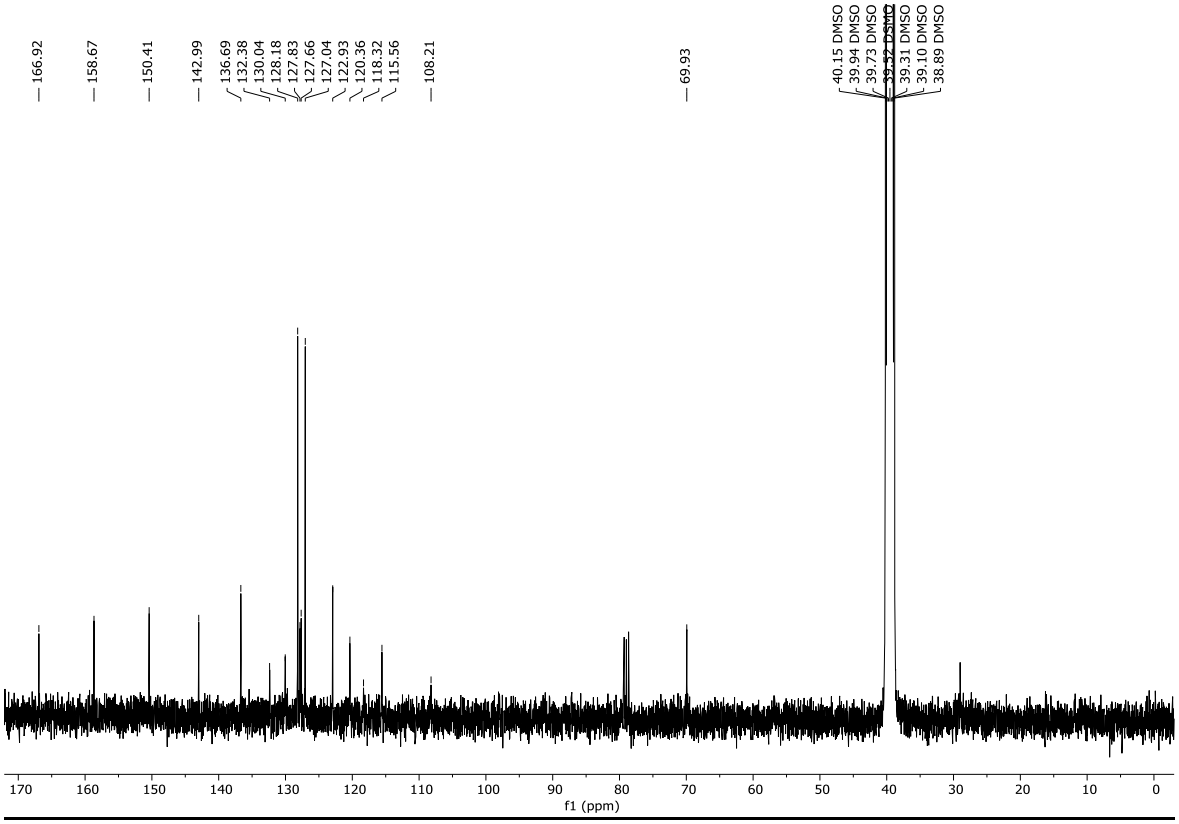

Figure X: ^{13}C NMR of molecule **63**.

6.4 Bibliography

1 R. M. Grotzfeld, N. Branda, J. Rebek Jr., *Science*, **1996**, *271*, 487-489.

2 S. Mecozzi, J. Rebek Jr., *Chem. Eur. J.*, **1998**, *4*, 1016-1022

3 C. H. Burgos, T. E. Barder, X. Huang, S. L. Buchwald, *Angew. Chem. Int. Ed.*, **2006**, *45*, 4321-4326.

4 G. V. López, E. M. Pandolfi, G. A. Seoane, *Synthesis*, **2000**, *10*, 1403-1408.

5 F. D. Bellamy, K. Ou, *Tetrahedron Letters*, **1984**, *8*, 839-842.

6 L. Fang, L. Qi, L. Ye, Z. Pan, W. Luo, F. Ling, W. Zhong, *J. Chem. Res.*, **2018**, *42*, 579-583.

7 D. E. Thurston, D. S. Bose, A. S. Thompson, P. W. Howard, A. Leoni, S. J. Croker, T. C. Jenkins, S. Neidle, J. A. Hartley, L. H. Hurley, *J. Org. Chem.*, **1996**, *61,* 8141-8147.

8 W. L. F. Armarego, C. Chai in *Purification of Laboratory Chemicals (Seventh Edition)*, Butterworth-Heinemann, Boston, **2013**.

9 W. C. Still, M. Kahn, A. Mitra, *J. Org. Chem.*, **1978**, *14*, 2923-2925.

7 Water-Soluble Triphenylenes and Micelles

The self-assembly of a precise number of homologous units for the construction of well-defined hollow capsules for transport, catalysis[1] and other supramolecular applications is a challenging task.[2,3] Usually, highly symmetric units are precisely adorned with specific functional groups to engage in weak attractive intermolecular forces like H-bonds,[4] ion-pairing,[5,6,7] metal-ligand coordination[8,9] and recently halogen bond.[10,11] Conversely, the self-assembly in water, even being facilitated by the hydrophobic effect, is characterized by a difficult prevision and a lack of directionality,[12] often providing variable aggregates with a wide distribution of the number of components. Precise self-assembly in water is obtained with amphiphilic units, where the hydrophilic moieties decorate one side of the molecule, leaving the other apolar.[13,14] Examples of well-defined self-assembled small capsules in water through the hydrophobic effect have been provided by the group of Yoshizawa,[15] where polyaromatic semi-rigid scaffolds with a limited flexibility are adorned with charged water-soluble ponytails,[16,17,18,19,20] leading to a large number of nanocontainers for several successful supramolecular applications (Figure 1).

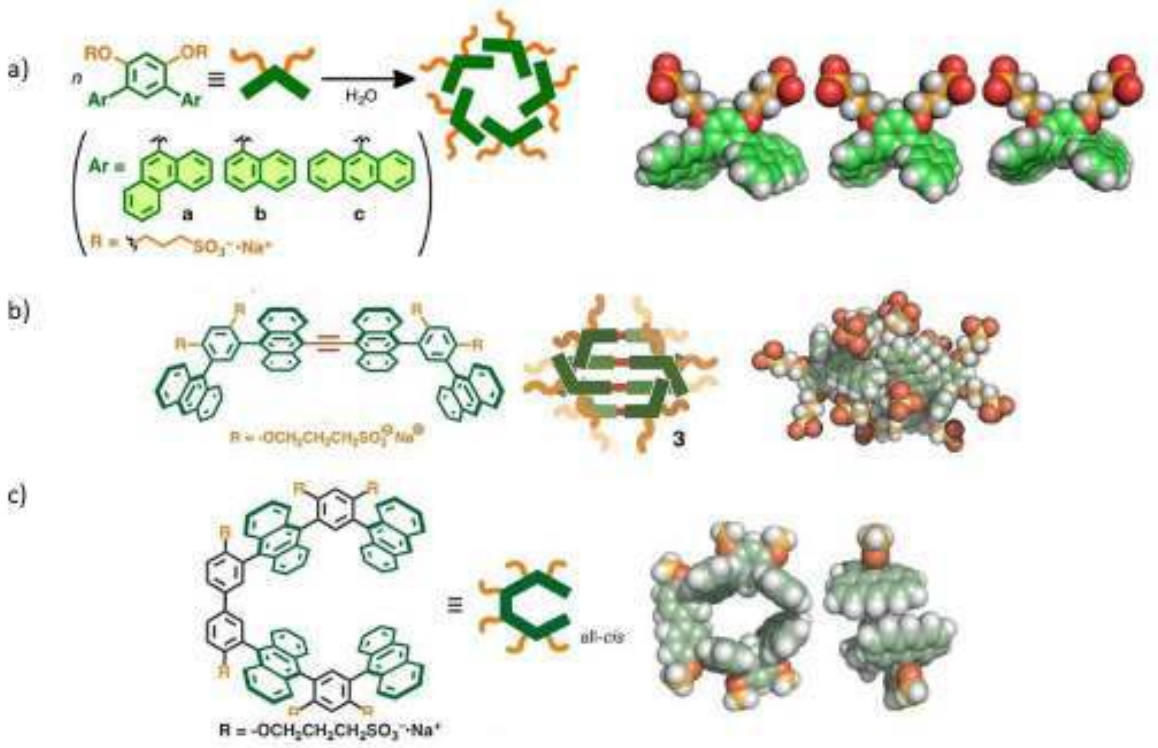

Figure 1: Cartoon representation and optimized structures of a) polyaromatic amphiphile units forming pentameric nanocapsules; b) polyaromatic gemini amphiphile for trimeric micelles; c) water-soluble polyaromatic molecular clip. Adapted respectively from [16], [17] and [18].

When the structure is more concave and decorated on the rim with several charges to impart water solubility, dimeric capsules in the presence of suitable guests are formed like in the examples provided by Gibb,[21] exploited for relevant examples of supramolecular catalysis (Figure 2).[22]

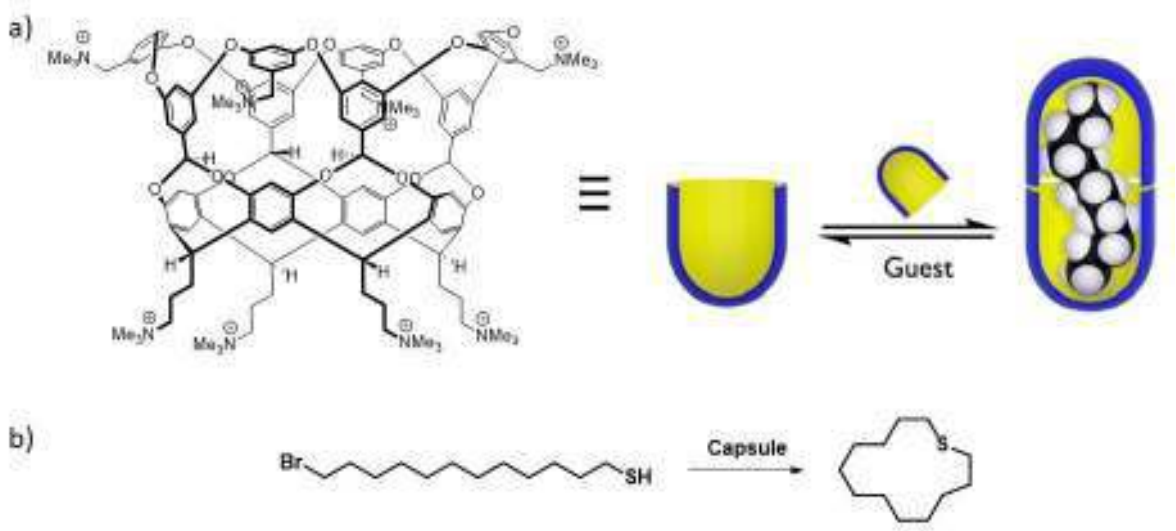

Figure 2: a) formation of Gibb's dimeric capsule; b) example of an intramolecular nucleophilic substitution reaction catalyzed within the cavity of the hydrophobic capsule. Adapted from [22].

The previous examples share a similar aromatic rigid and curved structure with hydrophilic appendages on the rim of the hydrophobic core. Differently, only few examples deal with the self-assembly in water of a precise number of units where the hydrophobic and hydrophilic portions of the amphiphilic monomer are alternated around a common organic core. Specifically, Shionoya and collaborators reported the aggregation of six hexa-substituted aromatic sub-components with alternating aromatic and pyridinium units, forming a nanometric cubic capsule with interdigitating groups (Scheme 1).[23,24]

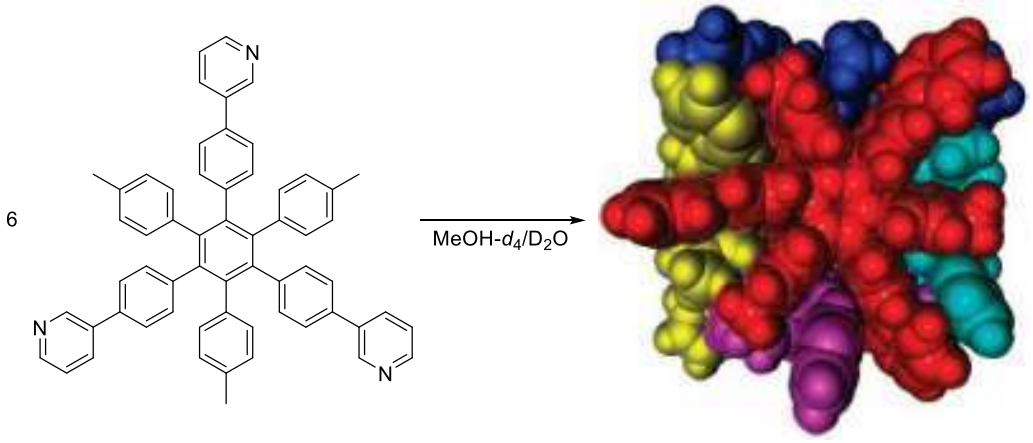

Scheme 1: Shionoya's nanometric cubic capsule aggregation in methanol/water. Adapted from [24].

It is worth to notice that similar organic units, in the presence of adamantane as an apolar smaller templating guest, led to the formation of a small tetrahedral capsule.[25]

A further example of alternated amphiphilic molecule was recently provided by Yoshizawa, based on a rigid *tris*-branched scaffold with an all-*syn* 1,3,5-trimethyl-2,4,6-triphenylbenzene core, forming a tetrameric capsule in water that enabled the hosting of stacked perylene guests, exhibiting unusual *Y*-type excimer-like emission at room temperature (Figure 3).[26]

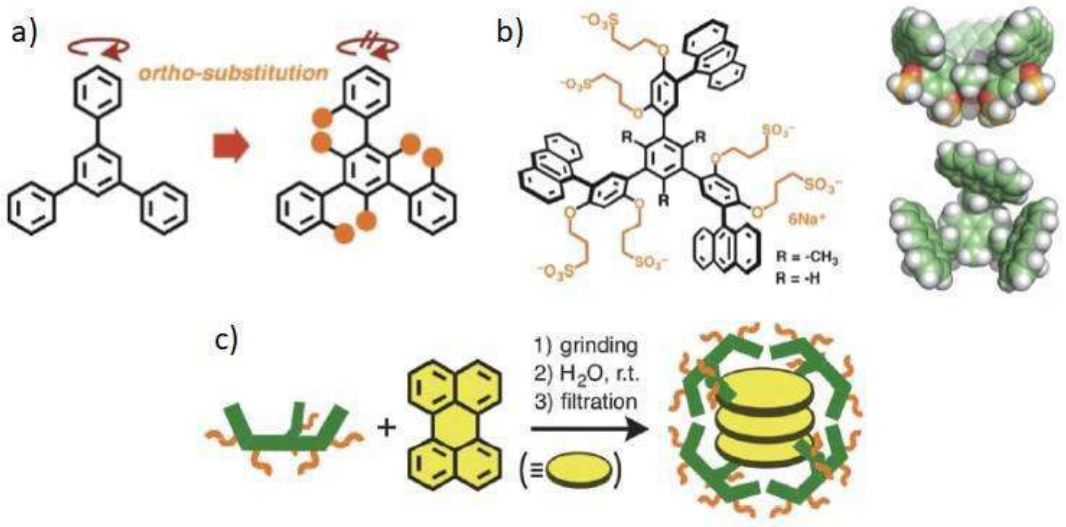

Figure 3: a) *Ortho* hexa-substituted 1,3,5-triphenylbenzene with restricted free rotation around the biphenyl single bonds; b) amphiphilic *tris*-branched scaffolds and optimized structures; c) encapsulation of perylene on the tetrameric assembly. Adapted from [26].

With the idea of creating very small micelle-like nanometric capsules in aqueous medium, based on ***C*$_3$-26** as a starting material, we considered the synthesis of different triphenylenes bearing hydrophilic units, like charged (anionic or cationic) or neutral (MPEG) moieties, alternated with apolar side-chains. It is likely to predict that once in water the three charged branches should move to one side of the triphenylene plane, while the apolar chains should move to the opposite side of the triphenylene. In this way, the polyaromatic central unit assumes a sort of Janus-type structure with a sort of polar side and an apolar side, mimicking the structure of a surfactant and thus enabling the self-assembly in water driven by the hydrophobic effect. However, triphenylenes are often used to create columnar assemblies in the formation of liquid crystal, thus the possibility of the presence of a pillar-like aggregate in water cannot be excluded *a priori* (Figure 4).

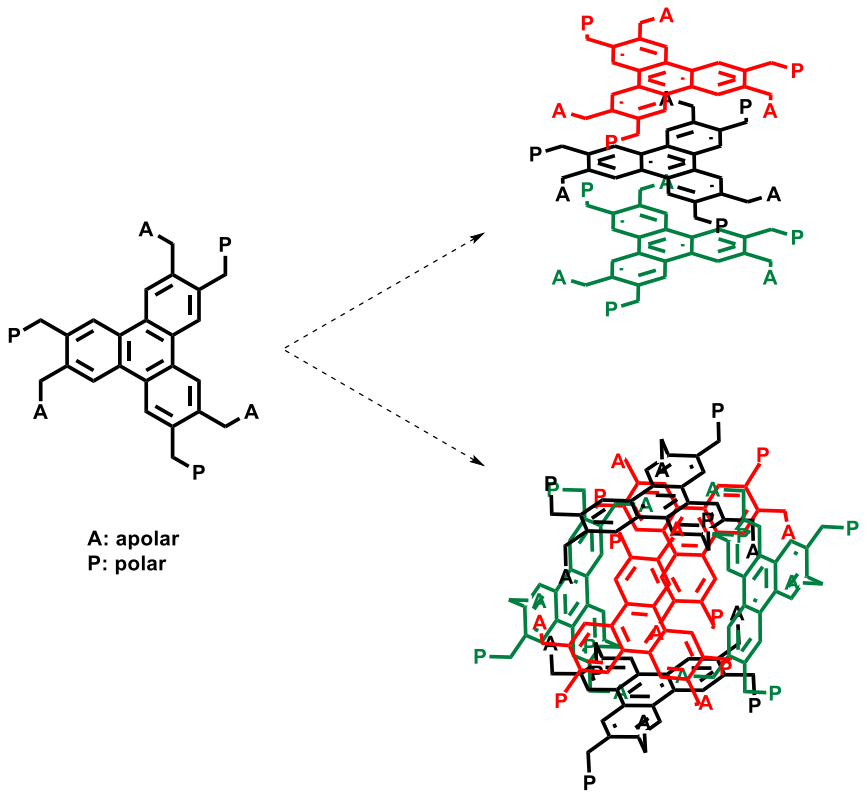

Figure 4: Schematic representation of possible aggregation structures of amphiphilic- triphenylenes in water.

A great part of this work, together with the work reported in Chapter 8, was carried out in collaboration with Prof. Pablo Ballester at the Istitut Català de Investigació Química (ICIQ), Tarragona, during a six-month internship in the second year of the PhD studies.

7.1 Synthesis of Water-Soluble Triphenylenes

Using ***C*$_3$-26** as starting material, the insertion of an anionic moiety resulted to be quite straightforward and it could be done in just one synthetic step. ***C*$_3$-26** was treated with butan sultone, heating at 70 °C in acetone, in the presence of K_2CO_3, for one week (Scheme 2).

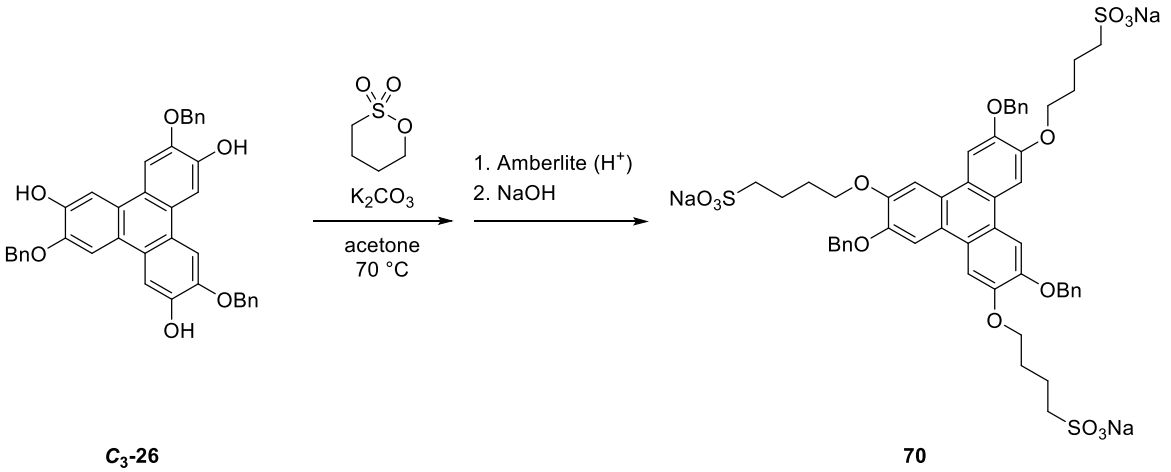

***C*$_3$-26** **70**

Scheme 2: Synthesis of sodium sulfonate **70**.

The crude was rinsed with Et_2O to remove the excess of sultone, then dissolved in water and passed through an Amberlite IR-120© column (acidic form) to remove the excess of K_2CO_3. The obtained conjugated acid was treated with NaOH until neutral pH measured with a pH-meter, achieving, after freeze-drying, the sodium sulfonate **70** in 94% yield.

In order to have another tris-anionic triphenylene with different apolar side chains, the C_3-symmetric *tris*-alkylated derivative **30b** described in Chapter 2 was further functionalized following an identical route (Scheme 3).

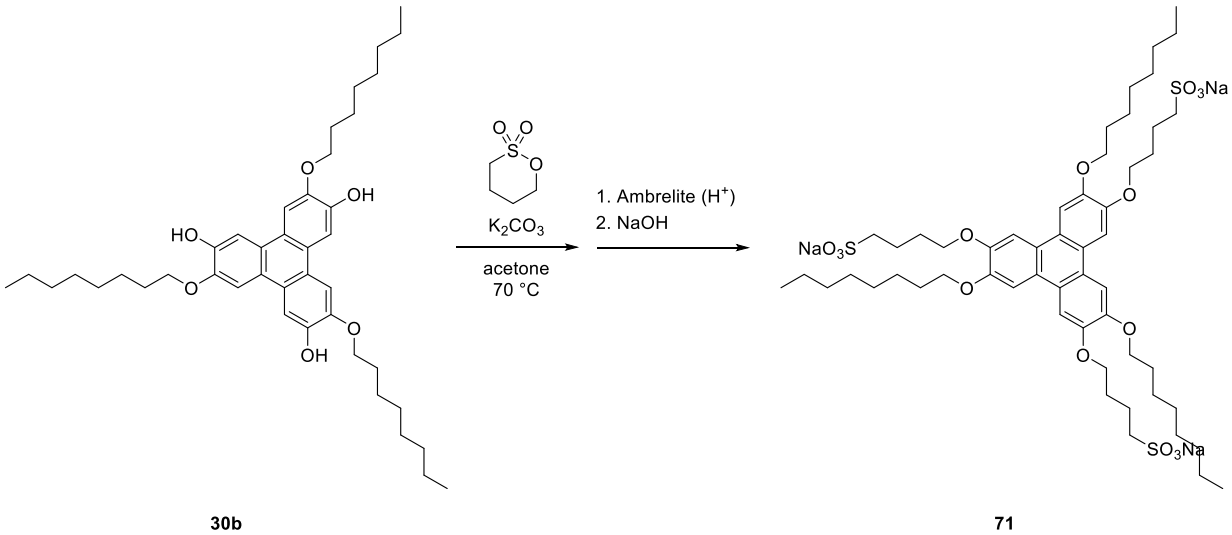

30b **71**

Scheme 3: Synthesis of sodium sulfonate derivative **71**.

After elaboration of the crude, the sodium sulfonate **71** was obtained, after freeze-drying, in 96% yield.

To further complement the two above described amphiphilic units, we decided to synthetize two more derivatives for comparison purposes: a negatively charged triphenylene not provided with the alkyl or benzyl chain, and a positively charged triphenylene. The first should be useful to understand the role of the apolar alkyl chain on the possible aggregation in water, the second to check the effect of positive rather than negative charges for the hydrophilic portion of the molecule.

The de-alkylated sulfonate **72** was obtained by hydrogenation of **70**, using palladium on activated charcoal as catalyst (Scheme 4).

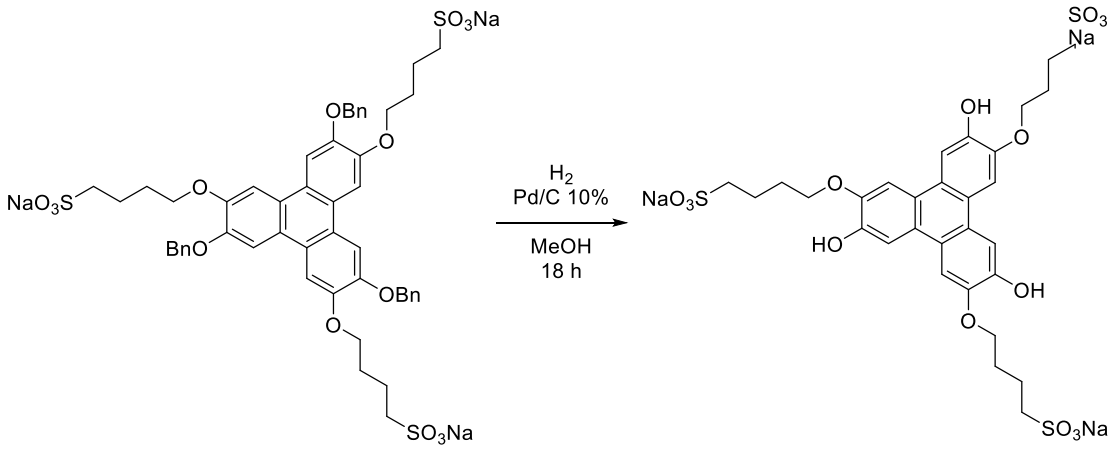

70 **72**

Scheme 4: Synthesis of sodium sulfonate **72** through hydrogenation of **70**.

Product **72** was recovered after filtration of the heterogeneous catalyst with a 90% yield.

For the synthesis of the cationic triphenylene, the synthetic route was not so straightforward, requiring overall three steps. Indeed, starting from ***C*$_3$-26** it was necessary firstly a hydroxy-alkylation, followed by chlorination and a final treatment with pyridine to achieve the corresponding pyridinium salt. The first step was carried out reacting together ***C*$_3$-26** and 4-chlorobutan-1-ol with K_2CO_3 in DMF, at 60 °C for 24 hours (Scheme 5).

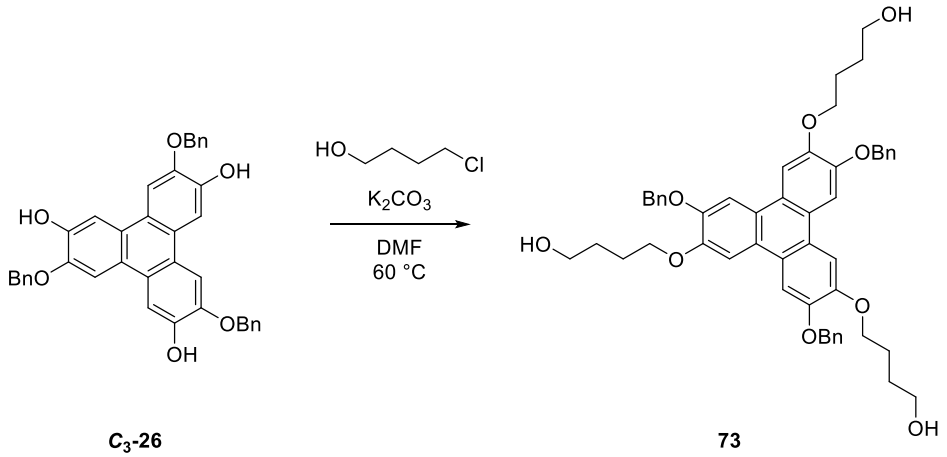

***C*$_3$-26** **73**

Scheme 5: Synthesis of alcohol **73**.

After precipitation from water, product **73** was filtered and recovered in 89% yield. The second step was the chlorination of **73**, which was achieved by treatment of the *tris*-alcohol with thionyl chloride (Scheme 6).[27]

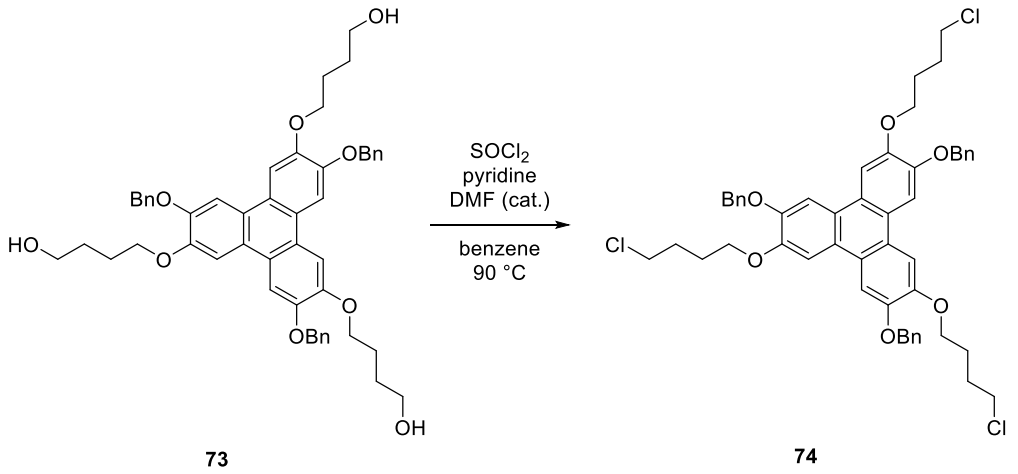

73 74

Scheme 6: Synthesis of chloride **74**.

The reaction crude was purified through column chromatography, affording the product in 48% yield. Last step was the nucleophilic substitution of the chloride with pyridine, that was obtained by heating **74** using pyridine as solvent, overnight at 110 °C (Scheme 7).[28]

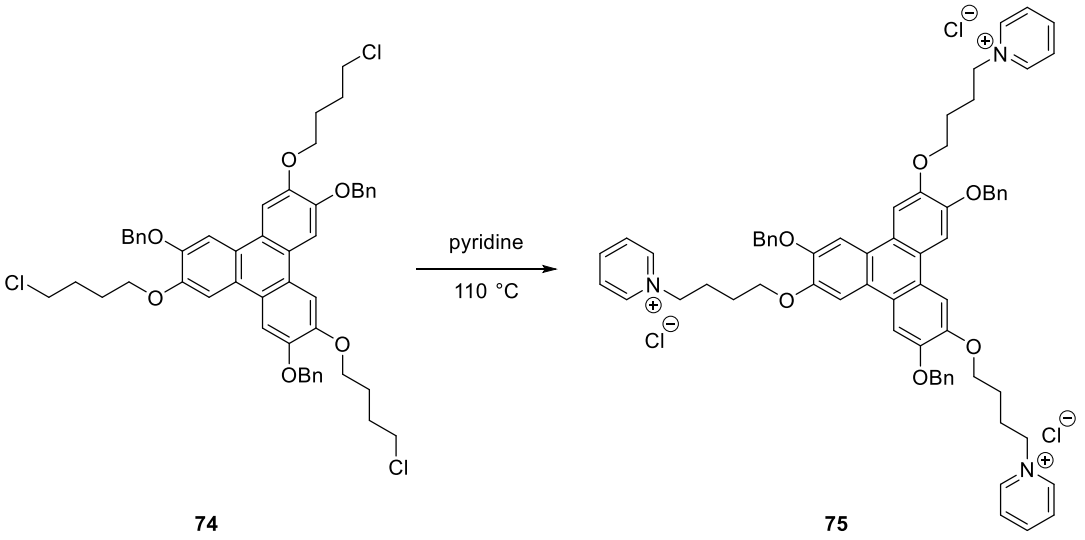

74 75

Scheme 7: Synthesis of pyridinium chloride salt **75**.

The pyridinium salt **75** was isolated in 78% yield after *vacuum* distillation of the excess of pyridine.

After the syntheses of all the ionic triphenylenes, the last synthetic effort was the preparation of a neutral water-soluble amphiphilic triphenylene, introducing a methyl-polyethylene glycol (MPEG) as hydrophilic side chain on the ***C*$_3$-26**. The synthesis started converting the terminal primary alcohol of MPEG 350 **76** into a good leaving group, by treatment with methanesulfonyl chloride (Scheme 8).[29]

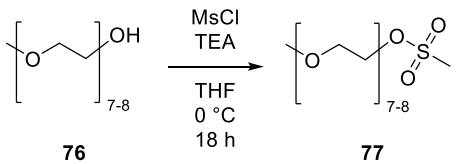

76 77

Scheme 8: Synthesis of methanesulfonated MPEG 350, **77**.

The methanesulfonylated chain **77** was obtained in 90% yield after a work-up procedure to neutralize the excess of methanesulfonyl chloride.

The MPEG chain **77** was linked to ***C*$_3$-26** with an alkylation reaction analogue to those reported in Chapter 2, promoting the substitution reaction with K_2CO_3 in DMF (Scheme 9).

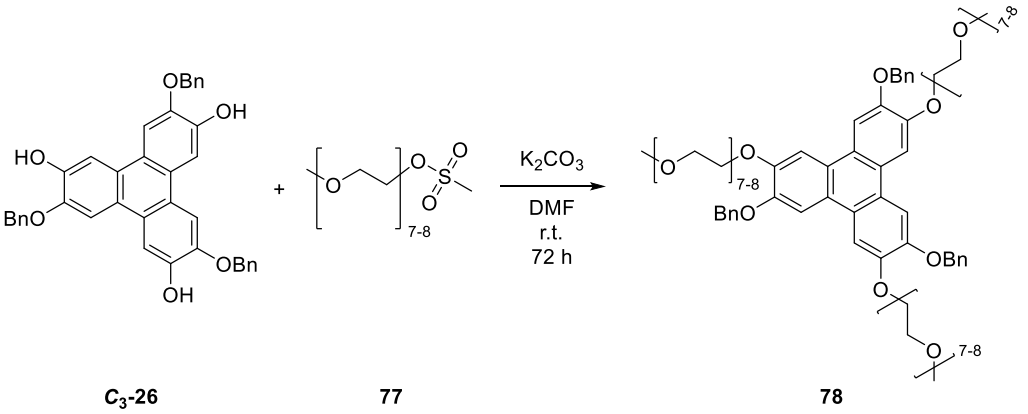

Scheme 9: Synthesis of MPEG 350 substituted triphenylene **78**.

After purification of the crude by exhaustive extraction with methanol, the product **78** was obtained in 50% yield.

All the four ionic and the neutral triphenylenes proved to be soluble in water, with maximum concentration in the range 10-15 mM for **71** and **78**, and up to 60 mM for **70**, **72** and **75**.

The solubility data are in good agreement with the behaviour of many other surfactants of the same nature, indeed ionic surfactants are usually more soluble than neutral ones with comparable apolar side chain and, as a consequence, they usually exhibit higher critical aggregation concentrations (c.a.c.).

7.2 ^{1}H NMR, DOSY, UV-Vis, AFM and DLS Characterization

Once the four water-soluble triphenylenes were available, several techniques were employed to understand their aggregation properties in aqueous medium, like ^{1}H NMR, pseudo 2D DOSY NMR, UV-Vis, dynamic light scattering (DLS) and atomic force microscopy (AFM) on dried samples.

To verify the aggregation of the triphenylenes in water, the first experiment was to register a series of ^{1}H NMR spectra for compound **70** at variable concentrations, since the shifts of the resonances could prove the presence of aggregation phenomena. Moreover, the inverse of the concentration against the chemical shift can give useful information also for the determination of the critical aggregation concentration (c.a.c.).[30] The ^{1}H NMR spectra of **70** in D_2O at different concentrations are reported in Figure 5.

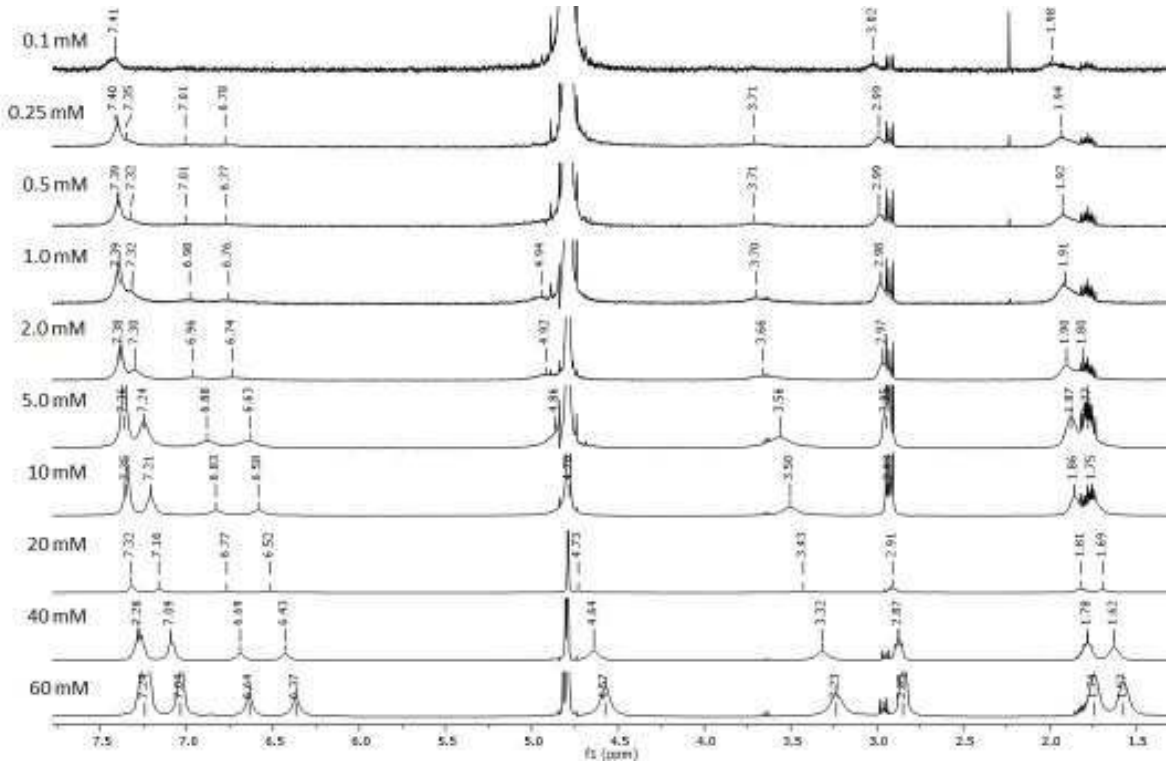

Figure 5: ^{1}H NMR spectra of **70** in D_2O at different concentrations reported in the picture.

As can be seen, by decreasing the concentration of **70**, a marked downfield shifting of the signals can be noticed, in particular for the resonances of the aromatic CH of the triphenylene and the entire benzyl units. Conversely, the resonances of the hydrophilic butyl sulfonate moieties were not heavily affected by the concentration. This effect is strongly indicative of an aggregation phenomena driven by the hydrophobic effect, where molecules of **70** interact with each other leaving the hydrophilic units towards the bulk water, with lower variation of the chemical environment on such residues, while forcing the hydrophobic aromatic units close to each other and thus explaining the up-field shift of the aromatic resonances. A c.a.c. of 3.9 mM was determined plotting the chemical shift of the phenyl CH proton with respect to the inverse of the concentration (see Experimental Section).

Similarly, ^{1}H NMR spectra of **71** in D_2O at different concentrations were recorded and are reported in Figure 6.

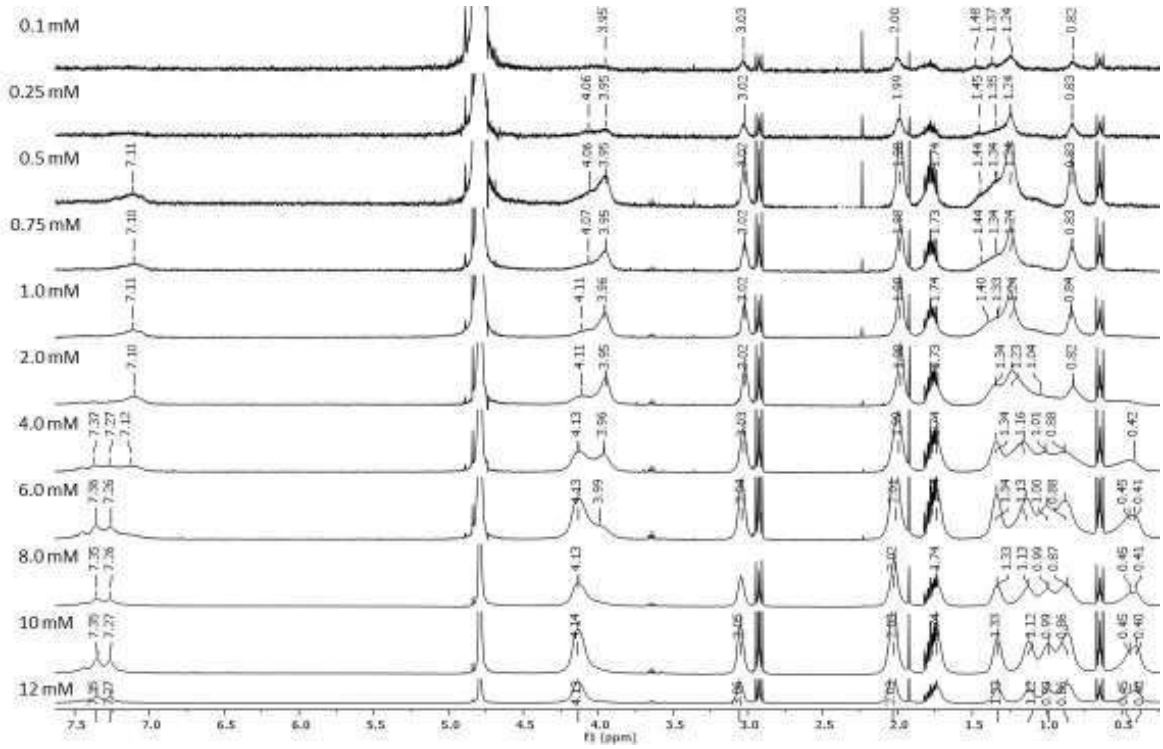

Figure 6: ^{1}H NMR spectra of **71** in D_2O at different concentrations reported on the picture.

For molecule **71**, the aggregation took place in a different fashion compared to **70**. The larger shifts were observed always for the aromatic CH of the triphenylene, indicative of aggregation phenomena driven by the hydrophobic effect. It is also worth to notice that the shielding effect observed on the aromatic CH residues with increasing the concentration were lower in the latter case compared to the benzyl derivative **70**, indicating a different role played by the benzyl units compared to the octyl units present in **71**. Nevertheless, looking more closely at the O-CH_2 resonances of **71** around 4.0 ppm, there seems to be the co-presence of at least two major species while diluting the samples, and this effect is somehow confirmed also considering in detail the aromatic portion of the spectra. Like the previous sample, the hydrophilic butyl sulfonate moieties did not show large chemical shift variation with the concentration of the sample. From the above data it was possible to calculate the c.a.c. 1.7 mM (see Experimental Section), which is lower than that of the previous compound, probably due to the presence of a larger apolar portion that promotes the aggregation in water at lower concentrations.

For the cationic amphiphilic triphenylene, **75**, the ^{1}H NMR spectra in D_2O at different concentrations are reported in Figure 7.

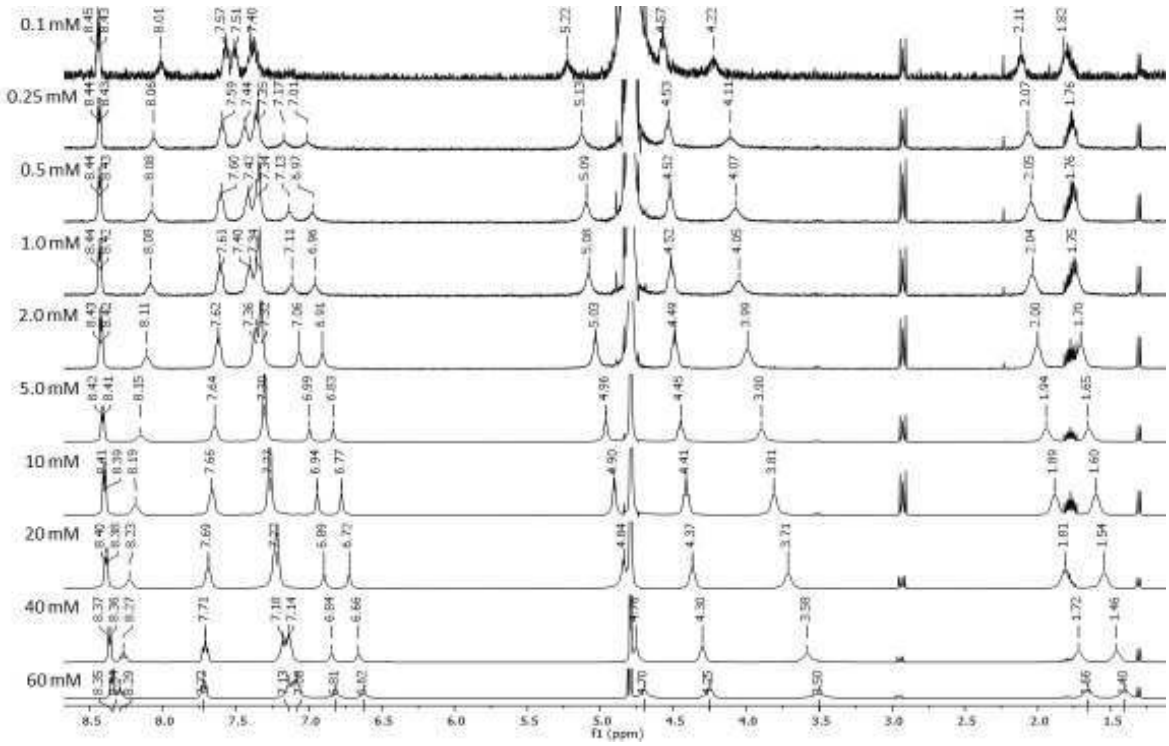

Figure 7: ^{1}H NMR spectra of **75** in D_2O at different concentrations reported on the picture.

The results collected for molecule **75** are similar to those obtained for molecule **70**. The larger shifts of the aromatic CH resonances of the triphenylene are once again indicative of aggregation phenomena driven by the hydrophobic effect. Conversely, the aromatic resonances attributed to the pyridinium units did not show large chemical shift variation in agreement with their rather constant solvation by water in the range of concentrations investigated. Also in this case, it was possible to calculate the c.a.c. value corresponding to 4.8 mM (see Experimental Section).

For the molecule **72**, lacking the hydrophobic alternating benzyl or octyl residues, the ^{1}H NMR spectra in D_2O at different concentrations are reported in Figure 8.

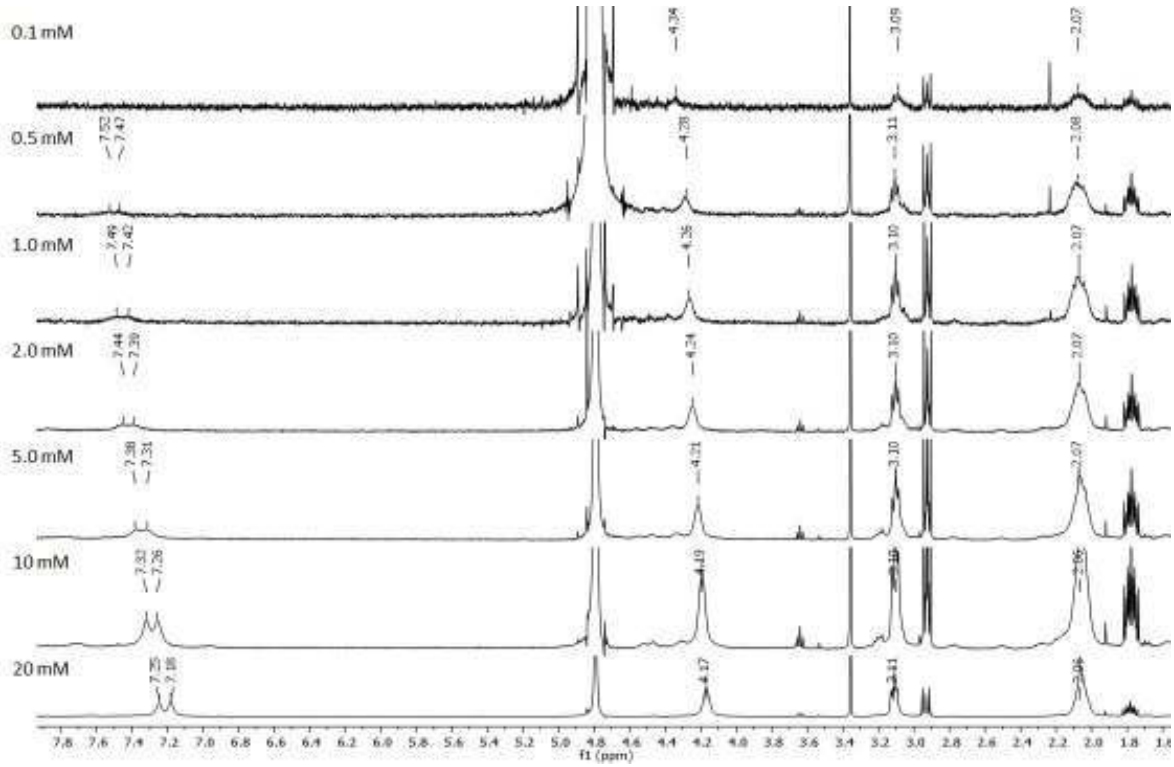

Figure 8: ^{1}H NMR spectra of **72** in D_2O at different concentrations reported on the picture.

In this case, higher shifts are observed for the triphenylene CH residues, probably indicating a more pronounced π-staking between two of these molecules in water. It is worth to notice that the aggregation properties of the latter triphenylene species **72**, lacking the presence of hydrophobic side chains, suggests that the aggregation phenomena taking place for **70**, **71** and **75** in water is highly dictated by the presence of such benzyl or octyl hydrophobic chains. For **72** the calculated c.a.c. was 3.3 mM (see Experimental Section), probably leading to different aggregates compared to the other amphiphilic triphenylene species.

Once the dilution NMR experiments on the ionic triphenylenes were concluded, we focused on the characterization of the neutral amphiphilic triphenylene derivative. The ^{1}H NMR spectra of **78** in D_2O at different concentrations are reported in Figure 9.

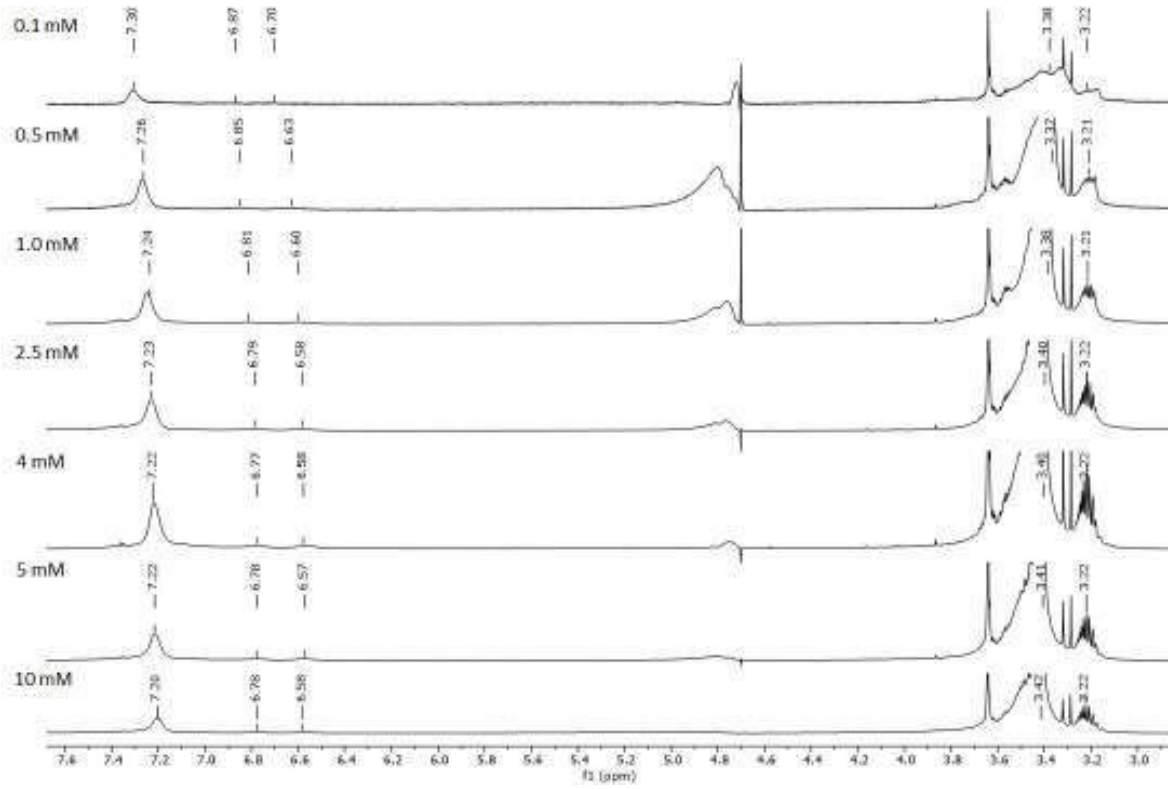

Figure 9: ^{1}H NMR spectra of **78** in D_2O at different concentrations. Relative concentrations are reported on the picture. The water signal was suppressed.

The results collected for the neutral triphenylene **78** are similar to those of molecule **70**, with the greater shifts observed for the aromatic CH of the triphenylene, even if at a less extent. To better understand the behaviour of all the water-soluble triphenylenes, the chemical shifts variations (Δδ) of the two triphenylenic CH residues are reported in Table 1, considering the same concentration range (from 0.5 mM to 10 mM).

Molecule	Δδ CH^1 [ppm]	Δδ CH^2 [ppm]
70	-0.19	-0.20
71	0.26	0.17
72	-0.29	-0.25
75	-0.23	-0.24
78	-0.09	-0.12

Table 1: Δδ of the two triphenylenic CH for all the water-soluble triphenylenes in a concentration range from 0.5 to 10 mM. CH^1 is referred to the triphenylenic CH with the higher δ, CH^2 with the lower δ.

As can be seen in Table 1, for all the triphenylenes, with the exception of **71**, the Δδ is negative, meaning that with the aggregation the triphenylene CH residues experience a more shielded environment, probably imparted by the positioning of the common benzyl residues present in all the triphenylene amphiphilic molecules but **71**. The latter shows positive Δδ values, which suggests that the triphenylene units are arranged in such a way that the CH of one residue fall in the deshielding region created by a second molecule, in a possible L reciprocal orientation. For the ionic derivatives bearing the benzyl substituents, the Δδ values are rather similar, while for the neutral benzyl substituted **78** the lower Δδ values immediately describes a different structure of the apolar core of the aggregates, for instance not excluding the presence of some of the PEG side chains pointing inward, or alternatively the formation of larger assemblies composed by a larger number of molecules

of **78**. Only with possible SANS experiments also on this derivative it could be possible to ascertain the real size of the core, the shell and other properties in water.

The c.a.c. calculated for **78** was 1.9 mM (see Experimental Section), which is lower than what observed for the other ionic derivatives, in agreement with the general observation that neutral surfactants and amphiphilic molecules tend to aggregate at lower concentrations compared to charged surfactant molecules. It is also worth noticing a peculiar behaviour in water of this molecule. Heating an aqueous solution of **78** leads to the precipitation of the compound, while the species is fully solubilized immediately back after cooling to room temperature. This apparently counter-intuitive behaviour is frequent among molecules characterized by the presence of PEG moieties and can be reconnected to the formation of aggregates in solution.[31] This effect, called inverse solubility, characterizes polymers having lower critical solution temperature (LCST)[32] and represents an important property for thermoresponsive polymers. For **78**, it is likely that at room temperature the molecule is soluble forming aggregates similar to micelles with the PEG units pointing outward, well solvated by water molecules, and the hydrophobic portions pointing inward in the apolar core of the aggregates. Upon heating, the aggregates start to be more labile, with the PEG residues undergoing a sort of retraction, changing in conformation and becoming more hydrophobic with concomitant precipitation. When the temperature lowers, the precipitate has time to self-assemble into stable soluble aggregates in water, thus leading to clear solutions.

Parallelly to ^{1}H NMR investigations, pseudo 2D DOSY NMR experiments in water were carried out, on a wide range of concentrations, for the five synthesized triphenylenes, in order to obtain data about the possible number of monomers aggregated in solution from diffusion coefficient determinations, the related hydrodynamic radius and thus the size of the aggregates.

For molecule **70**, the DOSY NMR were recorder in a concentration range from 60 mM to 0.1 mM. The trend of the diffusion coefficient (D) and hydrodynamic radius are reported in Figure 10. For all the reported DOSY (except for molecule **78**), average values and related uncertainties were calculated on two experiments for each concentration.

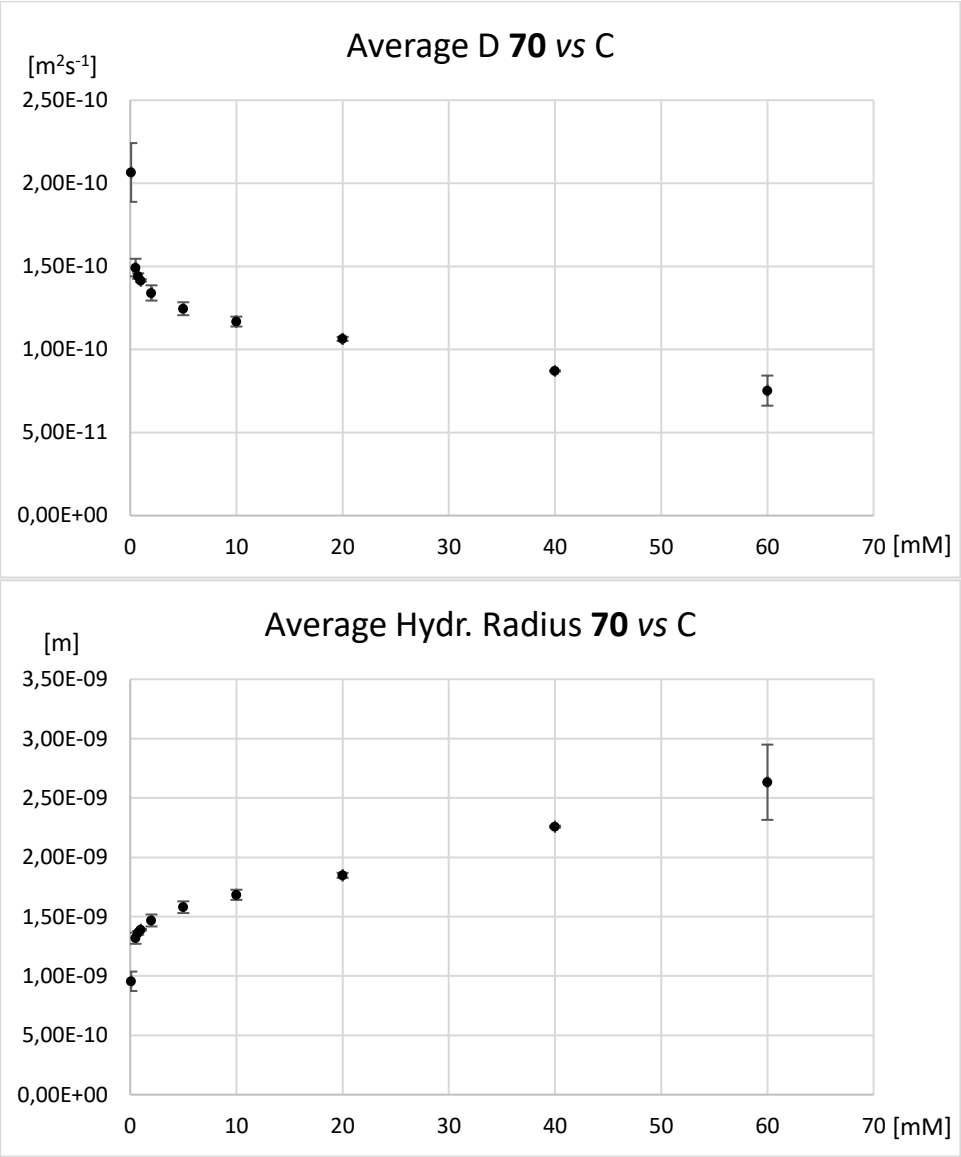

Figure 9: Average diffusion coefficient and hydrodynamic radius for molecule **70** at different concentrations in D_2O.

In all cases, the intensity decay of the resonances with the gradient strength was mono-exponential (see Experimental Part), thus supporting the presence in solution of just one major aggregation species. The average hydrodynamic radii of the species in solution showed a marked increase up to 1.5 nm for solutions in the range from 0.1 to 2 mM, with a subsequent less marked increase up to 2.5 nm for more concentrated solutions. Comparing the size of the solvated aggregates in solution and the size of the hydrophobic and hydrophilic units in the minimized structure of **70**, we can assume that the aggregates observed in water could be formed by a rather small number of molecules, probably not higher than 8 (Figure 11).

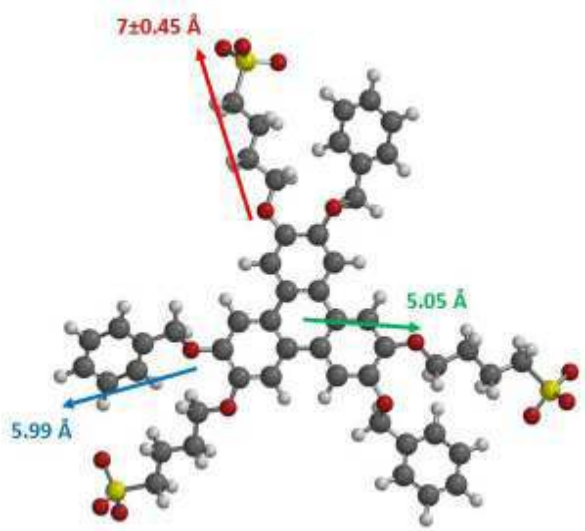

Figure 11: Molecular model of **70** reporting the sizes of hydrophobic and hydrophilic chains and the radius of the triphenylenic core.

For molecule **71**, bearing the octyl substituents, the DOSY NMR were recorder in a concentration range from 12 mM to 0.1 mM. The trend of the diffusion coefficient and hydrodynamic radius are reported in the Experimental Part. It is clear that also for **71** similar aggregation phenomena take place, considering that the intensity decay of the resonances with the gradient strength was still mono-exponential (see Experimental Part), but showing bigger aggregates in terms of hydrodynamic radius, probably due also to the observation of different kind of aggregates, as illustrated by the ^{1}H NMR spectra at variable concentrations.

For the cationic molecule **75**, the DOSY NMR were recorder in a concentration range from 60 mM to 0.1 mM (data reported in the Experimental Part), and the profile of diffusion coefficient and hydrodynamic radius as function of the concentration are perfectly superimposable to those of the anionic species **70**, with which they share the same benzyl hydrophobic side chains (Figure 12).

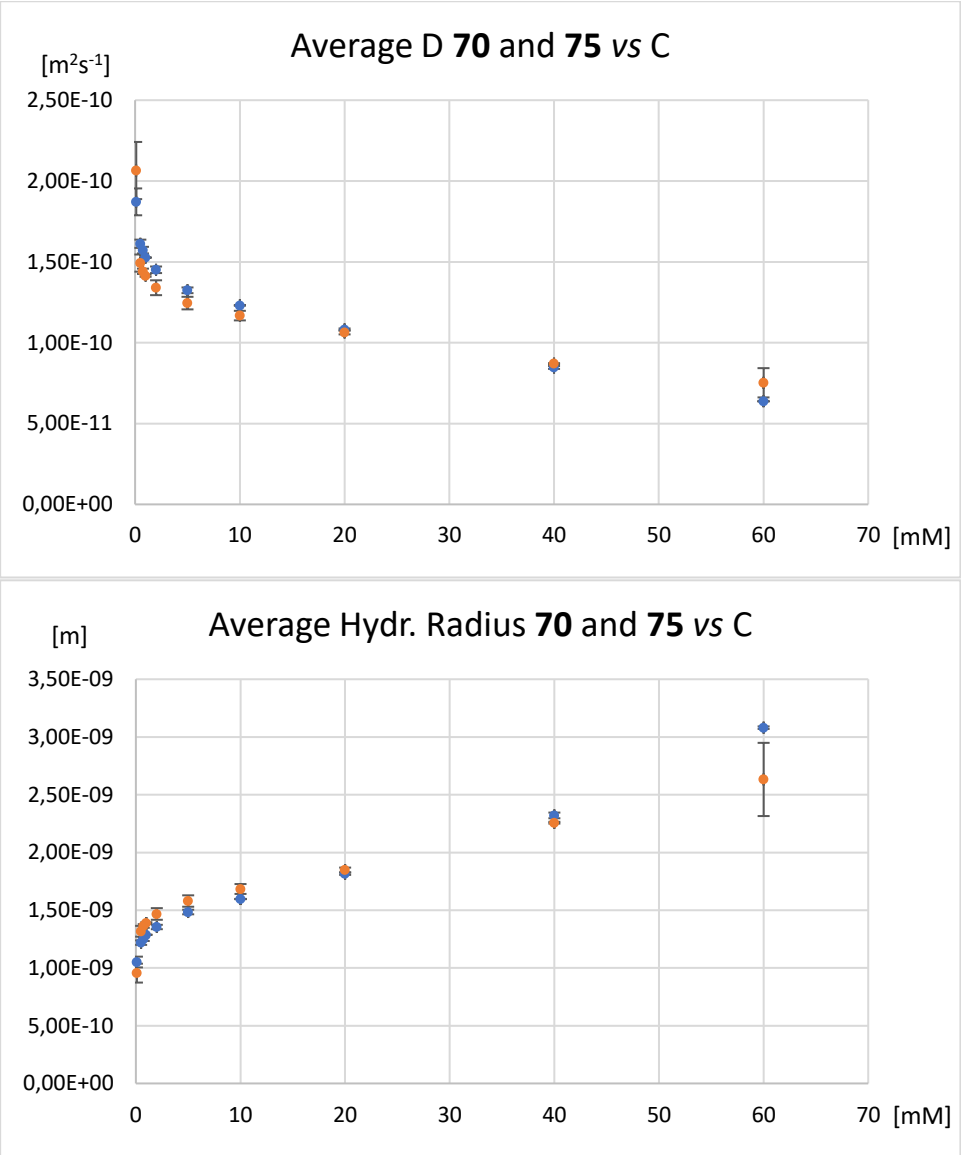

Figure 12: Comparison between diffusion coefficient and hydrodynamic radius of **70** (orange) and **75** (blue) as function of the concentration in D_2O.

This observation leads to the conclusion that it is not the charge type to control the assembly, but rather the hydrophobic moiety. Even in this case, the intensity decay of the resonances with the gradient strength was mono-exponential for molecule **75** (see Experimental Part), pointing out the presence of one prevalent species.

For molecule **72**, lacking hydrophobic alternating units connected to the triphenylene core, the DOSY NMR were recorder in a concentration range from 20 mM to 0.1 mM (data in the Experimental Part), evidencing in particular a multi-exponential decay indicative of the formation of several kind of aggregates in solution, with dimensions in the range of 1.2 nm (see Experimental Part). This is strikingly different to what observed for the other species described before, further confirming the importance of the presence of alternating residues on the triphenylene units with opposite polarity to induce ordered aggregation in water.

Preliminary DOSY experiments were run also on the more recently synthesized neutral **78** bearing PEG hydrophilic units (data in the Experimental Part), also in this case with an

intensity profile that followed a mono-exponential decay typical for the presence of a major aggregate in solution.

By looking at these provisional results, it is firstly evident that the presence of the long MPEG 350 chains increases the average hydrodynamic radii of the aggregates in water up to 2.7 nm, that appears to be about 1 nm bigger than the aggregates formed by **70** at the same concentration. In fact, considering the length of the PEG units, the neutral hydrophilic moiety of **78** is about 18 Å longer than the anionic side chain in **70** (Figure 13).

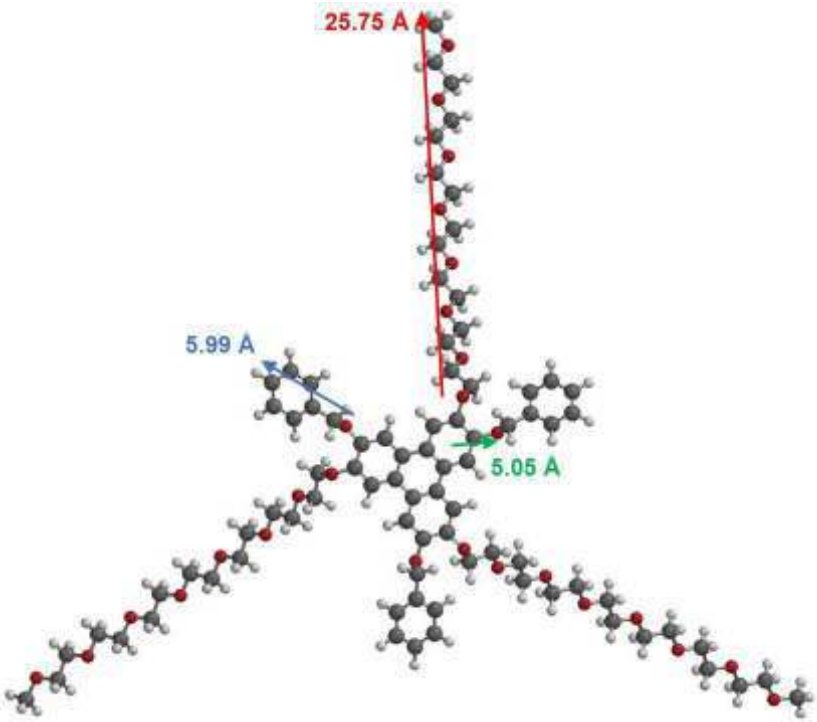

Figure 12: Molecular model of **78**, reporting the sizes of hydrophobic and hydrophilic chains, plus the radius of the triphenylenic core.

This could easily explain the difference of hydrodynamic radii observed for **70** and **78**, even if PEG chains usually assume a helical conformation when in water, thus causing the shortening of its length.

Once the DOSY experiments were completed, UV-Vis experiments in absorption and emission, at different concentrations and at variable temperature, were carried out in search for peculiar behaviours that could help understanding the type of aggregation in water of the triphenylenes. All the acquired experiments are reported into the Experimental Section.

Unfortunately, all the UV-Vis experiments at variable concentrations on **70** and **71** showed just a decrease of the absorption intensity with the decrease of the concentration, without showing any particular profile of the absorbance with the concentration thus giving non-interpretable results.

In the absorption experiment performed at variable temperatures on **70**, keeping the concentration constant to 60 mM, some changes are observed in the absorption profile, but not correlated to any precise event.

Seen the lack of results with the UV spectra, we decided to move to the analysis of the emission spectra at different concentrations. Again, experiments at variable concentrations on **70** and **71** showed just an overall decrease of the emission intensity with the decrease of the concentration, with an opposite trend observed in the beginning at high concentrations, probably caused by the presence of fluorescence self-quenching phenomena, that decrease with dilution, rather than something related with a precise aggregation mode. At a certain point, the self-quenching phenomena begin to fade, and the emission returns directly proportional to the concentration.

After these inconclusive results in the emission and absorption experiments, we decided to move to other techniques, without investigating also the other water-soluble triphenylenes **72**, **75** and **78** with the same methods.

Even though AFM measurements on samples require the complete removal of the solvent and this treatment can drastically change the aggregation properties, in particular for self-assembled species investigated in water, the use of such technique is rather commonly reported. In particular, the group of Yoshizawa supported the formation of nanometric capsules from amphiphilic units through the use of AFM.[16] Since our aggregates are characterized by similar properties, we submitted our sample to AFM analysis, working in tapping mode and using an ultra-sharp tip of 2 nm.

AFM samples of **70** were prepared drying a 5 mM aqueous solution over a mica layer. The recorded AFM picture is reported in Figure 14.

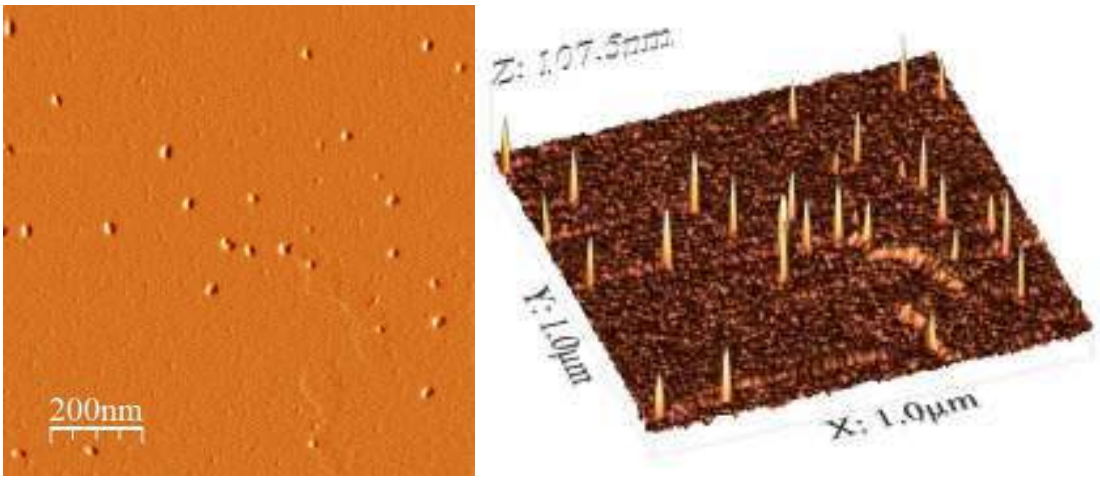

Figure 14: AFM picture of a 5 mM aqueous solution of **70** dried over mica.

Figure 14 shows that spherical aggregates with radius of about 4-5 nm are present on the surface of the mica. The average size is in agreement with what observed with DOSY NMR, being bigger from AFM measurements probably due to the evaporation process, which could cause a collapse of the micelles. Evaporation could also have caused the coalescence of some micelles, as shown by the presence of some bigger aggregates.

AFM samples of **71** were prepared drying a 5 mM aqueous solution over a mica layer. The recorded AFM picture is reported in Figure 15.

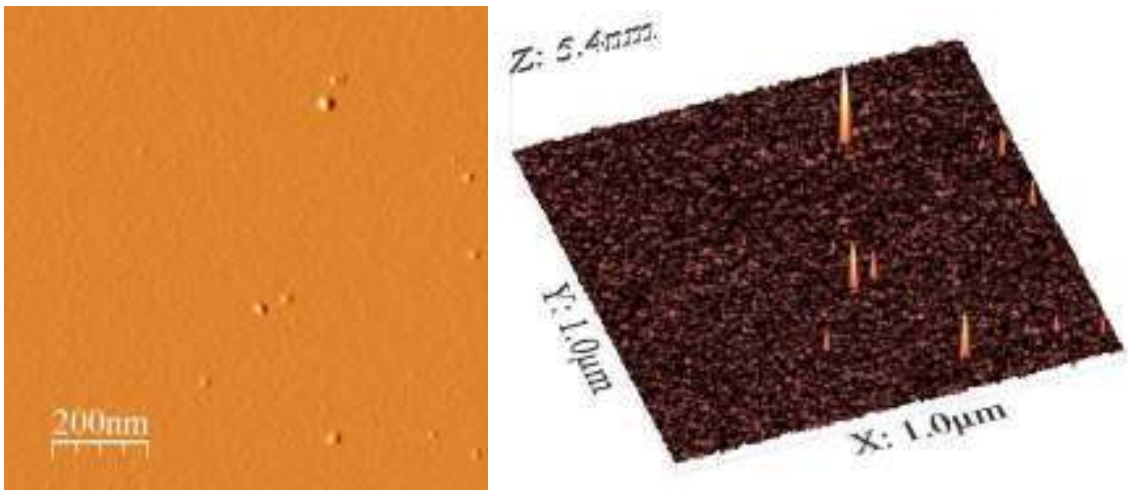

Figure 15: AFM picture of a 5 mM aqueous solution of **71** dried over mica.

Also in this case, spherical aggregates with radius of about 4-5 nm are present on the surface of the mica. These results suggest the existence of small spherical aggregates of the sulfonates **70** and **71**, that could collapse during the drying process. It is interesting to notice that, even if the two sulfonates have different hydrophobic moieties, the size of the formed aggregates are very similar. These results were somehow expected, since from DOSY NMR the calculated hydrodynamic radius for the two sulfonates, at the same concentrations, are slightly bigger for octyl sulfonate **71**, with a differences of ca. 0.3-0.4 nm.

AFM Experiments were run also on triphenylenes **72** and **75**, without highlighting the presence of aggregates of any sort. For molecule **75**, the absence of the alkyl apolar chains prevents the formation of visible aggregates in the AFM, confirming what was found during the DOSY experiments. For what regards the cationic **75**, its high hygroscopicity prevented the complete drying of the sample, not allowing the instrument to detect any signal on the surface of the mica sample. For what concerns the neutral triphenylene **78**, the AFM instrument was unfortunately no longer available at the time of its synthesis.

To acquire further information on the aggregation properties using a different analytical technique in solution, thanks to the collaboration with Dr. Claudia Mondelli from the Institut Laue-Langevin (ILL) in Grenoble it was possible to perform DLS measurements on the sample **70** in water. As reported in Figure 16, the sample at 25 mM clearly showed the presence of aggregates with average diameter of about 1.6 nm with a rather narrow size distribution.

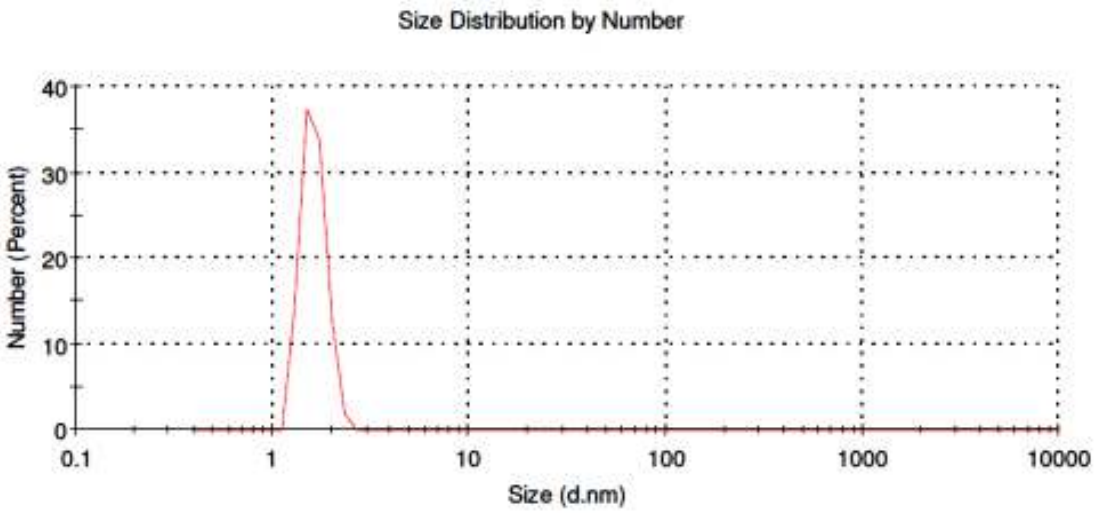

Figure 10: DLS report of a 25 mM aqueous solution of **70**.

This result is in agreement with the DOSY NMR calculation of the hydrodynamic radius. Indeed, even if the DOSY suggests a hydrodynamic diameter of about 3.6 nm for a 25 mM solution of **70** in D_2O, DLS measurements are relative mainly to the inner apolar core of the particle not considering the solvation sphere and the hydrophilic moieties. Conversely, the DOSY measurements reflect the interaction of the polar head groups with a layer of water molecules, thus leading to larger hydrodynamic radii.

Together, ^{1}H NMR, DOSY, AFM and DLS experiments on the *tris*-anionic derivative **70** agreed on the formation of nanometric aggregates in water solution, with some differences in size that are imputable to the intrinsic properties of each technique. However, these analyses could not exclude definitely the formation of small pillar-like structures, caused by the π-staking of few triphenylenic cores, rather than small pseudo-spherical micelles.

7.3 SANS Experiments

All the previous experiments proved the presence of small aggregates in solution, but the exact aggregation mode could not be unequivocally defined. To achieve this task, the use of a more sophisticated technique like the small angle neutron scattering (SANS) was necessary. In collaboration with Dr. Claudia Mondelli, we were able to get access to the proper facility at the ILL to have the opportunity to run SANS measurements, further investigating the effect of the concentration as we did with 2D DOSY experiments.

When a 25 mM solution of **70** in D_2O was subjected to SANS experiment, it showed clearly the presence of a main species in solution, with an average diameter of ca. 1.9 nm, thus further confirming the nanometric size of the capsules in water (Figure 17).

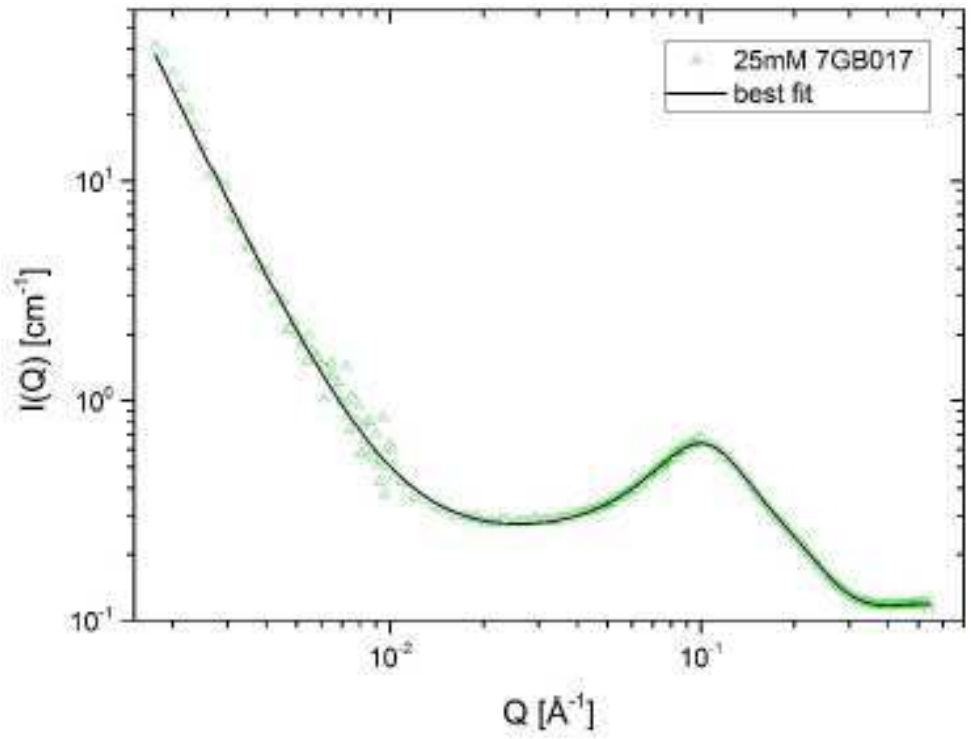

Figure 17: SANS intensity of a 25 mM solutions of **70** in D_2O.

The SANS I(Q) data were analysed with the SasView software packaging.[33] A full interpretation of the data was obtained combining a core-shell sphere model for the form factor (CSS) to describe the dimension of the nano-capsules and the Hyter-msa (Hmsa) model for the structure factor to describe the interaction between the charged micelles (see Experimental Section). A power law has been added to fit the scattering contribution coming from the aggregates of micelles. The results obtained from the best fit are reported in Table 2.

Radius of core [nm]	Thickness of shell [nm]	Radius Polydisp.	Thickness Polydisp.	SLD core·10^6 [Å^{-2}]	SLD shell·10^6 [Å^{-2}]	Effective Radius [nm]	Charge [e]
1.128±0.007	0.77±0.09	0.01±0.03	0.5±0.1	2.2±0.2	5.97±0.04	1.8±0.1	12.7±0.9

Table 2: SANS data analysis results for the nano-capsules of **1a** in D_2O.

According with SANS results, aggregates formed by **70** are made by a hydrophobic core with a radius of 1.128 nm and a hydrophilic shell of 0.77 nm thickness. The mean value of the effective radius of free nano-micelles is 1.8 ± 0.1 nm. The low value in the polydispersity of the core radius means a narrow distribution of radii values around the mean value. Therefore, micelles have averagely the same value of core radius, that remains unaffected by the interaction between charged micelles. Furthermore, the scattering length density (SLD) value of the core suggest that the nano-capsule are formed by a number of monomers between 6 and 8, most probably 7 (see Experimental Section).

The shells thickness presents a higher poly-dispersion, suggesting that the hydrophilic tails of the shell moves as bristles in the D_2O as the consequence of the interaction between charged micelles, changing the value of thickness dynamically over the time. Moreover, the model calculates an overall number of negative charges of about 13. With the charged

micelles being composed by 6 or 7 monomers (with three negative charges per monomer), this lack of charges can be explained considering that the hydrophilic shell could present few solvated sodium cations. Such cations reduce the electrostatic repulsion between monomers of **70** in the aggregate, providing a more stable capsule. The high value of SLD of the shell point out the presence of D_2O molecules between hydrophilic tails and sodium ions.

SANS results indicate that the shell constitute a dynamic system in which hydrophilic tails, immersed in the solvent with Na cations, ripple on the hydrophobic core when interacting charged micelles are close each other. When the aggregates are more separated, the hydrophilic tails stretch out, increasing the thickness of shell.

With the instrument used for the SANS experiments (see Experimental Section), the lower values of Q, at the left side of the graph in Figure 17, allow to investigate the possible existence of structures with an average size up to 200 nm due to the formation of aggregates of micelles. In the low-Q region, the scattering curve exhibited a power law behaviour $I(Q) \propto Q^{-D}$, with the value of the mass fractal dimension D = 2.71, suggesting a mass fractal behaviour. In this fractal picture of the system, the value of D suggests the presence of also some globular shaped aggregates of nano-micelles.

7.4 Molecular Modelling of the Aggregates in Water

With the aim of further supporting the experimental data with some in silico modelling of the aggregates in water, in collaboration with Prof. Achille Giacometti from Università Ca' Foscari we performed a series of molecular dynamics (MD) on the benzyl sulfonate **70**. MD simulations were run at a 25 mM concentration, corresponding to 41 molecules of **70** and 90196 water molecules, adding 121 sodium cations to make the system neutral, in a computational box of 14 nm of length. Details on the program are reported in the Experimental Section. Simulations were run for up to 50 ns after initial equilibration.

A snapshot of the results obtained after 45 ns of simulation, starting from an initial condition where single **70** molecules were randomly inserted in the computational box, is reported in Figure 18.

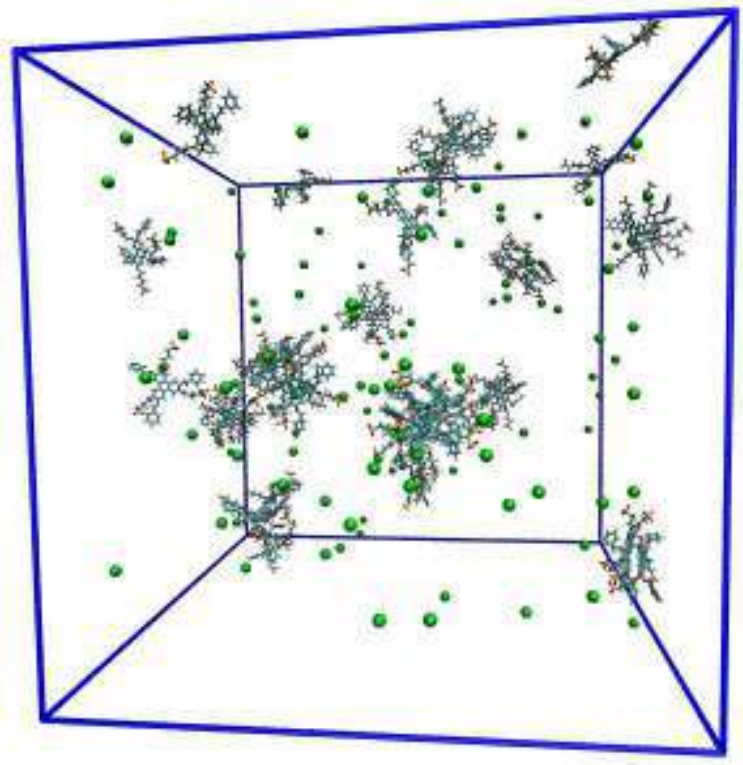

Figure 18: Snapshot of the molecular dynamics simulation after 45 ns. Water molecules have been removed for clarity.

The aggregation of the molecules in dimers, trimers and tetramers is clearly visible by zooming in the computational box, as shown in Figure 19.

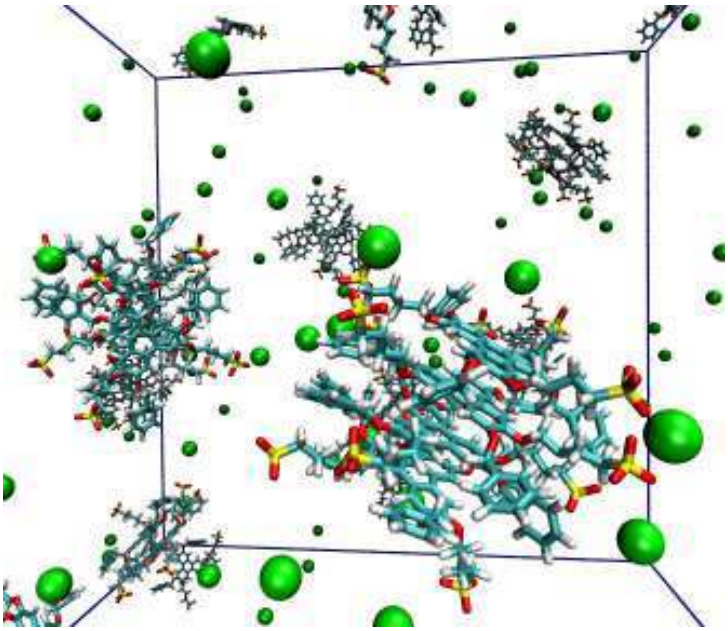

Figure 19: Blow-up of the simulation results after 45 ns.

This can be further confirmed by the calculation of the surface accessible area to the solvent (water) as a function of time as reported in the plot of Figure 20. A decrease in this area is a hallmark to prove the self-assembling process since it confirms the exclusion of water molecules around the triphenylene units due to their reciprocal aggregation.

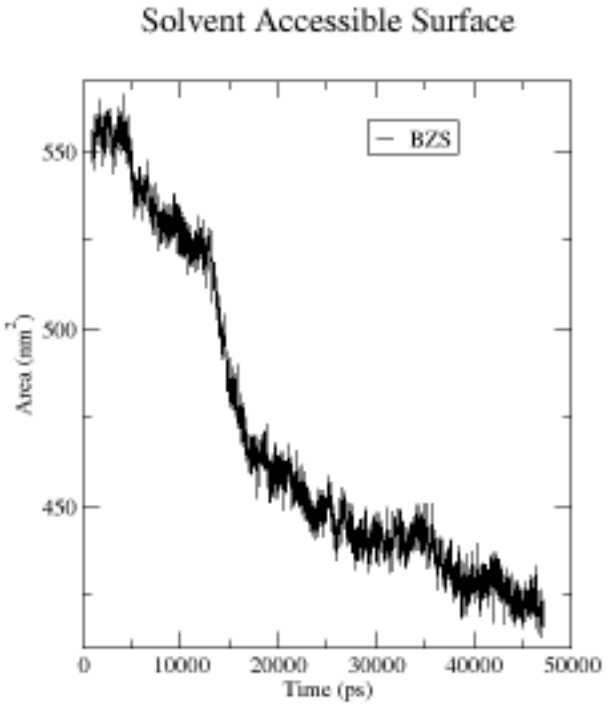

Figure 20: Solvent accessible area (nm^2) as a function of time (ps). BZS stands for benzyl sulfonate.

7.5 Host-Guest Chemistry

After completion of the synthesis of the water-soluble triphenylenes and the full characterization of the micelles for **70**, host-guest studies were run to understand the potentialities of the triphenylene based micelles in supramolecular chemistry and catalysis.

After a large screening of several possible guest molecules characterized by different size, shape, polarity and presence of different functional groups, the nano-capsules of **70** in water showed hosting properties towards highly hydrophobic guests like mesitylene. A 5 mM solution of **70** in D_2O in the presence of mesitylene showed two singlets, attributed respectively to the free aromatic hydrocarbon in water and two up-field shifted resonances for the encapsulated guest, as a consequence of a slow in-out exchange process on the NMR timescale (Figure 21 and NOESY spectrum in Experimental Section).

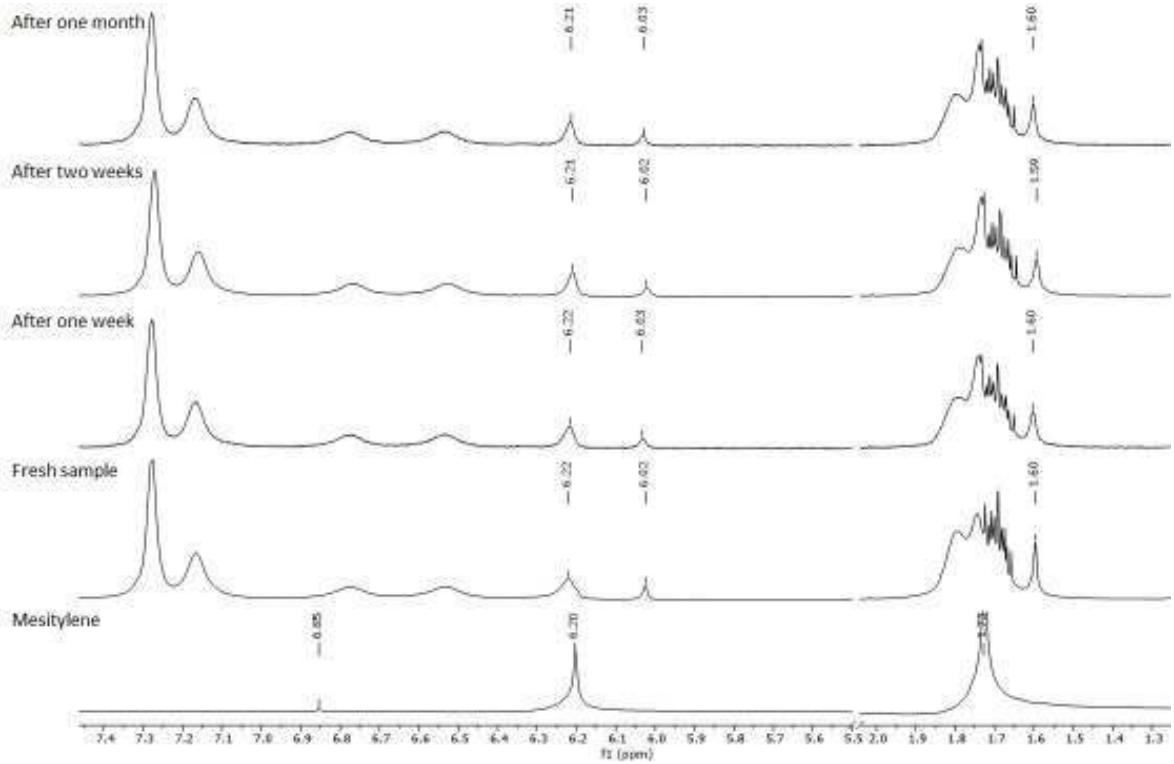

Figure 21: Detail of the ^{1}H NMR spectra of mesitylene (10 µL) in D_2O (bottom) and mesitylene (10 µL) in a 5 mM solution of **70** in D_2O (over time, top).

The spectra were unaltered for up to one month, confirming the stability of the capsule and its hosting properties. By integrating the signals of host and guest, a 12 to 1 molar ratio between the encapsulated molecules of mesitylene and the triphenylene **70** monomer was calculated. This means there is a molecule of mesitylene each two micelles, based on the assumption that a micelle is composed by six monomers.

Similar behaviour was observed with naphthalene-2,6-diol, whose resonances in the presence of **70** were highly shielded with a $\Delta\delta$ of -0.61 ppm, but this time under fast exchange on the NMR timescale probably due to the intrinsic higher solubility of the guest in water (Figure 22).

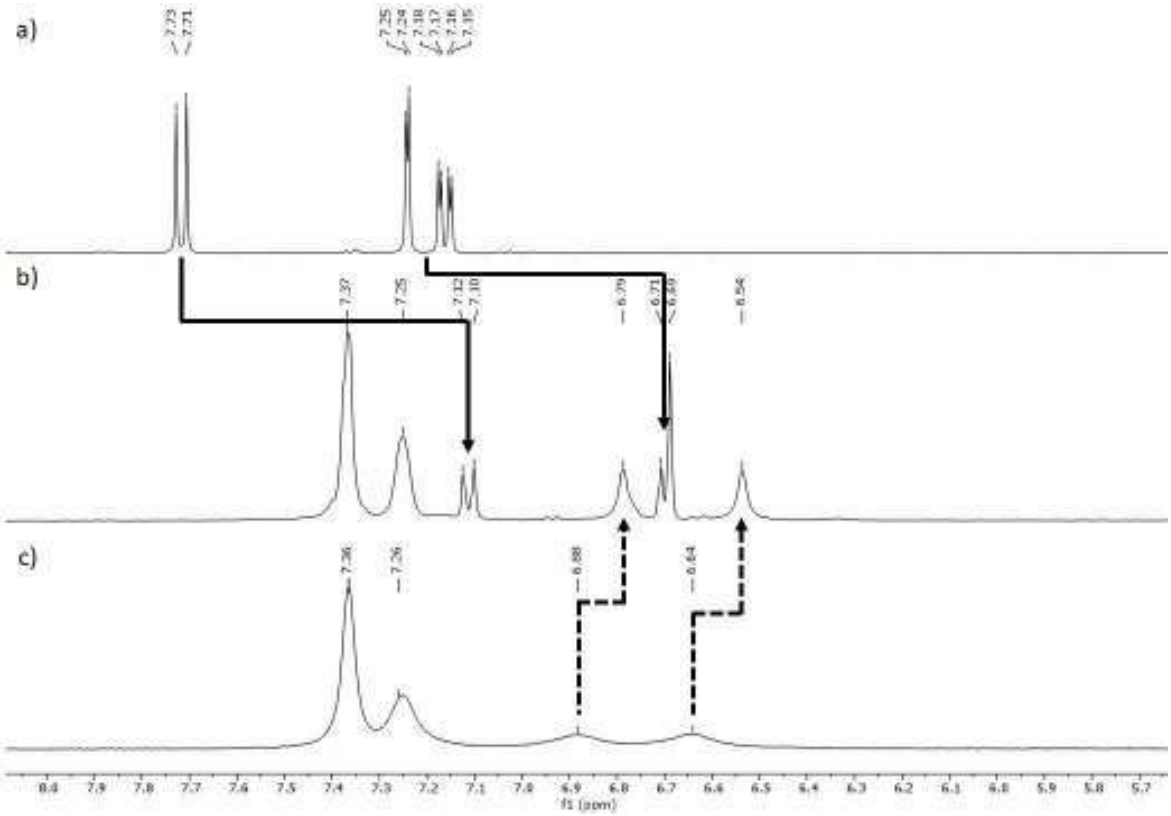

Figure 22: ^{1}H NMR of a) saturated aqueous naphthalene-2,6-diol, b) 5 mM **70** in saturated aqueous naphthalene-2,6-diol and c) 5 mM **70** in D_2O. The shifts of naphthalene-2,6-diol are highlighted with continue arrows while shifts **70** with dashed arrows.

Significant supramolecular interactions were also observed with naphthalene-1,5-diol which is characterized by a similar aromatic structure compared to 2,6-naphthalene diol (Figure 23).

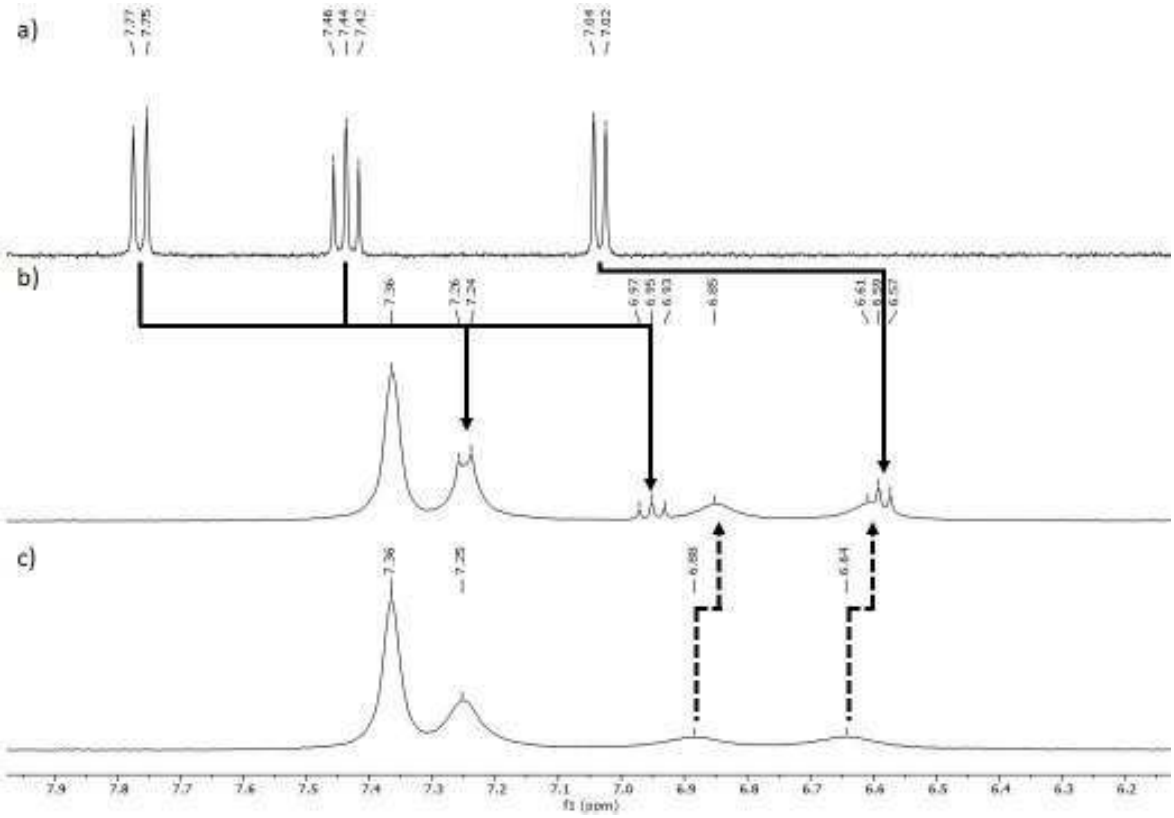

Figure 23: ^{1}H NMR of a) saturated aqueous naphthalene-1,5-diol, b) 5 mM **70** in saturated aqueous naphthalene-1,5-diol and c) 5 mM **70** in D_2O. The shifts of naphthalene-1,5-diol are highlighted with continue arrows while shifts **70** with dashed arrows.

Even in this case, the observation of large up-field shifts due to the shielding effect provided by the apolar core of the aggregates formed by the triphenylenic and benzyl units further supports the presence of an apolar aromatic cavity in the core of the micelles.

It is worth to notice that even non-aromatic guests turned out to show interactions with the nanometric capsules in water. In fact, 1-adamantanol in the presence of the nanocapsules showed important up-field shifts of all the resonances, respectively of -0.43, -0.25, -0.53 ppm (Figure 24).

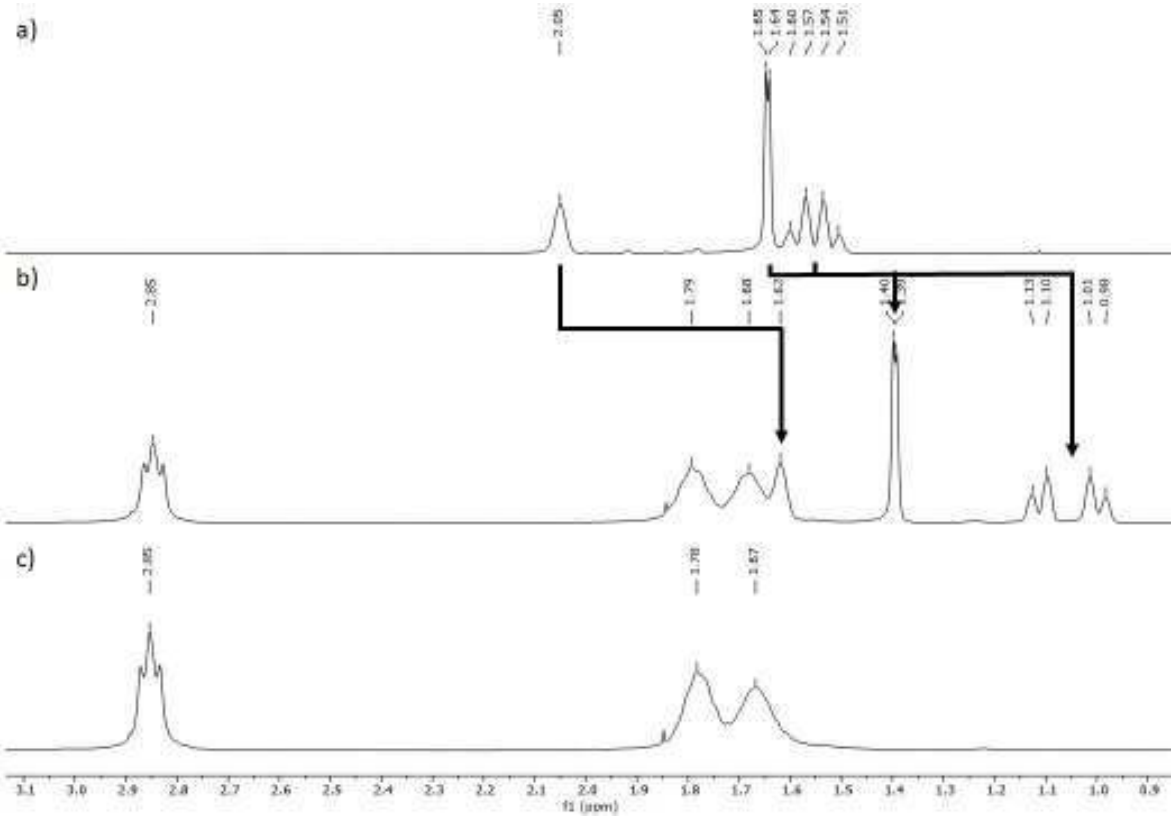

Figure 24: ^{1}H NMR of a) saturated aqueous 1-adamantanol, b) 10 mM **70** in saturated aqueous 1-adamantanol and c) 10 mM **70** in D_2O. The shifts of 1-adamantanol are highlighted with continue arrows.

In Figure 24 it is remarkable the effect of the capsule on the resonances of 1-adamantanol, that are much more resolved and separated compared to the free guest in water, as a further confirmation of the shielding effect imparted by the apolar core of the micellar nano-capsules of **70**. This time, with 1-adamantanol, no changes in the chemical shifts of the host were observed due to its aliphatic nature, that do not affect the host.

The similar anionic aggregate **71**, bearing the octyl moiety in place of the benzyl one, showed comparable host properties with mesitylene, indicating a somehow similar hydrophobic core. Conversely, the triphenylene anionic derivative **72** did not show any hosting properties in water with mesitylene, as a further evidence of the importance of the presence of a hydrophobic substituent on the triphenylene structure for the formation of a sufficiently large hydrophobic cavity, suitable for host guest interactions through the hydrophobic effect (see Experimental Section).

As long as the cationic amphiphilic triphenylene **75** is concerned, experiments were performed with mesitylene, observing the deshielding of the resonances of the aromatic guest, excluding the hosting in the core of the micelles with interactions probably due to π-π stacking between the electron-poor pyridinium moieties and the electron-rich mesitylene aromatic ring, that remained stable over time (Figure 25).

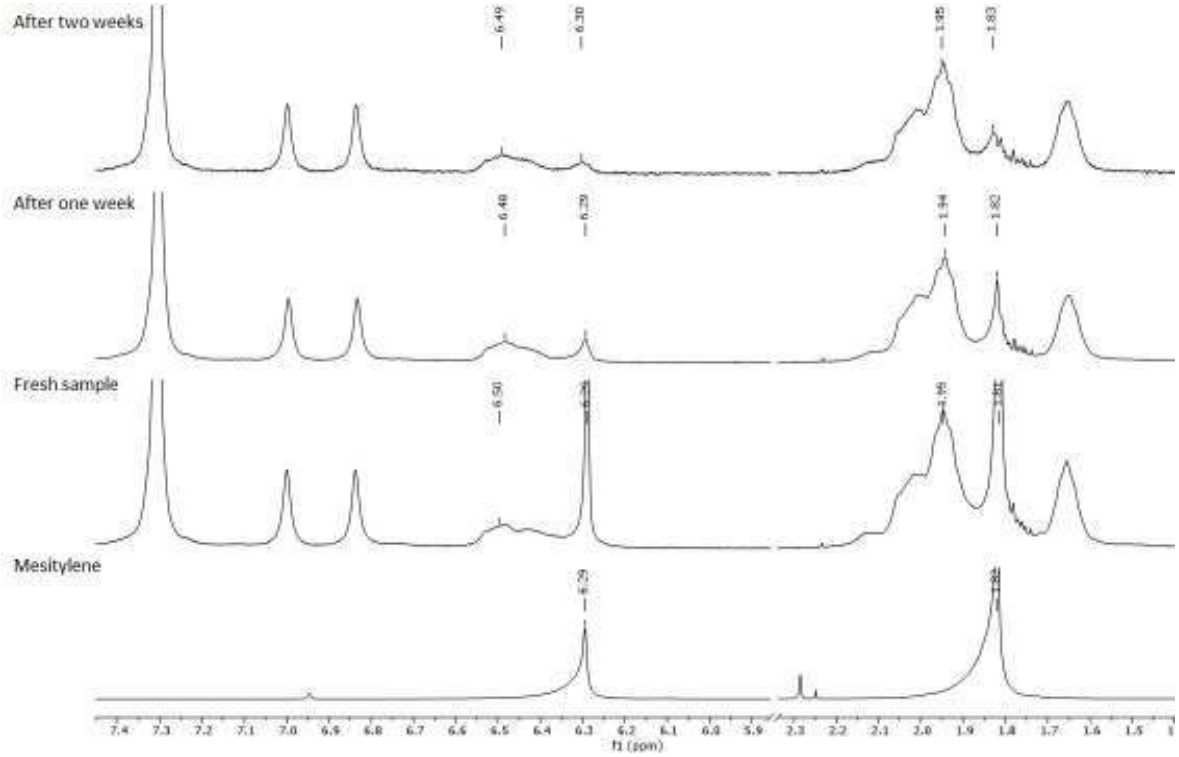

Figure 25: Detail of the ^{1}H NMR spectra of mesitylene (10 µL) in D_2O (bottom) and mesitylene (10 µL) in a 5 mM solution of **75** in D_2O (over time, top).

The peaks resulting from the interaction between **75** and mesitylene are similar to the those produced by **72**, consisting in broader and down-field shifted resonances, an opposite behaviour if compared with interaction of mesitylene with **70** and **71**.

Host-guest chemistry involving the neutral PEG containing triphenylene **78** was limited to trials with 1-adamantanol and mesitylene. In both cases, ^{1}H NMR showed no evidence of interaction between the guests and the micellar host, creating a stable emulsion in the case of mesitylene. This further underline the difference between the various kind of nano-capsules soluble in water, even sharing the same apolar core structure.

In this Chapter, we demonstrated the obtainment of water-soluble nano-capsules through the aggregation of few triphenylenic amphiphilic monomers, exploiting the hydrophobic effect. These capsules demonstrated to have host-guest properties, thus making them feasible for applications in supramolecular catalysis. Such experiments will start in the near future, while in the meantime the results here reported will be submitted to the attention of an editor.

7.6 Experimental Section

7.6.1 General Methods

The reactions were followed with TLC Polygram® Sil G/UV254, 0.25 mm thickness. ^{1}H NMR, ^{13}C NMR, and 2D spectra were recorded with a Bruker Avance II 400, Ascend 400 and Ascend 500 spectrometers, working at 400-500 and 100-126 MHz respectively. Resonance frequencies are referred to tetramethylsilane. IR spectra were recorded with a Perkin Elmer Spectrum One spectrophotometer. AFM images were recorded with an Agilent 5500. The instrument worked in tapping mode using an ultra-sharp tip Nanosensor SSS-SEIH-SPL, super-sharp silicon tip, Richness 5.0±1 µm, length 225±10 µm, width 33±7.5 µm; resonance frequency 96-175 kHz, Force constant 5-37 N/n; Tip height 10-15 µm; Tip radius: 2 nm (typical). Mass spectrometric measurements were performed using a Thermo Scientific LTQ Orbitrap XL equipped with HESI source. Regarding the Thermo Scientific LTQ Orbitrap XL, the compounds studied were dissolved in methanol or acetonitrile with a concentration of 5×10^{-3} M. They were injected into the HESI source by direct infusion with the syringe pump integrated in the mass spectrometer at a 5 mL·min^{-1} flow rate. Mass spectra were acquired in positive-polarity mode with the following tuning conditions: Temperature 40 °C, Sheath gas 8 (arbitrary units, arb), Aux gas and Sweep gas 0 arb, Spray Voltage 4.5 kV, Capillary temperature 275 °C, Capillary Voltage -9 V, Tube lence 150 V. In negative polarity the following tuning parameters were employed: Temperature 40 °C, Sheath gas 19 (arbitrary units, arb), Aux gas and Sweep gas 0 arb, Spray Voltage 3.0 kV, Capillary temperature 275 °C, Capillary Voltage 10 V, Tube lence 120 V. Mass spectra were collected in full scan with a resolution of 100000 at m/z 400. The Orbitrap MS was calibrated just before analysis and during the acquisition in order to improve mass accuracy lock masses were employed. All MD simulations were performed at the atomistic level using an in-house modification of the OPLS-AA/L force field within the GROMACS package. As the molecules are negatively charged, 121 Na cations were added to make the system neutral, and simulations were run up to 50 ns after an initial equilibration. Temperature and pressure were kept fixed during the simulations at the reference values 298.15 K and 1.13 bars, respectively. Reagents and solvents with high purity degree purchased by the providers were used as given. Otherwise, they were purified following the procedures reported in literature.[34]

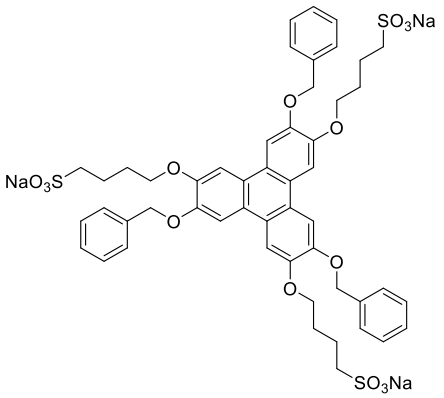

70

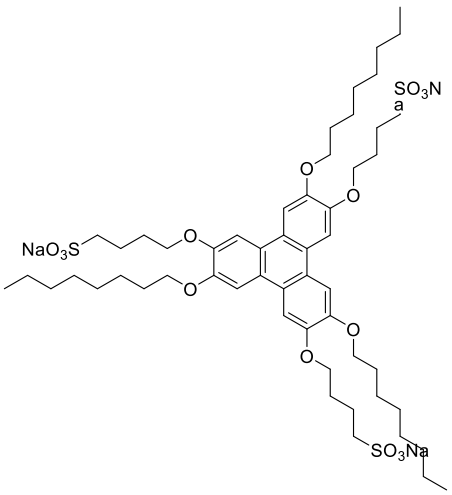

71

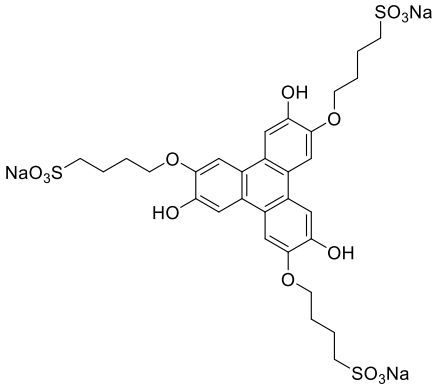

72

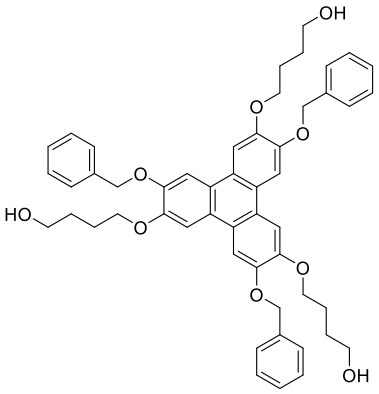

73

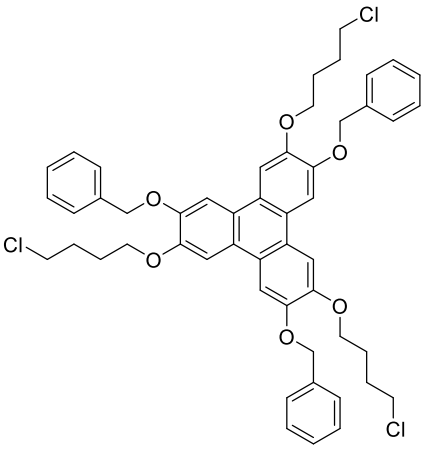

74

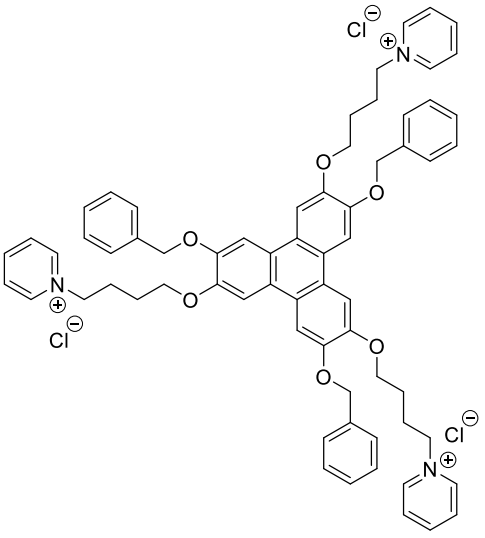

75

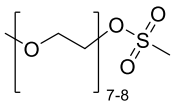

77

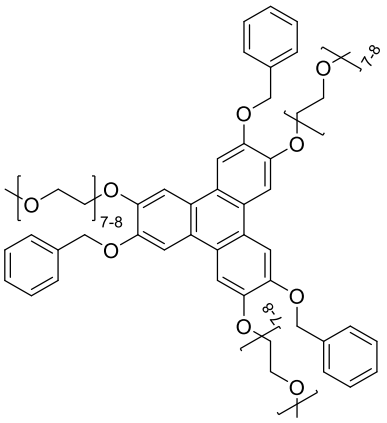

78

7.6.2 Experimental Procedures - Syntheses

General Procedure 1:

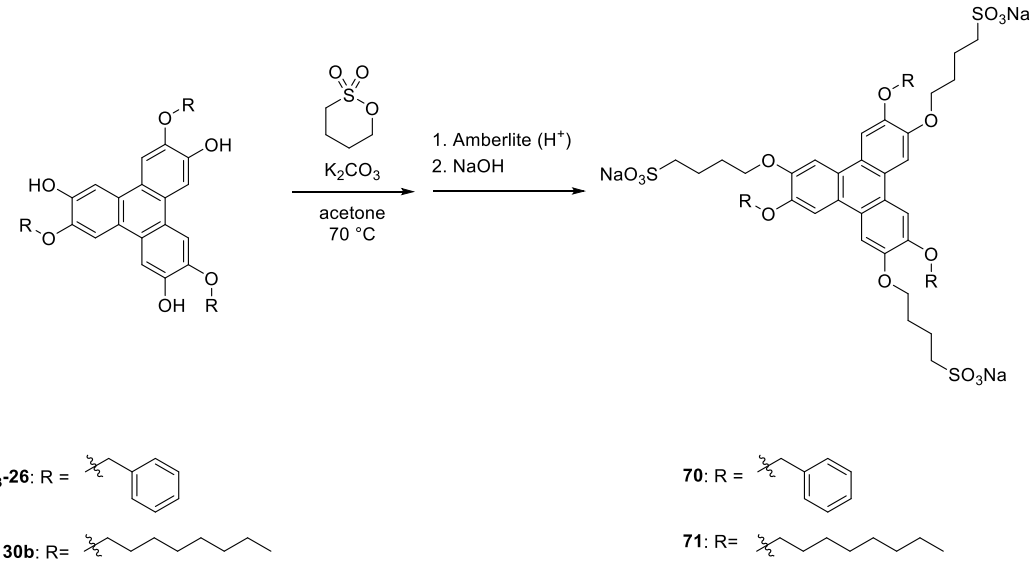

In a 25 mL round-bottomed flask, a suspension of 3,7,11-tris(alkyloxy)triphenylene-2,6,10-triol (0.64 mmol), butan sultone (0.59 mL, 0.78 g, 5.8 mmol), and K_2CO_3 (1.0 g, 7.2 mmol) in acetone (8 mL) was refluxed under inert atmosphere for 72h. The resulting mixture was diluted in 10 mL of absolute ethanol, filtered, washed with absolute ethanol (3×10 mL) and dried in *vacuum*. The resulting solid material was dissolved in 20 mL of water and passed through a wet Amberilite© IR 120 H^+ form column (d = 2 cm, h = 40 cm). The recovered pale-yellow acidic solution was carefully titrated with 0.1 M and 0.01 M aqueous NaOH to pH 7.0 with the aid of a pH-meter. The neutral solution was frozen in liquid nitrogen and lyophilized, affording a fluffy white solid.

Sodium 4,4',4''-((3,7,11-tris(benzyloxy)triphenylene-2,6,10-triyl)tris(oxy))tris(butane-1-sulfonate) (**70**): **GP1** was applied on 3,7,11-tris(benzyloxy)triphenylene-2,6,10-triol (***C*$_3$-26**), 94% yield. M.P. 230 °C (dec.). ^{1}H NMR (400 MHz, DMSO-d_6) δ 8.01 (3H, s), 7.85 (3H, s), 7.65-7.60 (6H, set of m), 7.43 (6H, t, *J* = 7.8 Hz), 7.35-7.29 (3H, set of m), 5.43 (6H, s), 4.24 (6H, t, *J* = 5.6 Hz), 2.58 (6H, t, *J* = 7.6 Hz), 2.01-1.83 (12H, set of m). ^{13}C{^{1}H} NMR (100 MHz): δ 149.1, 148.1, 138.1, 128.9, 128.1, 128.0, 123.4, 122.9, 108.4, 106.8, 70.7, 68.9, 51.7, 28.8, 22.6. IR (KBr): ν 3428, 2917, 2851, 1618, 1514, 1454, 1435, 1382, 1264, 1201, 1185, 1168, 1156, 1041,1023, 856, 743, 729, 696, 614, 598 cm^{-1}. HRMS (ESI-Orbitrap): calcd. for $C_{51}H_{51}Na_2O_{15}S_3$ [M^-] 1045.2191; found: 1045.2258; calcd. for $C_{51}H_{51}NaO_{15}S_3$ [M^{2-}] 511.1149; found: 511.1151; calcd. for $C_{51}H_{51}O_{15}S_3$ [M^{3-}] 333.0802; found: 333.0804.

Sodium 4,4',4''-((3,7,11-tris(octyloxy)triphenylene-2,6,10-triyl)tris(oxy))tris(butane-1-sulfonate) (**71**): **GP1** was applied on 3,7,11-tris(octyloxy)triphenylene-2,6,10-triol (**30b**), 96% yield. M.P. 240-250 °C (dec.). ^{1}H NMR (400 MHz, DMSO-d_6): δ 7.97 (3H, s), 7.96 (3H, s), 4.25 (6H, t, *J* = 6.3 Hz), 4.22 (6H, t, *J* = 6.4 Hz), 2.53 (6H, t, *J* = 7.5 Hz), 1.95-1.77 (18H, set of m), 1.57-1.47 (6H, set of m), 1.43-1.22 (24H, set of m), 0.87 (9H, t, *J* = 7.0 Hz). ^{13}C{^{1}H} NMR (100 MHz): δ148.6, 148.5, 122.9, 107.2, 107.1, 68.8, 68.7, 51.2, 38.9, 31.2, 28.9, 28.8, 28.7, 28.4, 25.7, 22.1, 22.0, 14.0. IR (KBr): ν 3447, 2922, 2852, 2543, 1931, 1698, 1665, 1620, 1518, 1467, 1437, 1399, 1383, 1360, 1263, 1169, 1045, 998, 834, 792, 707, 598, 532 cm^{-1}.

HRMS (ESI-Orbitrap): calcd. for $C_{54}H_{81}Na_2O_{15}S_3$ [M^-] 111.4538; found: 1111.4526; calcd. for $C_{54}H_{81}NaO_{15}S_3$ [M^{2-}] 544.2323; found: 544.2317; calcd. for $C_{54}H_{81}O_{15}S_3$ [M^{3-}] 355.1585; found: 355.1579.

Sodium 4,4',4''-((3,7,11-trihydroxytriphenylene-2,6,10-triyl)tris(oxy))tris(butane-1-sulfonate) (**72**)

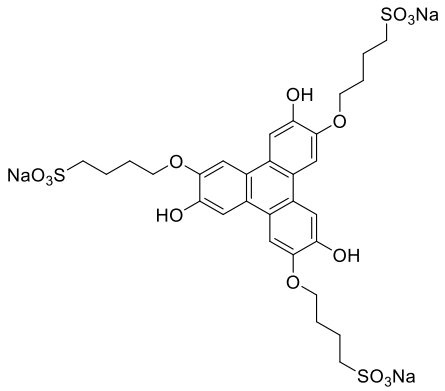

72

In a 50 mL round bottomed flask, a suspension of **72** (0.150 g, 0.14 mmol) and Pd/C 10% (50 mg) in MeOH (26 mL) was vigorously stirred under hydrogen atmosphere (1 Bar, balloon) at room temperature for 18 h. The resulting mixture was filtered on a celite plug, that was washed with MeOH. The resulting solution was concentrated in *vacuum*, to afford the product as a grey solid (0.100 g, 0.13 mmol, 90% yield). M.P. >300 °C. ^{1}H NMR (400 MHz, DMSO-d_6): δ 9.25 (3H, s), 7.77 (3H, s), 7.68 (3H, s), 4.12 (6H, t, *J* = 5.7 Hz), 2.56 (6H, t, *J* = 7.4 Hz), 1.96-1.86 (6H, m), 1.86-1.77 (6H, m). ^{13}C{^{1}H} NMR (100 MHz): δ 147.4, 123.8, 121.6, 121.5, 108.5, 106.1, 68.5, 51.6, 28.6, 22.4. IR (KBr): ν 3434, 1627, 1516, 1450, 1271, 1182, 1162, 1046, 850, 793, 608 cm^{-1}. HRMS (ESI-Orbitrap): calcd. for $C_{30}H_{33}NaO_{15}S_3$ [M^{2-}] 376.0445; found: 376.0441; calcd. for $C_{30}H_{33}O_{15}S_3$ [M^{3-}] 243.0333; found: 243.0337.

4,4',4''-((3,7,11-Tris(benzyloxy)triphenylene-2,6,10-triyl)tris(oxy))tris(butan-1-ol) (**73**)

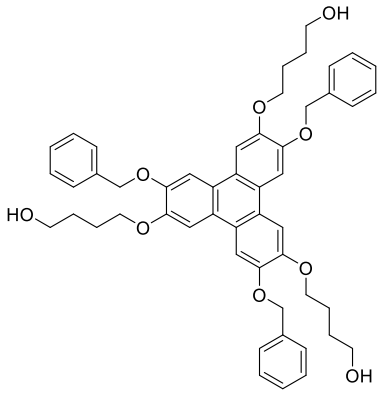

73

In a 25 mL round-bottomed two-necked flask, a suspension of ***C*$_3$-26** (0.50 g, 0.84 mmol), K_2CO_3 (1.05 g, 7.6 mmol) and 4-chlorobutan-1-ol (85%, 0.44 mL, 0.49 g, 3.8 mmol) in dry DMF (10 mL) was stirred under inert atmosphere for 24 hours at 60 °C. A further amount of K_2CO_3 (1.05 g, 7.6 mmol) and 4-chlorobutan-1-ol (85%, 0.44 mL, 0.49 g, 3.8 mmol) was added and the resulting mixture was stirred for 24 hours at 60 °C. The resulting crude material was cooled to room temperature and poured into 50 mL of water. The precipitate

was filtered, washed with water (3×5 mL) and dried in *vacuum*. Product **73** was obtained as a white solid and it was used without further purifications (0.61 g, 0.75 mmol, 89% yield). M.P. 162 °C. ^{1}H NMR (500 MHz, DMSO-d_6): δ 8.02 (3H, s), 7.87 (3H, s), 7.60 (6H, d, *J* = 7.2 H), 7.42 (6H, t, *J* = 7.5 Hz), 7.33 (3H, t, *J* = 7.4 Hz), 4.50 (3H, t, *J* = 5.2 Hz), 4.27 (6H, t, *J* = 6.5 Hz), 3.54 (6H, td, *J* = 6.5, 5.1 Hz), 1.95-1.86 (6H, set of m), 1.74-1.66 (6H, set of m). ^{13}C{^{1}H} NMR (126 MHz): δ 148.6, 147.7, 137.6, 128.4, 127.8, 127.6, 123.0, 122.5, 107.9, 106.5, 70.9, 68.5, 60.5, 29.2, 25.6. IR (KBr): ν 3436, 2920, 2844, 1650, 1617, 1518, 1450, 1438, 1380, 1261, 1197, 1050, 1025, 832, 736, 699, 615 cm^{-1}. HRMS (ESI-TOF): calcd. for $C_{51}H_{54}NaO_9$ [M^{+}] 833.3660; found: 833.3679.

2,6,10-Tris(benzyloxy)-3,7,11-tris(4-chlorobutoxy)triphenylene (**74**)

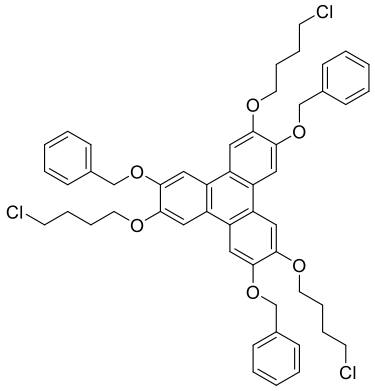

74

In a 25 mL round-bottomed flask, a mixture of **73** (0.7 g, 0.86 mmol), pyridine (0.23 mL, 0.23 g, 2.9 mmol), $SOCl_2$ (0.25 mL, 0.41 g, 3.45 mmol) and anhydrous DMF (one drop) in dry benzene (17 mL) was refluxed for 2 h under Ar. The resulting suspension was cooled to room temperature, poured in 240 mL of water and extracted with DCM (3×80 mL). The collected organic phases were dried over Na_2SO_4 and concentrated in *vacuum*. The crude product was purified by flash-chromatography (eluent DCM/*n*-hexane 6:4), affording the product as a light brown solid (0.36 g, 0.41 mmol, 48% yield). M.P. 130 °C. ^{1}H NMR (500 MHz, $CDCl_3$): δ 7.82 (3H, s), 7.66 (3H, s), 7.58-7.54 (6H, set of m), 7.44-7.39 (6H, set of m), 7.37-7.32 (3H, set of m), 5.34 (6H, s), 4.24 (6H, t, *J* = 5.6 Hz), 3.69 (6H, t, *J* = 6.2 Hz), 2.15-2.06 (12H, set of m). ^{13}C{^{1}H} NMR (126 MHz): δ 149.1, 148.5, 137.6, 128.8, 128.1, 127.5, 124.0, 123.5, 108.7, 107.0, 77.4, 77.2, 76.9, 72.1, 68.6, 45.0, 29.7, 26.9. IR (KBr): ν 3440, 2923, 2850, 1632, 1621, 1580, 1511, 1441, 1391, 1265, 1165, 1040, 1023, 820 cm^{-1}. HRMS (ESI-TOF): calcd. for $C_{51}H_{51}Cl_3NaO_6$ [M^{+}] 887.2643; found: 887.2663.

1,1',1''-(((3,7,11-Tris(benzyloxy)triphenylene-2,6,10-triyl)tris(oxy))tris(butane-4,1-diyl))tris(pyridin-1-ium) tris-chloride (**75**)

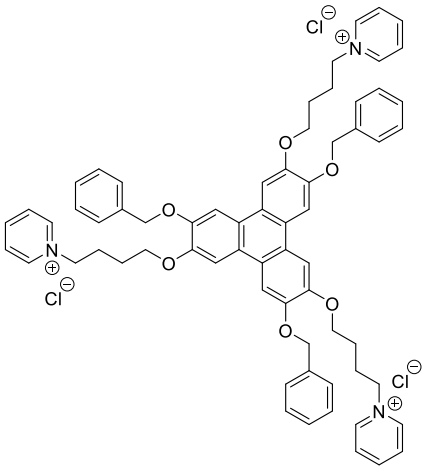

75

In a 10 mL round-bottomed flask, a solution of **74** (0.26 g, 0.30 mmol) in dry pyridine (6 mL) was stirred overnight at 110 °C under Ar. The mixture was cooled to room temperature, separating a brown oil from the solution. The crude product was isolated removing the most of pyridine at reduced pressure, dissolving the residue in a minimum amount of water and completing the removal of the pyridine/water azeotrope in *vacuum*. The sample was freeze-dried to remove completely water, affording the product as a fluffy light-brown solid (0.28 g, 0.26 mmol, 78% yield). ^{1}H NMR (500 MHz, methanol-d_4): δ 8.93 (6H, d, *J* = 5.3 Hz), 8.48 (3H, tt, *J* = 7.8, 1.4 Hz), 8.10 (3H, s), 7.96 (3H, s), 7.94-7.89 (6H, set of m), 7.57 (6H, d, *J* = 6.8 Hz), 7.28 (6H, t, *J* = 7.6 Hz), 7.19 (3H, t, *J* = 7.5 Hz), 5.39 (6H, s), 4.87 (6H, t, *J* = 7.1 Hz), 4.42 (6H, t, *J* = 5.4 Hz), 2.33-2.25 (6H, set of m), 1.93-1.87 (6H, set of m). ^{13}C{^{1}H} NMR (126 MHz): δ 149.8 (2C), 146.6, 146.0, 138.6, 129.8, 129.7, 129.5, 129.3, 125.0, 124.9, 107.6, 107.2, 72.5, 70.7, 62.8, 31.0, 25.6. HRMS (ESI-TOF): calcd. for $C_{66}H_{66}N_3O_6$ [M^{3+}]: 332.1645; Found: 332.1646.

2,5,8,11,14,17,20-heptaoxadocosan-22-yl methanesulfonate (**77**):

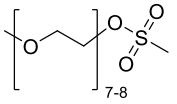

77

In a 100 mL round-bottomed flask, MPEG 350 (5.0 g, 15 mmol) was heated at 80 °C for 30 minutes under *vacuum*, in order to remove traces of moisture. The system was cooled to room temperature under Ar and dry THF (52 mL) and triethyl amine (2.83 g, 3.9 mL, 19 mmol) were added. The mixture was cooled to 0 °C and a solution of methanesulfonyl chloride (7.0 g, 4.7 mL, 61 mmol) in dry THF (10 mL) was added dropwise. The solution was allowed to return to room temperature overnight. The resulting mixture was filtered on a celite plug and the liquors were concentrated in *vacuum*. The residue was diluted in DCM (300 mL) and saturated aqueous $NaHCO_3$ (300 mL), maintaining the emulsion in vigorous stirring for 40 hours. The organic layer was separated, washed with saturated aqueous $NaHCO_3$ (3×100 mL), dried over $MgSO_4$, filtered and concentrated in *vacuum*. The product was obtained as a yellow oil (5.49 g, 13 mmol, 90% yield). ^{1}H NMR (400 MHz, $CDCl_3$): δ 5.27-

5.20 (3H, set of m), 4.33-4.22 (2H, set of m), 3.72-3.62 (2H, set of m), 3.59-3.50 (19H, set of m), 3.48-3.41 (2H, set of m), 3.32-3.24 (3H, set of m), 3.05- 2.92 (3H, set of m). $^{13}C\{^{1}H\}$ NMR (100 MHz): δ 71.7, 70.4, 70.4, 70.3, 69.3, 68.8, 58.8, 58.8, 53.5, 37.5, 37.5, 31.5, 30.1.

22,22',22''-((3,7,11-tris(benzyloxy)triphenylene-2,6,10-triyl)tris(oxy))tris(2,5,8,11,14,17,20-heptaoxadocosane) (**78**):

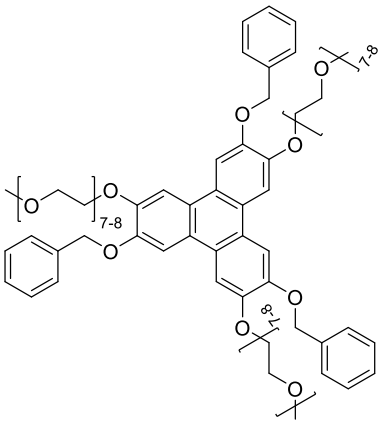

78

In a 25 mL pear-shaped, round-bottomed two-necked flask, a mixture of **77** (0.35 g, 0.85 mmol), ***C*$_3$-26** (0.10 g, 0.17 mmol) and K_2CO_3 (0.18 g, 1.3 mmol) in anhydrous DMF (2 mL) war stirred at room temperature for 72 hours under inert atmosphere. The DMF was removed in *vacuum* and the crude was absorbed on silica. The absorbed crude was extracted in a Soxhlet apparatus with DCM for 6 hours to remove the excess of **77**, and with methanol for 18 hours to recover the product. The methanol solution was dried in *vacuum*, affording the product as a waxy solid (0.13 g, 0.085 mmol, 50% yield). ^{1}H NMR (400 MHz, $CDCl_3$): δ 7.83 (3H, s), 7.71 (3H, s), 7.60-7.54 (6H, set of m), 7.44-7.37 (6H, set of m), 7.36-7.30 (3H, set of m), 5.33 (6H, s), 4.36 (6H, t, *J* = 5.1 Hz), 4.00 (6H, t, *J* = 5.1 Hz), 3.83-3.76 (6H, set of m), 3.70- 3.66 (6H, set of m), 3.66-3.56 (54H, set of m), 3.55-3.47 (6H, set of m), 3.38-3.31 (9H, set of m). $^{13}C\{^{1}H\}$ NMR (100 MHz): δ 148.9, 148.5, 137.5, 128.7, 128.0, 127.6, 124.0, 123.7, 108.8, 107.5, 77.5, 77.4, 77.2, 76.8, 72.0, 72.0, 71.1, 70.8, 70.7, 70.6 (5C), 69.9, 69.1, 59.1, 29.8. IR (KBr): ν 3435, 2876, 1617, 1508, 1433, 1353, 1264, 1166, 1105, 950, 847, 740, 701, 617 cm^{-1}.

7.6.3 NMR and MS

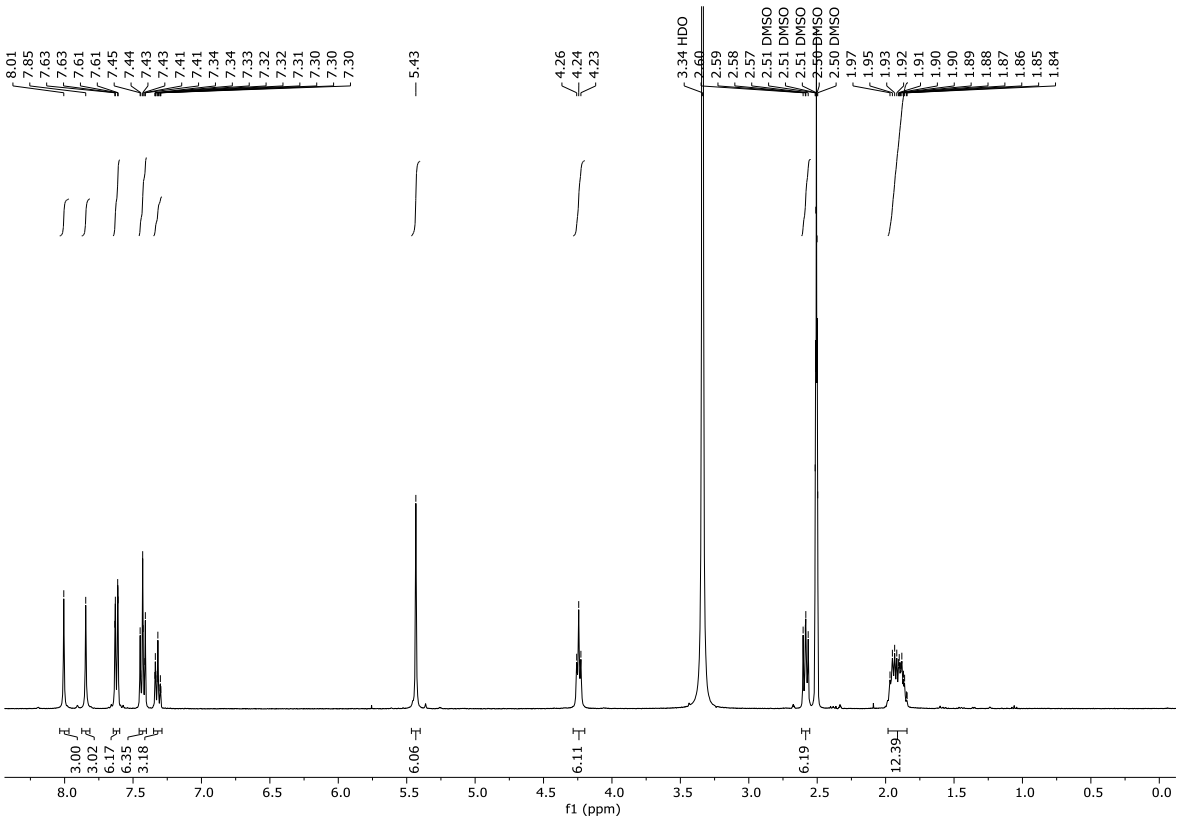

Figure I: ^{1}H NMR of molecule **70**.

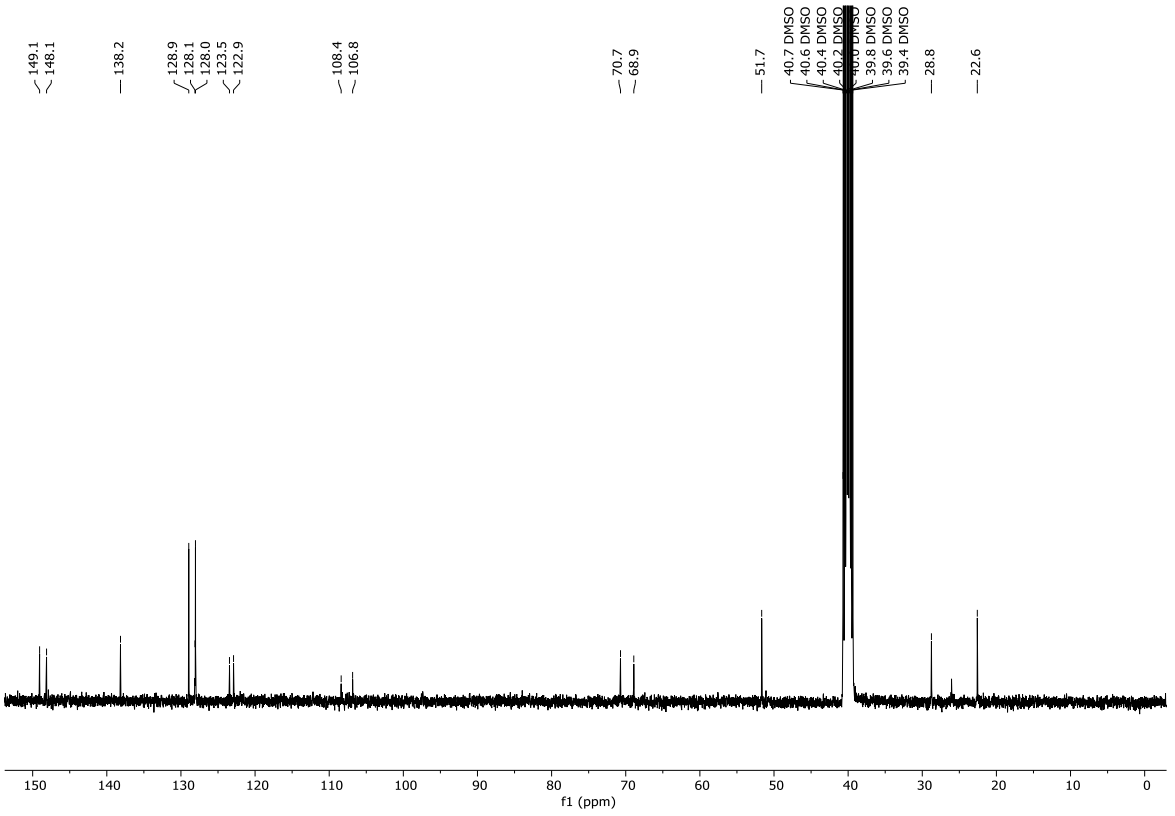

Figure II: ^{13}C NMR of molecule **70**.

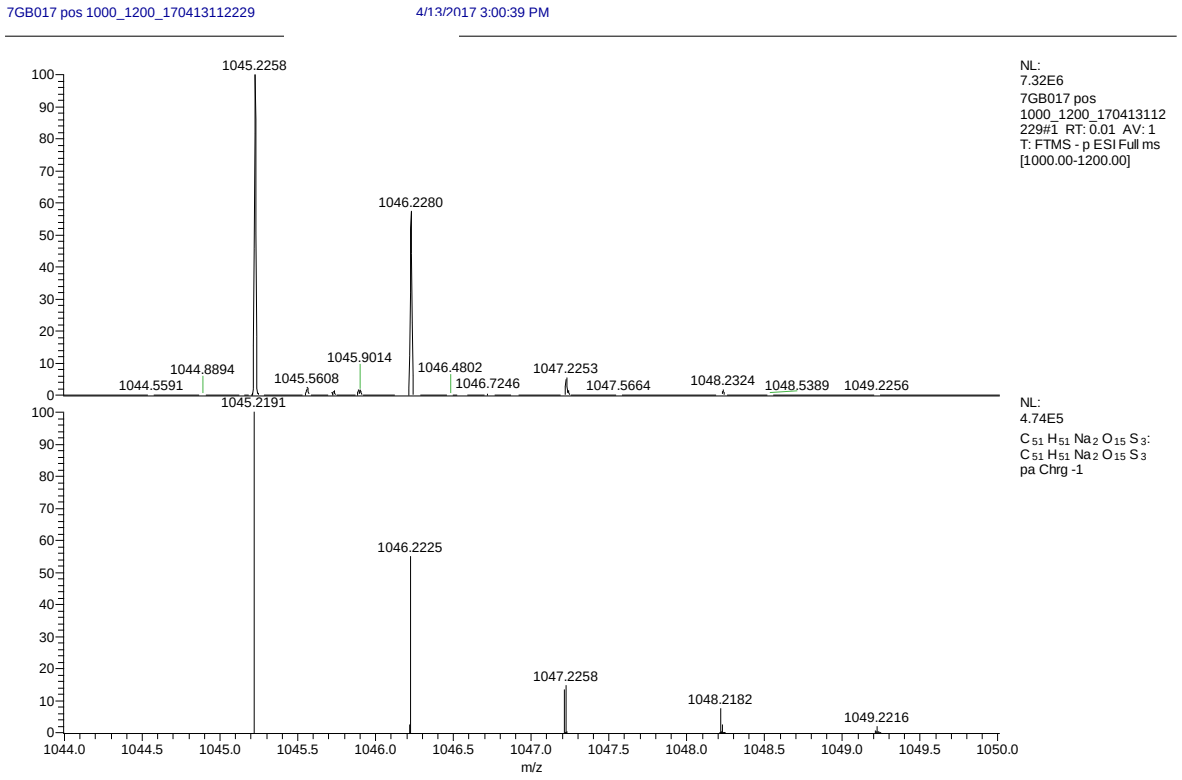

Figure III: ESI-HRMS of molecule **70**, detail of *m/z* = 1.

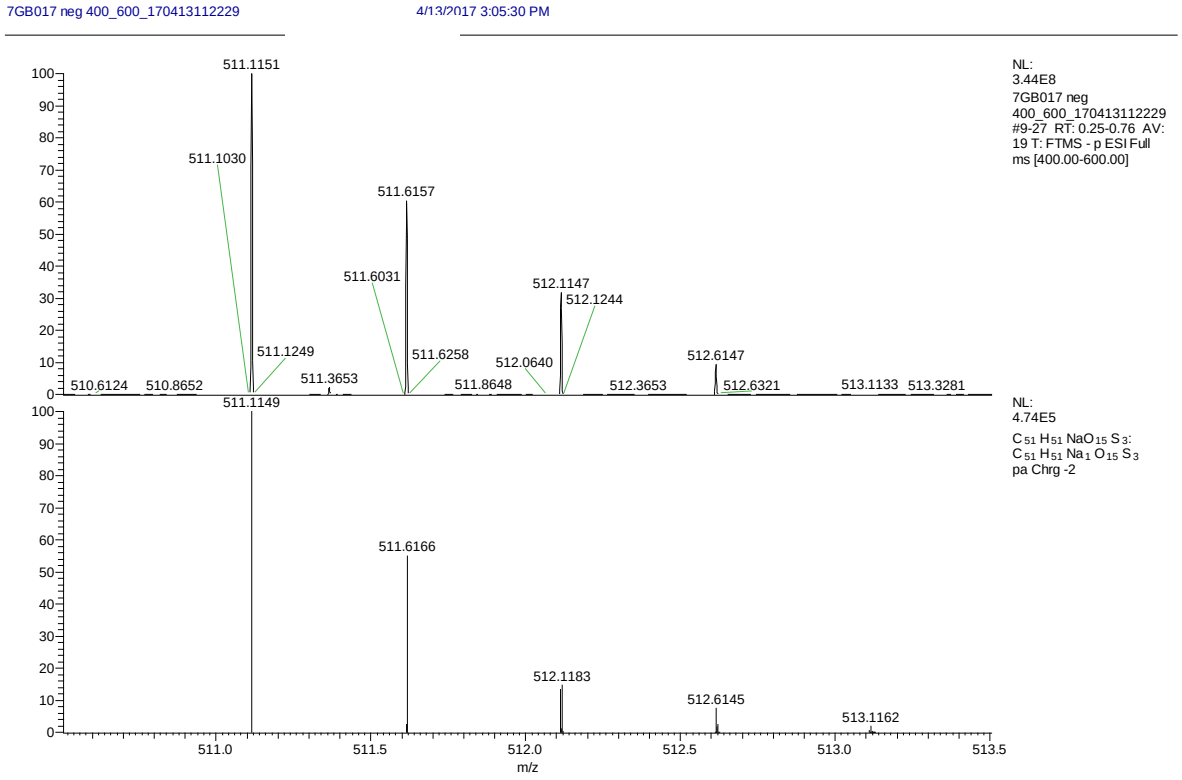

Figure IV: ESI-HRMS of molecule **70**, detail of *m/z* = 2.

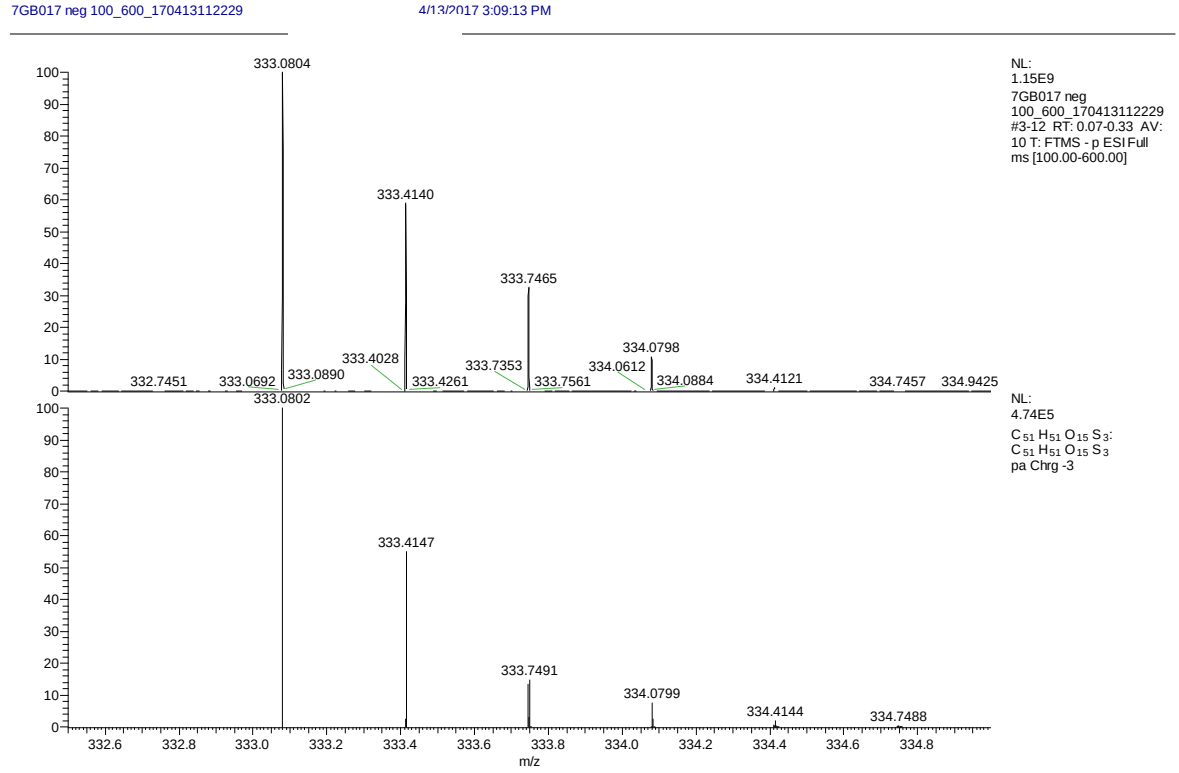

Figure V: ESI-HRMS of molecule **70**, detail of *m/z* = 3.

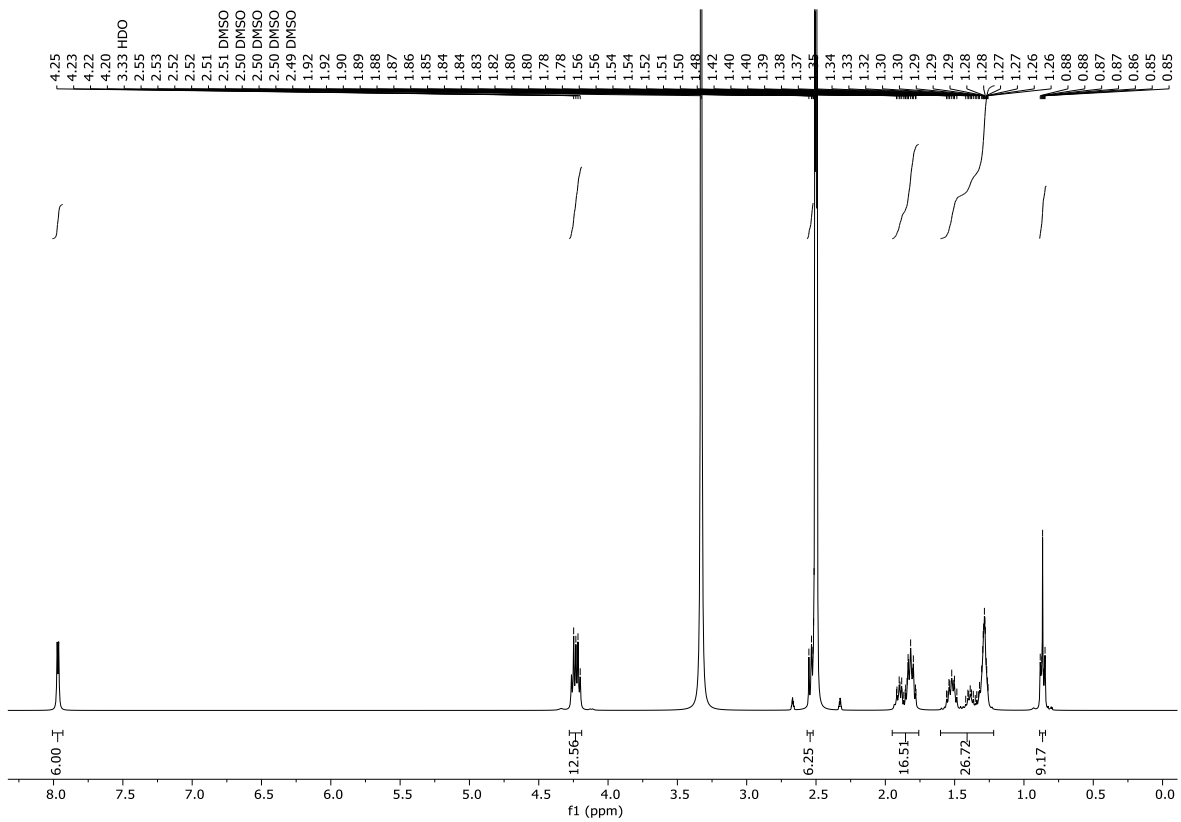

Figure VI: ^{1}H NMR of molecule **71**.

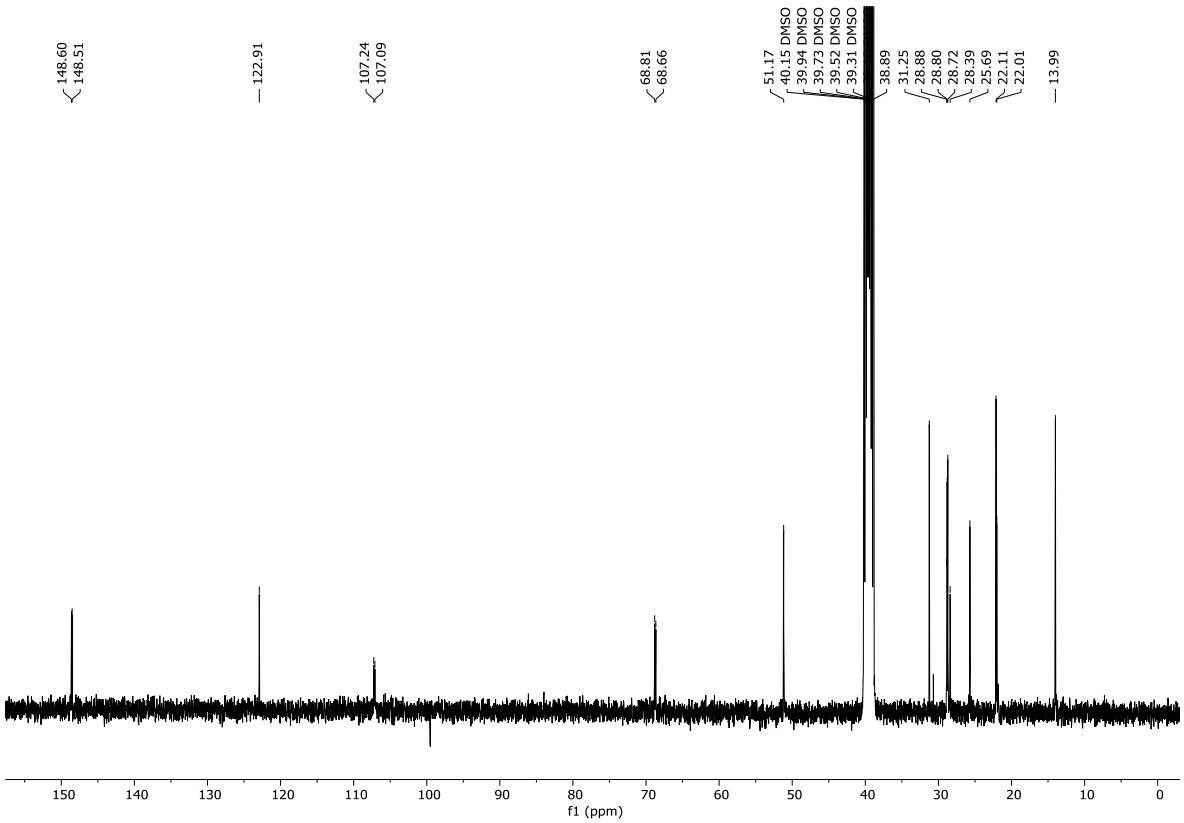

Figure VII: ^{13}C NMR of molecule **71**.

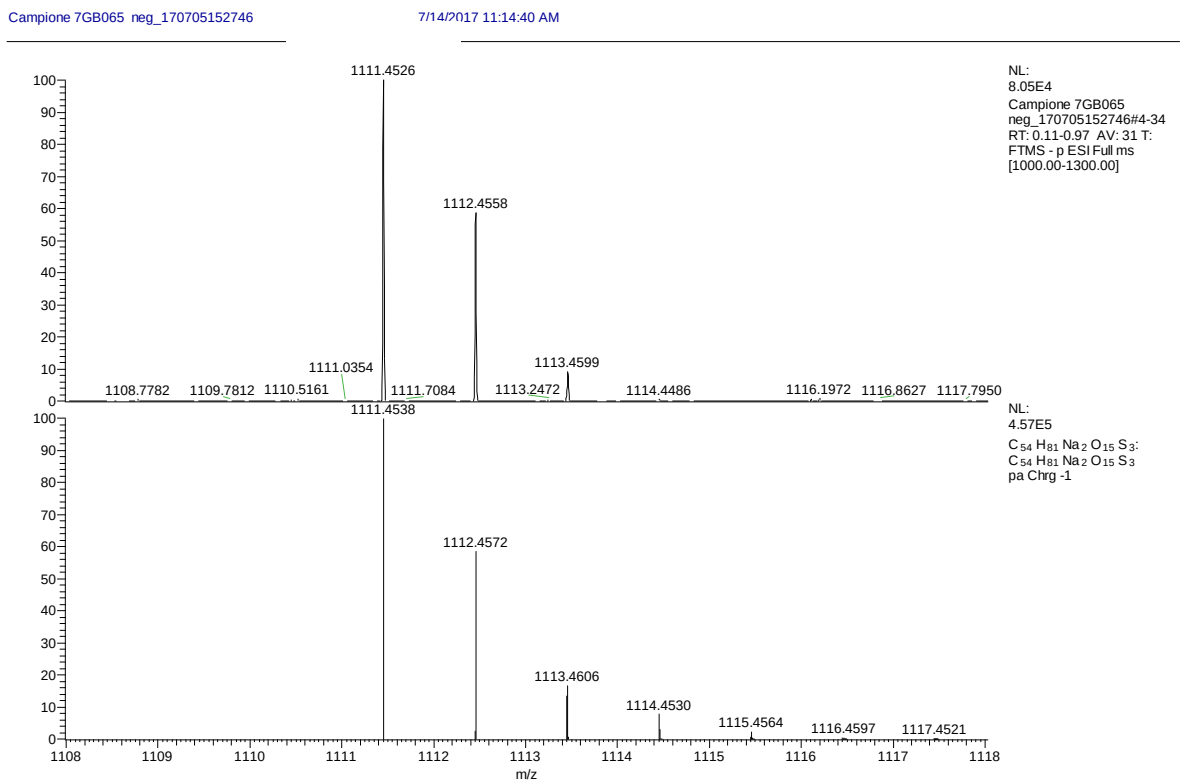

Figure VIII: ESI-HRMS of molecule **71**, detail of *m/z* = 1.

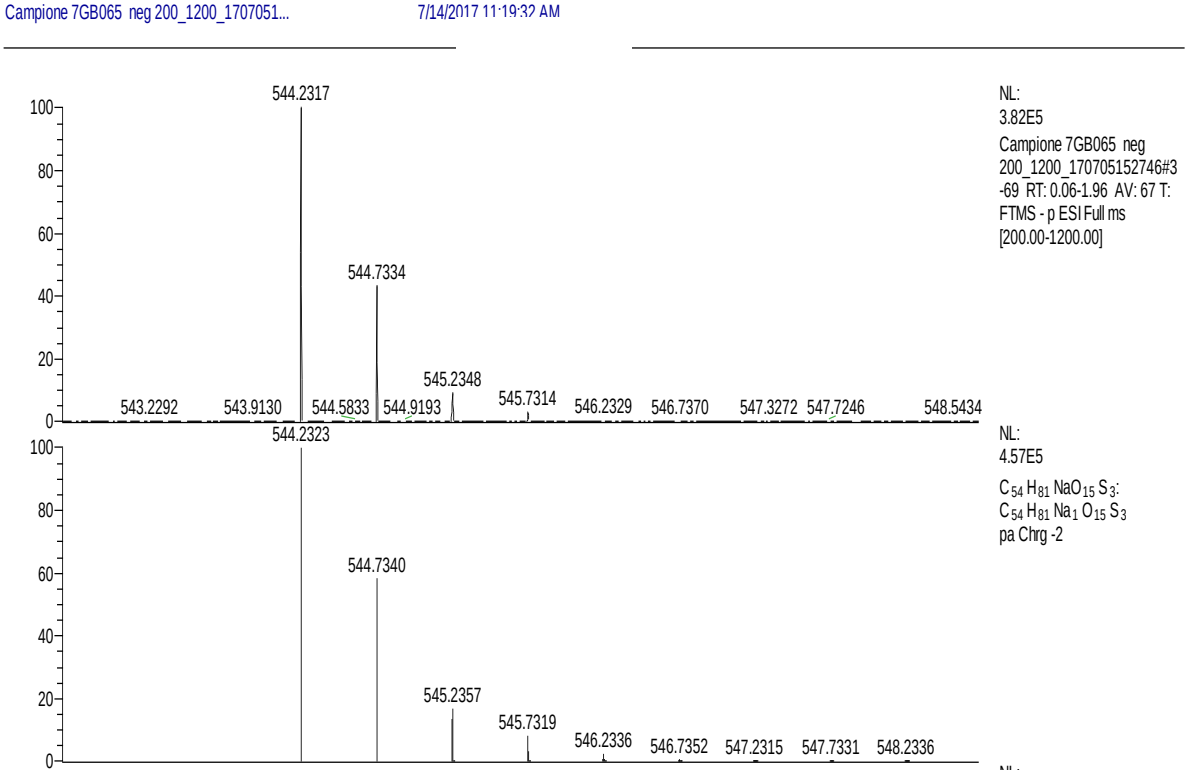

Figure IX: ESI-HRMS of molecule **71**, detail of *m/z* = 2.

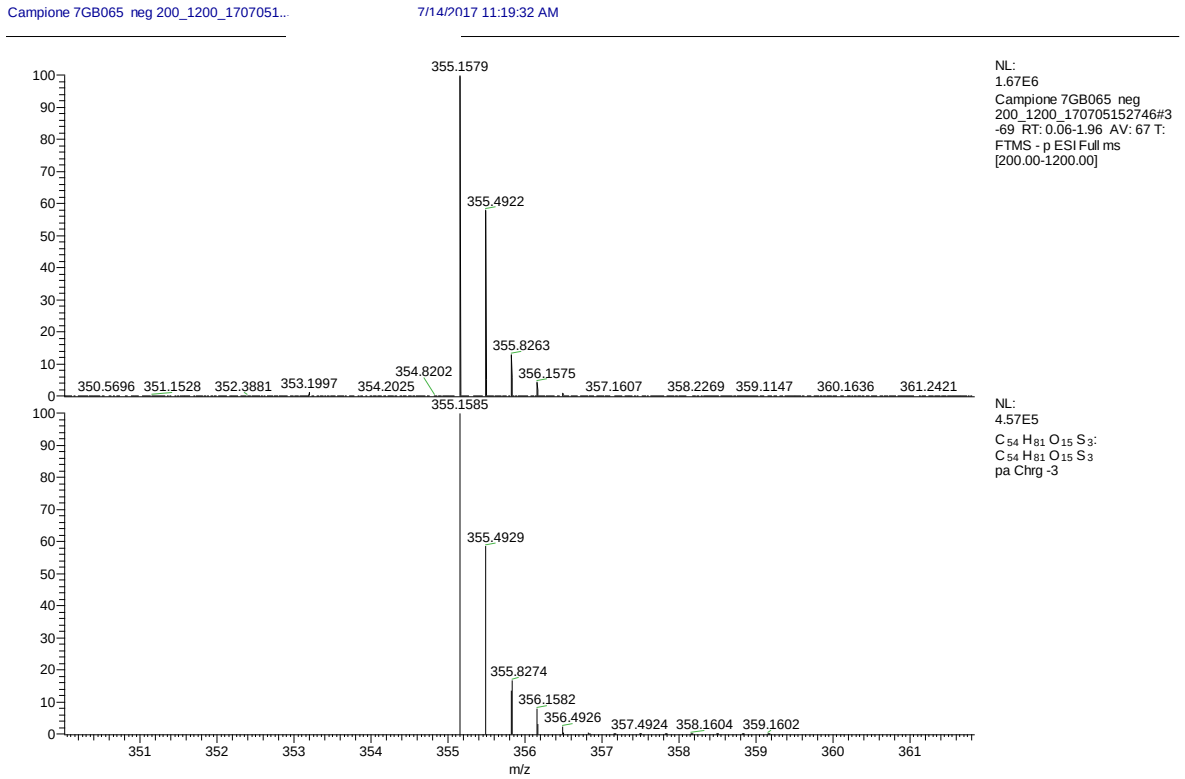

Figure X: ESI-HRMS of molecule **71**, detail of *m/z* = 3.

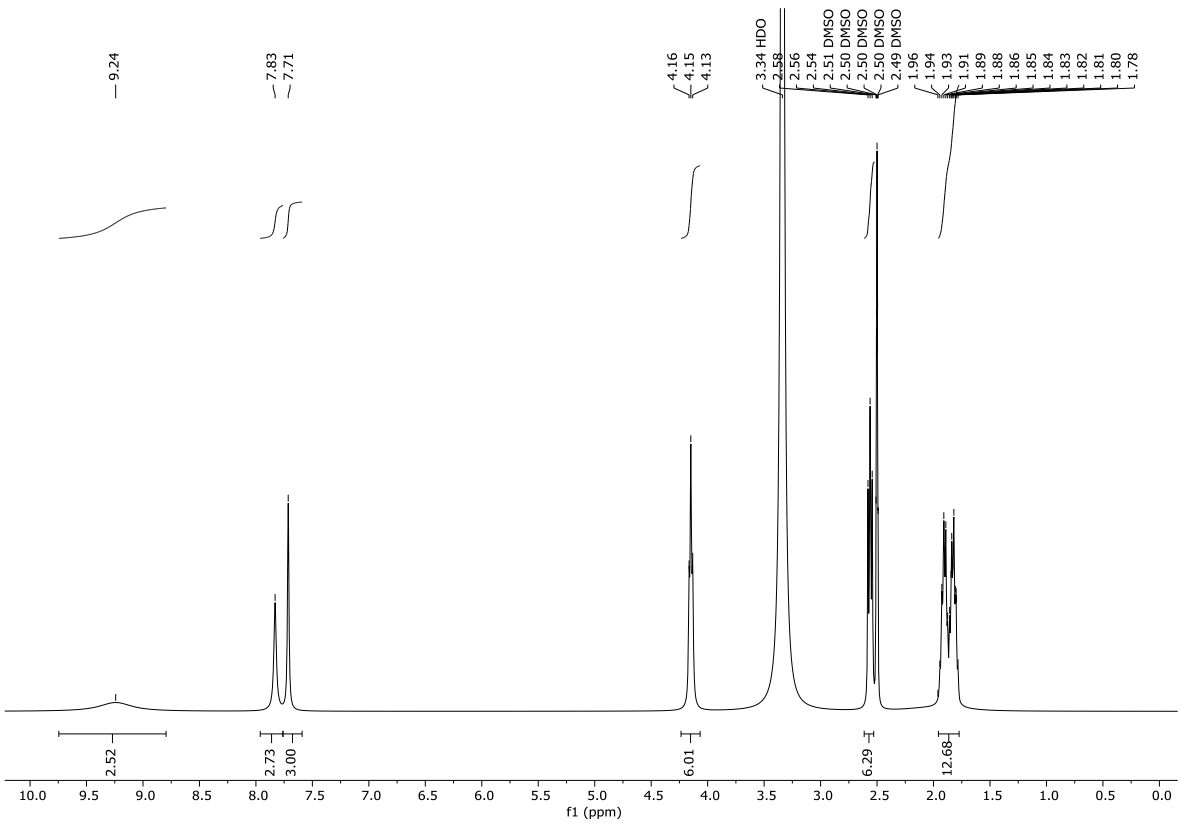

Figure XI: ^{1}H NMR of molecule **72**.

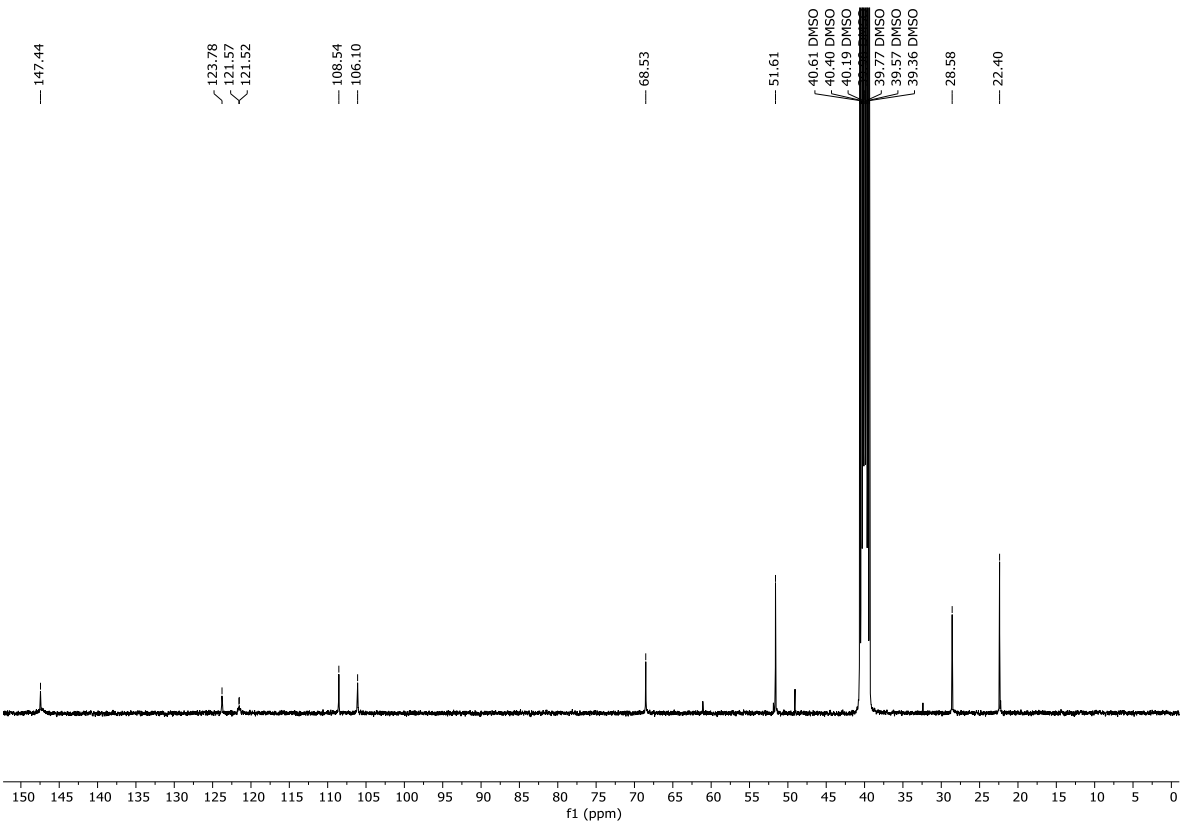

Figure XII: ^{13}C NMR of molecule **72**.

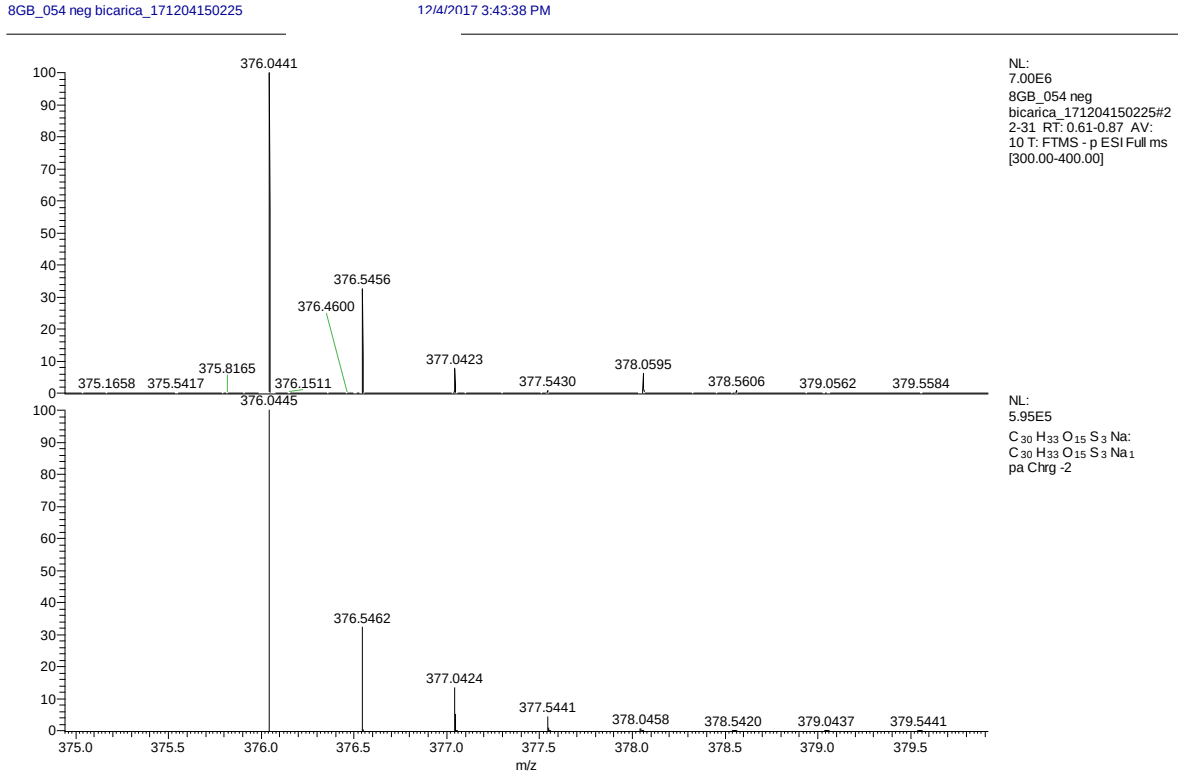

Figure XIII: ESI-HRMS of molecule **72**, detail of *m/z* = 2.

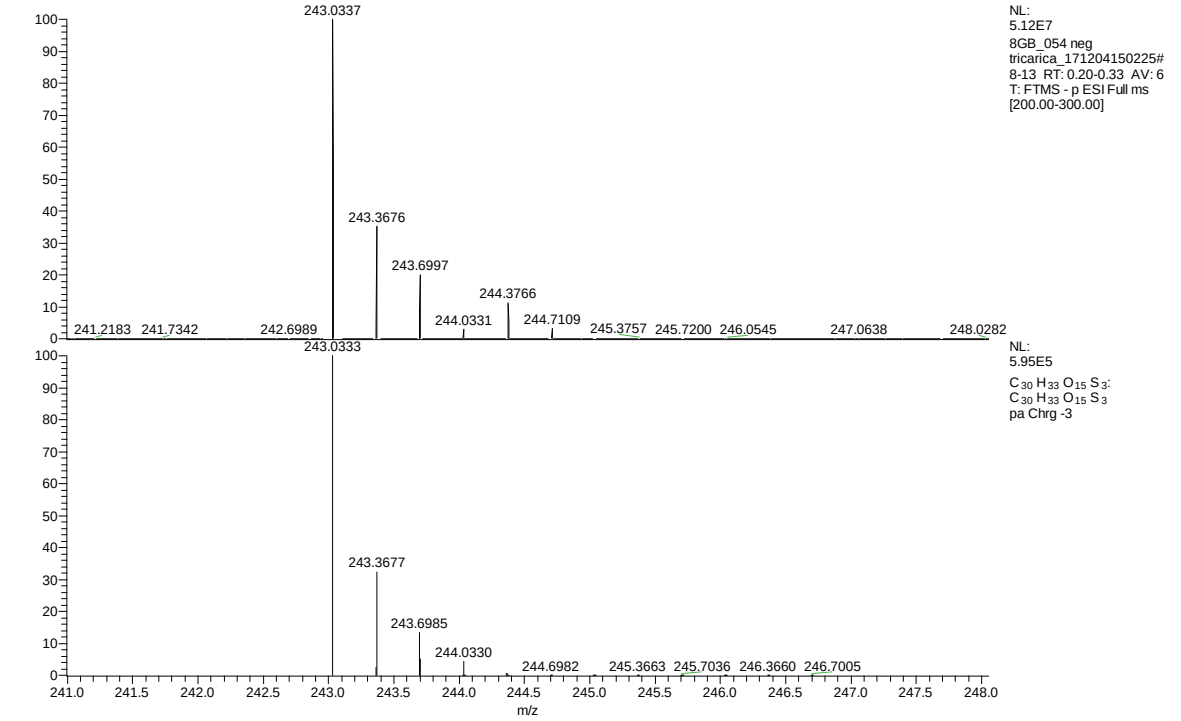

Figure XIV: ESI-HRMS of molecule **72**, detail of *m/z* = 3.

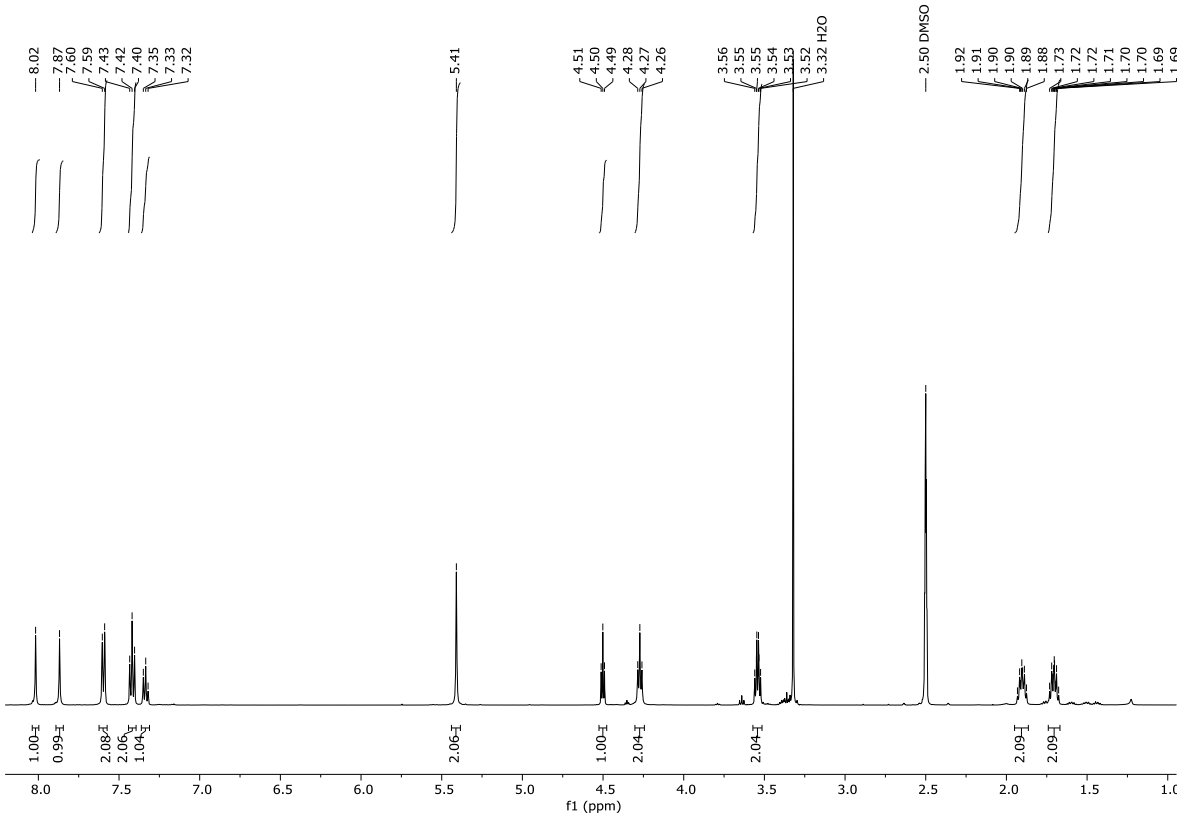

Figure XV: ^{1}H NMR of molecule **73**.

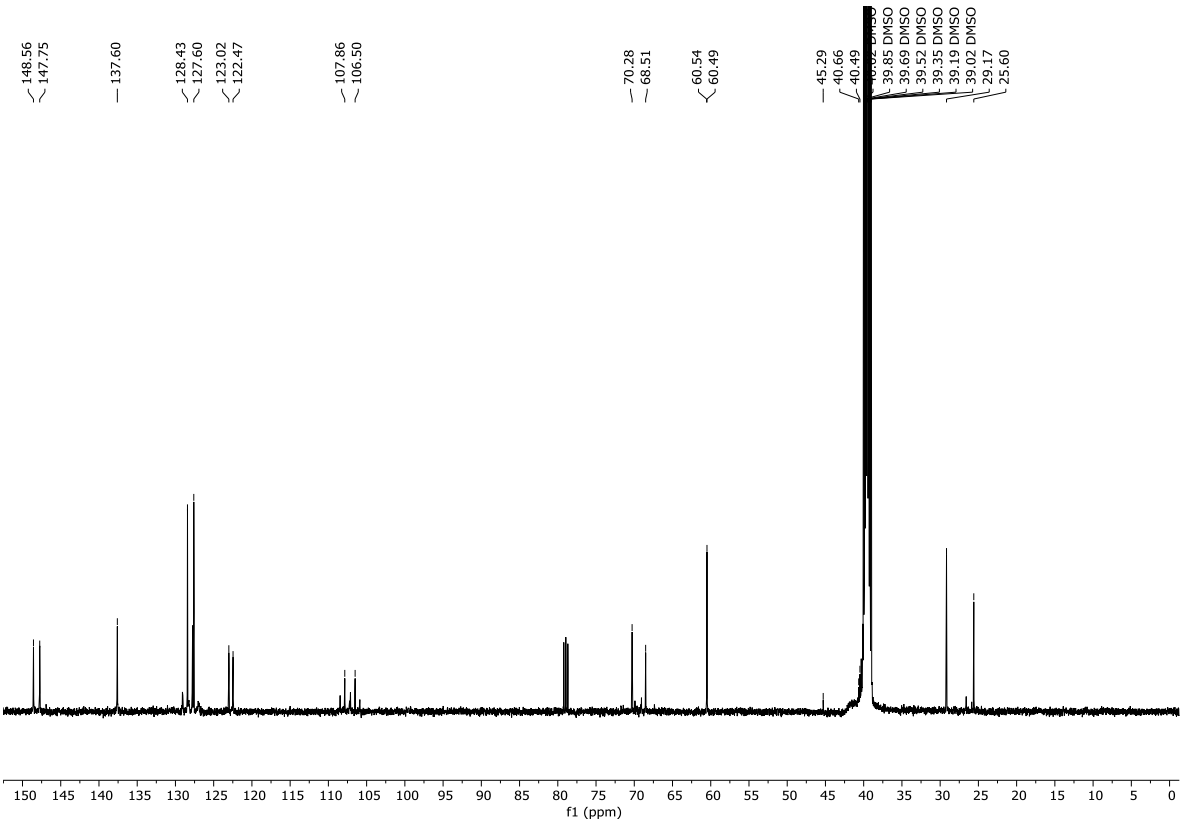

Figure XVI: ^{13}C NMR of molecule **73**.

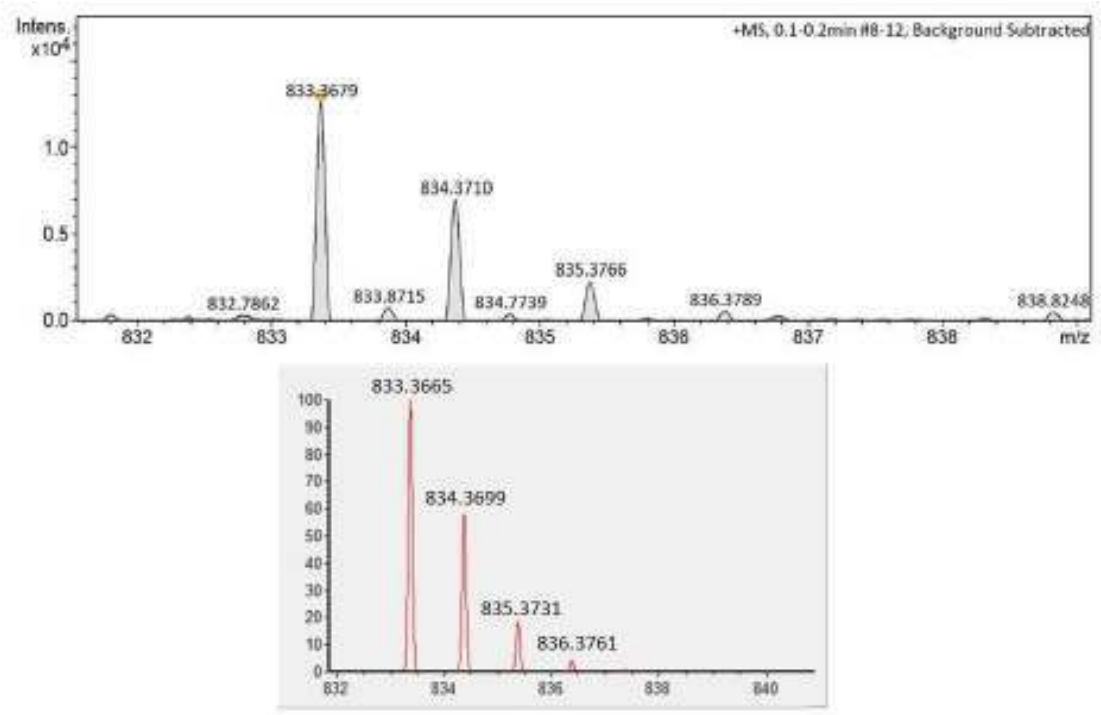

Figure XVII: ESI-HRMS of molecule **73**.

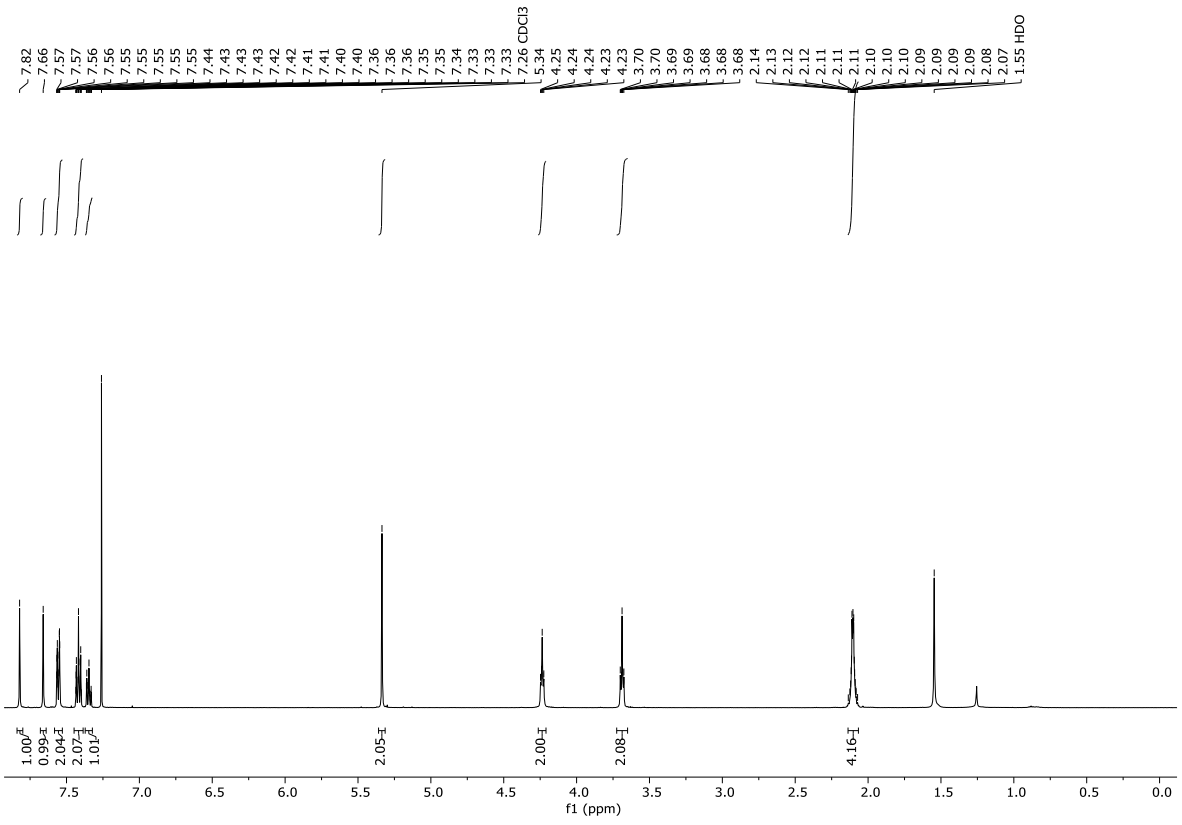

Figure XVIII: ^{1}H NMR of molecule **74**.

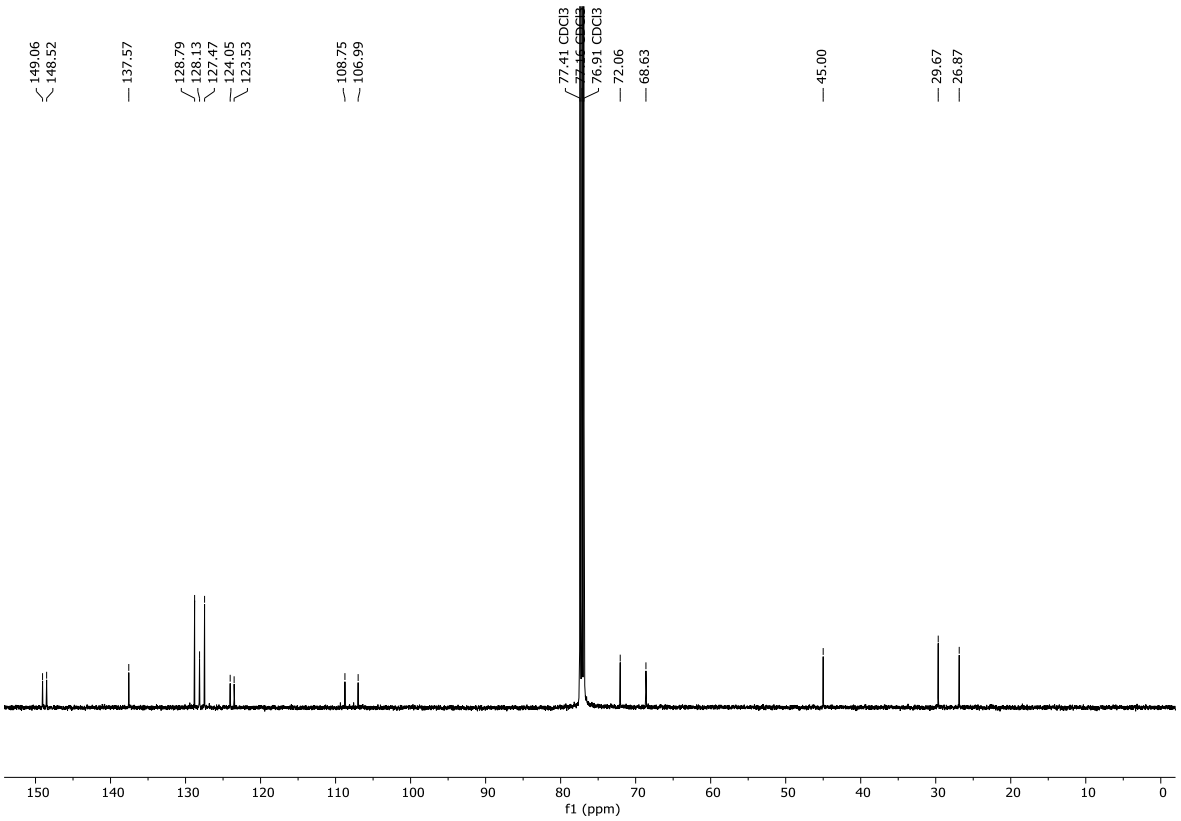

Figure XIX: ^{13}C NMR of molecule **74**.

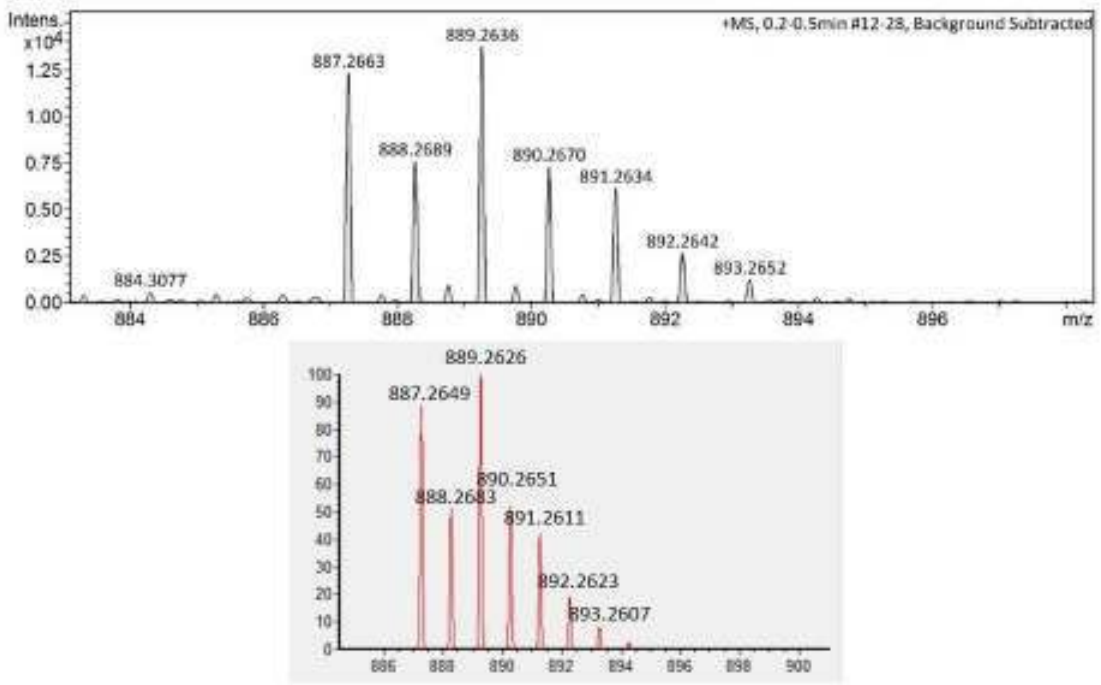

Figure XX: ESI-HRMS of molecule **74**.

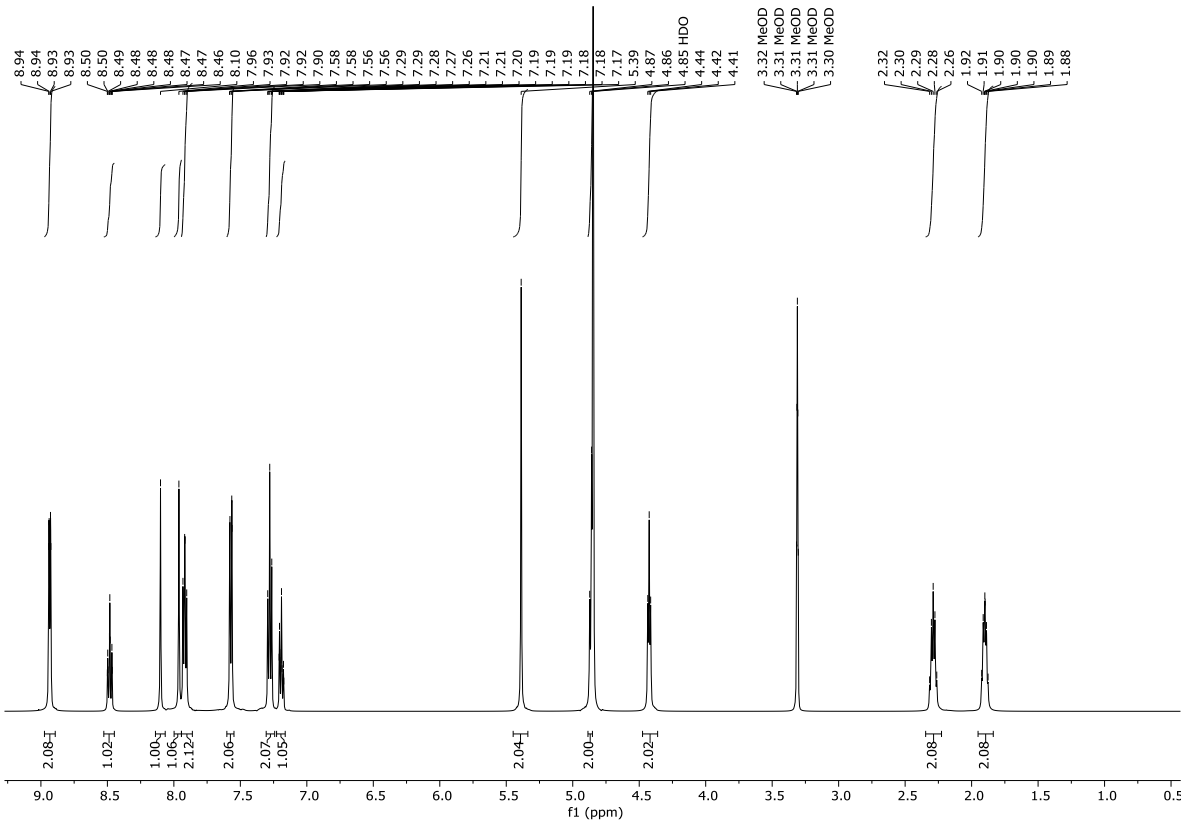

Figure XXI: ^{1}H NMR of molecule **75**.

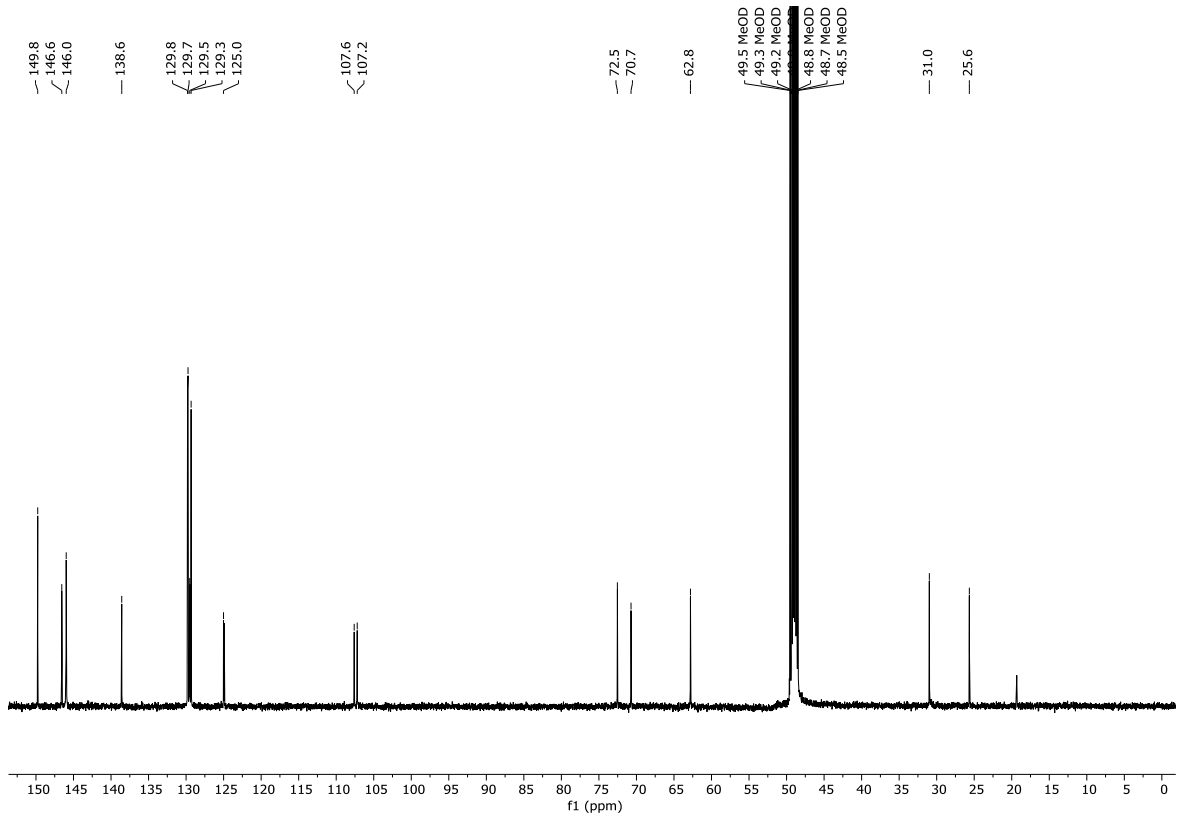

Figure XXII: ^{13}C NMR of molecule **75**.

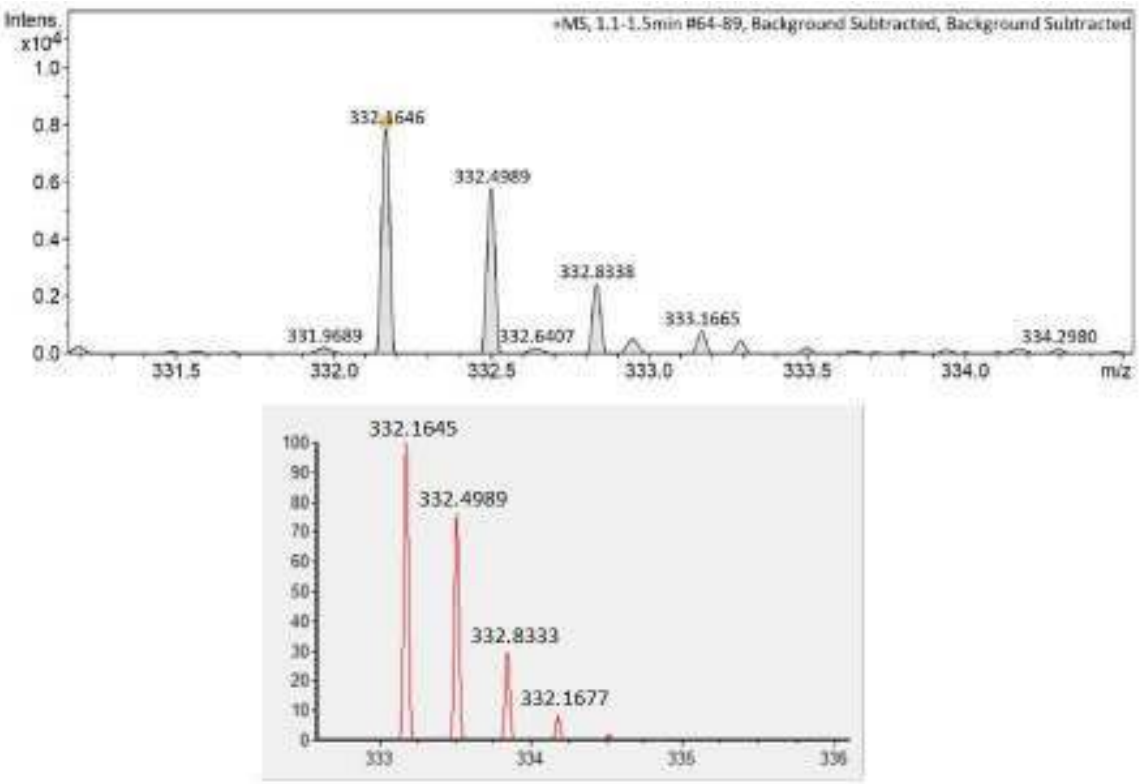

Figure XXIII: ESI-HRMS of molecule **75**.

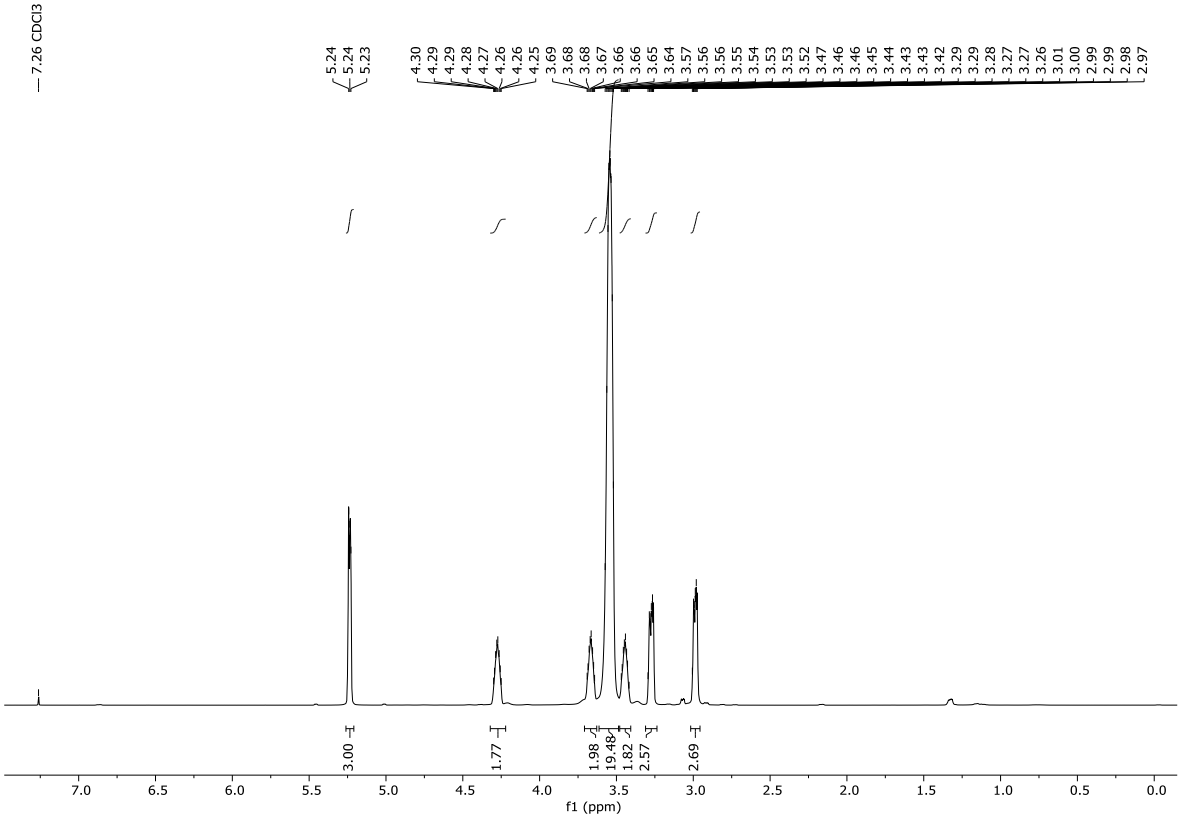

Figure XXIV: ^{1}H NMR of molecule **77**.

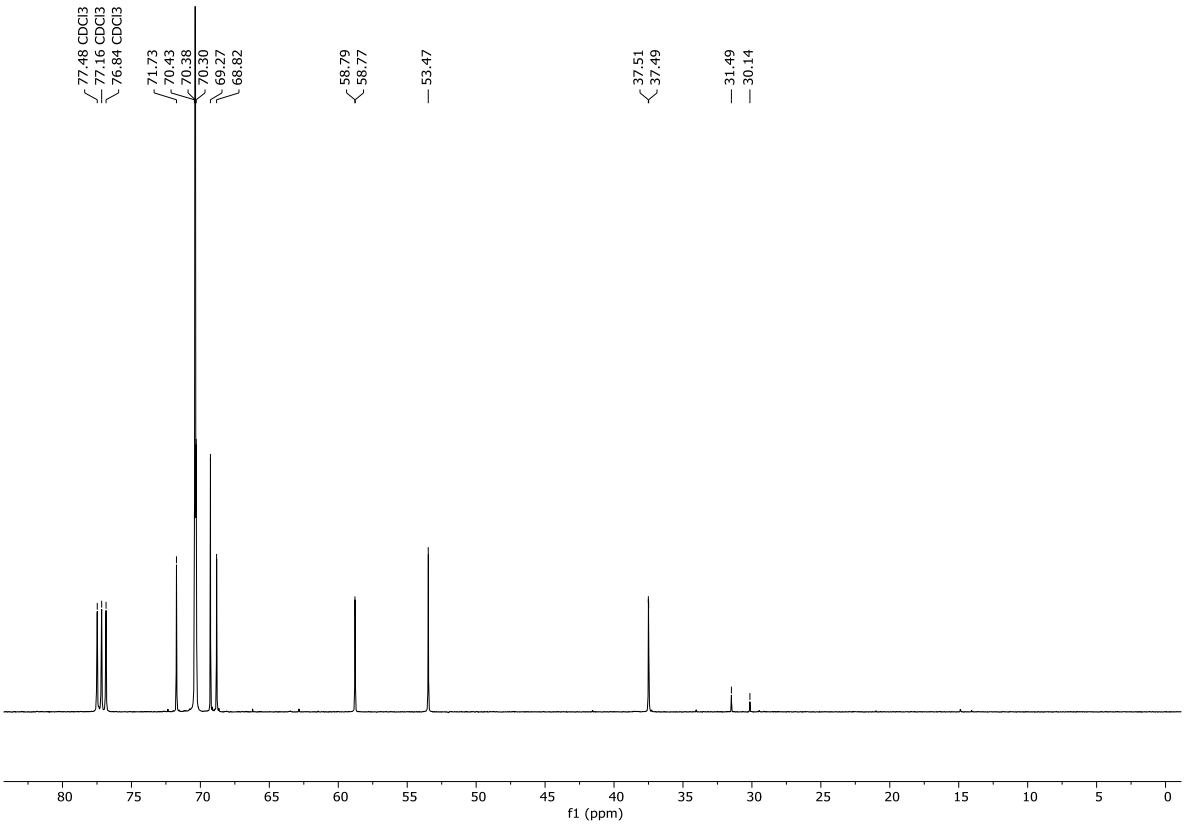

Figure XXV: ^{13}C NMR of molecule **77**.

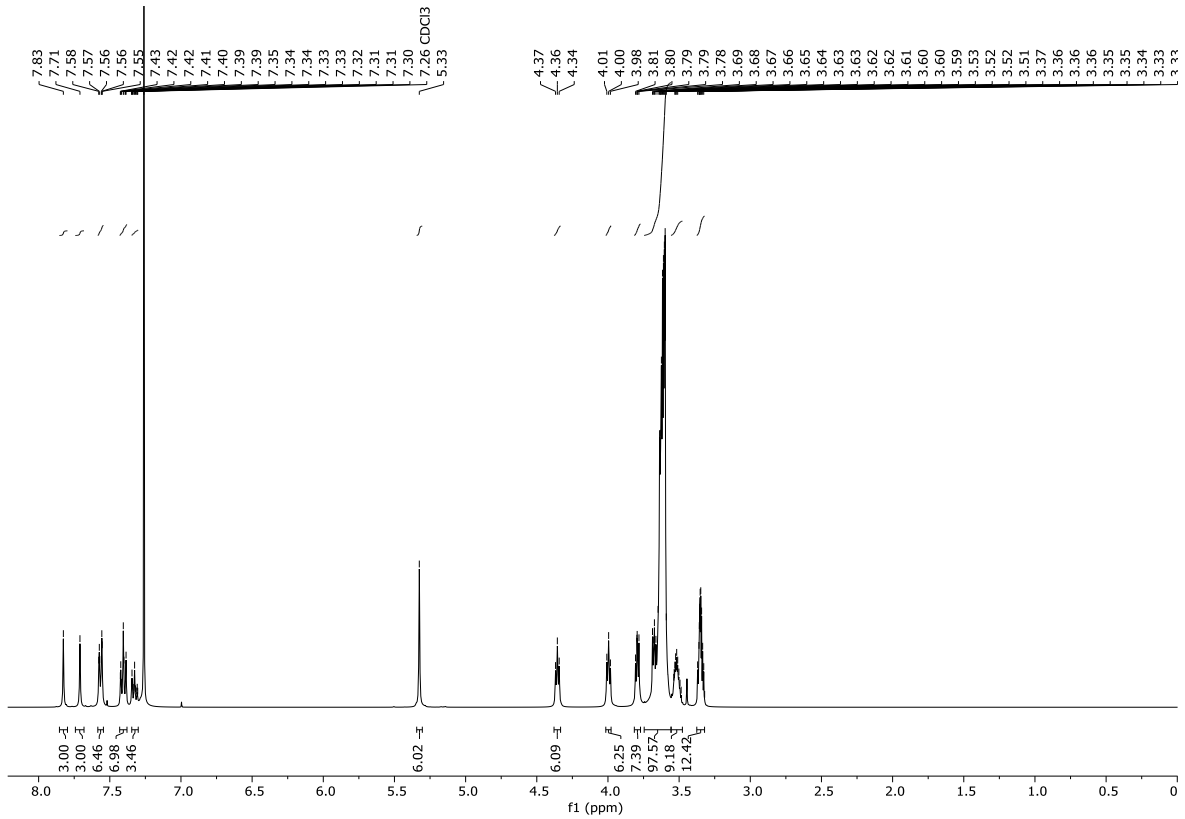

Figure XXVI: ^{1}H NMR of molecule **78**.

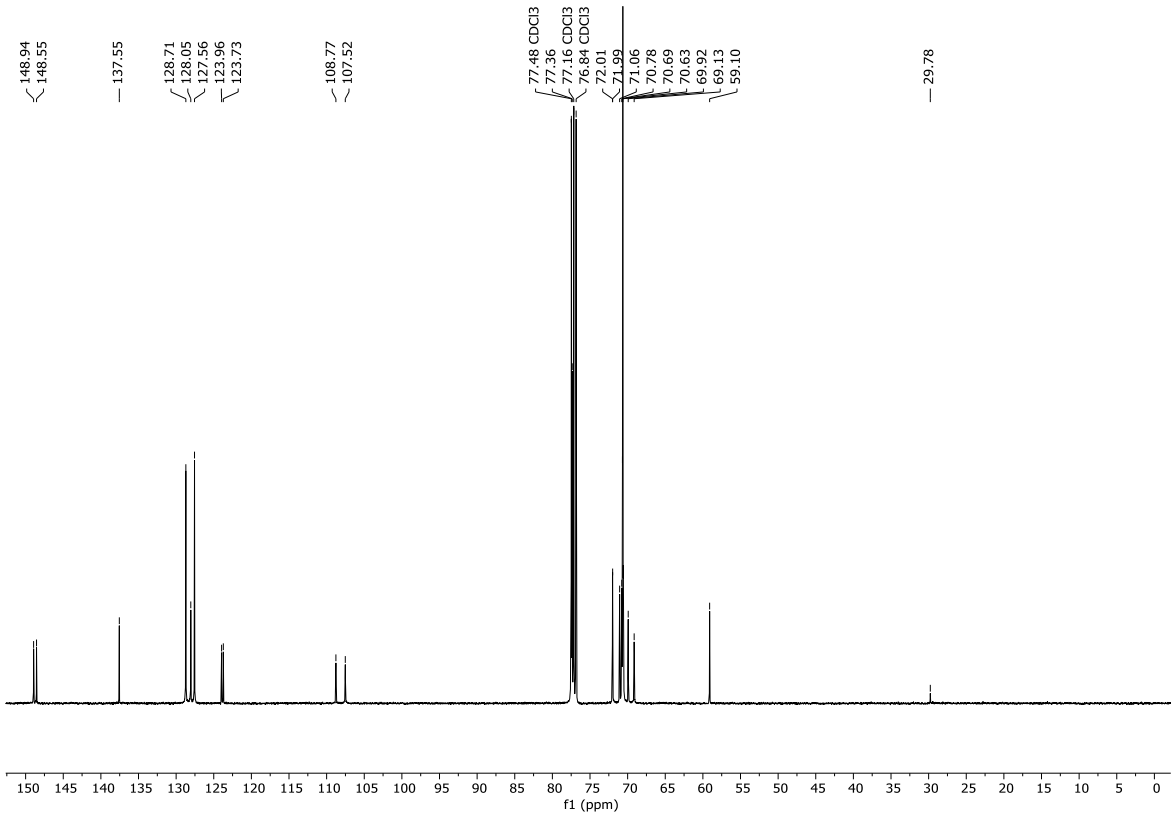

Figure XXVII: ^{13}C NMR of molecule **77**.

7.6.4 c.a.c., DOSY NMR and UV-Vis Spectra

c.a.c. and DOSY NMR 70

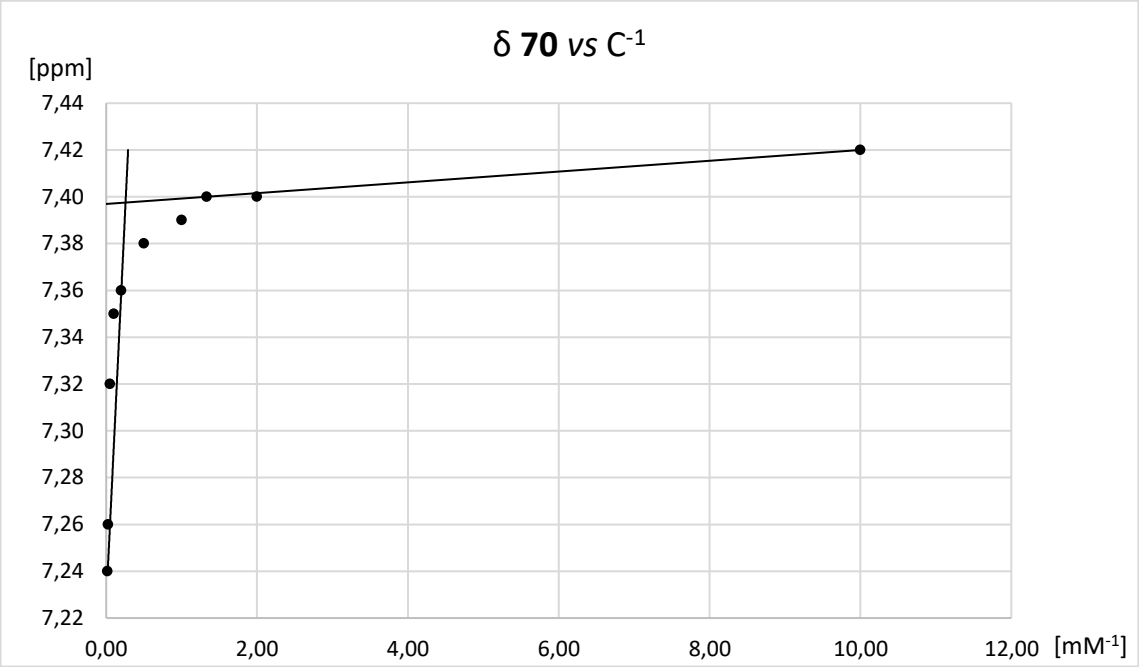

Figure *XXVIII*: Graph of triphenylenic CH chemical shift, δ, of **70** with respect to the inverse of the concentration. The two lines used to calculate the c.a.c. are reported.

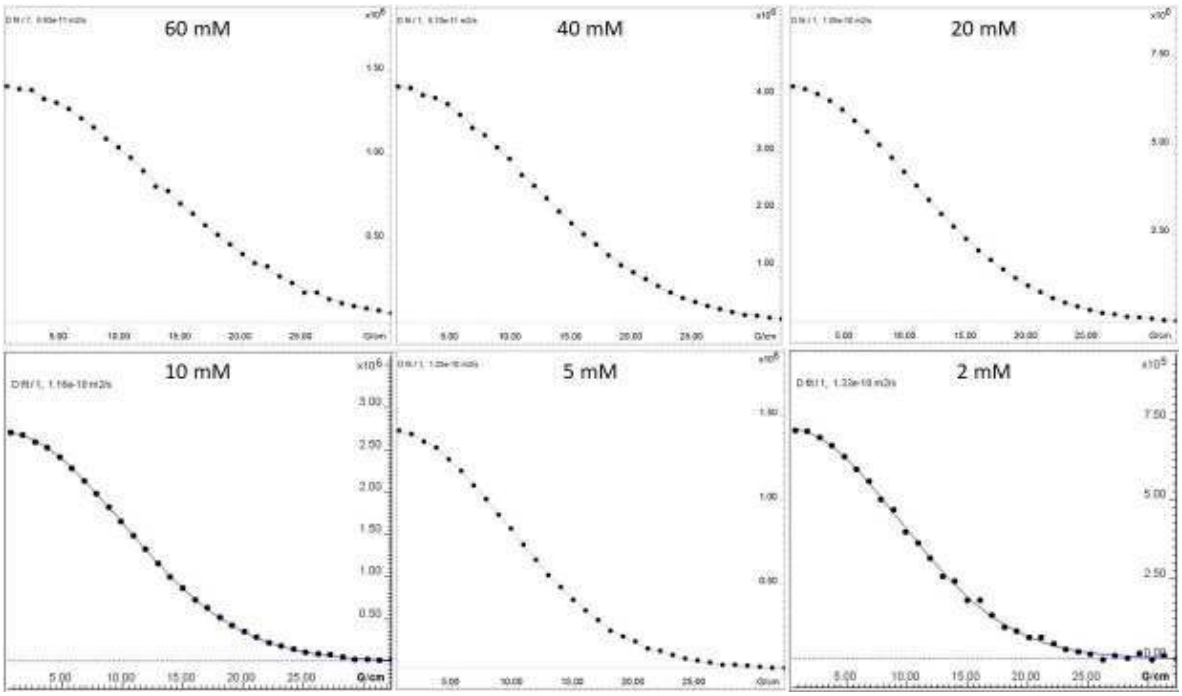

Figure XXIX: Pseudo2D-DOSY NMR monoexponential decay of **70** benzyl signals in D_2O at different concentrations.

First Round	Second Round	C [mM]	Average D First [m^2s^{-1}]	Average D Second [m^2s^{-1}]	Average D [m^2s^{-1}]	STD DEV D [m^2s^{-1}]	Error %
TGNGB008_60mM	TGNGB026_60mM	60	8.16E-11	6.88E-11	7.52E-11	9.06E-12	12.0
TGNGB008_40mM	TGNGB026_40mM	40	8.73E-11	8.68E-11	8.71E-11	2.99E-13	0.3
TGNGB008_20mM	TGNGB026_20mM	20	1.07E-10	1.06E-10	1.06E-10	1.22E-12	1.1
TGNGB008_10mM	TGNGB026_10mM_n2	10	1.19E-10	1.15E-10	1.17E-10	2.96E-12	2.5
TGNGB008_5mM	TGNGB026_5mM	5	1.27E-10	1.22E-10	1.25E-10	3.89E-12	3.1
TGNGB008_2mM	TGNGB026_2mM	2	1.37E-10	1.31E-10	1.34E-10	4.60E-12	3.4
TGNGB008_1mM	TGNGB026_1mM	1	1.42E-10	1.41E-10	1.42E-10	7.07E-13	0.5
TGNGB008_0,75mM_n2	TGNGB026_0,75mM	0.75	1.43E-10	1.45E-10	1.44E-10	1.65E-12	1.1
TGNGB008_0,5mM	TGNGB026_0,5mM	0.5	1.46E-10	1.53E-10	1.49E-10	5.30E-12	3.6
TGNGB008_0,1mM_n2	TGNGB026_0,1mM	0.1	2.19E-10	1.94E-10	2.07E-10	1.77E-11	8.6

Table I: Diffusion coefficients (D) of the two rounds of DOSY analysis of **70** in D_2O at different concentrations.

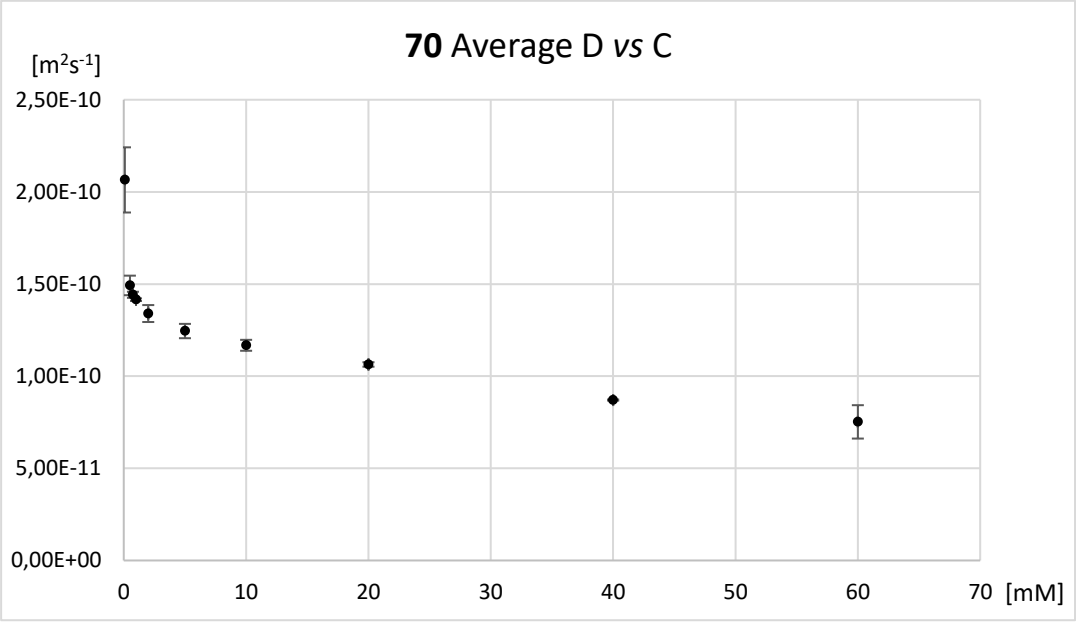

Figure XXX: Average diffusion coefficient of **70** vs concentration is reported.

First Round	Second Round	C [mM]	Hydr. Radius First [m]	Hydr. Radius Second [m]	Average Hydr. Radius [m]	STD DEV Hydr. Radius [m]	Error %
TGNGB008_60mM	TGNGB026_60mM	60	2.41E-09	2.86E-09	2.63E-09	3.17E-10	12.0
TGNGB008_40mM	TGNGB026_40mM	40	2.25E-09	2.26E-09	2.26E-09	7.74E-12	0.3
TGNGB008_20mM	TGNGB026_20mM	20	1.83E-09	1.86E-09	1.85E-09	2.12E-11	1.1
TGNGB008_10mM	TGNGB026_10mM_n2	10	1.65E-09	1.71E-09	1.68E-09	4.27E-11	2.5
TGNGB008_5mM	TGNGB026_5mM	5	1.54E-09	1.61E-09	1.58E-09	4.93E-11	3.1
TGNGB008_2mM	TGNGB026_2mM	2	1.43E-09	1.50E-09	1.47E-09	5.03E-11	3.4
TGNGB008_1mM	TGNGB026_1mM	1	1.38E-09	1.39E-09	1.39E-09	6.94E-12	0.5
TGNGB008_0,75mM_n2	TGNGB026_0,75mM	0.75	1.37E-09	1.35E-09	1.36E-09	1.56E-11	1.1
TGNGB008_0,5mM	TGNGB026_0,5mM	0.5	1.35E-09	1.28E-09	1.32E-09	4.68E-11	3.6
TGNGB008_0,1mM_n2	TGNGB026_0,1mM	0.1	8.97E-10	1.01E-09	9.55E-10	8.18E-11	8.6

Table II: Hydrodynamic radius of the two rounds of DOSY analysis of **70** in D_2O at different concentrations.

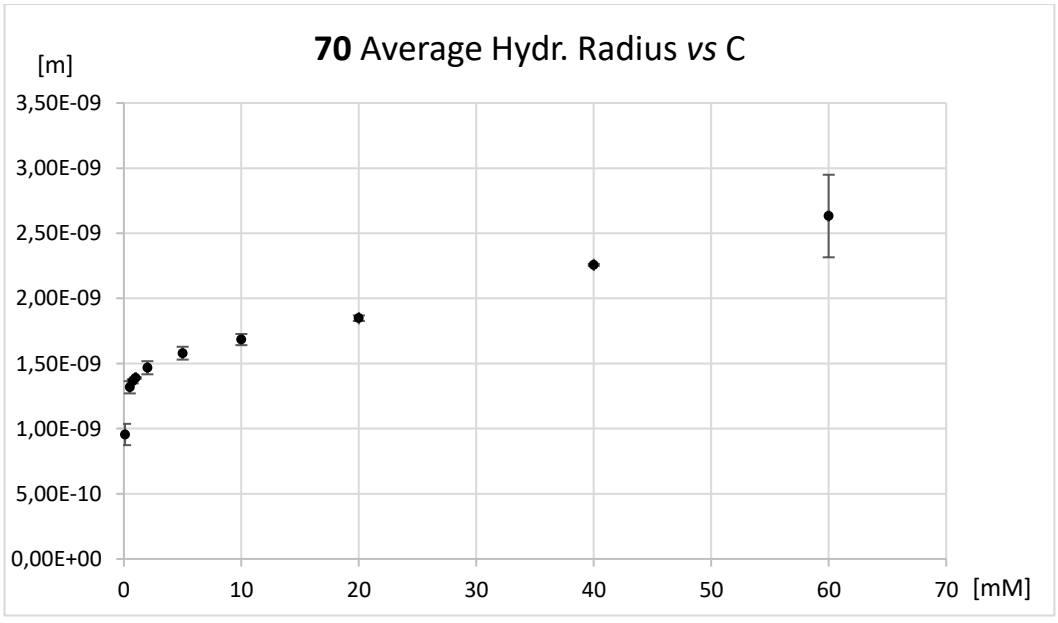

Figure XXXI: Average hydrodynamic radius of **70** *vs* concentration is reported.

c.a.c. and DOSY NMR 71

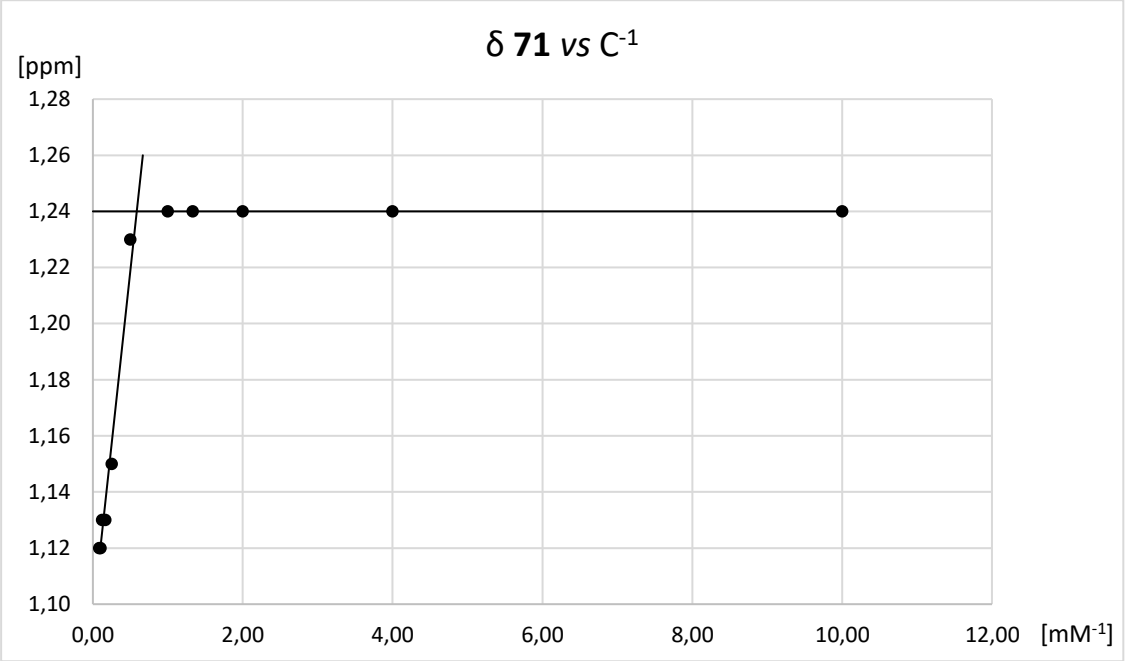

Figure XXXII: Graph of octyl CH_2 chemical shift, δ, of **71** with respect to the inverse of the concentration. The two lines used to calculate the c.a.c. are reported.

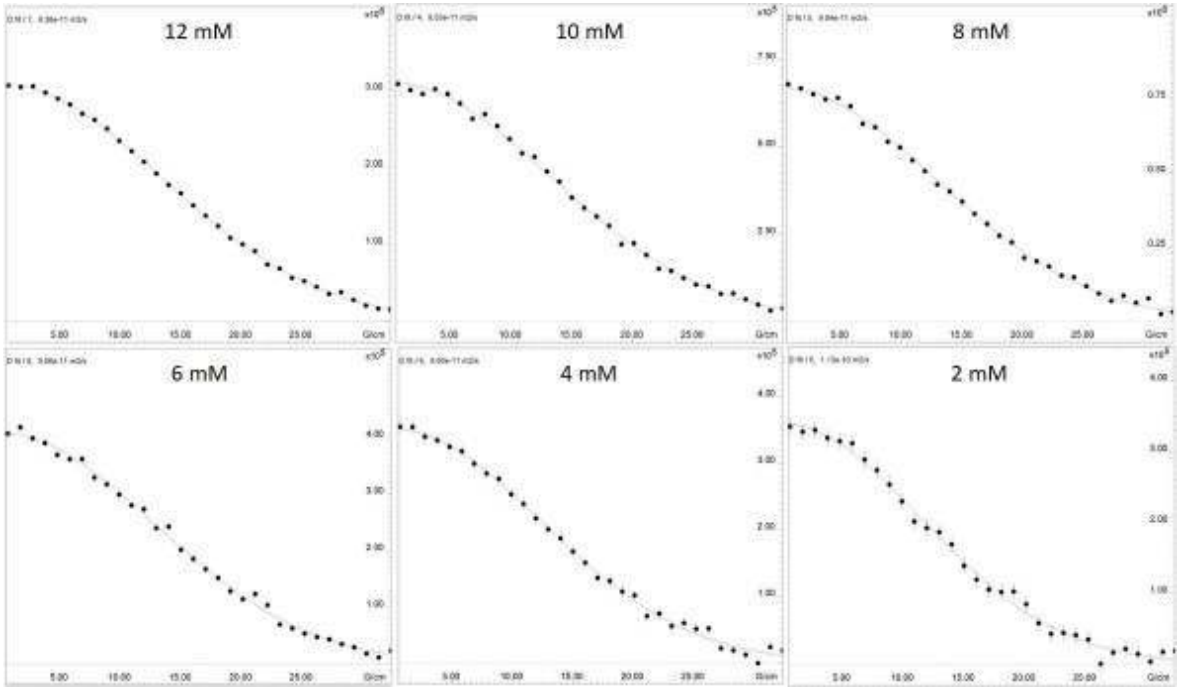

Figure XXXIII: Pseudo2D-DOSY NMR monoexponential decay of **71** triphenylenic signals in D_2O at different concentrations.

First Round	Second Round	C [mM]	Average D First [m^2s^{-1}]	Average D Second [m^2s^{-1}]	Average D [m^2s^{-1}]	STD DEV D [m^2s^{-1}]	Error %
TGNGB009_12mM	TGNGB044_12mM	12	8.63E-11	8.55E-11	8.59E-11	6.07E-13	0.7
TGNGB009_10mM	TGNGB044_10mM	10	8.73E-11	8.63E-11	8.68E-11	6.62E-13	0.8
TGNGB009_8mM	TGNGB044_8mM	8	8.87E-11	9.09E-11	8.98E-11	1.61E-12	1.8
TGNGB009_6mM	TGNGB044_6mM	6	9.27E-11	9.15E-11	9.21E-11	8.61E-13	0.9
TGNGB009_4mM	TGNGB044_4mM	4	1.00E-10	9.98E-11	1.00E-10	3.14E-13	0.3
TGNGB009_2mM	TGNGB044_2mM	2	1.16E-10	1.10E-10	1.13E-10	4.48E-12	4.0
TGNGB009_1mM_n2	TGNGB044_1mM	1	1.21E-10	1.18E-10	1.20E-10	1.84E-12	1.5
TGNGB009_0.75mM	TGNGB044_0.75mM	0.75	1.22E-10	1.24E-10	1.23E-10	1.38E-12	1.1
TGNGB009_0.5mM	TGNGB044_0.5mM	0.5	1.27E-10	1.25E-10	1.26E-10	1.18E-12	0.9
TGNGB009_0.25mM_n2	TGNGB044_0.25mM	0.25	1.57E-10	1.49E-10	1.53E-10	5.66E-12	3.7
TGNGB009_0.1mM	TGNGB044_0.1mM	0.1	1.57E-10	1.74E-10	1.66E-10	1.20E-11	7.3

Table III: Diffusion coefficients of the two rounds of DOSY analysis of **71** in D_2O at different concentrations.

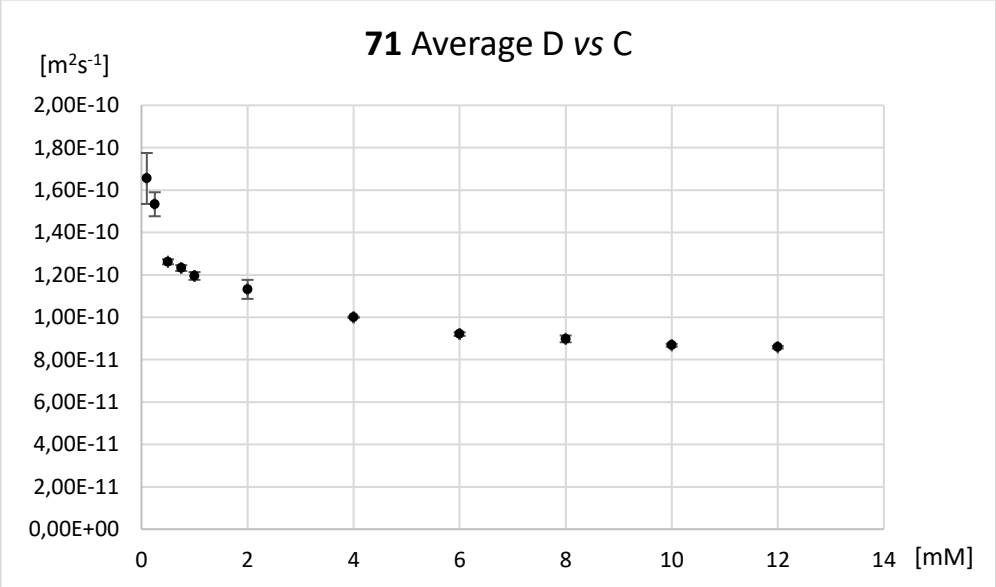

Figure XXXIV: Average diffusion coefficient of **71** *vs* concentration is reported.

First Round	Second Round	C [mM]	Hydr. Radius First [m]	Hydr. Radius Second [m]	Average Hydr. Radius [m]	STD DEV Hydr. Radius [m]	Error %
TGNGB009_12mM	TGNGB044_12mM	12	2.28E-09	2.30E-09	2.29E-09	1.62E-11	0.7
TGNGB009_10mM	TGNGB044_10mM	10	2.25E-09	2.28E-09	2.26E-09	1.73E-11	0.8
TGNGB009_8mM	TGNGB044_8mM	8	2.22E-09	2.16E-09	2.19E-09	3.92E-11	1.8
TGNGB009_6mM	TGNGB044_6mM	6	2.12E-09	2.15E-09	2.13E-09	2.00E-11	0.9
TGNGB009_4mM	TGNGB044_4mM	4	1.96E-09	1.97E-09	1.97E-09	6.18E-12	0.3
TGNGB009_2mM	TGNGB044_2mM	2	1.69E-09	1.79E-09	1.74E-09	6.88E-11	4.0
TGNGB009_1mM_n2	TGNGB044_1mM	1	1.63E-09	1.66E-09	1.64E-09	2.53E-11	1.5
TGNGB009_0.75mM	TGNGB044_0.75mM	0.75	1.61E-09	1.58E-09	1.60E-09	1.78E-11	1.1
TGNGB009_0.5mM	TGNGB044_0.5mM	0.5	1.55E-09	1.57E-09	1.56E-09	1.46E-11	0.9
TGNGB009_0.25mM_n2	TGNGB044_0.25mM	0.25	1.25E-09	1.32E-09	1.28E-09	4.73E-11	3.7
TGNGB009_0.1mM	TGNGB044_0.1mM	0.1	1.25E-09	1.13E-09	1.19E-09	8.65E-11	7.3

Table IV: Hydrodynamic radius of the two rounds of DOSY analysis of **71** in D_2O at different concentrations.

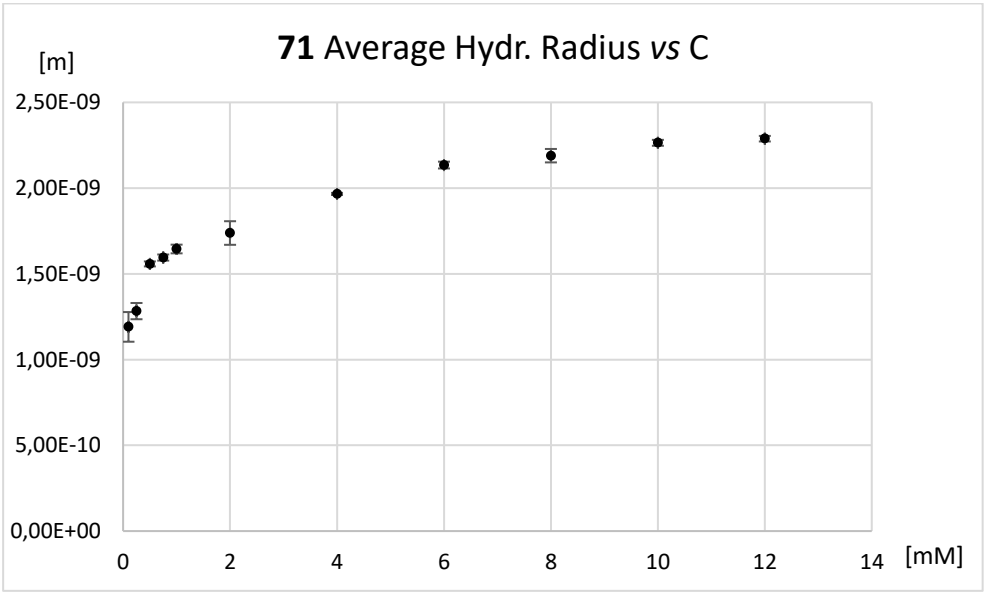

Figure XXXV: Average hydrodynamic radius of **71** *vs* concentration is reported.

c.a.c. and DOSY NMR 75

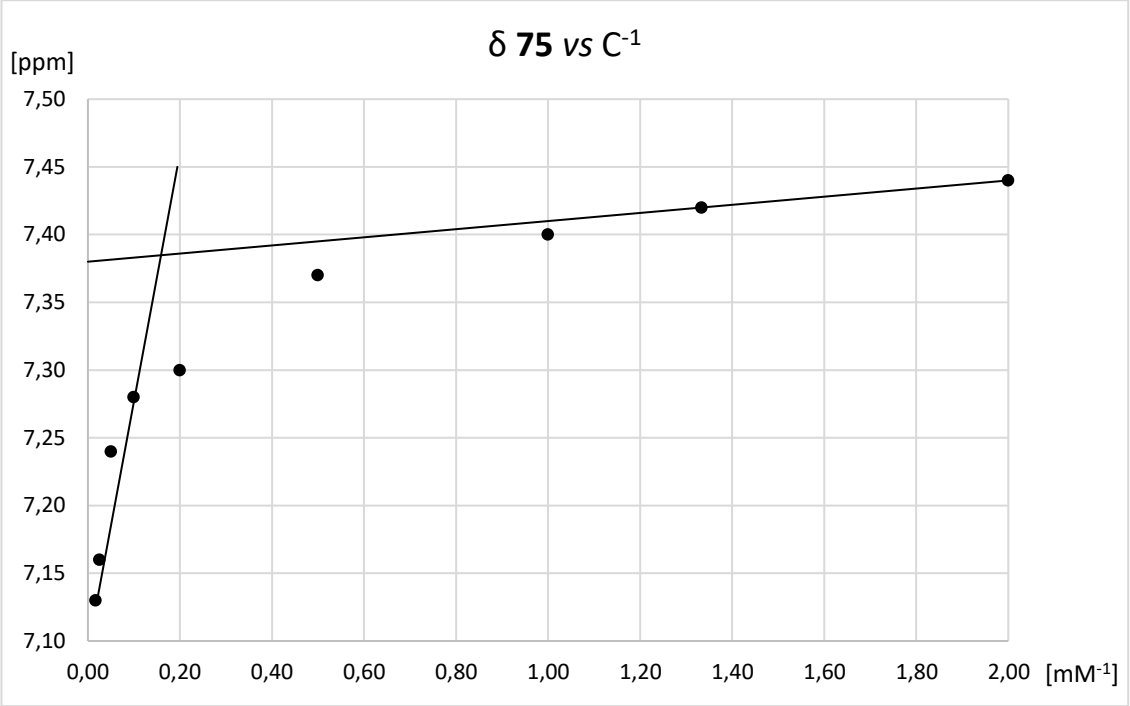

Figure XXXVI: Graph of aromatic CH chemical shift, δ, of **75** with respect to the inverse of the concentration. The two lines used to calculate the c.a.c. are reported.

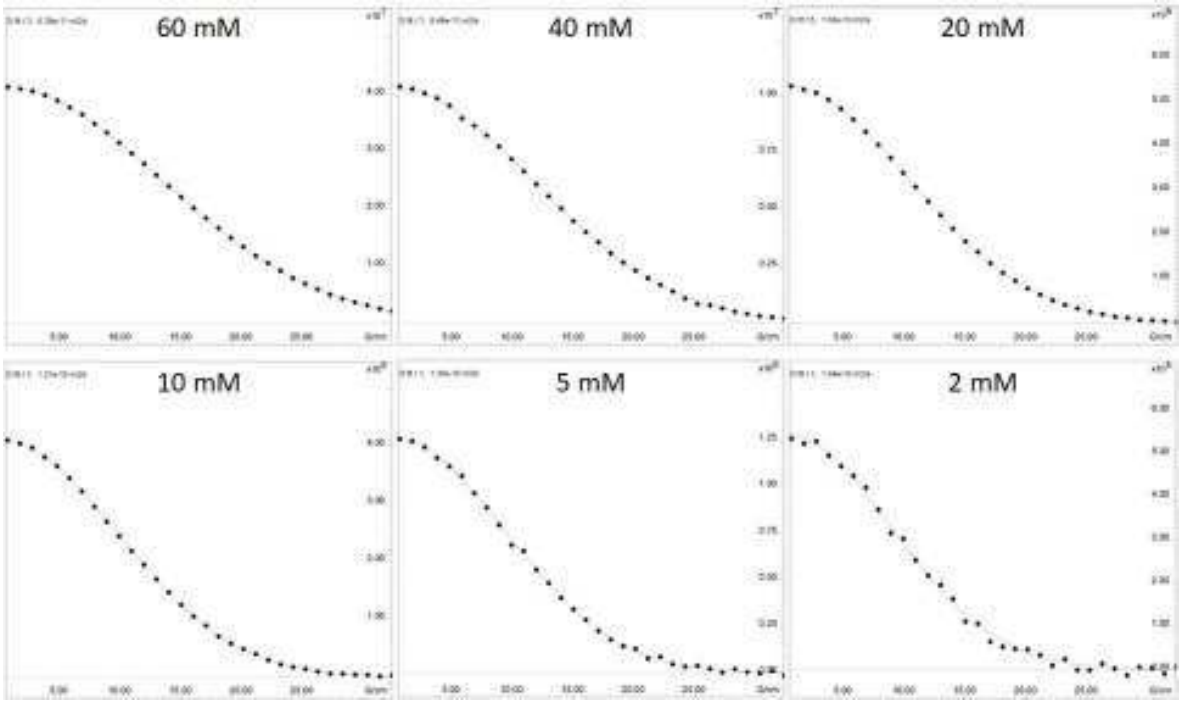

Figure XXXVII: Pseudo2D-DOSY NMR monoexponential decay of **75** triphenylenic signals in D_2O at different concentrations.

First Round	Second Round	C [mM]	Average D First [m^2s^{-1}]	Average D Second [m^2s^{-1}]	Average D [m^2s^{-1}]	STD DEV D [m^2s^{-1}]	Error %
TGNGB033_60mM	TGNGB034_60mM	60	6.36E-11	6.40E-11	6.38E-11	2.27E-13	0.4
TGNGB033_40mM	TGNGB034_40mM	40	8.41E-11	8.53E-11	8.47E-11	8.99E-13	1.1
TGNGB033_20mM	TGNGB034_20mM	20	1.09E-10	1.08E-10	1.08E-10	6.27E-13	0.6
TGNGB033_10mM	TGNGB034_10mM	10	1.23E-10	1.23E-10	1.23E-10	1.18E-13	0.1
TGNGB033_5mM	TGNGB034_5mM	5	1.34E-10	1.31E-10	1.32E-10	1.77E-12	1.3
TGNGB033_2mM	TGNGB034_2mM	2	1.44E-10	1.47E-10	1.45E-10	2.03E-12	1.4
TGNGB033_1mM	TGNGB034_1mM	1	1.53E-10	1.53E-10	1.53E-10	8.08E-14	0.1
TGNGB033_0.75mM	TGNGB034_0.75mM	0.75	1.56E-10	1.59E-10	1.57E-10	2.04E-12	1.3
TGNGB033_0.5mM_n3	TGNGB034_0.5mM	0.5	1.59E-10	1.63E-10	1.61E-10	2.55E-12	1.6
TGNGB033_0.1mM	TGNGB034_0.1mM	0.1	1.93E-10	1.81E-10	1.87E-10	8.31E-12	4.4

Table V: Diffusion coefficients of the two rounds of DOSY analysis of **75** in D_2O at different concentrations.

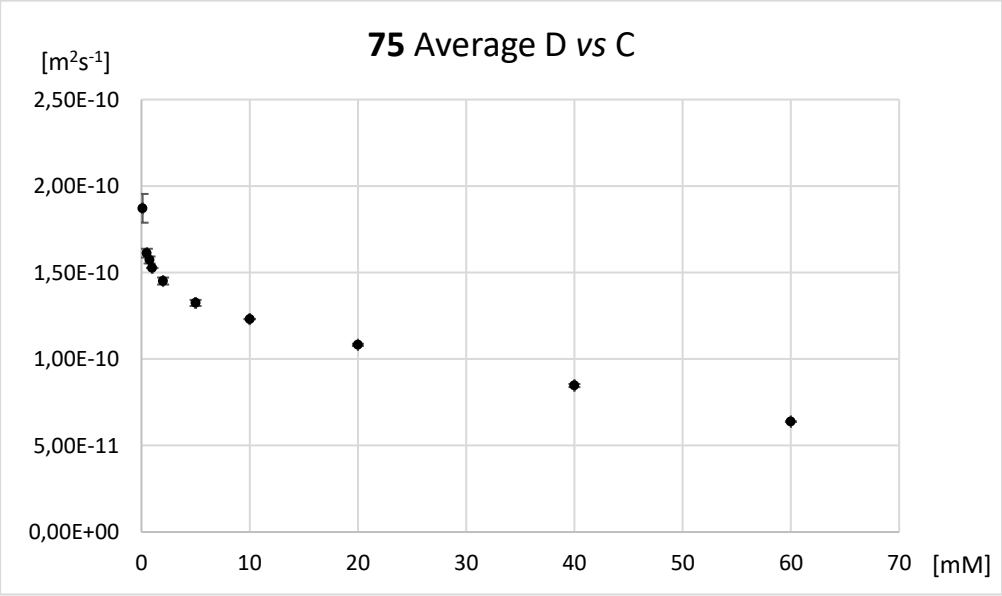

Figure XXXVIII: Average diffusion coefficient of **75** *vs* concentration is reported.

First Round	Second Round	C [mM]	Hydr. Radius First [m]	Hydr. Radius Second [m]	Average Hydr. Radius [m]	STD DEV Hydr. Radius [m]	Error %
TGNGB033_60mM	TGNGB034_60mM	60	3.09E-09	3.07E-09	3.08E-09	1.10E-11	0.4
TGNGB033_40mM	TGNGB034_40mM	40	2.34E-09	2.30E-09	2.32E-09	2.46E-11	1.1
TGNGB033_20mM	TGNGB034_20mM	20	1.81E-09	1.82E-09	1.82E-09	1.05E-11	0.6
TGNGB033_10mM	TGNGB034_10mM	10	1.60E-09	1.60E-09	1.60E-09	1.53E-12	0.1
TGNGB033_5mM	TGNGB034_5mM	5	1.47E-09	1.50E-09	1.48E-09	1.98E-11	1.3
TGNGB033_2mM	TGNGB034_2mM	2	1.37E-09	1.34E-09	1.35E-09	1.90E-11	1.4
TGNGB033_1mM	TGNGB034_1mM	1	1.29E-09	1.29E-09	1.29E-09	6.82E-13	0.1
TGNGB033_0.75mM	TGNGB034_0.75mM	0.75	1.26E-09	1.24E-09	1.25E-09	1.62E-11	1.3
TGNGB033_0.5mM_n3	TGNGB034_0.5mM	0.5	1.23E-09	1.21E-09	1.22E-09	1.93E-11	1.6
TGNGB033_0.1mM	TGNGB034_0.1mM	0.1	1.02E-09	1.08E-09	1.05E-09	4.67E-11	4.4

Table VI: Hydrodynamic radius of the two rounds of DOSY analysis of **75** in D_2O at different concentrations.

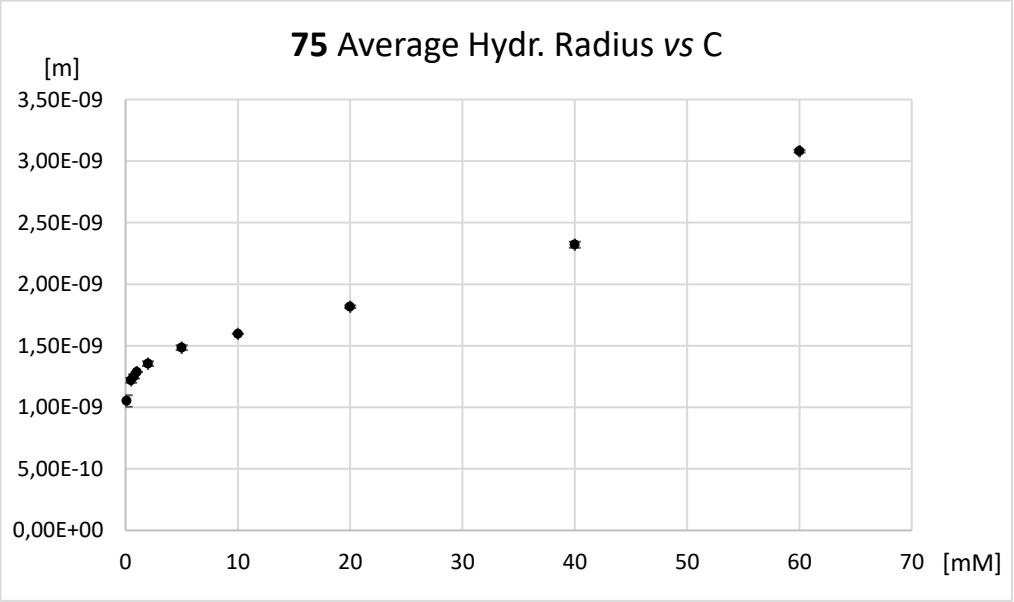

Figure XXXIX: Average hydrodynamic radius of **75** *vs* concentration is reported.

c.a.c. and DOSY NMR 72

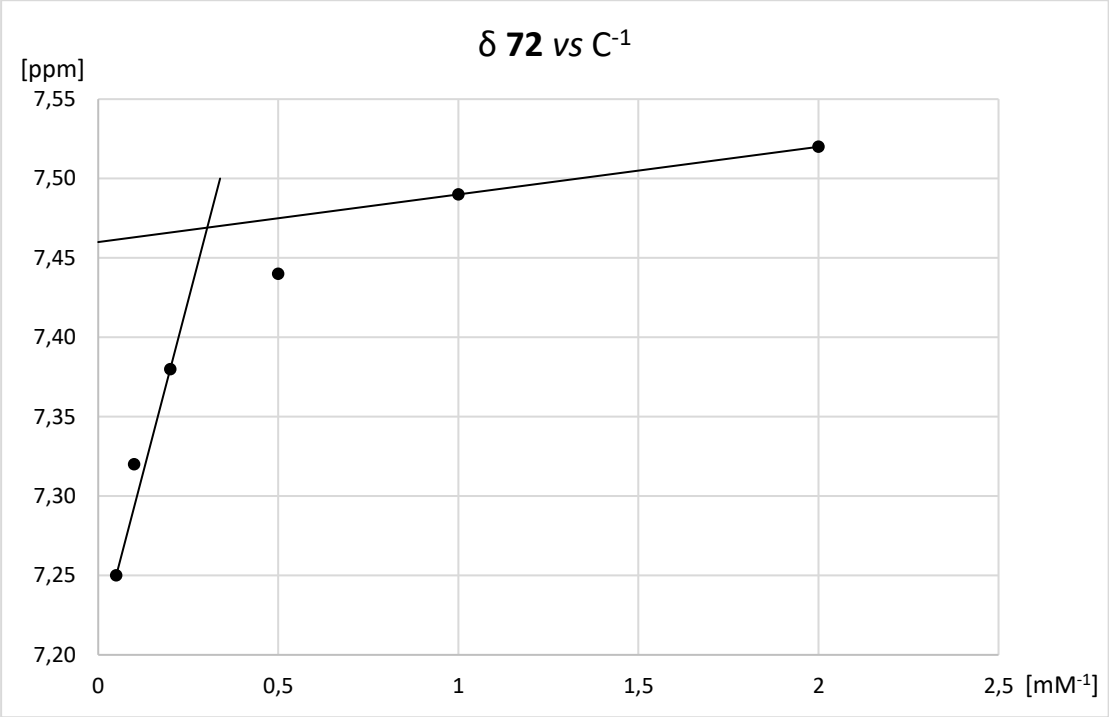

Figure XL: Graph of triphenylenic CH chemical shift, δ, of **72** with respect to the inverse of the concentration. The two lines used to calculate the c.a.c. are reported.

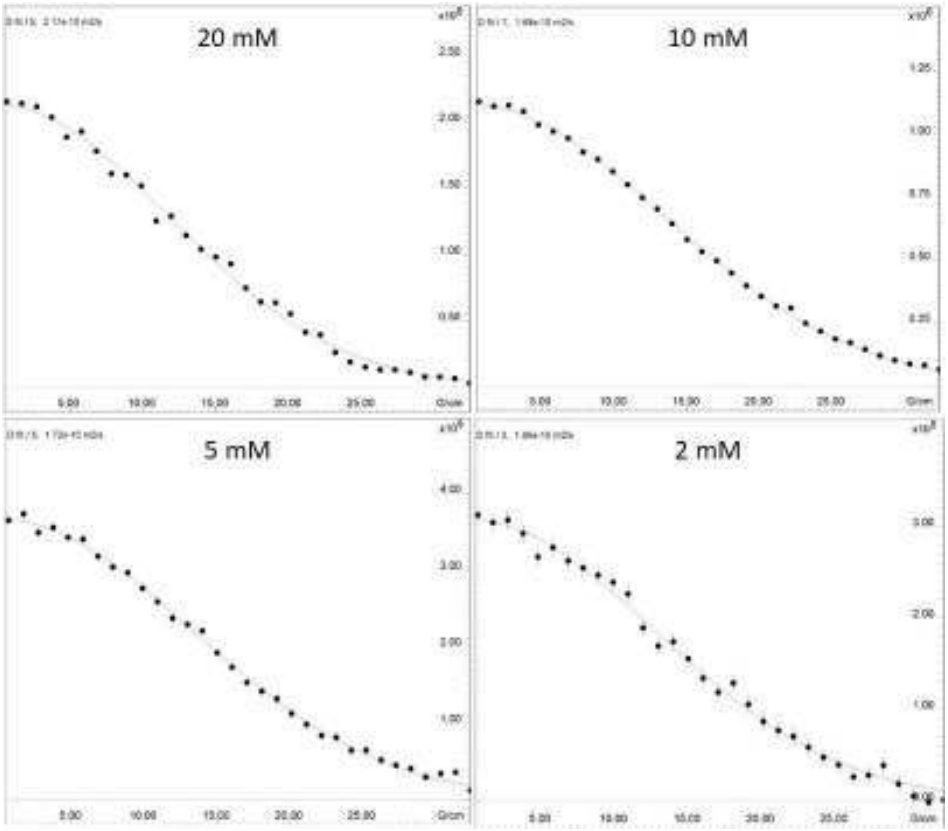

Figure XLI: Pseudo2D-DOSY NMR monoexponential decay of **72** triphenylenic signals in D_2O at different concentrations.

First Round	Second Round	C [mM]	Average D First [m^2s^{-1}]	Average D Second [m^2s^{-1}]	Average D [m^2s^{-1}]	STD DEV D [m^2s^{-1}]	Error %
TGNGB025_20mM	TGNGB043_20mM_n2	20	1.70E-10	2.16E-10	1.93E-10	3.31E-11	17.1
TGNGB025_10mM	TGNGB043_10mM	10	1.70E-10	1.69E-10	1.69E-10	8.49E-13	0.5
TGNGB025_5mM	TGNGB043_5mM	5	1.74E-10	1.73E-10	1.73E-10	9.43E-13	0.5
TGNGB025_2mM_n2	TGNGB043_2mM	2	1.73E-10	1.85E-10	1.79E-10	8.49E-12	4.7
TGNGB025_1mM_n2	TGNGB043_1mM	1	1.90E-10	2.22E-10	2.06E-10	2.26E-11	11.0
TGNGB025_0.5mM	TGNGB043_0.5mM	0.5	2.13E-10	2.21E-10	2.17E-10	5.66E-12	2.6
TGNGB025_0.1mM	TGNGB043_0.1mM	0.1	3.11E-10	3.26E-10	3.19E-10	1.06E-11	3.3

Table VII: Diffusion coefficients of the two rounds of DOSY analysis of **72** in D_2O at different concentrations.

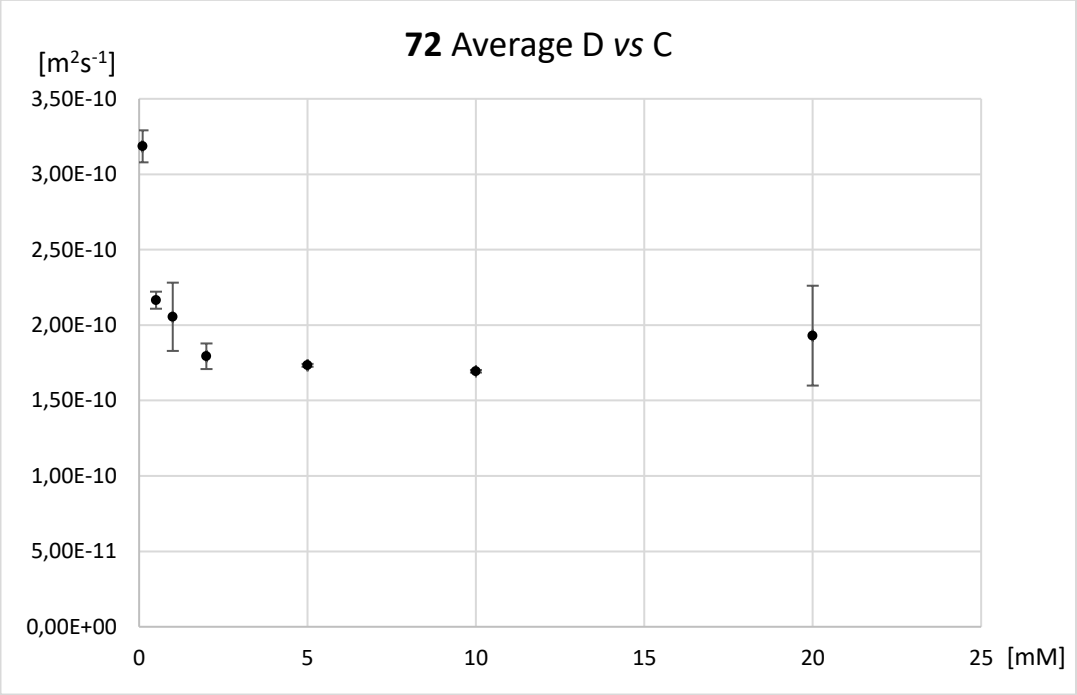

Figure XLII: Average diffusion coefficient of **72** *vs* concentration is reported.

First Round	Second Round	C [mM]	Hydr. Radius First [m]	Hydr. Radius Second [m]	Average Hydr. Radius [m]	STD DEV Hydr. Radius [m]	Error %
TGNGB025_20 mM	TGNGB043_ 20mM_n2	20	1.16E-09	9.08E-10	1.03E-09	1.77E-10	17.1
TGNGB025_10 mM	TGNGB043_ 10mM	10	1.16E-09	1.16E-09	1.16E-09	5.81E-12	0.5
TGNGB025_5 mM	TGNGB043_ 5mM	5	1.13E-09	1.14E-09	1.13E-09	6.17E-12	0.5
TGNGB025_2 mM_n2	TGNGB043_ 2mM	2	1.13E-09	1.06E-09	1.10E-09	5.19E-11	4.7
TGNGB025_1 mM_n2	TGNGB043_ 1mM	1	1.04E-09	8.87E-10	9.62E-10	1.06E-10	11.0
TGNGB025_0. 5mM	TGNGB043_ 0.5mM	0.5	9.25E-10	8.91E-10	9.08E-10	2.37E-11	2.6
TGNGB025_0. 1mM	TGNGB043_ 0.1mM	0.1	6.32E-10	6.03E-10	6.17E-10	2.06E-11	3.3

Table VIII: Hydrodynamic radius of the two rounds of DOSY analysis of **72** in D_2O at different concentrations.

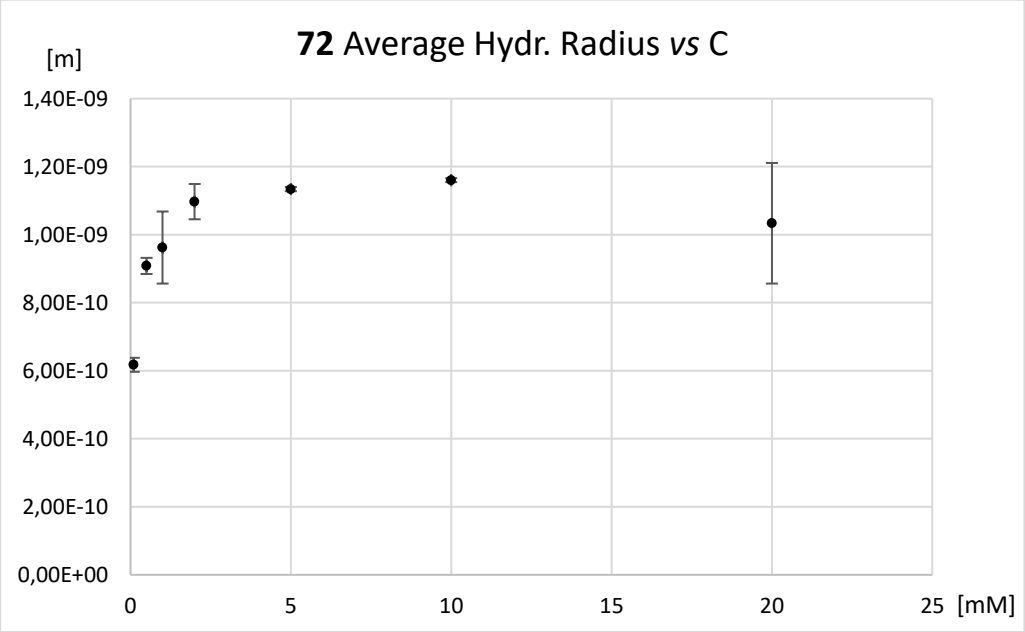

Figure XLIII: Average hydrodynamic radius of **72** *vs* concentration is reported.

c.a.c. and DOSY NMR 78

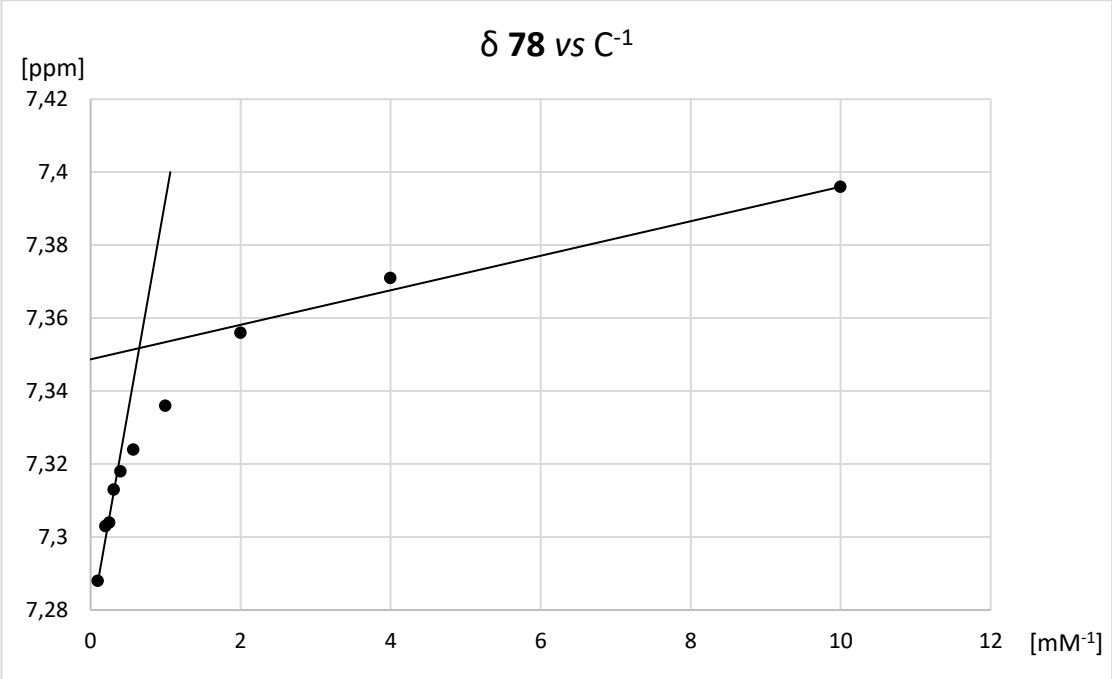

Figure XLV: Graph of aromatic CH chemical shift, δ, of **78** with respect to the inverse of the concentration. The two lines used to calculate the c.a.c. are reported.

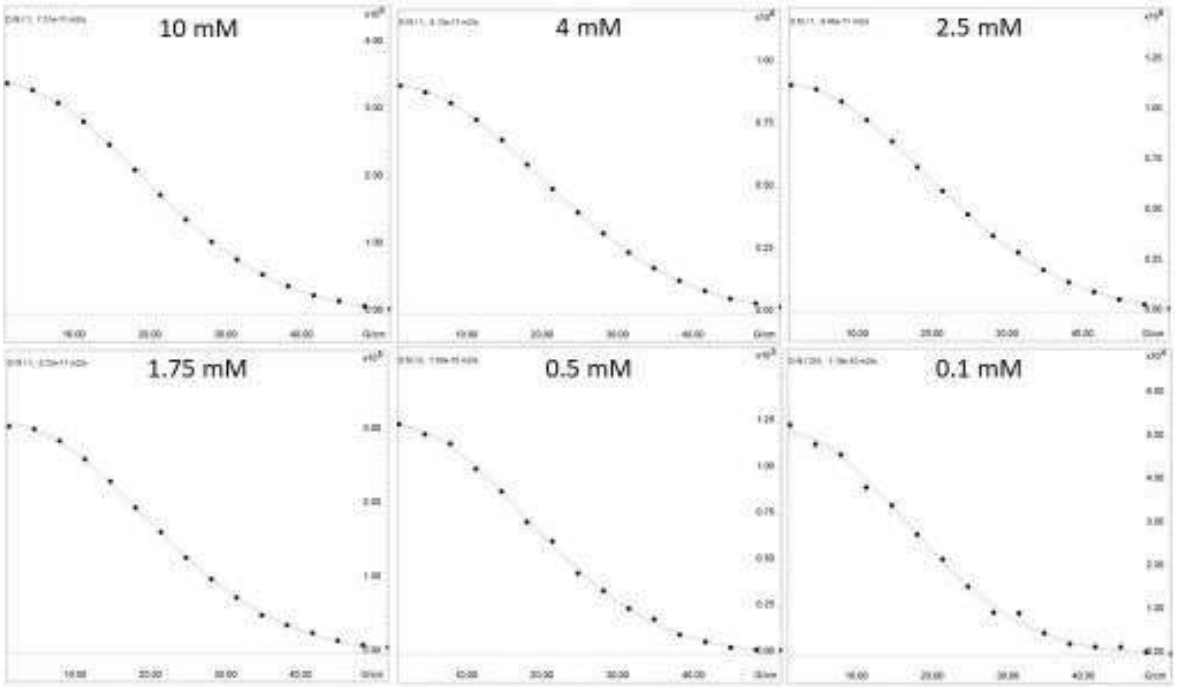

Figure XLV: Pseudo2D-DOSY NMR monoexponential decay of **78** triphenylenic signals in D_2O at different concentrations.

File Name	C [mM]	Average D [m^2s^{-1}]	STD DEV D [m^2s^{-1}]	Error %
1SS019_TP-MPEG350 10mM DOSY	10	7.30E-11	1.38E-12	1.9
1SS019_TP-MPEG350 4mM DOSY	4	8.10E-11	1.01E-12	1.3
1SS019_TP-MPEG350 2.5mM DOSY	2.5	8.56E-11	9.42E-13	1.1
1SS019_TP-MPEG350 1.75mM DOSY	1.75	8.95E-11	1.45E-12	1.6
1SS019_TP-MPEG350 0.5mM DOSY	0.5	9.98E-11	1.30E-12	1.3
1SS019_TP-MPEG350 0.1mM DOSY	0.1	1.16E-10	2.13E-12	1.8

Table IX: Diffusion coefficients of one round of DOSY analysis of **78** in D_2O at different concentrations.

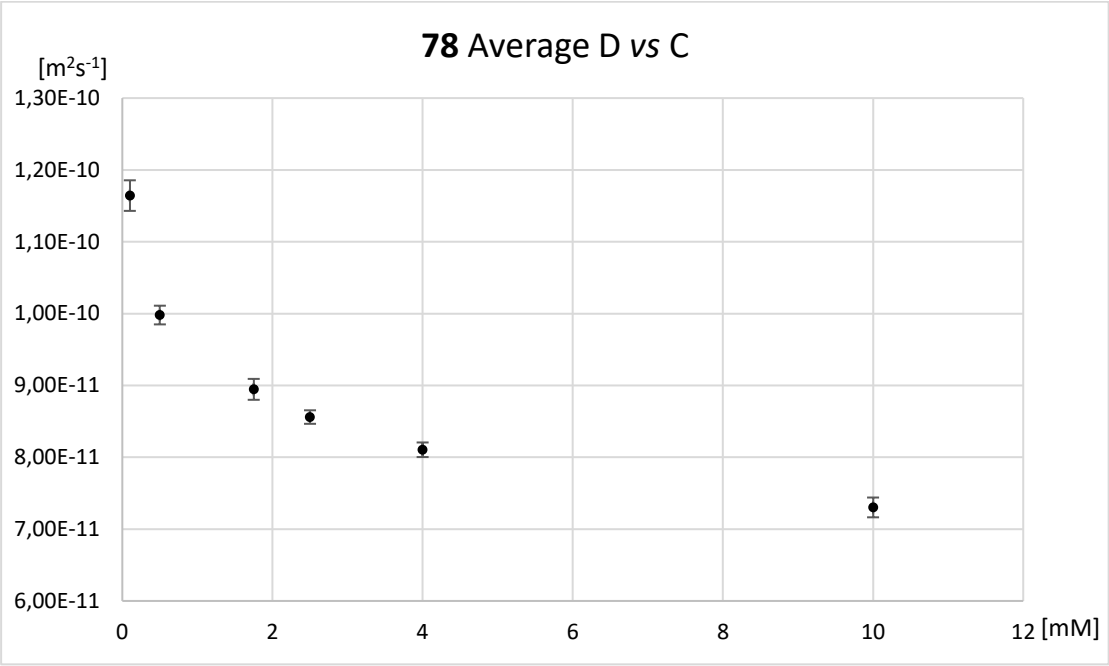

Figure XLVI: Average diffusion coefficient of **78** *vs* concentration is reported.

File Name	C [mM]	Hydrodynamic radius [m]	STD DEV Hydr. Radius [m]	Error %
1SS019_TP-MPEG350 10mM DOSY	10	2.69E-09	5.08E-11	1.89
1SS019_TP-MPEG350 4mM DOSY	4	2.43E-09	3.03E-11	1.25
1SS019_TP-MPEG350 2.5mM DOSY	2.5	2.30E-09	2.53E-11	1.10
1SS019_TP-MPEG350 1.75mM DOSY	1.75	2.20E-09	3.57E-11	1.63
1SS019_TP-MPEG350 0.1mM DOSY	0.5	1.97E-09	2.57E-11	1.30
1SS019_TP-MPEG350 0.1mM DOSY	0.1	1.69E-09	3.09E-11	1.83

Table X: Hydrodynamic radius of one round of DOSY analysis of **78** in D_2O at different concentrations.

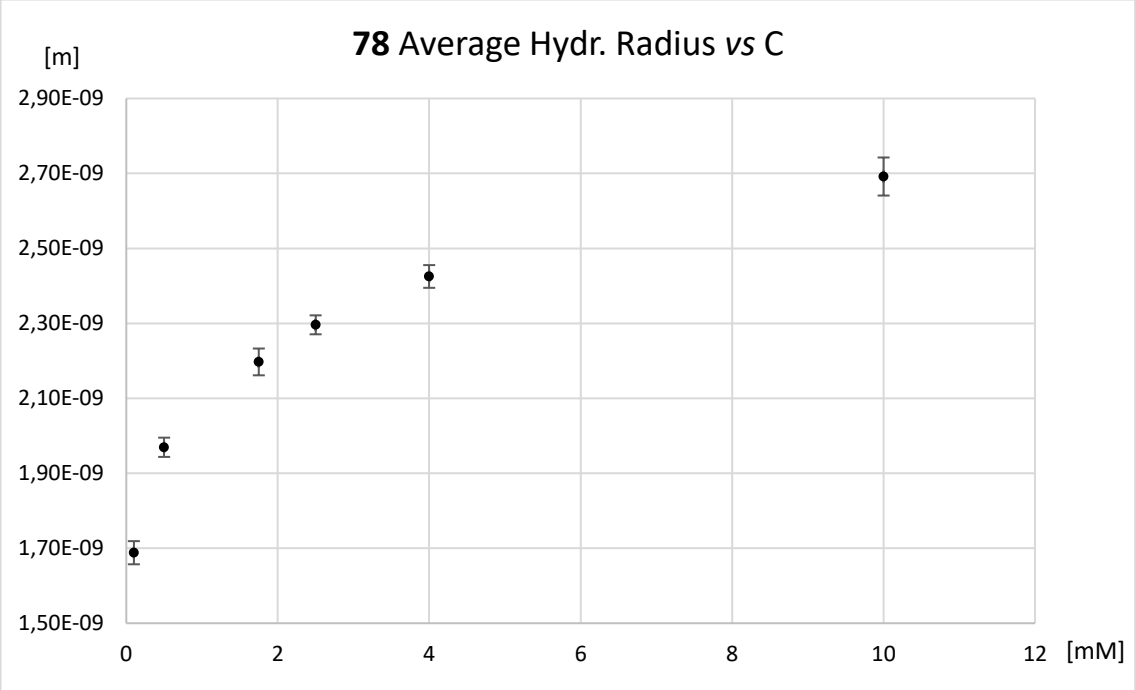

Figure XLVII: In the graphic below, average hydrodynamic radius of **78** *vs* concentration is reported.

Absorption/Emission of 70:

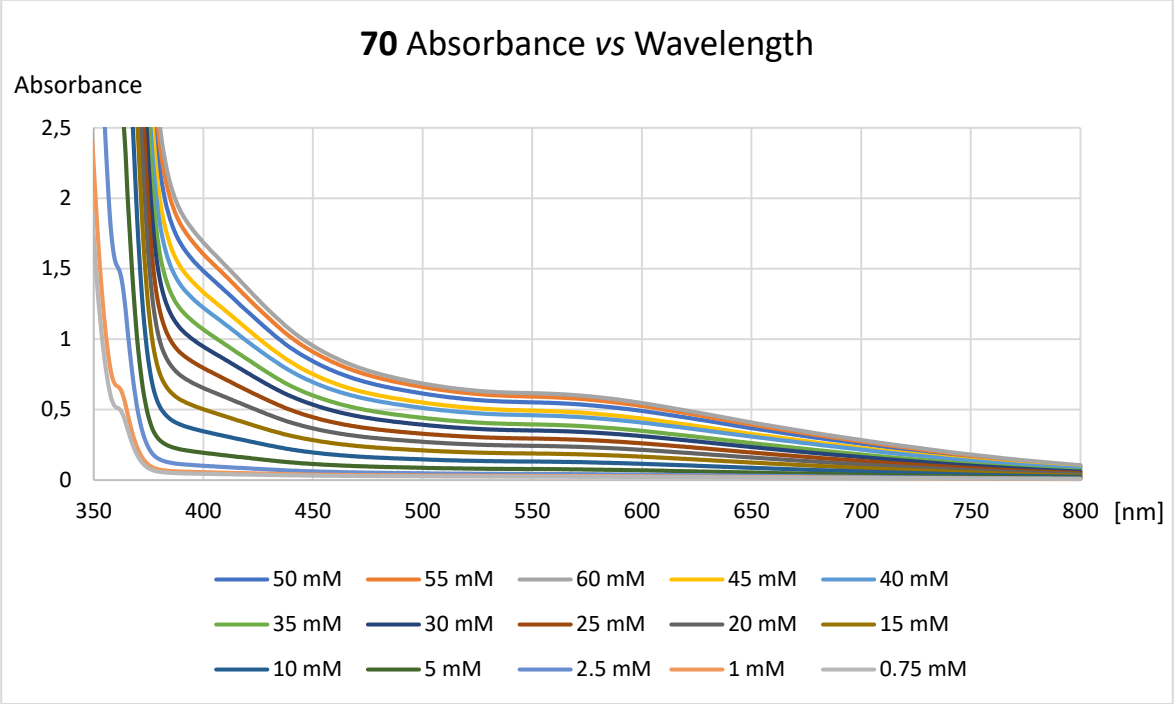

Figure XLVIII: UV-Vis absorbance of **70** in water at different concentrations at 297 K.

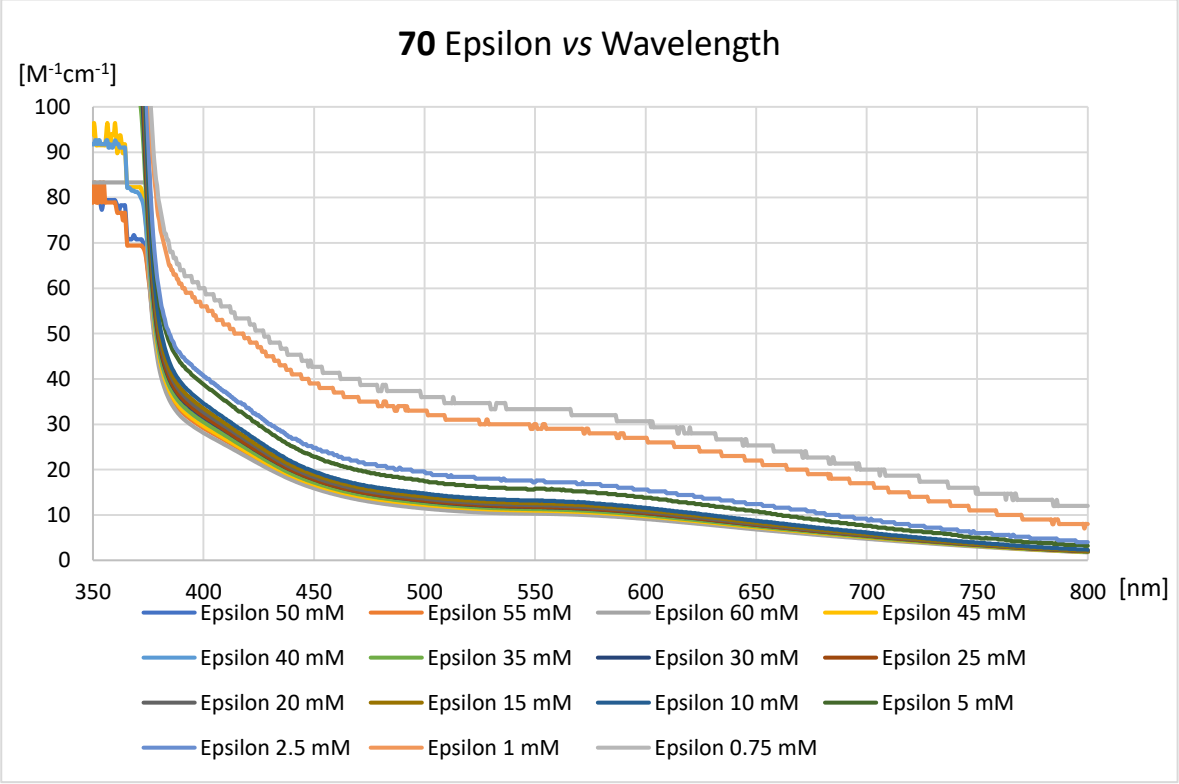

Figure XLIX: UV-Vis epsilon of **70** in water at different concentrations at 297 K.

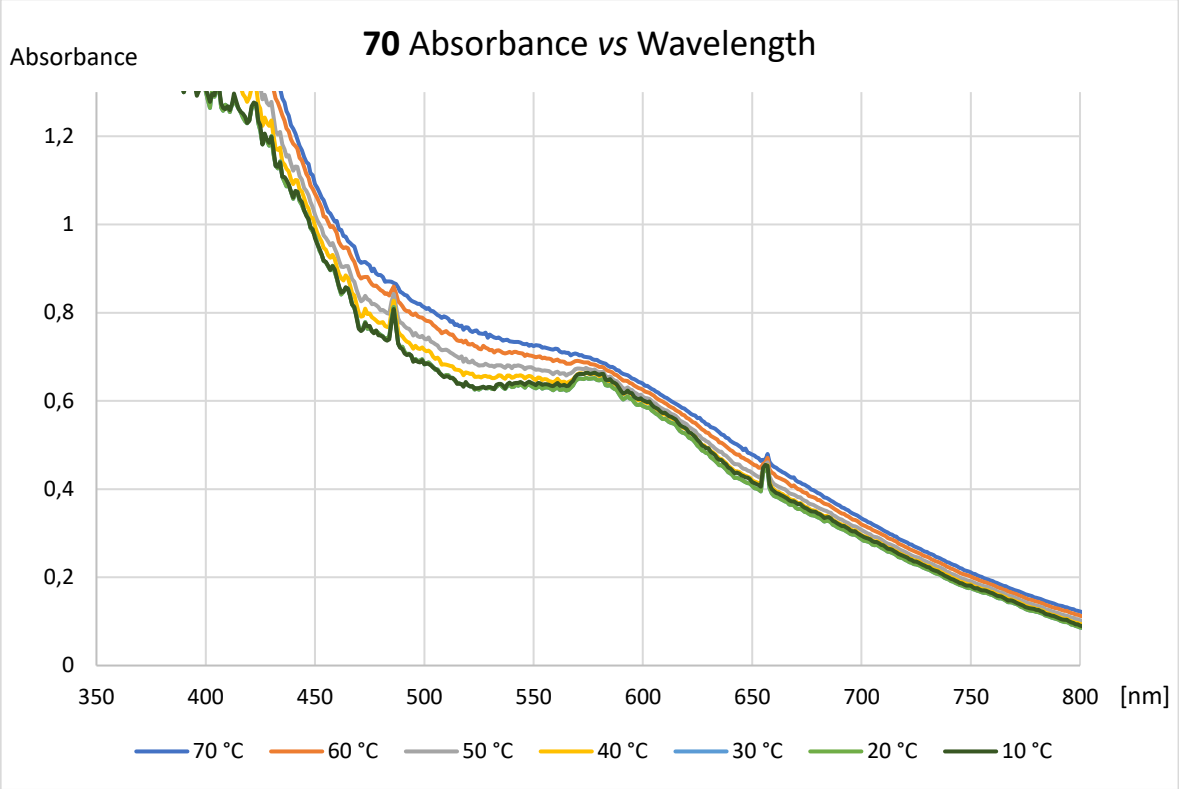

Figure L: UV-Vis epsilon of **70** 60 mM solution in water at different temperatures.

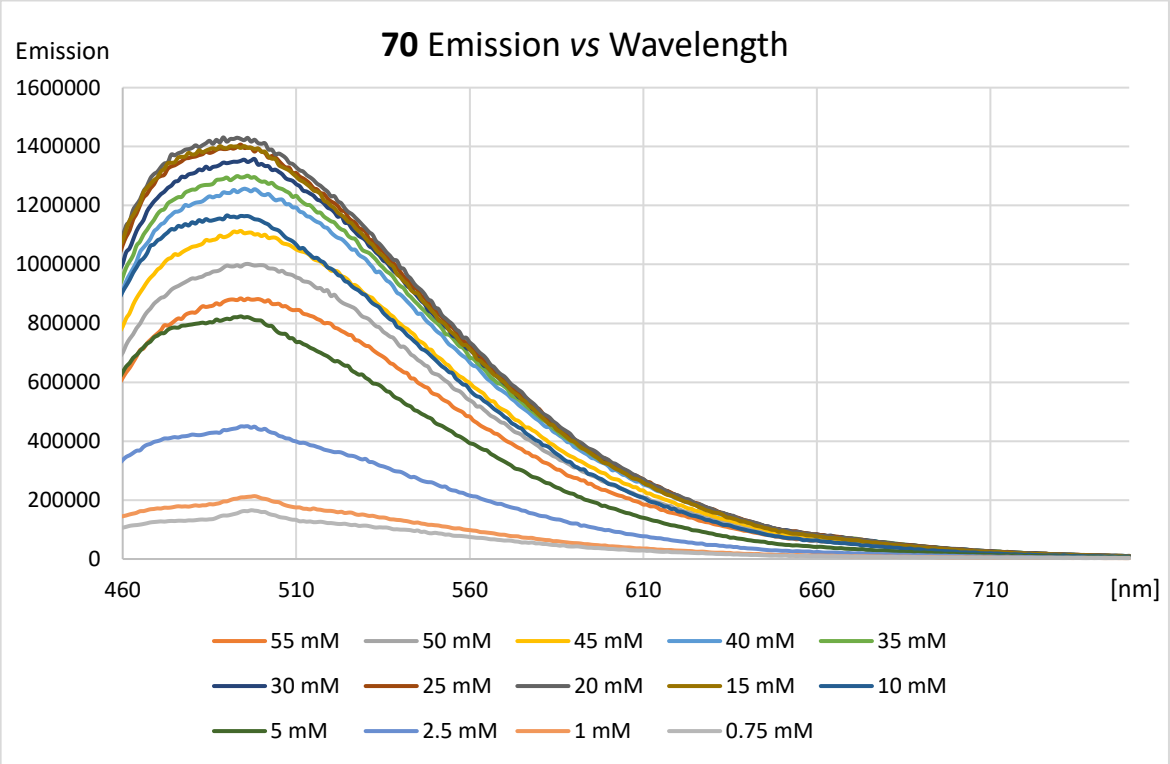

***Figure* LI**: Emission spectra of **70** in water at different concentrations at 297 K. Excitation wavelength 425 nm.

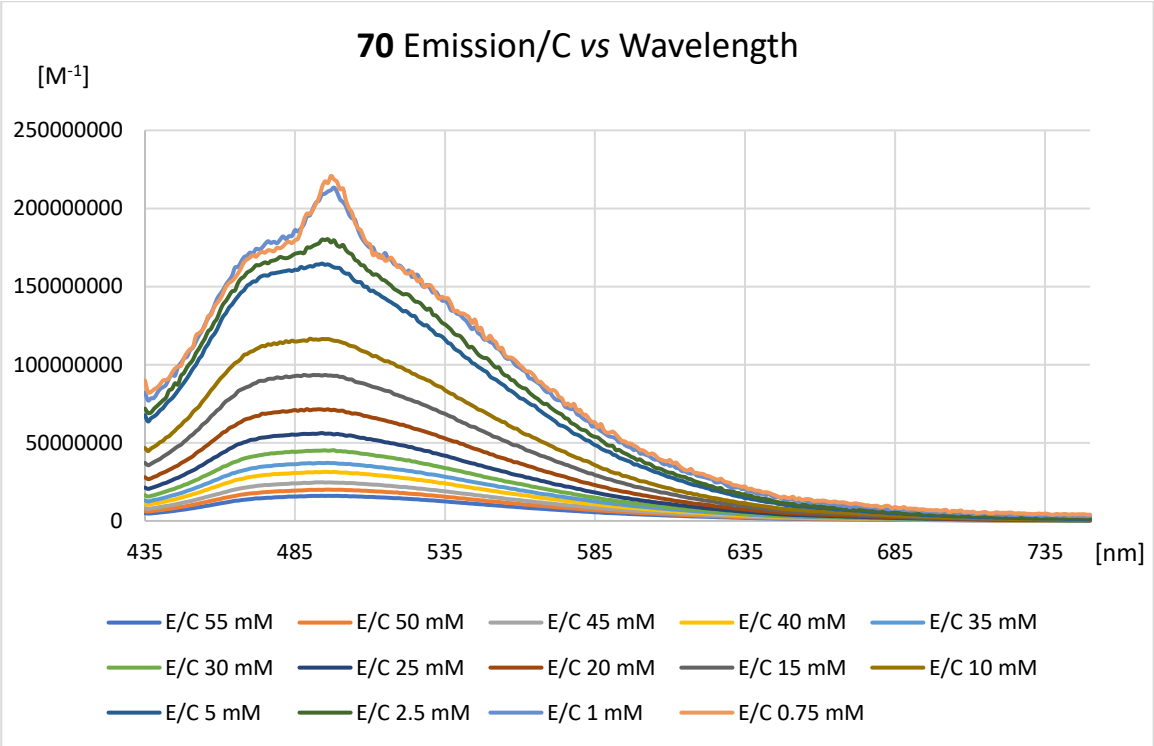

Figure LII: Emission divided for concentration of **70** in water at different concentrations at 297 K. Excitation wavelength 425 nm.

Absorption/Emission of 71:

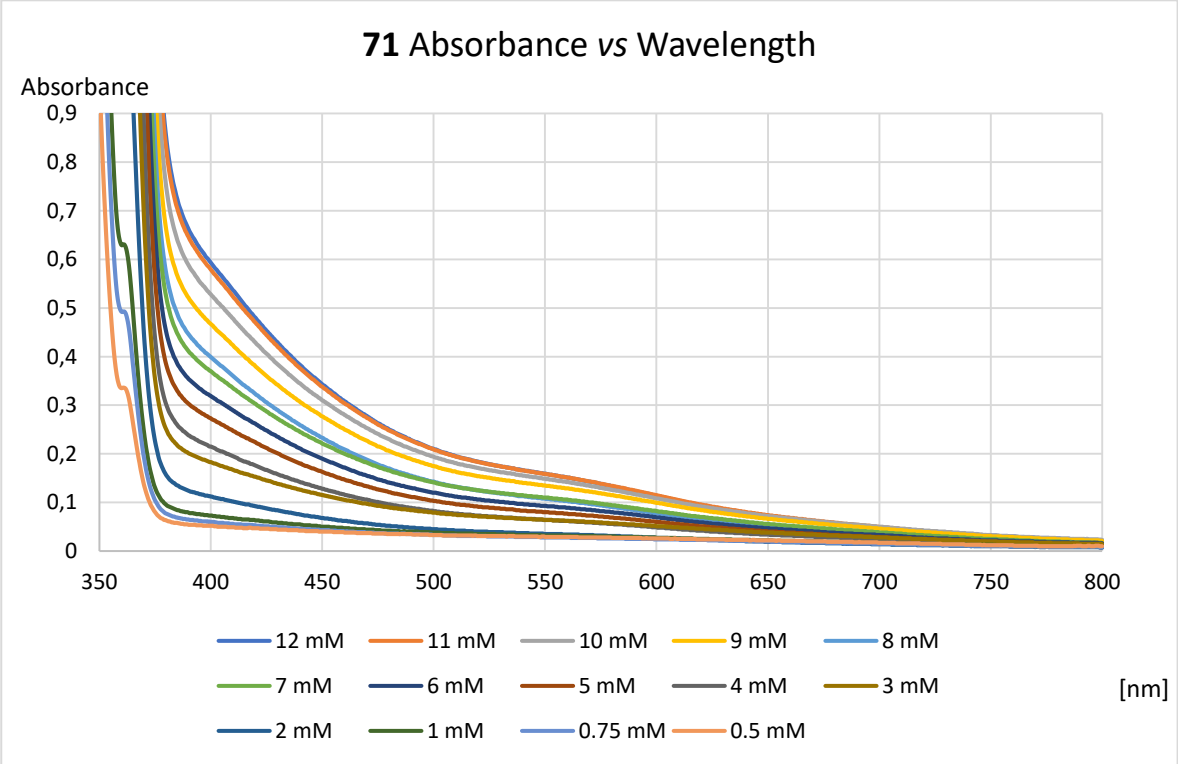

***Figure* LIII**: *UV-Vis absorbance of **71** in water at different concentrations at 297 K.*

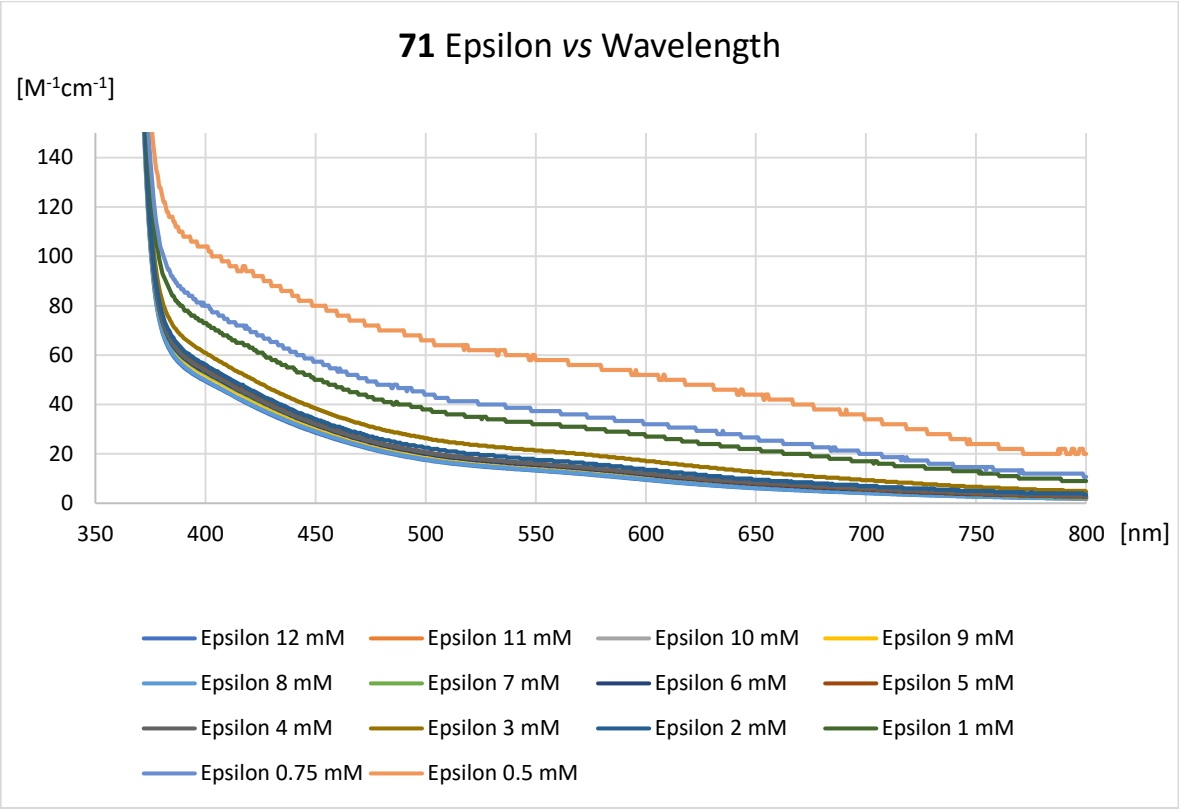

Figure LIV: UV-Vis epsilon of **71** in water at different concentrations at 297 K.

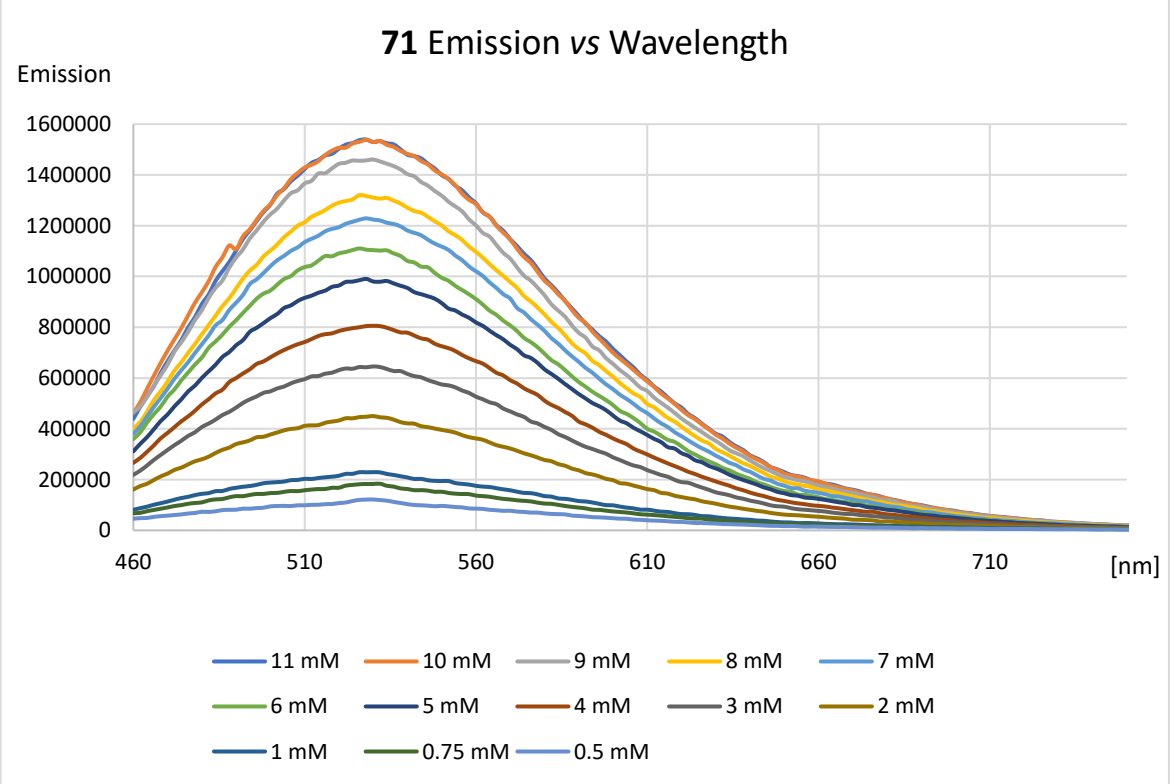

Figure LV: Emission spectra of **71** in water at different concentrations at 297 K. Excitation wavelength 450 nm.

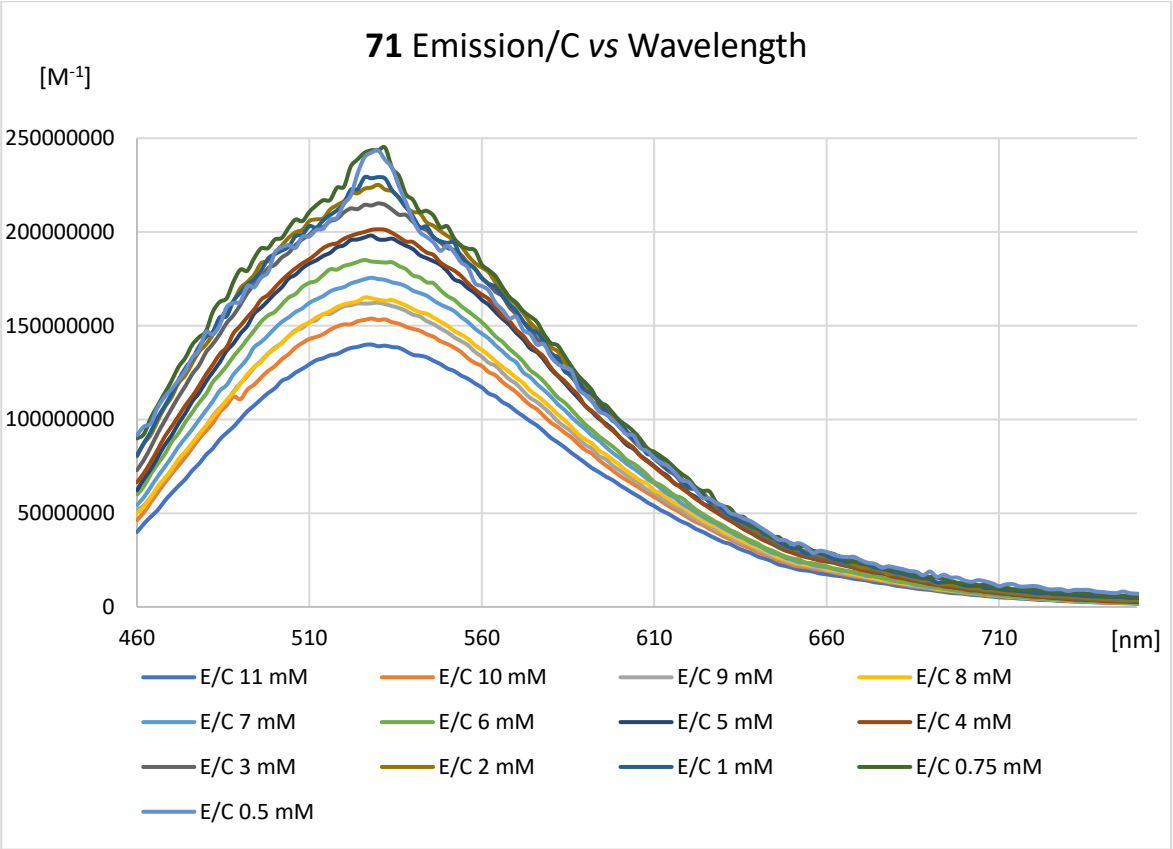

Figure* LVI:* Emission divided for concentration of **71** in water at different concentrations at 297 K. Excitation wavelength 450 nm.

7.6.5 SANS analysis

The SANS measurements on **70** were performed on the Instrument D11 at the Institut Laue-Langevin (ILL), a large scale facility situated in Grenoble, France. The measure has been obtained at a fixed wavelength of 0.6 nm, for three sample to detector distances (SDD) of 1.2, 8 and 39 m, in order to cover a large region of scattering vector Q, from 0.0025 to 0.5 $Å^{-1}$. The transmission of the sample was obtained at an SDD of 8 m. The data reduction was performed with the software package LAMP.[35] The calibration procedure was done by mean of a H_2O measurement to determine the absolute scale and the detector efficiencies.[36]

The modelization of the SANS curve has involved different models founded on SasView software. The curve was fitted employing the following function:

$$I(Q) = P(Q)S(Q) + PL(Q)$$

Where P(Q) is the form factor for a core shell sphere, S(Q) is the Hyter-msa structure factor describing the interaction between charged macroion and PL(Q) is the power law function involved to fit the scattering contribution from the larger aggregates.

The form factor for a core shell sphere $P(Q)=F^2(Q)$, is related to the scattering amplitude F(Q), given by:[37]

$$F(Q) = \frac{3}{V_s}\left[V_c(\rho_c - \rho_s)\frac{sin(qr_c) - qr_c cos\,(qr_c)}{(qr_c)^3} + V_s(\rho_s - \rho_{solv})\frac{sin(qr_s) - qr_s cos\,(qr_s)}{(qr_s)^3}\right]$$

where V_s is the volume of the micelle, V_c is the core volume, r_s is the total radius of the particle (radius of core and thickness of shell), r_c is the radius of the core, ρ_c is the scattering length density (SLD) of the core, ρ_s is the SLD of the shell, ρ_{solv} is the SLD of the solvent. For this model is possible to calculate the average distribution of core radius and shell thickness defined as polydispersity of core radius and shell, respectively PD_{core} and PD_{shell}. The meaning of polydispersity parameter PD has not to be confused with a molecular weight distribution in polymer science. The distribution function used to describe the PD_{core} and PD_{shell} is a Gaussian distribution function and the polydispersity is defined as follows:

$$PD = \frac{\sigma}{\bar{x}}$$

Where σ is the standard deviation and $\bar{x}$ the mean value of the distribution.

The structure factor S(Q) was involved to study the interaction between the charged (spherical) micelles by means of a repulsive screened Coulomb potential. The analytical solution of the structure factor was given by Hayter and Penford.[38,39] The structure factor is calculated for a system of charged spheroidal micelles (dissolved) in a dielectric medium. The ionic strength of the solution is computed by means of the salt concentration (25 mM) and it is valid only for monovalent salt. For this model the counterions have also to be monovalent and, in this case, they are represented by the sodium cations.

The evaluation of the number of monomers composing a nano-capsule has been done comparing the SLD core value obtained from the fit SLD_F (2.2 ± 0.2) with the Theoretical one SLD_T. The SLD_T has been obtained by:[40]

$$SLD_T = \rho_c N_a \frac{\sum_{i=1}^{N} b_i}{\sum_{i=1}^{N} M_i}$$

where M_i is the atomic molar mass fo each element, ρ_c is the density of core, b_i the scattering length of atoms (Table XI) and N_a the Avogadro constant. The core density ρ_c has been computed for a core spherical volume of 1.13 nm radius (extract from the fit) and the mass of the core has been estimated for 6, 7 and 8 monomers. Values of core mass, volume, density and SLD_T have been reported in Table XII, and relative errors related to these quantities are not shown because less than 1%. The comparison between the SLD_T and SLD_F suggest the presence of 7 monomers per micelle.

	MW
$C_{39}O_6H_{27}$	591.62
	b_i [10-15m]
C	6.646
O	-3.739
H	5.803

Table XI: Molecular weight of the hydrophobic part of a monomer and scattering lengths of its atoms.[41]

n° monomers	**Estimated core mass [g]**	**Estimated core volume [cm^3]**	**Estimated core density [$g \cdot cm^{-3}$]**	**SLD_T [10-6 $Å^{-2}$]**
6	5.889E-21	6.041E-21	0.975	1.916
7	6.878E-21	6.041E-21	1.138	2.235
8	7.859E-21	6.041E-21	1.301	2.532

Table XII: Estimated core mass, volume and density and SLD_T for different number of monomers.

7.6.6 Host-Guest Experiments

Host-guest experiments with mesitylene were run shaking 10 µL of mesitylene with 0.5 mL of host solution in D_2O followed by 10 minutes of ultrasound bath.

The saturated solutions of solid guests were prepared suspending the solid in 2 mL of D_2O followed by 10 minutes of ultrasound bath, centrifugation and filtration. The resulted saturated solutions were used to record the ^1H NMR of the lone guest and to prepare the host solution for the host-guest experiments.

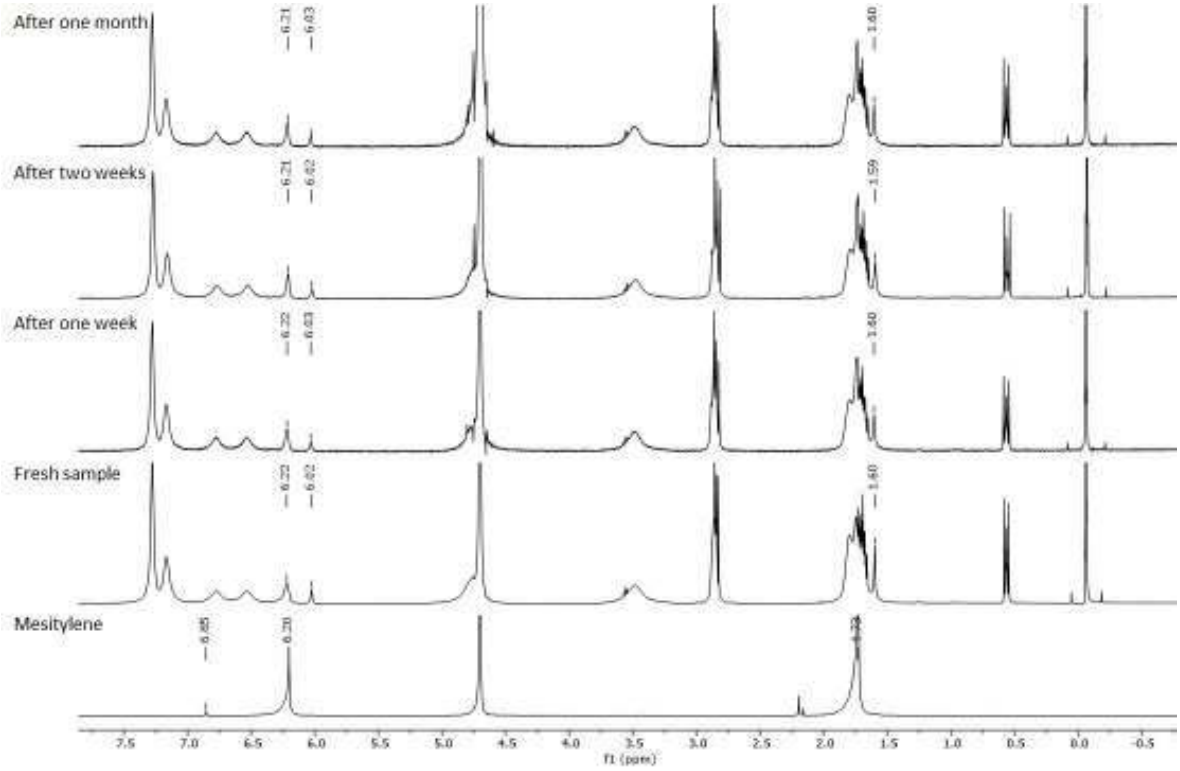

Figure LVII: Complete ^1H NMR spectra of mesitylene in D_2O (bottom) and mesitylene (10 µL) in 0.5 mL of a 5 mM solution of **70** in D_2O (over time, top).

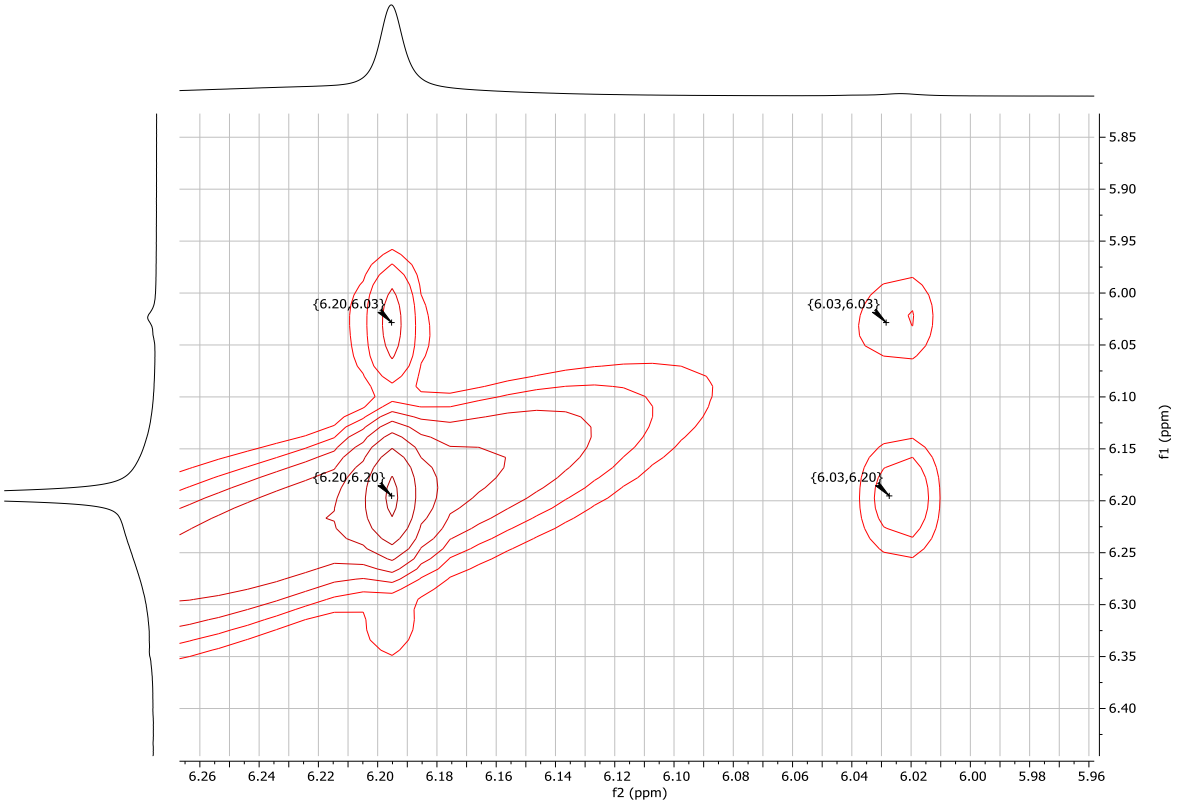

Figure LVIII: NOESY NMR of mesitylene (10 µL) in 0.5 mL of a 5 mM solution of **70** in D_2O. detail of the NOE interaction between the two mesitylene signals.

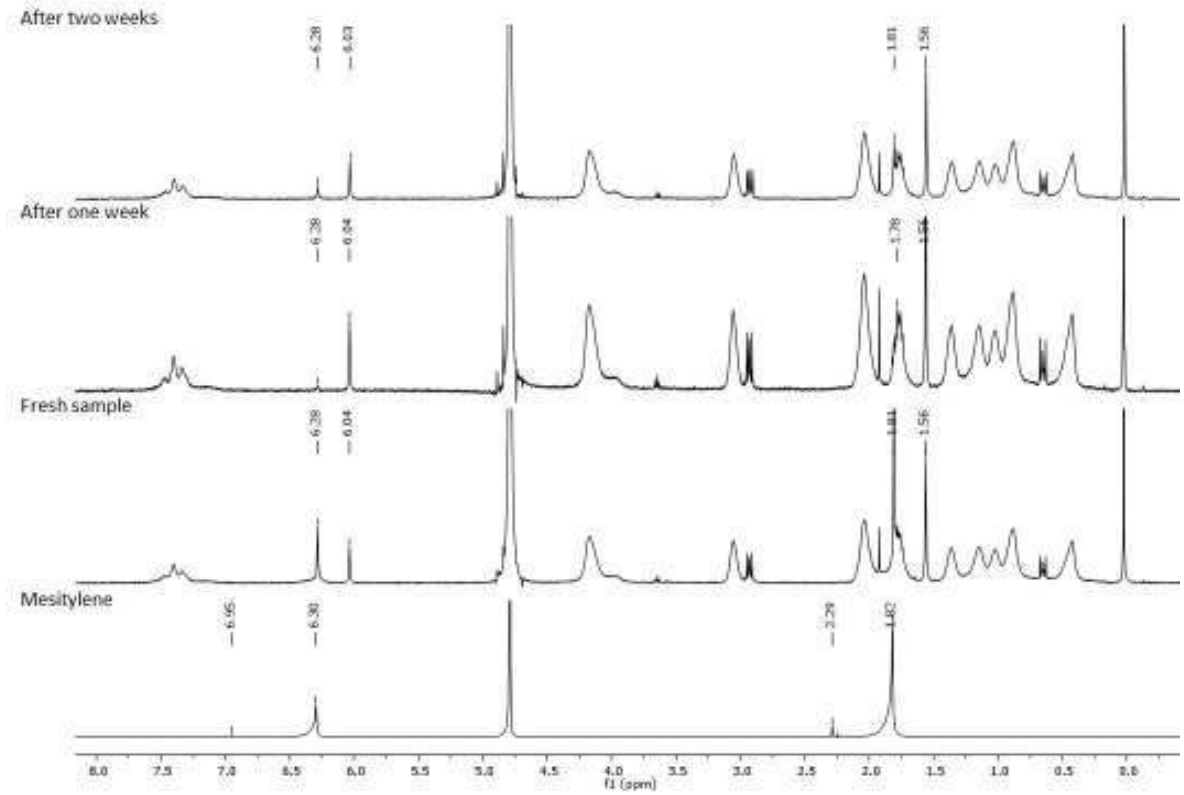

Figure LIX: ^1H NMR spectra of mesitylene in D_2O (bottom) and mesitylene (10 µL) in 0.5 mL of a 5 mM solution of **71** in D_2O (over time, top).

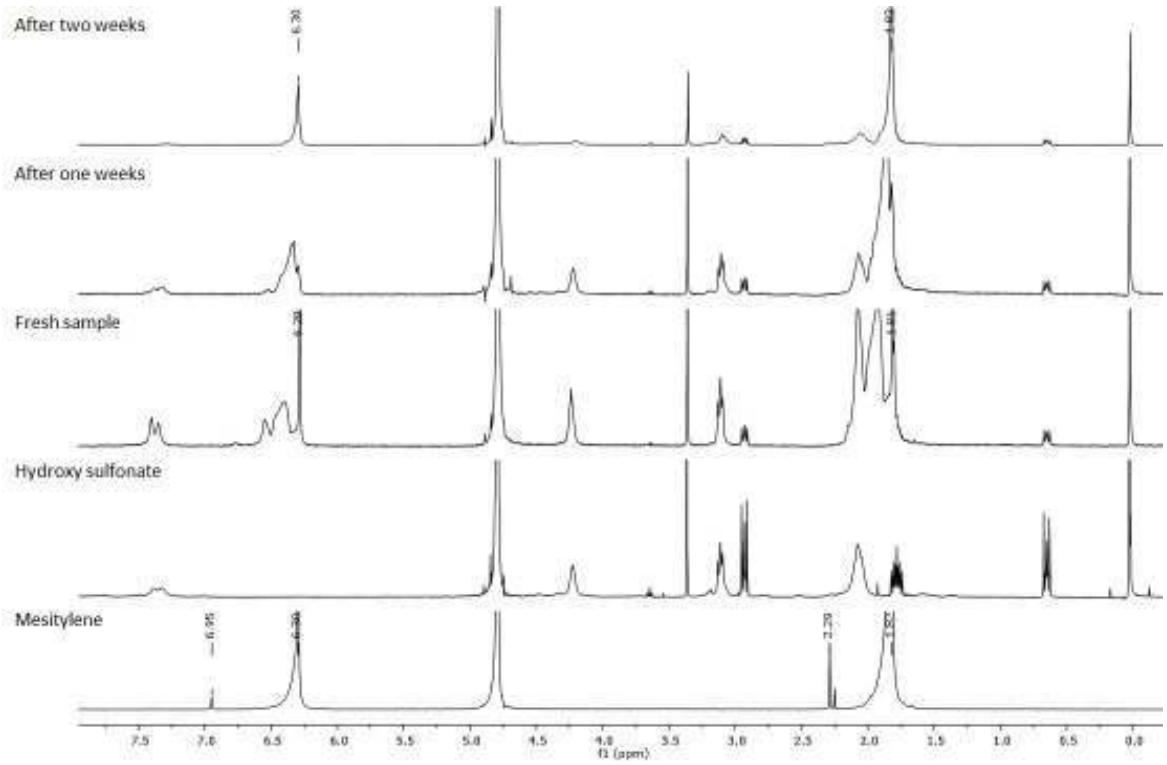

Figure LX: ^{1}H NMR spectra of mesitylene in D_2O (bottom) and mesitylene (10 µL) in 0.5 mL of a 5 mM solution of **72** in D_2O (over time, top).

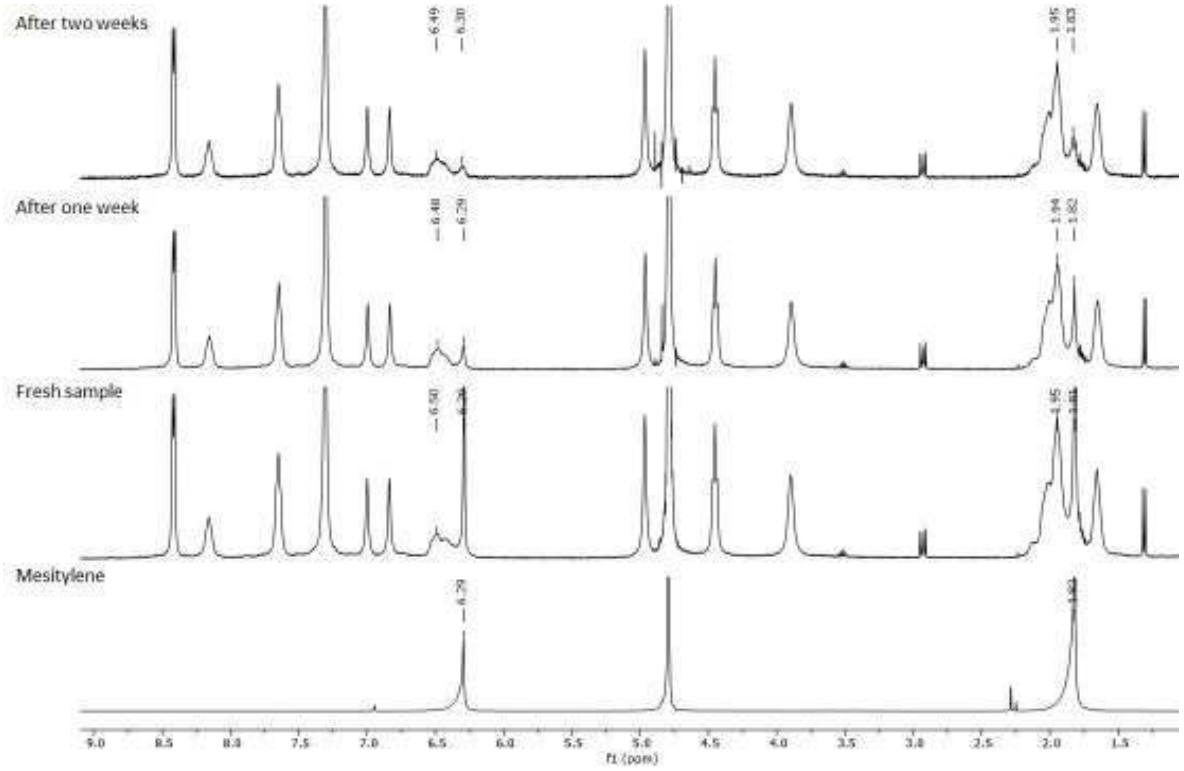

Figure LXI: Complete ^{1}H NMR spectra of mesitylene in D_2O (bottom) and mesitylene (10 µL) in 0.5 mL of a 5 mM solution of **75** in D_2O (over time, top).

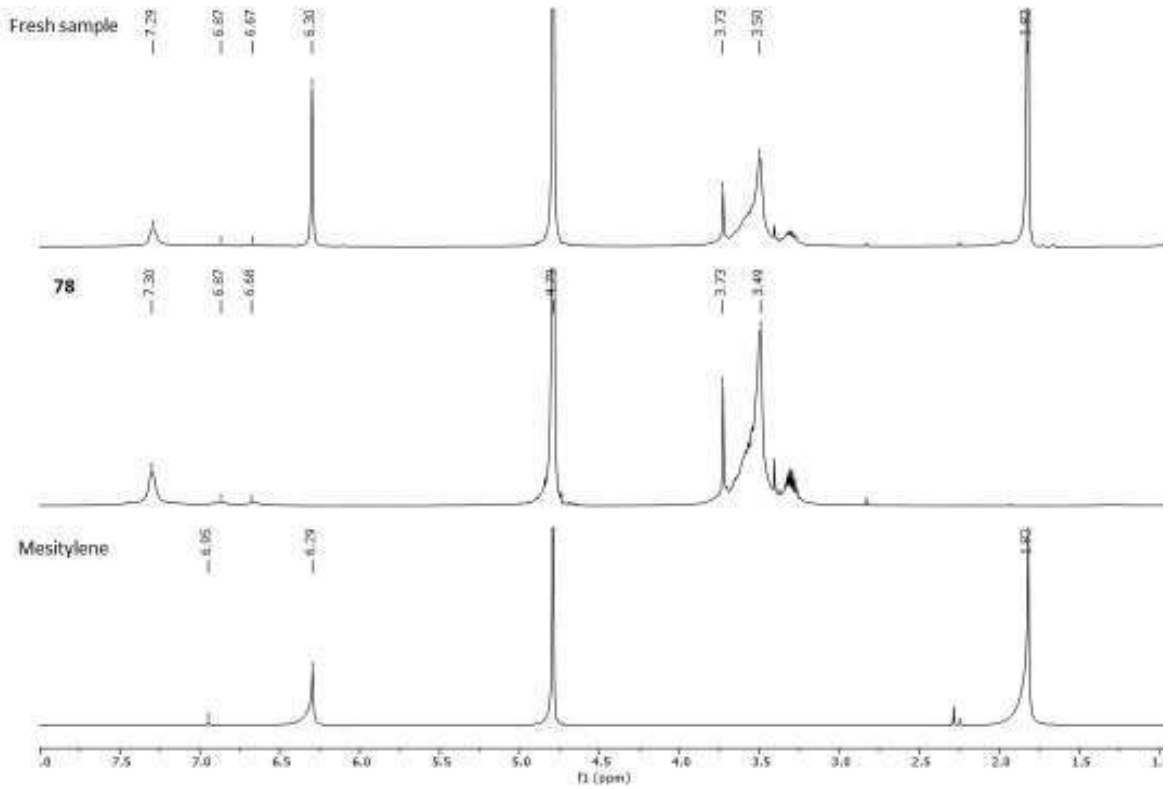

Figure LXII: Complete ^{1}H NMR spectra of mesitylene in D_2O (bottom), 5 mM solution of **78** in D_2O (centre) and mesitylene (10 µL) in 0.5 mL of a 5 mM solution of **78** in D_2O (top).

7.7 Bibliography

1 F. Schwizer, Y. Okamoto, T. Heinisch, Y. Gu, M. M. Pellizzoni, V. Lebrun, R. Reuter, V. Köhler, J. C. Lewis, T. R. Ward, *Chem. Rev.*, **2018**, *118*, 142-231.

2 S. Zarra, D. M. Wood, D. Roberts, J. R. Nitschke, *Chem. Soc. Rev.*, **2014**, *44*, 419-432.

3 P. Zhang, *Chem.*, **2017**, *3*, 15-16.

4 D. Ajami, L. Liu, J. Rebek Jr, *Chem. Soc. Rev.*, **2015**, *44*, 490-499.

5 F. Corbellini, L. Di Costanzo, M. Crego-calama, S. Geremia, D. N. Reinhoudt, S. Chimiche, V. Uni, *J. Am. Chem. Soc.*, **2003**, *125*, 9946-9947.

6 T. Grawe, T. Schrader, R. Zadmard, A. Kraft, *J. Org. Chem.*, **2002**, *67*, 3755-3763.

7 F. Corbellini, R. M. A. Knegtel, P. D. J. Grootenhuis, M. Crego-calama, D. N. Reinhoudt, *Chem. - A Eur. J.*, **2005**, *11*, 298-307.

8 C. J. Brown, F. D. Toste, R. G. Bergman, K. N. Raymond, *Chem. Rev.*, **2015**, *115*, 3012-3035.

9 A. J. McConnell, C. S. Wood, P. P. Neelakandan, J. R. Nitschke, *Chem. Rev.*, **2015**, *115*, 7729-7793.

10 O. Dumele, B. Schreib, U. Warzok, N. Trapp, C. A. Schalley, F. Diederich, *Angew. Chemie - Int. Ed.*, **2017**, *56*, 1152-1157.

11 L. Turunen, A. Peuronen, S. Forsblom, E. Kalenius, M. Lahtinen, K. Rissanen, *Chem. – A Eur. J.*, **2017**, *23*, 11714-11718.

12 F. Biedermann, W. M. Nau, H. Schneider, *Angew. Chemie – Int. Ed.*, **2014**, *53*, 11158-11171.

13 M. B. Hillyer, B. C. Gibb, *Annu. Review Phys. Chem.*, **2016**, *67*, 307-329.

14 K. Kondo, J. K. Klosterman, M. Yoshizawa, *Chem. – A Eur. J.*, **2017**, *23*, 16710-16721.

15 M. Yoshizawa, L. Catti, *Acc. Chem. Res.*, **2019**, *52*, 2392-2404.

16 Y. Okazawa, K. Kondo, M. Akita, M. Yoshizawa, *J. Am. Chem. Soc.*, **2015**, *137*, 98-101.

17 T. Nishioka, K. Kuroda, M. Akita, M. Yoshizawa, *Angew. Chemie - Int. Ed.*, **2019**, *58*, 6579–6583.

18 K. Jono, A. Suzuki, M. Akita, K. Albrecht, K. Yamamoto, M. Yoshizawa, *Angew. Chemie - Int. Ed.*, **2017**, *56*, 3570–3574.

19 Y. Satoh, L. Catti, M. Akita, M. Yoshizawa, *J. Am. Chem. Soc.*, **2019**, 141, 12268-12273.

20 K. Kondo, M. Akita, T. Nakagawa, Y. Matsuo, *Chem. - A Eur. J.*, **2015**, *21*, 12741-12746.

21 J. H. Jordan, B. C. Gibb, *Chem. Soc. Rev.*, **2015**, *44*, 547-585.

22 K. Wang, X. Cai, W. Yao, D. Tang, R. Kataria, H. S. Ashbaugh, L. D. Byers, B. C. Gibb, *J. Am. Chem. Soc.*, **2019**, *141*, 6740-6747.

23 S. Hiraoka, T. Nakamura, M. Shiro, M. Shionoya, *J. Am. Chem. Soc.*, **2010**, *132*, 13223-13225.

24 S. Hiraoka, K. Harano, M. Shiro, M. Shionoya, *J. Am. Chem. Soc.*, **2008**, *130*, 14368-14369.

25 S. Hiraoka, K. Harano, T. Nakamura, M. Shiro, M. Shionoya, *Angew. Chemie - Int. Ed.*, **2009**, *48*, 7006-7009.

26 A. Suzuki, M. Akita, M. Yoshizawa, *Chem. Commun.*, **2016**, *52*, 10024-10027.

27 S. O. Alapafuja, S. P. Nikas, V. G. Shukla, I. Papanastasiou, A. Makriyannis, *Tetrahedron Lett.*, **2009**, *50*, 7028-7031.

28 G. Peñuelas-Haro, P. Ballester, *Chem. Sci.*, **2019**, *10*, 2413-2423.

29 Z. Yuanyuan, C. Xiang, L. Yuhui, T. Zhiwei, CN108034283, **2018**.

30 J. Zhao, B. M. Fung, *Langmuir*, **1993**, *9*, 1228-1231.

31 M. I. Gibson, R. K. O'Reilly, *Chem. Soc. Rev.,* 2013, **42**, 7204-7213.

32 Y. Koda, T. Terashima, M. Sawamoto, *ACS Macro Lett.*, **2015**, *4*, 1366-1369.

33 http://www.sasview.org/

34 W. L. F. Armarego, C. Chai in *Purification of Laboratory Chemicals (Seventh Edition)*, Butterworth-Heinemann, Boston, **2013**.

35 D. Richard, M. Ferrand, G. J. Kearley, *J. Neut. Res.*, **1996**, *4*, 33-39.

36 P. Lindner, R. Schweins, *Org. Neut. News*, **2010**, *21*, 15-18.

37 V. Castelletto, I.W. Hamley, *Current Opinion in Colloid & Interface Science*, **2002**, *7*, 167-172.

38 J. B. Hayter, J. Penfold, *Mol. Phys.*, **1981**, *42*, 109-118.

39 J. P. Hansen, J. B. Hayter, *Mol. Phys.*, **1982**, *6*, 651-656.

40 http://www.ncnr.nist.gov/resources/sldcalc.html

41 V. F. Sears, *Neut. News,* **1992**, *3*, 26-37.

8 Ionic Dimeric Capsule

In contrast to hydrogen bonds[1] and metal-ligand interactions,[2] ionic interactions have been seldomly exploited for the construction of well-defined supramolecular containers. Several years ago, ionic capsules based on calix[4]arene scaffolds were reported. The capsule's assembly exploited the establishment of four coulombic (charge-charge) interactions, assisted by hydrogen bonding between a *tetra*-sulfonate and *tetra*-amidinium units[3] or a tetra-carboxylate and, again, a tetra-amidinium components,[4] thus enabling the persistence of the dimeric capsules even in water solution (Figure 1).[5]

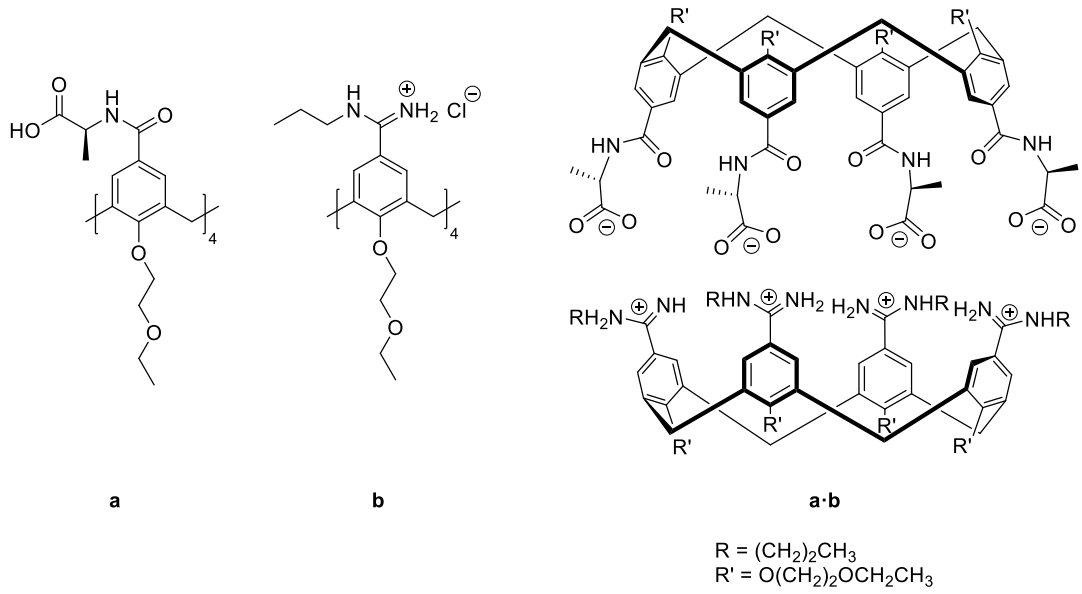

Figure 1: Tetra-carboxylate calix[4]arene, **a**, and tetra-amidinium calix[4]arene, **b**, forming the dimeric capsule **a·b** in water. Adapted from [5a].

Two additional examples rely on the establishment of only three coulombic interactions between components based on mesitylene or calix[3]arene scaffolds.[6]

The presence of complementary ionic (coulombic) interactions ensures the formation of heterodimeric aggregates. However, for assemblies based on ionic-units (supramolecular hosts), its binding properties are limited compared to non-ionic counterparts owing to the possible existence of repulsive interactions with charged guests.

After the synthesis of the anionic and cationic triphenylenes, reported in the previous Chapter 7, we wondered what could happen by mixing together in water the benzyl sulfonate **70** with the benzyl pyridinium **75**, basically if the hydrophobic effect or the ionic interaction will prevail. In the latter case, it could be possible to obtain an ionic dimeric capsule by the interaction of three purely ionic (coulombic) interactions.

8.1 Synthesis of the Ionic Capsule

To ascertain whether an ionic capsule was possible from the two opposite charged triphenylenes **70** and **75**, the first experiment was to mix two equimolar solution in D_2O of

the ionic triphenylenes **70** and **75** (5 mM) observing the immediate formation of a white precipitate. ^{1}H NMR of the suspension proved the absence of any material in solution, meaning the quantitative precipitation of an aggregate of any sort between **70** and **75** (Figure 2).

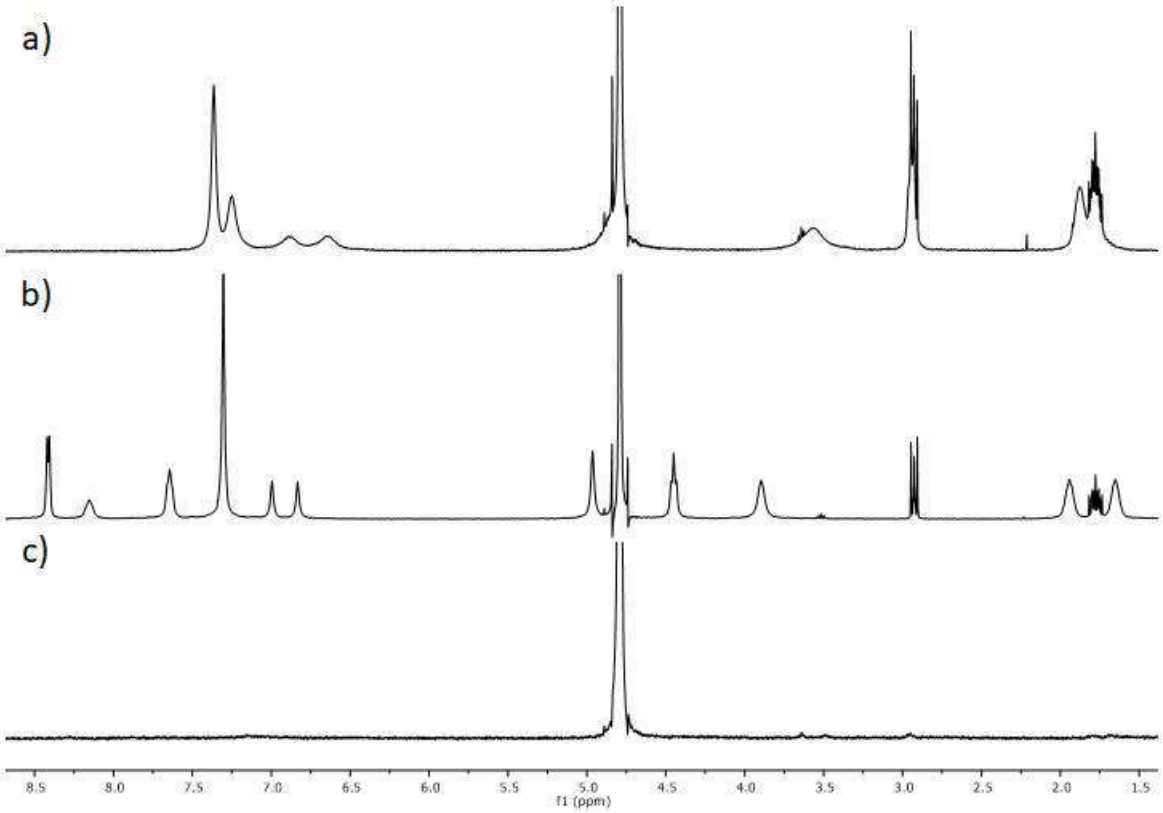

Figure 2: a) ^{1}H NMR of **70**, 5 mM, in D_2O; b) ^{1}H NMR of **75**, 5 mM, in D_2O; c) ^{1}H NMR of an equimolar mixture of **70** and **75** in D_2O.

The obtained precipitate was isolated by filtration and proved to be soluble in polar solvents such as DMSO and MeOH. The ^{1}H NMR spectra of the solution revealed the presence of both components **70** and **75** in a 1:1 molar ratio. This observation suggested the formation of a **70·75** neutral dimeric assembly that was insoluble in water. The ^{1}H NMR spectrum of an equimolar mixture of **70** and **75** in methanol-d_4 showed significant up-field shifted resonances for all the proton signals with respect to those of the two separate components in the same solvent (Figure 3).

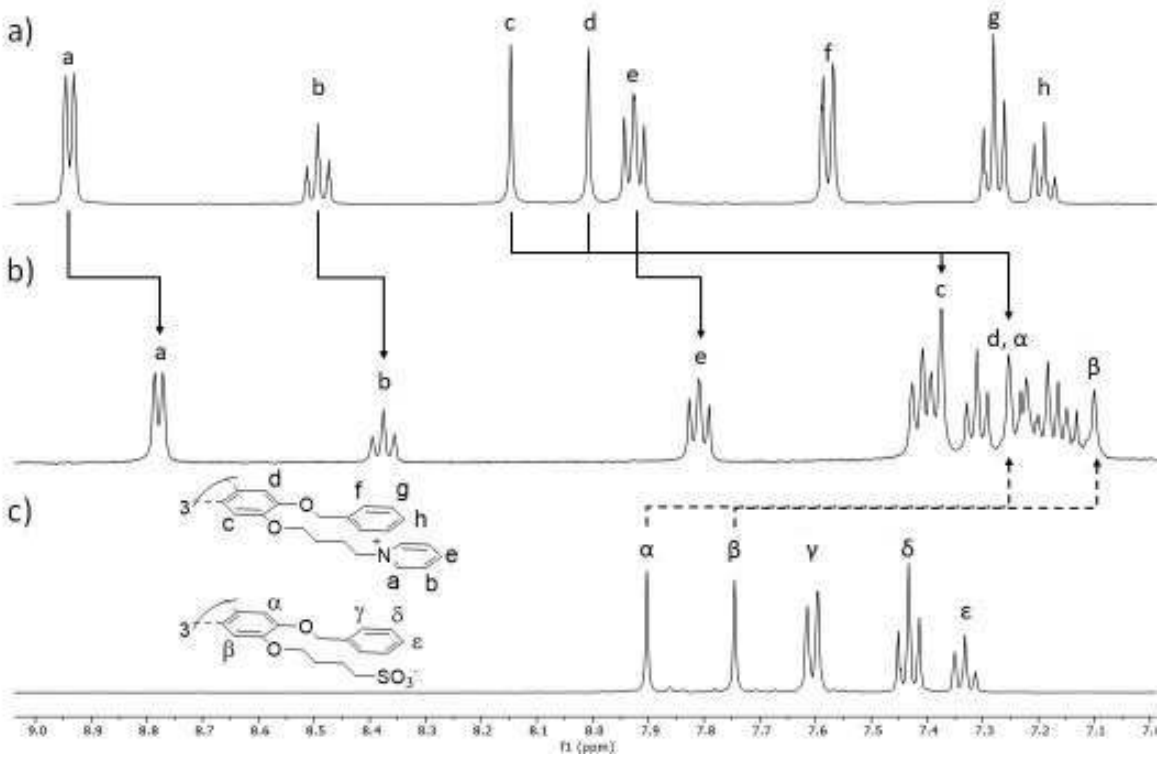

Figure 3: a) ^{1}H NMR of **75**, 2.5 mM, in methanol-d_4; b) ^{1}H NMR of an equimolar mixture of **70** and **75** in methanol-d_4; b) ^{1}H NMR of **70**, 2.5 mM, in methanol-d_4. The resonances are assigned, and shifts are highlighted with continue arrows for **75** and with dashed arrows for **70**.

In detail, the signals of the hydrogen atoms of the two triphenylene units showed a chemical shift change of $\Delta\delta_{\alpha,\beta}$ = 0.65 ppm for **70** and $\Delta\delta_{c,d}$ = 0.77 ppm for **75**. Moreover, the signals for the hydrogen atoms of the butyl and benzyl substituents experienced up-field shifts in the range of 0.50-0.15 ppm. The sum of all these observations suggested the formation of a complex between **70** and **75**. Analogous behaviour of the assembly was observed in the ^{1}H NMR in DMSO-d_6 of the stoichiometric **70·75** assembly (see Experimental Section). In order to characterize the nature of the complex, DOSY experiments were performed on the equimolar mixture in methanol-d_4.[7] The signal decay of the triphenylene protons of **70** and **75** in the equimolar mixture *vs* the gradient strength showed a good fit to a mono-exponential function, and provided identical diffusion coefficients for the two triphenylene partners, 2.10(±0.14)·10^{-10} $m^2 \cdot s^{-1}$ (Figure 4).

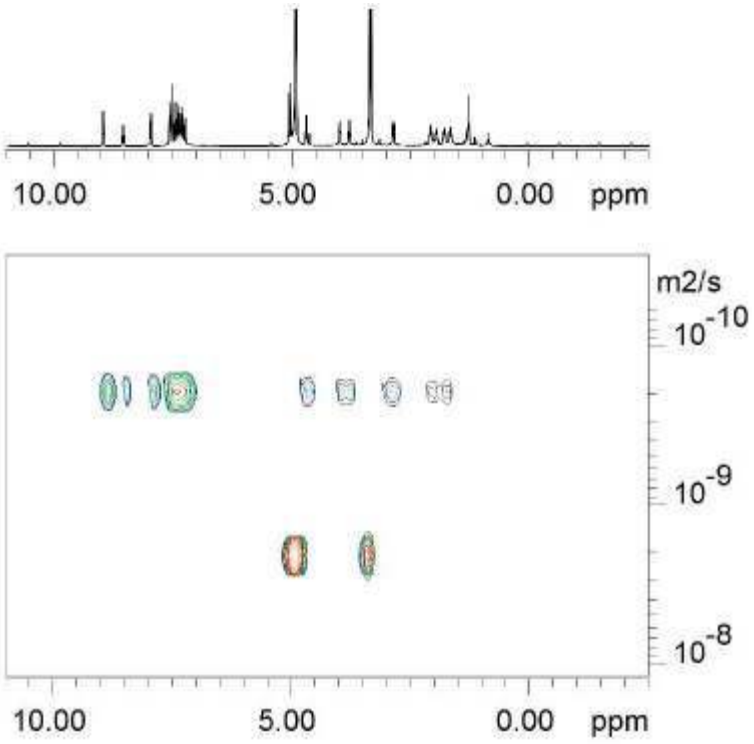

Figure 4: DOSY experiment of a 2.5 mM equimolar mixture of **70** and **75** in methanol-d_4.

This result indicated that both compounds were involved in the formation of the same diffusing species. Previously, we determined the diffusion coefficients of **70** and **75** at 1 mM in methanol-d_4 resulting respectively $4.50(\pm0.04)\cdot10^{-10}$ $m^2\cdot s^{-1}$ and $4.00(\pm0.10)\cdot10^{-10}$ $m^2\cdot s^{-1}$. Using the Stokes-Einstein equation, we estimated 19.2 Å the radius of for the putative heterodimeric spherical diffusing species and 10 Å radius the diffusing spherical species of both monomers. Analogous results were obtained using DMSO-d_6 as solvent (see Experimental Section).

8.2 NMR, MS and X-Ray Characterization

Once the first indications of the presence of a **70·75** aggregate were gathered, we performed a ^{1}H NMR titration of a 1 mM solution of **70** in methanol-d_4 using a 10 mM solution of **75** in the same solvent. The addition of incremental amounts of **75** induced upfield changes to the proton signals of **70**, and a set of signals assigned to the protons of **75** grew in intensity. After the addition of 1 equiv. of **75**, the signals of the protons of **70** did not experience additional chemical shift changes, while the aromatic proton signals of **75** started to move downfield. Taken all together, these observations are indicative of the formation of 1:1 complex for which a binding constant larger than 10^4 M^{-1} can be estimated in methanol-d_4. In addition, the chemical exchange between the free and bound components of the cage complex is fast on the chemical shift timescale (Figure 5).

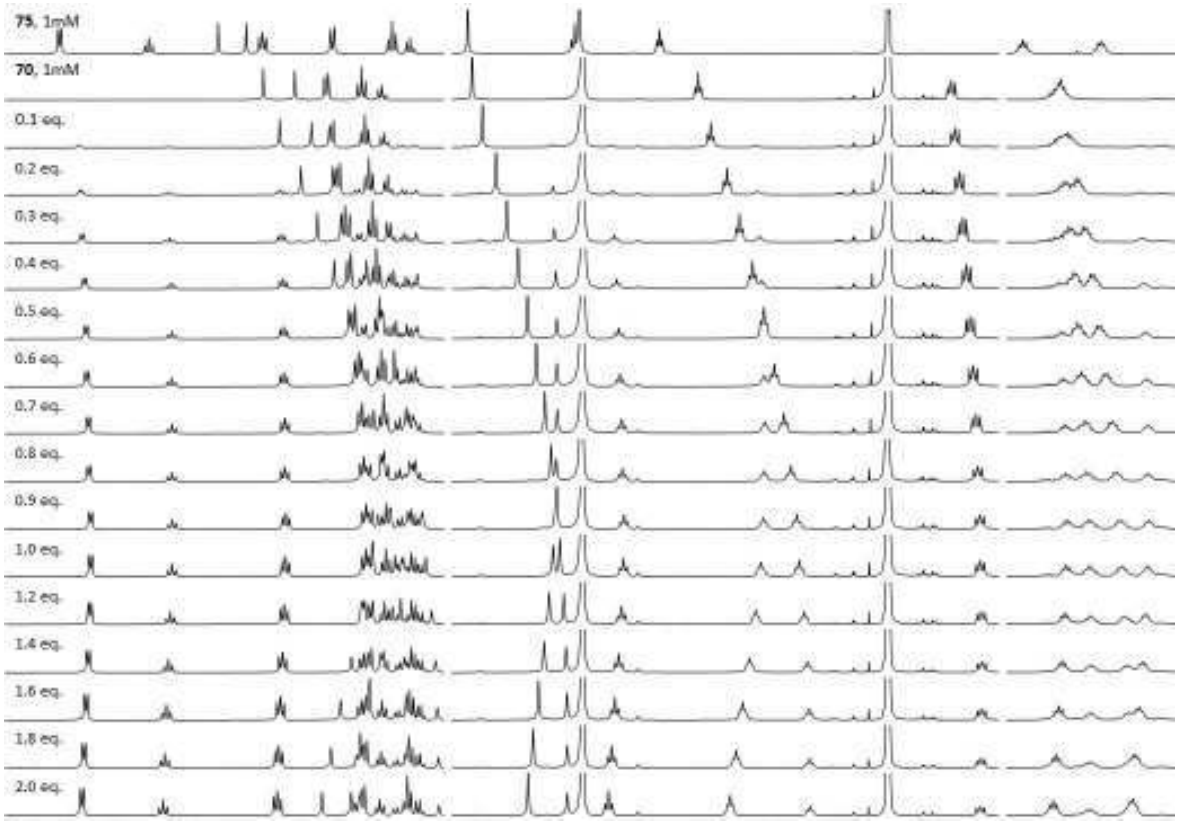

Figure 5: ^{1}H NMR titration of **70** (1 mM) with **75** (10 mM, 0.1 eq. = 5 µL) in methanol-d_4.

At mM concentrations, the equimolar mixture of **70** and **75** produced almost a quantitative assembly of the cage in methanol-d_4 and DMSO-d_6 solutions. However, we did not observe NOE cross-peaks between the proton signals of **70** and **75** in the assembly.

The **70·75** cage assembly was further characterized by ESI-TOF-MS, from an equimolar solution in methanol. The analysis of the mixture using the positive ion mode showed an intense peak at *m/z* 688.2359, corresponding to tripled charged ion [**70·75** + 3Na]$^{3+}$ (Figure 6).

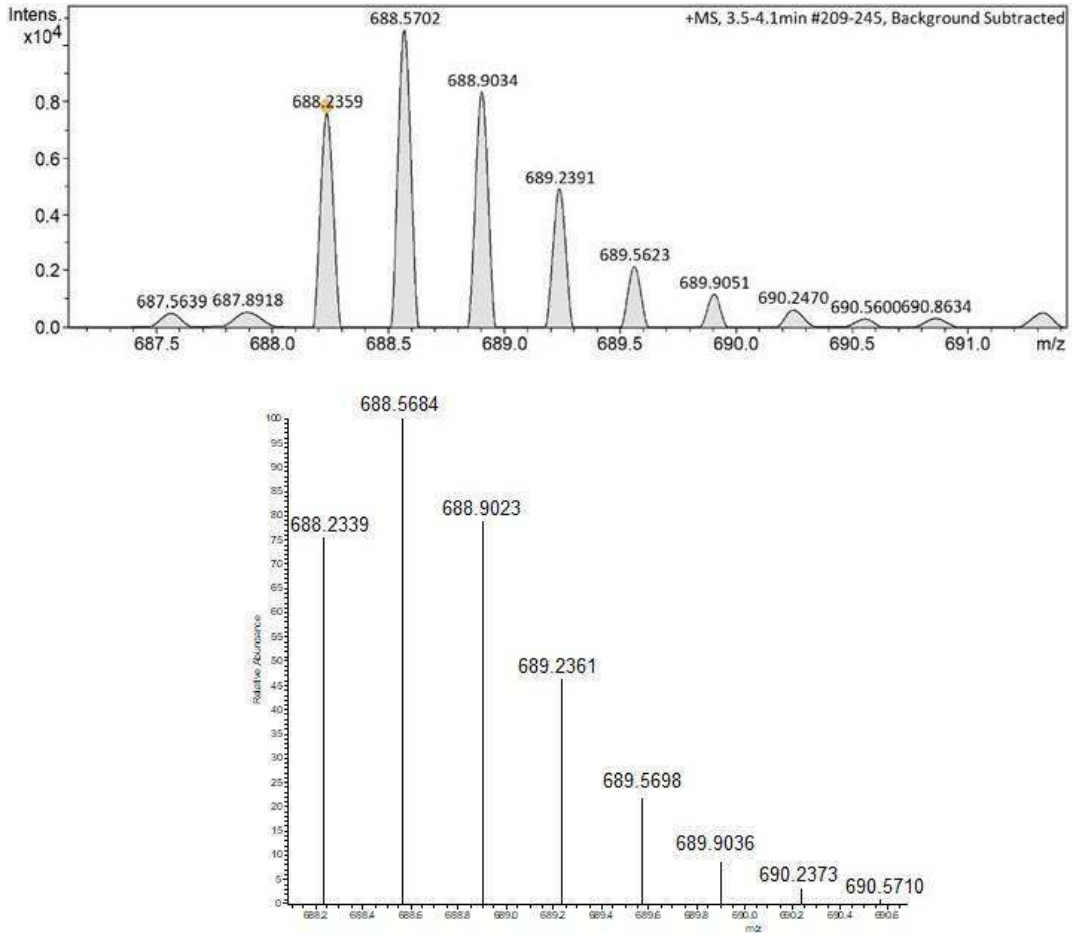

Figure 6: ESI-MS of a methanol solution of **70·75**. Top: isotopic cluster of the aggregate [**70·75**+ 3Na]$^{3+}$; bottom: simulation of the cluster.

Peaks at *m/z* 1020.9 and 2018.7, corresponding respectively to the ions [**70·75** + 2Na]$^{2+}$ and [**70·75** + Na]$^{+}$ were also observed, together with those of the oligomer ions, [**75·70·75**]$^{3+}$ (*m/z* 997.4), [**70·75 ·70·75** + 3Na]$^{3+}$ (*m/z* 1353.5) and [**70·75·70** + 5Na]$^{2+}$ (*m/z* 1555.0).

Slow evaporation of an equimolar 2.5 mM solution of **70·75** in methanol produced single crystals suitable for X-ray diffraction. The solution of the diffracted data confirmed the formation of the 1:1 cage complex held together by three ion-paired interactions in the solid-state (Figure 7).

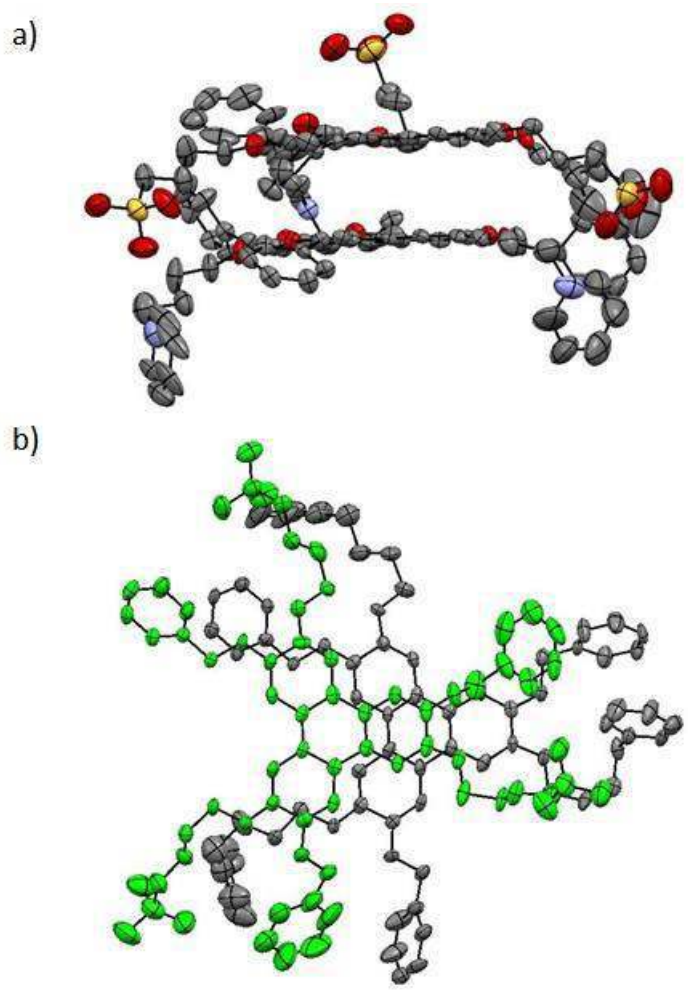

Figure 7: X-Ray crystal structure of **70·75** cage complex. a) Side view; b) Top view (**70** is highlighted in green, **75** in grey). Hydrogens are omitted for clarity.

In the solid phase, triphenylenes **70** and **75** are staked on their triphenylenic core, with their charged moieties facing each other. Indeed, the interaction observed in solution is present also in the crystals. The crystal cell repeats with the same configuration in all the directions.

8.3 Host-Guest Chemistry

Once the formation of **70·75** cage complex was evidenced in solution, we investigated the host-guest properties of this new supramolecular host. Neutral and anionic flat aromatic guests, like potassium phthalimide, potassium hydrogen phthalate or 2,6-naphtalene diol did not provide spectral evidence for their interaction with the cage. On the contrary, flat aromatic cations, such as methylene blue (MB) and methyl viologen, induced chemical shift changes of the protons of the **70·75** cage that were consistent with the formation of host-guest complexes. In Figure 6 it is reported the ^{1}H NMR spectra of methylene blue and methyl viologen in methanol-d_4 and in the presence of **70·75**, showing both the shielding of the resonances of the cationic guests ($\Delta\delta$ = 0.20 ppm and $\Delta\delta$ = 0.10 ppm respectively) and the concomitant complementary de-shielding of the resonances of both halves of the capsule ($\Delta\delta_{\alpha,\beta,c,d}$ = 0.05 ppm and $\Delta\delta_{\alpha,\beta,c,d}$ = 0.20 ppm respectively). The latter effect is a further confirmation that the cationic guest is bound within the heterodimeric capsule and it is not only recognized by the *tris*-anionic species **70**.

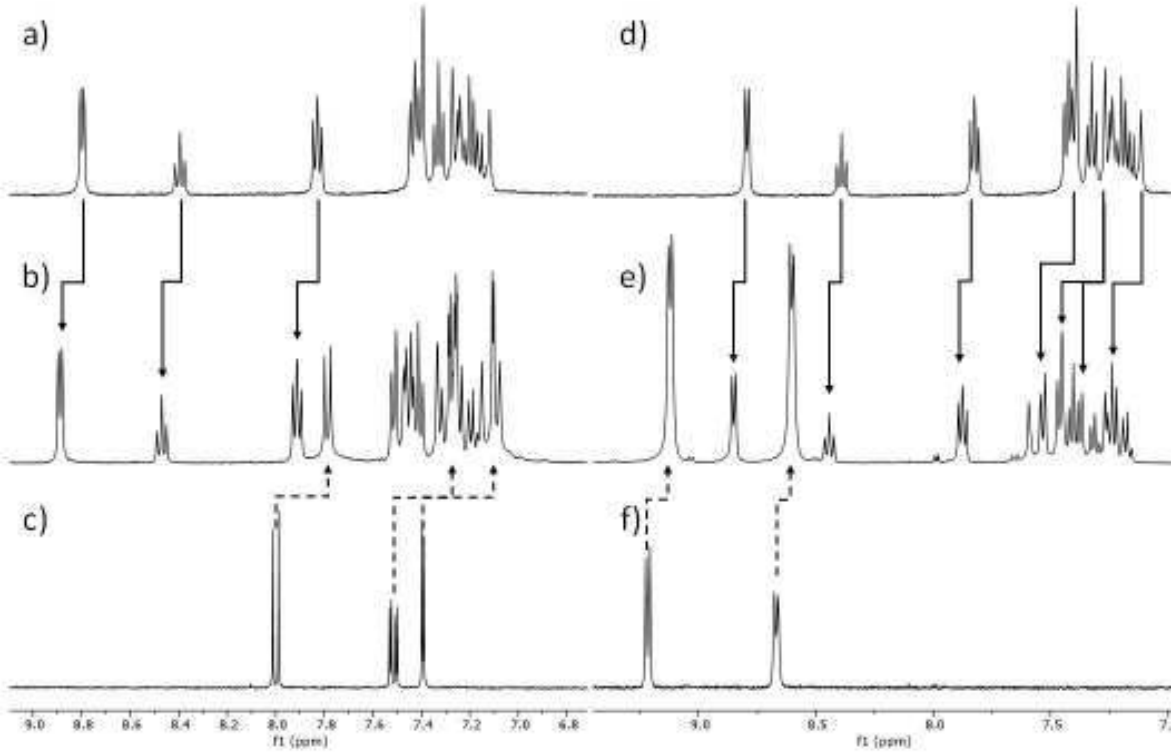

Figure 8: Aromatic region of the ^{1}H NMR spectra in methanol-d_4 for a) and d) **70·75** 1 mM; b) methylene blue 5 mM + **70·75** 1 mM; c) methylene blue 1 mM; e) methyl viologen 5 mM + **70·75** 1 mM; f) methyl viologen 1 mM. The shifts of **70·75** are highlighted with continue arrows while shifts of the guest with dashed arrows.

^{1}H NMR titrations for a 1:1 binding model provided binding constants K_a = 121 ± 3 M^{-1} for methylene blue and a K_a = 53 ± 4 M^{-1} for methyl viologen (see Experimental Section, Titrations 1 and 2).[8] The observed values are comparable to what observed in some examples for calix[4]arene ionic cages with tetramethylammonium salts or *N*-methylquinuclidinium chloride as guests.[3a,4b,4c,6b] On the contrary, alternative guests such as acetyl choline, *bis*(2,4,6-trimethylphenyl)iodonium triflate and 5-(trifluoromethyl) dibenzothiophenium trifluoromethanesulfonate (Umemoto's reagent), characterized by a more rounded shape, failed to show encapsulation, further underlying the shape selectivity imparted by the capsule in this host guest recognition phenomena.

8.4 MS Investigation on the Host-Guest Aggregate

In collaboration with Prof. Christoph Schalley of the Freie Universität Berlin, we were able to carry-out an accurate mass-spectroscopy investigation on the host-guest adduct formed by the ionic capsule and MB.

Preliminary measurements were done at first on the single components, separated capsule and guest, in order to have the corresponding reference spectra. In Figure 9 is reported the MS spectrum of the ionic capsule **70·75**.

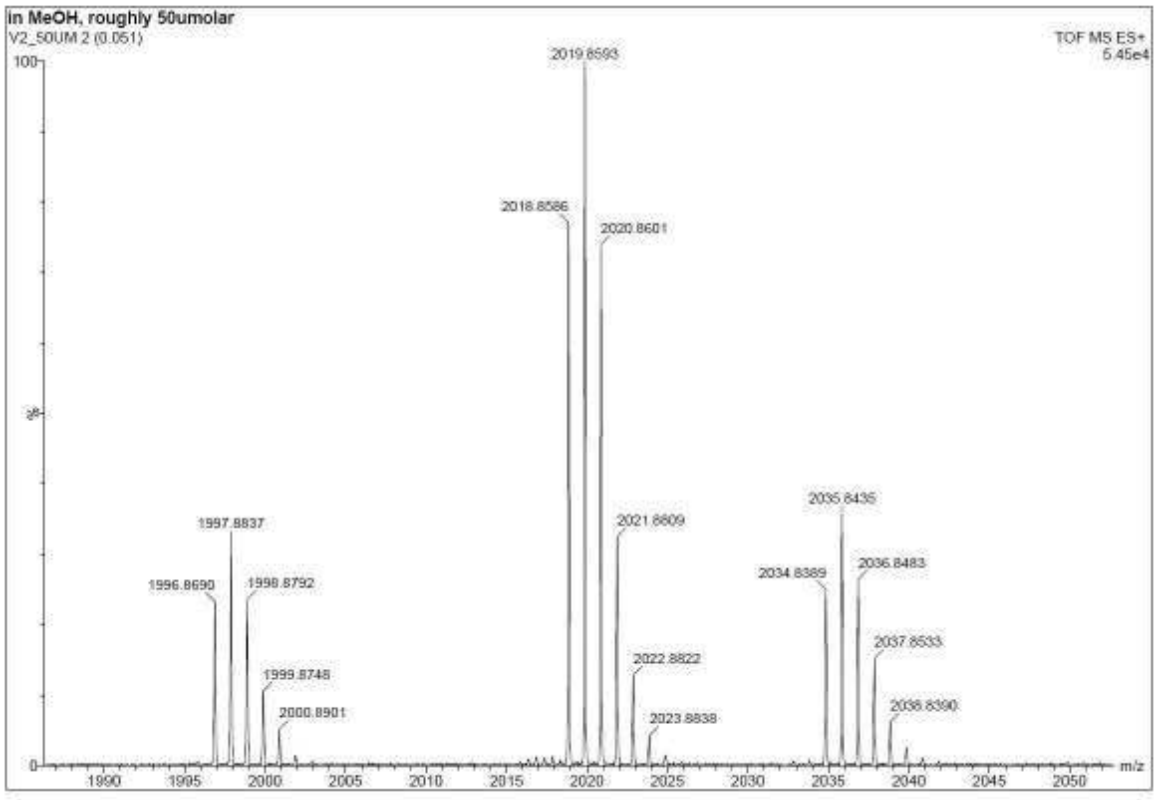

Figure 9: Detail of the MS analysis on host **70·75**. [**70·75** + H]$^+$, [**70·75** + Na]$^+$ and [**70·75** + K]$^+$ adduct are visible.

With the instrument present in Berlin, the capsule was observed in three different adducts: *m/z* 1996.8690, *m/z* 2018.8586 and *m/z* 2034.8389, corresponding to [**70·75** + H]$^+$, [**70·75** + Na]$^+$ and [**70·75** + K]$^+$, respectively. Subsequently, a solution of **70·75** and MB was subjected to the same analysis. The resulting MS spectrum is reported in Figure 10.

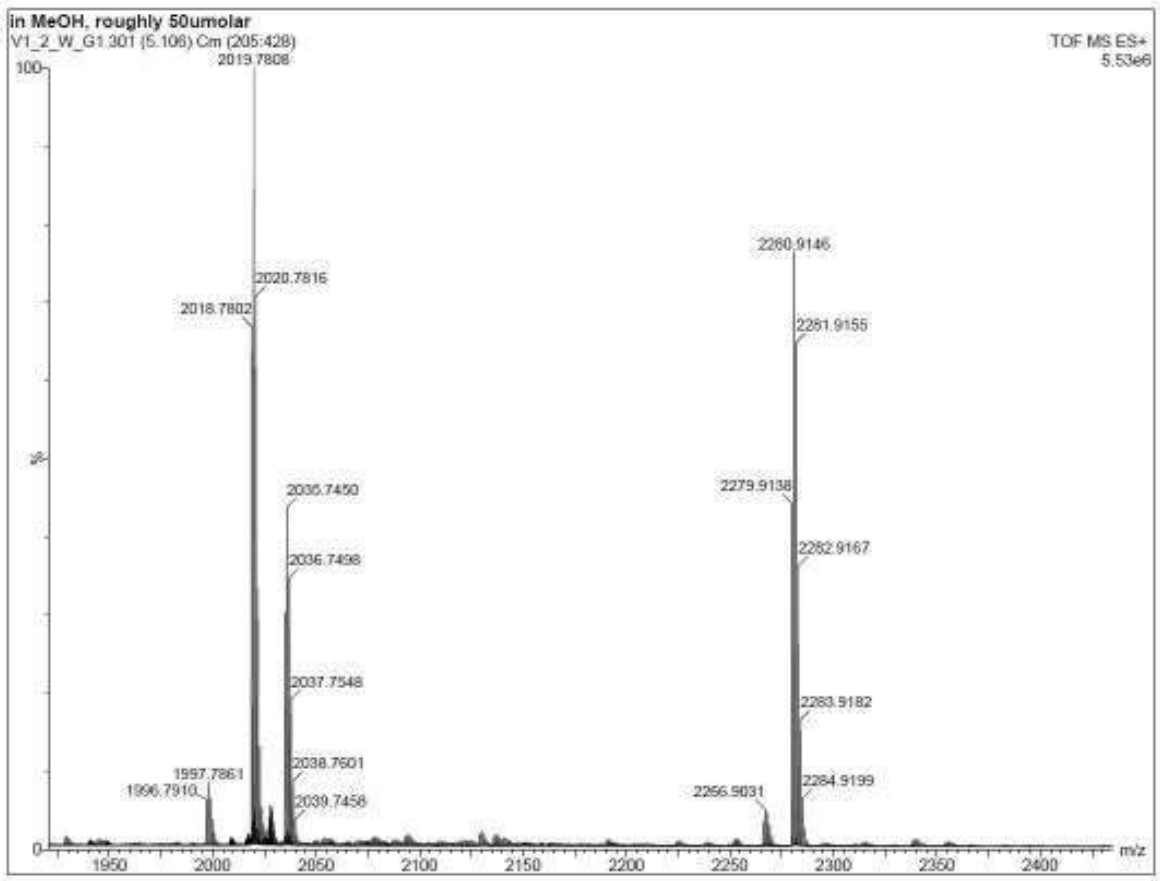

Figure 10: Detail of the MS spectrum on host **70·75** in the presence of MB. Adducts [**70·75** + Na]$^+$, [**70·75** + K]$^+$ and [**70·75** + MB]$^+$ are visible.

As can be seen in Figure 10, the *m/z* 2280.9146 signal refers clearly to the host-guest adduct [**70·75** + MB]$^+$. This is in fact a further strong support for the hosting properties of the ionic capsule for cationic guests. Nevertheless, even if the MS analysis showed clearly the host-guest adduct, the exact location of the guest on the host, if inside the cavity or on the surface, is still uncertain. For this reason, ion mobility spectroscopy (IMS) experiments will be run in the near future within the collaboration with Prof. Schalley. The planned experiments, based on the determination of the collisional diameter of the species in gas phase, will provide a possible solution. Indeed, the capsule with the guest located within the two triphenylene units, and the capsule with the guest located on its surface, are characterized by molecular models with different size and shape. This will enable the determination of the exact position of the guest in the host.

8.5 Experimental Section

8.5.1 General Methods

The reactions were followed with TLC Polygram® Sil G/UV254, 0.25 mm thickness. ^{1}H NMR, ^{13}C NMR, and 2D spectra were recorded with a Bruker Avance II 400, Ascend 400 and Ascend 500 spectrometers, working at 400-500 and 100-126 MHz respectively. Resonance frequencies are referred to tetramethylsilane. IR spectra were recorded with a Perkin Elmer Spectrum One spectrophotometer. Crystal structure determinations were carried out using a Rigaku MicroMax-007HF diffractometer equipped with a PILATUS 200K detector and a Bruker Apex II Duo equipped with an APEX II detector. Both using Mo*Kα* radiation. Crystal structure solution was achieved using VLD and Patterson methods as implemented in SIR2014 v14.10. Mass spectrometric measurements were performed using a Thermo Scientific LTQ Orbitrap XL equipped with HESI source, or Bruker HPLC-TOF (MicroTOF Focus). MS analysis on the host-guest adduct were performed with a Synapt G2-S HDMS (Waters Co., Milford, MA, USA) travelling wave ion mobility mass spectrometer. Regarding the Thermo Scientific LTQ Orbitrap XL, the compounds studied were dissolved in methanol or acetonitrile with a concentration of $5 \cdot 10^{-3}$ M. They were injected into the HESI source by direct infusion with the syringe pump integrated in the mass spectrometer at a 5 $mL \cdot min^{-1}$ flow rate. Mass spectra were acquired in positive-polarity mode with the following tuning conditions: Temperature 40 °C, Sheath gas 8 (arbitrary units, arb), Aux gas and Sweep gas 0 arb, Spray Voltage 4.5 kV, Capillary temperature 275 °C, Capillary Voltage -9 V, Tube lence 150 V. In negative polarity the following tuning parameters were employed: Temperature 40 °C, Sheath gas 19 (arbitrary units, arb), Aux gas and Sweep gas 0 arb, Spray Voltage 3.0 kV, Capillary temperature 275 °C, Capillary Voltage 10 V, Tube lence 120 V. Mass spectra were collected in full scan with a resolution of 100000 at m/z 400. The Orbitrap MS was calibrated just before analysis and during the acquisition in order to improve mass accuracy lock masses were employed. Regarding the Synapt G2-S HDMS, ions were generated by electrospray ionisation (ESI). Ionisation conditions varied depending on the complex to be measured but typical values were as follows: capillary voltage of 2.5-3 kV; source temperature of 80-100 °C, sampling cone voltage of 10-20 V, source offset of 10-20 V; desolvation gas temperature 180 °C. The concentration of the host was 50 µM in MeOH with host guest experiments conducted with a 2x excess of guest. The injection rate was 10 µL/min. Collision induced dissociation (CID) was completed in the trap cell with Nitrogen as the collision gas with collision voltages ranging from 0-50 eV. Reagents and solvents with high purity degree purchased by the providers were used as given. Otherwise, they were purified following the procedures reported in literature. Anhydrous solvents were prepared by adding activated 3 Å molecular sieves to the solvent under inert atmosphere, or distillated following the procedures reported in literature.[9] Molecular sieves were activated shortly before the use by continuous heating under *vacuum*. Flash chromatography were performed with silica gel Merk 60, 230-400 mesh, following procedures reported in literature.[10]

8.5.2 Experimental Procedures - Syntheses

Synthesis of the ionic dimeric capsule (**70·75**):

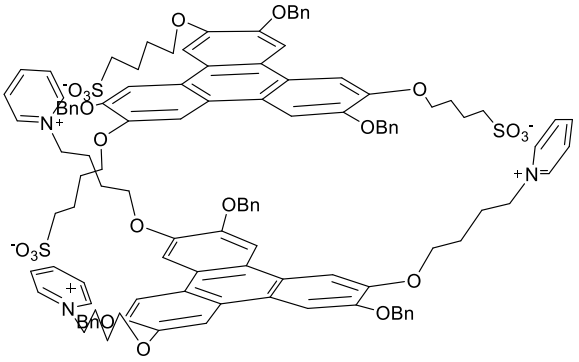

70·75

In two separate vials, **70** (0.028 g, 0.025 mmol) and **75** (0.029 mg, 0.025 mmol) were dissolved in water (2 mL each) to afford the respective solutions. The two solutions were mixed together, the resulting precipitate was filtered, washed with water (3×10 mL) and dried in *vacuum* overnight. The product was obtained as a grey solid, without the need of further purification (0.050 g, 0.025 mmol, quantitative yield). ^{1}H NMR (400 MHz, methanol-d_4): δ 8.79 (6H, d, *J* = 5.9 Hz), 8.38 (3H, t, *J* = 7.8 Hz), 7.81 (6H, t, *J* = 7.1 Hz), 7.45-7.08 (48 H, set of m), 5.00 (6H, s), 4.94 (6H, s), 4.64 (6H, t, *J* = 7.0 Hz), 3.74 (6H, t, *J* = 6.3 Hz), 2.88-2.81 (6H, set of m), 2.15-2.04 (6H, set of m), 2.02-1.89 (6H, set of m), 1.85-1.74 (6H, set of m), 1.72-1.64 (6H, set of m). ^{1}H NMR (400 MHz, DMSO-d_6): δ 9.15-9.08 (6H, set of m), 8.57 (3H, tt, *J* = 7.8, 1.4 Hz), 8.09 (6H, dd, *J* = 7.7, 6.5 Hz), 8.02 (3H, s), 7.90 (3H, s), 7.89 (3H, s), 7.75 (3H, s), 7.62-7.56 (6H, set of m), 7.56-750 (6H, set of m), 7.39 (t, *J* = 7.6 Hz, 1H), 7.35-7.17 (12 H, set of m), 5.37 (6H, s), 5.37 (6H, s), 4.77 (6H, t, *J* = 7.2 Hz), 4.32 (6H, t, *J* = 6.0 Hz), 4.20 (6H, t, *J* = 5.4 Hz), 2.59 (6H, t, *J* = 7.2 Hz), 2.22-2.13 (6H, set of m), 1.96-1.79 (18H, set of m). HRMS (ESI): calcd. for $C_{117}H_{117}N_3Na_3O_{21}S_3$ [M^{3+}] 688.5684; found: 688.5702.

8.5.3 NMR and MS Spectrum

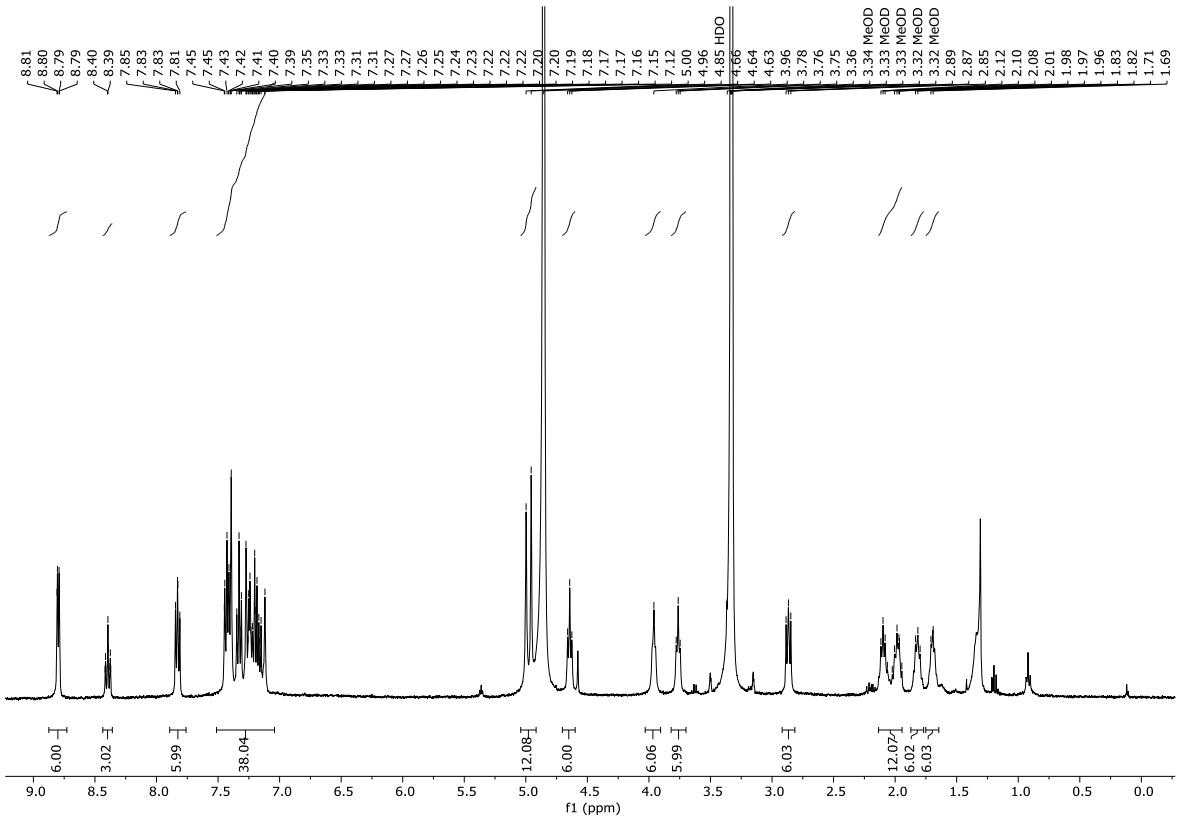

Figure I: ^{1}H NMR of dimeric capsule **70·75** in methanol-d_4.

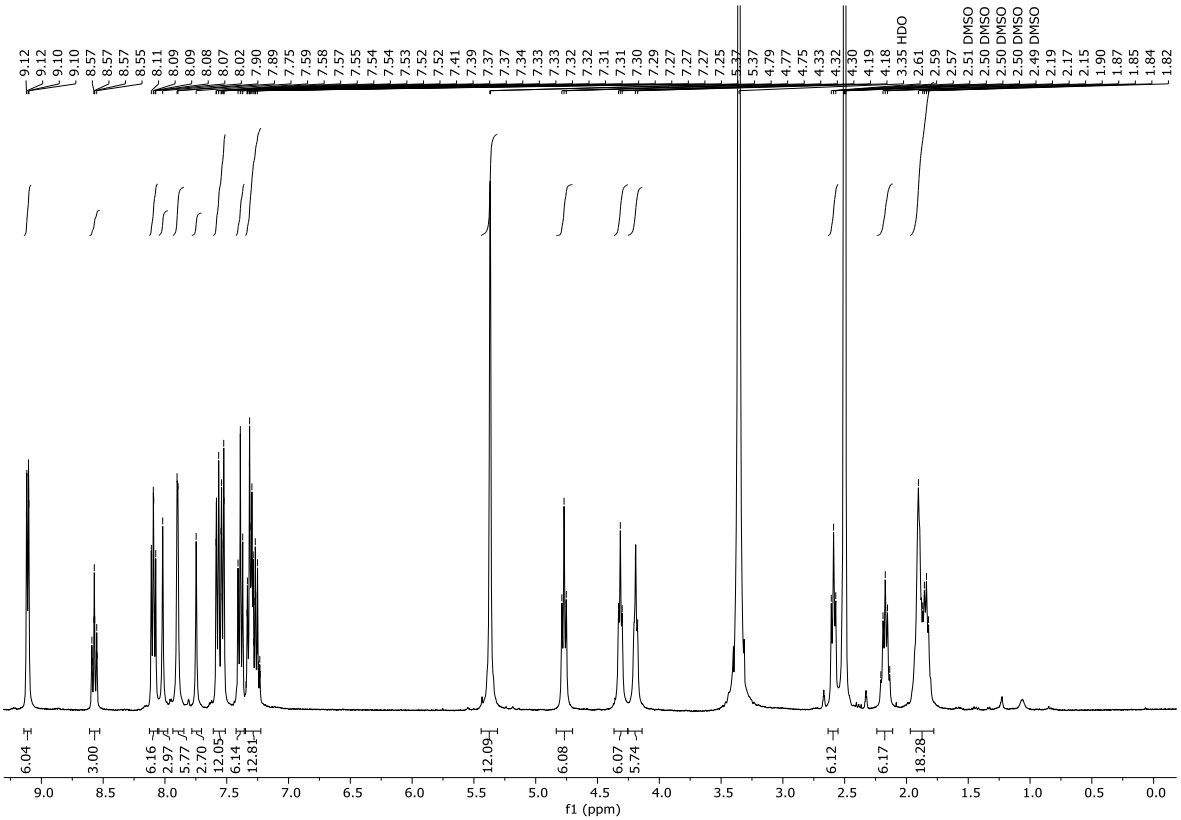

Figure II: ^{1}H NMR of dimeric capsule **70·75** in DMSO-d_6.

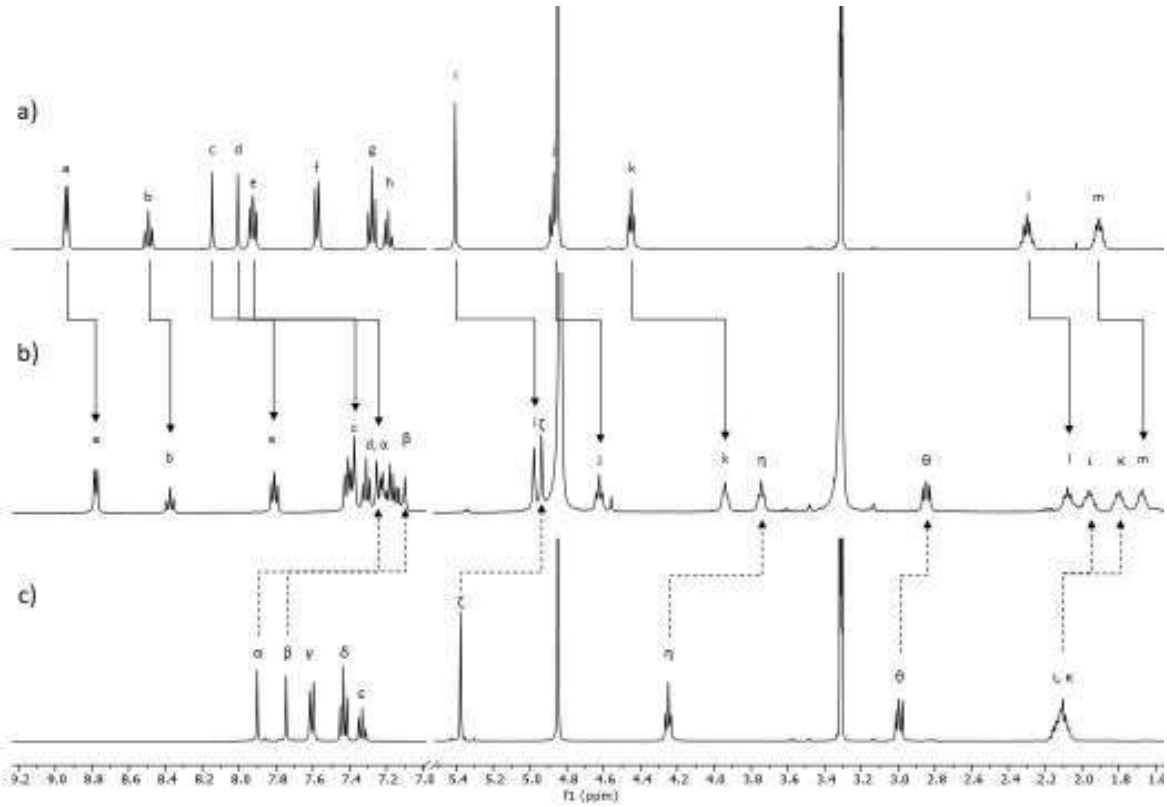

Figure III: Figure 3, complete. ^{1}H NMR spectra in MeOH-d_4 of a) **75**; b) **70·75**; c) **70**. The shifts are highlighted with arrows.

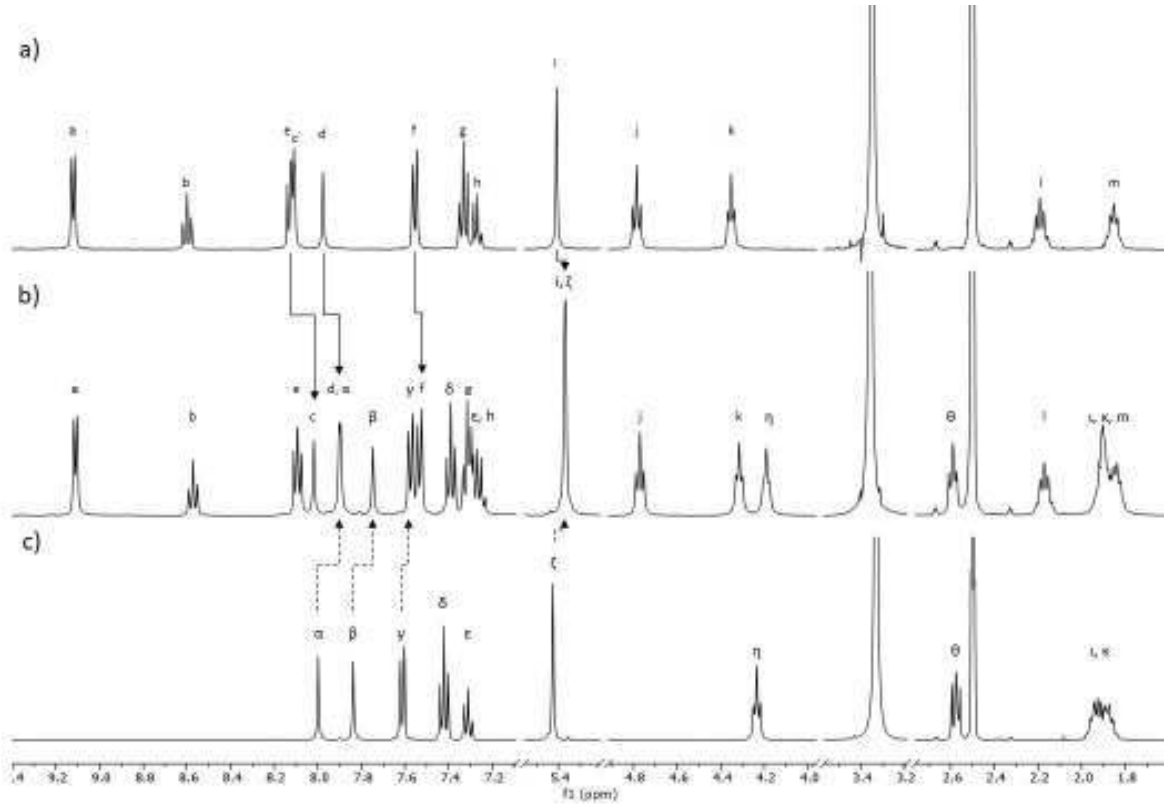

Figure IV: ^{1}H NMR spectra in DMSO-d_4 of a) **75**; b) **70·75**; c) **70**. The shifts are highlighted with arrows.

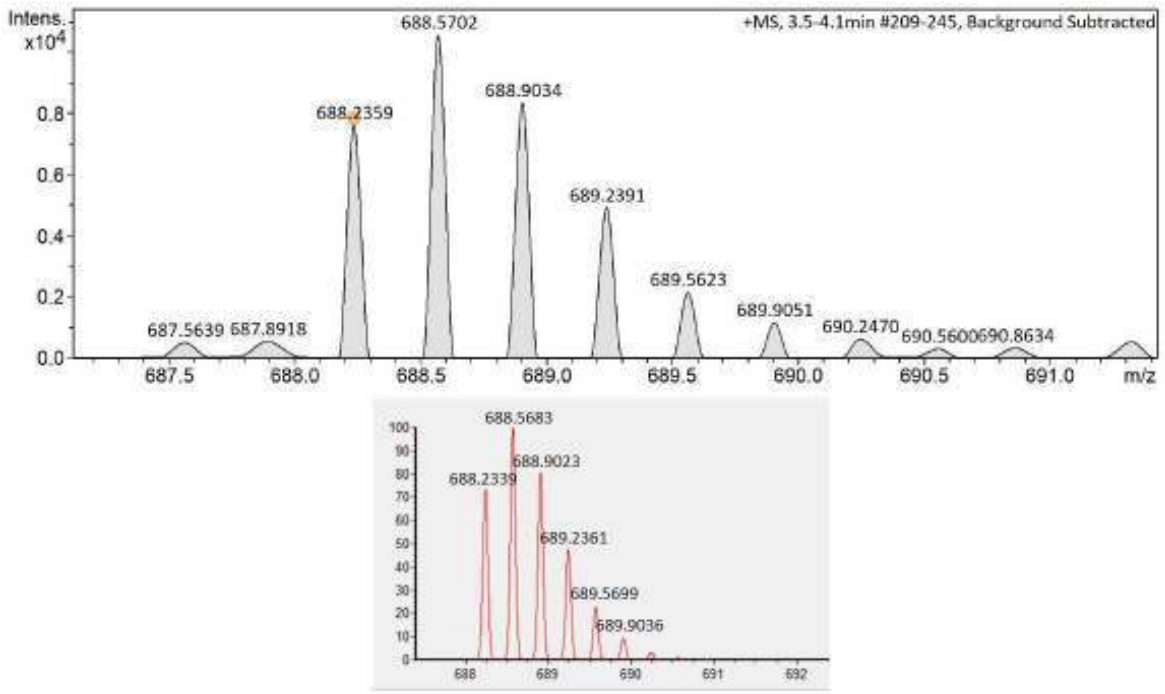

***Figure V**: ESI-HRMS* of dimeric capsule ***70·75**, [**70·75**+ 3Na]$^{3+}$ ion.*

8.5.4 DOSY NMR

DOSY NMR 1: 70·75 in MeOH-d_4

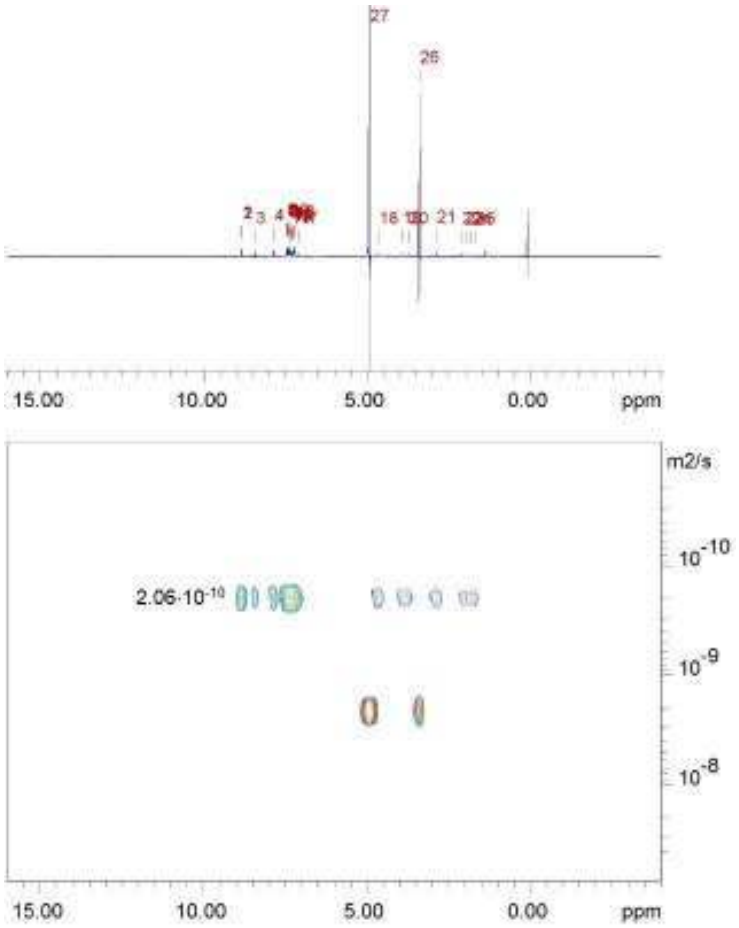

Figure VI: DOSY NMR 1, pseudo 2D-DOSY NMR.

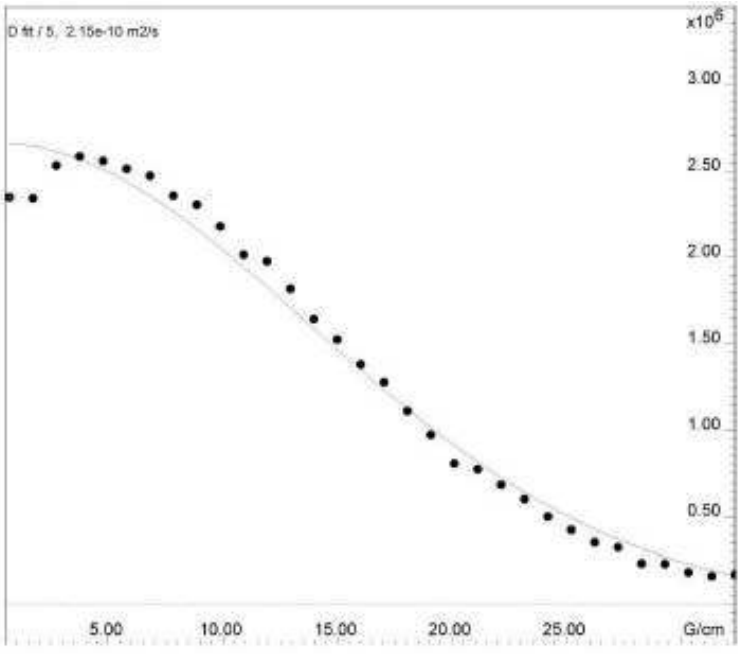

Figure VII: DOSY NMR 1, monoexponential signal decay.

DOSY NMR 2: 70 in MeOH-d_4

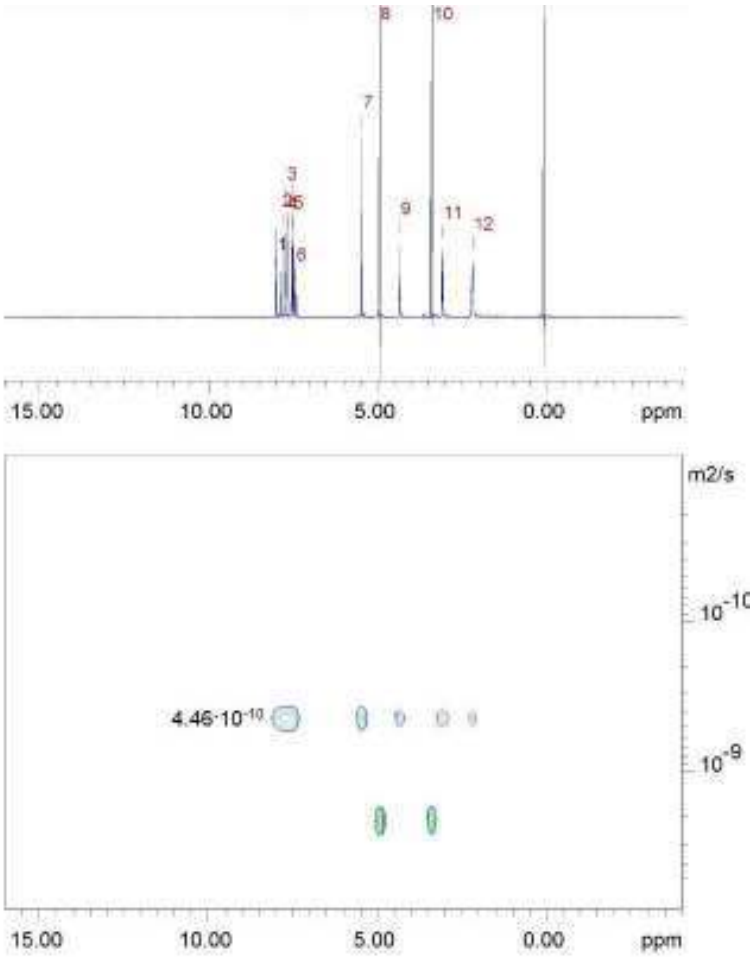

Figure VIII: DOSY NMR 2, pseudo 2D-DOSY NMR.

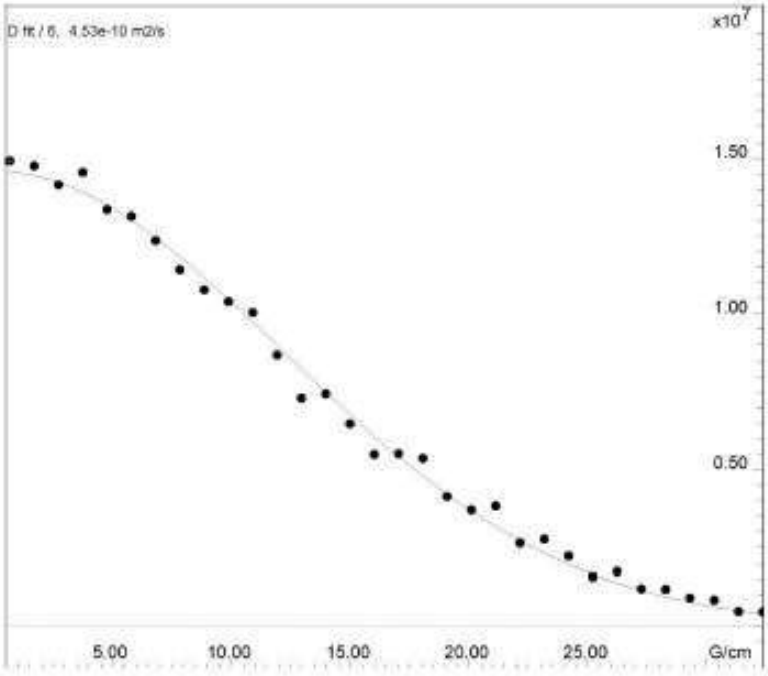

Figure IX: DOSY NMR 2, monoexponential signal decay.

DOSY NMR 3: 75 in MeOH-d_4

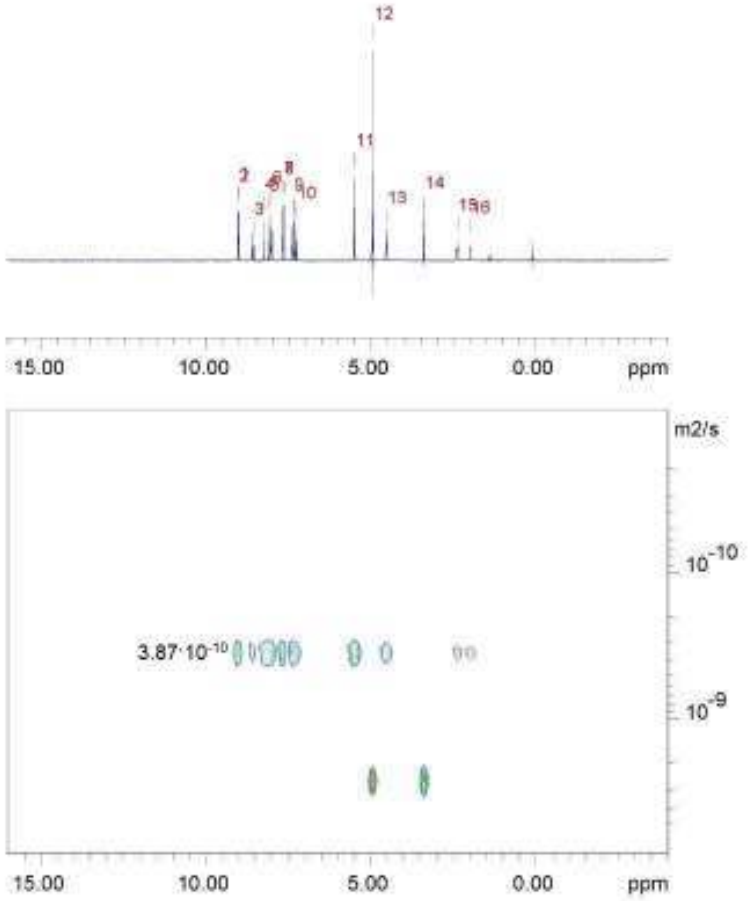

Figure X: DOSY NMR 3, pseudo 2D-DOSY NMR.

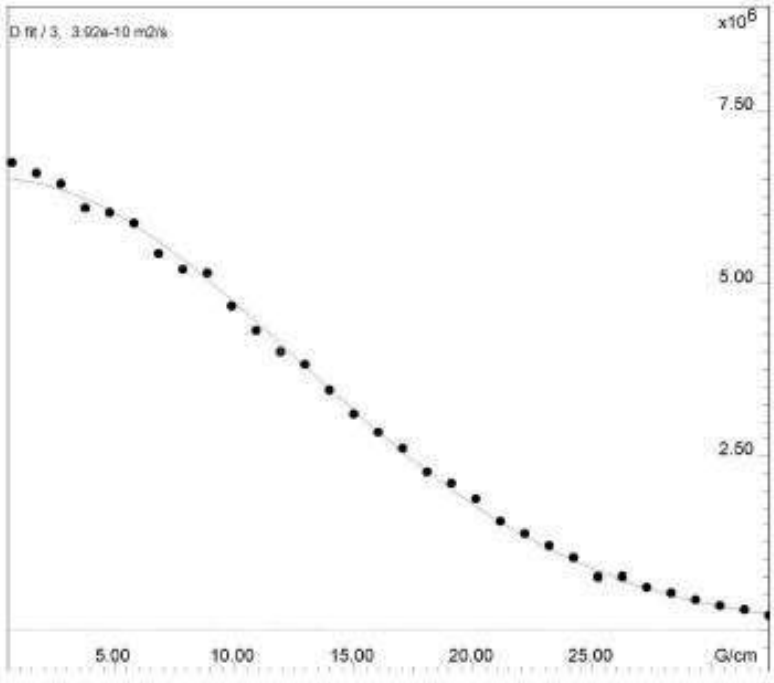

***Figure* XI**: DOSY NMR 3, monoexponential signal decay.

DOSY NMR 4: 70·75 in DMSO-d_4

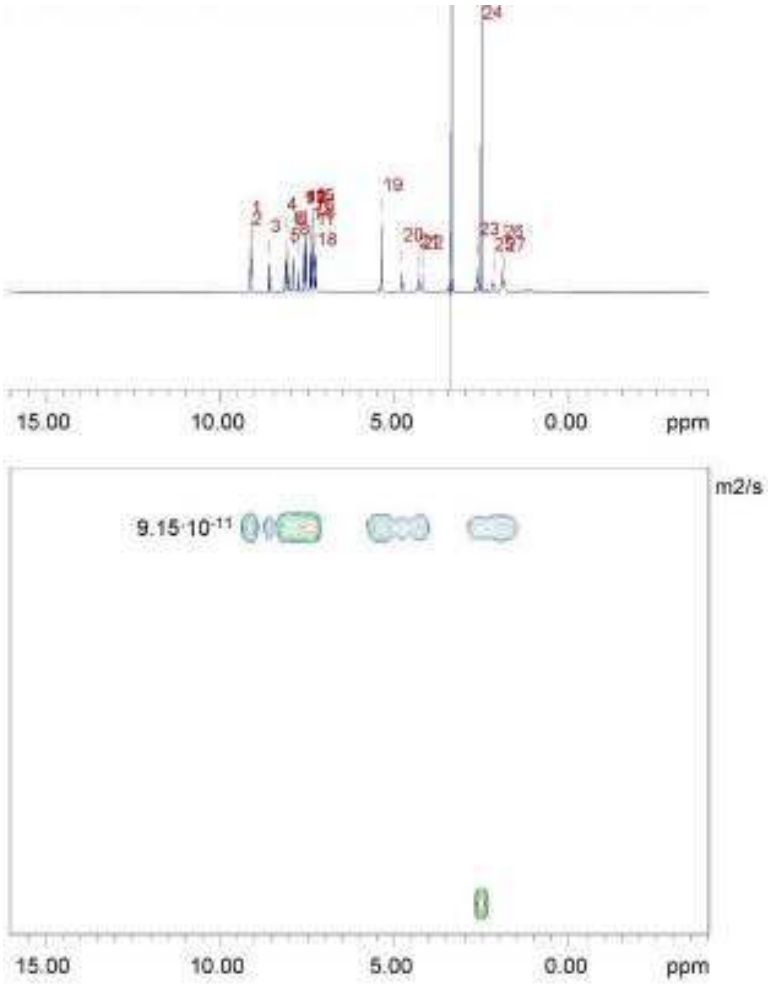

Figure XII: DOSY NMR 4, pseudo 2D-DOSY NMR.

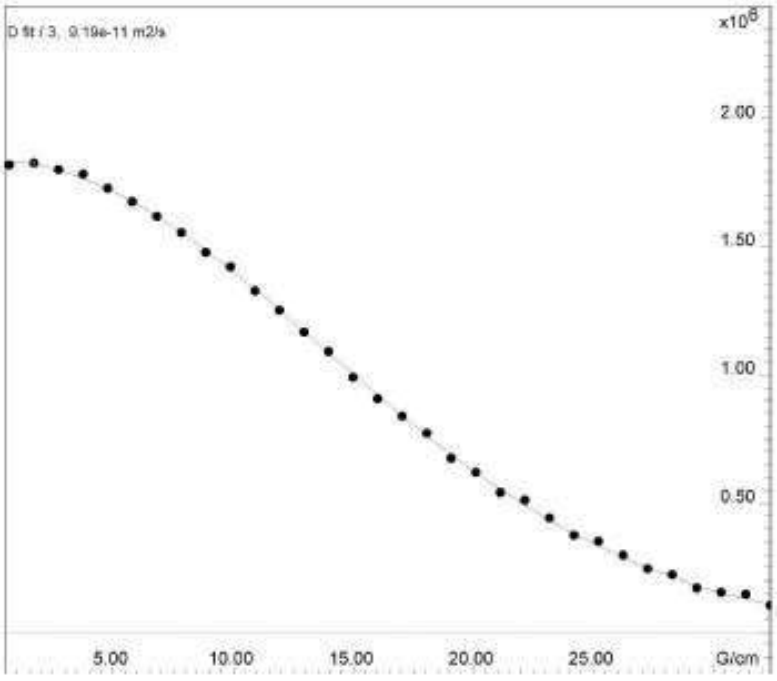

Figure XIII: DOSY NMR 4, monoexponential signal decay.

DOSY NMR 5: 70 in DMSO-d_4

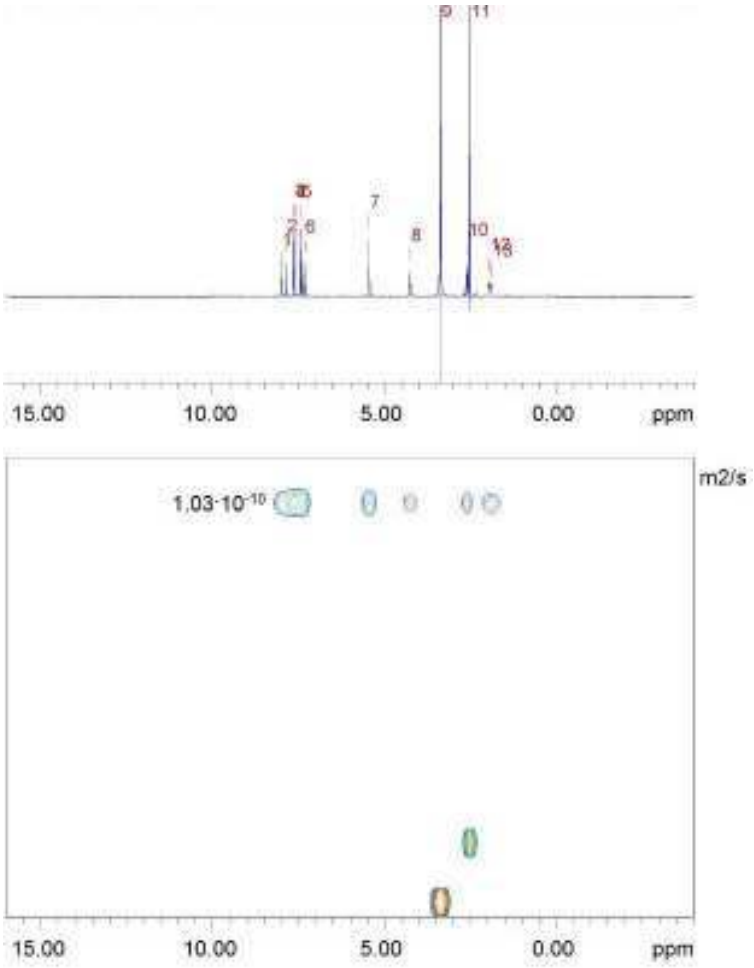

Figure XIV: DOSY NMR 5, pseudo 2D-DOSY NMR.

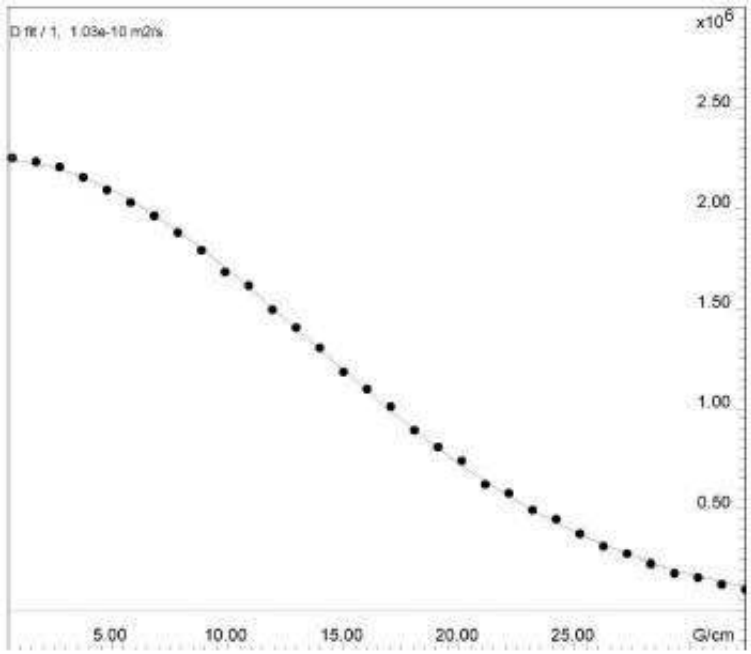

Figure XV: DOSY NMR 5, monoexponential signal decay.

DOSY NMR 6: 75 in DMSO-d_4

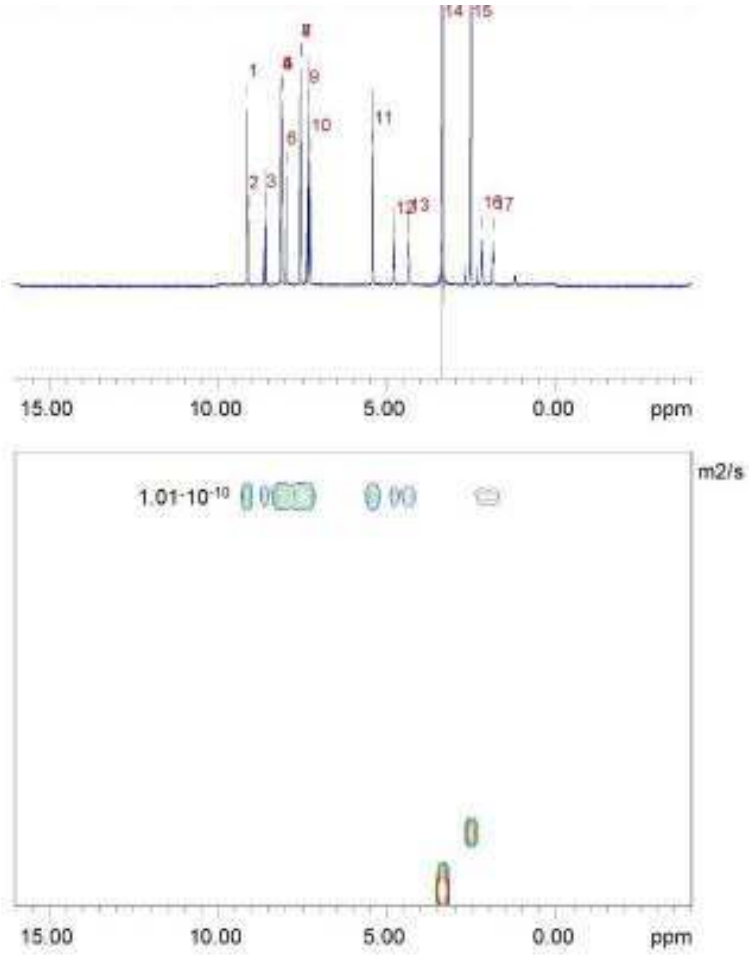

Figure XVI: DOSY NMR 6, pseudo 2D-DOSY NMR.

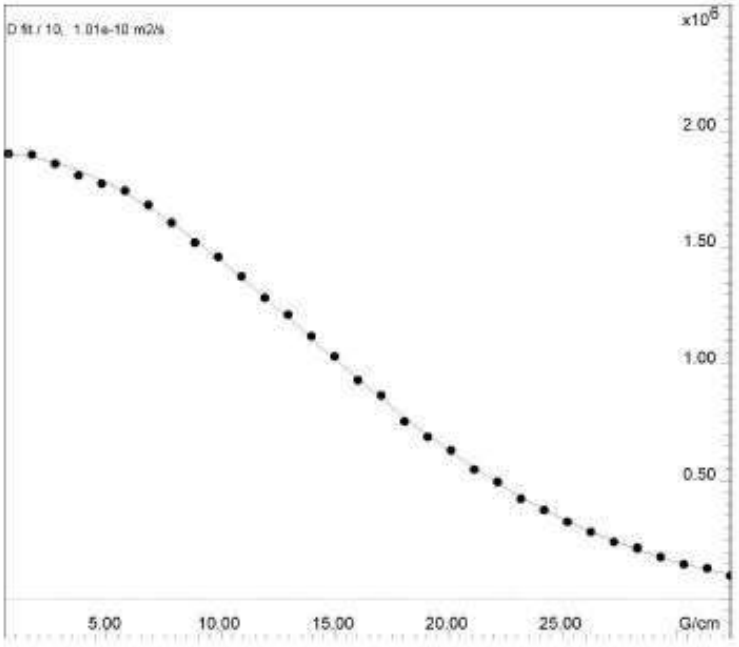

Figure XVII: DOSY NMR 6, monoexponential signal decay.

8.5.5 Titrations

Titration 1: **70** 1 mM + **75** (10 mM, 0.1 eq. = 5 µL)**,** MeOH-d_4

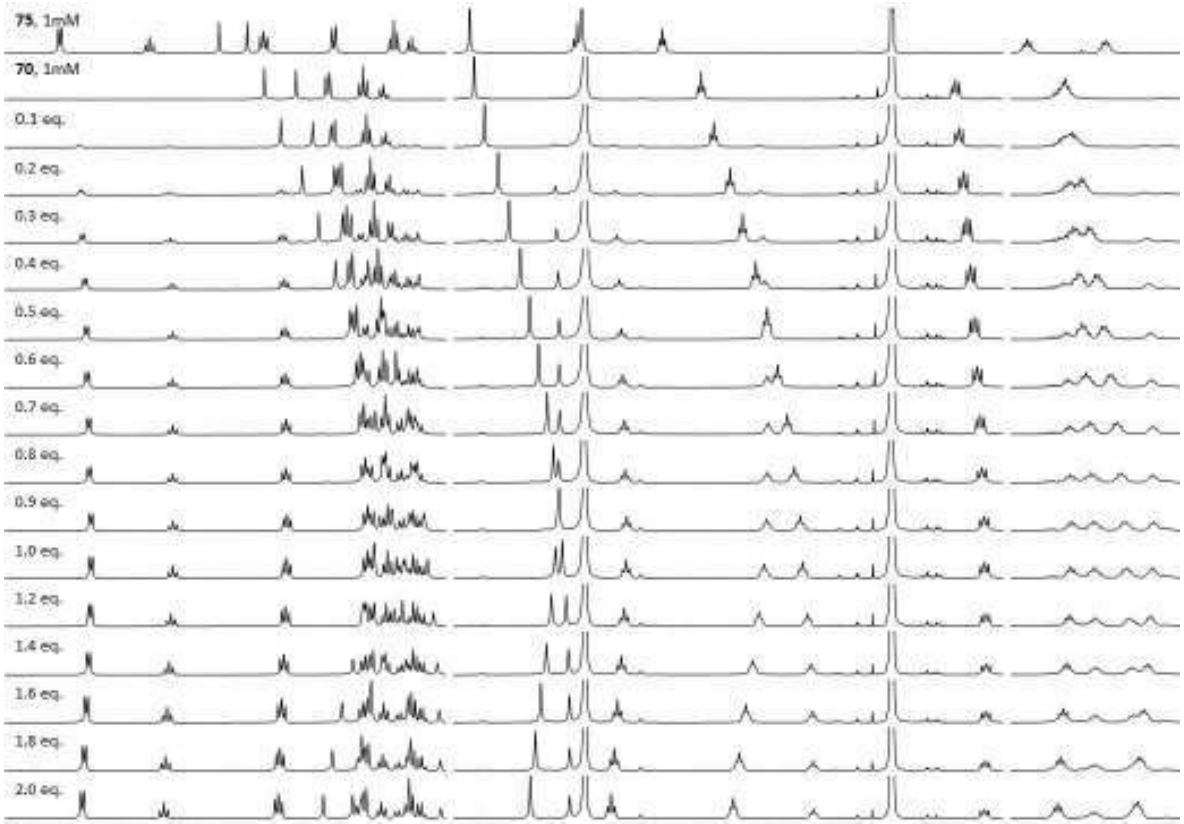

Figure XVIII: Titration 1, ^{1}H NMR.

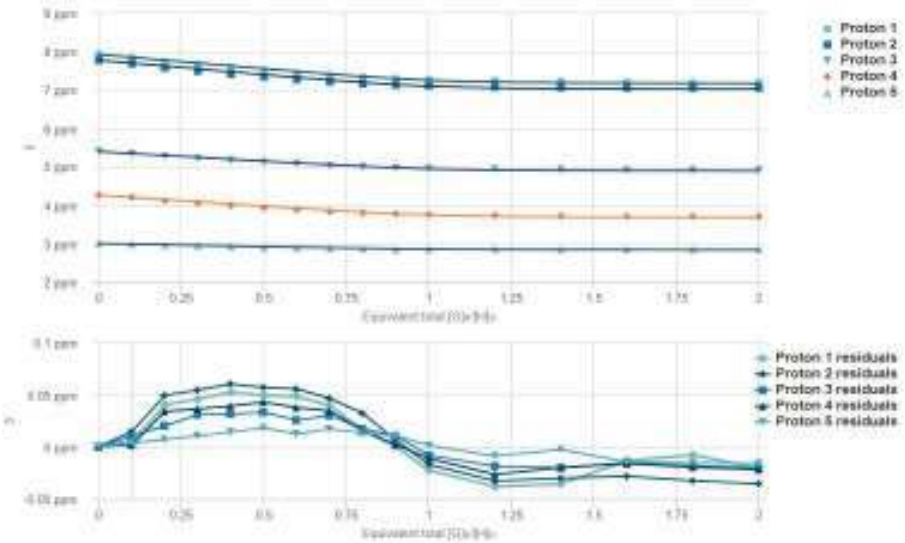

Figure XIX: Titration 1, ^{1}H NMR shifts and Δδ.

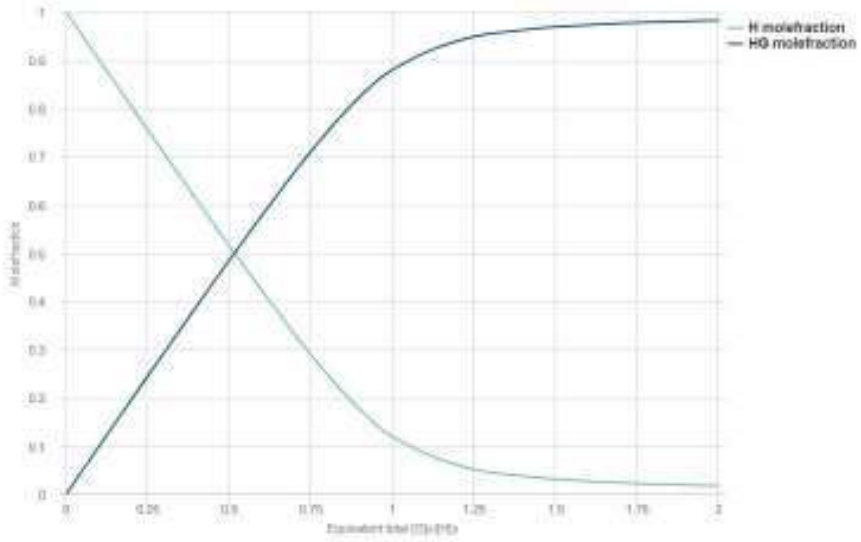

Figure XX: Titration 1, molefraction chart.

Quality of fit

Fit	RMS	Covariance
Proton 1	3.2479e-2	1.7304e-2
Proton 2	3.6791e-2	2.4885e-2
Proton 3	2.1303e-2	1.6707e-2
Proton 4	2.6194e-2	1.8841e-2
Proton 5	1.1740e-2	4.9120e-2
Total	**2.7703e-2**	**1.3124e-2**

Coefficients

Fit	H	HG
Proton 1	7.8200	7.1982
Proton 2	7.7700	7.0013
Proton 3	5.3900	4.8809
Proton 4	4.2600	3.6681
Proton 5	3.0000	2.8926

Figure XXI: Titration 1, titration fit data.

Titration 2: 70·75 1 mM + methylene blue (10 mM, 0.1 eq. = 5 µL)**,** MeOH-d_4

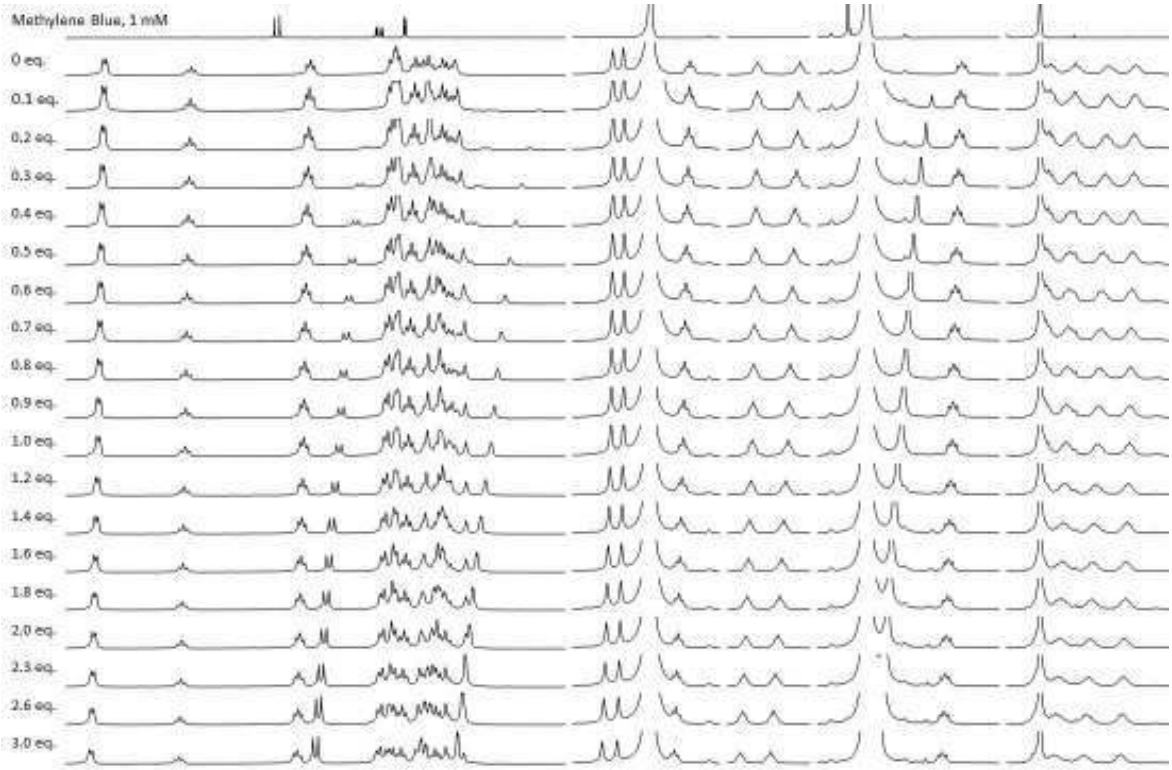

***Figure* XXII**: *Titration 2, ^{1}H NMR.*

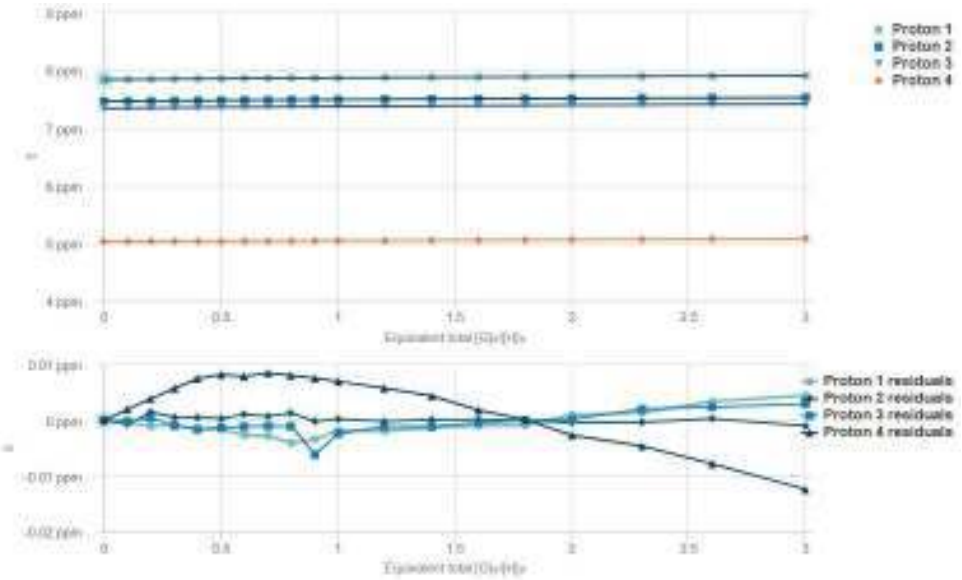

Figure XXIII: Titration 2, ^{1}H NMR shifts and Δδ.

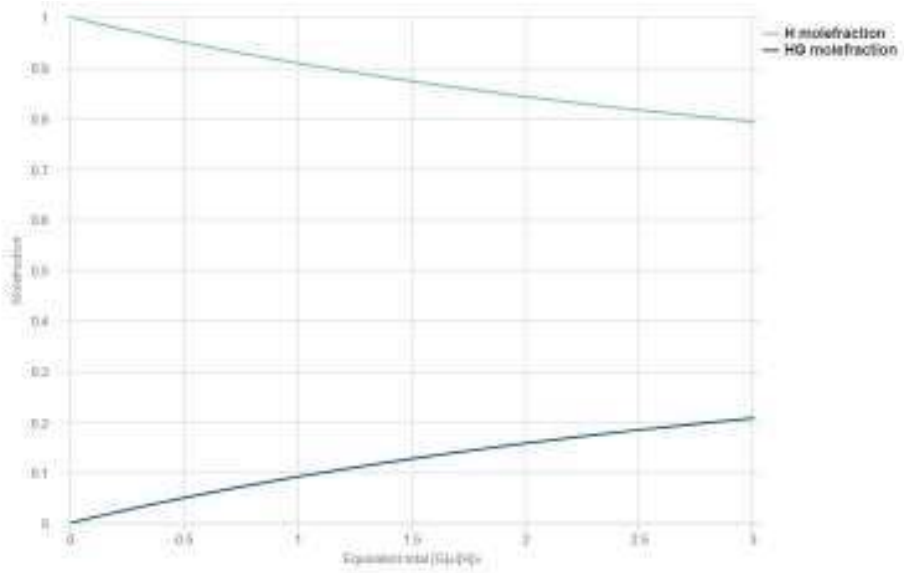

Figure XXIV: Titration 2, molefraction chart.

Quality of fit

Fit	RMS	Covariance
Proton 1	2.2421e-3	1.2309e-2
Proton 2	6.5417e-4	1.0896e-3
Proton 3	1.9782e-3	8.3032e-3
Proton 4	6.4150e-3	0.1344
Total	**3.5539e-3**	**3.0868e-2**

Coefficients

Fit	H	HG
Proton 1	7.8400	8.1705
Proton 2	7.4640	7.7730
Proton 3	7.3420	7.6991
Proton 4	5.0330	5.2193

Figure XXV: Titration 2, titration fit data.

Titration 3: 70·75 1 mM + methyl viologen (10 mM, 0.1 eq. = 5 µL)**,** MeOH-d_4

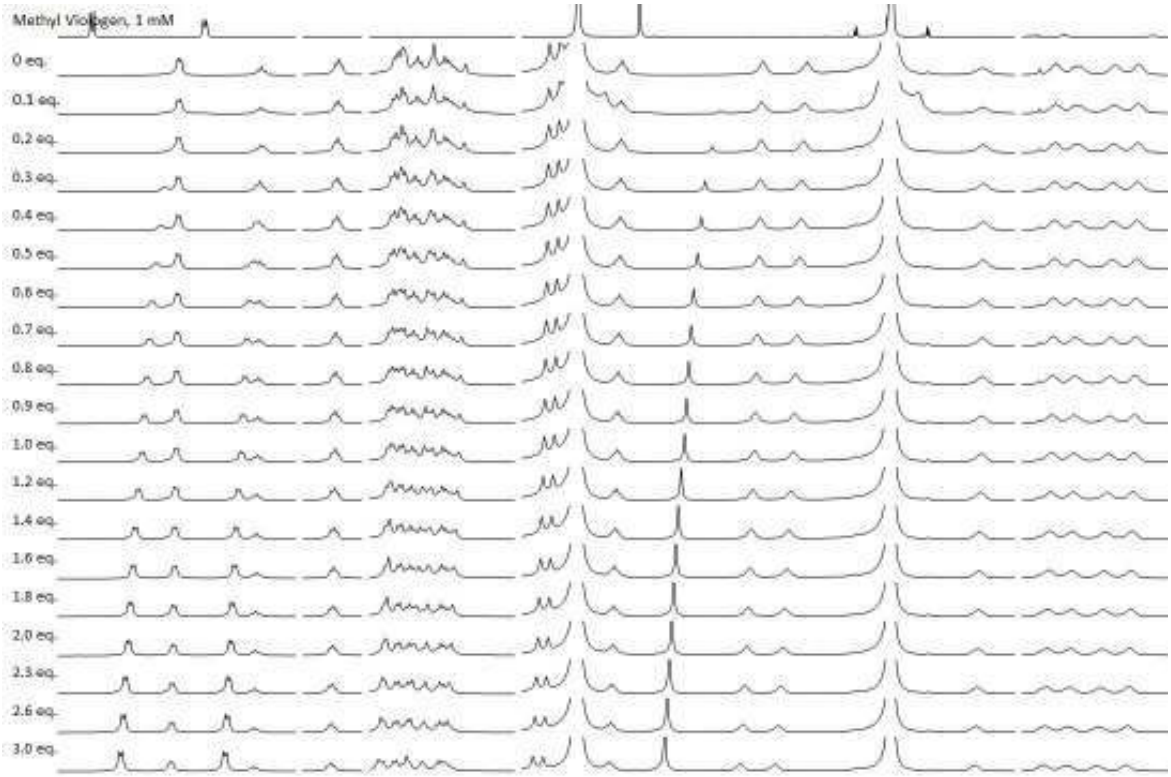

Figure XXVI: Titration 3, ^{1}H NMR.

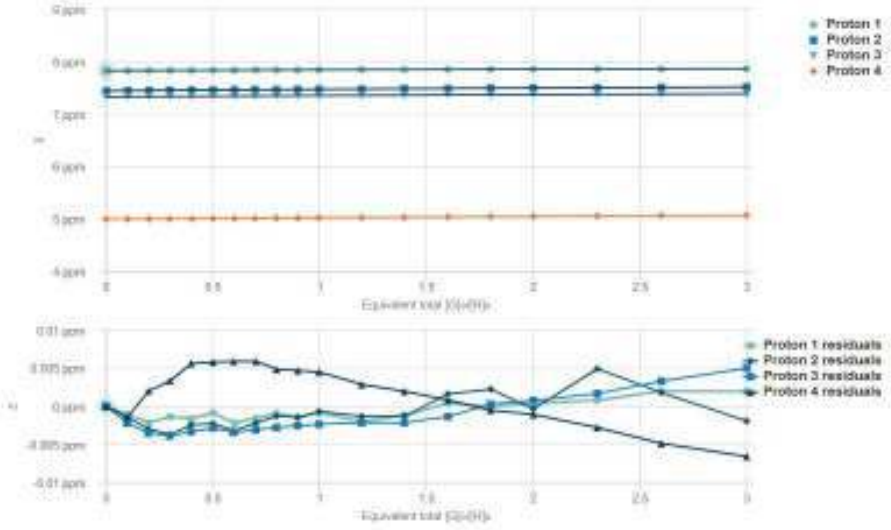

Figure XXVII: Titration 3, ^{1}H NMR shifts and Δδ.

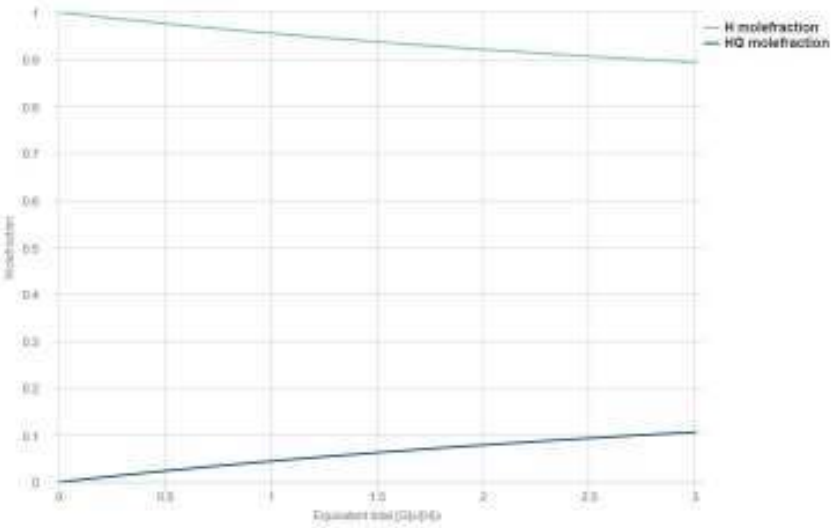

Figure XXVIII: Titration 3, molefraction chart.

Quality of fit

Fit	RMS	Covariance
Proton 1	1.3853e-3	1.2536e-2
Proton 2	2.2682e-3	1.0356e-2
Proton 3	2.7516e-3	2.5003e-2
Proton 4	4.0156e-3	2.2467e-2
Total	2.7731e-3	2.0093e-2

Coefficients

Fit	H	HG
Proton 1	7.8250	6.2097
Proton 2	7.4400	6.1449
Proton 3	7.3260	7.8802
Proton 4	4.9600	5.6583

Figure XXIX: Titration 3, titration fit data.

8.5.6 X-Rays Diffraction

Identification code	GB047	
Empirical formula	C123.80 H144.20 N3 O27.80 S3	
Formula weight	2215.19	
Temperature	100(2)K	
Wavelength	0.71073 Å	
Crystal system	triclinic	
Space group	P 1	
Unit cell dimensions	a = 9.8688(4)Å	a = 112.216(4)°.
	b = 17.2408(8)Å	b = 100.526(3)°.
	c = 19.4655(6)Å	g = 98.676(3)°.
Volume	2925.2(2) $Å^3$	
Z	1	
Density (calculated)	1.257 mg/m^3	
Absorption coefficient	0.139 mm^{-1}	
F(000)	1178	
Crystal size	0.400 x 0.050 x 0.050 mm^3	
Theta range for data collection	2.155 to 29.204°.	
Index ranges	-12<=h<=13,-23<=k<=21,-26<=l<=24	
Reflections collected	89292	
Independent reflections	21374 [R(int) = 0.0756]	
Completeness to theta =29.204°	83.9%	
Absorption correction	Multi-scan	
Max. and min. transmission	1.00 and 0.64	
Refinement method	Full-matrix least-squares on F^2	
Data / restraints / parameters	21374/ 1315/ 1604	
Goodness-of-fit on F^2	1.376	
Final R indices [I>2sigma(I)]	R1 = 0.0963, wR2 = 0.2235	
R indices (all data)	R1 = 0.1857, wR2 = 0.2489	
Largest diff. peak and hole	0.800 and -0.433 $e·Å^{-3}$	

8.6 Bibliography

1 a) R. Wyler, J. de Mendoza, J. Rebek, Jr., *Angew. Chem. Int. Ed*., **1993**, *32*, 1699-1701. b) F. Hof, S. L. Craig, C. Nuckolls, J. Rebek, Jr., *Angew. Chem. Int. Ed.*, **2002**, *41*, 1488-1508. c) O. Mogck, V. Bçhmer, W. Vogt, *Tetrahedron*, **1996**, *52*, 8489-8496. d) V. Bçhmer, M. O. Vysotsky, *Aust. J. Chem.* **2001**, *54*, 671-677. e) L. J. Prins, D. N. Reinhoudt, P. Timmerman, *Angew. Chem. Int. Ed.*, **2001**, *40*, 2382-2426.

2 M. Fujita, S. Nagao, K. Ogura, *J. Am. Chem. Soc.*, **1995**, *117*, 1649-1650. b) M. Fujita, *Chem. Soc. Rev.*, **1998**, *27*, 417-425. c) P. Jacopozzi, E. Dalcanale, *Angew. Chem. Int. Ed.*, **1997**, *36*, 613-615. d) D. L. Caulder, K. N. Raymond, *J. Chem. Soc. Dalton Trans.*, **1999**, 1185-1200. e) S. R. Seidel, P. J. Stang, *Acc. Chem. Res.*, **2002**, *35*, 972-983. f) M. M. J. Smulders, I. A. Riddell, C. Browne, J. R. Nitschke, *Chem. Soc. Rev.*, **2013**, *42*, 1728-1754.

3 a) F. Corbellini, R. Fiammengo, P. Timmerman, M. Crego-Calama, K. Versluis, A. J. R. Heck, I. Luyten, D. N. Reinhoudt, *J. Am. Chem. Soc.*, **2002**, *124*, 6569-6575. b) R. Fiammengo, P. Timmerman, J. Huskens, K. Versluis, A. J. R. Heck, D. N. Reinhoudt, *Tetrahedron*, **2002**, *58*, 757-764. c) R. Fiammengo, K. Wojciechowski, M. Crego-Calama, P. Timmerman, A. Figoli, M. Wessling, D. N. Reinhoudt, *Org. Lett.,* **2003**, *19*, 3367-3370. d) G. V. Oshovsky, D. N. Reinhoudt, W. Verboom, *J. Am. Chem. Soc.*, **2006**, *128*, 5270-5278. e) G. V. Oshovsky, D. N. Reinhoudt, W. Verboom, *J. Org. Chem.* **2006**, *71*, 7441-7448. f) G. V. Oshovsky, D. N. Reinhoudt, W. Verboom, *Eur. J. Org. Chem.* **2006**, 2810–2816. g) T. S. Koblenz, H. L. Dekker, C. G. de Koster, P. W. N. M. van Leeuwen, J. N. H. Reek, *Chem. Commun.*, **2006**, 1700-1702.

4 a) R. Zadmard, T. Schrader, T. Grawe, A. Kraft, *Org. Lett.,10*, **2002**, 1687-1690. b) R. Zadmard, M. Junkers, T. Schrader, T. Grawe, A. Kraft, *J. Org. Chem.* **2003**, *68*, 6511-6521. c) F. Corbellini, F. W. B. van Leeuwen, H. Beijleveld, H. Kooijman, A. L. Spek, W. Verboom, M. Crego-Calama, D. N. Reinhoudt, *New J. Chem.*, **2005**, *29*, 243–248. d) B. Kuberski, A. Szumna, *Chem. Commun.*, **2009**, 1959-1961. e) T. S. Koblenz, H. L. Dekker, C. G. de Koster, P. W. N. M. van Leeuwen, J. N. H. Reek, *Chem. Asian J.*, **2011**, *6*, 2444-2462. f) T. S. Koblenz, H. L. Dekker, C. G. de Koster, P. W. N. M. van Leeuwen, J. N. H. Reek, *Chem. Asian J.*, **2011,** *6*, 2431-2443.

5 a) F. Corbellini, L. Di Costanzo, M. Crego-Calama, S. Geremia, D. N. Reinhoudt, *J. Am. Chem. Soc.*, **2003**, *125*, 9946-9947. b) F. Corbellini, R. M. A. Knegtel, P. D. J. Grootenhuis, M. Crego-Calama, D. N. Reinhoudt, *Chem. Eur. J.*, **2005**, *11*, 298-307.

6 a) T. Grawe, T. Schrader, R. Zadmard, A. Kraft, *J. Org. Chem.* **2002**, *67,* 3755-3763. b) T. Kusukawa, C. Katano, C. Kim, *Tetrahedron*, **2012**, *68*, 1492-1501.

7 A. Chen, D. H. Wu, C. S. Johnson, *J. Am. Chem. Soc.*, **1995**, *117*, 7965-7970.

8 a) P. Thordarson, *Chem. Soc. Rev.*, **2011**, *40*, 1305-1323. b) D. B. Hibbert, P. Thordarson, *Chem. Commun.*, **2016**, *52*, 12792-12805.

9 W. L. F. Armarego, C. Chai in *Purification of Laboratory Chemicals (Seventh Edition)*, Butterworth-Heinemann, Boston, **2013.**

10 W. C. Still, M. Kahn, A. Mitra, *J. Org. Chem.*, **1978**, *14*, 2923-2925.

Conclusions and Future Perspectives

C.1 Development of a New Synthetic Route to C_3-Triphenylenes

In the first chapter of this Doctoral Thesis, the development of a new synthetic route to 3,7,11-tris(benzyloxy)triphenylene-2,6,10-triol, ***C*$_3$-26** as a very useful and versatile molecule for its application in supramolecular chemistry was reported.

This result was obtained after a systematic study of different cyclization methods for the preparation of the central triphenylenic core. After selecting the tris-benzylidene **18** as a suitable scaffold for the following reduction reaction, the latter was optimized changing several parameters such as kind of reductant, Lewis acid, reaction temperature and time in order to optimize the yield of the final product. The final setup resulted to be a good compromise between reaction time and temperature in order to obtain the best yield, with the possibility of recycling the undesired ***C*$_S$-26** co-product.

At the same time, studies regarding the stereochemistry of the tris-benzylidene **18** were carried out in order to understand the number of possible stereoisomers and their distribution. To fulfil this target, the fluorinated tris-benzylidene **23** was obtained following an alternative synthetic way, demonstrating that the molecule, despite ^{1}H NMR isocronicity, exists in two isomers, *syn* and *anti*, with a distribution of 1:3 in favour of the *anti*, as predicted by theory and statistic.

C.2 Mannich Reactions on C_3-triphenylenes

The second chapter focused on the functionalization of the ***C*$_3$-26** product, obtained in the first chapter, through Mannich reaction. It is worth to mention that this kind of functionalization is one of the few reporting successfully a reaction involving sterically hindered triphenylene CH residues. The optimized synthetic procedure enabled the synthesis of a wide range of highly functionalized cyclic derivatives, in medium to high yields.

Even if in the proposed small library of compounds did not show liquid crystals properties, we are confident that in the near future, by using the developed efficient functionalization method and making a delicate balance between the size, and flexibility, of the substituents of the triphenylene core, a new class of liquid crystals could be realistically obtained with possible unique interesting applications.

However, the introduction on the triphenylene unit of six-member heterocyclic rings caused the new substituents to bend outside the triphenylene plane, making the class of molecules more three-dimensional from a substrate that was perfectly flat in the beginning. This peculiarity was exploited in Chapter 5 for the preparation of metal-ligand capsules in solution.

C.3 Other Derivatizations on the Triphenylene Core

In this Chapter, new derivatization methods for the triphenylene CH residues was investigated, aiming of widening the reactivity of the aromatic unit and also at the development of alternative methods for the preparation of sumanene derivatives, useful concave molecules for supramolecular applications.

Unfortunately, none of our trials led to the final product, but during this study a good knowledge of the reactivity of the triphenylene was achieved, enabling the optimization of an amido-methylation of the ***C*$_3$-26** product forming a new *C*$_3$-symmetric triphenylene, endowed with electrophilic chloro-acetamido functionalities, thus opening for future studies on the functionalization of this new triphenylene scaffold. In fact, nucleophilic substitution reactions on such electrophilic units was proved to be possible, and the next steps will be the functionalization of this triphenylene derivative with bulky residues in order to force the latter to reside on one side or the other of the plane of the triphenylene core. This will lead to different stereoisomers, potentially characterized by *P* and *M* stable helicity due to out-of-plane arrangement of the substituents (which are potentially helpful for diastereomeric functionalization).

C.4 Sulphide and Disulphide Cages

After the synthesis of three different thiol-substituted triphenylenes, the *tris*-thiol **49** was successfully employed for the synthesis of two covalent cages, one based on the dimerization of **49** through disulphide bonds, the second obtained through nucleophilic substitution reaction with a *tris*-halogenated mesitylene in order to obtain a smaller sulphide cage. The disulphide cage **50** resulted to exists in a mixture of stereoisomers, (*PP,MM*) and (*meso-PM*), due to the prochirality of the precursor ***C*$_3$-26**.

Once obtained, the molecules were fully characterized and subjected to host-guest experiments in order to understand also this behaviour. The experiments did not provide so far clear examples of suitable guests for disulphide **50**, and for sulphide **52** the interactions observed with cationic species were fairly modest. For this reason, more host-guest experiments will be carried out in the future, trying different and more soluble guests in order to match the rather small cavity of the capsules.

C.5 Pt and Pd Ligands from *C*$_3$-Triphenylenes

After the obtainment of Mannich-substituted triphenylenes, by using different amino-pyridines we were able to synthesize efficiently three *C*$_3$-symmetric triphenylene tridentate pyridine ligands that were employed for the synthesis of coordination cages in solution with Pd(II) or Pt(II) metal centres as coordination corners. Among the three ligands considered, ***m*-54** provided in solution the formation of M_3L_2 cages both with Pd(II) or Pt(II) metal corners, when using dppe as a ligand for the metal. In contrast, the ***o*-54** ligand led to more unstable assemblies and the ***p*-54** ligands led only to the formation of coordination polymers, that eventually precipitated from the solution, regardless the use of Pd(II) or Pt(II) metal centres. As far as the ***m*-54** ligand is concerned, ^{1}H NMR pseudo-2D-DOSY

experiments and $^{19}F\{^1H\}$ NMR titrations demonstrated the formation of clear M_3L_2 aggregates in solution, even though the $^{31}P\{^1H\}$ NMR and ^1H NMR spectra were not informative due to exchange processes. The latter were attributed to the formation of diastereoisomeric cages, derived by the prochiral nature of the tris-pyridine triphenylene ligand once coordinated, forming the trigonal bipyramidal unit and conformational equilibria of the ligand itself and of the diphosphane, as supported by quanto-mechanical calculations. No clear-cut evidence of guest binding was observed due to the dynamic properties of the assemblies, although it cannot be excluded that, in the narrow cavity, binding of solvent molecules or more probably of counter-anions could occur.

In the future, other metalorganic cages will be taken in consideration, designing other C_3-symmetric triphenylenic ligands.

C.6 Hydrogen Bonded Capsules

Starting from the precursor ***C*$_3$-26**, after functionalization with carboxylic functional groups, the monomer **69** turned out to self-assemble into dimers through hydrogen bond interactions. What is remarkable is the fact that this molecule, albeit insoluble in chloroform but fairly soluble in methanol, demonstrated to aggregate in the latter solvent through the establishment of six hydrogen bonds between the carboxylic moieties, as demonstrated by the observation of an AB system by the benzylic methylene in the ^1H NMR spectra, which was even more clear by lowering the temperature. The obtained species is likely to be homochiral based on quanto-mechanical calculations of the possible stereoisomeric dimeric capsules. Titration of a solution of **69** in methanol with chloroform gave further support to the formation of the dimeric capsule in solution, observing a 1:1 mixture of the solvents as best conditions for the formation of the capsule. In the future, host-guest trials will be carried out at low temperature and in the 1:1 methanol/chloroform mixture to highlight possible uses of this capsule in supramolecular chemistry, based on the presence of a cavity of about 540 $Å^3$ as determined by quantomechanical calculations.

C.7 Water-Soluble Triphenylenes and Micelles

In this Chapter of Doctoral Thesis, the design and the synthesis of C_3-symmetric triphenylene units endowed with alternating hydrophilic (neutral, cationic and anionic) and hydrophobic substituents was reported, aiming to the promotion of spontaneous self-assembly in water, driven by the hydrophobic effect, to obtain nanometric capsules formed by only few amphiphilic units. Several analyses with various techniques, like ^1H NMR, pseudo-2D-DOSY NMR, DLS, AFM and SANS revealed the presence of nanometric capsules in water at least for the *tris*-sulfonate species **70**, endowed with three hydrophobic benzyl moieties. In particular, with hydrophobic benzyl units pointing inward and the hydrophilic sulfonated units outward, the micelles are characterized by a hydrodynamic radius of 1.8 nm in water and an organic core of 1.13 nm as determined by SANS experiments, which is compatible with the aggregation of only six molecules of **70** in solution. Quantomechanical calculations and molecular dynamic studies supported the experimental data. Results on the other water-soluble triphenylenes suggest a behavior similar to **70**, except for molecule

72, which is not provided of hydrophobic moieties and that showed formation of only dimers, with no cavity to host additional species.

The nano-micelles could host hydrophobic guests like mesitylene, aromatic naphthols and 1-adamantanol, with different exchange properties as function of the solubility of the guests in water. In the near future, these properties will be the base for supramolecular catalysis trials for different reactions, in particular for those involving apolar substrates and cationic intermediate species.

C.8 Ionic Dimeric Capsule

In Chapter 8, the spontaneous assembly of a novel ion-paired capsule **70·75** at mM concentration was disclosed. The new capsule is based on two C_3-symmetric triphenylene units whose synthesis is reported in Chapter 7, held together by three ionic interactions. The **70·75** cage is stable both in polar-protic and aprotic solvent like methanol and DMSO, featuring an electron rich internal cavity displaying high selectivity for flat cationic aromatic guests like methylene blue or methyl viologen. The structure of the capsule was further supported by the X-ray structure of the dimeric assembly obtained by evaporation of a sample in methanol. After these positive results, we envisage that C_3-symmetric triphenylene units will spur further developments and applications in supramolecular recognition phenomena and eventually supramolecular catalysis in polar media.

In conclusion of this doctoral thesis, through several examples of new chemical modifications, characterized by high yields and selectivities and new supramolecular structures, held together by a wide range of intermolecular forces forming several new host systems, has reached its target to revamp triphenylene and derivatives as a new molecular scaffold in supramolecular chemistry. We are sure that this will spur future investigation on the capsules and cages presented in this work, enriching the scientific community involved in this interdisciplinary field of research.